Identification of a Novel Metastasis Enhancer, CDCP1, and Analysis of Its Functions during Melanoma Metastasis

by

Hui Liu

M.S. Biology
University of Georgia, 2001

SUBMITTED TO THE DEPARTMENT OF BIOLOGY
IN PARTIAL FULFILLMENT OF THE REQUIREMENTS FOR THE DEGREE OF

DOCTOR OF PHILOSOPHY IN BIOLOGY
AT THE
MASSACHUSETTS INSTITUTE OF TECHNOLOGY

ARCHIVES

May 2009

Signature of Author: _____
Department of Biology
May 22, 2009

Certified by: _____
Richard O. Hynes
Professor of Biology
Thesis Supervisor

Certified by: _____
Forest M. White
Associate Professor of Biological Engineering
Thesis Supervisor

Accepted by: _____
Stephen P. Bell
Professor of Biology
Chairman, Committee for Graduate Studies

Identification of a Novel Metastasis Enhancer, CDCP1, and Analysis of Its Functions during Melanoma Metastasis

by

Hui Liu

Submitted to the Department of Biology on May 22nd 2008,
In Partial Fulfillment of the Requirements for the
Degree of Doctor of Philosophy in Biology

ABSTRACT

Nearly 90% of cancer mortality from solid tumors is due to metastasis of malignant cells to the distant vital organs. It is now well established that a plethora of stromal cells are present within the tumor, and contribute in various ways to tumor initiation and progression, and plasma membrane proteins are the mediators for tumor-stromal communications. In this thesis, I focused on plasma membrane proteins that may contribute to tumor metastasis. I applied quantitative mass spectrometry technology to first identify plasma proteins that are expressed at different levels in melanoma cells with high versus low metastatic abilities. Using SILAC (stable isotope labeling with amino acids in culture) coupled with nano-spray tandem mass spectrometry, this work led to the discovery of Cub Domain Containing Protein 1 (CDCP1) as one of those differentially expressed transmembrane proteins. We found that CDCP1 is not only a surface marker for cells with higher metastatic potential, it is also functionally engaged in enhancing tumor metastasis. When searching for the underlying mechanisms, we found that CDCP1 is important for soft agar colony-forming abilities, suggesting that CDCP1 might regulate the balance between cell proliferation and anoikis. Making use of 3D Matrigel culture system, we found that CDCP1 also regulates scattered growth of melanoma cells. We speculate these two factors may contribute to enhanced-metastatic ability observed in mice. When investigating signaling pathways that may mediate the functions of CDCP1, we found that overexpression of CDCP1 correlates with hyper-activation of Src family kinases. While wild-type CDCP1 enhances SFK activation, point mutation that abolished CDCP1 functions (in scattered growth and in metastasis) also abolished SFK hyper-activation, suggesting that CDCP1 might function through the activation of SFKs. Such notion was further supported since pharmacological reagents PP2 and Dasatinib, which are two SFK inhibitors, blocked *in vitro* functions of CDCP1 in scattered growth. Thus the work in this thesis has identified a novel metastasis enhancer, CDCP1, and has gained insight into the mechanisms by which CDCP1 functions.

Thesis supervisors:

Richard Hynes: **Professor of Biology**

Forest White: **Associate Professor of Biological Engineering**

ACKNOWLEDGEMENTS

This thesis would not have been possible without the help and support from many people. First and foremost, I want to thank my thesis advisers – Richard Hynes and Forest White. I want to thank Richard for his support and guidance, and also the independence he gave me to pursue my scientific interests. I also want to thank him for always being patient and calm… I sincerely appreciated his effort in ensuring the lab being a pleasant place for every member, and I simply admire his critical yet fair judgments of science in general.

When experiments were particularly challenging at the beginning of the thesis, Forest came and rescue me. With his experience, his eager of sharing that experience, and his laughter and openness, he guided me through the rough spots.

I would like to thank my thesis committee members, Tyler Jacks and Michael Yaffe for their time and advice, and for their critical evaluation of my work. I am also grateful to Michael Hemann and Karen Cichowski for giving the time and effort to be on my defense committee.

I want to thank Richard Cook and Alla Leshinsky in the biopolymer facility. Dick generously allowed me to learn and use their instrument for my mass spectrometry work; and Alla has being there for me – we worked side-by-side and learned mass spectrometry step-by-step together. I am grateful to Shao-En Ong at the Broad Institute for providing invaluable suggestions, and for being a great person to talk to when having mass spectrometry problems. Many thanks go to the proteomics facility as well.

It has been great pleasure working in the Hynes lab for the past years and I want to thank all the Hynes lab members for making it such a friendly, supportive and stimulating working environment. Many thanks to Jane, for her loving and caring for all the lab members, and for fulfilling my requests of having bourbon sauce on all my birthday cakes. I want to thank the past and present fellow graduate students, Sarah, Chris, Sunny, Olga, and Jeff, for sharing the wonderful graduate school experiences. I also want to thank previous and current Hynes lab members, Lei, Patrick, Sophie, Yueyi, Aaron, Shahin, Mariette, Myriam, Joe, Josh, Adam and John in our side of the lab, and Kaan, Chris, Arjan, Hamid, Jessica, and Kwabena in "the other side" of the lab, they are all fantastic people to work with.

Our Koch Institute support facilities have made many of the experiments possible. I am particularly grateful for Denise Crowley, Charlie Whittaker, Elisa Vasile, and MIT Division of Comparative Medicine for their help. Also, I would like to thank Dr. Donna Stoltz, Dr. James Quigley, and Dr. Ryuichi Sakai for generously providing various reagents for my work.

Lastly, I want to thank my family – my parents for their endless support and encouragement and giving me the freedom of pursuing my interests since I was little; my husband for his love, patience (when are you going to get a real job?) and tolerance ☺; and my little David for making me understand the simplicity of happiness, and giving me a different perspective on almost everything, even other drivers honking me on the street!

Table of Contents

Title Page	----------	1
Abstract	----------	3
Acknowledgement	----------	5
Table of Contents	----------	7
Chapter 1:	Introduction ----------	9
Chapter 2:	Application of Quantitative Mass Spectrometry to Identify Membrane Proteins That are Differentially Expressed Between Poorly and Highly Metastatic Tumor Cells ----------	55
Chapter 3:	A Direct Test for the Role of CDCP1 in Melanoma Metastasis -------	93
Chapter 4:	Cellular Mechanisms by which CDCP1 May Function to Enhance Metastasis ----------	135
Chapter 5:	Molecular Mechanisms by which CDCP1 May Function to Enhance Metastasis ----------	171
Chapter 6:	Discussions and Future Directions ----------	233
Appendix A:	Role of Yes Associate Protein (YAP) in Melanoma Metastasis ------	253
Appendix B:	Protocols for SILAC and Mass Spectrometry ----------	267
Appendix C:	Proteins that were Identified by Mass Spectrometry ----------	273
Appendix D:	Materials and Methods ----------	293

CHAPTER 1.

INTRODUCTION

The contents of this chapter were written by Hui Liu, with editing by Richard Hynes.

The Basics of Cancer Metastasis

Despite significant improvement in local treatments for cancer, many patients still succumb to this disease. In 2008 alone, it was estimated by the American Cancer Society that 565,000 cancer-related deaths occurred. Nearly 90% of cancer mortality from solid tumors is due to tumor metastasis to the distant organs that are resistant to conventional therapies, begging for a more thorough understanding of this deadly disease. Indeed, the studies of cancer metastasis began over 100 years ago, but only in the past thirty years have we seen an explosion of research advances and started to gain insights into the mechanisms of the fatal disease. This lag is not due to lack of effort, but rather, it reflects the complicated nature of cancer metastasis.

It has long been observed that tumor cells metastasize to specific organs; breast cancer cells primarily metastasize to bone, lungs, liver and brain; lung adenocarcinomas frequently form tumors in brain, bone, adrenal gland and liver. While both colorectal and pancreatic cancer cells tend to grow secondary tumors in the liver and lungs, prostate caner cells almost exclusively migrate to bones and form tumors there (Hess et al., 2006; Nguyen et al., 2009). This tissue tropism has sparked various hypotheses, and numerous experiments have been carried out, particularly with the development of microarray technology, to address this issue (Gupta et al., 2005; Kang et al., 2003; Muller et al., 2001), and I will focus on this topic first. Another important feature of metastasis concerns the kinetic differences among various types of tumors. Breast cancer recurrences are often observed after years or decades of tumor remission, while lung cancer patients and patients with melanoma often suffer swift and multi-organ metastasis months after initial diagnosis (Hoffman et al., 2000; Karrison et al., 1999). This topic has just started to receive more attention and factors that account for the temporal differences among different tumors remain obscure.

Dividing Cancer Metastasis to Three Major Steps

Tumor metastasis is a complicated process, presumably involving tumor cell detachment and migration/invasion from the primary site (local invasion); intravasation, survival in the circulation, arrest and sometimes extravasation from the circulation (systemic traveling); and growth, survival and angiogenesis at the distant organ(s) (colonization) (Gupta and Massague, 2006; Hynes, 2003; Nguyen et al., 2009; Weiss, 2000).

It has become increasingly clear that tumor cells coordinate with environmental factors, such as other cells (in particular, fibroblasts, macrophages, platelets and endothelial cells) and extracellular matrix proteins to metastasize (Bissell et al., 2005; Bissell and Radisky, 2001; Condeelis and Pollard, 2006; Fata et al., 2004; Fidler et al., 2007; Haviv et al., 2009; Kenny and Bissell, 2003; Nelson and Bissell, 2006; Zumsteg and Christofori, 2009). In the past decade, with the development of microarray and other large-scale profiling technologies such as array-CGH and SNP arrays, a large number of genes/proteins have been found contributing to various steps of metastasis; both tumor cell-intrinsic factors and components derived from the stroma. Here I will describe three major steps through which tumor cells progress in order to make successful metastases, and give examples of factors that are involved in each step (see Figure 1 for an overview of these steps).

Step I - Local Migration and Invasion

The journey of cancer cell metastasis starts when cells detach from the primary tumor and begin to invade into neighboring connective tissues and blood vessels or lymphatics. Almost all cells have an intrinsic ability to perform some level of migration, and different cells may utilize different forms of migration; however, such activities are greatly augmented in invasive tumors.

Numerous *in vitro* studies using fibroblasts and keratinocytes migrating on 2D substrates have established the principal events leading to effective cell migration, which have recently been extended to migration in a 3D matrix (Friedl and Wolf, 2003; Lauffenburger and Horwitz, 1996). Migration in general can be divided into five steps that form a continuous cycle – 1) localized actin polymerization drives the formation of lamellipodia or filopodia, followed by 2) integrin-mediated focal-contact formation, engaging the intracellular actin-based cytoskeleton with extracellular matrix proteins. 3) Surface proteases such as membrane-type I matrix metalloproteinase are recruited near focal adhesions to perform localized matrix degradation. 4) Actin filaments engage cross-linking proteins to stabilize actin strands, and interact with contractile proteins such as myosin II, for contracting and shortening of actin strands. 5) Such contraction of membrane-anchored actin strands co-ordinates with turnover of focal adhesions at the rear ends, thus generating cell translocation along the substrate (Friedl, 2004). This type of movement is typical mesenchymal cell movement, where integrins and matrix matalloproteases have been

shown to play critical roles in migration (Hynes, 2002; Sabeh et al., 2004). Adhesion by integrins to ECM proteins presents a bimodal relationship – while weak interaction between integrins and ECM is not supportive for effective cell migration, high affinity also damps cell migration.

This 5-step model and *in vitro* migration systems have helped to decipher molecular players involved in each step of migration and have generated a large body of knowledge regarding effective cell migration. Initially, the actin-nucleating ARP2/3 complex together with a multifunctional adaptor protein N-WASP, are critical for the generation of actin protrusions (Bompard and Caron, 2004; Le Clainche and Carlier, 2008; Stradal and Scita, 2006), and phosphoinositides (PIPs) are important for both anchoring Arp2/3/WASP complexes to the membrane, and for activation of small GTPases RAC, CDC42 and Rho through binding and activating their activator GEFs (guanine-nucleotide exchange factors)(Kaibuchi et al., 1999). The accumulation of membrane metalloproteases has been shown to regulate fibroblast and tumor cell migration in 3D matrices *in vitro* (Friedl et al., 1997; Hotary et al., 2000; Sabeh et al., 2004), and regulates normal mammary gland development *in vivo* (Bissell et al., 2005; Fata et al., 2004).

The hypothesis that epithelial-mesenchymal transition (EMT) may play major roles during cancer metastasis further highlighted the importance of mesenchymal migration (Thiery, 2002; Yang et al., 2004). During EMT, epithelial cells reduce expression of the cell-cell adhesion molecule E-cadherin, acquire elongated morphology and migrate as single spindle-shaped cells. In humans, there seems to be an inverse relationship between E-cadherin levels and tumor grade or patient survival (Birchmeier and Behrens, 1994; Hirohashi, 1998). In the RipTag pancreatic mouse model, a loss of E-cadherin during adenoma-to-carcinoma transition was observed. When crossed with mice expressing E-cadherin under the Rip-promoter, tumors that developed in double-transgenic mice were arrested at adenoma stage; when RipTag mice were crossed with mice expressing dominant-negative E-cadherin, more tumors progress to carcinoma, with some of them invading to lymph nodes (Perl et al., 1998). These data are consistent with the model that EMT has a functional role during tumor progression and metastasis. In addition, transcription factors Twist, Snail and Slug, which induce EMT during normal development, have been shown to induce EMT in tumor cells and render these cells highly metastatic (Alves et al., 2009; Peinado et al., 2007; Yang et al., 2004). The importance of EMT has

been emphasized over the past years to understand how normally non-mobile epithelial cells become invasive.

Recently, a slightly different view of how tumor cells migrate *in vivo* has emerged, owing to the development of novel imaging technologies and use of fluorophore-labeled cells in live organisms (Sahai, 2007). Using multiphoton confocal microscopy, it has been observed that, *in vivo*, the speed and character of mammary carcinoma cell motility is quite different from what has been observed *in vitro* (Condeelis and Segall, 2003; Farina et al., 1998; Wyckoff et al., 2007). *In vivo*, cancer cells migrate in amoeboid fashion, with velocity up to 10 times that observed *in vitro*. The highest velocity was observed when cells move along linear ECM fibers, and such movement was not restricted by ECM networks in the mammary tumors. This type of amoeboid movement is quite different from the traditional mesenchymal movement described above. In amoeboid movement, cells make weak and transient interactions with ECM, lack stress fibers and focalized proteolytic activity (which are typical for mesenchymal migration), and the physical movement is generated by cortical filamentous actin (Friedl and Wolf, 2003).

It is, perhaps, not surprising to see a different mode of migration, since several different types of migration have long been observed during development and in human tumor samples. Migration can be categorized as individual cell migration (such as mesenchymal and amoeboid migration mentioned above) or collective cell migration. For example, during mammary gland morphogenesis, cells migrate together as a column; and following closure of the neural tube, blastoderm cells migrate as a sheet of cells (Davidson and Keller, 1999); both are collective migrations. In tumor samples, both single-cell and collective migrations have been observed, showing the heterogeneous nature of tumor cell migration.

In addition, tumor cells have shown great plasticity in mode of movement. In 3D collagen matrix, HT-1080 fibrosarcoma cells or MDA-MB-231 mammary carcinoma cells display a mesenchymal type of migration, dependent on β1 integrins and degrading matrix by MT1-MMPs. However, when such collagen proteolysis was blocked using a range of protease inhibitors, the cells completely changed their mode of migration and migrated in amoeboid fashion independent of proteolysis, "elbowing" their way through the collagen matrix. This newly adapted movement is instead dependent on the activation of ROCK (possibly by activation of RhoA), and myosin-generated force (Wolf et al., 2003; Wyckoff et al., 2006).

Primary melanoma tumor explants growing in collagen lattices migrate as multi-cellular clusters, with preferential β1 integrin localization at the leading edge. When blocking antibody was used against β1 integrins, instead of blocking cell migration, the melanoma cells took off as individual amoeboid cells and disseminated (Hegerfeldt et al., 2002). These observations suggest that tumor cells can use different migration patterns, depending on what tools are available to them.

It is safe to conclude that there is no "one-size-fits-all" for cancer cell migration and invasion *in vivo*. There are different modes of migration, each with different molecular requirements– mesenchymal migration is dependent on activation of integrins, Rac and MMPs, while amoeboid movement needs activities of Rho, and cells possess remarkable plasticity to switch between different methods. Therefore, studying tumor cell migration *in vivo* or *in vivo*–like 3D matrix settings will be useful to deduce common features and requirements for migration, in the hopes to develop therapeutic reagents to block tumor cell metastasis.

But what makes some carcinoma cells more invasive than others, if all cells have intrinsic abilities of migration? What are the factors that mobilize such migration abilities? The answers may lie both in the microenvironment in which tumor cells reside and in the ability of some tumor cells to activate their migration machinery more efficiently than others.

It is now well established that a plethora of stromal cells are present within the tumor, and contribute in various ways to tumor initiation and progression (Tlsty and Coussens, 2006). Cancer-associated fibroblasts (CAFs) have previously been shown to contribute to tumor growth (Camps et al., 1990; Haviv et al., 2009; Olumi et al., 1999) and invasiveness of colon cancer cells (Nakajima et al., 1990). Tumor cell interactions with fibroblasts regulate the secretion of type IV collagenase *in vitro* and presumably contribute to the differential production of this enzyme in *vivo* (Fabra et al., 1992). Recently, it was observed that fibroblasts lead collective squamous cell carcinoma invasion in 3D matrix, generating remodeled matrix tracks to enhance the carcinoma cells' invasion (Gaggioli et al., 2007).

The presence of innate immune cells, especially mast cells and macrophages, has been documented in numerous clinical studies, and has been correlated with angiogenesis and poor clinical outcomes (Duncan et al., 1998; Takanami et al., 2000; Talmadge et al., 2007). In experimental models (MMTv-PyMT mammary carcinoma model, or in lung cancer cells),

selectively deleting tumor-associated macrophages reduces tumor angiogenesis, invasion and lung metastasis, highlighting the pivotal roles of macrophages in tumor metastasis (Hiraoka et al., 2008; Lin et al., 2006; Lin et al., 2001; Miselis et al., 2008; Zeisberger et al., 2006). *In vivo*, direct observation of primary mammary tumors revealed enhanced infiltration of macrophages in tumors generated by highly metastatic cells relative to poorly metastatic cells.

On the tumor side, establishing cell polarity was suggested to be one of the essential functions for effective migration, and one important factor to differentiate tumor cells with different metastatic potentials (Friedl, 2004). Comparing mammary carcinoma cells with high metastatic ability (MTLn3 cells) to cells with low metastatic potential (MTC cells) revealed interesting differences (Farina et al., 1998; Neri et al., 1982). While MTLn3 cells migrate in a completely amoeboid manner without intrinsic polarity, once they come close to blood vessels, these cells polarize toward them (Wyckoff et al., 2000), and MTLn3 cells only invade blood vessels where perivascular macrophages are located (Wyckoff et al., 2007); MTC cells have some residual polarity with partial mesenchymal movement, but they do not respond to the blood vessel cue. Mechanistically, a paracrine loop has been identified between macrophages and breast carcinoma cells. These macrophages have been shown to produce epidermal growth factor (EGF), which will reorientate tumor cells expressing EGF-receptors, and attract them toward the blood vessels. Macrophages are recruited to the tumor site due to production of a powerful chemoattractant, colony-stimulating factor 1 (CSF-1) (Goswami et al., 2005; Wyckoff et al., 2004). Figure 2 shows the crosstalk between tumor cells and macrophages that enhances tumor cell local invasion.

Once polarity is established, it stimulates local activation of cofilin resulting in actin polymerization and membrane protrusion. Wyckoff et al have developed an *in vivo* invasion assay where needles containing EGF were inserted into the mammary gland to collect primary tumor cells that are actively in the process of invasion. This assay was combined with microarray technology to profile the cells that are most invasive from the primary tumors (Wyckoff et al., 2004). Through such analyses, the cofilin pathway was identified and shown to be a major determinant of metastasis (Wang et al., 2007; Wang et al., 2006). Cofilin is a small ubiquitous protein that can sever actin filaments, increasing the number of free barbed ends for future actin polymerization (Ghosh et al., 2004; Yamaguchi et al., 2005). In addition, cofilin can synergize with the dendritic nucleation acitivity of Arp2/3 complexes

(Ichetovkin et al., 2002). The end result of cofilin activation is a large increase in actin polymerization, generating protrusions at the membrane. It was shown that EGF stimulation of mammary carcinoma cells induces phosphorylation-dependent global inactivation of cofilin, while stimulating local phospholipase Cγ-mediated activation of cofilin. Such spatial control will direct actin polymerization toward the source of EGF, mediating directional cell migration (Wang et al., 2007). The importance of the cofilin pathway in mammary cancer metastasis was shown by experimentally manipulating LIM kinase 1 (LIMK1), which negatively regulates cofilin activity by phosphorylating cofilin. Mammary tumor cells expressing LIMK1 or kinase-dead LIMK1 have decreased or enhanced cofilin activation, respectively, which caused proportional reduction or increase in motility (both *in vitro* and *in vivo*), intravasation, and metastasis of tumor cells (Wang et al., 2006).

In addition, RhoC has been identified as a metastasis enhancer through microarray analysis comparing melanoma cells with low or high metastatic ability. When poorly metastatic melanoma cells over-express RhoC, these cells became more migratory and more metastatic when injected intravenously. Conversely, when highly metastatic cells express dominant-negative RhoC, there was a strong reduction in both cell migration and number of metastasis in the lungs, supporting the hypothesis that RhoC functions to enhance motility and metastasis (Clark et al., 2000). These experimental metastasis results were confirmed using an endogenous mammary tumor model crossed with RhoC knockout mice – many fewer metastases were observed when RhoC expression was abolished (Hakem et al., 2005).

In summary, current data support the idea that there exist intrinsic differences in cell migration machinery among tumor cells with different metastatic abilities. There also exist differences in how various tumor cells co-ordinate with their microenvironment – how they change the microenvironment, and how they respond to the different factors contributed by the cells in that local community. All these factors contribute to the ability of the tumor cells to migrate/invade through their tissue stroma to gain access to the circulation, which is the first step toward systemic dissemination.

Step II - Systemic Traveling and Arresting

The next hurdle tumor cells encounter before they gain access to the blood stream for systemic dissemination is the endothelial barrier. Tumor cell migration slows down significantly when tumor cells come near the blood vessels, possibly due to the thick basement membrane surrounding the blood vessels. When interacting with endothelial cells that express DARC (Duffy antigen receptor for chemokines), tumor cells may stop proliferation and senesce if they express tetraspanin CD82 (KAI1) (Bandyopadhyay et al., 2006). Trans-endothelial migration of tumor cells is one of the mechanisms that tumor cells use to intravasate, and in fact, angiopoietin-like 4 produced by tumor cells in response to TGF-β has been shown to induce dissociation of endothelial cell-cell junctions to facilitate tumor entrance to the blood stream (Padua et al., 2008). However, this is not the only mechanism by which tumor cells gain access to the bloodstream. Work by Chang et al has clearly shown that a high percentage of tumor vessels contain "mosaic" vessels, where part of the vessels lack CD31/CD105 and lectin staining, and are replaced by tumor cells (Chang et al., 2000). Although it is not clear whether the tumor cells are a functional part of the blood vessels, these data certainly suggest that tumor cells can directly face the blood stream without the barrier of endothelial cells, which is also in agreement with the fact that some tumor vessels are leaky. In other cases, tumor cells are thought first to enter rather porous lymphatics before draining into systemic circulation.

Whether or not entering the bloodstream is a rate-limiting step is still controversial, partly due to technical difficulties of direct observation. In some situations, large numbers of tumor cells have been observed in the blood. It has been estimated that nearly 4*10e6 cells were released from each gram of primary tumor per day (Butler and Gullino, 1975; Glaves et al., 1988; Weiss and Glaves, 1983). In other work, the number of tumor cells in circulation correlates with the number of lung metastases (Wyckoff et al., 2000), and correlates with poor prognosis (Denis et al., 1997; Racila et al., 1998), suggesting that it may be one of the rate-limiting steps in metastasis. It was observed that 32% of poorly metastatic MTC cells were fragmented while entering the blood stream, compared with 6% of highly metastatic MTLn3 cells, suggesting that intravasation is at least an inefficient, if not rate-limiting, step (Wyckoff et al., 2000). With new technology that efficiently captures circulating tumor cells (Nagrath et al., 2007), revisiting this question will certainly provide more information.

Once in the bloodstream, tumor cells are devoid of assembled extracellular matrix proteins with which they were familiar at the primary site, and endure shear stress that they have

never encountered before. It is speculated that activation of Rho, and thus stronger cortical acto-myosin contraction that promotes amoeboid movement discussed above, may physically help the tumor cells withstand mechanical stress (Sahai, 2007). In addition, increased expression of cytokeratin in highly metastatic cells relative to poorly metastatic cells was also suggested to play a role in physically counteracting the shear force in the circulation (Condeelis and Segall, 2003). Furthermore, genes involved in apoptosis pathways may also contribute to tumor cell survival.

James Ewing suggested that blood-flow pathways between primary and secondary tumors were sufficient to account for organ-specific metastasis (Fidler, 2003). Although it is clear that circulatory patterns do not fully explain tissue tropism, flow patterns certainly contribute to where tumor cells go once they are in the circulation. For example, colon cancer cells are taken by the hepatic-portal circulatory system first to the liver and indeed, 78% of colon cancer metastases are in liver (Hess et al., 2006). However, such blood-flow patterns cannot explain fully the distribution of metastases (Weiss, 2000). As will be discussed later, the tissue microenvironment where disseminated cells end up is another important determinant.

Eventually, circulating tumor cells arrest, making contacts with endothelial cells. In some situations, this can be a passive process – while the diameter of capillaries ranges from 3-8μm, the sizes of most tumor cells are around 15-20μm, and tumor cells can be arrested in the capillary due to physical constriction (Chambers et al., 2002; Ito et al., 2001). Alternatively, tumor cells may actively adhere to endothelial cells, similar to what has been observed for leukocytes. Selectins have been shown to be crucial for leukocyte tethering and rolling in response to inflammatory cytokines, which is essential for subsequent integrin activation and firm adhesion to endothelial cells (Sperandio, 2006). Tumor cells with reduced selectin ligands were less metastatic (Witz, 2008; Zipin et al., 2004). Spontaneous pancreatic tumors metastasize to lymph nodes when expressing L-selectin (Qian et al., 2001). Mice lacking P- and/or L-selectins were resistant to metastasis by colon cancer cells (Borsig et al., 2002), supporting the idea that selctin-mediated interactions with tumor cells may be actively involved in arresting in the blood vessels. Recently, it was shown that phage presenting metadherin home specifically to lung microvasculature and that breast cancer cells whose metadherin was blocked using antibody or siRNA showed reduced lung metastasis, in agreement with tumor-vasculature interaction being important for cancer cell

metastasis (Brown and Ruoslahti, 2004). *In vivo* imaging showed that within the bone marrow, there exist specialized discontinuous endothelial regions that express E-selectin and stromal-cell-derived factor 1 (SDF-1). When tumor cells (including leukemia cells and prostate cancer cells) were introduced to the mice through tail-vein injection, cells were localized to these regions within 1 hour of injection, and remained there for a period of time. Disrupting the interaction between SDF-1 and its receptor CXCR4 on the tumor cells inhibited localization of tumor cells to these discrete sites, suggesting that tumor cells are actively "homing" to regions in the bone marrow (Sipkins et al., 2005). These data support the idea that tumor cells can home to specific anatomic areas via active protein-protein or protein-carbohydrate interactions.

Several lines of evidence suggest that platelets may facilitate tumor cell metastasis through various means. Platelets have been observed to surround tumor cells (Honn et al., 1992a; Kitagawa et al., 1989), possibly providing physical protection and preventing attack by immune cells(Nieswandt et al., 1999); such tumor-platelet aggregates may help in tethering to endothelial cells, slowing down their movement, adhering to the blood vessel, and may help facilitating growth at the site, or extravasation. In addition, platelets are a rich source of various growth factors, such as platelet-derived growth factor (PDGF) and VEGF, which have been shown to promote tumor cell proliferation, survival, invasion (Lip et al., 2002; Nash et al., 2002) and angiogenesis (Sierko and Wojtukiewicz, 2004), all of which can potentially contribute to tumor metastasis (Honn et al., 1992b; Sierko and Wojtukiewicz, 2007).

Recently an intriguing observation was reported – in mice bearing subcutaneous tumors of either B16 melanoma or Lewis lung carcinoma (LLC), "pre-metastatic niches" were observed in the lungs, which contain bone-marrow-derived cells that are VEGFR1- and integrin $\alpha4\beta1$- positive. In these niches, strong fibronectin expression was also reported. This finding is surprising because such niches could apparently be detected before individual tumor cells were seen in the lungs. In addition, conditioned media from melanoma could re-direct LLC cells to organs to which melanomas frequently metastasize (Kaplan et al., 2005). These results suggested that "primary" tumors can secrete factors that mobilize bone-marrow-derived progenitor cells, which in turn dictate where the future metastases arise. In another paper, it was shown that tumor cells secrete growth factors such as VEGFA, TGFβ, and TNFα, which stimulate endothelial cells and Mac1+ myeloid

cells to produce chemokines S100A8, S100A9. These chemokines in turn stimulate tumor cell migration, and neutralizing antibodies reduced the colonization of tumor cells in the lung (Hiratsuka et al., 2006). This new observation suggests that primary tumor cells themselves, in part, determine where the future metastases arise through systemic release of factors, although a generalization of this idea requires many more experiments. There are many important questions unanswered. Given the systemic release of chemokines by the growth factors, why do "pre-metastatic" niches develop in specific sites? Are these sites that have different types of endothelial cells relative to their neighbors (Sipkins et al., 2005), or are these sites that experience different blood flow and thus different shear forces and respond differently to the systemic signals than do endothelial cells at other locations? Or are these sites of spontaneous lesions constantly occurring in normal organisms that attract platelets, which together with endothelial cells determine where these niches are? Are these sites indeed where the future metastasis are located? What are the roles of bone-marrow derived cells at these niches? Do they function like the macrophages in the primary tumor to generate a permissive environment? What are the functions of the fibronectin observed in these "pre-metastatic" niches? A deeper understanding of these questions will have important clinical implications in terms of preventing tumor cells from lodging at distant organs and preventing metastasis.

Step III - Colonization of Distant Organ(s)

As mentioned earlier, one of the characteristics of cancer metastasis is tissue tropism. In 1889, Stephen Paget found that out of 735 breast cancer necropsies, "241 had cancer of the liver, only 17 had cancer of the spleen, and 30 had cancer of the kidneys or suprarenals", and 70 had lung cancer (Weiss, 2000). Based on earlier work and ideas of Fuchs, he proposed the "seed-and-soil" theory - "When a plant goes to seed, its seeds are carried in all directions; but they can only live and grow if they fall on congenial soil" (Paget, 1989), thus tumor cells cannot flourish on their own unless they encounter a suitable organ environment. The "seed-and-soil" theory suggests that, in addition to the properties of the "seeds", additional factors at the "soil" or target organs will contribute greatly to the growth of metastases. I mentioned earlier the determinants of where tumor cells finally settle, which is certainly part of where the 'seeds" go, and now I will focus on the factors that contribute to whether these "seeds" can eventually flourish.

Given the large body of knowledge that tissue microenvironment contributes to tumor initiation and progression at the primary site, it is not hard to imagine similar cooperation at work at the metastatic sites, although work has just started to elucidate these factors. Recognizing similarities between circulating tumor cells and circulating leukocytes, Muller et al analyzed the chemokine receptor expression levels of a panel of human breast carcinoma cells, and found markedly enhanced expression of CXCR4 and CCR7. Their ligands (SDF-1α and CCL21, respectively) are highly enriched in lymph nodes, to which tumor cells normally metastasize. When blocking antibody was used to disrupt SDF1α – CXCR4 interactions, a significant reduction in lung and lymph node metastasis was observed, using both an experimental metastasis model and an orthotropic implantation model, supporting the important roles these chemokines play during mammary carcinoma metastasis (Muller et al., 2001). Melanoma and other mammary carcinoma cells that metastasize to the bone have been shown to express RANK (receptor), and in response to the ligand RANKL, the cells show increased migration. In vivo, disrupting RANK-RANKL signals by over-expression of the decoy receptor OPG on melanoma cells significantly decreased bone metastasis. These experiments clearly showed the importance of cytokines/chemokines in metastasis formation, although it is still not clear if these cytokines/chemokines just function in tumor cell "homing" to a particular organ, or if they also contribute to the growth of these cells upon their arrival (Jones et al., 2006).

Kang et al expanded the early studies by *in vivo* selection of mammary carcinoma cells that traffic specifically to the bones, and analyzed the expression profiles of these cells using microarrays, which was followed by functional evaluation of identified gene signatures (Kang et al., 2003; Lu and Kang, 2007). Together with Yin et al and Park et al, a co-operative network between mammary carcinoma cells and osteoclasts in the bone marrow was suggested to facilitate osteolytic metastasis (Lu and Kang, 2007; Pantschenko et al., 2003; Park et al., 2007; Yin et al., 1999). In this particular microenvironment, factors secreted by tumor cells (including IL-11, TNF-α, IL-6 and parathyroid hormone-related protein (PTHRP) stimulate the release of RANKL by osteoblasts. RANKL functions on myeloid precursor cells, promoting maturation of osteoclasts, which degrade the bone matrix and release a plethora of growth factors that benefit the tumor cells (Nguyen et al., 2009). Although different players are involved compared to the invasive microenvironment at the primary tumor site, a similar scheme is employed, involving both the tumor cells and tissue-resident cells and crosstalk among these cells. Recently, a different gene signature was discovered

marking mammary carcinoma cells that target specifically to the lungs (Minn et al., 2005). Comparison between this gene set with the "bone-metastasis" gene set revealed little commonality, suggesting that different molecules are involved in successful colonization in different organs. Given that many of the "lung signature" genes are secreted or membrane proteins, it is plausible that these factors invoke crosstalk between tumor cells and the lung-resident cells, together contributing to the formation of lung metastasis, although the details of such crosstalk await further elucidation. Figure 3 depicts such an "excited" microenvironment where various growth factors, cytokines and chemokines produced by tumor cells and tissue-resident cells provide a fertile "soil" for metastasis formation.

Another common site of metastasis is liver – almost all common tumors metastasize to the liver, and in particular, uveal melanoma, pancreatic and colorectal carcinomas preferentially form secondary tumors there. This may be partly due to the blood-flow pattern of liver – approximately 75% of all its blood supply comes from the hepatic portal vein, which drains from spleen and gastrointestinal tract and is rich in nutrients (Shneider 2008). It is the first microvascular bed that gastrointestinal tumor cells encounter once they have intravasated, and the rich nutrients in the blood could certainly help tumor survival and growth. The anatomy of the liver sinusoid may also contribute to establishment of metastases. Liver sinusoidal capillaries are fenestrated, lined with discontinuous endothelial cells, thus facilitating traverse of tumor cells into the organ (Paku et al., 2000).

Kupffer cells, which are liver-resident macrophages making up almost 10-15% of all liver cells, lining the liver sinusoids in addition to endothelial cells. As mentioned earlier, macrophages have been shown to play pivotal roles for mammary tumor initiation, angiogenesis and progression due to secretion of cytokines, growth factors and metalloproteases (Joyce and Pollard, 2009). Knowing the importance of macrophages in those circumstances, and drawing similarities here, can we speculate that Kupffer cells may also contribute to liver metastasis by providing rich sources of growth factors and cytokines to contribute to tumor cell colonization in the liver? There is some evidence supporting this hypothesis – tumor cells have been shown to stimulate Kupffer cells to release TNFα and to upregulate endothelial adhesion molecules such as E-selectin, mediating enhanced tumor-endothelial interactions (Auguste et al., 2007; Gangopadhyay et al., 1998; Gjoen et al., 1989; Khatib et al., 2005). A recent study suggests that Kupffer cell-derived MMP9 contributes to liver metastasis of colorectal cancer (Gorden et al., 2007). However, it was

also argued that Kupffer cells might function to suppress metastasis formation in the liver due to endocytosis-mediated tumor cell destruction (van der Bij et al., 2005).

These observations may sound contradictory at first, but probably reflect temporal differences in Kupffer cell functions. In work by Timmers et al investigating the early events of rat colon carcinoma cells injected intramesenterically into rats, they found that between 1 hr to 8 hr, about 70% of all tumor cells are in phagosomes of the Kupffer cells, which increases to approximately 90% by 24 hours, supporting their function as first-line immune defense at early time points. However, about 6% of all tumor cells remain untouched by Kupffer cells (or by Natural killer cells), suggesting this might be the population of tumor cells that persist and become metastases (Timmers et al., 2004), potentially through stimulating Kupffer cells to produce a variety of cytokines over a period of time. It is clear that, in order to understand why many different types tumor cells can flourish in the liver, more work is needed to investigate tumor-liver cell interactions. One starting point might be extending works by Kang et al and Minn et al, to isolate mammary carcinoma cells that specifically metastasize to the liver and profile those cells for "liver signatures". Furthermore, a more vigorous test of the function of Kupffer cells in metastasis establishment is necessary before research can be carried out to address the mechanisms of such involvement, if any.

Laborious approaches such as cDNA subtraction and microcell-mediated chromosomal transfer have been applied early on to identify genes that are involved in metastasis (Yoshida et al., 2000). Since then, new technologies such as genome sequencing and microarray analysis have accelerated the pace by which new discoveries were made. In the past decades, a large number of genes/proteins have been found to potentially contribute to metastasis by functioning in the above-mentioned steps. These are both cell-intrinsic factors (such as cofilin pathway, RhoC) and factors such as chemokines/chemokine receptors that allow for tumor-environment crosstalk. And some of these discoveries may open the gate toward better treatment. However, many questions still remain – in addition to tissue tropism, another observation is that different tumors metastasize at different rates. So what are the factors contributing to such temporal differences?

Kinetic Differences Among Different Tumor Metastases and Tumor Dormancy

It was observed that although breast cancer and lung cancer metastasize to similar organs (Hess et al., 2006), such as bone, liver and brain, they do so with distinct kinetics. In breast cancer, metastasis might be manifest years or decades after the initial removal of even a small primary tumor (Karrison et al., 1999); while for lung cancer, distant metastases can be established within months of diagnosis (Feld et al., 1984; Hoffman et al., 2000), and similar swift metastasis is observed in pancreatic and colorectal cancers (Fearon and Vogelstein, 1990; Nieto et al., 2008). Although early diagnosis accounts for some of the differences, the striking temporal variability among different types of tumors suggests mechanistic differences among the tumor cells forming metastases slowly or quickly.

One question concerning such variability is whether or not tumor cells from breast or prostate cancer disseminate at different time points relative to lung or colorectal or intestinal cancers? In breast and prostate cancers, it has been recently appreciated that dissemination of tumor cells can occur early during primary tumor progression (Klein, 2008; Riethdorf et al., 2008). This became apparent with better technology to identify disseminated tumor cells (DTCs) or circulating tumor cells (CTCs) from the bone marrow or the blood of cancer patients respectively, followed by single-cell genomic analysis including CGH (comparative genomic hybridization), LOH (loss of heterozygosity), and microarray analyses. Analyses of human DTCs have found that DTCs present different genomic changes compared to the primary tumors, suggesting that they may have disseminated early and evolved independently at the distant site (Schardt et al., 2005) (Schmidt-Kittler et al., 2003). In addition, early DTCs can also be found in transgenic mice bearing a constitutively activated HER-2 gene under control of MMTV promoter before the transition from epithelial hyperplasia to carcinoma *in situ*. Investigations following DTCs in mice have shown that they can eventually become overt metastases, supporting the idea that (at least some) early-disseminated cells from breast cancer are indeed metastasis-competent. These data showed that in breast cancer, tumor cells can achieve the first two steps (local invasion and systemic traveling and landing) of metastasis early, but the competence to colonize at the distant organ may take time to develop (Nguyen et al., 2009).

Colorectal carcinoma, on the other hand, seems to take decades to transit from colorectal hyperplasia to adenoma to invasive carcinoma; however, when colon tumor cells invade the underlying colonic wall, metastasis can proceed quickly. Once they become invasive, few, if any further genetic mutations are required for them to become metastatic (Jones et al.,

2008; Kinzler and Vogelstein, 1996). Although minimal residual disease has been observed from some colorectal patients, it is not clear whether they disseminated from early or late stages of tumors (Merrie et al., 1999). Currently studies to investigate DTCs in the liver for human patients and using colorectal mouse models have not been performed to the same extent as has been done for mammary tumors.

The temporal differences among different tumors may suggest mechanistic differences in the way that these primary tumor cells become metastatic. Maybe, for breast cancers, infiltration can be achieved early but the cells are kept "dormant", while for colorectal or lung cancer cells, ability to infiltrate is gained later during tumor progression while colonization is relatively efficient for these cells. Therefore, for breast cancer cells (and perhaps prostate cancer cells), tumor dormancy is of particular interest, since this step may represent a critical step amenable to clinical intervention. Identifying the capacities of different tumor cells at various stages of tumor progression will be particularly useful to design effective treatment, perhaps targeting the rate-limiting step(s) during metastasis for different tumor types.

Tumor Dormancy

Metastasis is an inefficient process, and it has been estimated that approximately 0.01% of cancer cells directly injected into circulation eventually form metastases (Fidler, 1970). Work by Cameron et al (Cameron et al., 2000) and Luzzi et al (Luzzi et al., 1998) showed that using an experimental metastasis assay where tumor cells were introduced into circulation directly, the initial "trapping " of the cells was efficient, with approximately 90% of cells observed 1 hour post injection. However, on day 3, only 2% of the cells persist as "micrometastases" or "seeds" and by two weeks, about 0.1% of the cells grow into micro- or macro-metastases in the liver, although a much higher percentage of solitary cells were observed (~80% on day3 and ~40% by two weeks, respectively) (Luzzi et al., 1998). Similar results were observed when tumor cells were introduced to the lungs, although the numbers are slightly different (Cameron et al., 2000). It was suggested that failure of these solitary cells to initiate growth and inefficiency of micrometastasis in progressing into macrometastasis, are the primary reasons for metastasis inefficiency.

In fact, persistent presence of tumor cells in cancer patients has long been observed, particularly in breast and prostate cancer patients, where 20-45% of patients will relapse years or even decades after initial tumor removal (Karrison et al., 1999). After initial treatments, tumor deposits that remain in the body (minimum residual disease) have been observed for breast, prostate, colon, head and neck, neuroblastoma, melanoma, non-small cell lung cancer, leukemia and lymphoma patients (Aguirre-Ghiso, 2007), threatening the recurrence of tumors in the patients. The long latency between the time of initial treatment and the manifestation of metastasis can not be explained by continuous tumor cell proliferation (Aguirre-Ghiso, 2007), and detected circulating tumor cells after surgery are often negative for the proliferation marker Ki67, suggesting that the state of "dormancy" exists in human patients (Muller et al., 2005).

Does tumor dormancy exist in mouse models that are commonly used for metastasis studies? The answer is yes. With fluorescence-marked mammary carcinoma cells, tumor cells can be seen by microscopy as single cells in the lungs upon tail-vein injection for up to 6 months; when recovered from the lungs, these cells retain the ability to proliferate *in vitro*, forming primary tumors at the subcutaneous site and in the fat pad (Goodison et al., 2003). This is true in the liver, since poorly metastatic mammary carcinoma cells were observed to persist in the liver as solitary cells for up to 11 weeks without proliferation (Ki67-negative), while highly metastatic cells progress to tumors (Naumov et al., 2002). Using magnetic resonance imaging (MRI) to track breast cancer cells in the brain and follow them overtime, Heyn et al have shown that while some cells become sizable tumors in the brain, others remain as single cells over the course of a month, representing a reservoir of dormant cells (Heyn et al., 2006).

Then the important questions are: 1) Why the disseminated cells are in a dormant state? 2) What triggers the exit from such a state?

Why disseminated tumor cells remain dormant?

It was appreciated that two types of dormancies exist – cellular dormancy as described above, where solitary cells remain alive but withdraw from the cell cycle; and tumor mass dormancy, when tumor cell proliferation and apoptosis are balanced, probably due to lack of

angiogenesis (Naumov et al., 2008). They are not mutually exclusive, and can co-exist both in mouse models and in human patients (Aguirre-Ghiso, 2007).

Currently the understanding of why individual tumor cells are dormant is still limited, and an emerging theme seems to be the lack of proper cell-microenvironment interactions, most notably cell–ECM (extracellular matrix protein) crosstalk. *In vitro*, 40% of tumorigenic T4-2 mammary cells proliferate continuously after 10-12days in Matrigel, while most non-malignant S1 cells stopped proliferation and assumed acinar structures. When integrin β1 blocking antibody was used to interfere with tumor cell and ECM interactions, T4-2 cells upregulated $p21^{cip}$ and withdrew from the cell cycle, which was reversible if the blocking antibody is removed. These observations suggest that, at least *in vitro*, the ability of cells to engage proper ECM is critical for cell proliferation (Weaver et al., 1997). *In vivo*, concomitant deletion of β1 integrin (MMTV-$\beta1^{loxP/loxP}$) and expression of polyoma-virus middle T oncogene (MMTV-Cre-PyMT) in mammary epithelial cells resulted in reduced hyperplastic nodules in the mammary glands; when the hyperplastic nodules were analyzed for β1 integrin expression, they remained positive (due to the mosaic pattern of Cre expression, thus a mosaic pattern of β1 integrin deletion). When β1 was deleted *in vitro* by infecting tumor cells with adenovirus expressing Cre, these cells failed to proliferate *in vitro*; and when orthotopically implanted into the mammary fat pad, cells deleted of β1 integrins failed to proliferate *in vivo*, although remaining as single cells (White et al., 2004). These data showed that disrupting integrin and ECM interaction renders the cells dormant, both *in vitro* and *in vivo* at the primary tumor site.

Along the same line, reduction of urokinase plasminogen activator receptor (uPAR) in human epidermoid carcinoma cells resulted in loss of tumor growth in chick CAM, which is probably due to much reduced cell proliferation judging by BrdU incorporation. This loss of tumor growth can last up to 5 months before spontaneous resumption of growth occurs (Yu et al., 1997). Work by Aguirre-Ghiso et al led to the conclusion that μPAR is involved in activation of integrin α5β1, which activates the ERK (mitogenic extracellular regulated kinase) signaling pathway. When disrupting μPAR-β1 integrin interactions with blocking peptides, activation of ERK is reduced (Aguirre Ghiso et al., 1999). Furthermore, activation of integrin α5β1 promotes fibronectin fibril assembly, and results in reduced signaling through stress-activated kinase $p38^{MAPK}$ activation (Aguirre-Ghiso et al., 2001). *In vivo* imaging in chick CAM and in nude mice has shown the activation of ERK or p38MAPK in

growing or dormant tumors, respectively (Aguirre-Ghiso et al., 2004). It was proposed by Aguirre-Ghiso et al that a balance between oncogenic activated ERK pathway and stress-activated $p38^{MAPK}$ pathway determines whether cells enter proliferation or dormancy (Ranganathan et al., 2006a; Ranganathan et al., 2006b).

Conceptually, it is logical to think that when disseminated tumor cells land in foreign organs, where integrins encounter incompatible ECM, the cells may activate a "stress pathway". As a result, the cells withdraw from cell cycle and become dormant. The above-mentioned experiments certainly support this hypothesis. Further support of this idea came from work by Vander Griend et al (Vander Griend et al., 2005). They found that over-expression of JNK (c-Jun NH2-teminal kinase) – specific kinase MKK7 in prostate carcinoma cells, which activates the JNK pathway, significantly suppressed formation of overt lung metastasis. Lungs bearing these tumor cells formed microscopic metastasis, but could not progress to full-blown tumors. The same metastasis-suppression was observed when MKK4 was over-expressed, which activated both JNK and $p38^{MAPK}$ pathways (Vander Griend et al., 2005; Yamada et al., 2002; Yoshida et al., 1999). Recently the same group showed that, in human ovarian cancer cell lines, activation of $p38^{MAPK}$ (by MKK6) and JNK (by MKK4) suppressed tumor metastasis in the lungs via activation of p21cip and p26kip in tumor cells and withdrawal from cell cycle (Hickson et al., 2006; Lotan et al., 2008).

In addition to the role of tumor-ECM interactions in inducing tumor dormancy, other cells in the microenvironment that the tumor cells encounter are likely to contribute as well. The tetraspanin KAI1 (or CD82) has been found to be a metastasis suppressor for prostate, breast, lung, pancreatic tumors and for melanomas and the mechanism of such suppression has recently been elucidated after the ligand of KAI1 was found (Dong et al., 1995; Tonoli and Barrett, 2005). It turns out the Duffy antigen receptor for chemokines (DARC) is localized specifically on the endothelial cells, and interaction between KAI1 localized on the tumor cells with DARC leads to inhibition of tumor proliferation and tumor cell senescence (Bandyopadhyay et al., 2006). These data suggest that interactions between tumor cells and endothelial cells are likely to induce tumor cell dormancy as well, although it is not clear why KAI1 does not affect primary tumor growth and functions to suppress metastasis specifically. One possible link is that KAI1 has been shown to regulate μPAR activities and to interact with integrins and disrupt integrin signaling (Bass et al., 2005; Sridhar and Miranti,

2006), reflecting the recurring theme of disrupted tumor-microenvironment communications mentioned earlier, but the detailed mechanisms are not clear.

KiSS-1 is another metastasis suppressor gene that has been shown to suppress melanoma, mammary and ovarian cancer metastasis, but did not affect primary tumor growth (Lee et al., 1996; Lee and Welch, 1997; Nash and Welch, 2006). It encodes several secreted peptides, among which is metastin, a 54-amino acid peptide that binds to G-protein-coupled-receptor 54 (GPR54) (Kotani et al., 2001; Muir et al., 2001; Ohtaki et al., 2001). Although the early report suggested that GRP54 mediates the metastasis-suppression function of KISS1 in melanomas (Ohtaki et al., 2001), other reports have shown KISS-1 can still suppress tumor metastases even when they lack GPR54 expression (Jiang et al., 2005; Nash et al., 2007; Nash and Welch, 2006). It was found that melanoma cells expressing KiSS1 persist in the lungs as solitary cells for up to 120 days after intravenous injection, suggesting the induction of cellular dormancy by KISS1. Interestingly, these tumor cells do not express the receptor GPR54, and only when KISS1 is secreted can it function as a metastasis suppressor. In addition, such suppression is manifested in multiple organs such as lung, eye, kidney and bones (Horak et al., 2008; Nash et al., 2007). It is possible that other unknown receptor(s) on the tumor cells may be mediating KiSS1 functions as a metastasis suppressor. It is also conceivable, given known tumor-microenvironment communications, that secreted KISS1 acts on other cells in the microenvironment, which in turn, mediate tumor cell dormancy.

The relationships between primary tumors and their metastases are complicated – on the one hand, primary tumors have been claimed to mobilize bone marrow-derived cells to set up "pre-metastatic niches" to facilitate future metastasis; on the other hand, primary tumors have been shown to systemically secrete factors that keep metastases in check. Husemann et al found that in mice bearing primary tumors, the number of DTCs is small (approximately 0.002% of the bone marrow cells). However, when transferred into naïve mice, these DTCs quickly expand into tumors and can make up to 30% of the bone marrow in the recipient mice. This work suggested that in mice with primary tumors, the DTCs are kept in a dormant state, which can be released experimentally by transferring DTCs to naive mice without primary tumors (Husemann et al., 2008). Angiogenesis inhibitors secreted by the primary tumors, such as angiostatin and endostatin, have been shown to maintain metastases in tumor mass dormancy, with proliferation balanced by cell apoptosis due to

lack of angiogenesis (Holmgren et al., 1995; Naumov et al., 2008; O'Reilly et al., 1994). A short burst of angiogensis factors, which occurs after surgical removal of the primary tumors, can tip such a balance and result in overt metastasis formation (Demicheli et al., 2008; Indraccolo et al., 2006).

What wakes the cells from dormant state?

Another important question concerning tumor dormancy is what are the factors that wake up those cells from their dormant state and restores competency to become full-blown tumors? Unfortunately, we only have very limited knowledge on this question.

One intriguing observation though, may shed some light on this question. Work by Podsypanina in the Varmus group showed that normal mammary epithelial cells, when injected into the tail vein of immunocompromised mice, are able to persist in the lungs for up to 4 months with slow proliferation. However, when these cells were induced to express ongogenic Ras and Myc, the cells proliferate quickly and develop into ectopic mammary tumors in the lung (Podsypanina et al., 2008). Although this scenario is different from dormant metastasis cells in that 1) presumably clusters of mammary epithelial cells were introduced to the lung, rather than single solitary cells and 2) the existence of a basal level of mitosis in the cells that is lacking in dormant disseminated cancer cells, these data suggested that acute oncogenic stimulation can quickly "wake up" the cells to become competent for intensive proliferation. It is conceivable that for dormant disseminated tumor cells that reside in the body, maybe a local or systemic "stimulation" can functionally fulfill what is achieved here (by inducing K-Ras and Myc), and thus act as a switch to turn on the proliferative competence of the dormant cells. The nature of this stimulation is not clear. But one can speculate that changes in the microenvironment due to inflammation or aging could be part of the "stimulus package". It was shown that induction of lung inflammation through activation of macrophages enhanced lung metastases formation (Stathopoulos et al., 2008); hyperoxic injury to the lung and allergen-induced pulmonary inflammation also increased lung metastasis (Adamson et al., 1987; Taranova et al., 2008). Furthermore, cells expressing senescent markers accumulate with age (Dimri et al., 1995; Mishima et al., 1999; Pendergrass et al., 1999), and senescent fibroblasts have been shown to produce inflammatory cytokines and proteases, promoting tumor cell growth (Campisi, 2005; Krtolica

et al., 2001). These data suggest that changes in the microenvironment of tumor cells may contribute to waking the cells from dormant state, although the mechanisms are not clear.

The ultimate goal of studying metastasis is to slow the progress of the disease, and ideally coax tumor cells into "peaceful existence" within host organs, and the naturally-occurring tumor dormancy offers some hope toward such a goal. It is fair to say that, although tumor dormancy has been recognized for half a century (Hadfield, 1954), mechanistic studies of this phenomenon have just started to yield fruit, and we still have very limited knowledge on this subject. With currently available technologies, such as live imaging technology, *in vivo* functional screening using barcoded RNAi and cDNA expression libraries, and global expression profiling, we can expect to see an explosion of research on this topic, which will undoubtedly extend our understanding of this intriguing phenomenon.

Outstanding questions

Despite significant enrichment of knowledge about cancer metastasis, many questions remain and some have been outlined above. As mentioned earlier, different tumor cells preferentially metastasize to defined sets of organs (tissue tropism), and this could be due to preferential landing and /or preferential growth at these organs, and may often involve both the tumor cells and other cell types such as macrophages, fibroblasts and endothelial cells present in the distant organs. Much work has been done on mammary carcinomas to understand metastasis toward bone and lung, but research on this front for other types of tumors is still lacking. In addition, tissue tropism toward liver has not been extensively studied, although almost all tumor types metastasize to this organ.

When investigating tumor-stromal interactions, many factors, most noticeably soluble factors such as chemokines and growth factors, have been shown to contribute greatly to initial invasion and ultimately to tumor growth at distant sites. However, research on membrane-localized adhesion molecules has not been done to the same level. Recently "cancer stem cells (CSC)" have been hypothesized to contribute to solid tumor initiation and maintenance (Visvader and Lindeman, 2008), and to tumor metastasis (Brabletz et al., 2005). Adult stem cells have been shown to exist in various tissues such as skin (Blanpain and Fuchs, 2009), prostate, breast (Shackleton et al., 2006), lung (Kim et al., 2005), brain, and in several cases, expansion of adult stem cells has been observed upon oncogenic stimulation (Kim et

al., 2005; Malanchi et al., 2008; Shackleton et al., 2006), suggesting they may be the precursors for these tumors. *In vitro* sorting of tumor cells based on different surface markers (such as CD44, CD133, Thy-1, CD24, CD49) has shown that certain cell populations marked by "stem cell markers" are more efficient at forming tumors in immunocompromised mice (Al-Hajj et al., 2003; Bao et al., 2006; Cho et al., 2008; Fang et al., 2005; Hermann et al., 2007; Malanchi et al., 2008; Schatton et al., 2008; Singh et al., 2004; Wright et al., 2008; Yang et al., 2008). Although the "cancer stem cell" theory was recently challenged (Kelly et al., 2007; Quintana et al., 2008) and the question of whether they are real "stem cells" is still debated, it remains true that cells with certain surface markers can initiate tumors better than cells that do not express these surface markers. Elucidating the common roles of these "markers" may provide additional targets for cancer treatment.

What are these "markers"? One commonly used marker is CD44 – CD44 is a receptor for hyaluronic acid, which is a major component of extracellular matrix of most mammalian tissues. It has been shown to be involved in adhesion and motility, cell proliferation, and cell survival, and over-expression of CD44 variant forms has been shown to enhance metastasis in pancreatic and mammary tumors (Gunthert et al., 1991; Klingbeil et al., 2009), potentially through activation of c-Met (Matzke et al., 2007; Orian-Rousseau et al., 2002), Src (Lee et al., 2008) and/or Rho-ROCK (Visvader and Lindeman, 2008). Therefore, it is possible that CD44 expression on the "cancer stem cells" confers functional advantage for these cells to be better equipped for tumor formation and invasion. Another routinely used "cancer stem cell" marker is CD133, or prominin. Although not many functional studies have been done on this molecule, recent work showed that reducing CD133 expression by siRNA in metastatic melanoma significantly reduced lung metastasis, supporting a functional role of this molecule during metastasis (Rappa et al., 2008). Perhaps in addition to being surface markers, these membrane proteins are actually involved in communication with their environment, providing selective advantages for these cells during the course of tumor formation and metastasis.

Although many membrane adhesion molecules have been identified to be involved in cancer metastasis (E-cadherin, ICAM, integrins etc), putting them in the context of a complicated *in vivo* environment and investigating tumor cell behavior in such an environment will be one step further toward an integrated view of metastasis formation. In particular, in the context

of tumor dormancy when tumor cells fail to recognize the new environment, adhesion molecules will undoubtedly be interesting targets to investigate, to understand if some of them provide "this is home" information and allow the outgrowth of metastasis, or transduce stress signals to retain dormancy. Currently, this research is still lacking

Finally, although I did not elaborate upon it in this review, the host immune system can both positively and negatively affect tumor initiation, progression and metastasis, and that is certainly an area of intensive investigation (Dunn et al., 2004; Smyth et al., 2006).

Plasma membrane proteins in melanoma metastasis

As described earlier, tumor microenvironment contributes greatly to tumor initiation, progression and metastasis formation. Many of the genes in the "gene signature" derived from mammary carcinoma cells metastasizing to the lungs encode secreted and membrane proteins (Minn et al., 2005); a "metastasis signature" that correlates with clinical outcomes of melanoma patients is also highly enriched for secreted and membrane proteins (Xu et al., 2008). Given that these factors (secreted proteins, plasma membrane proteins) potentially mediate the interactions between tumor cells and their microenvironment, this thesis aims to investigate plasma membrane proteins and their roles in melanoma metastasis. The subsequent chapters are structured in the following manner:

- In **Chapter 2**, I will describe a strategy that we applied to enrich for plasma membrane proteins. I will also describe a quantitative mass spectrometry method we applied to identify membrane proteins that are differentially expressed on melanoma cells with high versus low metastatic potentials. Finally, I will discuss the identification of one membrane protein – Cub domain containing protein 1 (CDCP1) - through such a process and focus on this protein for subsequent functional analysis.

- In **Chapter 3**, I will provide an overview of CDCP1 and CUB domains – including proteins containing CUB domain and CUB domain structures. I will also provide evidence that CDCP1 is a surface marker for melanoma cells with higher metastatic ability. I will further test the functional involvement of CDCP1 using both shRNA-mediated knock-down, and using retrovirus-mediated over-expression. It was found, by both methods, that CDCP1 plays a causal role to enhance melanoma metastasis.

- In **Chapter 4**, I will describe our attempts to understand, at a cell biological level, the functions of CDCP1 that contribute to its metastasis-enhancer activity. I will describe our work with both conventional 2D assays and eventually turn to 3D Matrigel assays to understand the roles of the CDCP1.

- In **Chapter 5**, I will provide an overview of activation mechanisms of Src and PKCδ, and I will describe our attempts at understanding the functions of CDCP1 at the molecular level. I will provide evidence that Src activation possibly contributes to the functions of CDCP1, both *in vitro* and *in vivo*.

- In **Chapter 6**, I will summarize the work described in this thesis, the unanswered questions that came from this study, and possible avenues for future research that could be undertaken to answer these questions.

REFERENCES

Adamson, I. Y., Young, L., and Orr, F. W. (1987). Tumor metastasis after hyperoxic injury and repair of the pulmonary endothelium. Lab Invest *57*, 71-77.
Aguirre Ghiso, J. A., Kovalski, K., and Ossowski, L. (1999). Tumor dormancy induced by downregulation of urokinase receptor in human carcinoma involves integrin and MAPK signaling. J Cell Biol *147*, 89-104.
Aguirre-Ghiso, J. A. (2007). Models, mechanisms and clinical evidence for cancer dormancy. Nat Rev Cancer *7*, 834-846.
Aguirre-Ghiso, J. A., Liu, D., Mignatti, A., Kovalski, K., and Ossowski, L. (2001). Urokinase receptor and fibronectin regulate the ERK(MAPK) to p38(MAPK) activity ratios that determine carcinoma cell proliferation or dormancy in vivo. Mol Biol Cell *12*, 863-879.
Aguirre-Ghiso, J. A., Ossowski, L., and Rosenbaum, S. K. (2004). Green fluorescent protein tagging of extracellular signal-regulated kinase and p38 pathways reveals novel dynamics of pathway activation during primary and metastatic growth. Cancer Res *64*, 7336-7345.
Al-Hajj, M., Wicha, M. S., Benito-Hernandez, A., Morrison, S. J., and Clarke, M. F. (2003). Prospective identification of tumorigenic breast cancer cells. Proc Natl Acad Sci U S A *100*, 3983-3988.
Alves, C. C., Carneiro, F., Hoefler, H., and Becker, K. F. (2009). Role of the epithelial-mesenchymal transition regulator Slug in primary human cancers. Front Biosci *14*, 3035-3050.
Auguste, P., Fallavollita, L., Wang, N., Burnier, J., Bikfalvi, A., and Brodt, P. (2007). The host inflammatory response promotes liver metastasis by increasing tumor cell arrest and extravasation. Am J Pathol *170*, 1781-1792.
Bandyopadhyay, S., Zhan, R., Chaudhuri, A., Watabe, M., Pai, S. K., Hirota, S., Hosobe, S., Tsukada, T., Miura, K., Takano, Y., *et al.* (2006). Interaction of KAI1 on tumor cells with DARC on vascular endothelium leads to metastasis suppression. Nat Med *12*, 933-938.
Bao, S., Wu, Q., McLendon, R. E., Hao, Y., Shi, Q., Hjelmeland, A. B., Dewhirst, M. W., Bigner, D. D., and Rich, J. N. (2006). Glioma stem cells promote radioresistance by preferential activation of the DNA damage response. Nature *444*, 756-760.
Bass, R., Werner, F., Odintsova, E., Sugiura, T., Berditchevski, F., and Ellis, V. (2005). Regulation of urokinase receptor proteolytic function by the tetraspanin CD82. J Biol Chem *280*, 14811-14818.
Birchmeier, W., and Behrens, J. (1994). Cadherin expression in carcinomas: role in the formation of cell junctions and the prevention of invasiveness. Biochim Biophys Acta *1198*, 11-26.
Bissell, M. J., Kenny, P. A., and Radisky, D. C. (2005). Microenvironmental regulators of tissue structure and function also regulate tumor induction and progression: the role of extracellular matrix and its degrading enzymes. Cold Spring Harb Symp Quant Biol *70*, 343-356.
Bissell, M. J., and Radisky, D. (2001). Putting tumours in context. Nat Rev Cancer *1*, 46-54.
Blanpain, C., and Fuchs, E. (2009). Epidermal homeostasis: a balancing act of stem cells in the skin. Nat Rev Mol Cell Biol *10*, 207-217.
Bompard, G., and Caron, E. (2004). Regulation of WASP/WAVE proteins: making a long story short. J Cell Biol *166*, 957-962.
Borsig, L., Wong, R., Hynes, R. O., Varki, N. M., and Varki, A. (2002). Synergistic effects of L- and P-selectin in facilitating tumor metastasis can involve non-mucin ligands and implicate leukocytes as enhancers of metastasis. Proc Natl Acad Sci U S A *99*, 2193-2198.

Brabletz, T., Jung, A., Spaderna, S., Hlubek, F., and Kirchner, T. (2005). Opinion: migrating cancer stem cells - an integrated concept of malignant tumour progression. Nat Rev Cancer *5*, 744-749.
Brown, D. M., and Ruoslahti, E. (2004). Metadherin, a cell surface protein in breast tumors that mediates lung metastasis. Cancer Cell *5*, 365-374.
Butler, T. P., and Gullino, P. M. (1975). Quantitation of cell shedding into efferent blood of mammary adenocarcinoma. Cancer Res *35*, 512-516.
Cameron, M. D., Schmidt, E. E., Kerkvliet, N., Nadkarni, K. V., Morris, V. L., Groom, A. C., Chambers, A. F., and MacDonald, I. C. (2000). Temporal progression of metastasis in lung: cell survival, dormancy, and location dependence of metastatic inefficiency. Cancer Res *60*, 2541-2546.
Campisi, J. (2005). Senescent cells, tumor suppression, and organismal aging: good citizens, bad neighbors. Cell *120*, 513-522.
Camps, J. L., Chang, S. M., Hsu, T. C., Freeman, M. R., Hong, S. J., Zhau, H. E., von Eschenbach, A. C., and Chung, L. W. (1990). Fibroblast-mediated acceleration of human epithelial tumor growth in vivo. Proc Natl Acad Sci U S A *87*, 75-79.
Chambers, A. F., Groom, A. C., and MacDonald, I. C. (2002). Dissemination and growth of cancer cells in metastatic sites. Nat Rev Cancer *2*, 563-572.
Chang, Y. S., di Tomaso, E., McDonald, D. M., Jones, R., Jain, R. K., and Munn, L. L. (2000). Mosaic blood vessels in tumors: frequency of cancer cells in contact with flowing blood. Proc Natl Acad Sci U S A *97*, 14608-14613.
Cho, R. W., Wang, X., Diehn, M., Shedden, K., Chen, G. Y., Sherlock, G., Gurney, A., Lewicki, J., and Clarke, M. F. (2008). Isolation and molecular characterization of cancer stem cells in MMTV-Wnt-1 murine breast tumors. Stem Cells *26*, 364-371.
Clark, E. A., Golub, T. R., Lander, E. S., and Hynes, R. O. (2000). Genomic analysis of metastasis reveals an essential role for RhoC. Nature *406*, 532-535.
Condeelis, J., and Pollard, J. W. (2006). Macrophages: obligate partners for tumor cell migration, invasion, and metastasis. Cell *124*, 263-266.
Condeelis, J., and Segall, J. E. (2003). Intravital imaging of cell movement in tumours. Nat Rev Cancer *3*, 921-930.
Davidson, L. A., and Keller, R. E. (1999). Neural tube closure in Xenopus laevis involves medial migration, directed protrusive activity, cell intercalation and convergent extension. Development *126*, 4547-4556.
Demicheli, R., Retsky, M. W., Hrushesky, W. J., Baum, M., and Gukas, I. D. (2008). The effects of surgery on tumor growth: a century of investigations. Ann Oncol *19*, 1821-1828.
Denis, M. G., Lipart, C., Leborgne, J., LeHur, P. A., Galmiche, J. P., Denis, M., Ruud, E., Truchaud, A., and Lustenberger, P. (1997). Detection of disseminated tumor cells in peripheral blood of colorectal cancer patients. Int J Cancer *74*, 540-544.
Dimri, G. P., Lee, X., Basile, G., Acosta, M., Scott, G., Roskelley, C., Medrano, E. E., Linskens, M., Rubelj, I., Pereira-Smith, O., and et al. (1995). A biomarker that identifies senescent human cells in culture and in aging skin in vivo. Proc Natl Acad Sci U S A *92*, 9363-9367.
Dong, J. T., Lamb, P. W., Rinker-Schaeffer, C. W., Vukanovic, J., Ichikawa, T., Isaacs, J. T., and Barrett, J. C. (1995). KAI1, a metastasis suppressor gene for prostate cancer on human chromosome 11p11.2. Science *268*, 884-886.
Duncan, L. M., Richards, L. A., and Mihm, M. C., Jr. (1998). Increased mast cell density in invasive melanoma. J Cutan Pathol *25*, 11-15.
Dunn, G. P., Old, L. J., and Schreiber, R. D. (2004). The three Es of cancer immunoediting. Annu Rev Immunol *22*, 329-360.

Fabra, A., Nakajima, M., Bucana, C. D., and Fidler, I. J. (1992). Modulation of the invasive phenotype of human colon carcinoma cells by organ specific fibroblasts of nude mice. Differentiation *52*, 101-110.
Fang, D., Nguyen, T. K., Leishear, K., Finko, R., Kulp, A. N., Hotz, S., Van Belle, P. A., Xu, X., Elder, D. E., and Herlyn, M. (2005). A tumorigenic subpopulation with stem cell properties in melanomas. Cancer Res *65*, 9328-9337.
Farina, K. L., Wyckoff, J. B., Rivera, J., Lee, H., Segall, J. E., Condeelis, J. S., and Jones, J. G. (1998). Cell motility of tumor cells visualized in living intact primary tumors using green fluorescent protein. Cancer Res *58*, 2528-2532.
Fata, J. E., Werb, Z., and Bissell, M. J. (2004). Regulation of mammary gland branching morphogenesis by the extracellular matrix and its remodeling enzymes. Breast Cancer Res *6*, 1-11.
Fearon, E. R., and Vogelstein, B. (1990). A genetic model for colorectal tumorigenesis. Cell *61*, 759-767.
Feld, R., Rubinstein, L. V., and Weisenberger, T. H. (1984). Sites of recurrence in resected stage I non-small-cell lung cancer: a guide for future studies. J Clin Oncol *2*, 1352-1358.
Fidler, I. J. (1970). Metastasis: guantitative analysis of distribution and fate of tumor embolilabeled with 125 I-5-iodo-2'-deoxyuridine. J Natl Cancer Inst *45*, 773-782.
Fidler, I. J. (2003). The pathogenesis of cancer metastasis: the 'seed and soil' hypothesis revisited. Nat Rev Cancer *3*, 453-458.
Fidler, I. J., Kim, S. J., and Langley, R. R. (2007). The role of the organ microenvironment in the biology and therapy of cancer metastasis. J Cell Biochem *101*, 927-936.
Friedl, P. (2004). Prespecification and plasticity: shifting mechanisms of cell migration. Curr Opin Cell Biol *16*, 14-23.
Friedl, P., Maaser, K., Klein, C. E., Niggemann, B., Krohne, G., and Zanker, K. S. (1997). Migration of highly aggressive MV3 melanoma cells in 3-dimensional collagen lattices results in local matrix reorganization and shedding of alpha2 and beta1 integrins and CD44. Cancer Res *57*, 2061-2070.
Friedl, P., and Wolf, K. (2003). Tumour-cell invasion and migration: diversity and escape mechanisms. Nat Rev Cancer *3*, 362-374.
Gaggioli, C., Hooper, S., Hidalgo-Carcedo, C., Grosse, R., Marshall, J. F., Harrington, K., and Sahai, E. (2007). Fibroblast-led collective invasion of carcinoma cells with differing roles for RhoGTPases in leading and following cells. Nat Cell Biol *9*, 1392-1400.
Gangopadhyay, A., Lazure, D. A., and Thomas, P. (1998). Adhesion of colorectal carcinoma cells to the endothelium is mediated by cytokines from CEA stimulated Kupffer cells. Clin Exp Metastasis *16*, 703-712.
Ghosh, M., Song, X., Mouneimne, G., Sidani, M., Lawrence, D. S., and Condeelis, J. S. (2004). Cofilin promotes actin polymerization and defines the direction of cell motility. Science *304*, 743-746.
Gjoen, T., Seljelid, R., and Kolset, S. O. (1989). Binding of metastatic colon carcinoma cells to liver macrophages. J Leukoc Biol *45*, 362-369.
Glaves, D., Huben, R. P., and Weiss, L. (1988). Haematogenous dissemination of cells from human renal adenocarcinomas. Br J Cancer *57*, 32-35.
Goodison, S., Kawai, K., Hihara, J., Jiang, P., Yang, M., Urquidi, V., Hoffman, R. M., and Tarin, D. (2003). Prolonged dormancy and site-specific growth potential of cancer cells spontaneously disseminated from nonmetastatic breast tumors as revealed by labeling with green fluorescent protein. Clin Cancer Res *9*, 3808-3814.
Gorden, D. L., Fingleton, B., Crawford, H. C., Jansen, D. E., Lepage, M., and Matrisian, L. M. (2007). Resident stromal cell-derived MMP-9 promotes the growth of colorectal metastases in the liver microenvironment. Int J Cancer *121*, 495-500.

Goswami, S., Sahai, E., Wyckoff, J. B., Cammer, M., Cox, D., Pixley, F. J., Stanley, E. R., Segall, J. E., and Condeelis, J. S. (2005). Macrophages promote the invasion of breast carcinoma cells via a colony-stimulating factor-1/epidermal growth factor paracrine loop. Cancer Res *65*, 5278-5283.
Gunthert, U., Hofmann, M., Rudy, W., Reber, S., Zoller, M., Haussmann, I., Matzku, S., Wenzel, A., Ponta, H., and Herrlich, P. (1991). A new variant of glycoprotein CD44 confers metastatic potential to rat carcinoma cells. Cell *65*, 13-24.
Gupta, G. P., and Massague, J. (2006). Cancer metastasis: building a framework. Cell *127*, 679-695.
Gupta, G. P., Minn, A. J., Kang, Y., Siegel, P. M., Serganova, I., Cordon-Cardo, C., Olshen, A. B., Gerald, W. L., and Massague, J. (2005). Identifying site-specific metastasis genes and functions. Cold Spring Harb Symp Quant Biol *70*, 149-158.
Hadfield, G. (1954). The dormant cancer cell. Br Med J *2*, 607-610.
Hakem, A., Sanchez-Sweatman, O., You-Ten, A., Duncan, G., Wakeham, A., Khokha, R., and Mak, T. W. (2005). RhoC is dispensable for embryogenesis and tumor initiation but essential for metastasis. Genes Dev *19*, 1974-1979.
Haviv, I., Polyak, K., Qiu, W., Hu, M., and Campbell, I. (2009). Origin of carcinoma associated fibroblasts. Cell Cycle *8*, 589-595.
Hegerfeldt, Y., Tusch, M., Brocker, E. B., and Friedl, P. (2002). Collective cell movement in primary melanoma explants: plasticity of cell-cell interaction, beta1-integrin function, and migration strategies. Cancer Res *62*, 2125-2130.
Hermann, P. C., Huber, S. L., Herrler, T., Aicher, A., Ellwart, J. W., Guba, M., Bruns, C. J., and Heeschen, C. (2007). Distinct populations of cancer stem cells determine tumor growth and metastatic activity in human pancreatic cancer. Cell Stem Cell *1*, 313-323.
Hess, K. R., Varadhachary, G. R., Taylor, S. H., Wei, W., Raber, M. N., Lenzi, R., and Abbruzzese, J. L. (2006). Metastatic patterns in adenocarcinoma. Cancer *106*, 1624-1633.
Heyn, C., Ronald, J. A., Ramadan, S. S., Snir, J. A., Barry, A. M., MacKenzie, L. T., Mikulis, D. J., Palmieri, D., Bronder, J. L., Steeg, P. S., *et al.* (2006). In vivo MRI of cancer cell fate at the single-cell level in a mouse model of breast cancer metastasis to the brain. Magn Reson Med *56*, 1001-1010.
Hickson, J. A., Huo, D., Vander Griend, D. J., Lin, A., Rinker-Schaeffer, C. W., and Yamada, S. D. (2006). The p38 kinases MKK4 and MKK6 suppress metastatic colonization in human ovarian carcinoma. Cancer Res *66*, 2264-2270.
Hiraoka, K., Zenmyo, M., Watari, K., Iguchi, H., Fotovati, A., Kimura, Y. N., Hosoi, F., Shoda, T., Nagata, K., Osada, H., *et al.* (2008). Inhibition of bone and muscle metastases of lung cancer cells by a decrease in the number of monocytes/macrophages. Cancer Sci *99*, 1595-1602.
Hiratsuka, S., Watanabe, A., Aburatani, H., and Maru, Y. (2006). Tumour-mediated upregulation of chemoattractants and recruitment of myeloid cells predetermines lung metastasis. Nat Cell Biol *8*, 1369-1375.
Hirohashi, S. (1998). Inactivation of the E-cadherin-mediated cell adhesion system in human cancers. Am J Pathol *153*, 333-339.
Hoffman, P. C., Mauer, A. M., and Vokes, E. E. (2000). Lung cancer. Lancet *355*, 479-485.
Holmgren, L., O'Reilly, M. S., and Folkman, J. (1995). Dormancy of micrometastases: balanced proliferation and apoptosis in the presence of angiogenesis suppression. Nat Med *1*, 149-153.
Honn, K. V., Tang, D. G., and Chen, Y. Q. (1992a). Platelets and cancer metastasis: more than an epiphenomenon. Semin Thromb Hemost *18*, 392-415.
Honn, K. V., Tang, D. G., and Crissman, J. D. (1992b). Platelets and cancer metastasis: a causal relationship? Cancer Metastasis Rev *11*, 325-351.

Horak, C. E., Lee, J. H., Marshall, J. C., Shreeve, S. M., and Steeg, P. S. (2008). The role of metastasis suppressor genes in metastatic dormancy. APMIS *116*, 586-601.
Hotary, K., Allen, E., Punturieri, A., Yana, I., and Weiss, S. J. (2000). Regulation of cell invasion and morphogenesis in a three-dimensional type I collagen matrix by membrane-type matrix metalloproteinases 1, 2, and 3. J Cell Biol *149*, 1309-1323.
Husemann, Y., Geigl, J. B., Schubert, F., Musiani, P., Meyer, M., Burghart, E., Forni, G., Eils, R., Fehm, T., Riethmuller, G., and Klein, C. A. (2008). Systemic spread is an early step in breast cancer. Cancer Cell *13*, 58-68.
Hynes, R. O. (2002). Integrins: bidirectional, allosteric signaling machines. Cell *110*, 673-687.
Hynes, R. O. (2003). Metastatic potential: generic predisposition of the primary tumor or rare, metastatic variants-or both? Cell *113*, 821-823.
Ichetovkin, I., Grant, W., and Condeelis, J. (2002). Cofilin produces newly polymerized actin filaments that are preferred for dendritic nucleation by the Arp2/3 complex. Curr Biol *12*, 79-84.
Indraccolo, S., Favaro, E., and Amadori, A. (2006). Dormant tumors awaken by a short-term angiogenic burst: the spike hypothesis. Cell Cycle *5*, 1751-1755.
Ito, S., Nakanishi, H., Ikehara, Y., Kato, T., Kasai, Y., Ito, K., Akiyama, S., Nakao, A., and Tatematsu, M. (2001). Real-time observation of micrometastasis formation in the living mouse liver using a green fluorescent protein gene-tagged rat tongue carcinoma cell line. Int J Cancer *93*, 212-217.
Jiang, Y., Berk, M., Singh, L. S., Tan, H., Yin, L., Powell, C. T., and Xu, Y. (2005). KiSS1 suppresses metastasis in human ovarian cancer via inhibition of protein kinase C alpha. Clin Exp Metastasis *22*, 369-376.
Jones, D. H., Nakashima, T., Sanchez, O. H., Kozieradzki, I., Komarova, S. V., Sarosi, I., Morony, S., Rubin, E., Sarao, R., Hojilla, C. V., *et al.* (2006). Regulation of cancer cell migration and bone metastasis by RANKL. Nature *440*, 692-696.
Jones, S., Chen, W. D., Parmigiani, G., Diehl, F., Beerenwinkel, N., Antal, T., Traulsen, A., Nowak, M. A., Siegel, C., Velculescu, V. E., *et al.* (2008). Comparative lesion sequencing provides insights into tumor evolution. Proc Natl Acad Sci U S A *105*, 4283-4288.
Joyce, J. A., and Pollard, J. W. (2009). Microenvironmental regulation of metastasis. Nat Rev Cancer *9*, 239-252.
Kaibuchi, K., Kuroda, S., and Amano, M. (1999). Regulation of the cytoskeleton and cell adhesion by the Rho family GTPases in mammalian cells. Annu Rev Biochem *68*, 459-486.
Kang, Y., Siegel, P. M., Shu, W., Drobnjak, M., Kakonen, S. M., Cordon-Cardo, C., Guise, T. A., and Massague, J. (2003). A multigenic program mediating breast cancer metastasis to bone. Cancer Cell *3*, 537-549.
Kaplan, R. N., Riba, R. D., Zacharoulis, S., Bramley, A. H., Vincent, L., Costa, C., MacDonald, D. D., Jin, D. K., Shido, K., Kerns, S. A., *et al.* (2005). VEGFR1-positive haematopoietic bone marrow progenitors initiate the pre-metastatic niche. Nature *438*, 820-827.
Karrison, T. G., Ferguson, D. J., and Meier, P. (1999). Dormancy of mammary carcinoma after mastectomy. J Natl Cancer Inst *91*, 80-85.
Kelly, P. N., Dakic, A., Adams, J. M., Nutt, S. L., and Strasser, A. (2007). Tumor growth need not be driven by rare cancer stem cells. Science *317*, 337.
Kenny, P. A., and Bissell, M. J. (2003). Tumor reversion: correction of malignant behavior by microenvironmental cues. Int J Cancer *107*, 688-695.
Khatib, A. M., Auguste, P., Fallavollita, L., Wang, N., Samani, A., Kontogiannea, M., Meterissian, S., and Brodt, P. (2005). Characterization of the host proinflammatory response to tumor cells during the initial stages of liver metastasis. Am J Pathol *167*, 749-759.

Kim, C. F., Jackson, E. L., Woolfenden, A. E., Lawrence, S., Babar, I., Vogel, S., Crowley, D., Bronson, R. T., and Jacks, T. (2005). Identification of bronchioalveolar stem cells in normal lung and lung cancer. Cell *121*, 823-835.
Kinzler, K. W., and Vogelstein, B. (1996). Lessons from hereditary colorectal cancer. Cell *87*, 159-170.
Kitagawa, H., Yamamoto, N., Yamamoto, K., Tanoue, K., Kosaki, G., and Yamazaki, H. (1989). Involvement of platelet membrane glycoprotein Ib and glycoprotein IIb/IIIa complex in thrombin-dependent and -independent platelet aggregations induced by tumor cells. Cancer Res *49*, 537-541.
Klein, C. A. (2008). The direct molecular analysis of metastatic precursor cells in breast cancer: a chance for a better understanding of metastasis and for personalised medicine. Eur J Cancer *44*, 2721-2725.
Klingbeil, P., Marhaba, R., Jung, T., Kirmse, R., Ludwig, T., and Zoller, M. (2009). CD44 variant isoforms promote metastasis formation by a tumor cell-matrix cross-talk that supports adhesion and apoptosis resistance. Mol Cancer Res *7*, 168-179.
Kotani, M., Detheux, M., Vandenbogaerde, A., Communi, D., Vanderwinden, J. M., Le Poul, E., Brezillon, S., Tyldesley, R., Suarez-Huerta, N., Vandeput, F., *et al.* (2001). The metastasis suppressor gene KiSS-1 encodes kisspeptins, the natural ligands of the orphan G protein-coupled receptor GPR54. J Biol Chem *276*, 34631-34636.
Krtolica, A., Parrinello, S., Lockett, S., Desprez, P. Y., and Campisi, J. (2001). Senescent fibroblasts promote epithelial cell growth and tumorigenesis: a link between cancer and aging. Proc Natl Acad Sci U S A *98*, 12072-12077.
Lauffenburger, D. A., and Horwitz, A. F. (1996). Cell migration: a physically integrated molecular process. Cell *84*, 359-369.
Le Clainche, C., and Carlier, M. F. (2008). Regulation of actin assembly associated with protrusion and adhesion in cell migration. Physiol Rev *88*, 489-513.
Lee, J. H., Miele, M. E., Hicks, D. J., Phillips, K. K., Trent, J. M., Weissman, B. E., and Welch, D. R. (1996). KiSS-1, a novel human malignant melanoma metastasis-suppressor gene. J Natl Cancer Inst *88*, 1731-1737.
Lee, J. H., and Welch, D. R. (1997). Suppression of metastasis in human breast carcinoma MDA-MB-435 cells after transfection with the metastasis suppressor gene, KiSS-1. Cancer Res *57*, 2384-2387.
Lee, J. L., Wang, M. J., Sudhir, P. R., and Chen, J. Y. (2008). CD44 engagement promotes matrix-derived survival through the CD44-SRC-integrin axis in lipid rafts. Mol Cell Biol *28*, 5710-5723.
Lin, E. Y., Li, J. F., Gnatovskiy, L., Deng, Y., Zhu, L., Grzesik, D. A., Qian, H., Xue, X. N., and Pollard, J. W. (2006). Macrophages regulate the angiogenic switch in a mouse model of breast cancer. Cancer Res *66*, 11238-11246.
Lin, E. Y., Nguyen, A. V., Russell, R. G., and Pollard, J. W. (2001). Colony-stimulating factor 1 promotes progression of mammary tumors to malignancy. J Exp Med *193*, 727-740.
Lip, G. Y., Chin, B. S., and Blann, A. D. (2002). Cancer and the prothrombotic state. Lancet Oncol *3*, 27-34.
Lotan, T., Hickson, J., Souris, J., Huo, D., Taylor, J., Li, T., Otto, K., Yamada, S. D., Macleod, K., and Rinker-Schaeffer, C. W. (2008). c-Jun NH2-terminal kinase activating kinase 1/mitogen-activated protein kinase kinase 4-mediated inhibition of SKOV3ip.1 ovarian cancer metastasis involves growth arrest and p21 up-regulation. Cancer Res *68*, 2166-2175.
Lu, X., and Kang, Y. (2007). Organotropism of breast cancer metastasis. J Mammary Gland Biol Neoplasia *12*, 153-162.
Luzzi, K. J., MacDonald, I. C., Schmidt, E. E., Kerkvliet, N., Morris, V. L., Chambers, A. F., and Groom, A. C. (1998). Multistep nature of metastatic inefficiency: dormancy of solitary

cells after successful extravasation and limited survival of early micrometastases. Am J Pathol *153*, 865-873.
Malanchi, I., Peinado, H., Kassen, D., Hussenet, T., Metzger, D., Chambon, P., Huber, M., Hohl, D., Cano, A., Birchmeier, W., and Huelsken, J. (2008). Cutaneous cancer stem cell maintenance is dependent on beta-catenin signalling. Nature *452*, 650-653.
Matzke, A., Sargsyan, V., Holtmann, B., Aramuni, G., Asan, E., Sendtner, M., Pace, G., Howells, N., Zhang, W., Ponta, H., and Orian-Rousseau, V. (2007). Haploinsufficiency of c-Met in cd44-/- mice identifies a collaboration of CD44 and c-Met in vivo. Mol Cell Biol *27*, 8797-8806.
Merrie, A. E., Yun, K., van Rij, A. M., and McCall, J. L. (1999). Detection and significance of minimal residual disease in colorectal cancer. Histol Histopathol *14*, 561-569.
Minn, A. J., Gupta, G. P., Siegel, P. M., Bos, P. D., Shu, W., Giri, D. D., Viale, A., Olshen, A. B., Gerald, W. L., and Massague, J. (2005). Genes that mediate breast cancer metastasis to lung. Nature *436*, 518-524.
Miselis, N. R., Wu, Z. J., Van Rooijen, N., and Kane, A. B. (2008). Targeting tumor-associated macrophages in an orthotopic murine model of diffuse malignant mesothelioma. Mol Cancer Ther *7*, 788-799.
Mishima, K., Handa, J. T., Aotaki-Keen, A., Lutty, G. A., Morse, L. S., and Hjelmeland, L. M. (1999). Senescence-associated beta-galactosidase histochemistry for the primate eye. Invest Ophthalmol Vis Sci *40*, 1590-1593.
Muir, A. I., Chamberlain, L., Elshourbagy, N. A., Michalovich, D., Moore, D. J., Calamari, A., Szekeres, P. G., Sarau, H. M., Chambers, J. K., Murdock, P., *et al.* (2001). AXOR12, a novel human G protein-coupled receptor, activated by the peptide KiSS-1. J Biol Chem *276*, 28969-28975.
Muller, A., Homey, B., Soto, H., Ge, N., Catron, D., Buchanan, M. E., McClanahan, T., Murphy, E., Yuan, W., Wagner, S. N., *et al.* (2001). Involvement of chemokine receptors in breast cancer metastasis. Nature *410*, 50-56.
Muller, V., Stahmann, N., Riethdorf, S., Rau, T., Zabel, T., Goetz, A., Janicke, F., and Pantel, K. (2005). Circulating tumor cells in breast cancer: correlation to bone marrow micrometastases, heterogeneous response to systemic therapy and low proliferative activity. Clin Cancer Res *11*, 3678-3685.
Nagrath, S., Sequist, L. V., Maheswaran, S., Bell, D. W., Irimia, D., Ulkus, L., Smith, M. R., Kwak, E. L., Digumarthy, S., Muzikansky, A., *et al.* (2007). Isolation of rare circulating tumour cells in cancer patients by microchip technology. Nature *450*, 1235-1239.
Nakajima, M., Morikawa, K., Fabra, A., Bucana, C. D., and Fidler, I. J. (1990). Influence of organ environment on extracellular matrix degradative activity and metastasis of human colon carcinoma cells. J Natl Cancer Inst *82*, 1890-1898.
Nash, G. F., Turner, L. F., Scully, M. F., and Kakkar, A. K. (2002). Platelets and cancer. Lancet Oncol *3*, 425-430.
Nash, K. T., Phadke, P. A., Navenot, J. M., Hurst, D. R., Accavitti-Loper, M. A., Sztul, E., Vaidya, K. S., Frost, A. R., Kappes, J. C., Peiper, S. C., and Welch, D. R. (2007). Requirement of KISS1 secretion for multiple organ metastasis suppression and maintenance of tumor dormancy. J Natl Cancer Inst *99*, 309-321.
Nash, K. T., and Welch, D. R. (2006). The KISS1 metastasis suppressor: mechanistic insights and clinical utility. Front Biosci *11*, 647-659.
Naumov, G. N., Folkman, J., Straume, O., and Akslen, L. A. (2008). Tumor-vascular interactions and tumor dormancy. APMIS *116*, 569-585.
Naumov, G. N., MacDonald, I. C., Weinmeister, P. M., Kerkvliet, N., Nadkarni, K. V., Wilson, S. M., Morris, V. L., Groom, A. C., and Chambers, A. F. (2002). Persistence of solitary mammary carcinoma cells in a secondary site: a possible contributor to dormancy. Cancer Res *62*, 2162-2168.

Nelson, C. M., and Bissell, M. J. (2006). Of extracellular matrix, scaffolds, and signaling: tissue architecture regulates development, homeostasis, and cancer. Annu Rev Cell Dev Biol *22*, 287-309.
Neri, A., Welch, D., Kawaguchi, T., and Nicolson, G. L. (1982). Development and biologic properties of malignant cell sublines and clones of a spontaneously metastasizing rat mammary adenocarcinoma. J Natl Cancer Inst *68*, 507-517.
Nguyen, D. X., Bos, P. D., and Massague, J. (2009). Metastasis: from dissemination to organ-specific colonization. Nat Rev Cancer *9*, 274-284.
Nieswandt, B., Hafner, M., Echtenacher, B., and Mannel, D. N. (1999). Lysis of tumor cells by natural killer cells in mice is impeded by platelets. Cancer Res *59*, 1295-1300.
Nieto, J., Grossbard, M. L., and Kozuch, P. (2008). Metastatic pancreatic cancer 2008: is the glass less empty? Oncologist *13*, 562-576.
O'Reilly, M. S., Holmgren, L., Shing, Y., Chen, C., Rosenthal, R. A., Moses, M., Lane, W. S., Cao, Y., Sage, E. H., and Folkman, J. (1994). Angiostatin: a novel angiogenesis inhibitor that mediates the suppression of metastases by a Lewis lung carcinoma. Cell *79*, 315-328.
Ohtaki, T., Shintani, Y., Honda, S., Matsumoto, H., Hori, A., Kanehashi, K., Terao, Y., Kumano, S., Takatsu, Y., Masuda, Y., *et al.* (2001). Metastasis suppressor gene KiSS-1 encodes peptide ligand of a G-protein-coupled receptor. Nature *411*, 613-617.
Olumi, A. F., Grossfeld, G. D., Hayward, S. W., Carroll, P. R., Tlsty, T. D., and Cunha, G. R. (1999). Carcinoma-associated fibroblasts direct tumor progression of initiated human prostatic epithelium. Cancer Res *59*, 5002-5011.
Orian-Rousseau, V., Chen, L., Sleeman, J. P., Herrlich, P., and Ponta, H. (2002). CD44 is required for two consecutive steps in HGF/c-Met signaling. Genes Dev *16*, 3074-3086.
Padua, D., Zhang, X. H., Wang, Q., Nadal, C., Gerald, W. L., Gomis, R. R., and Massague, J. (2008). TGFbeta primes breast tumors for lung metastasis seeding through angiopoietin-like 4. Cell *133*, 66-77.
Paget, S. (1989). The distribution of secondary growths in cancer of the breast. 1889. Cancer Metastasis Rev *8*, 98-101.
Paku, S., Dome, B., Toth, R., and Timar, J. (2000). Organ-specificity of the extravasation process: an ultrastructural study. Clin Exp Metastasis *18*, 481-492.
Pantschenko, A. G., Pushkar, I., Anderson, K. H., Wang, Y., Miller, L. J., Kurtzman, S. H., Barrows, G., and Kreutzer, D. L. (2003). The interleukin-1 family of cytokines and receptors in human breast cancer: implications for tumor progression. Int J Oncol *23*, 269-284.
Park, B. K., Zhang, H., Zeng, Q., Dai, J., Keller, E. T., Giordano, T., Gu, K., Shah, V., Pei, L., Zarbo, R. J., *et al.* (2007). NF-kappaB in breast cancer cells promotes osteolytic bone metastasis by inducing osteoclastogenesis via GM-CSF. Nat Med *13*, 62-69.
Peinado, H., Olmeda, D., and Cano, A. (2007). Snail, Zeb and bHLH factors in tumour progression: an alliance against the epithelial phenotype? Nat Rev Cancer *7*, 415-428.
Pendergrass, W. R., Lane, M. A., Bodkin, N. L., Hansen, B. C., Ingram, D. K., Roth, G. S., Yi, L., Bin, H., and Wolf, N. S. (1999). Cellular proliferation potential during aging and caloric restriction in rhesus monkeys (Macaca mulatta). J Cell Physiol *180*, 123-130.
Perl, A. K., Wilgenbus, P., Dahl, U., Semb, H., and Christofori, G. (1998). A causal role for E-cadherin in the transition from adenoma to carcinoma. Nature *392*, 190-193.
Podsypanina, K., Du, Y. C., Jechlinger, M., Beverly, L. J., Hambardzumyan, D., and Varmus, H. (2008). Seeding and propagation of untransformed mouse mammary cells in the lung. Science *321*, 1841-1844.
Qian, F., Hanahan, D., and Weissman, I. L. (2001). L-selectin can facilitate metastasis to lymph nodes in a transgenic mouse model of carcinogenesis. Proc Natl Acad Sci U S A *98*, 3976-3981.
Quintana, E., Shackleton, M., Sabel, M. S., Fullen, D. R., Johnson, T. M., and Morrison, S. J. (2008). Efficient tumour formation by single human melanoma cells. Nature *456*, 593-598.

Racila, E., Euhus, D., Weiss, A. J., Rao, C., McConnell, J., Terstappen, L. W., and Uhr, J. W. (1998). Detection and characterization of carcinoma cells in the blood. Proc Natl Acad Sci U S A *95*, 4589-4594.
Ranganathan, A. C., Adam, A. P., and Aguirre-Ghiso, J. A. (2006a). Opposing roles of mitogenic and stress signaling pathways in the induction of cancer dormancy. Cell Cycle *5*, 1799-1807.
Ranganathan, A. C., Adam, A. P., Zhang, L., and Aguirre-Ghiso, J. A. (2006b). Tumor cell dormancy induced by p38SAPK and ER-stress signaling: an adaptive advantage for metastatic cells? Cancer Biol Ther *5*, 729-735.
Rappa, G., Fodstad, O., and Lorico, A. (2008). The stem cell-associated antigen CD133 (Prominin-1) is a molecular therapeutic target for metastatic melanoma. Stem Cells *26*, 3008-3017.
Riethdorf, S., Wikman, H., and Pantel, K. (2008). Review: Biological relevance of disseminated tumor cells in cancer patients. Int J Cancer *123*, 1991-2006.
Sabeh, F., Ota, I., Holmbeck, K., Birkedal-Hansen, H., Soloway, P., Balbin, M., Lopez-Otin, C., Shapiro, S., Inada, M., Krane, S., *et al.* (2004). Tumor cell traffic through the extracellular matrix is controlled by the membrane-anchored collagenase MT1-MMP. J Cell Biol *167*, 769-781.
Sahai, E. (2007). Illuminating the metastatic process. Nat Rev Cancer *7*, 737-749.
Schardt, J. A., Meyer, M., Hartmann, C. H., Schubert, F., Schmidt-Kittler, O., Fuhrmann, C., Polzer, B., Petronio, M., Eils, R., and Klein, C. A. (2005). Genomic analysis of single cytokeratin-positive cells from bone marrow reveals early mutational events in breast cancer. Cancer Cell *8*, 227-239.
Schatton, T., Murphy, G. F., Frank, N. Y., Yamaura, K., Waaga-Gasser, A. M., Gasser, M., Zhan, Q., Jordan, S., Duncan, L. M., Weishaupt, C., *et al.* (2008). Identification of cells initiating human melanomas. Nature *451*, 345-349.
Schmidt-Kittler, O., Ragg, T., Daskalakis, A., Granzow, M., Ahr, A., Blankenstein, T. J., Kaufmann, M., Diebold, J., Arnholdt, H., Muller, P., *et al.* (2003). From latent disseminated cells to overt metastasis: genetic analysis of systemic breast cancer progression. Proc Natl Acad Sci U S A *100*, 7737-7742.
Shackleton, M., Vaillant, F., Simpson, K. J., Stingl, J., Smyth, G. K., Asselin-Labat, M. L., Wu, L., Lindeman, G. J., and Visvader, J. E. (2006). Generation of a functional mammary gland from a single stem cell. Nature *439*, 84-88.
Shneider , S. (2008). Pediatric Gastrointestinal Disease., (Connecticut: PMPH-USA).
Sierko, E., and Wojtukiewicz, M. Z. (2004). Platelets and angiogenesis in malignancy. Semin Thromb Hemost *30*, 95-108.
Sierko, E., and Wojtukiewicz, M. Z. (2007). Inhibition of platelet function: does it offer a chance of better cancer progression control? Semin Thromb Hemost *33*, 712-721.
Singh, S. K., Hawkins, C., Clarke, I. D., Squire, J. A., Bayani, J., Hide, T., Henkelman, R. M., Cusimano, M. D., and Dirks, P. B. (2004). Identification of human brain tumour initiating cells. Nature *432*, 396-401.
Sipkins, D. A., Wei, X., Wu, J. W., Runnels, J. M., Cote, D., Means, T. K., Luster, A. D., Scadden, D. T., and Lin, C. P. (2005). In vivo imaging of specialized bone marrow endothelial microdomains for tumour engraftment. Nature *435*, 969-973.
Smyth, M. J., Dunn, G. P., and Schreiber, R. D. (2006). Cancer immunosurveillance and immunoediting: the roles of immunity in suppressing tumor development and shaping tumor immunogenicity. Adv Immunol *90*, 1-50.
Sperandio, M. (2006). Selectins and glycosyltransferases in leukocyte rolling in vivo. FEBS J *273*, 4377-4389.

Sridhar, S. C., and Miranti, C. K. (2006). Tetraspanin KAI1/CD82 suppresses invasion by inhibiting integrin-dependent crosstalk with c-Met receptor and Src kinases. Oncogene *25*, 2367-2378.
Stathopoulos, G. T., Sherrill, T. P., Han, W., Sadikot, R. T., Yull, F. E., Blackwell, T. S., and Fingleton, B. (2008). Host nuclear factor-kappaB activation potentiates lung cancer metastasis. Mol Cancer Res *6*, 364-371.
Stradal, T. E., and Scita, G. (2006). Protein complexes regulating Arp2/3-mediated actin assembly. Curr Opin Cell Biol *18*, 4-10.
Takanami, I., Takeuchi, K., and Naruke, M. (2000). Mast cell density is associated with angiogenesis and poor prognosis in pulmonary adenocarcinoma. Cancer *88*, 2686-2692.
Talmadge, J. E., Donkor, M., and Scholar, E. (2007). Inflammatory cell infiltration of tumors: Jekyll or Hyde. Cancer Metastasis Rev *26*, 373-400.
Taranova, A. G., Maldonado, D., 3rd, Vachon, C. M., Jacobsen, E. A., Abdala-Valencia, H., McGarry, M. P., Ochkur, S. I., Protheroe, C. A., Doyle, A., Grant, C. S., *et al.* (2008). Allergic pulmonary inflammation promotes the recruitment of circulating tumor cells to the lung. Cancer Res *68*, 8582-8589.
Thiery, J. P. (2002). Epithelial-mesenchymal transitions in tumour progression. Nat Rev Cancer *2*, 442-454.
Timmers, M., Vekemans, K., Vermijlen, D., Asosingh, K., Kuppen, P., Bouwens, L., Wisse, E., and Braet, F. (2004). Interactions between rat colon carcinoma cells and Kupffer cells during the onset of hepatic metastasis. Int J Cancer *112*, 793-802.
Tlsty, T. D., and Coussens, L. M. (2006). Tumor stroma and regulation of cancer development. Annu Rev Pathol *1*, 119-150.
Tonoli, H., and Barrett, J. C. (2005). CD82 metastasis suppressor gene: a potential target for new therapeutics? Trends Mol Med *11*, 563-570.
van der Bij, G. J., Oosterling, S. J., Meijer, S., Beelen, R. H., and van Egmond, M. (2005). Therapeutic potential of Kupffer cells in prevention of liver metastases outgrowth. Immunobiology *210*, 259-265.
Vander Griend, D. J., Kocherginsky, M., Hickson, J. A., Stadler, W. M., Lin, A., and Rinker-Schaeffer, C. W. (2005). Suppression of metastatic colonization by the context-dependent activation of the c-Jun NH2-terminal kinase kinases JNKK1/MKK4 and MKK7. Cancer Res *65*, 10984-10991.
Visvader, J. E., and Lindeman, G. J. (2008). Cancer stem cells in solid tumours: accumulating evidence and unresolved questions. Nat Rev Cancer *8*, 755-768.
Wang, W., Eddy, R., and Condeelis, J. (2007). The cofilin pathway in breast cancer invasion and metastasis. Nat Rev Cancer *7*, 429-440.
Wang, W., Mouneimne, G., Sidani, M., Wyckoff, J., Chen, X., Makris, A., Goswami, S., Bresnick, A. R., and Condeelis, J. S. (2006). The activity status of cofilin is directly related to invasion, intravasation, and metastasis of mammary tumors. J Cell Biol *173*, 395-404.
Weaver, V. M., Petersen, O. W., Wang, F., Larabell, C. A., Briand, P., Damsky, C., and Bissell, M. J. (1997). Reversion of the malignant phenotype of human breast cells in three-dimensional culture and in vivo by integrin blocking antibodies. J Cell Biol *137*, 231-245.
Weiss, L. (2000). Metastasis of cancer: a conceptual history from antiquity to the 1990s. Cancer Metastasis Rev *19*, I-XI, 193-383.
Weiss, L., and Glaves, D. (1983). Cancer cell damage at the vascular endothelium. Ann N Y Acad Sci *416*, 681-692.
White, D. E., Kurpios, N. A., Zuo, D., Hassell, J. A., Blaess, S., Mueller, U., and Muller, W. J. (2004). Targeted disruption of beta1-integrin in a transgenic mouse model of human breast cancer reveals an essential role in mammary tumor induction. Cancer Cell *6*, 159-170.
Witz, I. P. (2008). The selectin-selectin ligand axis in tumor progression. Cancer Metastasis Rev *27*, 19-30.

Wolf, K., Mazo, I., Leung, H., Engelke, K., von Andrian, U. H., Deryugina, E. I., Strongin, A. Y., Brocker, E. B., and Friedl, P. (2003). Compensation mechanism in tumor cell migration: mesenchymal-amoeboid transition after blocking of pericellular proteolysis. J Cell Biol *160*, 267-277.
Wright, M. H., Calcagno, A. M., Salcido, C. D., Carlson, M. D., Ambudkar, S. V., and Varticovski, L. (2008). Brca1 breast tumors contain distinct CD44+/CD24- and CD133+ cells with cancer stem cell characteristics. Breast Cancer Res *10*, R10.
Wyckoff, J., Wang, W., Lin, E. Y., Wang, Y., Pixley, F., Stanley, E. R., Graf, T., Pollard, J. W., Segall, J., and Condeelis, J. (2004). A paracrine loop between tumor cells and macrophages is required for tumor cell migration in mammary tumors. Cancer Res *64*, 7022-7029.
Wyckoff, J. B., Jones, J. G., Condeelis, J. S., and Segall, J. E. (2000). A critical step in metastasis: in vivo analysis of intravasation at the primary tumor. Cancer Res *60*, 2504-2511.
Wyckoff, J. B., Pinner, S. E., Gschmeissner, S., Condeelis, J. S., and Sahai, E. (2006). ROCK- and myosin-dependent matrix deformation enables protease-independent tumor-cell invasion in vivo. Curr Biol *16*, 1515-1523.
Wyckoff, J. B., Wang, Y., Lin, E. Y., Li, J. F., Goswami, S., Stanley, E. R., Segall, J. E., Pollard, J. W., and Condeelis, J. (2007). Direct visualization of macrophage-assisted tumor cell intravasation in mammary tumors. Cancer Res *67*, 2649-2656.
Xu, L., Shen, S. S., Hoshida, Y., Subramanian, A., Ross, K., Brunet, J. P., Wagner, S. N., Ramaswamy, S., Mesirov, J. P., and Hynes, R. O. (2008). Gene expression changes in an animal melanoma model correlate with aggressiveness of human melanoma metastases. Mol Cancer Res *6*, 760-769.
Yamada, S. D., Hickson, J. A., Hrobowski, Y., Vander Griend, D. J., Benson, D., Montag, A., Karrison, T., Huo, D., Rutgers, J., Adams, S., and Rinker-Schaeffer, C. W. (2002). Mitogen-activated protein kinase kinase 4 (MKK4) acts as a metastasis suppressor gene in human ovarian carcinoma. Cancer Res *62*, 6717-6723.
Yamaguchi, H., Lorenz, M., Kempiak, S., Sarmiento, C., Coniglio, S., Symons, M., Segall, J., Eddy, R., Miki, H., Takenawa, T., and Condeelis, J. (2005). Molecular mechanisms of invadopodium formation: the role of the N-WASP-Arp2/3 complex pathway and cofilin. J Cell Biol *168*, 441-452.
Yang, J., Mani, S. A., Donaher, J. L., Ramaswamy, S., Itzykson, R. A., Come, C., Savagner, P., Gitelman, I., Richardson, A., and Weinberg, R. A. (2004). Twist, a master regulator of morphogenesis, plays an essential role in tumor metastasis. Cell *117*, 927-939.
Yang, Z. F., Ho, D. W., Ng, M. N., Lau, C. K., Yu, W. C., Ngai, P., Chu, P. W., Lam, C. T., Poon, R. T., and Fan, S. T. (2008). Significance of CD90+ cancer stem cells in human liver cancer. Cancer Cell *13*, 153-166.
Yin, J. J., Selander, K., Chirgwin, J. M., Dallas, M., Grubbs, B. G., Wieser, R., Massague, J., Mundy, G. R., and Guise, T. A. (1999). TGF-beta signaling blockade inhibits PTHrP secretion by breast cancer cells and bone metastases development. J Clin Invest *103*, 197-206.
Yoshida, B. A., Dubauskas, Z., Chekmareva, M. A., Christiano, T. R., Stadler, W. M., and Rinker-Schaeffer, C. W. (1999). Mitogen-activated protein kinase kinase 4/stress-activated protein/Erk kinase 1 (MKK4/SEK1), a prostate cancer metastasis suppressor gene encoded by human chromosome 17. Cancer Res *59*, 5483-5487.
Yoshida, B. A., Sokoloff, M. M., Welch, D. R., and Rinker-Schaeffer, C. W. (2000). Metastasis-suppressor genes: a review and perspective on an emerging field. J Natl Cancer Inst *92*, 1717-1730.
Yu, W., Kim, J., and Ossowski, L. (1997). Reduction in surface urokinase receptor forces malignant cells into a protracted state of dormancy. J Cell Biol *137*, 767-777.

Zeisberger, S. M., Odermatt, B., Marty, C., Zehnder-Fjallman, A. H., Ballmer-Hofer, K., and Schwendener, R. A. (2006). Clodronate-liposome-mediated depletion of tumour-associated macrophages: a new and highly effective antiangiogenic therapy approach. Br J Cancer *95*, 272-281.
Zipin, A., Israeli-Amit, M., Meshel, T., Sagi-Assif, O., Yron, I., Lifshitz, V., Bacharach, E., Smorodinsky, N. I., Many, A., Czernilofsky, P. A., *et al.* (2004). Tumor-microenvironment interactions: the fucose-generating FX enzyme controls adhesive properties of colorectal cancer cells. Cancer Res *64*, 6571-6578.
Zumsteg, A., and Christofori, G. (2009). Corrupt policemen: inflammatory cells promote tumor angiogenesis. Curr Opin Oncol *21*, 60-70.

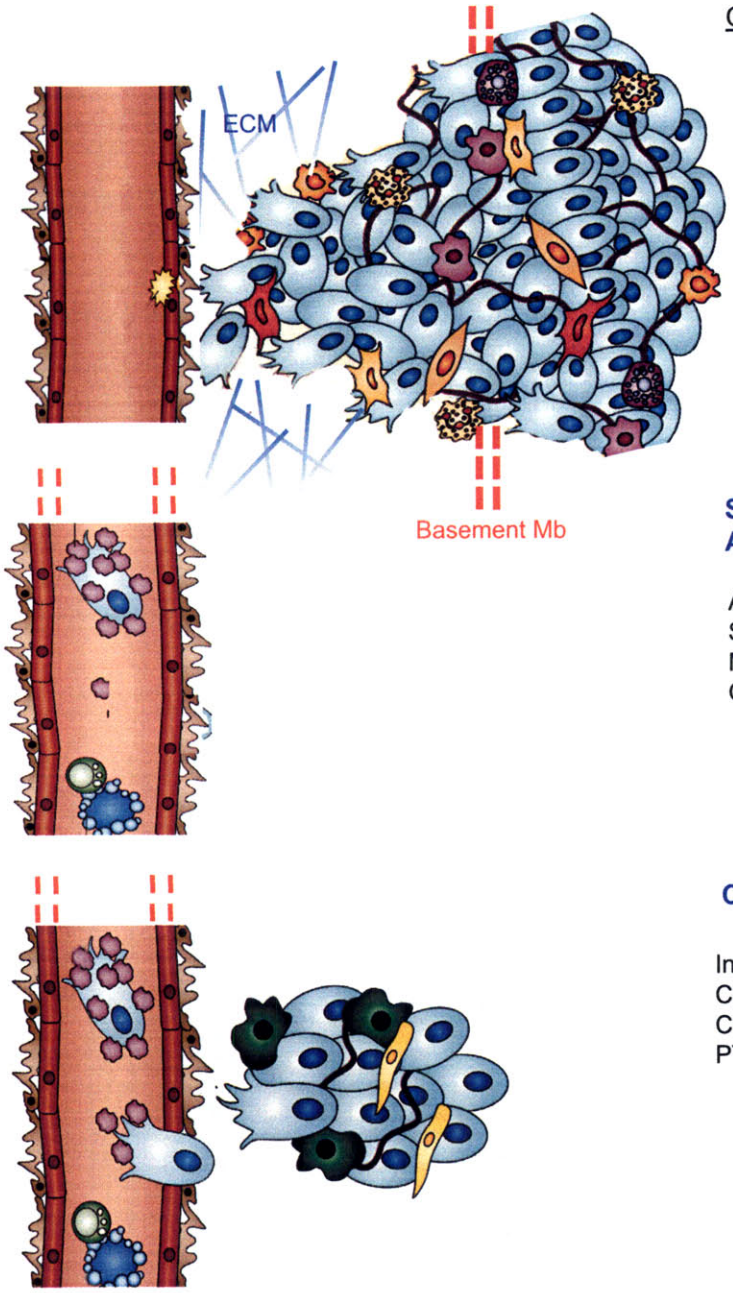

Genes/Proteins involved:

Local Invasion

Integrins
E-cadherin,Twist, Snail
MMPs
Growth factor receptors
RhoC, cofilin pathway proteins

Systemic Travelling and Arresting

ANGPTL4
Selectins
Metadherin
Chemokines /cytokine -receptors

Colonization

Integrins, uPAR
Cytokine – receptors (GMCSF, IL6)
Chemokines - receptors
PTHrP

Figure 1. General review of three major steps in tumor metastasis and genes/proteins that have been shown to be involved in each step. (Adapted from Joyce JA and Pollard JW, Nature Reviews Cancer, 2009.

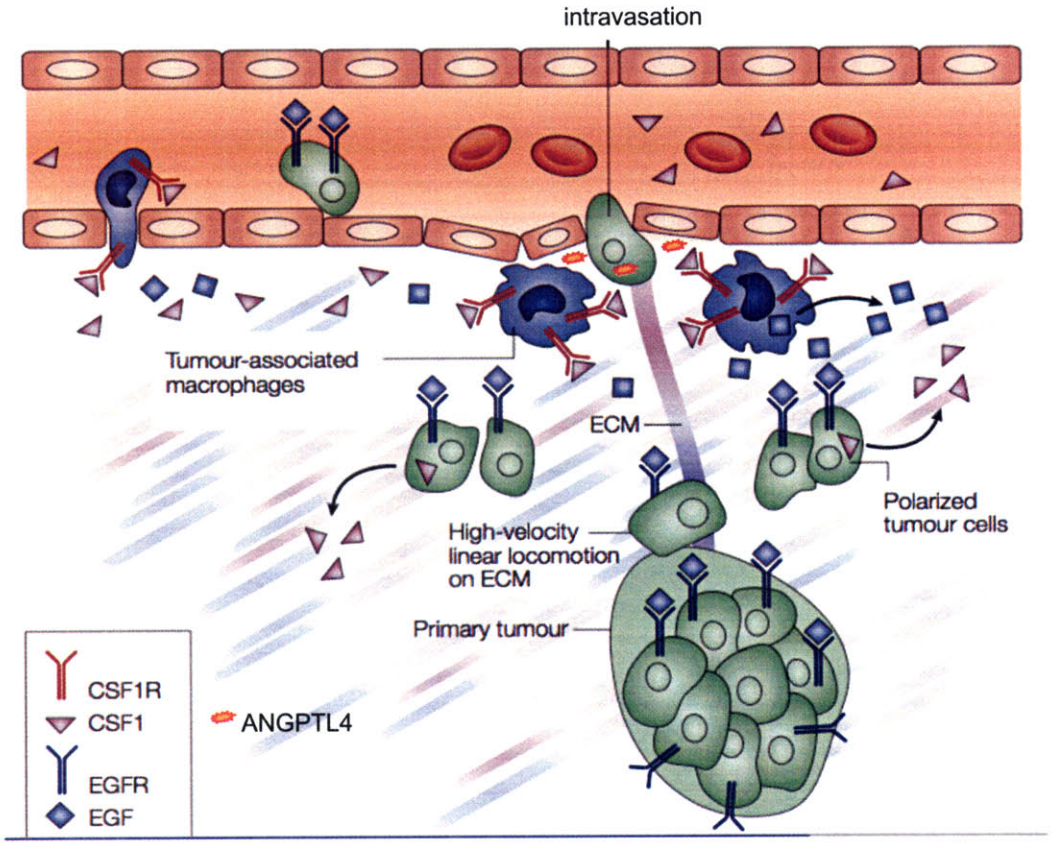

Figure 2. Crosstalk between tumor cells and macrophages that augments local invasiveness. Primary tumor cells secrete CSF1, which attracts macrophages to the site of the primary tumor, and are often associated with blood vessels. Macrophages in turn produce EGF, which orientate the primary tumor cells and induce migration of tumor cells toward the blood vessels. Tumor cells can also secrete angiopoietin-like 4 (upon stimulation by TGFβ) to induce dissociation of endothelial cell-cell junctions, facilitating tumor cell intravasation. (Adapted from Condeelis J and Segall JE, Nature Reviews Cancer, 2003)

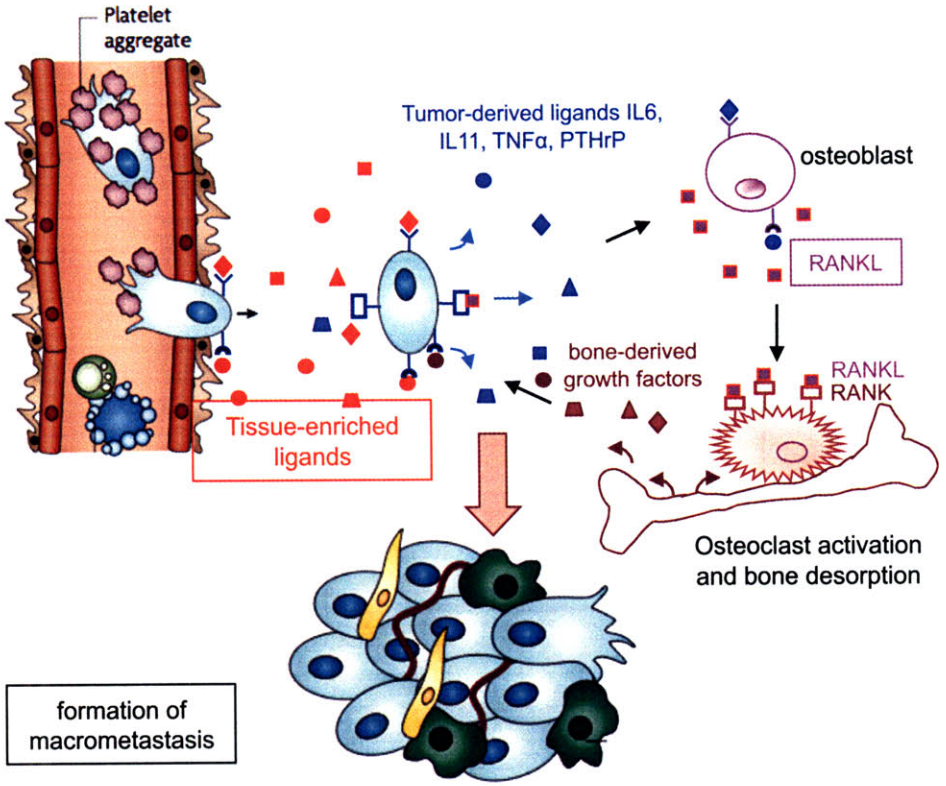

Figure 3. Colonization of distant organs. Depicted here is the presence various growth factors, cytokines, chemokines and their receptors cooperate to create an microenvironment at the distant organs that facilitate tumor metastasis formation. In response to tissue-enriched ligands such as SDF-1 and CXL21, tumor cells may be "attracted" to these particular organs. Once the cells are arrested in particular organ, for example in the bone marrow, tumor cells are capable of secreting cytokines and chemokines such as IL6, IL11, parathyroid hormone related protein (PTHrP), which stimulate the release of RANKL by osteoblasts. RANKL in turn promotes the maturation of osteoclasts, resulting in bone desorption and release of growth factors embedded in the bone marrow matrix, thus stimulating metastases formation in the bone.

CHAPTER 2.

APPLICATION OF QUANTITATIVE MASS SPECTROMETRY TO IDENTIFY MEMBRANE PROTEINS THAT ARE DIFFERENTIALLY EXPRESSED BETWEEN POORLY AND HIGHLY METASTATIC TUMOR CELLS

The work in this chapter was conceived by Hui Liu and Richard Hynes. The colloidal silica beads were kindly provided by Dr. Stolz at University of Pittsburgh. Mass spectrometry analyses were assisted by Richard Cook and Alla Leshinsky, and bioinformatics analysis was assisted by Charlie Whittaker. The contents of this chapter were written by Hui Liu, with editing by Richard Hynes.

INTRODUCTION

As mentioned in the first chapter, although metastasis has been recognized for more than 100 years, the tools for mechanistic understanding of the contributors were just not there until the past twenty years or so. Equipped with molecular biology technologies, various methods have been used over the years to identify the underlying genetic and epigenetic changes that enhance or suppress metastatic abilities in mouse models.

Experimental Mouse Models

Three basic experimental models have been applied to study metastasis in mice. The most convenient method is introducing tumor cells directly into the circulation, the so-called "experimental metastasis assay". Using this assay, for example, tumor cells can be injected into mice via tail vein, and the first microvascular bed the cells encounter is the lung. Tumor cells can also be injected intraportally to target mouse liver, or injected into the left cardiac ventricle to target the bones. The advantage of this method is that cells can be experimentally manipulated to over-express or down-regulate genes-of-interest and used to test the causative relationship between particular proteins/genes and metastasis. It is the most widely used method because of the simplicity of the experiment. However, this method does not capture the whole metastatic process; rather, it focuses on the later steps of metastasis (systemic traveling and arresting, and colonization as described in Chapter 1). The other commonly used metastasis model involves implantation of primary tumor either at an ectopic or orthotopic site, followed by analyzing the target organs to which those tumor cells normally metastasize. This method allows researchers to investigate the whole metastasis process, and is often used to investigate mammary and prostate metastasis. This method suffers temporal restrictions, since sometimes the experiments have to be stopped due to large primary tumors, and therefore primary tumor resection is required to observe full metastasis. Such surgical removal of primary tumors may change the course of metastasis. Nevertheless, this method is also widely used to test causality of particular genes/proteins. Once these data are in hand, and if transgenic or knockout mice are available for the gene/protein-of-interest, endogenous tumor models are often crossed with the transgenic or knockout mice to confirm their functions in metastasis.

Technologies used to Identify Metastasis Enhancers and Suppressors

Many technologies have been applied to understand metastasis, each with its own merits and caveats. For simplicity, I will divide the techniques used into three categories, focusing on DNA, mRNA, or protein, respectively.

Changes at DNA Level

Several techniques have been used to investigate chromosomal changes, which reveal copy number and structural differences at the whole-genome level, as well as regional chromosome gain or loss. Conventional banding karyotyping has been used to identify chromosomal changes. Although suffering from poor resolution, such analysis has narrowed one of the early-identified tumor suppressors to chromosome 11p11.2-13 (Ichikawa et al., 1992), which eventually led to the discovery of *KAI1*, a metastasis suppressor gene (Dong et al., 1995). Currently this method has largely been replaced by molecular cytogenetic techniques, including comparative genomic hybridization (CGH), spectral karyotyping (SKY), multicolor fluorescence *in situ* hybridization (FISH), and single nucleotide polymorphism arrays (SNP arrays). Essentially FISH consists of labeling DNA probes (usually using bacterial artificial chromosomes or BACs) with different fluorescence (red or green) directly or indirectly, followed by hybridization on chromosomal preparations previous fixed on slides, which will be visualized *in situ* by microscope (Volpi and Bridger, 2008). FISH is best suited for detecting and localizing specific DNA sequences on the chromosomes, and identifying numerical and structural chromosomal abnormalities. Traditionally the resolution of FISH is limited by the size of BACs, which are usually 100s of thousands of base pairs; however currently more than 30 different types of FISH have been developed, some with resolution down to 1000bp (Volpi and Bridger, 2008). SKY uses optical spectroscopy and chromosomal paint to examine the orderly arrangement of all chromosomes, a nice tool to investigate chromosomal translocations. SKY can detect DNA fragments as small as 1.5 million base pairs and can detect the origin of extrachromosomal fragments present in tumor cells (Rutka et al., 2009).

CGH is another molecular cytogenetic technique, which traditionally involves labeling total genomic DNA from two samples (for example, from cells with low or high metastatic abilities) with different fluorescence directly or indirectly (red or green), and hybridizing to pre-fixed metaphase chromosome spreads. The results are visualized with fluorescence microscopy – any gain or loss of genetic material will be visualized and calculated as enhanced or

dimmed fluorescence (Gebhart, 2004). CGH has been used to examine chromosome imbalance. Although this traditional method has quite coarse resolution and cannot detect differences below 3-5 mega base pairs, currently an improvement of this method has been developed, which is array-CGH. In this technique, instead of hybridizing to metaphase spreads, the probes are incubated with glass slides that have thousands of DNA sequences spanning all chromosomes, offering unprecedented resolution of less than 100 kilobases. Copy number changes (deletions, gains or amplifications) can be easily detected; however, balanced chromosome translocations and inversions cannot be detected. Another genomic array, SNP array, is frequently used for genetic linkage analysis to map disease-susceptibility genes, and for loss of heterozygosity (LOH) analysis due to uniparental disomy in cancer research. Using high-density SNP arrays to analyze large collections of human lung adenocarcinomas, 57 recurrent events including large-scale chromosome arm-copy number gain and loss and local amplification and homozygous deletions have been observed. Through this work, a novel putative oncogene was identified which is located at a frequently amplified region (chromosome 14q13.3), and encodes a transcription factor (Andersen et al., 2007; Lindblad-Toh et al., 2000; Weir et al., 2007).

Recent breakthroughs in new sequencing methods have led to the development of "next generation" sequencing technologies, including 454, Solexa or SOLiD sequencing. The end results of such massive sequencing are tens of gigabases of sequencing data in a single run, allowing genome-wide screening for point mutations, copy number changes and rearrangement in a single experiment. The power of this technology has been shown recently – Campbell et al have found more than 100 somatic rearrangements in two lung cancer patients, and some of those resulted in fusion transcripts that may be involved in oncogenesis. In another paper, Hodges et al combined exon-capture arrays with deep sequencing, and re-sequenced ~ 200,000 exons in a single experiment (Campbell et al., 2008; Hodges et al., 2007).

Since the goal of genomic analysis is to identify changes that may eventually result in functional changes (by proteins and microRNAs), and due to the prevalence of repetitive sequences and non-coding sequences in the human genome, chromosomal changes found at the DNA level do not always yield functional consequences. Therefore, DNA analyses are often combined with mRNA analyses in practice.

Changes at the mRNA Level

cDNA library construction and subsequent screening with mRNA probes from highly or poorly metatastic cells have been used to identify cDNA clones that showed differential hybridization. This method (although painfully tedious) has been used successfully to isolate the first metastasis suppressor gene *NM23* (Steeg et al., 1988). Subtractive hybridization, which relies on the removal of cDNA-mRNA hybrids formed between the control and test samples, can also be used to detect differentially expressed transcripts. Using this method, Kiss-1, another metastasis suppressor has been identified (Lee et al., 1996).

Although these methods have been useful in identifying transcriptional alterations, a powerful new technique emerged in the 1990s has essentially replaced them. DNA microarrays enabled the detection of changes in the whole transcriptome in one simple experiment, and current advances in software not only allow the identification of individual gene-expression changes, but also allow the recognition of signaling pathways that may be altered (Subramanian et al., 2007). Since their development, DNA microarrays have been applied efficiently to identity numerous genes that enhance or suppress metastasis. Early work by Clark found that a small GTPase, RhoC, is upregulated in highly metastatic melanoma cells and shown to be functionally involved in metastasis (Clark et al., 2000). Following that, a large number of genes have been found to be up- or down-regulated in metastasis, involving motility, survival, proliferation and angiogenesis (Nguyen et al., 2009). Data from microarray analyses have helped to dissect some of the molecular mechanisms of tissue tropism of metastasis (Gupta et al., 2005), and help define molecular interactions of tumor-cell and microenvironment interactions (Joyce and Pollard, 2009), both are fundamental questions regarding cancer metastasis.

In addition, microarray analyses have proven valuable in the clinic; profiling of the primary tumors has shown the presence of gene signatures that predict the clinical outcomes of the patients, thus providing an additional tool for patient therapy decision-making (Ramaswamy et al., 2003; van 't Veer et al., 2002; Weir et al., 2007), and cathepsin cysteine proteases identified from array analysis have been used in mouse lung adenocarcinoma models to image the presence and progress of lung cancers (Grimm et al., 2005). Applying laser-capture microdissection to isolate particular regions within the tumors, researchers have analyzed the expression profiles of heterogeneous populations of cell in a given tumor, to

identify tumor progression genes. For example, Schuetz et al have microdissected ductal carcinomas *in situ* and invasive ductal carcinoma within breast tumors and performed microarray analysis, and identified genes that are potentially involved in invasiveness (Schuetz et al., 2006). The versatility and flexibility of arrays have been shown in work by Hoshida et al, where formalin-fixed, paraffin-embedded, human samples,that have been archived for up to 24 years can be used to perform array analyses, and yielded predictive power for disease recurrence (Hoshida et al., 2008). In fact, work has been started to take advantage of the predictive power of the gene signatures and to use that in clinical trials in order to select breast cancer patients who might benefit from adjuvant chemotherapy (Mook et al., 2007).

As mentioned earlier, combination analyses of chromosomal changes and expression profiling are often used together, and ideally, changes in chromosomes show correlative changes in mRNA transcription. Often, this is followed by analyses of corresponding proteins to see if changes found in the above-mentioned process result in mutation, truncation, or alteration in expression levels of the proteins. The reason for this indirect approach to identify protein changes is that nucleotides are much easier to manipulate experimentally and can be analyzed at large-scale genomic levels. On the contrary, traditional protein-sequencing using Edman degradation is not suitable for high-throughput screening. With recent technological improvements in protein-array and mass spectrometry, direct protein comparisons are now becoming feasible.

Changes at the Protein Level

It needs to be mentioned that researches have cleverly taken advantage of the immune system to identify proteins that are differentially expressed (either at different quantity or in different forms). The development of monoclonal antibodies has been an invaluable tool to identify novel proteins, and if high specificity is confirmed, they can be used to deliver toxins or radio-isotopes selectively to cells expressing those antigens. For example, tenascin was found to be overexpressed by human malignant gliomas (Bourdon et al., 1985; Bourdon et al., 1983), and when conjugated with radio-isotopes, monoclonal antibodies to tenascin have been used in clinical trials in glioma patients with significant efficacy (Bigner et al., 1995; Cokgor et al., 2000). Other methods, including subtractive immunization and whole-cell panning with subtraction, have been developed to look specifically for proteins

differentially expressed on closely related cells. When searching for proteins that may contribute to metastasis, mice were first immunized with poorly metastatic cells and treated with immuno-suppressant drugs, followed by immunizing with highly metastatic cells and generation of monoclonal antibodies from those mice (subtractive immunization). Through this work, one monoclonal antibody was found to inhibit HEp3 cell metastasis, which was later identified to be anti-CD151 antibody (Testa et al., 1999; Zijlstra et al., 2008).

Mass Spectrometry

Mass spectrometers measure the mass-to-charge ratios (m/z) of ions; therefore the very first step of using mass spectrometers in biological analyses is converting neutral proteins- or peptides-of-interest usually present in liquid to gas-phase charged molecules. This can be accomplished by electrospray ionization (ESI) or matrix-assisted laser desorption/ionization (MALDI). Indeed, it was the development of such ionization technologies that led to the share of the 2002 Nobel Prize in Chemistry and finally application of mass spectrometry to efficient biological analyses (Glish and Vachet, 2003). Currently there are many different types of mass spectrometers, each with its own advantages and drawbacks, thus better suited for different purposes. For example, linear ion-trap mass analyzer possesses great sensitivity and fast data acquisition, but has limited resolution and is very useful for high-throughput protein identification. On the other hand, quadropole time-of-flight (Q-TOF) mass spectrometer exhibits high resolution and mass accuracy, and performs well for quantitative analysis as well as posttranslational modification analysis (Domon and Aebersold, 2006).

The basic procedures for protein identification using linear ion-trap type of mass spectrometry is outlined below: 1) Enzymatic digestion of protein complexes (usually by trypsin) to reduce the sizes to peptides; 2) Separation of complex peptide mixtures to simplify the population of peptides introduced into the mass analyzer. This is typically achieved by loading peptide mixtures onto reverse-phase HPLC and eluting with increasing concentrations of organics, thus peptides are separated by their hydrophobicity; 3) Ionization of peptides using electrospray ionization (ESI), which introduces (usually) positive charges on the peptides, allowing the subsequent analysis; 4) Peptides (ions) fly into the mass spectrometer and are focused along the way to enter the mass analyzers, where the m/z (molecular weight/charge) is analyzed for all peptides present in the analyzer. This step

is called an MS scan; 5) Particular peptides (ions) are then enriched in the ion trap followed by collision-induced-dissociation (CID), which breaks the selected peptides to smaller fragments at peptide bonds. The m/z of these smaller ions are again analyzed, and this step is called an MS/MS scan. MS scan and MS/MS scan are repeated thousands of times until all peptides from the HPLC are eluted. 6) Following this data-gathering stage, the resulting thousands of spectra (where m/z is plotted against ion intensity) are searched against protein/nucleotide databases using computer programs. The programs take the MS/MS spectra as input and score them against theoretical fragmentation patterns, which are computed for peptides in the databases. If a high confidence match is found for a particular spectrum, it will be assigned with a peptide sequence, which will be matched to a particular protein (Nesvizhskii et al., 2007; Steen and Mann, 2004).

This basic identification process can be modified to meet quantification needs. This usually involves chemically or metabolically labeling one population of proteins/peptides with "heavy" isotope entities (such as ^{13}C, ^{15}N), while the other population remains "light" (with ^{12}C or ^{14}N). When these two populations are mixed and subjected to mass spectrometric analysis, they can be separated by their m/z difference in the spectrum, thus allowing for relative quantification (Ong and Mann, 2005).

In the past 10 years, significant technological improvements in mass spectrometers and the completion of genomic sequencing have pushed mass spectrometry to the center stage of protein identification and quantification at the system level. The impressive sensitivity (attomoles of peptides can be detected), the ability to identify proteins and their modifications, coupled with novel quantitative methods, has enabled mass spectrometry to perform high-throughput analysis to identify and simultaneously quantify large numbers of proteins in given cells or tissues (Andersen and Mann, 2006; Cox and Mann, 2007; Cravatt et al., 2007; Domon and Aebersold, 2006; Han et al., 2008). To date, mass spectrometry has been applied successfully to investigate protein-protein interactions (Burckstummer et al., 2006; Danial et al., 2003; Drakas et al., 2005; Honey et al., 2001), to understand organelle components and dynamic changes of organelles in response to stimulations (Andersen et al., 2005; Andersen and Mann, 2006; de Hoog et al., 2004; Foster et al., 2003), to investigate protein-level changes during disease progression, such as during tumor progression and metastasis (Conn et al., 2008; Everley et al., 2006; Everley et al., 2004; Hastie et al., 2005; Leth-Larsen et al., 2009; Lund et al., 2009; Rahbar and Fenselau,

2004), to understand cell signaling pathways in response to particular stimulation ((Macek et al., 2009; Nita-Lazar et al., 2008; White, 2008), and to characterize known and novel post-translational modifications of proteins, such as ubiquitination, SUMOylation, methylation (Denison et al., 2005; Makhnevych et al., 2009; Miranda and Sorkin, 2007; Ong et al., 2004). Recent focus on biomarker identification from blood or tissue fluid will undoubtedly help with early disease diagnosis in the future.

One challenge that mass spectrometry faces is that proteins are present in the cells with much higher complexity than at the mRNA level, due to various post-translational modifications and splice variants, and are also present with large concentration differences. For example, the dynamic range in serum reaches 10 orders of magnitude (Wright et al., 2005). Due to these difficulties, one-experiment-analyze-all approaches such as DNA microarrays are not feasible using mass spectrometry. Instead, analyzing a defined subset of proteins usually yields deeper and often more useful information. In addition, proteins often have different functions when localized at different subcellular localizations - for example, ErbB-1 functions as the epidermal growth factor receptor on the plasma membrane, transducing signals to activate the MAPK signaling pathway; however, ErbB-1 bound to ligand can translocate to the nucleus and function as a transcription activator for activation of cyclin D1, and C-terminal fragment of ErbB-4 can also translocate to the nucleus, and regulate the transcription factor Yes-associated-protein (Aqeilan et al., 2005; Carpenter, 2003; Komuro et al., 2003; Omerovic et al., 2004). Therefore analyzing specific organelles not only functionally simplifies samples for mass spectrometry analyses, but also provides information about protein localization, which is one important part of protein function. This type of inventory analysis can be coupled with large-scale protein-protein interaction profiling, to shed light on the complex protein networks within each organelle and among different organelles (Andersen and Mann, 2006).

Cancer Membrane Proteomics

As mentioned in Chapter 1, membrane proteins play important roles during various stages of tumor progression and metastasis. In a sense, they function as the 'antennae" for cells to detect their environment and determine the cellular outcome, such as cell proliferation, migration or apoptosis, in response to the stimuli present in the environment.

Studying plasma membranes at the proteomics level has only been made possible by the advances in the mass spectrometry and 2D electrophoresis fields. Using 2D electrophoresis, two populations of complex protein mixtures can be differentially labeled using fluorophores before electrophoresis and relative protein quantities can be detected based on the fluorescence ratios present at each protein spot. The spots can then be excised for identification using mass spectrometry. Such analyses have proven useful to identify membrane proteins involved in tumor progression and metastasis (Blonder et al., 2006; Dowling et al., 2007; Jiang et al., 2003; Roesli et al., 2008).

Using quantitative mass spectrometry, more membrane proteins have been discovered to change expression among tumor cells (Dowling et al., 2008; Everley et al., 2006; Everley et al., 2004; Hastie et al., 2005; Keshamouni et al., 2006; Leth-Larsen et al., 2009; Lund et al., 2009; Patra, 2008; Rahbar and Fenselau, 2004). For example, recently the Quigley group have isolated plasma membrane from HT-1080 fibrosarcoma cells that are highly disseminating or poorly disseminating, and have identified 47 membrane proteins that are differentially expressed. Among them, tissue factor (TF) has been shown to be functional involved in tumor cell intravasation in a chick CAM (chorioallantoic membrane) metastasis model (Conn et al., 2008).

Currently, application of quantitative mass spectrometry has yielded a large amount of information, however, in most cases, this information remains un-validated. Very few of these identifications have been followed up with functional tests for their actual involvement in metastases, or followed up to test their efficacies as disease markers. However, as more researchers become dissatisfied with merely inventorying membrane proteins, we may see improvements over the current analyses.

EXPERIMENTAL GOALS AND APPROACHES

We are interested in understanding differences between tumor cells with high versus low metastatic abilities. In particular, given known interactions between tumor cells and their microenvironment, we are particularly interested in plasma membrane proteins that show differential expression levels. We would like to focus on potential adhesion molecules, as mentioned in Chapter 1, I believe that a better understanding of adhesion molecules (cell-cell adhesion and cell-matrix adhesion) – their functions in metastasis formation, and the

molecular mechanisms of such functions - should shed light on the mechanisms that tumor cells use to communicate with their microenvironment.
With this goal in mind, I first identified membrane proteins that are present on melanoma cells using membrane enrichment, proteolysis, followed by liquid chromatography coupled to tandem mass spectrometry (LC-MS/MS). Then I applied newly developed quantitative mass spectrometry methods to screen for membrane proteins that showed expression-level differences between poorly metastatic A375 cells and highly metastatic MA2 cells. These analyses were followed by confirming changes using other conventional methods and eventually I focused on one particular membrane protein for functional studies, which will be described in Chapter 3.

RESULTS

Plasma Membrane Enrichment

Previously a series of melanoma cells with different metastatic abilities have been established in our lab (Xu et al., 2006). A375 cells are poorly metastatic when introduced into the mice via tail-vein injection, while MA2 cells form large numbers of lung tumors using the same assay. To enrich for plasma membrane proteins, we decided to apply a colloidal silica method since this method introduces minimum alteration of the proteins, as compared with surface biotinylation; and this method has been shown to remove intracellular membranes, such as ER and Golgi membranes and to enrich for plasma membranes specifically. Contamination by internal membranes is the major caveat for microsome fractionation protocols that enrich for membranes.

The colloidal silica protocol was developed by the Jacobson group, which took advantage of the electrostatic interactions between positively charged colloidal silica beads and negatively charged plasma membranes (Chaney and Jacobson, 1983; Rahbar and Fenselau, 2004; Sambuy and Rodriguez-Boulan, 1988; Stolz et al., 1992; Stolz and Jacobson, 1992). Briefly A375 or MA2 cells were dissociated from the culture plates by incubating in PBS for 5-10min, and cell numbers were determined. After coating the cells with colloidal silica beads, the cells were over-coated with anionic polyacrylic acid to stabilize colloidal pellicles and to minimize contaminations between exposed colloidal silica beads and cell debris. Following resuspension in hypotonic lysis buffer, cells were lysed with a Parr nitrogen bomb and the

cell lysate was centrifuged at low speed (900g) to remove cytosolic proteins (supernatant I or Supt I). Pellets from this low-speed centrifugation (pellet I or PI) were loaded onto 70% Nycodenz, and were centrifuged at 15000g to pellet plasma membranes. Membranes from other organelles concentrate at the interface between the two layers. After removing top, middle and bottom layers, the pellet was washed three times with basic buffer to remove loosely associated proteins, and the final pellet (pellet II) was stored at -80^{0}C until analysis. The membrane isolation procedure is shown in Figure 1A.

Western blot experiments were performed using a list of antibodies against different subcellular organelle markers (Figure 1B), among which, integrin α2 was used as marker for plasma membrane, Golgin 97 as the Golgi marker, and Sec61β was used as ER marker. Images of the western blots are shown in Figure 1C, and the relative plasma membrane enrichment was determined based on the densitometry measurements compared to the whole cell lysate, and a 10-15 fold enrichment was routinely achieved.

Mass Spectrometry and Protein Identifications

Enriched membrane proteins were separated on 4-20% gradient gels and stained with Coomassie blue SafeStain (Figure 2A). 30 gel slices were dissected from the sample gel, reduced, alkylated, and in-gel digested with trypsin. Peptides were extracted and dried using Speed-vac, and were then reconstituted in 0.1% formic acid in deionized H_2O. One-third of the peptides from each gel slice were analyzed with LTQ ion-trap mass spectrometer from Thermo Finnigan, using in-line liquid chromatography- tandem mass spectrometry (LC-MS/MS). Data were collected by the mass spectrometer in data-dependent acquisition mode, with 10 most abundant ions collected for MS/MS scan following a survey scan (MS scan) in each cycle. These data were analyzed using Sequest software, and annotated for subcellular localization. A total of 1325 proteins were identified, with 384 (37.8%) identified by one peptide, 355 (34.9%) identified by two peptides and 586 (57.7%) proteins identified with three or more peptides (Figure 2B). Among the 586 proteins, 56.3% were identified with 3-5 peptides, 29% were identified with 6-10 peptides and 14.7% were identified with more than 10 peptides (Figure 2C).

Next, we analyzed the subcellular localization of identified proteins using GO term analysis (Figure 2D). We found approximately 26% of GO-term associated proteins are plasma membrane proteins, while ~10% are cytoskeleton proteins. The significant contamination came

from cytosol (8.8%) and nucleus (23.1%). See appendix C for the full list of proteins that were identified in this work.

Stable Isotope Labeling by Amino Acids in cell Culture (SILAC) and Quantitative Mass Spectrometry

SILAC was developed in the Mann group (Ong et al., 2002; Ong et al., 2003), where heavy isotope-enriched amino acids were fed to the cells in tissue culture. After extended periods of time, almost all proteins are labeled with "heavy" amino acids. Currently, the most commonly used amino acids are arginine and lysine, because tryptic peptides usually contain at least one of these two residues. Since its development, this technique has been widely applied to measure relative protein and phospho-protein abundances (Aggelis et al., 2009; Cox et al., 2009; Gioia et al., 2009; Ong et al., 2009; Oppermann et al., 2009; Pimienta et al., 2009). Compared with other chemical labeling techniques, SILAC is best used for in vitro culture systems since it requires at least five passages in the medium to ensure full incorporation of the heavy amino acids, although recently SILAC mice have been developed – the mice were fed with a heavy amino-acid-enriched diet and thus all cells in the mice are "heavier" than those from littermates that were given regular diet – thus opening the door for in vivo quantification (Kruger et al., 2008). Because SILAC labeling occurs at the protein level, differentially labeled cells can be mixed early on before any manipulations are done, thereby minimizing errors introduced by experimental procedure. For these reasons, we chose to use SILAC to fulfill our quantification needs, and a schematic is outlined in Figure 3A.

To determine empirically the cut-off value for quantification, "light" and "heavy" peptides with the same sequence were synthesized by the Biopolymer Lab at the Koch Institute. The heavy peptides were synthesized in the presence of "heavy"-L-Leucine-N-FMOC (U-$^{13}C_6$, ^{15}N –L-leucine), therefore the molecular weights of heavy peptides are 7 daltons heavier than light peptide. These two peptides were mixed at equal amount and 20 femtomole, 200 femtomole, or 2 picomole of the mixture were introduced into the mass spectrometer. Upon data collection and database search, relative quantities of these two peptides were obtained using PepQuan software, which is part of the BioWorks Browser package (Agilent). Based on this information, we choose to define a conservative ratio ≤0.75 as showing decreased expression, and a ratio ≥1.25 as defining enhanced expression (Figure 3B).

Passage-matched A375 (low metastatic cells) and MA2 (high metastatic cells) were grown in "light" (Arg0, Lys 0) and "heavy" (Arg10, Lys 8) media, respectively; equal amounts of total cell lysate from these two cell lines were mixed and plasma membrane preparations were made. A total of 80μg of membrane proteins were separated on 4-20% gel and 20 gel slices were cut and in-gel digested. Samples were analyzed with LC-MS/MS as mentioned above; with slight modification of sample-acquisition method. Briefly, during gradient elution from the HPLC, followed by an MS scan, zoom scan spectra and MS/MS spectra were obtained for each of the top 5 abundant ions per data-dependent cycle. Data were analyzed using Sequest software for identification and with PepQuan for quantification. Figure 3C and 3D show examples of the identification and quantification of SILAC peptide pairs from EphA2. Table 1 and table 2 show proteins that are downregulated or upregulated in highly metastatic MA2 cells relative to poorly metastatic A375 cells, respectively. In total, we found approximately 60% of all proteins generated quantitative information, while the relative quantities of 40% of the identified proteins could not be determined, most likely due to their low abundance. Out of all proteins that were quantitated, 23% have shown differential expression between A375 cells and MA2 cells.

Confirmation of Mass Spectrometry Analysis

To confirm the mass spectrometry data, western analysis and flow cytometry (FACS) analyses were performed. Equal amounts of total protein lysates from passage-matched A375 and MA2 cells were loaded onto SDS-PAGE gels, and western analysis was carried out using antibodies against integrin α3 and EphA2 (Figure 4A). We found reduction in integrin α3 (top panel) and EphA2 (bottom panel) protein levels in MA2 cells relative to A375 cells. These results are in agreement with the mass spectrometry quantifications. However, we did not observe total protein expression change in CDCP1 using cells *in vitro* by western blotting (Figure 4B). We then carried out FACS analysis to investigate specifically protein abundance at the cell membrane, on which the mass spectrometry analyses were done. Indeed, flowcytometry showed that surface CDCP1 is upregulated in MA2 cells compared to A375 cells, confirming the mass spectrometry results (Figure 4C). We also found that surface expression of integrin α3 is reduced in MA2 cells, again agreeing with mass spectrometry results (Figure 4D). To compare *in vitro* and *in vivo* protein expression levels, we generated subcutaneous tumors using A375 cells or MA2 cells and blotted for CDCP1 and EphA2 expression using the tumor samples. In line with the in vitro mass spectrometry data, we saw increased CDCP1 and decreased EphA2 total protein levels in the subcutaneous tumors generated from MA2 cells relative to those from

A375 cells (Figure 4E).

DISCUSSION

Plasma membrane constitutes only about 2% of the cellular proteins, and a small percentage of the total cellular membrane content (Kearney and Thibault, 2003). This low abundance relative to internal membranes, its similarity to other organelle membrane components, and its propensity to exist in different structures (open sheets, closed vesicles) have made plasma membrane isolation a challenge to researchers (Rahbar and Fenselau, 2004). Strategically, two methods have been developed for this purpose. One based on the density differences between membranes and other subcellular organelles, usually achieved by (ultra)centrifugation in sucrose gradient. Membrane preparations obtained with this method are typically heavily contaminated with internal membranes such as mitochondria and ER membranes due to their similarity in densities (Macher and Yen, 2007). The colloidal silica method we applied is one step above this traditional microsome preparation, which significantly removes internal membrane contamination (Chaney and Jacobson, 1983; Stolz et al., 1992; Stolz and Jacobson, 1992). The other method applies affinity purification with or without up-front modifications. Lectin affinity purification has been developed based on the presence of glycosylation on membrane proteins (Macher and Yen, 2007). Initially we tried this method early on without much success, and also due to concerns that different lectins may selectively bind to a subset of proteins, thus biasing our enrichment effort. Another available affinity-based method took advantage of membrane-impermeable biotinylation followed by high-affinity biotin-avidin interaction for purification (Conn et al., 2008; Zhang et al., 2003). We also tried this method, which offered similar results compared to the colloidal silica method (data not shown). Due to the same worry of selective enrichment, we decided to choose colloidal silica method as our primary method. But I believe that surface biotinylation is a good complementary technique.

In this work, we applied a colloidal silica pellicle method to enrich for plasma membrane. Western analysis showed significant removal of ER and Golgi proteins, as well as nuclear and cytosolic (data not shown) proteins, while retaining plasma membrane proteins. We routinely achieved 10-15 fold enrichment, although >20 fold enrichment has been reported (Durr et al., 2004; Oh et al., 2004), suggesting room for improvements. As suggested in the original publications, the caveat of this protocol is contamination by nuclear proteins, because of density similarity of coated plasma membrane and nuclei. And this is certainly manifested in our protein

identification results – nearly 23% of identified proteins are nuclear proteins, which comprise the major contaminants.

We identified a large number of proteins through this work, among which 941 were mapped by two or more peptides to that particular protein with good confidence. This confidence came from 1) stringent search criteria – we used Sequest search software and applied cutoffs of 2, 2.5 and 3.5 for ions with charges of 1, 2, or 3; and ΔCn of higher than 0.1. We also applied a cutoff p value of less than 0.0001; and 2) additional visual inspection of the spectrum when less than 3 peptides were found to match a particular protein. Recently it was suggested that probability-determining software that provide statistical measures of confidence and estimate false discovery rates may need to applied as well for large datasets (Nesvizhskii et al., 2007). We would like to try such statistical software in our future analyses, to see if it offers advantage compared with our current method.

In our quantification, we found that nearly 40% of proteins identified did not generate quantitative information. This is probably due to low abundance of these ions in the original spectrum – although low abundance ions can be sequenced with good confidence, believable quantification is not feasible if they are near or below the baseline. Another reason lies in how the quantitative information was extracted: in an MS experiment, the ion intensity of a particular peptide can be plotted against the time when the peptide is eluted from the HPLC. Therefore effective quantification depends on the continued presence of that ion over a period of time, and sometimes due to the complexity of the mixtures, this is not possible (Ong and Mann, 2005). As a result, the quantitative information could not all be extracted with high confidence. We also noticed that the majority of the changes are less than 2 fold, in part, this may due to the intrinsic capability (or incapability) of the particular type of instrument that we used. We used a linear ion-trap mass spectrometer for our analyses, which is very useful for high-throughput protein identification, but is known to have limited resolution and low dynamic range. Future work with improved instrumentation will offer more precise quantifications.

Despite these caveats, we were pleased to identify proteins that have previously been implicated in metastasis, such as melanoma adhesion molecule (CD146/MUC18) (Wu et al., 2004) and CD44, a receptor for hyaluronic acid (Hill et al., 2006), as well as EphA2 (Brantley-Sieders et al., 2005; Brantley-Sieders et al., 2008; Vaught et al., 2008) and integrin β3 (Felding-Habermann et al., 2001; Li et al., 2001; Pecheur et al., 2002; Switala-Jelen et al., 2004).

For reasons that will be detailed in the next chapter, I focused on a transmembrane protein CDCP1 (cub-domain-containing protein 1) for further analysis. We found from our membrane mass spectrometry that CDCP1 expression is increased in highly metastatic MA2 cells relative to the parental poorly metastatic A375 cells. Investigating total expression levels using whole cell lysates and western blotting suggested that total protein levels are not significantly changed between these two cells lines, rather, surface expression levels are different using flow cytometry analysis. This type of data highlights the importance of analyzing proteins at the subcellular localizations where they are functional. Interestingly, previous microarray analysis by Dr. Lei Xu had found that the mRNA level of CDCP1 is reduced in subcutaneous tumors generated by MA2 cells compared with those by A375 cells. However, protein quantitation of CDCP1 showed that it is indeed increased in tumors generated by MA2 cells. Perhaps such a discrepancy is not unexpected, Gygi et al have shown that for low abundance transcripts/proteins, changes in the quantity of mRNAs are not reliable indicators of protein abundance (Gygi et al., 1999). This discrepancy indicates that translational and post-translational regulation of CDCP1 may occur, which awaits further elucidation. We are interested in knowing how often this kind of difference occurs and what are the characteristics of the transcripts /proteins that present such discrepancies. For this purpose, I have carried out microarray analysis using passage-matched A375 cells and MA2 cells (data not shown), and systematic comparison between protein abundances and mRNA levels will be the obvious next step.

In summary, we have applied cutting-edge quantitative mass spectrometry analysis to identify plasma membrane proteins, but also to investigate quantitative differences between tumor cells with low or high metastatic potentials. Out of a list of proteins that showed differential expression, we have confirmed such changes using other conventional methods, and we are focusing on one of these proteins, CDCP1, for functional characterization and molecular dissection, which will be detailed in the next three chapters.

REFERENCES

Aggelis, V., Craven, R. A., Peng, J., Harnden, P., Cairns, D. A., Maher, E. R., Tonge, R., Selby, P. J., and Banks, R. E. (2009). Proteomic identification of differentially expressed plasma membrane proteins in renal cell carcinoma by stable isotope labelling of a von Hippel-Lindau transfectant cell line model. Proteomics *9*, 2118-2130.
Andersen, C. L., Wiuf, C., Kruhoffer, M., Korsgaard, M., Laurberg, S., and Orntoft, T. F. (2007). Frequent occurrence of uniparental disomy in colorectal cancer. Carcinogenesis *28*, 38-48.
Andersen, J. S., Lam, Y. W., Leung, A. K., Ong, S. E., Lyon, C. E., Lamond, A. I., and Mann, M. (2005). Nucleolar proteome dynamics. Nature *433*, 77-83.
Andersen, J. S., and Mann, M. (2006). Organellar proteomics: turning inventories into insights. EMBO Rep *7*, 874-879.
Aqeilan, R. I., Donati, V., Palamarchuk, A., Trapasso, F., Kaou, M., Pekarsky, Y., Sudol, M., and Croce, C. M. (2005). WW domain-containing proteins, WWOX and YAP, compete for interaction with ErbB-4 and modulate its transcriptional function. Cancer Res *65*, 6764-6772.
Bigner, D. D., Brown, M., Coleman, R. E., Friedman, A. H., Friedman, H. S., McLendon, R. E., Bigner, S. H., Zhao, X. G., Wikstrand, C. J., Pegram, C. N., and et al. (1995). Phase I studies of treatment of malignant gliomas and neoplastic meningitis with 131I-radiolabeled monoclonal antibodies anti-tenascin 81C6 and anti-chondroitin proteoglycan sulfate Me1-14 F (ab')2--a preliminary report. J Neurooncol *24*, 109-122.
Blonder, J., Chan, K. C., Issaq, H. J., and Veenstra, T. D. (2006). Identification of membrane proteins from mammalian cell/tissue using methanol-facilitated solubilization and tryptic digestion coupled with 2D-LC-MS/MS. Nat Protoc *1*, 2784-2790.
Bourdon, M. A., Matthews, T. J., Pizzo, S. V., and Bigner, D. D. (1985). Immunochemical and biochemical characterization of a glioma-associated extracellular matrix glycoprotein. J Cell Biochem *28*, 183-195.
Bourdon, M. A., Wikstrand, C. J., Furthmayr, H., Matthews, T. J., and Bigner, D. D. (1983). Human glioma-mesenchymal extracellular matrix antigen defined by monoclonal antibody. Cancer Res *43*, 2796-2805.
Brantley-Sieders, D. M., Fang, W. B., Hicks, D. J., Zhuang, G., Shyr, Y., and Chen, J. (2005). Impaired tumor microenvironment in EphA2-deficient mice inhibits tumor angiogenesis and metastatic progression. FASEB J *19*, 1884-1886.
Brantley-Sieders, D. M., Zhuang, G., Hicks, D., Fang, W. B., Hwang, Y., Cates, J. M., Coffman, K., Jackson, D., Bruckheimer, E., Muraoka-Cook, R. S., and Chen, J. (2008). The receptor tyrosine kinase EphA2 promotes mammary adenocarcinoma tumorigenesis and metastatic progression in mice by amplifying ErbB2 signaling. J Clin Invest *118*, 64-78.
Burckstummer, T., Bennett, K. L., Preradovic, A., Schutze, G., Hantschel, O., Superti-Furga, G., and Bauch, A. (2006). An efficient tandem affinity purification procedure for interaction proteomics in mammalian cells. Nat Methods *3*, 1013-1019.
Campbell, P. J., Stephens, P. J., Pleasance, E. D., O'Meara, S., Li, H., Santarius, T., Stebbings, L. A., Leroy, C., Edkins, S., Hardy, C., *et al.* (2008). Identification of somatically acquired rearrangements in cancer using genome-wide massively parallel paired-end sequencing. Nat Genet *40*, 722-729.
Carpenter, G. (2003). Nuclear localization and possible functions of receptor tyrosine kinases. Curr Opin Cell Biol *15*, 143-148.
Chaney, L. K., and Jacobson, B. S. (1983). Coating cells with colloidal silica for high yield isolation of plasma membrane sheets and identification of transmembrane proteins. J Biol Chem *258*, 10062-10072.
Clark, E. A., Golub, T. R., Lander, E. S., and Hynes, R. O. (2000). Genomic analysis of metastasis reveals an essential role for RhoC. Nature *406*, 532-535.

Cokgor, I., Akabani, G., Kuan, C. T., Friedman, H. S., Friedman, A. H., Coleman, R. E., McLendon, R. E., Bigner, S. H., Zhao, X. G., Garcia-Turner, A. M., *et al.* (2000). Phase I trial results of iodine-131-labeled antitenascin monoclonal antibody 81C6 treatment of patients with newly diagnosed malignant gliomas. J Clin Oncol *18*, 3862-3872.
Conn, E. M., Madsen, M. A., Cravatt, B. F., Ruf, W., Deryugina, E. I., and Quigley, J. P. (2008). Cell surface proteomics identifies molecules functionally linked to tumor cell intravasation. J Biol Chem *283*, 26518-26527.
Cox, J., and Mann, M. (2007). Is proteomics the new genomics? Cell *130*, 395-398.
Cox, J., Matic, I., Hilger, M., Nagaraj, N., Selbach, M., Olsen, J. V., and Mann, M. (2009). A practical guide to the MaxQuant computational platform for SILAC-based quantitative proteomics. Nat Protoc *4*, 698-705.
Cravatt, B. F., Simon, G. M., and Yates, J. R., 3rd (2007). The biological impact of mass-spectrometry-based proteomics. Nature *450*, 991-1000.
Danial, N. N., Gramm, C. F., Scorrano, L., Zhang, C. Y., Krauss, S., Ranger, A. M., Datta, S. R., Greenberg, M. E., Licklider, L. J., Lowell, B. B., *et al.* (2003). BAD and glucokinase reside in a mitochondrial complex that integrates glycolysis and apoptosis. Nature *424*, 952-956.
de Hoog, C. L., Foster, L. J., and Mann, M. (2004). RNA and RNA binding proteins participate in early stages of cell spreading through spreading initiation centers. Cell *117*, 649-662.
Denison, C., Kirkpatrick, D. S., and Gygi, S. P. (2005). Proteomic insights into ubiquitin and ubiquitin-like proteins. Curr Opin Chem Biol *9*, 69-75.
Domon, B., and Aebersold, R. (2006). Mass spectrometry and protein analysis. Science *312*, 212-217.
Dong, J. T., Lamb, P. W., Rinker-Schaeffer, C. W., Vukanovic, J., Ichikawa, T., Isaacs, J. T., and Barrett, J. C. (1995). KAI1, a metastasis suppressor gene for prostate cancer on human chromosome 11p11.2. Science *268*, 884-886.
Dowling, P., Meleady, P., Dowd, A., Henry, M., Glynn, S., and Clynes, M. (2007). Proteomic analysis of isolated membrane fractions from superinvasive cancer cells. Biochim Biophys Acta *1774*, 93-101.
Dowling, P., Walsh, N., and Clynes, M. (2008). Membrane and membrane-associated proteins involved in the aggressive phenotype displayed by highly invasive cancer cells. Proteomics *8*, 4054-4065.
Drakas, R., Prisco, M., and Baserga, R. (2005). A modified tandem affinity purification tag technique for the purification of protein complexes in mammalian cells. Proteomics *5*, 132-137.
Durr, E., Yu, J., Krasinska, K. M., Carver, L. A., Yates, J. R., Testa, J. E., Oh, P., and Schnitzer, J. E. (2004). Direct proteomic mapping of the lung microvascular endothelial cell surface in vivo and in cell culture. Nat Biotechnol *22*, 985-992.
Everley, P. A., Bakalarski, C. E., Elias, J. E., Waghorne, C. G., Beausoleil, S. A., Gerber, S. A., Faherty, B. K., Zetter, B. R., and Gygi, S. P. (2006). Enhanced analysis of metastatic prostate cancer using stable isotopes and high mass accuracy instrumentation. J Proteome Res *5*, 1224-1231.
Everley, P. A., Krijgsveld, J., Zetter, B. R., and Gygi, S. P. (2004). Quantitative cancer proteomics: stable isotope labeling with amino acids in cell culture (SILAC) as a tool for prostate cancer research. Mol Cell Proteomics *3*, 729-735.
Felding-Habermann, B., O'Toole, T. E., Smith, J. W., Fransvea, E., Ruggeri, Z. M., Ginsberg, M. H., Hughes, P. E., Pampori, N., Shattil, S. J., Saven, A., and Mueller, B. M. (2001). Integrin activation controls metastasis in human breast cancer. Proc Natl Acad Sci U S A *98*, 1853-1858.

Foster, L. J., De Hoog, C. L., and Mann, M. (2003). Unbiased quantitative proteomics of lipid rafts reveals high specificity for signaling factors. Proc Natl Acad Sci U S A *100*, 5813-5818.
Gebhart, E. (2004). Comparative genomic hybridization (CGH): ten years of substantial progress in human solid tumor molecular cytogenetics. Cytogenet Genome Res *104*, 352-358.
Gioia, M., Foster, L. J., and Overall, C. M. (2009). Cell-Based Identification of Natural Substrates and Cleavage Sites for Extracellular Proteases by SILAC Proteomics. Methods Mol Biol *539*, 1-23.
Glish, G. L., and Vachet, R. W. (2003). The basics of mass spectrometry in the twenty-first century. Nat Rev Drug Discov *2*, 140-150.
Grimm, J., Kirsch, D. G., Windsor, S. D., Kim, C. F., Santiago, P. M., Ntziachristos, V., Jacks, T., and Weissleder, R. (2005). Use of gene expression profiling to direct in vivo molecular imaging of lung cancer. Proc Natl Acad Sci U S A *102*, 14404-14409.
Gupta, G. P., Minn, A. J., Kang, Y., Siegel, P. M., Serganova, I., Cordon-Cardo, C., Olshen, A. B., Gerald, W. L., and Massague, J. (2005). Identifying site-specific metastasis genes and functions. Cold Spring Harb Symp Quant Biol *70*, 149-158.
Gygi, S. P., Rochon, Y., Franza, B. R., and Aebersold, R. (1999). Correlation between protein and mRNA abundance in yeast. Mol Cell Biol *19*, 1720-1730.
Han, X., Aslanian, A., and Yates, J. R., 3rd (2008). Mass spectrometry for proteomics. Curr Opin Chem Biol *12*, 483-490.
Hastie, C., Saxton, M., Akpan, A., Cramer, R., Masters, J. R., and Naaby-Hansen, S. (2005). Combined affinity labelling and mass spectrometry analysis of differential cell surface protein expression in normal and prostate cancer cells. Oncogene *24*, 5905-5913.
Hill, A., McFarlane, S., Johnston, P. G., and Waugh, D. J. (2006). The emerging role of CD44 in regulating skeletal micrometastasis. Cancer Lett *237*, 1-9.
Hodges, E., Xuan, Z., Balija, V., Kramer, M., Molla, M. N., Smith, S. W., Middle, C. M., Rodesch, M. J., Albert, T. J., Hannon, G. J., and McCombie, W. R. (2007). Genome-wide in situ exon capture for selective resequencing. Nat Genet *39*, 1522-1527.
Honey, S., Schneider, B. L., Schieltz, D. M., Yates, J. R., and Futcher, B. (2001). A novel multiple affinity purification tag and its use in identification of proteins associated with a cyclin-CDK complex. Nucleic Acids Res *29*, E24.
Hoshida, Y., Villanueva, A., Kobayashi, M., Peix, J., Chiang, D. Y., Camargo, A., Gupta, S., Moore, J., Wrobel, M. J., Lerner, J., *et al.* (2008). Gene expression in fixed tissues and outcome in hepatocellular carcinoma. N Engl J Med *359*, 1995-2004.
Ichikawa, T., Ichikawa, Y., Dong, J., Hawkins, A. L., Griffin, C. A., Isaacs, W. B., Oshimura, M., Barrett, J. C., and Isaacs, J. T. (1992). Localization of metastasis suppressor gene(s) for prostatic cancer to the short arm of human chromosome 11. Cancer Res *52*, 3486-3490.
Jiang, D., Ying, W., Lu, Y., Wan, J., Zhai, Y., Liu, W., Zhu, Y., Qiu, Z., Qian, X., and He, F. (2003). Identification of metastasis-associated proteins by proteomic analysis and functional exploration of interleukin-18 in metastasis. Proteomics *3*, 724-737.
Joyce, J. A., and Pollard, J. W. (2009). Microenvironmental regulation of metastasis. Nat Rev Cancer *9*, 239-252.
Kearney, P., and Thibault, P. (2003). Bioinformatics meets proteomics--bridging the gap between mass spectrometry data analysis and cell biology. J Bioinform Comput Biol *1*, 183-200.
Keshamouni, V. G., Michailidis, G., Grasso, C. S., Anthwal, S., Strahler, J. R., Walker, A., Arenberg, D. A., Reddy, R. C., Akulapalli, S., Thannickal, V. J., *et al.* (2006). Differential protein expression profiling by iTRAQ-2DLC-MS/MS of lung cancer cells undergoing epithelial-mesenchymal transition reveals a migratory/invasive phenotype. J Proteome Res *5*, 1143-1154.

Komuro, A., Nagai, M., Navin, N. E., and Sudol, M. (2003). WW domain-containing protein YAP associates with ErbB-4 and acts as a co-transcriptional activator for the carboxyl-terminal fragment of ErbB-4 that translocates to the nucleus. J Biol Chem *278*, 33334-33341.
Kruger, M., Moser, M., Ussar, S., Thievessen, I., Luber, C. A., Forner, F., Schmidt, S., Zanivan, S., Fassler, R., and Mann, M. (2008). SILAC mouse for quantitative proteomics uncovers kindlin-3 as an essential factor for red blood cell function. Cell *134*, 353-364.
Lee, J. H., Miele, M. E., Hicks, D. J., Phillips, K. K., Trent, J. M., Weissman, B. E., and Welch, D. R. (1996). KiSS-1, a novel human malignant melanoma metastasis-suppressor gene. J Natl Cancer Inst *88*, 1731-1737.
Leth-Larsen, R., Lund, R., Hansen, H. V., Laenkholm, A. V., Tarin, D., Jensen, O. N., and Ditzel, H. J. (2009). Metastasis-related plasma membrane proteins of human breast cancer cells identified by comparative quantitative mass spectrometry. Mol Cell Proteomics.
Li, X., Regezi, J., Ross, F. P., Blystone, S., Ilic, D., Leong, S. P., and Ramos, D. M. (2001). Integrin alphavbeta3 mediates K1735 murine melanoma cell motility in vivo and in vitro. J Cell Sci *114*, 2665-2672.
Lindblad-Toh, K., Tanenbaum, D. M., Daly, M. J., Winchester, E., Lui, W. O., Villapakkam, A., Stanton, S. E., Larsson, C., Hudson, T. J., Johnson, B. E., *et al.* (2000). Loss-of-heterozygosity analysis of small-cell lung carcinomas using single-nucleotide polymorphism arrays. Nat Biotechnol *18*, 1001-1005.
Lund, R., Leth-Larsen, R., Jensen, O. N., and Ditzel, H. J. (2009). Efficient Isolation and Quantitative Proteomic Analysis of Cancer Cell Plasma Membrane Proteins for Identification of Metastasis-Associated Cell Surface Markers. J Proteome Res.
Macek, B., Mann, M., and Olsen, J. V. (2009). Global and site-specific quantitative phosphoproteomics: principles and applications. Annu Rev Pharmacol Toxicol *49*, 199-221.
Macher, B. A., and Yen, T. Y. (2007). Proteins at membrane surfaces-a review of approaches. Mol Biosyst *3*, 705-713.
Makhnevych, T., Sydorskyy, Y., Xin, X., Srikumar, T., Vizeacoumar, F. J., Jeram, S. M., Li, Z., Bahr, S., Andrews, B. J., Boone, C., and Raught, B. (2009). Global map of SUMO function revealed by protein-protein interaction and genetic networks. Mol Cell *33*, 124-135.
Miranda, M., and Sorkin, A. (2007). Regulation of receptors and transporters by ubiquitination: new insights into surprisingly similar mechanisms. Mol Interv *7*, 157-167.
Mook, S., Van't Veer, L. J., Rutgers, E. J., Piccart-Gebhart, M. J., and Cardoso, F. (2007). Individualization of therapy using Mammaprint: from development to the MINDACT Trial. Cancer Genomics Proteomics *4*, 147-155.
Nesvizhskii, A. I., Vitek, O., and Aebersold, R. (2007). Analysis and validation of proteomic data generated by tandem mass spectrometry. Nat Methods *4*, 787-797.
Nguyen, D. X., Bos, P. D., and Massague, J. (2009). Metastasis: from dissemination to organ-specific colonization. Nat Rev Cancer *9*, 274-284.
Nita-Lazar, A., Saito-Benz, H., and White, F. M. (2008). Quantitative phosphoproteomics by mass spectrometry: past, present, and future. Proteomics *8*, 4433-4443.
Oh, P., Li, Y., Yu, J., Durr, E., Krasinska, K. M., Carver, L. A., Testa, J. E., and Schnitzer, J. E. (2004). Subtractive proteomic mapping of the endothelial surface in lung and solid tumours for tissue-specific therapy. Nature *429*, 629-635.
Omerovic, J., Puggioni, E. M., Napoletano, S., Visco, V., Fraioli, R., Frati, L., Gulino, A., and Alimandi, M. (2004). Ligand-regulated association of ErbB-4 to the transcriptional co-activator YAP65 controls transcription at the nuclear level. Exp Cell Res *294*, 469-479.
Ong, S. E., Blagoev, B., Kratchmarova, I., Kristensen, D. B., Steen, H., Pandey, A., and Mann, M. (2002). Stable isotope labeling by amino acids in cell culture, SILAC, as a simple and accurate approach to expression proteomics. Mol Cell Proteomics *1*, 376-386.

Ong, S. E., Kratchmarova, I., and Mann, M. (2003). Properties of 13C-substituted arginine in stable isotope labeling by amino acids in cell culture (SILAC). J Proteome Res *2*, 173-181.
Ong, S. E., and Mann, M. (2005). Mass spectrometry-based proteomics turns quantitative. Nat Chem Biol *1*, 252-262.
Ong, S. E., Mittler, G., and Mann, M. (2004). Identifying and quantifying in vivo methylation sites by heavy methyl SILAC. Nat Methods *1*, 119-126.
Ong, S. E., Schenone, M., Margolin, A. A., Li, X., Do, K., Doud, M. K., Mani, D. R., Kuai, L., Wang, X., Wood, J. L., *et al.* (2009). Identifying the proteins to which small-molecule probes and drugs bind in cells. Proc Natl Acad Sci U S A *106*, 4617-4622.
Oppermann, F. S., Gnad, F., Olsen, J. V., Hornberger, R., Greff, Z., Keri, G., Mann, M., and Daub, H. (2009). Large-scale proteomics analysis of the human kinome. Mol Cell Proteomics.
Patra, S. K. (2008). Dissecting lipid raft facilitated cell signaling pathways in cancer. Biochim Biophys Acta *1785*, 182-206.
Pecheur, I., Peyruchaud, O., Serre, C. M., Guglielmi, J., Voland, C., Bourre, F., Margue, C., Cohen-Solal, M., Buffet, A., Kieffer, N., and Clezardin, P. (2002). Integrin alpha(v)beta3 expression confers on tumor cells a greater propensity to metastasize to bone. FASEB J *16*, 1266-1268.
Pimienta, G., Chaerkady, R., and Pandey, A. (2009). SILAC for global phosphoproteomic analysis. Methods Mol Biol *527*, 107-116, x.
Rahbar, A. M., and Fenselau, C. (2004). Integration of Jacobson's pellicle method into proteomic strategies for plasma membrane proteins. J Proteome Res *3*, 1267-1277.
Ramaswamy, S., Ross, K. N., Lander, E. S., and Golub, T. R. (2003). A molecular signature of metastasis in primary solid tumors. Nat Genet *33*, 49-54.
Roesli, C., Mumprecht, V., Neri, D., and Detmar, M. (2008). Identification of the surface-accessible, lineage-specific vascular proteome by two-dimensional peptide mapping. FASEB J *22*, 1933-1944.
Rutka, J. T., Kongkham, P., Northcott, P., Carlotti, C., Guduk, M., Osawa, H., Moreno, O., Seol, H. J., Restrepo, A., Weeks, A., *et al.* (2009). The evolution and application of techniques in molecular biology to human brain tumors: a 25 year perspective. J Neurooncol *92*, 261-273.
Sambuy, Y., and Rodriguez-Boulan, E. (1988). Isolation and characterization of the apical surface of polarized Madin-Darby canine kidney epithelial cells. Proc Natl Acad Sci U S A *85*, 1529-1533.
Schuetz, C. S., Bonin, M., Clare, S. E., Nieselt, K., Sotlar, K., Walter, M., Fehm, T., Solomayer, E., Riess, O., Wallwiener, D., *et al.* (2006). Progression-specific genes identified by expression profiling of matched ductal carcinomas in situ and invasive breast tumors, combining laser capture microdissection and oligonucleotide microarray analysis. Cancer Res *66*, 5278-5286.
Steeg, P. S., Bevilacqua, G., Kopper, L., Thorgeirsson, U. P., Talmadge, J. E., Liotta, L. A., and Sobel, M. E. (1988). Evidence for a novel gene associated with low tumor metastatic potential. J Natl Cancer Inst *80*, 200-204.
Steen, H., and Mann, M. (2004). The ABC's (and XYZ's) of peptide sequencing. Nat Rev Mol Cell Biol *5*, 699-711.
Stolz, D. B., Bannish, G., and Jacobson, B. S. (1992). The role of the cytoskeleton and intercellular junctions in the transcellular membrane protein polarity of bovine aortic endothelial cells in vitro. J Cell Sci *103 (Pt 1)*, 53-68.
Stolz, D. B., and Jacobson, B. S. (1992). Examination of transcellular membrane protein polarity of bovine aortic endothelial cells in vitro using the cationic colloidal silica microbead membrane-isolation procedure. J Cell Sci *103 (Pt 1)*, 39-51.

Subramanian, A., Kuehn, H., Gould, J., Tamayo, P., and Mesirov, J. P. (2007). GSEA-P: a desktop application for Gene Set Enrichment Analysis. Bioinformatics *23*, 3251-3253.
Switala-Jelen, K., Dabrowska, K., Opolski, A., Lipinska, L., Nowaczyk, M., and Gorski, A. (2004). The biological functions of beta3 integrins. Folia Biol (Praha) *50*, 143-152.
Testa, J. E., Brooks, P. C., Lin, J. M., and Quigley, J. P. (1999). Eukaryotic expression cloning with an antimetastatic monoclonal antibody identifies a tetraspanin (PETA-3/CD151) as an effector of human tumor cell migration and metastasis. Cancer Res *59*, 3812-3820.
van 't Veer, L. J., Dai, H., van de Vijver, M. J., He, Y. D., Hart, A. A., Mao, M., Peterse, H. L., van der Kooy, K., Marton, M. J., Witteveen, A. T., *et al.* (2002). Gene expression profiling predicts clinical outcome of breast cancer. Nature *415*, 530-536.
Vaught, D., Brantley-Sieders, D. M., and Chen, J. (2008). Eph receptors in breast cancer: roles in tumor promotion and tumor suppression. Breast Cancer Res *10*, 217.
Volpi, E. V., and Bridger, J. M. (2008). FISH glossary: an overview of the fluorescence in situ hybridization technique. Biotechniques *45*, 385-386, 388, 390 passim.
Weir, B. A., Woo, M. S., Getz, G., Perner, S., Ding, L., Beroukhim, R., Lin, W. M., Province, M. A., Kraja, A., Johnson, L. A., *et al.* (2007). Characterizing the cancer genome in lung adenocarcinoma. Nature *450*, 893-898.
White, F. M. (2008). Quantitative phosphoproteomic analysis of signaling network dynamics. Curr Opin Biotechnol *19*, 404-409.
Wright, M. E., Han, D. K., and Aebersold, R. (2005). Mass spectrometry-based expression profiling of clinical prostate cancer. Mol Cell Proteomics *4*, 545-554.
Wu, G. J., Peng, Q., Fu, P., Wang, S. W., Chiang, C. F., Dillehay, D. L., and Wu, M. W. (2004). Ectopical expression of human MUC18 increases metastasis of human prostate cancer cells. Gene *327*, 201-213.
Xu, L., Begum, S., Hearn, J. D., and Hynes, R. O. (2006). GPR56, an atypical G protein-coupled receptor, binds tissue transglutaminase, TG2, and inhibits melanoma tumor growth and metastasis. Proc Natl Acad Sci U S A *103*, 9023-9028.
Zhang, W., Zhou, G., Zhao, Y., and White, M. A. (2003). Affinity enrichment of plasma membrane for proteomics analysis. Electrophoresis *24*, 2855-2863.
Zijlstra, A., Lewis, J., Degryse, B., Stuhlmann, H., and Quigley, J. P. (2008). The inhibition of tumor cell intravasation and subsequent metastasis via regulation of in vivo tumor cell motility by the tetraspanin CD151. Cancer Cell *13*, 221-234.

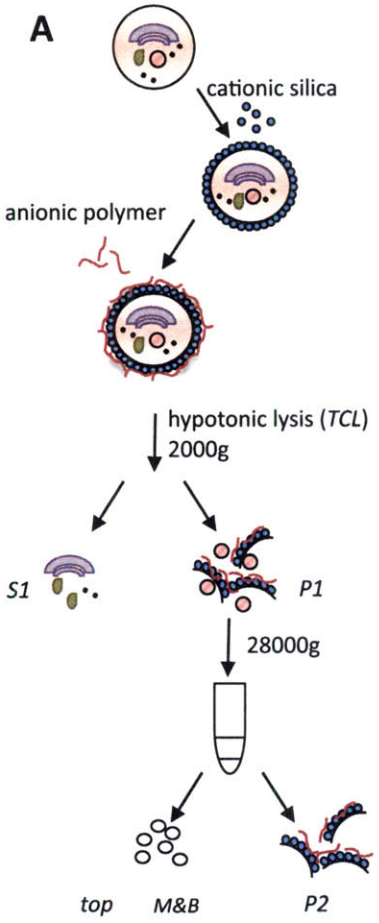

B

antibody	marker
Integrin α2	plasma membrane
Golgin 97	Golgi
Nucleoporin p62	nucleus
Annexin II	plasmalmma
Bcl-2	mitochondria
Sec61β	ER

C

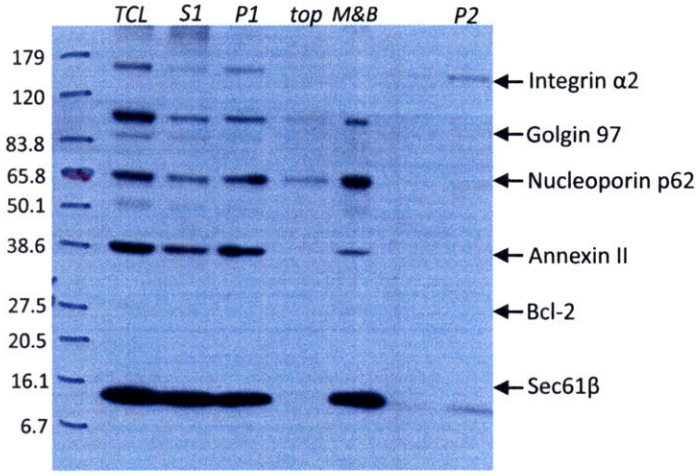

Figure 1. Plasma membrane enrichment. (A) Schematic of colloidal silica membrane enrichment protocol. **(B) and (C)** Antibodies used (B) in western blotting to show removal of intracellular membranes and cytosolic proteins, and enrichment of plasma membrane proteins).

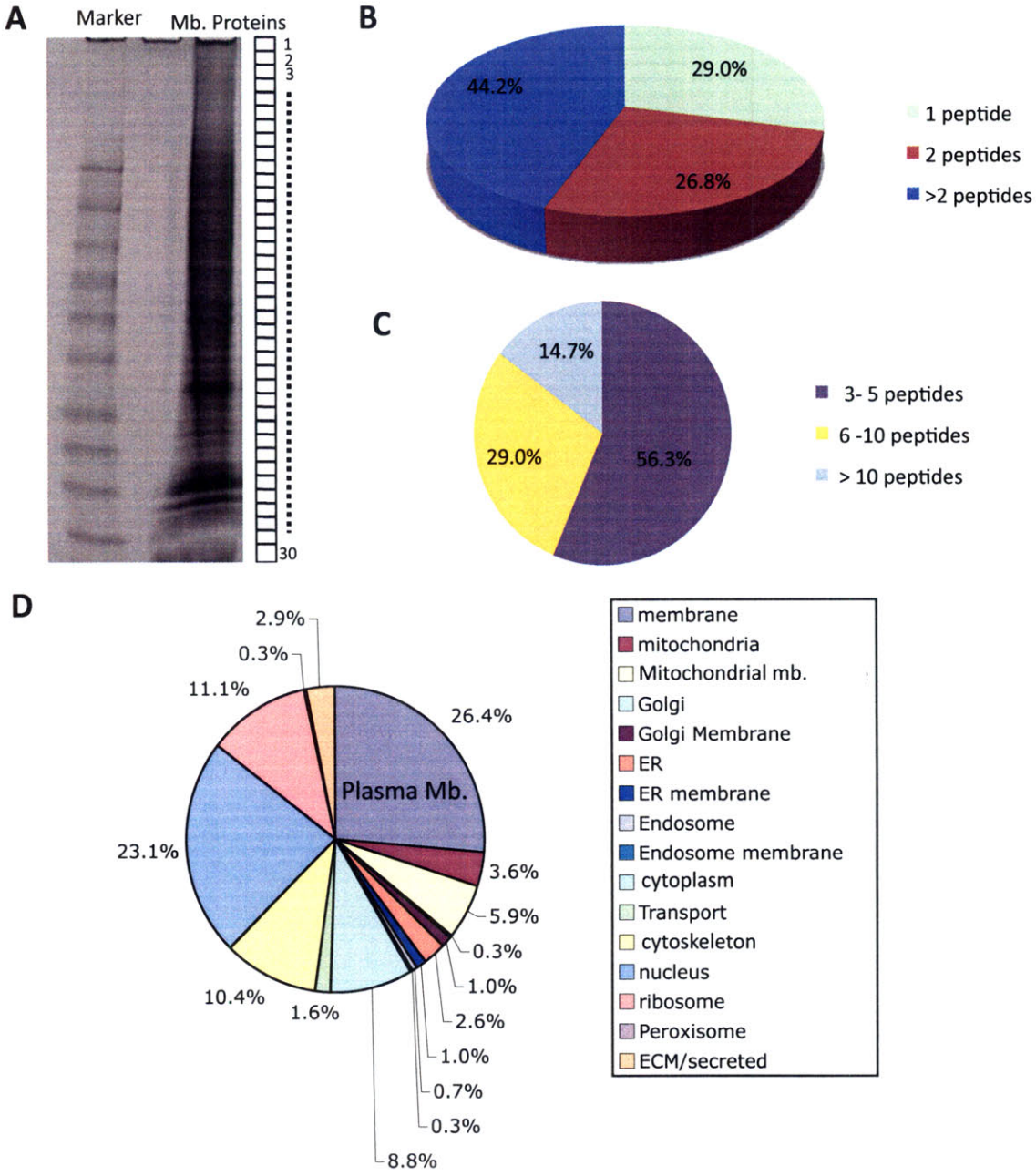

Figure 2. Identification of membrane-enriched proteins. (A) The pellet that contains the enriched membrane proteins was separated on 1D SDS-PAGE gel, cut into 20-30 gel slices and each gel slice was in-gel digested with trypsin, and peptides were extracted. **(B)** Distribution of proteins identified by number of peptides. Approximately 70% of the proteins were identified with 2 or more peptides. **(C)** Among the proteins that were identified by more than 2 peptides, 56.3% were identified with 3-5 peptides, 29% were identified with 6-10 peptides and 14.7% were found with more than 10 peptides matching a particular protein. (D) Distribution of proteins identified in this work, categorized by their subcellular localizations.

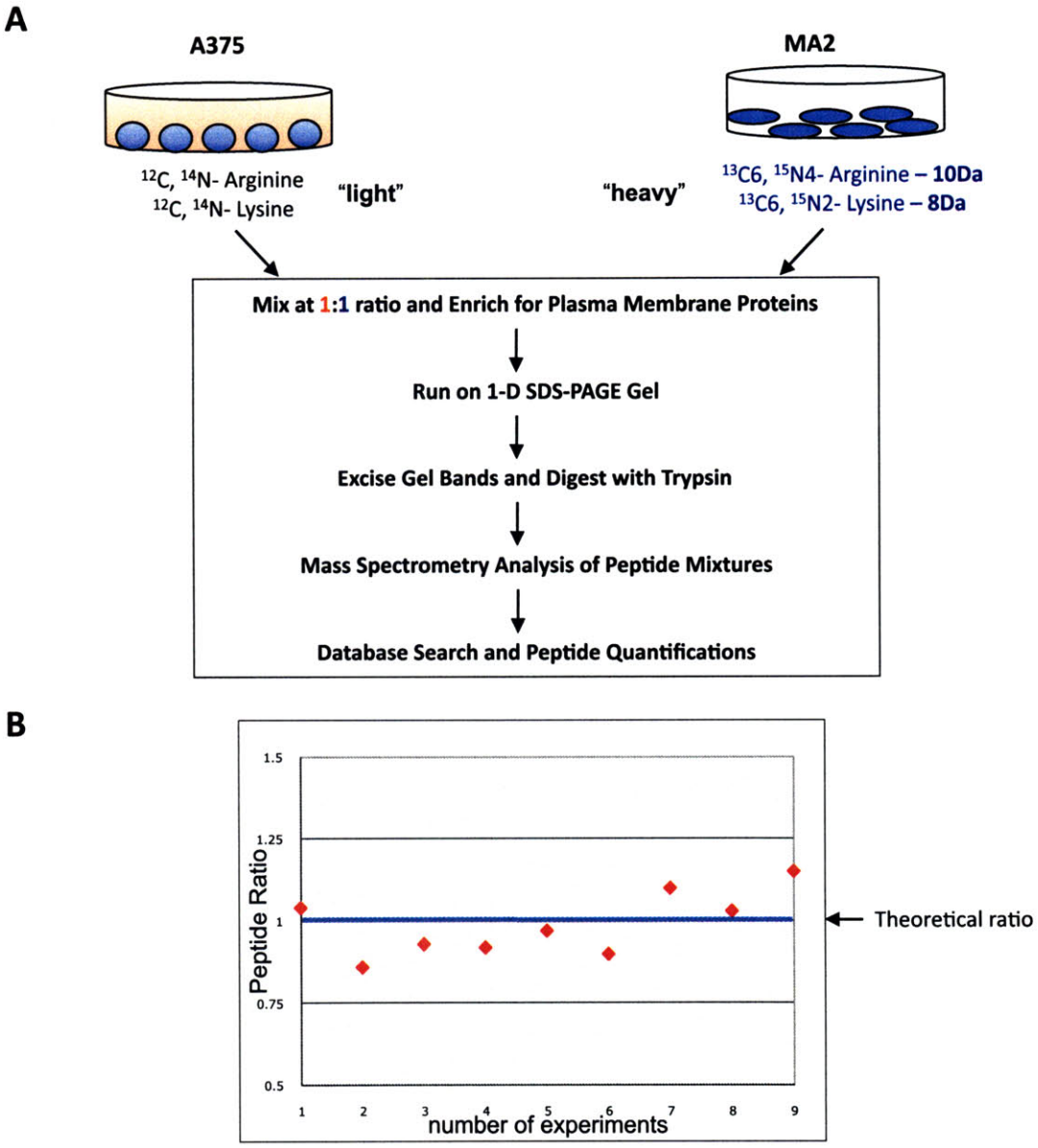

Figure 3. SILAC coupled with LC-MS/MS for protein quantification. (A) Schematic SILAC strategy to label A375 and MA2 cells and subsequent sample processing for quantitative analysis. **(B)** Ratios of synthetic heavy/light peptides were determined using PepQuant, and plotted against the theoretical ratio. Based on this result, heavy/light ratios that are ≤0.75 or ≥1.25 are considered different between two samples.

C

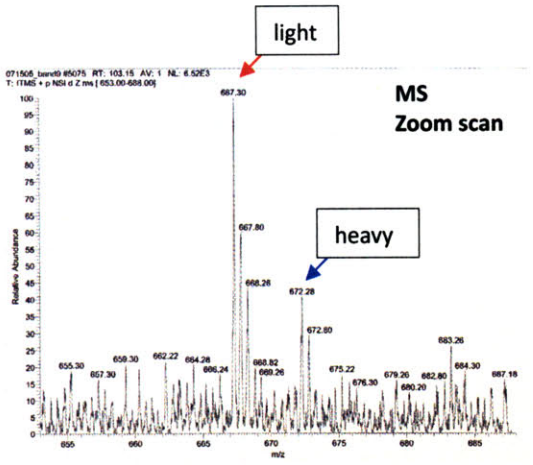

D

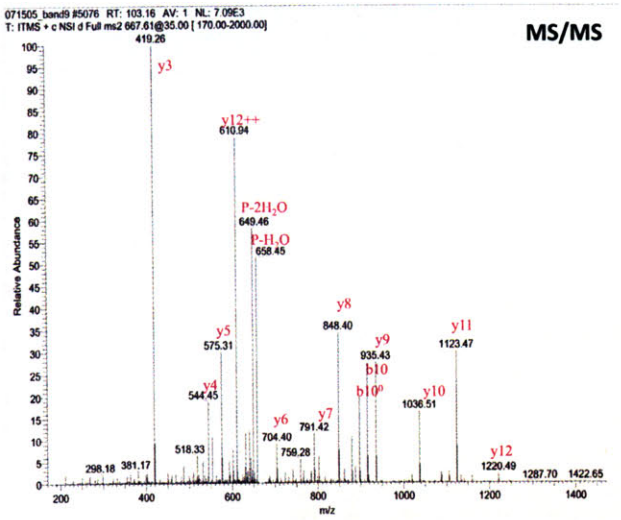

Figure 3. SILAC coupled with LC-MS/MS for protein quantification. (C) Representative zoom scan spectrum showing SILAC peptide pair from EphA2. The peptide pair shown has a charge of 2+, giving rise to an m/z difference of 5. (D) Tandem mass spectrum (MS/MS) of the peptide shown in C. Masses of expected b- and y-type fragment ions are shown.

Accession	protein name	# of peptides	ratio (H/L)
P29317	EPHA2_ Ephrin type-A receptor 2	8	0.18
Q59H77	Chaperonin containing TCP1, subunit 3 (Gamma) variant	7	0.28
Q01650	Large neutral amino acids transporter small subunit 1	4	0.29
P32970	Tumor necrosis factor ligand superfamily member 7 (CD70)	4	0.29
Q5JWF2	Guanine nucleotide-binding protein G(s) subunit alpha isoforms	13	0.45
Q96MN4	CDNA FLJ32119 fis,similar to RNA binding protein EWS	4	0.47
Q7Z3V1	Integrin beta 1	7	0.5
Q13765	Nascent polypeptide-associated complex subunit alpha	4	0.51
Q03405	Urokinase plasminogen activator surface receptor	3	0.52
P55290	Cadherin-13	7	0.52
Q99623	Prohibitin-2 (B-cell receptor-associated protein BAP37)	6	0.55
Q15417	Calponin-3 (Calponin, acidic isoform)	4	0.55
O43809	Cleavage and polyadenylation specificity factor 5	8	0.58
P35232	Prohibitin	5	0.59
P38159	Heterogeneous nuclear ribonucleoprotein G (hnRNP G)	4	0.6
Q53X65	GAPD protein	8	0.64
P23246	Splicing factor, proline- and glutamine-rich	14	0.66
P22087	rRNA 2'-O-methyltransferase fibrillarin (EC 2.1.1.-)	13	0.66
P30825	High-affinity cationic amino acid transporter 1	2	0.66
P09471	Guanine nucleotide-binding protein G(o) subunit alpha 1	6	0.67
Q14157	Ubiquitin-associated protein 2-like (Protein NICE-4)	5	0.68
P33176	Kinesin heavy chain (Ubiquitous kinesin heavy chain) (UKHC)	3	0.68
O95183	Vesicle-associated membrane protein 5 (VAMP-5)	3	0.69
P00505	Aspartate aminotransferase, mitochondrial precursor	5	0.7
P05026	Sodium/potassium-transporting ATPase subunit beta-1	6	0.7
P14625	Endoplasmin precursor, Heat shock protein 90 kDa beta member 1	11	0.71
P50443	Sulfate transporter (Diastrophic dysplasia protein)	8	0.71
P26006	Integrin alpha-3	3	0.72
Q5CAQ7	Heat shock protein HSP 90-alpha 2	26	0.73
Q4LE56	MYO1C variant protein	7	0.74
Q8ND56	Protein FAM61A (Putative alpha synuclein-binding protein)	4	0.74
P54136	Arginyl-tRNA synthetase, cytoplasmic	4	0.74
Q96PD2	Discoidin, CUB and LCCL domain-containing protein 2	2	0.74
Q99832	T-complex protein 1 subunit eta (TCP-1-eta)	6	0.75
Q96FZ7	Charged multivesicular body protein 6, Vacuolar protein sorting-associated protein 20	3	0.75
Q9Y266	Nuclear migration protein nudC	4	0.75
P31689	Heat shock 40 kDa protein	4	0.75
Q9UHX1	Ro ribonucleoprotein-binding protein 1 (SIAHBP1 protein)	5	0.75
P15880	40S ribosomal protein S2 (S4) (LLRep3 protein)	16	0.75
P51149	Ras-related protein Rab-7	5	0.75

Table I. Proteins that are down-regulated in highly metastatic MA2 cells relative to poorly metastatic A375 cells.

Accession	protein name	# of peptides	ratio (H/L)
Q6ZNL4	FLJ00279 protein	11	1.25
P62249	40S ribosomal protein S16	6	1.25
Q59GM9	Brain glycogen phosphorylase variant	8	1.26
Q5VVD0	Ribosomal protein	4	1.26
P60866	40S ribosomal protein S20	6	1.26
P17301	Integrin alpha-2 precursor (Platelet membrane glycoprotein	10	1.26
Q14254	Flotillin-2 (Epidermal surface antigen) (ESA)	5	1.26
P49588	Alanyl-tRNA synthetase, cytoplasmic (EC 6.1.1.7) (Alanine-	5	1.27
Q53G25	Ribosomal protein S5 variant (Fragment)	8	1.29
P20020	Plasma membrane calcium-transporting ATPase 1 (EC 3.6.3.8)	5	1.3
P42766	60S ribosomal protein L35	4	1.32
Q71UI9	Histone H2AV (H2A.F/Z)	5	1.33
P01903	HLA class II histocompatibility antigen, DR alpha chain	16	1.35
Q96AG4	Leucine-rich repeat-containing protein 59	5	1.35
Q5VWA5	Dolichyl-diphosphooligosaccharide-protein glycosyltransfe	5	1.38
P23634	Plasma membrane calcium-transporting ATPase 4 (EC 3.6.3.8)	5	1.39
Q548L2	CTCL tumor antigen HD-CL-06 (Vimentin variant)	17	1.4
O00161	Synaptosomal-associated protein 23 (SNAP-23) (Vesicle-mem	10	1.42
Q59GJ2	HLA class I histocompatibility antigen, A-1 alpha chain v	4	1.44
P05106	Integrin beta-3	11	1.5
Q30180	MHC class II HLA-SB-beta-1 gene (untyped), clone LC11	3	1.52
Q58J86	Elongation factor 2	16	1.54
P18085	ADP-ribosylation factor 4	4	1.55
Q6W6M8	Antigen MLAA-42	7	1.68
Q6N0B3	Hypothetical protein DKFZp686P03159	15	1.68
Q07065	P63 protein (Cytoskeleton-associated protein 4)	4	1.73
P62826	GTP-binding nuclear protein Ran (GTPase Ran)	5	1.79
P43121	MUC18, Melanoma-associated antigen MUC18	13	1.9
Q9H5V8	CUB domain containing protein 1 (CDCP1)	2	2.03
P16070	CD44 antigen precursor (Phagocytic glycoprotein I) (PGP-1)	7	2.23
P13987	CD59 glycoprotein precursor (Membrane attack complex inhibitor)	3	2.24
P06396	Gelsolin precursor (Actin-depolymerizing factor)	19	2.33
P47895	Aldehyde dehydrogenase 1A3	10	2.42
Q9UKS6	Protein kinase C and casein kinase substrate in neurons protein 3, Endophilin I	5	2.52
Q96B97	SH3-domain kinase-binding protein 1 (Cbl-interacting protein)	5	2.77

Table II. Proteins that are up-regulated in highly metastatic MA2 cells relative to poorly metastatic A375 cells.

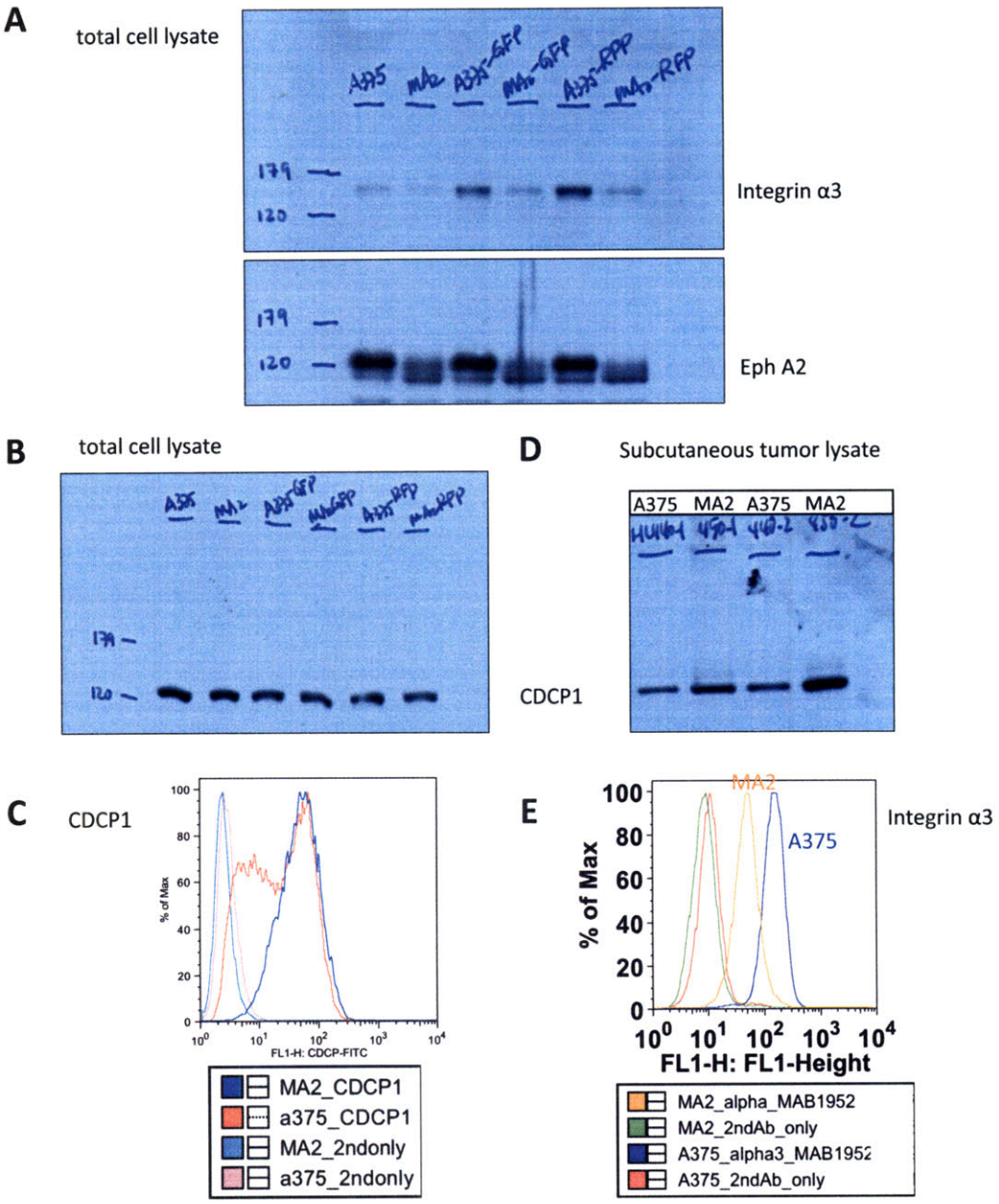

Figure 4. Western blotting and FACS confirming quantitative results obtained from mass spectrometry. (A) Total cell lysates were blotted using antibodies against integrin α3 and EphA2, confirming that both proteins are downregulated in MA2 cells relative to A375 cells. **(B)** Anti-CDCP1 western blot showed that total CDCP1 protein levels did not change. **(C)** However, cell surface CDCP1 expression level on average, is enhanced in MA2 cells, thus confirming our mass spectrometry results. **(D)** When subcutaneous tumors generated from MA2 cells or A375 cells were blotted for the expression levels of CDCP1, they also showed increased expression in MA2 cells. **(E)** Flow cytometry analysis of integrin α3 revealed reduced surface expression in MA2 cells compared to A375 cells, in agreement with mass spectrometry result.

CHAPTER 3.

A TEST FOR THE ROLE OF CDCP1 IN MELANOMA METASTASIS

The work in this chapter is conceived by Hui Liu and Richard Hynes. The contents of this chapter were written by Hui Liu, with editing by Richard Hynes.

INTRODUCTION

As described in Chapter 2, we have identified proteins that are differentially expressed between tumor cells with high versus low metastatic potentials, and we have confirmed the changes in expression levels using conventional western blotting and flow cytometry analyses. One of the proteins, cub-domain-containing protein 1 (CDCP1) attracted our attention. In this chapter, I will detail the rationales of choosing CDCP1 for further functional analyses, and summarize current knowledge on cub domains.

CUB DOMAIN CONTAINING PROTEIN 1 (CDCP1)

Early works leading to the discovery of CDCP1 – CDC1 in cell adhesion and in cancer and cancer metastasis

CDCP1 is a type I transmembrane protein, with extracellular N-terminal signal peptide (amino acid residues1-29), one high score CUB domain and two low score CUB domains (approximately residue ranges 220-350, 425-523, and 545-660), followed by a single transmembrane domain (residues 666-691) and a cytoplasmic domain (residues 692-836) (Figure 1A). Northern blots show that CDCP1 is expressed most highly in skeletal muscle and colon, followed by small intestine, lung, kidney and placenta (Hooper et al., 2003). Prostate, thyroid and tongue also express CDCP1**. Although the function of CDCP1 is largely unclear, the works that led to the discovery of this protein may shed some light.

CDCP1 was discovered through four independent researches. In the earliest work in 1996, Xia et. al. found that when human foreskin keratinocytes (HFK) were detached from laminin 5 using trypsin, a strongly tyrosine-phosphorylated protein band at 80kDa was detected, but disappeared when the cells were allowed to re-adhere. This is in marked contrast to focal adhesion kinase (FAK), which is strongly phosphorylated when HFK cells are attached, and de-phosphorylated with cells are in suspension (Xia et al., 1996). The same group identified p80 as CDCP1 eight years later, with a precursor at 140kDa. It was shown that Src family kinases (SFKs) are responsible for the phosphorylation and phosphoprotein phosphatase

** **Source:** Genomics Institute of the Novartis Research Foundation, provided by Steve Sheng.

(PTPs) are responsible for the dephosphorylation of CDCP1, but the identity of the PTP was not clear (Brown et al., 2004). These two papers showed correlation between cell de-adhesion and phosphorylation of CDCP1, but the cause-effect relationship was not analyzed.

In agreement with the idea that SFKs phosphorylate CDCP1, Bhatt et al when searching for novel Src substrates during mitosis, found that CDCP1 is in the same immuno-precipitated complex as Yes during mitosis. *In vivo* phosphorylation of CDCP1 is inhibited by three different SFK inhibitors (PP1, PD173955 and PD179483) and, *in vitro*, CDCP1 can be directly phosphorylated by Src. When CDCP1 was over-expressed in adherent mammary carcinoma MDA-468 cells, the cells detached from the plate and proliferated in a loosely adherent suspension, suggesting a causal role of CDCP1 in cell de-adhesion (Bhatt et al., 2005).

CDCP1 was also shown to be overexpressed in human colorectal and lung cancer by Schweifer's group. Using representational difference analysis (RDA) together with cDNA array technology, Scherl-Mostageer et. al. found CDCP1 is over expressed in human lung carcinoma and colon carcinoma (Scherl-Mostageer et al., 2001). In addition, using whole-cell panning of antibody libraries against human prostate cancer PC3 cells subtracted by normal prostate cells, Siva et. al. identified an antibody that reacts with CDCP1, suggesting that CDCP1 may be differentially or over- expressed on human prostate cancer cells (Siva et al., 2008).

Hooper et al used subtractive immunization and discovered that CDCP1 is more abundantly expressed on highly metastatic human epidermoid carcinoma cells line, M^{+}HEp3, as compared with the poorly metastatic parental line HEp3. SFK-dependent tyrosine phosphorylation of CDCP1 in these cells was also confirmed. Together these studies suggest that CDCP1 is upregulated in several different cancers relative to the normal tissue, and over-expressed in highly metastatic cells compared with the poorly metastatic counterpart.

These early works on CDCP1 did not assign a functional role to CDCP1 during tumor formation or metastasis, but present it as an interesting molecule, especially in light of the fact that proteins involved in adhesion/migration have frequently been found playing roles

during metastasis. These data prompted us to select CDCP1 as one of the candidate proteins, to test for functional involvement in melanoma metastasis.

CUB DOMAINS

As mentioned earlier, CDCP1 contains three extracellular CUB domains. Although the functions of CDCP1 were not clear, we hoped to gain insights in this manner by knowing what are the other proteins that contain CUB domain, and the function of CUB domain in those proteins, and by understanding the structural features of CUB domains.

The name CUB domain comes from three proteins where the domain was originally defined – complement proteins C1s/C1r, sea urchin protein uEGF, and bone morphogenesis protein 1 (Bork, 1991). This domain contains approximately 110 amino acids and is almost exclusively found in membrane proteins and secreted proteins (SMART domain analysis). At the amino acid level, the conserved features of CUB domains include 1) the presence of four conserved cysteines, which suggests the presence of two disulfide bridges, and 2) conserved hydrophobic and aromatic amino acids throughout the domain, which is a pattern typical for proteins with anti-parallel beta sheets (Bork and Beckmann, 1993). It is found in functionally diverse proteins such as a family of spermadhesins that are involved fertilization, complement subcomponents, dorso-ventral patterning proteins Tolloids, and in endocytic receptor cubilin, and is believed to function in protein-protein and/or protein/carbohydrate interactions.

Proteins Containing CUB domains

Analysis of CUB domains through the PFAM database showed that more than 900 proteins have CUB domains in their architectures (Pfam 23.0, July 2008, 10340 families). Among those, most of the proteins are from eukaryotes, especially from metazoans.

Among all 940 metazoan proteins that contain CUB domains, we can roughly divide into four subfamilies. The first family contains CUB domains only, ranging between one to 15 CUB domains, with the majority of this family having one (134 out of 206 proteins). This family includes CDCP1, as described above.

Proteins harboring protease domains, such as trypsin/chymotrypsin-like serine protease domain or Zn^{++}-dependent metalloprotease domain, belong to the second family. This family has more than 260 proteins, making up approximately 25% of all CUB-containing proteins. The founding members of CUB domain - complement system proteins C1s/C1r and bone morphogenesis protein 1(BMP-1) belong to this family. Proteins containing these enzymatic domains most likely function as proteases cleaving other cellular proteins or extracellular matrix proteins in regulated fashion.

The third family is the largest family, comprising approximately half of all CUB-containing proteins. All of them have one or more domains known to be involved in protein-protein interactions, such as Sushi domains (Kirkitadze and Barlow, 2001), Fibronectin III repeats (Hynes et al., 1984), discoidin domains, and low density lipoprotein receptor domains; or involved in protein-carbohydrate interaction such as lectin domains (Kogelberg and Feizi, 2001). Although the functions of many of these proteins are not known, they are speculated to be involved in protein-protein interaction or protein-carbohydrate interactions. In some cases, these interactions may transmit signals through transmembrane domains. One example is G-protein coupled receptor 126 (GPR126). It belongs to an orphan G-protein coupled receptor family that has exceptionally long extracellular domains N-terminal to their seven trans-membrane segments (Bockaert et al., 2002; Oh et al., 2006). Proteins in this orphan receptor family have recently been shown bind to tissue transglutaminase 2 and suppresses melanoma metastasis (Xu et al., 2006).

The last family is small, with only 14 members, but unique, in that all family members contain one growth factor domain. Platelet derived growth factor C and D (PDGF-C and -D) are two such proteins, with a C-terminal PDGF domain and an N-terminal CUB domain, which requires proteolytic removal before the PDGF-DD dimer can activate PDGF receptors (LaRochelle et al., 2001; Li et al., 2000). Figure 1B shows examples for each family of proteins containing CUB-domains.

In addition to eukaryotes, two viral proteins and several bacterial proteins from *Flavobacteria bacterium, Pseudoalteromonas atlantica, Chlorobium phaeobacteroide, and Bdellovibrio bacteriovorus* also contain CUB domains. Often these proteins contain either CUB domain alone, or with fibronectin III repeat, laminin G domain, or in one case, repeats in polycystic kidney disease 1 (PDK domain), suggesting adhesion-related functions.

Functions of CUB domains

The functions of CUB domains have been attributed to protein-carbohydrate, protein-phospholipid, protein-protein interactions and in some cases, protein trafficking and localization.

Roles of CUB domains in protein-carbohydrate and protein-phopsholipid binding were mostly elucidated in the spermadhesin family of proteins found on the surface of ungulate sperm (Topfer-Petersen et al., 2008; Topfer-Petersen et al., 1998). Spermadhesins are 12-16 kDa proteins involved in fertilization, which have a single CUB domain in each protein. In pigs there are five members - AQN-1, AQN-3, AWN, PSP-1, PSP-II. It has been shown that non-aggregated AWN-1 and AQN-3 are capable of interacting with phosphorylethanolamine (Dostalova et al., 1995), and the binding region was mapped to residues 6-12 and 104-108 of the CUB domain (Ensslin et al., 1995).

Porcine spermadhesins also present diverse carbohydrate-interacting capacities. AQN-1 recognizes both α- and β- linked galactose, as well as Man α1-3 (Manα 1-6) Man structure (Ekhlasi-Hundrieser et al., 2005); AQN-3 interacts with Gal β1-3 GlcNAc and Gal β1-4 GlcNAc sequences; and AWN binds only galactose. Isolated PSP-II is capable of interacting with Mannose-6-phopsphate and heparin(Solis et al., 1998). **

Although CUB domains can function as protein-carbohydrate, protein-phospholipid interaction protein modules, these seem to be unique properties in spermadhesin family of proteins. Rather, it seems more common for CUB domains to serve as protein-protein binding domains, since this feature has been shown in a much broader range of proteins involved in various biological functions.

** Binding of PSP-II with mannose-6-phopshpate is lost upon heterodimerization with PSP-1. However, recently it is shown that in normal physiological Zn++ concentration, there is a decreased PSP-1/PSP-II heterodimer stability (Campanero-Rhodes et al., 2005), suggesting the relevance of Man-6-P binding in physiological conditions.

With twenty-seven CUB domains, Cubilin obtained its name. Cubilin is a 460kDa membrane glycoprotein that functions as an endocytic receptor(Christensen and Birn, 2002). Many of these CUB domains have been shown to interact with various protein ligands, including intrinsic factor-vitamin B12 complex (Kozyraki et al., 1999; Kristiansen et al., 1999; Seetharam et al., 1997), apolioprotein A-I (Kozyraki et al., 1999), vitamin D (Nykjaer et al., 2001), and myeloma light chain (Batuman et al., 1998). The Kd between CUB5-8 and intrinsic factor –vitaminB12 is in the 40nM range, suggesting high affinity interactions (Kristiansen et al., 1999). Moreover, mutation in CUB8 has been found responsible for Megaloblastic anaemia 1 (MAG1), a disease characterized by selective intestinal vitamin B12 malabsorption, supporting the involvement of CUB8 in specific protein interaction (Aminoff et al., 1999).

Mannan-binding lectin-associated serine proteases (MASP) belong to the above-mentioned family II, which function as proteases in the carbohydrate-initiated complement system. Carbohydrates on the surface of pathogens are recognized by oligomeric lectins, which in turn interact with MASPs, thus initiating the complement activation cascade. Interactions between MASPs and lectins have been mapped to the CUB domains (Feinberg et al., 2003; Gregory et al., 2004; Stengaard-Pedersen et al., 2003; Teillet et al., 2008), and mutation in CUB1 of MASP-2 has been shown in patients who suffer from chronic infection and inflammatory disease(Stengaard-Pedersen et al., 2003), supporting roles of CUB domains in protein-protein interactions.

The model that CUB domains serve as protein-protein interaction modules is further supported by studies with tolloid metalloprotease, including *Drosophila* tolloid (TLC), mammalian tolloid (mTLD) and bone morphogenesis protein 1 (BMP1). This family of proteins plays important roles in development due to their ability to cleave transforming growth factor β (TGFβ) antagonists(Dale and Wardle, 1999; Mullins, 1998). Human BMP-1 cleaves procollagen (Kessler et al., 1996), and CUB domains are responsible for substrate binding (Sieron et al., 2000). In addition, CUB-1 domain in another metalloprotease ADAMTS13 has been shown to bind directly with unusually large von Willebrand factor (ULVWF) under static and flow conditions (Tao et al., 2005), CUB domain from platelet-endothelial cell surface protein SCUBE1 are necessary for interaction with BMP (Tu et al., 2008). Together, these data support a common role of CUB domains in protein-protein interaction.

In addition to the notion that CUB domains are involved in protein-substrate interaction, domain analyses in several proteins have shown that they are also important for protein secretion and localization. For example, CUB1 domain from BMP-1 is important for the secretion of BMP-1. When expressed in 293-EBNA cells, BMP-1 truncated in the first CUB domain fails to be detected in the culture medium (Hartigan et al., 2003). Mutant PDGF-D production (without the N-terminal CUB domain) was not successful due to intracellular retention of the protein, suggesting a role of CUB domain in protein secretion (Bergsten et al., 2001). Furthermore, ADAMTS13 without the C-terminus CUB domains fails to be secreted specifically from the apical face of transfected MDCK cells, and is no longer localized to the lipid rafts in these cells (Shang et al., 2006). Mutation resulting in loss of the second CUB domain in ADAMTS13 was detected in patients with thrombotic thrombocytopenic purpura (TTP) condition, and secretion of the protein was severely impaired, further supporting the role of CUB domains in protein secretion (Pimanda et al., 2004). However, it is not clear whether CUB domains are directly involved in protein sorting and secretion machinery, or are important for the folding and thus the integrity of the proteins. Misfolded proteins are often retained in the ER and Golgi for degradation. It is largely speculation that CUB domains may be involved in proper protein folding, as CUB domain from cubillin has been shown to interact with receptor-associated protein (RAP) (Kristiansen et al., 1999), which is a molecular chaperone. It is possible that CUB domains are capable of recruiting molecular chaperones, which facilitate protein folding, thus secretion. Further analysis is required to sort out among these possibilities.

Structure of CUB domains

To understand the broad interaction capability shown by different CUB domains, we have to turn to the structure of CUB domains. The crystal structures of CUB domains have been solved under several conditions – CUB domain alone, CUB-EGF together, and CUB-EGF-CUB together (Feinberg et al., 2003; Gregory et al., 2003; Romero et al., 1997; Teillet et al., 2008).

The basic structure of CUB domains was elucidated for two members of the spermadhesins, PSP-I and PSP-II, revealing a compact ellipsoidal structure (Figure1C). Each CUB domain is formed by 10 ß-strands arranged into a sandwich of two 5- ß strand sheets, with all the

hydrophobic residues buried inside the sandwich, and two disulfide bridges located on opposite edges of the same face of the sandwich (Romero et al., 1997).

Studies of MASP2 and MASP 1/3 have shown that CUB1-EGF-CUB2 segments within these proteins are responsible for homo-dimerization and interaction with the binding partner MBP (mannose-binding protein). Crystal structures of CUB1-EGF-CUB2 from MASP2 and MASP1/3 show these CUB domains have a similar ß-sandwich fold with disulfide bridges as that of spermadhesins, only that they lack the first 1 or 2 ß strands. Each CUB1-EGF-CUB2 has the shape of an elongated "C" and they dimerize in head-to-tail fashion, involving the CUB1 domain of one monomer with the EGF of its counterpart through hydrophobic interactions. This dimerization generates a concave surface, which was proposed to be the binding site for MBP (Feinberg et al., 2003) (Imagine two elongated "C" in mirror symmetry, Figure 1D). In addition, highly conserved acidic amino acids (Glu, Asp) were also identified in many CUB domains, which have been shown to co-ordinate Ca^{++} in the loops connecting the β strands (Blanc et al., 2007; Teillet et al., 2008). Mutation of those sites abolishes or severely decreases interaction with MBP, suggesting they are either involved in direct binding, or in stabilizing the CUB domain structures (Teillet et al., 2008).

From these structural studies, it appears that β-sheets are involved in homo- and hetero-dimerization of the CUB domains. Also, it was proposed that the loop regions -loop LC, LE, LG and LI defined in the Romero paper- are the principal regions involved in ligand interaction. However, more structural and mutagenesis studies are necessary to further understand the differences in binding with a variety of partners – proteins versus carbohydrates, and pinpoint amino acids that are involved in these interactions.

Our current understanding of proteins containing CUB domains and CUB domain structures and functions indicates that CDCP1 might function as a membrane adhesion molecule with extracellular ligand(s), although the identity of which is not clear. These data provided further incentives for pursuing the functions of CDCP1.

EXPERIMENTAL GOALS AND APPROACHES

Our proteomics analysis comparing membrane proteins between high versus low metastatic melanoma cells revealed that CDCP1 is upregulated in highly metastatic MA2 cells. We

wished to expand this work to other highly metastatic melanoma cells to see if such elevation is a common theme. Equally importantly, we wished to establish a functional role of CDCP1 during melanoma metastasis. Understandably, a fraction of expression level changes we found through the proteomics screen are potentially bystander changes that are not functionally involved. We hoped to identify the underlying differences that drive metastasis, therefore laying a foundation for the development of potential treatment. In this study, we used a tail-vein injection model to investigate metastatic abilities of melanoma cells. This model gives us the flexibility to experimentally manipulate the expression levels of CDCP1 using either shRNA-based knockdown, or retrovirus-based over-expression.

RESULTS

CDCP1 expression is significantly altered in a variety of different tumor types

Oncomine is a public database, which contains data from 28880 microarrays and from 41 cancer types. Our initial comparison of tumor versus normal samples from Oncomine revealed that CDCP1 mRNA levels are altered in many different tumor types (Table 1). Out of 51 studies, 20 of them showed that CDCP1 mRNA levels changed significantly, and in most cases, is increased in cancer comparing to normal tissues, in agreement with previous studies. In addition, comparison of CDCP1 expression levels in brain, breast and bladder tumors showed that CDCP1 is elevated in patients with poor prognosis (www.oncomine.org). These data are in agreement with previous reports that CDPC1 is upregulated in lung and colorectal cancers, and provided further support for choosing CDCP1 as a candidate to test its functions.

Melanoma cells with enhanced metastatic potential express elevated surface CDCP1 relative to cells with low metastatic ability

As discussed in the previous chapter, highly metastatic MA2 cells have enhanced CDCP1 expression levels compared to A375 cells. However, we would like to test whether this is an isolated incidence, as we are trying to identify common proteins that are potentially involved in cancer metastasis. For this reason, we investigated the surface expression of CDCP1 on other melanoma cells lines that were derived through *in vivo* selection by Dr. Lei Xu. After 1 or 2 rounds of selection, MA1, MC1 and MA2, MC2 were generated, respectively (Figure

2A) and all of them produce more lung metastases when intravenously injected into nude mice (Xu et al., 2006). Early passages of MA1, MA2, MC1 and MC2 were obtained and $0.5*10^6$ cells were analyzed by FACS to investigate the expression levels of CDCP1. All these cells express higher surface CDCP1 compared to A375 cells (Figure 2B).

Noticeably, flow cytometry analysis of the parental A375 cells grown *in vitro* reveals two subpopulations. As shown in Figure 2B and 2C, one population of A375 cells have lower surface expression of CDCP1 ($CDCP1^{low}$) than the other ($CDCP1^{high}$). And this appears to be a stable feature for the cells cultured *in vitro*. When parental A375 cells were continuously passed every three days for up to four passages and surface expression of CDCP1 was analyzed with each passage, we always observed the presence of two subpopulations (data not shown).

However, the picture was quite different when A375 cells were passed *in vivo*. $1x10^6$ A375 cells were intravenously injected into NOD/SCID mice, and five weeks later, the lungs of the mice were dissected and tumor nodules were surgically removed, and dispersed using the blunt end of 1ml syringes. The cells were allowed to propagate in E4Hg-10 medium, and passed once before analyzing surface expression of CDCP1. From this experiment, we generated HL1720-1, -2 and HL1740-1, -2, -3, a total of 5 cell lines. Surprisingly, all these cells showed up as $CDCP1^{high}$ population (Figure 2D), and have similar mean fluorescent intensity (MFI) to MA2 cells (Figure 2E). Thus it is the $CDCP1^{high}$ cells that generate metastases.

CDCP1 can be used as a surface marker to select cells with higher metastatic ability

We were intrigued yet delighted at this finding since two people using two different mouse strains (nude mice and NOD/SCID mice), at different times isolated tumor cells from the lungs, yet all 9 cell lines (MA1, MA2, MC1, MC2, HL1720-1, -2, and HL1740-1, -2, -3) express high CDCP1 levels. Therefore, the fact that all tumor cells derived from the lung have higher CDCP1 expression is unlikely to be a stochastic event. Rather, it suggests that CDCP1 might be a surface marker for cells with higher metastatic potential.

To test this hypothesis, we sorted the parental A375 cells based on CDCP1 expression levels into $CDCP1^{high}$ and $CDCP1^{low}$ using flow cytometry (Figure 3A), and intravenously

injected these two populations into NOD/SCID mice to assay for the metastatic potential of either population. As shown in Figure 3B, indeed mice injected with CDCP1^{high} cells harbor more lung metastases than those injected with CDCP1^{low} cells ($p = 0.043$, student t test), supporting our hypothesis. Again, all cells derived from these lung tumors retain high CDCP1 expression levels (Figure 3C). These data suggested that CDCP1 is a surface marker for cells with high metastatic potential, at least in our system.

Down-regulation of CDCP1 in highly metastatic MA2 cells significantly reduces lung metastasis while it has no effect on subcutaneous tumor growth.

To test whether CDCP1 is functionally involved in melanoma metastasis, I first tested whether experimental down-regulation of CDCP1 in MA2 cells reduces their metastatic potential in the tail-vein injection model using stable CDCP1 knockdown cell lines.

We chose a mir30-based shRNA knockdown system, as this system has shown greater p53 knockdown, generating cells with phenotype reminiscent of p53 null, which has not been achieved by other knockdown systems (Hemann et al., 2003). A schematic of the vector is shown in figure 4A, and the resulting knockdown cells are GFP$^+$ and were selected with 2.5μg/ml of puromycin. Out of four knockdown cell lines generated, we chose to work with knockdown line 6 and 10 (MA2-KD6 and MA2-KD10, arrows), as they showed most severe reduction of CDCP1 compared to cells expressing stable shRNA against the firefly luciferase gene (MA2-Ctrl-KD) (Figure 4B). We found no significant difference in cell proliferation *in vitro* among the cell lines (Figure 4C), and subcutaneous tumors derived from these cells reached the same size at the end of 33 days (Figure 4D). When the cells were dissociated at the time of dissection and analyzed for surface CDCP1 expression by FACS analysis, they all maintained lower expression levels compared to control knockdowns (Figure 4E).

Next, we injected $1*10^6$ cells of each cell line intravenously into ten NOD/SCID mice, and five weeks later, the mice were sacrificed and surface lung nodules on the left lobe were counted in blinded fashion. As shown in figure 4F, mice injected with MA2-KD6 and MA2-KD10 produced significantly fewer surface lung nodules (mean = 42.8±10.7 and 51.4±7.3, respectively) compared to MA2-Ctrl-KD (mean = 110.8±7.8, $p = 0.0002$ and 0.0001

respectively). These data suggest that CDCP1 is partly necessary for A375 melanoma cells to metastasis.

Up-regulation of CDCP1 in poorly metastatic A375 cells significantly enhances lung metastasis while it has no effect on subcutaneous tumor growth.

Conversely, we wanted to test whether overexpression of CDCP1 enhanced the metastasis ability in poorly metastatic A375 cells. We cloned full-length CDCP1 into a retroviral vector MIGw, and generated pools of A375 cells harboring either control virus (A375-Vector-Ctrl) or CDCP1 virus (A375-CDCP1). GFP-positive cells were sorted using flow cytometry and surface expression levels of CDCP1 were confirmed using FACS (Figure 5A). *In vitro*, A375-CDCP1 cells proliferate more slowly *in vitro* than do A375-Vector- Ctrl cells. When cells were harvested every 3 or 4 days and cell numbers were counted, A375-CDCP1 cells on average reach 65.13% (±4.95%) of A375-vector Ctrl cells (Figure 5B and a full description of the phenotype of A375-CDCP1 cells will be described in the next chapter). When 0.5*10e6 cells were injected at subcutaneous sites, tumors derived from both cell types reached similar weight at the end of each experiment, although tumors from A375-CDCP1 cells are slightly smaller than that from A375-vector Ctrl cells, but the difference was not statistically significant (Figure 5C). We then injected 1*10e6 of either A375-vector Ctrl cells or A375-CDCP1 cells into NOD/SCID mice via the tail vein and 5 weeks later, the numbers of GFP+ nodules on all lobes of the lungs were counted under UV dissecting microscope (Figure 5D). A375-CDCP1 cells formed significantly more metastasis (mean = 375±48.7, Figure 5F) in the lungs than did A375-vector Ctrl cells (mean = 74.9±28.4, $p = 0.0011$ Figure 5E). Overall, these results indicated that CDCP1 enhances melanoma metastasis and up-regulation of CDCP1 is sufficient to increase the metastatic potential of poorly metastatic A375 cells.

DISCUSSION

In this work, we showed that CDCP1 expression in elevated in highly metastatic melanoma cells relative to their poorly metastatic counterparts, and that CDCP1 is a marker for cells with higher metastatic potential. These results are in agreement with and significantly extend the previous studies. CDCP1 has been discovered to be elevated in lung, colon, and gastric cancer, and in metastatic squamous cell carcinomas (Hooper et al., 2003; Perry et

al., 2007; Scherl-Mostageer et al., 2001; Siva et al., 2008) – all these cells are epithelial of origin. Developmentally, melanoma cells are derived from neural crest cells, a completely different cell type from epithelial cells. Our current data that CDCP1 expression is enhanced in metastatic melanoma cells extended these earlier works, suggesting that over-expression of CDCP1 may be a more common phenomenon than has been researched. In fact, data mining using Oncomine has shown that levels of CDCP1 are increased in pancreatic, ovarian, bladder, breast, lung and brain tumors compared to the normal tissues, and support this notion. Future studies investigating these types of tumors are needed to generalize the correlation between CDCP1 expression levels and disease states.

Using clinical samples, Awakura and Ikeda recently showed that CDCP1 is a prognostic marker for renal cell carcinoma and lung adenocarcinoma (Awakura et al., 2008; Ikeda et al., 2009). There is an inverse relationship between the expression levels detected by immunohistochemical methods and the length of survival of the patients. And CDCP1 can be used as a prognostic marker for patients. Although we showed that CDCP1 could be used as a marker to separate melanoma cells with different metastatic abilities, which is in agreement with these two studies, we have not yet performed immuno-histochemical staining of human melanoma samples. Such analysis using clinical samples including primary and metastasis melanoma is required to establish the prognostic significance of CDCP1 in melanomas. We have obtained human tumor samples along with normal samples, and tumors of different grades and we will use those samples for such analysis.

Tumor cells do not survive on their own; numerous studies have shown that tumor microenvironment including different cell types such as fibroblasts (Haviv et al., 2009; Olumi et al., 1999), macrophages (Condeelis and Pollard, 2006), endothelial cells (Nyberg et al., 2008) to name a few, and proteins such as extracellular proteins (ECM) (Bissell et al., 2005; Butcher et al., 2009; Xu et al., 2006) and growth factors such as TGFβ (Massague, 2008) contribute greatly to the tumor cell behaviors. In our study, we found that A375-CDCP1 cells proliferate more slowly *in vitro* compared to A375-Ctrl-vector cells, but subcutaneous tumors derived from either cell type reach the same size. However, in the lungs, A375-CDCP1 cells form significantly more metastases than do the control cells. These differences support the notion that factors in different tissues play important roles in tumor growth and metastasis formation. CUB domains in other proteins have been shown to be involved in protein-protein and protein-carbohydrate interactions. It is conceivable that three

CUB domains that CDCP1 possess are able to interact with components in the microenvironment, therefore transmitting signals to the cells and affecting the tumor growth. In fact, as will be detailed in chapter V (data not shown here), we have generated hybrid CDCP1 where extracellular and transmembrane domains were replaced with those from IL2-receptor α(Tac-CDCP1). Cells expressing hybrid CDCP1 failed to elicit the effects seen by wild-type CDCP1, supporting our hypothesis (although we have not eliminated the possibility that cis- or trans- interaction between CDCP1 is enough to initiate signals). It will be of great interest to identify the ligand of CDCP1, which will shed light on the nature of such microenvironment interactions with the tumor cells. In fact, work has been initiated in our lab to search for CDCP1 ligand(s).

There are several obvious extensions based on our current work and work by the Sakai group.

1) Does CDCP1 function as a metastasis enhancer in other types of tumors in addition to melanoma, lung adenocarcinoma and gastric cancer? Oncomine is a public database, which contains data from 28880 microarrays and from 41 cancer types. Comparison of CDCP1 expression levels in brain, breast and bladder tumors showed that CDCP1 is elevated in patients with poor prognosis (www.oncomine.org). It is worth investigating the function of CDCP1 in these types of tumors to establish a broader role during metastasis.
2) Does CDCP1 play a role in metastasis in *in vivo* tumor models? This is temporarily hindered by the absence of CDCP1 knockout mice, although such mouse strain generation is underway through the KOMP project by NIH (WWW.knockoutmouse.org). With the generation of such a strain (or conditional knockout strains), we will be able to evaluate the role of CDCP1 in melanoma progression and metastasis, and in lung and gastric cancers.
3) Going back to the observation that CDCP1 expression is enhanced in several types of tumors (Perry et al., 2007; Scherl-Mostageer et al., 2001; Siva et al., 2008) (and Oncomine analysis), it will be interesting to test if CDCP1 confers tumorigenesity.
4) And importantly, what is the mechanism that CDCP1 function as a metastasis enhancer in our system? We began to address this question and have started to gain insight on this front, which will be detailed in the next two chapters.

In conclusion, we have shown that CDCP1 is a surface marker for melanoma cells with high metastatic potential. By both partial loss-of-function and gain-of-function studies, we also showed for the first time, that CDCP1 plays a causal role in metastasis of melanoma cells. It is very satisfying to see that proteins identified through our proteomics screen induced causal changes, and is not simply a bystander change. In the next chapter, we will attempt to understand the underlying mechanisms by which CDCP1 contributes to metastasis, first at cellular biology level then at molecular biology level.

REFERENCES

Aminoff, M., Carter, J. E., Chadwick, R. B., Johnson, C., Grasbeck, R., Abdelaal, M. A., Broch, H., Jenner, L. B., Verroust, P. J., Moestrup, S. K., *et al.* (1999). Mutations in CUBN, encoding the intrinsic factor-vitamin B12 receptor, cubilin, cause hereditary megaloblastic anaemia 1. Nat Genet *21*, 309-313.

Awakura, Y., Nakamura, E., Takahashi, T., Kotani, H., Mikami, Y., Kadowaki, T., Myoumoto, A., Akiyama, H., Ito, N., Kamoto, T., *et al.* (2008). Microarray-based identification of CUB-domain containing protein 1 as a potential prognostic marker in conventional renal cell carcinoma. J Cancer Res Clin Oncol *134*, 1363-1369.

Batuman, V., Verroust, P. J., Navar, G. L., Kaysen, J. H., Goda, F. O., Campbell, W. C., Simon, E., Pontillon, F., Lyles, M., Bruno, J., and Hammond, T. G. (1998). Myeloma light chains are ligands for cubilin (gp280). Am J Physiol *275*, F246-254.

Benes, C. H., Wu, N., Elia, A. E., Dharia, T., Cantley, L. C., and Soltoff, S. P. (2005). The C2 domain of PKCdelta is a phosphotyrosine binding domain. Cell *121*, 271-280.

Bergsten, E., Uutela, M., Li, X., Pietras, K., Ostman, A., Heldin, C. H., Alitalo, K., and Eriksson, U. (2001). PDGF-D is a specific, protease-activated ligand for the PDGF beta-receptor. Nat Cell Biol *3*, 512-516.

Bhatt, A. S., Erdjument-Bromage, H., Tempst, P., Craik, C. S., and Moasser, M. M. (2005). Adhesion signaling by a novel mitotic substrate of src kinases. Oncogene *24*, 5333-5343.

Bissell, M. J., Kenny, P. A., and Radisky, D. C. (2005). Microenvironmental regulators of tissue structure and function also regulate tumor induction and progression: the role of extracellular matrix and its degrading enzymes. Cold Spring Harb Symp Quant Biol *70*, 343-356.

Blanc, G., Font, B., Eichenberger, D., Moreau, C., Ricard-Blum, S., Hulmes, D. J., and Moali, C. (2007). Insights into how CUB domains can exert specific functions while sharing a common fold: conserved and specific features of the CUB1 domain contribute to the molecular basis of procollagen C-proteinase enhancer-1 activity. J Biol Chem *282*, 16924-16933.

Bockaert, J., Claeysen, S., Becamel, C., Pinloche, S., and Dumuis, A. (2002). G protein-coupled receptors: dominant players in cell-cell communication. Int Rev Cytol *212*, 63-132.

Bork, P. (1991). Complement components C1r/C1s, bone morphogenic protein 1 and Xenopus laevis developmentally regulated protein UVS.2 share common repeats. FEBS Lett *282*, 9-12.

Bork, P., and Beckmann, G. (1993). The CUB domain. A widespread module in developmentally regulated proteins. J Mol Biol *231*, 539-545.

Brown, T. A., Yang, T. M., Zaitsevskaia, T., Xia, Y., Dunn, C. A., Sigle, R. O., Knudsen, B., and Carter, W. G. (2004). Adhesion or plasmin regulates tyrosine phosphorylation of a novel membrane glycoprotein p80/gp140/CUB domain-containing protein 1 in epithelia. J Biol Chem *279*, 14772-14783.

Butcher, D. T., Alliston, T., and Weaver, V. M. (2009). A tense situation: forcing tumour progression. Nat Rev Cancer *9*, 108-122.

Campanero-Rhodes, M. A., Menendez, M., Saiz, J. L., Sanz, L., Calvete, J. J., and Solis, D. (2005). Analysis of the stability of the spermadhesin PSP-I/PSP-II heterodimer. Effects of Zn2+ and acidic pH. FEBS J *272*, 5663-5670.

Christensen, E. I., and Birn, H. (2002). Megalin and cubilin: multifunctional endocytic receptors. Nat Rev Mol Cell Biol *3*, 256-266.

Condeelis, J., and Pollard, J. W. (2006). Macrophages: obligate partners for tumor cell migration, invasion, and metastasis. Cell *124*, 263-266.

Dale, L., and Wardle, F. C. (1999). A gradient of BMP activity specifies dorsal-ventral fates in early Xenopus embryos. Semin Cell Dev Biol *10*, 319-326.
Dostalova, Z., Calvete, J. J., and Topfer-Petersen, E. (1995). Interaction of non-aggregated boar AWN-1 and AQN-3 with phospholipid matrices. A model for coating of spermadhesins to the sperm surface. Biol Chem Hoppe Seyler *376*, 237-242.
Ekhlasi-Hundrieser, M., Gohr, K., Wagner, A., Tsolova, M., Petrunkina, A., and Topfer-Petersen, E. (2005). Spermadhesin AQN1 is a candidate receptor molecule involved in the formation of the oviductal sperm reservoir in the pig. Biol Reprod *73*, 536-545.
Ensslin, M., Calvete, J. J., Thole, H. H., Sierralta, W. D., Adermann, K., Sanz, L., and Topfer-Petersen, E. (1995). Identification by affinity chromatography of boar sperm membrane-associated proteins bound to immobilized porcine zona pellucida. Mapping of the phosphorylethanolamine-binding region of spermadhesin AWN. Biol Chem Hoppe Seyler *376*, 733-738.
Feinberg, H., Uitdehaag, J. C., Davies, J. M., Wallis, R., Drickamer, K., and Weis, W. I. (2003). Crystal structure of the CUB1-EGF-CUB2 region of mannose-binding protein associated serine protease-2. EMBO J *22*, 2348-2359.
Gregory, L. A., Thielens, N. M., Arlaud, G. J., Fontecilla-Camps, J. C., and Gaboriaud, C. (2003). X-ray structure of the Ca2+-binding interaction domain of C1s. Insights into the assembly of the C1 complex of complement. J Biol Chem *278*, 32157-32164.
Gregory, L. A., Thielens, N. M., Matsushita, M., Sorensen, R., Arlaud, G. J., Fontecilla-Camps, J. C., and Gaboriaud, C. (2004). The X-ray structure of human mannan-binding lectin-associated protein 19 (MAp19) and its interaction site with mannan-binding lectin and L-ficolin. J Biol Chem *279*, 29391-29397.
Hartigan, N., Garrigue-Antar, L., and Kadler, K. E. (2003). Bone morphogenetic protein-1 (BMP-1). Identification of the minimal domain structure for procollagen C-proteinase activity. J Biol Chem *278*, 18045-18049.
Haviv, I., Polyak, K., Qiu, W., Hu, M., and Campbell, I. (2009). Origin of carcinoma associated fibroblasts. Cell Cycle *8*, 589-595.
Hemann, M. T., Fridman, J. S., Zilfou, J. T., Hernando, E., Paddison, P. J., Cordon-Cardo, C., Hannon, G. J., and Lowe, S. W. (2003). An epi-allelic series of p53 hypomorphs created by stable RNAi produces distinct tumor phenotypes in vivo. Nat Genet *33*, 396-400.
Hooper, J. D., Zijlstra, A., Aimes, R. T., Liang, H., Claassen, G. F., Tarin, D., Testa, J. E., and Quigley, J. P. (2003). Subtractive immunization using highly metastatic human tumor cells identifies SIMA135/CDCP1, a 135 kDa cell surface phosphorylated glycoprotein antigen. Oncogene *22*, 1783-1794.
Hynes, R. O., Schwarzbauer, J. E., and Tamkun, J. W. (1984). Fibronectin: a versatile gene for a versatile protein. Ciba Found Symp *108*, 75-92.
Ikeda, J., Oda, T., Inoue, M., Uekita, T., Sakai, R., Okumura, M., Aozasa, K., and Morii, E. (2009). Expression of CUB domain containing protein (CDCP1) is correlated with prognosis and survival of patients with adenocarcinoma of lung. Cancer Sci *100*, 429-433.
Kessler, E., Takahara, K., Biniaminov, L., Brusel, M., and Greenspan, D. S. (1996). Bone morphogenetic protein-1: the type I procollagen C-proteinase. Science *271*, 360-362.
Kirkitadze, M. D., and Barlow, P. N. (2001). Structure and flexibility of the multiple domain proteins that regulate complement activation. Immunol Rev *180*, 146-161.
Kogelberg, H., and Feizi, T. (2001). New structural insights into lectin-type proteins of the immune system. Curr Opin Struct Biol *11*, 635-643.
Kozyraki, R., Fyfe, J., Kristiansen, M., Gerdes, C., Jacobsen, C., Cui, S., Christensen, E. I., Aminoff, M., de la Chapelle, A., Krahe, R., *et al.* (1999). The intrinsic factor-vitamin B12 receptor, cubilin, is a high-affinity apolipoprotein A-I receptor facilitating endocytosis of high-density lipoprotein. Nat Med *5*, 656-661.

Kristiansen, M., Kozyraki, R., Jacobsen, C., Nexo, E., Verroust, P. J., and Moestrup, S. K. (1999). Molecular dissection of the intrinsic factor-vitamin B12 receptor, cubilin, discloses regions important for membrane association and ligand binding. J Biol Chem *274*, 20540-20544.
LaRochelle, W. J., Jeffers, M., McDonald, W. F., Chillakuru, R. A., Giese, N. A., Lokker, N. A., Sullivan, C., Boldog, F. L., Yang, M., Vernet, C., *et al.* (2001). PDGF-D, a new protease-activated growth factor. Nat Cell Biol *3*, 517-521.
Li, X., Ponten, A., Aase, K., Karlsson, L., Abramsson, A., Uutela, M., Backstrom, G., Hellstrom, M., Bostrom, H., Li, H., *et al.* (2000). PDGF-C is a new protease-activated ligand for the PDGF alpha-receptor. Nat Cell Biol *2*, 302-309.
Massague, J. (2008). TGFbeta in Cancer. Cell *134*, 215-230.
Mullins, M. C. (1998). Holy Tolloido: Tolloid cleaves SOG/Chordin to free DPP/BMPs. Trends Genet *14*, 127-129.
Nyberg, P., Salo, T., and Kalluri, R. (2008). Tumor microenvironment and angiogenesis. Front Biosci *13*, 6537-6553.
Nykjaer, A., Fyfe, J. C., Kozyraki, R., Leheste, J. R., Jacobsen, C., Nielsen, M. S., Verroust, P. J., Aminoff, M., de la Chapelle, A., Moestrup, S. K., *et al.* (2001). Cubilin dysfunction causes abnormal metabolism of the steroid hormone 25(OH) vitamin D(3). Proc Natl Acad Sci U S A *98*, 13895-13900.
Oh, D. Y., Kim, K., Kwon, H. B., and Seong, J. Y. (2006). Cellular and molecular biology of orphan G protein-coupled receptors. Int Rev Cytol *252*, 163-218.
Olumi, A. F., Grossfeld, G. D., Hayward, S. W., Carroll, P. R., Tlsty, T. D., and Cunha, G. R. (1999). Carcinoma-associated fibroblasts direct tumor progression of initiated human prostatic epithelium. Cancer Res *59*, 5002-5011.
Perry, S. E., Robinson, P., Melcher, A., Quirke, P., Buhring, H. J., Cook, G. P., and Blair, G. E. (2007). Expression of the CUB domain containing protein 1 (CDCP1) gene in colorectal tumour cells. FEBS Lett *581*, 1137-1142.
Pimanda, J. E., Maekawa, A., Wind, T., Paxton, J., Chesterman, C. N., and Hogg, P. J. (2004). Congenital thrombotic thrombocytopenic purpura in association with a mutation in the second CUB domain of ADAMTS13. Blood *103*, 627-629.
Romero, A., Romao, M. J., Varela, P. F., Kolln, I., Dias, J. M., Carvalho, A. L., Sanz, L., Topfer-Petersen, E., and Calvete, J. J. (1997). The crystal structures of two spermadhesins reveal the CUB domain fold. Nat Struct Biol *4*, 783-788.
Scherl-Mostageer, M., Sommergruber, W., Abseher, R., Hauptmann, R., Ambros, P., and Schweifer, N. (2001). Identification of a novel gene, CDCP1, overexpressed in human colorectal cancer. Oncogene *20*, 4402-4408.
Seetharam, B., Christensen, E. I., Moestrup, S. K., Hammond, T. G., and Verroust, P. J. (1997). Identification of rat yolk sac target protein of teratogenic antibodies, gp280, as intrinsic factor-cobalamin receptor. J Clin Invest *99*, 2317-2322.
Shang, D., Zheng, X. W., Niiya, M., and Zheng, X. L. (2006). Apical sorting of ADAMTS13 in vascular endothelial cells and Madin-Darby canine kidney cells depends on the CUB domains and their association with lipid rafts. Blood *108*, 2207-2215.
Sieron, A. L., Tretiakova, A., Jameson, B. A., Segall, M. L., Lund-Katz, S., Khan, M. T., Li, S., and Stocker, W. (2000). Structure and function of procollagen C-proteinase (mTolloid) domains determined by protease digestion, circular dichroism, binding to procollagen type I, and computer modeling. Biochemistry *39*, 3231-3239.
Siva, A. C., Kirkland, R. E., Lin, B., Maruyama, T., McWhirter, J., Yantiri-Wernimont, F., Bowdish, K. S., and Xin, H. (2008). Selection of anti-cancer antibodies from combinatorial libraries by whole-cell panning and stringent subtraction with human blood cells. J Immunol Methods *330*, 109-119.

Solis, D., Romero, A., Jimenez, M., Diaz-Maurino, T., and Calvete, J. J. (1998). Binding of mannose-6-phosphate and heparin by boar seminal plasma PSP-II, a member of the spermadhesin protein family. FEBS Lett *431*, 273-278.
Stengaard-Pedersen, K., Thiel, S., Gadjeva, M., Moller-Kristensen, M., Sorensen, R., Jensen, L. T., Sjoholm, A. G., Fugger, L., and Jensenius, J. C. (2003). Inherited deficiency of mannan-binding lectin-associated serine protease 2. N Engl J Med *349*, 554-560.
Tao, Z., Peng, Y., Nolasco, L., Cal, S., Lopez-Otin, C., Li, R., Moake, J. L., Lopez, J. A., and Dong, J. F. (2005). Recombinant CUB-1 domain polypeptide inhibits the cleavage of ULVWF strings by ADAMTS13 under flow conditions. Blood *106*, 4139-4145.
Teillet, F., Gaboriaud, C., Lacroix, M., Martin, L., Arlaud, G. J., and Thielens, N. M. (2008). Crystal structure of the CUB1-EGF-CUB2 domain of human MASP-1/3 and identification of its interaction sites with mannan-binding lectin and ficolins. J Biol Chem *283*, 25715-25724.
Topfer-Petersen, E., Ekhlasi-Hundrieser, M., and Tsolova, M. (2008). Glycobiology of fertilization in the pig. Int J Dev Biol *52*, 717-736.
Topfer-Petersen, E., Romero, A., Varela, P. F., Ekhlasi-Hundrieser, M., Dostalova, Z., Sanz, L., and Calvete, J. J. (1998). Spermadhesins: a new protein family. Facts, hypotheses and perspectives. Andrologia *30*, 217-224.
Tu, C. F., Yan, Y. T., Wu, S. Y., Djoko, B., Tsai, M. T., Cheng, C. J., and Yang, R. B. (2008). Domain and functional analysis of a novel platelet-endothelial cell surface protein, SCUBE1. J Biol Chem *283*, 12478-12488.
Uekita, T., Jia, L., Narisawa-Saito, M., Yokota, J., Kiyono, T., and Sakai, R. (2007). CUB domain-containing protein 1 is a novel regulator of anoikis resistance in lung adenocarcinoma. Mol Cell Biol *27*, 7649-7660.
Uekita, T., Tanaka, M., Takigahira, M., Miyazawa, Y., Nakanishi, Y., Kanai, Y., Yanagihara, K., and Sakai, R. (2008). CUB-domain-containing protein 1 regulates peritoneal dissemination of gastric scirrhous carcinoma. Am J Pathol *172*, 1729-1739.
Xia, Y., Gil, S. G., and Carter, W. G. (1996). Anchorage mediated by integrin alpha6beta4 to laminin 5 (epiligrin) regulates tyrosine phosphorylation of a membrane-associated 80-kD protein. J Cell Biol *132*, 727-740.
Xu, L., Begum, S., Hearn, J. D., and Hynes, R. O. (2006). GPR56, an atypical G protein-coupled receptor, binds tissue transglutaminase, TG2, and inhibits melanoma tumor growth and metastasis. Proc Natl Acad Sci U S A *103*, 9023-9028.

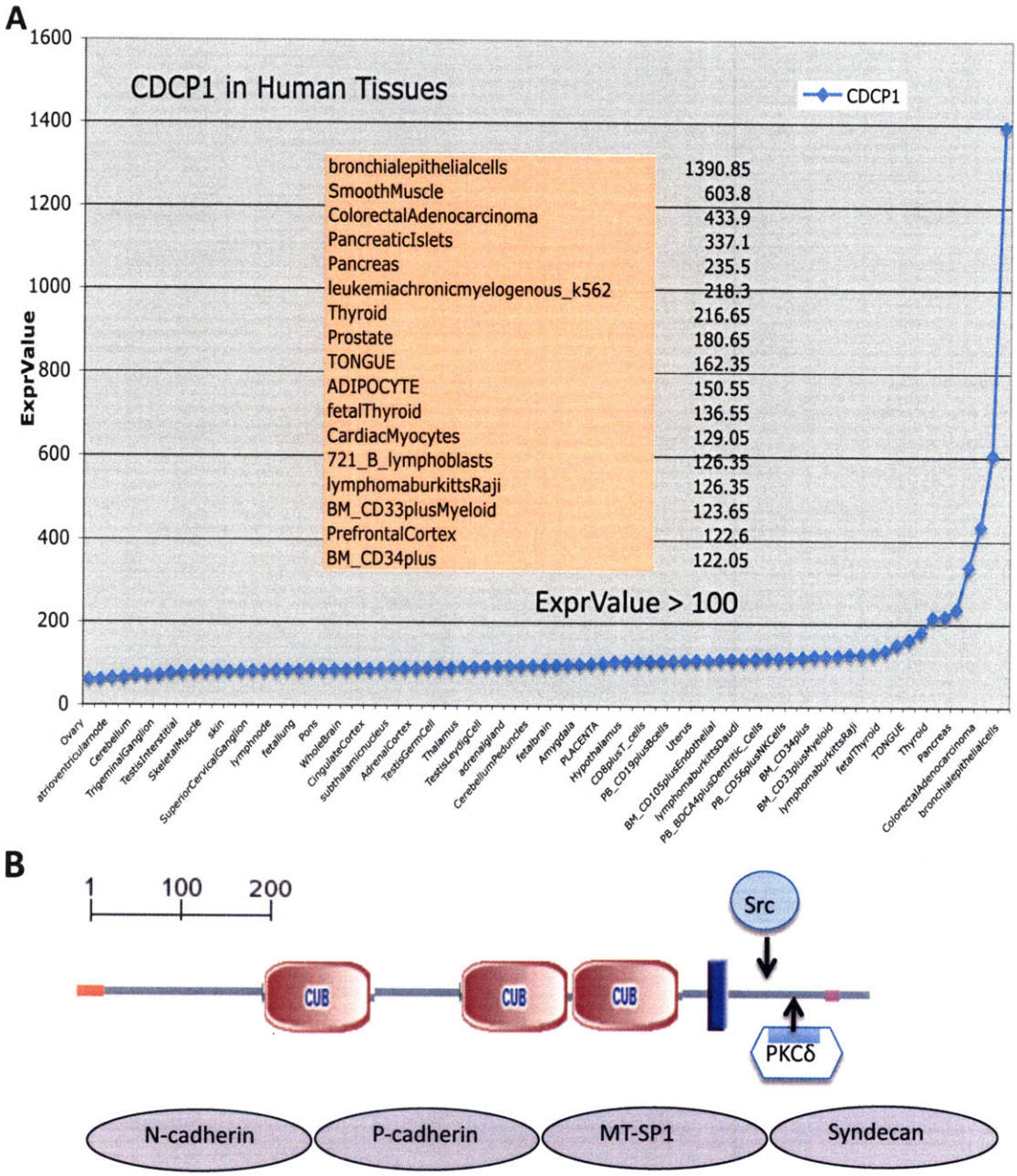

Figure 1. CUB domain Containing protein 1 (CDCP1) expression profile and proteins with CUB domains in their architectures. (A) Normal human tissues that express CDCP1 at mRNA level. Data were obtained from Novartis Gene Atlas Dataset and figure was created by Steve Shen. **(B)** Structure outline of CDCP1. It contains (from N-terminus to the C-terminus): signal peptide, 3 extracellular CUB domains, a transmembrane domain and intracellular domain. Src family kinase and PKCδ have been shown interact with CDCP1 through intracellular tyrosines. Purple ovals represent proteins interacting with CDCP1 by Co-immunoprecipitation experiments.

C Family I: AWN

Family II: TLL1

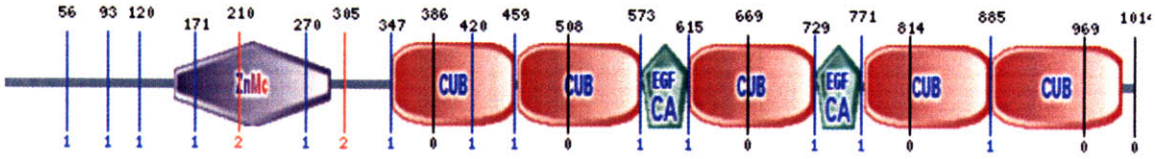

Family II: C1r

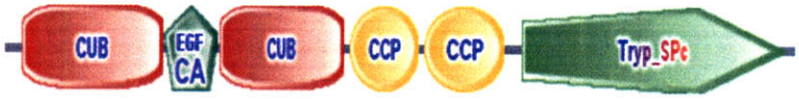

Family III: LRP10

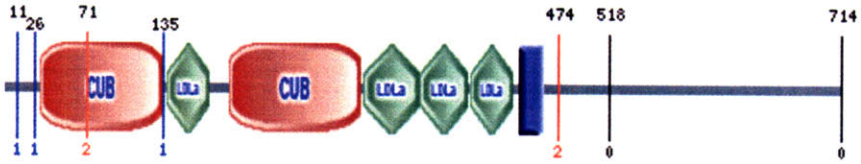

Family III: Neuropilin-1

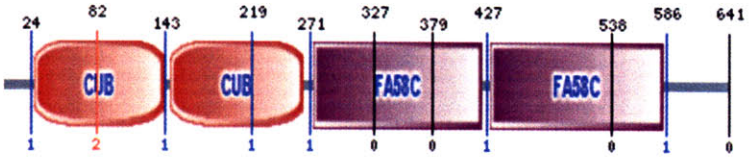

Famiily IV: PDGF-D

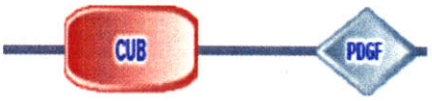

Figure 1. CUB domain Containing protein 1 (CDCP1) expression profile and proteins with CUB domains in their architectures. (C) Examples of subfamilies of proteins that contain CUB domains as described in the text.

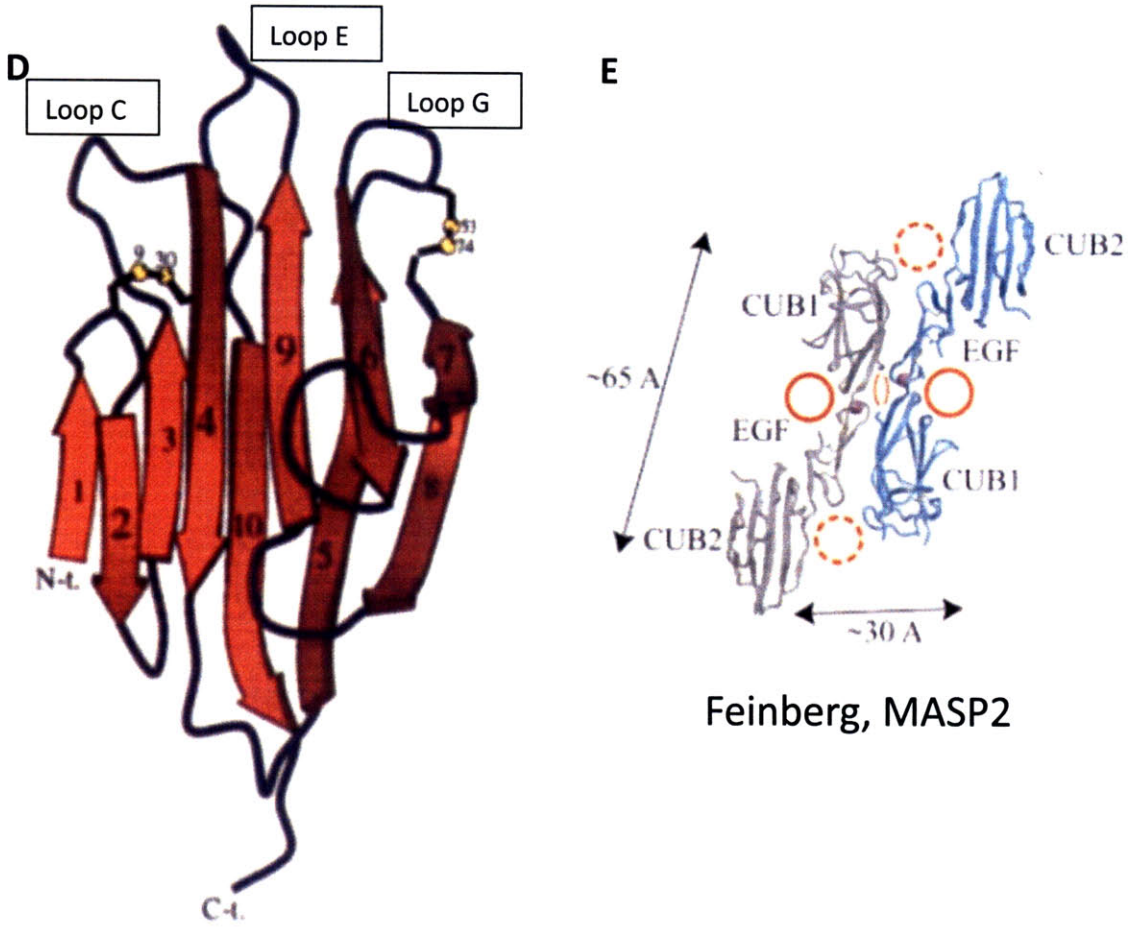

Figure 1. CUB domain Containing protein 1 (CDCP1) expression profile and proteins with CUB domains in their architectures. (D) Crystal structure of porcine PSPI shows the overall fold of CUB domains. Loop C, E and G are proposed to be involved in interaction with binding partners. Adapted from Romero et al, 1997. **(E)** Crystal structure of MASP2. CUB1-EGF-CUB2, notice the closed orange circles indicate where the substrates are likely to interact. Adapted from Feinberg et al, 2003

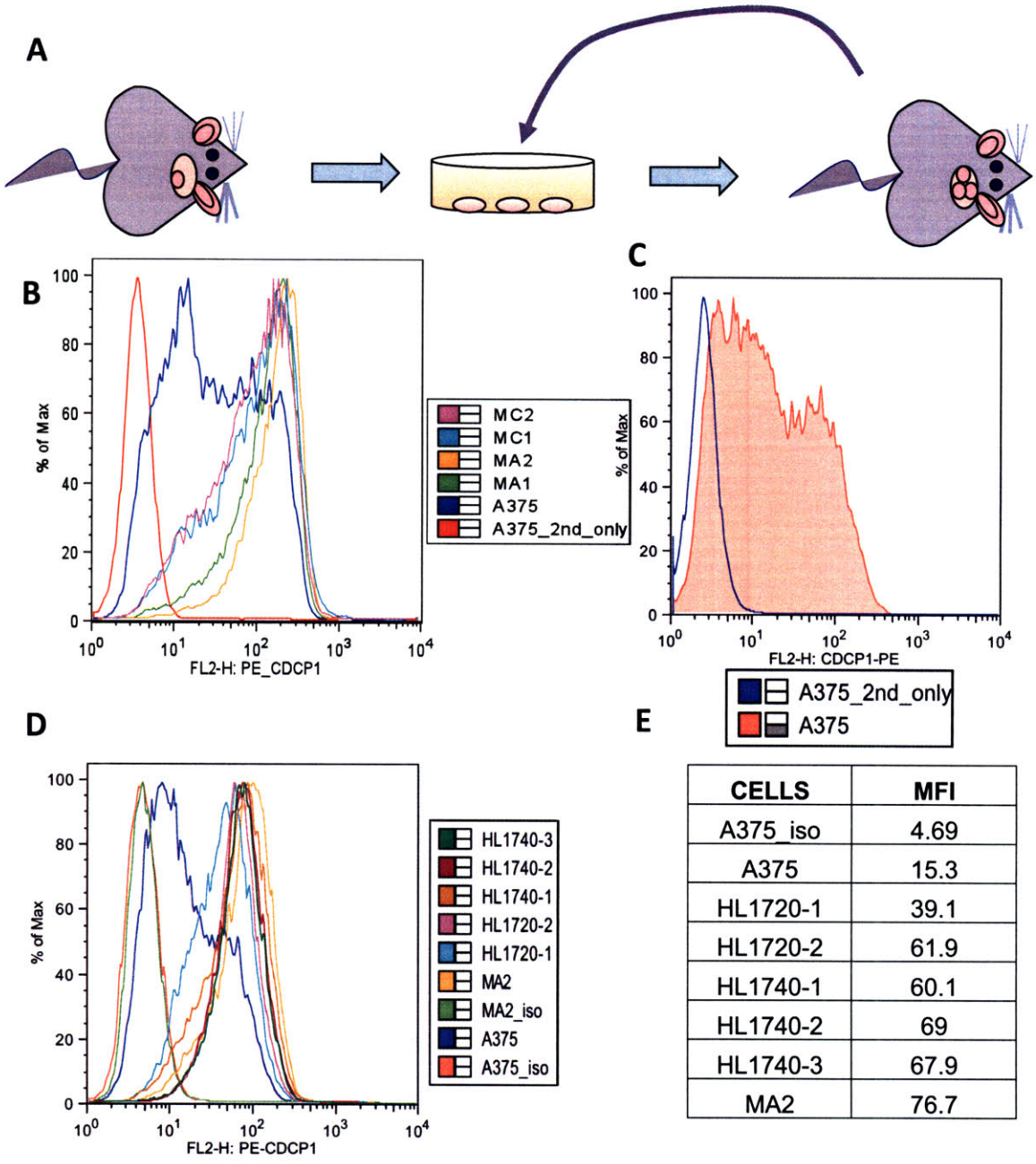

CELLS	MFI
A375_iso	4.69
A375	15.3
HL1720-1	39.1
HL1720-2	61.9
HL1740-1	60.1
HL1740-2	69
HL1740-3	67.9
MA2	76.7

Figure 2. CDCP1 expression levels are upregulated in highly metastatic melanoma cell lines compared to cells with low metastatic potential, and all cells derived from lung metastasis show high CDCP1 expression levels. **(A)** A schematic of in vivo derivation of MA1, MC1, MA2 and MC2 cells from parental A375 cells. All derived cells have higher metastatic potential compared to A375 cells. **(B)** Flow cytometry analysis of CDCP1 expression shows CDCP1 surface levels are increased in all highly metastatic cells (MA1, MA2, MC1 and MC2) comparing to low-metastatic parental A375. **(C)** Surface expression of CDCP1 on A375 cells reveals two peaks; **(D)** All tumor cells derived from in vivo lung metastasis show high expression levels of CDCP1 compared to A375 cells. **(E)** Mean fluorescence intensity of CDCP1 for figure 2D.

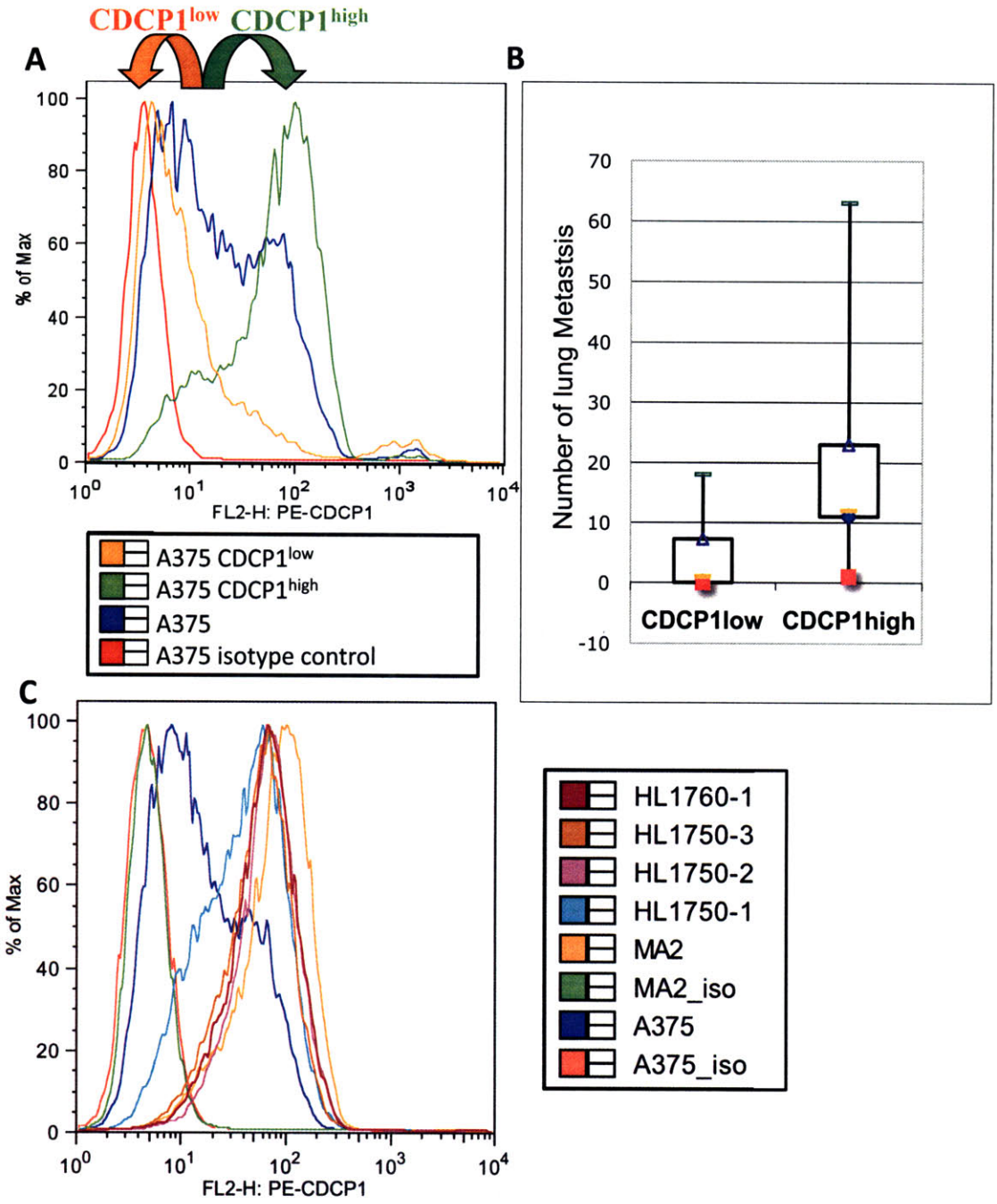

Figure 3. CDCP1 is a surface marker for melanoma cells with higher metastatic potentials. (A) Parental A375 cells can be sorted into CDCP1^{high} and CDCP1^{low} sub-populations. **(B)** CDCP1^{high} cells form more lung metastasis when intravenously injected into NOD/SCID mice. **(C)** Cells isolated from lung metastasis from mice injected with CDCP1^{high} (HL1750-1,-2, HL1760-1,-2) maintain higher CDCP1 expression levels that are equivalent to MA2 cells.

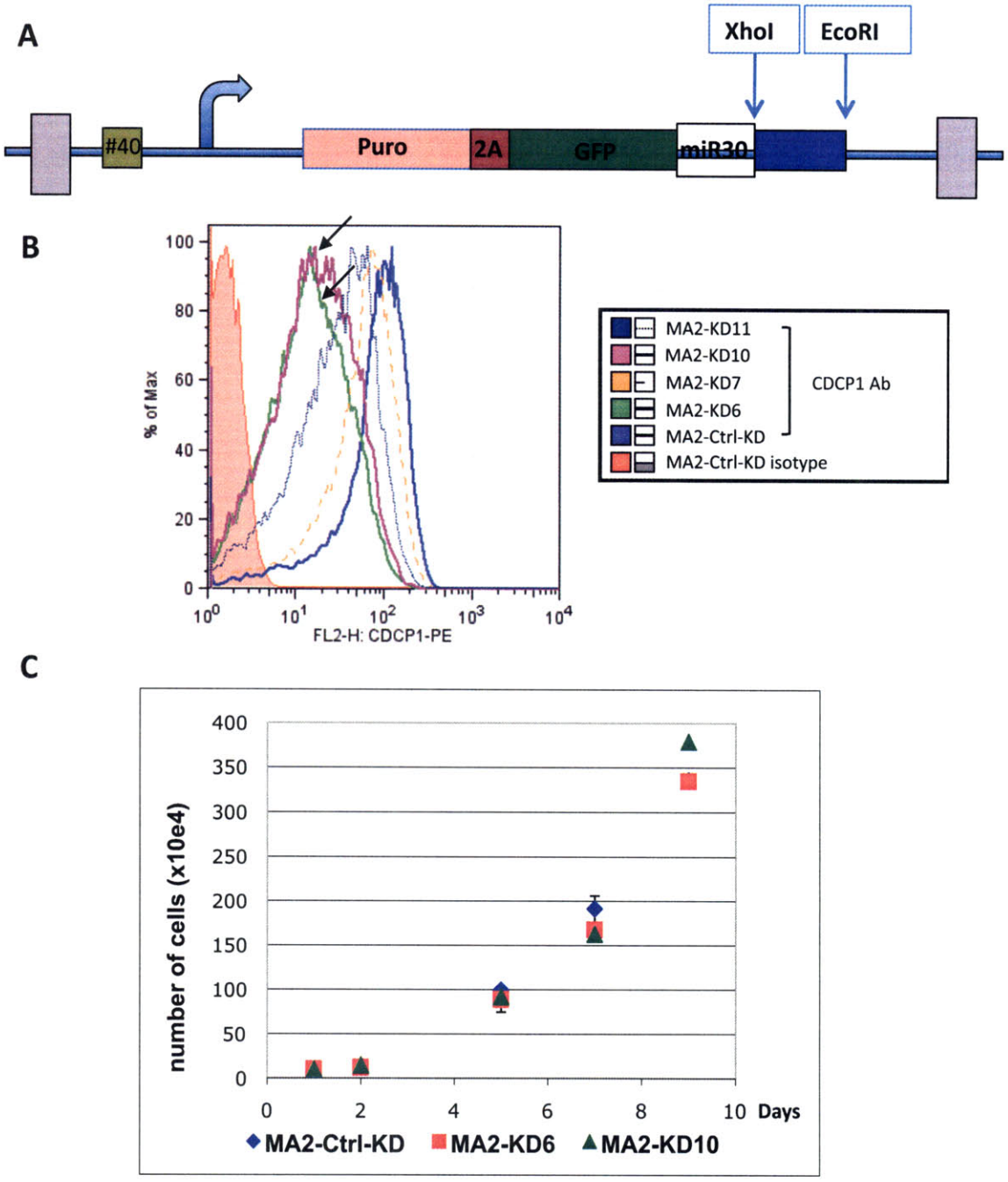

Figure 4. Downregulation of CDCP1 in highly metastatic cells significantly reduced lung metastasis, while having no effect on *in vitro* cell proliferation and subcutaneous tumor. (A) A schematic of the vector used to generate CDCP1 knock-down MA2 cells. Gene specific shRNA sequences were cloned between XhoI and EcoRI sites. **(B)** FACS plot showing down-regulation of surface CDCP1 in MA2 cells. Arrows indicate the two knock-down lines used in our studies. **(C)** Reducing CDCP1 expression in MA2 cells does not affect cell proliferation *in vitro*.

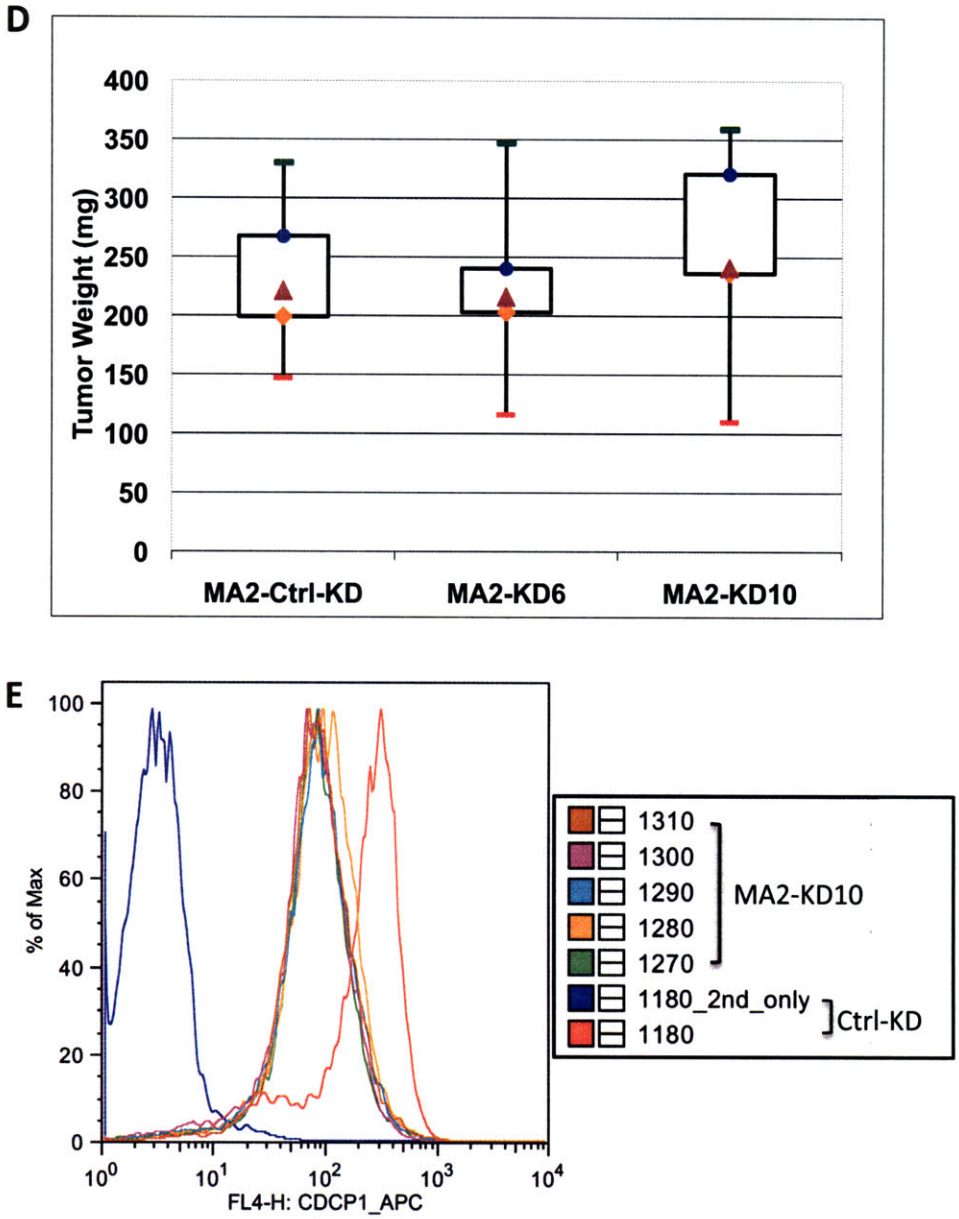

Figure 4. Downregulation of CDCP1 in highly metastatic cells significantly reduced lung metastasis, while having no effect on *in vitro* cell proliferation and subcutaneous tumor. **(D)** Subcutaneous tumors from MA2-Ctrl-KD and MA2-KD6, 10 reach the same weight after 33 days. **(E)** At the time of dissection, subcutaneous tumor cells from MA2-KD6 (data not shown here for simplicity) and MA2-KD10 maintain their lower CDCP1 expression compared to subcutaneous tumors generated from MA2-Ctrl-KD cells.

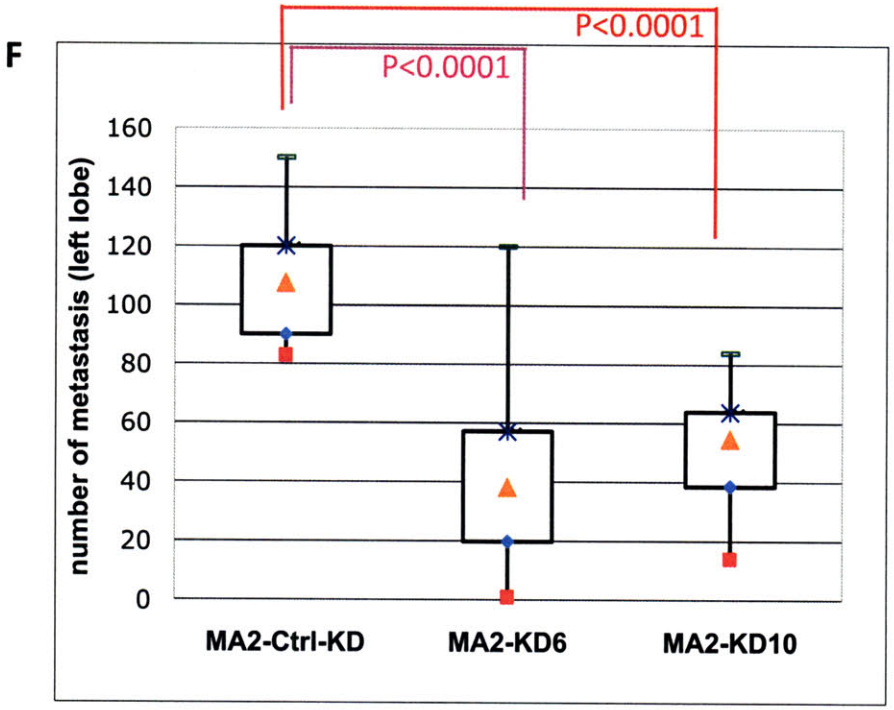

Figure 4. Downregulation of CDCP1 in highly metastatic cells significantly reduced lung metastasis, while having no effect on *in vitro* cell proliferation and subcutaneous tumor. (F) Numbesr of surface tumors in mice injected with MA2-KD6 and MA2-KD10 cells are significantly smaller than with MA2-Ctrl-KD cells.

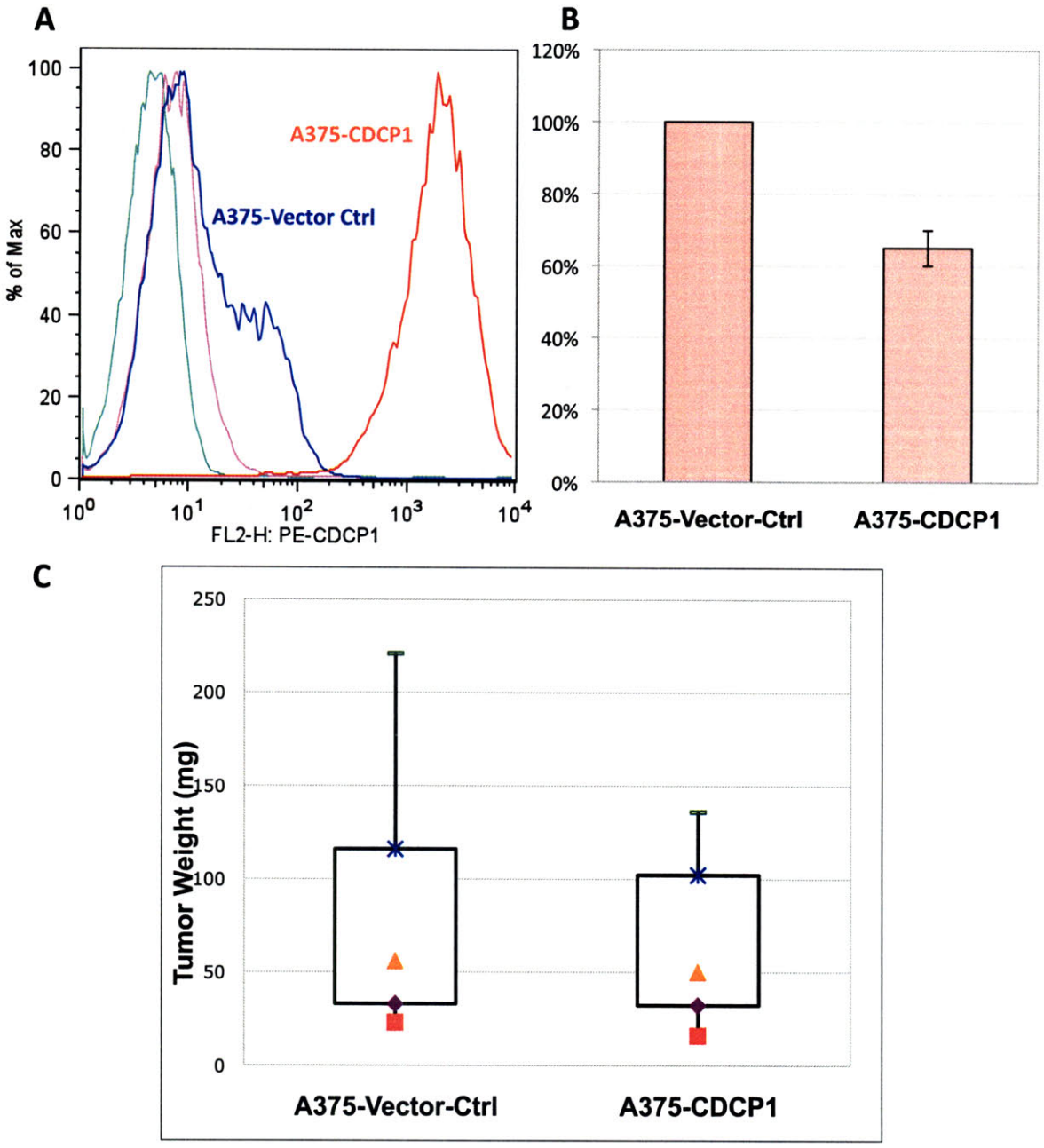

Figure 5. Overexpression of CDCP1 in poorly metastatic A375 cells decreases cell proliferation *in vitro*, does not affect tumor growth at the subcutaneous site, but significantly enhances lung metastasis of the cells . (A) A375 cells carrying MIGw-CDCP1 vector express higher surface CDCP1 than those carrying control vectors. **(B)** *In vitro*, A375-CDCP1 typically reach 65% in cell number comparing to A375-Vector-Ctrl on day 3 when equal numbers of cells were plated on day 1. **(C)** Tumors derived from A375-CDCP1 cells reach the same size as those from A375-Vector-Ctrl cells.

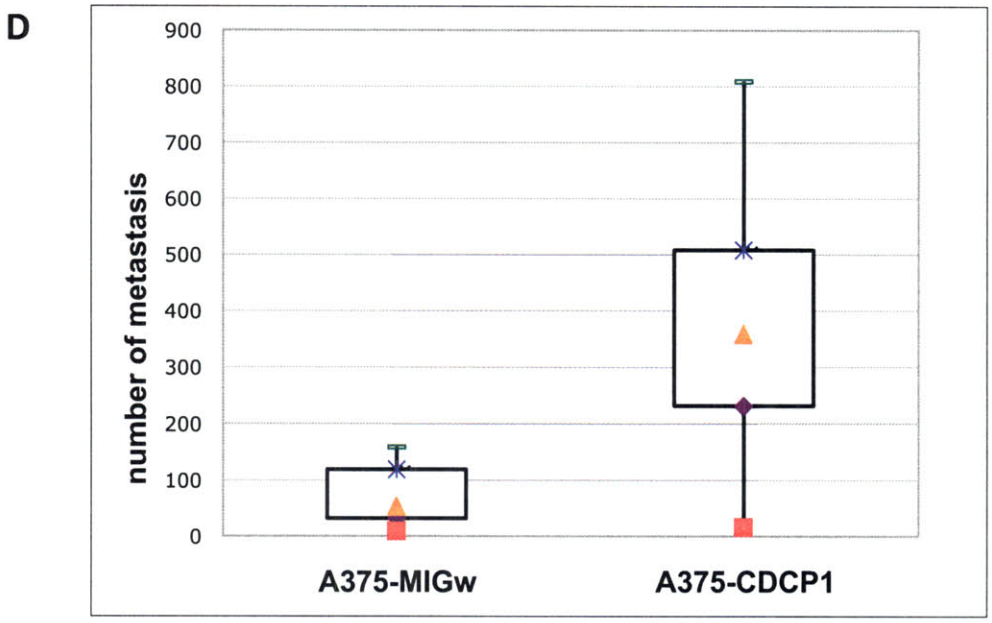

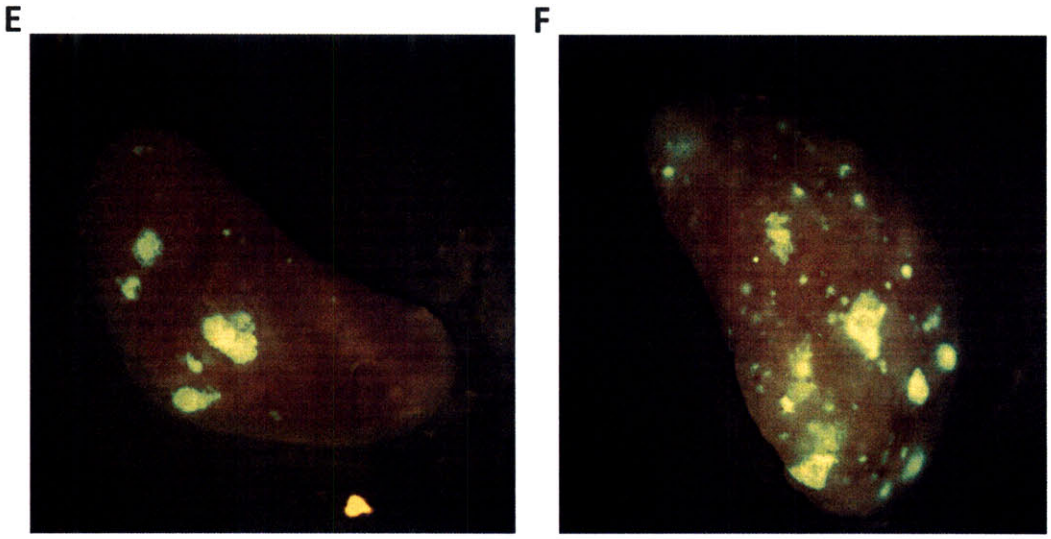

Figure 5. Overexpression of CDCP1 in poorly metastatic A375 cells decreases cell proliferation in vitro, does not affect tumor growth at the subcutaneous site, but significantly enhances lung metastasis of the cells . **(D)** Mice injected with A375-CDCP1have significantly more lung metastasis at the end of five weeks compared to mice injected with control cells. **(E) (F)** Representative image of lung from mice injected with control cells (E) or A375-CDCP1 cells (F).

CHAPTER 4.

CELLULAR MECHANISMS BY WHICH CDCP1 FUNCTIONS TO ENHANCE METASTASIS

The work in this chapter was conceived by Hui Liu and Richard Hynes. The contents of this chapter were written by Hui Liu, with editing by Richard Hynes.

As discussed in Chapter 1, metastasis is a complicated process involving multiple steps, with each step being accomplished by various genetic and epigenetic changes of the tumor cells and by support from the tumor microenvironment. Many membrane proteins have been shown involved in various steps along the way, as has been discussed in Chapter 1. The major cellular pathways that have been implicated in cancer metastasis are cell proliferation, apoptosis resistance, cell migration /invasion, and angiogenesis.

EXPERIMENTAL GOALS AND APPROACHES

In the previous chapter, I have shown that CDCP1 is a novel metastasis enhancer, and I am interested in further understanding the cellular pathways that CDCP1 uses to achieve such an effect. To start addressing this question, we utilized two sets of cells used in the metastasis assays (MA2-Ctrl-KD and MA2-KD6/10, and A375 cells and A375-CDCP1), and asked whether we can observe differences in cell adhesion to substrates, in cell proliferation, in anoikis-resistance, and in migration/invasion.

RESULTS

Using these two series of cells, we found that, in some situations, both series of cells yield the same information; while in other situations, we only observed effects when CDCP1 is overexpressed, but not when downregulated, suggesting that in these conditions CDCP1 is sufficient but not necessary.

CDCP1 is involved in regulating the abilities of cells to form soft agar colonies – by both over-expression and knocking-down experiments

Soft agar colony forming assay is commonly used to measure the transformed state of the cells – normal cells fail to form colonies in soft agar due to lack of proper cell-substrate interactions, while transformed cells can. The assay measures the combination of cell proliferation and survival in the absence of cell-substratum anchorage. We performed soft agar colony assay by embedding MA2-Ctrl-KD cells and MA2-KD6, -KD10 cells in 0.3% agarose in normal growth medium (containing 10% bovine serum). The assays were performed in blind fashion, with the plates coded by other members in the lab. Colony numbers were recorded after a week, and MA2-KD10 (mean = 18.69 ±0.64) produced

significantly fewer colonies comparing to MA2-Ctrl-KD cells (mean =24.15±0.82, p=0.0001, N=3, Figure 1A). Conversely, A375 cells overexpressing CDCP1 formed more soft-agar colonies than did A375-vector-Ctrl cells (Figure 1B). These data suggested that CDCP1 might be involved in regulating the balance between cell proliferation and cell death, in favor of cell proliferation.

CDCP1 plays a role in cell proliferation and apoptosis within the metastasis in the lungs

To support our *in vitro* findings, we performed immunohistological staining using anti-Ki67 antibody, which recognizes all cells undergoing active mitosis. When comparing percent Ki67+ cell in the mouse lungs receiving MA2-Ctrl-KD cells versus MA2-KD6 and KD10 cells, we found that there is a significant reduction in the mitosis index comparing MA2-KD10 (mean = 3.32% ± 0.94%, p=0.03) to Ctrl-KD (mean = 6.33% ± 0.89%). There is also a small reduction comparing MA2-KD6 (mean 4.28% ± 0.86%) to Ctrl-KD, but it is not statistically significant (p= 0.1) (Figure 2A and 2B). Next, we analyzed cell apoptosis in these lungs using ApopTag®, which measures the presence of free DNA ends in apoptosing/dead cells (Figure 2C). We found a very small but statistically significant increase in percent cells undergoing apoptosis within the metastasis when comparing MA2-KD6 (mean = 1.8%±0.162%), MA2-KD10 (mean = 1.981%±0.268%) to MA2-Ctrl-KD (mean = 1.145%±0.089%) with p=0.0016 and =0.0017 respectively.

In both over-expression and knowdown systems, CDCP1 was found to regulate soft agar colony formation, suggesting it may function to tilt the balance of proliferation and apoptosis favoring proliferation. This idea was also supported by *in vivo* data, where lung metastases generated from MA2 cells with reduced CDCP1 showed decreased proliferation index and slightly enhanced apoptosis. Although these differences are not very impressive, over a long period of time, these small differences may indeed contribute to tumor metastasis.

Although the aforementioned phenomena were observed using both series of cells, the following findings are only applicable in over-expression system.

CDCP1-overexpressing cells proliferate more slowly *in vitro*

When cell proliferation was analyzed either by plating the same number of cells and counting after 3 days, or using CellTiter 96® AQue kit from Promega, we found that A375-CDCP1 cells proliferate more slowly than A375-Ctrl-vector cells. Cell number is usually 65.13(±4.95%) that of A375-Vector-Ctrl cells after three days in culture (Figure 3A, N=7). However, we did not observe proliferation difference comparing MA2-Ctrl-KD cells to CDCP1 knockdown cell lines (Figure 3B).

CDCP1-overexpressing cells are bigger in size

Cell size analysis was performed using Coulter Counter and mean diameter of A375-CDCP1 and control cells were analyzed. A375-Ctrl-vector cells were allowed to grow to 70-80% confluence before being detached from the plate with PBS/EDTA, while A375-CDCP1 cells were collected from suspension. Mean diameter for A375-CDCP1 is 15.6μm (±0.22μm, N=13) while mean diameter for A375-Vector-Ctrl is 14.4μm (±0.23μ m, N=14), representing 30% increase in cell volume comparing to the control cells (Figure 3C and 3D).

Overexpression of CDCP1 in poorly metastatic A375 cells causes the cells to detach and proliferate in suspension

To understand further the role of CDCP1 during metastasis *in vitro*, we overexpressed CDCP1 in poorly metastatic A375 cells (A375-CDCP1). A375 cells are adherent cells with a small population loosely adherent or in suspension, which presumably are cells undergoing mitosis. When cells were infected to express CDCP1 and GFP (not as fusion proteins), we found that on day 1, when the cells are weakly green, they remain attached to the plate. However, on day 2, when the cells become bright green, the majority of the cells completely detached and became free-floating suspension cells (mean = 66.6%± 10.3% of total cells, N=5). This is not the case for cells expressing the 2A-GFP vector (A375-Ctrl-vector), where cells remained adherent (mean = 9.5%±2.7% of total cells, N=5, Figure 4A and 4B). A375-CDCP1 cells are alive because they are negative for trypan blue staining, negative for Annexin V and PI staining (data not shown). Moreover, propagation of these cells was performed by simply diluting the suspension cells into fresh culture medium from then on. In agreement with the observations of Bhatt, CDCP1 seems to function as an anti-adhesion molecule (Bhatt et al., 2005).

We decided to investigate this apparent anti-adhesion function further using standard adhesion assays. We coated 96 -well plates with common ECM proteins - fibronectin (FN), vitronectin (VN), and with BSA as negative control, poly D-lysine as positive control. The cells were allowed to adhere for 10min, 30min or 1 hour before being gently washed off. Cells remaining bound to the plates were fixed and stained with Crystal Violet, which was extracted with Triton X-100 and absorbance of A540 was analyzed. Over-expression of CDCP1 slightly reduced cell adhesion to fibronectin over the concentration range of 2.5μg/ml to 40μg/ml (Figure 5A). However, adhesion to vitronectin over the same concentration range was not affected by expression of CDCP1 (n=3) (Figure 5B). To our surprise, such reduction in adhesion to FN (Figure 5C) disappeared when adhesion assays were carried out for 1 hour (Figure 5D)(n=3).

Integrins are the major receptors involved in cell adhesion on fibronectin and vitronectin. A375 cells express α5β1, α3β1, αVβ3 integrins. We tested the effect of CDCP1 over-expression on the surface integrin levels using flow cytometry, and found A375-CDCP1 cells express similar levels of integrin αvβ3, and a small reduction (approximately 2 fold) in α5β1 surface expression. We also analyzed integrin activation status using an antibody that specifically recognizes activated integrin β1, and again, we observed a similarly small reduction in activated β1 on the surface, corresponding the reduced expression levels (Figure 6). These data agree with the adhesion results, that adhesion to fibronectin is slightly affected by overexpressing CDCP1.

When investigating the cells ability to spread on fibronectin and vitronectin, we found that A375-CDCP1 cells almost completely failed to spread. While A375-Vector-Ctrl spread quickly on FN or VN coated glass slides with apparent membrane ruffles, A375-CDCP1 cells remain round and appear to sit on top of the glass slides (Figure 7). We also used live imaging to investigate further whether A375-CDCP1 cells simply have slower kinetics for spreading. Over 6 hours of imaging, A375-CDCP1 cells remain as round cells, while A375-Vector-Ctrl remain spread over the period of imaging (data not shown).

Our data suggest that although CDCP1 only has a small effect on cell adhesion kinetics and on cell adhesion strength, it severely decreased the ability of the cells to spread on extracellular matrix proteins. This may help explain the adhesion-to-suspension transition we observed in tissue culture.

Direct test of anoikis using melanoma cells did not reveal significant effect by CDCP1

Uekita et al reported that in lung adenocarcinoma A549 cells, decreasing CDCP1 expression has a detrimental effect on the cells' ability to resist anoikis – apoptosis induced by lack of cell-substrate interaction (Uekita et al., 2007). The fact that CDCP1 overexpression causes the cells to lose adhesion and proliferate in suspension suggests that CDCP1 expression may allow the cells to circumvent anchorage-dependence. In other words, CDCP1 provides anoikis resistance. To test this idea experimentally, we performed an anoikis-resistance test by plating 0.1*10e6 cells in poly 2-hydroxyethyl methacrylate (polyHEMA) coated 6-well plates in serum-free medium, the cells were stained for surface Annexin V and propidium iodide (PI), and the percentage of cells that are Annexin V-positive but PI-negative were calculated as apoptosing cells, and percent cells that are positive for both Annexin V and PI were calculated as dead cells. However, this direct test of anoikis did not yield results that we expected – both cells types showed similar level of apoptosing cells (data not shown). Noticeably, these cells formed large cell aggregates in polyHEMA-coated plates.

We also investigated potential involvement of CDCP1 in melanoma migration and invasion using Boyden-chamber transwell migration and invasion assays, and we did not observe consistent effect using a series of cells (data not shown).

In conclusion, our *in vitro* work with CDCP1 showed that CDCP1 overexpression slightly enhances cells' anchorage-independence growth in the soft agar, and downregulation of CDCP1 decreases this ability, suggesting a role of CDCP1 in altering the balance between proliferation and anoikis. And we speculate that this ability potentially contributes to metastasis-enhancing activity seen *in vivo*.

A375-CDCP1 cells grow in scattered manner in 3D Matrigel with decreased N-cadherin and β-catenin at cell-cell junctions

When considering our experimental approaches, we realized that soft agar colony assay might be the one that best mimics *in vivo* situation during metastasis - namely the ability of single cells scattered in a foreign environment to grow into colonies. We reasoned that

applying a 3-dimensional culture system (3D) using physiologically relevant substrates such as Matrigel (matrix proteins secreted by Engelbroth-Holm-Swarm tumor cells) instead of agarose might be a more relevant approach to understand *in vivo* functions of CDCP1. This system has been used extensively in mammary gland development and carcinogenesis, but not so with melanoma. With this idea in mind, we coated 8-well chamber glass slides with Matrigel at 4^0C and allowed solidifying at 37^0C before single-cell suspensions of A375-Vector-Ctrl and A375-CDCP1 were seeded on the gels. Cells were cultured with this on-top-of Matrigel method for 6 days to 10 days and cell morphologies were analyzed. A375-Vector-Ctrl grow into "balls" with strong N-cadherin and β-catenin at cell-cell junctions, while A375-CDCP1 grow in a scattered fashion like "clusters-of-grapes", with reduced N-cadherin and β-catenin at cell-cell junctions, although the total levels of these two proteins are not changed (Figure 8A, 8B and 8C).

From these *in vitro* and 3D studies, we concluded that CDCP1 promotes dispersive growth in three-dimensional extracellular matrix. Together with its role in altered balance between proliferation and anoikis in favor of cell growth, it is conceivable that these two effects of CDCP1 may ultimately function in enhancement of metastasis.

CDCP1 has a small effect on the early cell seeding/surviving in the lungs

In an attempt to pinpoint temporally when CDCP1 plays a major role in promoting metastasis, we investigated if CDCP1 has any effect during early survival (in the circulation) and seeding phase, or during tumor initiation and growth phase of metastasis. A375-Vector-Ctrl and A375-CDCP1 cells were labeled with red or green fluorescent dyes and mixed at 1:1 ratio before intravenous injection into NOD/SCID mice. Mice were sacrificed at 40min, 4hr, and 5hrs, the left lobes were sandwiched between glass-bottom dishes and cover glasses, and 10 random fields for each lobe were imaged using a DeltaVision microscope. We found for all three time points, that there are more A375-CDCP1 in the lungs than A375-Control-Vector cells and the difference is statistically significant, although the difference is less than 2 fold for all time points (Figure 9A, 9B). We also performed the same experiment using MA2-Ctrl-KD cells and MA2-KD10 cells but we did not observe difference between the number of MA2-Ctrl-KD cells and MA2-KD10 cells at 30min, 3 hours, 4 hours, 5 hours or 6 hours (Figure 9C, 9D).

These data suggest that although over-expression of CDCP1 has an effect on the early retention of cells in the lung, the difference is small (less than 2 fold) and less likely by itself to explain the large difference (5.3 fold difference in number of metastasis) we observe at the end of five weeks. Thus, the stronger effect of CDCP1 on lung metastasis is probably manifested later than the first several hours.

DISCUSSION

To gain insight into how CDCP1 promotes melanoma metastasis, we performed various *in vitro* assays comparing MA2 cells to CDCP1 knock-downs and A375 cells to CDCP1 over-expressers. We found that CDCP1 has no effect on migration/invasion in short-term assays, nor does it change anoikis resistance in polyHEMA-coating assays. However, CDCP1 does seem to have a small effect on the balance between cell proliferation and anoikis, because it positively regulates soft-agar colony formation abilities of melanoma cells. We found that in 3D culture, CDCP1 expression allows the cells to grow in scattered manner. These properties, together, might contribute to the *in vivo* metastasis-enhancing ability of CDCP1. This is supported by *in vivo* analysis of proliferation and apoptosis – when CDCP1 expression is reduced, within the tumor, there is somewhat increased apoptosis and reduced proliferation in the lungs.

Uekita et al have reported that downregulation of CDCP1 in lung adenocarcinoma A549 cells significantly decreased anoikis resistance in polyHEMA assay (Uekita et al., 2007). However, we did not find the same using melanoma cells. Although polyHEMA has been widely used to assay for anoikis in different cell types such as mammary epithelial/cancer cells, lung cancer cells, and colon cancer cells, melanoma seems to present a particular problem. A375 melanoma cells aggregate in polyHEMA coated culture vessels, forming "melanospheres". It has been thought that such aggregates enhance cell survival due to signals by cell-cell contacts and localized secretion of ECM proteins in the aggregates. In fact, new methods have been developed specifically to address this problem (Tzukert et al., 2008). However, our *in vitro* data that CDCP1 positively regulates soft agar colony formation, and *in vivo* data that downregulation of CDCP1 enhanced cell apoptosis, are broadly consistent with results from the Sakai group, supporting the idea that CDCP1 plays some role in apoptosis resistance.

We also found that overexpression of CDCP1 causes the cells to detach from tissue culture plates and proliferate in suspension, a function we termed anti-adhesion. This is particularly interesting for several reasons. First, this is consistent with its proposed function in anoikis resistance. Normal cells require cell-substrate engagement in order to survive and proliferate, widely known as anchorage-dependent growth. When deprived of such substrate interactions, normal cells die from apoptosis – a process known as anoikis. The fact that overexpression of CDCP1 allows A375 cells and mammary carcinoma cells (Bhatt et al., 2005) to detach and proliferate in suspension suggests that CDCP1 may provide extra signals to circumvent the requirement for cell-substrate engagement. It will be interesting to express CDCP1 in untransformed cells to see if CDCP1 is sufficient for such anoikis resistance in normal cells.

Secondly, understanding the mechanisms through which CDCP1 antagonizes adhesion will provide additional information to understand the complicated process of cell adhesion, cell spreading and processes related to these two. Almost all cells express integrin hetrodimers, which are the major transmembrane proteins that interact with extracellular matrix proteins (ECM), regulating cell adhesion (Hynes, 2002; Hynes, 2004). Signals from extracellular matrix such as the identity of the ECM proteins and the physical status of ECM proteins (assembled or not, rigidity of the ECM) regulates the activation of integrins (outside-in signals) and signals from inside the cells such as activation of various small GTPases, the presence of talin and kindlin (inside-out signals) regulate the activation status of integrins (Hynes, 2004). As a result, cells precisely regulate the timing and strength of adhesion to ECM (Cantor et al., 2008; Larjava et al., 2008). Failures in such regulations are causes of many diseases, such as bullous pemphigoid (Dowling et al., 1996; Smith, 1993; Venning et al., 1992) and Glanzmann thrombasthenia (Hodivala-Dilke et al., 1999). The process of adhesion is complicated. At the cellular level, the initial adhesion is followed by subsequent spreading. At the molecular level, the initial adhesion is mediated by integrin-ECM interaction at the periphery of the cells, forming small and transient focal contacts. Some of the focal contacts mature into focal adhesions, which are more stable complexes mediating stronger interactions. Eventually stable fibrillar adhesions form in the middle of the cells in contact with ECM. Different structural and signal proteins are present in these complexes (van der Flier and Sonnenberg, 2001). For example, integrin $\alpha v\beta 3$ is enriched in the focal contacts and focal adhesions, but integrin $\alpha 5\beta 1$ is more abundant in the fibrillar adhesions. A recent proteomics study found several hundreds of proteins in these complexes,

presenting a daunting job trying to understand the precise spatial and temporal regulation of these complexes (Zaidel-Bar et al., 2007). We found that CDCP1 does not affect the initial adhesion per se, rather, it inhibits the cells from spreading, suggest that signals from/by CDCP1 inhibit signals that are required for later steps of cell adhesion. Thus, understanding mechanistically how CDCP1 exerts such functions will provide useful information to tease out the complicated process mentioned above.

We found that when A375 cells overexpress CDCP1, the cells are bigger than control cells. At this point, we do not know if this is a direct effect of CDCP1, namely if CDCP1 impinges on cell growth pathway such as mTOR pathway (Ma and Blenis, 2009; Sarbassov et al., 2005), or it is a secondary effect due to lack of cell-substrate interaction, which activates RhoGTPase and controls the contractility of the cells. Further investigations are required to tease out these possibilities.

We also observed that when introduced into the lungs of the mice via tail vein injection, there were more A375-CDCP1 after 40min compared to the control. However, the fact that we did not see the opposite to be true using MA2 and knock-down cells, and the increased cell size in A375-CDCP1 suggest that this effect may be secondary to the increase in cell diameter. The possibility remains that CDCP1 expression enhances the cells' survival in the blood stream. Further work is required to stain for the presence of apoptotic cells at early time points (40min) post injection.

In an attempt to understand when CDCP1 exerts its major function *in vivo* to enhance metastasis, we found that the very early effect is small at best, if any. When metastasis number and size of lung metastases derived from A375-Vector-Ctrl cells or A375-CDCP1 cells were analyzed, we noticed that the biggest difference is in the number of tumors in the lung. When we find tumors derived from A375-vector-Ctrl, they often can grow to the same size as tumors derived from A375-CDCP1 cells, suggesting that maybe CDCP1 function in initiation of metastasis. However, we will need more tumors from A375-Vector-Ctrl cells for this to be conclusive.

3D Matrigel culture is currently accepted to mimic *in vivo* environment. For example, mammary epithelial cells grown in Matrigel have been shown to closely recapitulate *in vivo* mammary gland morphogenesis (Mailleux et al., 2008). A large panel of mammary tumor

cell lines were used by the Bissell group to assay their morphologies in 3D Matrigel, and it was shown that the growth patterns of these cells correlate with their gene expression profiles, and cells that grow in "grape" or "stellate" morphology represent more aggressive carcinoma cells (Kenny et al., 2007). When analyzing the behavior of A375-CDCP1 and control cells in Matrigel 3D assays, we found a dramatic difference between the growth patterns of these cells; while the control cells grow into tight balls of cells, expression of CDCP1 completely changes these structures. Almost all A375-CDCP1 cells look like clusters of grapes, with much reduced cell-cell localization of N-cadherins and β-catenin, suggesting that overexpression of CDCP1 resulted in a more aggressive phenotype.

In conclusion, we investigated at the cellular biology level, the mechanisms by which CDCP1 may contribute to enhanced melanoma metastasis and we found that altered balance between cell proliferation and apoptosis, and scattered proliferation pattern in *in vivo*-like environment could contribute to such a function. In the next chapter, we will present data utilizing this system to understand at the molecular level what are the signals activated by CDCP1 and how they may contribute to the metastasis-enhancing activity of CDCP1 *in vivo*.

Bhatt, A. S., Erdjument-Bromage, H., Tempst, P., Craik, C. S., and Moasser, M. M. (2005). Adhesion signaling by a novel mitotic substrate of src kinases. Oncogene *24*, 5333-5343.
Cantor, J. M., Ginsberg, M. H., and Rose, D. M. (2008). Integrin-associated proteins as potential therapeutic targets. Immunol Rev *223*, 236-251.
Dowling, J., Yu, Q. C., and Fuchs, E. (1996). Beta4 integrin is required for hemidesmosome formation, cell adhesion and cell survival. J Cell Biol *134*, 559-572.
Hodivala-Dilke, K. M., McHugh, K. P., Tsakiris, D. A., Rayburn, H., Crowley, D., Ullman-Cullere, M., Ross, F. P., Coller, B. S., Teitelbaum, S., and Hynes, R. O. (1999). Beta3-integrin-deficient mice are a model for Glanzmann thrombasthenia showing placental defects and reduced survival. J Clin Invest *103*, 229-238.
Hynes, R. O. (2002). Integrins: bidirectional, allosteric signaling machines. Cell *110*, 673-687.
Hynes, R. O. (2004). The emergence of integrins: a personal and historical perspective. Matrix Biol *23*, 333-340.
Kenny, P. A., Lee, G. Y., Myers, C. A., Neve, R. M., Semeiks, J. R., Spellman, P. T., Lorenz, K., Lee, E. H., Barcellos-Hoff, M. H., Petersen, O. W., *et al.* (2007). The morphologies of breast cancer cell lines in three-dimensional assays correlate with their profiles of gene expression. Mol Oncol *1*, 84-96.
Larjava, H., Plow, E. F., and Wu, C. (2008). Kindlins: essential regulators of integrin signalling and cell-matrix adhesion. EMBO Rep *9*, 1203-1208.
Ma, X. M., and Blenis, J. (2009). Molecular mechanisms of mTOR-mediated translational control. Nat Rev Mol Cell Biol *10*, 307-318.
Mailleux, A. A., Overholtzer, M., and Brugge, J. S. (2008). Lumen formation during mammary epithelial morphogenesis: insights from in vitro and in vivo models. Cell Cycle *7*, 57-62.
Sarbassov, D. D., Ali, S. M., and Sabatini, D. M. (2005). Growing roles for the mTOR pathway. Curr Opin Cell Biol *17*, 596-603.
Smith, L. T. (1993). Ultrastructural findings in epidermolysis bullosa. Arch Dermatol *129*, 1578-1584.
Tzukert, K., Gorodestky, R., Avrahami, I., Krasny, L., Shimony, N., Elkin, G., Nettelbeck, D. M., and Haviv, Y. S. (2008). A novel dynamic matrix detachment model reveals a shift from apoptosis to necrosis in melanoma cells. Cancer Lett *272*, 345-354.
Uekita, T., Jia, L., Narisawa-Saito, M., Yokota, J., Kiyono, T., and Sakai, R. (2007). CUB domain-containing protein 1 is a novel regulator of anoikis resistance in lung adenocarcinoma. Mol Cell Biol *27*, 7649-7660.
van der Flier, A., and Sonnenberg, A. (2001). Function and interactions of integrins. Cell Tissue Res *305*, 285-298.
Venning, V. A., Allen, J., Aplin, J. D., Kirtschig, G., and Wojnarowska, F. (1992). The distribution of alpha 6 beta 4 integrins in lesional and non-lesional skin in bullous pemphigoid. Br J Dermatol *127*, 103-111.
Zaidel-Bar, R., Itzkovitz, S., Ma'ayan, A., Iyengar, R., and Geiger, B. (2007). Functional atlas of the integrin adhesome. Nat Cell Biol *9*, 858-867.

A

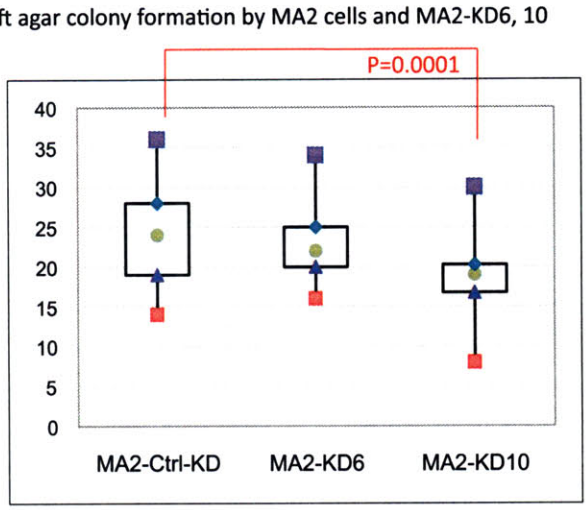

B

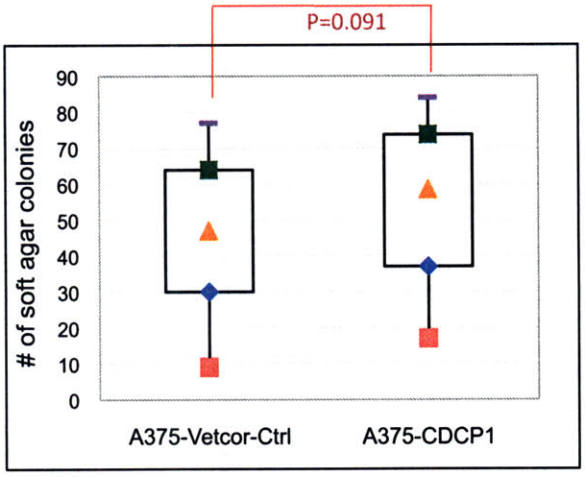

Figure 1. CDCP1 regulates soft agar colony formation abilities. (A) Downregulation of CDCP1 significantly decreased the number of colonies formed by MA2 cells. **(B)** Over-expression of CDCP1 slightly increased the number of colonies formed by A375 cells. N=4

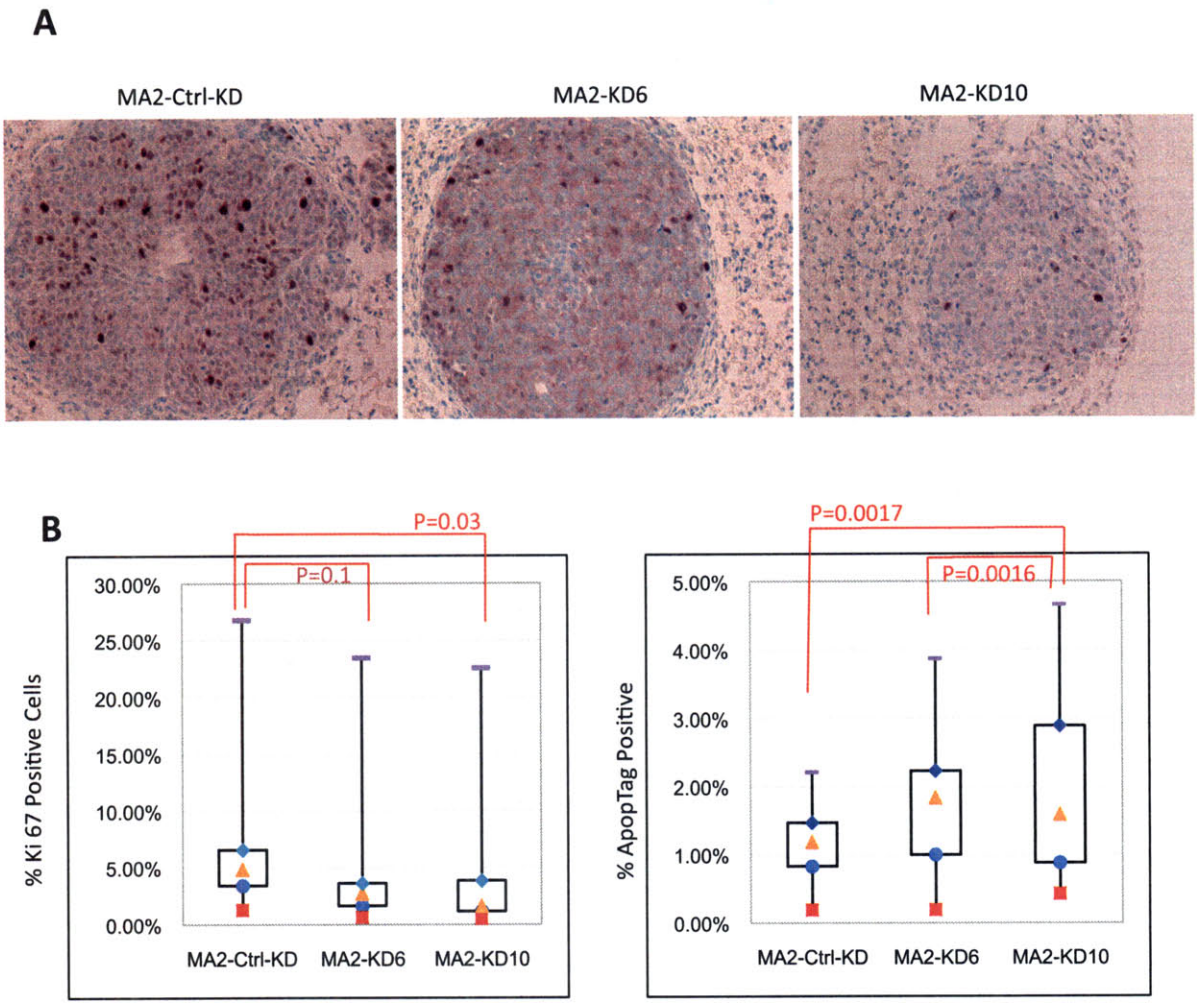

Figure 2. Downregulation of CDCP1 in vivo decreased cell proliferation index and increased apoptosis within lung metastases. (A) Typical lung metastases sections are shown following staining with the proliferation marker Ki67(top) or by TUNEL, using ApopTag detection kit (bottom). (B) Quantitation of staining results for Ki67(left panel) and TUNEL (right panel) are shown for mouse lungs 5 weeks after tail vein injection.

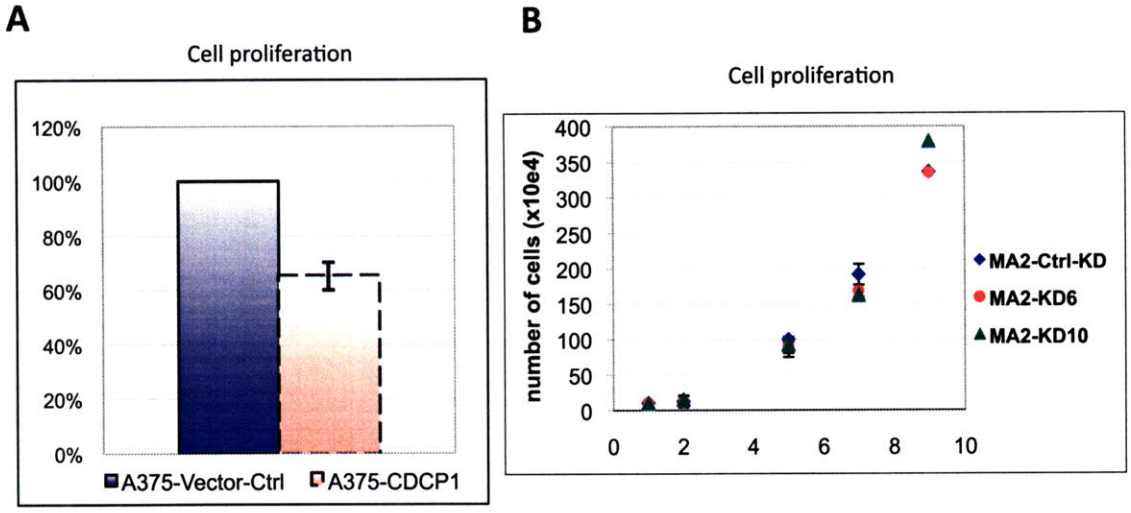

Figure3. CDCP1 overexpression reduced A375 proliferation; while down-regulation of CDCP1 did not affect proliferation in MA2 cells. (A) 1*10e6 A375-CDCP1 or A375-Vector-Ctrl cells were seeded in 10-cm plates in E4Hg-10 medium on day0 ad cells were collected on day3. Cell numbers were counted and A375-Vector-Ctrl were set as 100%. On average, the number of A375-CDCP1 cells reach 65.13%(±4.95%) that of A375-Vector-Ctrl cells (N=7). **(B))** MA2-Ctrl-KD and MA2-KD6, -10 cells proliferate at similar rate *in vitro*

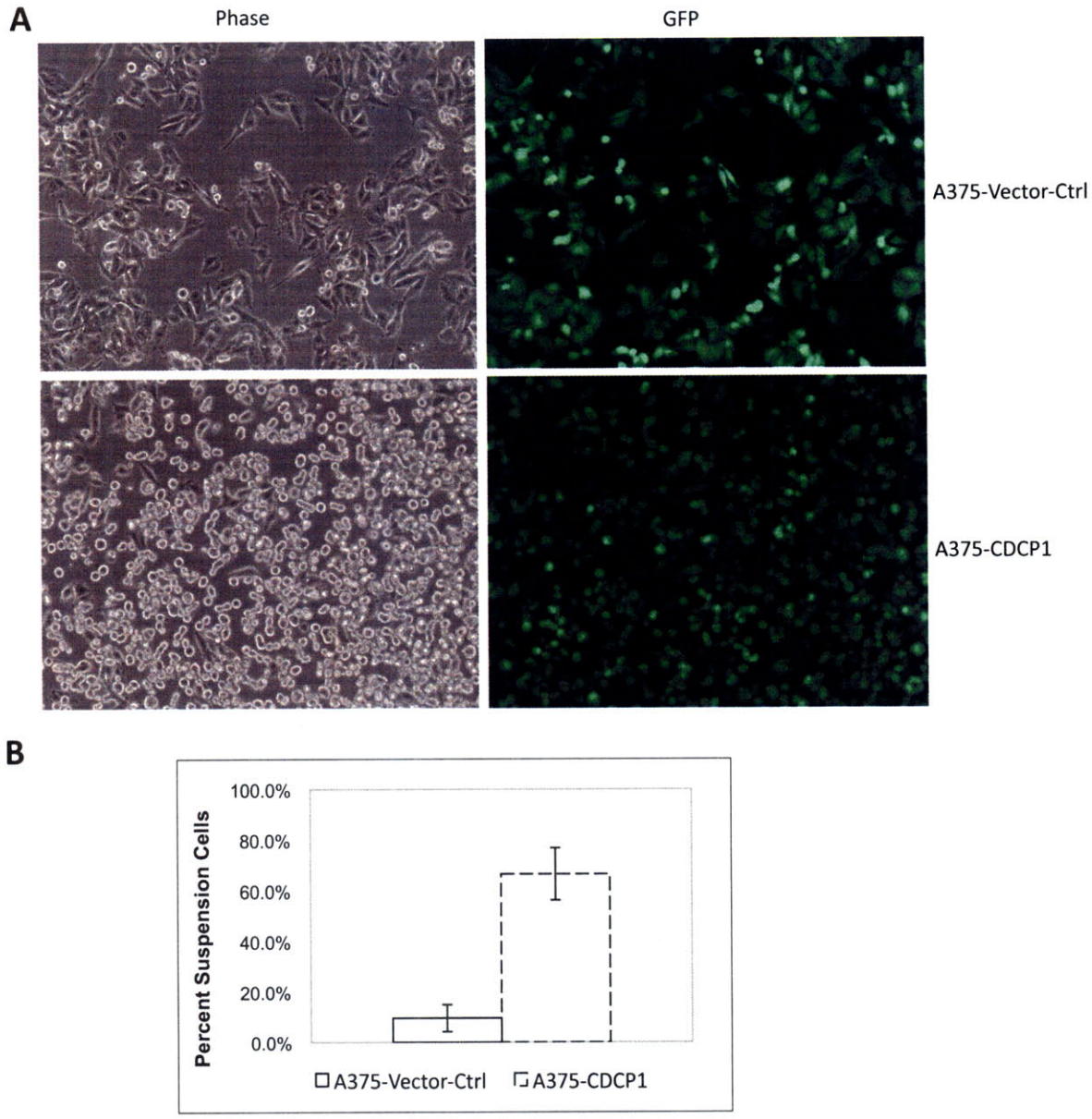

Figure 4. Overexpression of CDCP1 in poorly metastatic A375 cells causes the cells to de-adhere in culture. **(A)** Two days after A375 cells were infected with either Vector-Ctrl virus or CDCP1 virus, majority of A375-Vector-Ctrl cells remain attached, while most A375-CDCP1 cells detach from culture plate and proliferate in suspension; **(B)** Quantification of percentage of total cells that are in suspension (N=5).

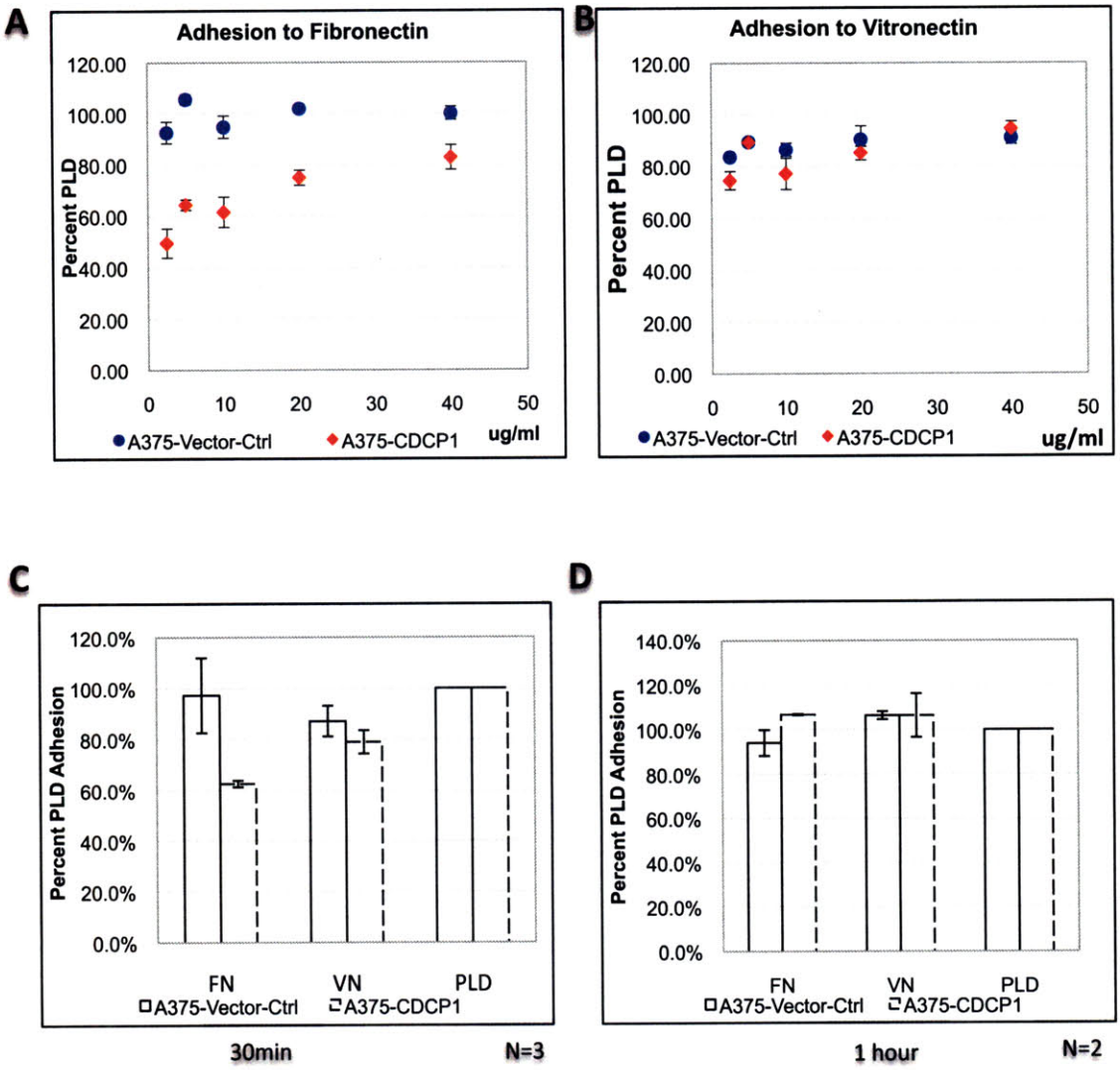

Figure 5. CDCP1-overexpressing cells show time- and concentration-dependent adhesion defect on fibronectin, but not on vitronectin. **(A)** A375-CDCP1 cells show a modest reduction in adhesion to fibronectin in concentration-dependent manner. **(B)** Adhesion to vitronectin was not affected by CDCP1 over-expression. **(C)** There are less A375-CDCP1 cells adhere to Fibronectin at 30min compared to the control cells, and this difference was resolved after 1hr of adhesion **(D).** No difference was observed in cells ability to adhere to vitronectin.

A

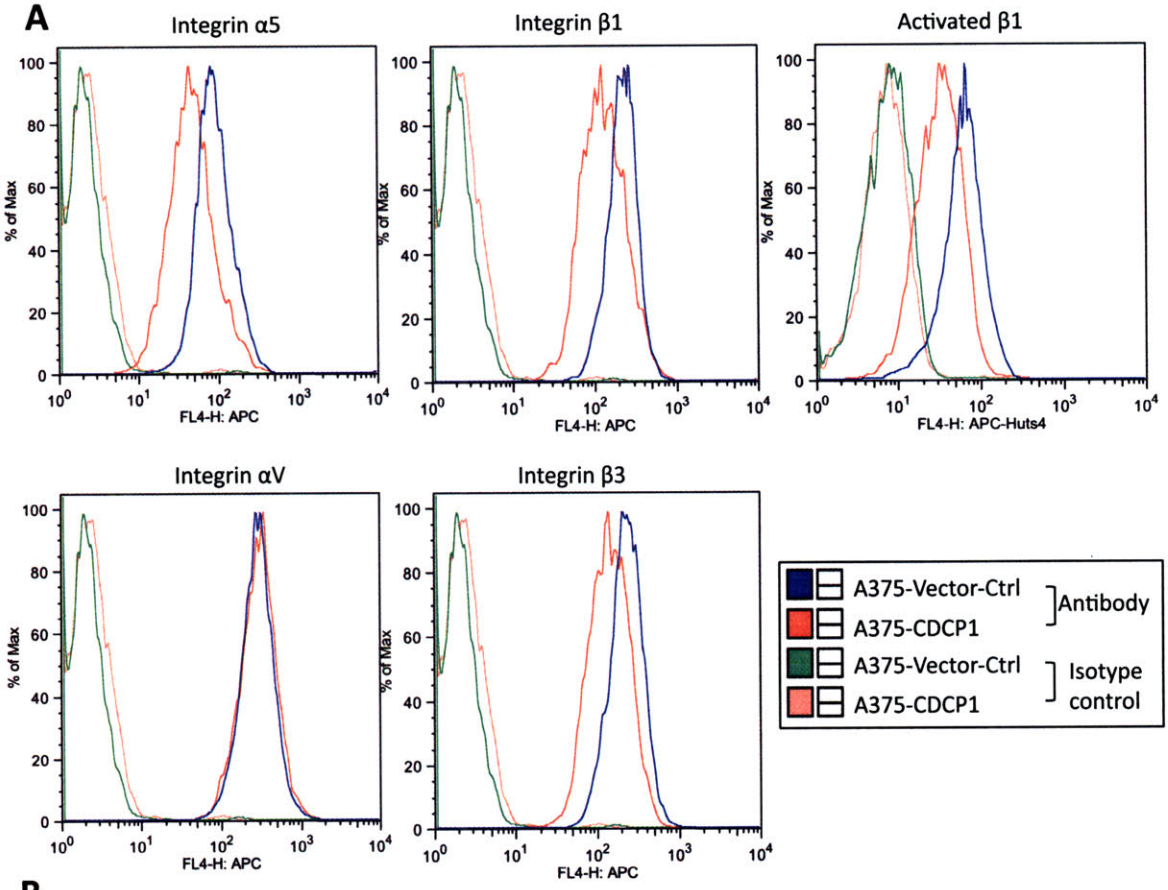

B

Integrin	A375-Vector-Ctrl (MFI)	A375-CDCP1 (MFI)	percent change relative to Ctrl
α5	90	46.2	-48.67%
β1	76.8	49.4	-35.68%
activated β1	59.4	31.4	-47.14%
αV	287	298	3.83%
β3	75.3	50	-33.60%

Figure 6. A375-CDCP1 cells express reduced surface levels in a subset of integrins relative to A375-Vector-Ctrl cells, and such reductions correlate with adhesion defects. (A) A375-CDCP1 and A375-Vector-Ctrl cells were incubated with antibodies specific to each integrin and analyzed using flow cytometry. Integrin α5, β1, β3 and activated β1 showed reduced levels, while αV surface level was not changed. **(B)** Comparison of mean fluorescence intensity (MFI) of surface integrins and percent change relative to A375-Vector-Ctrl cells shows that in most cases, the difference is less than 2-fold.

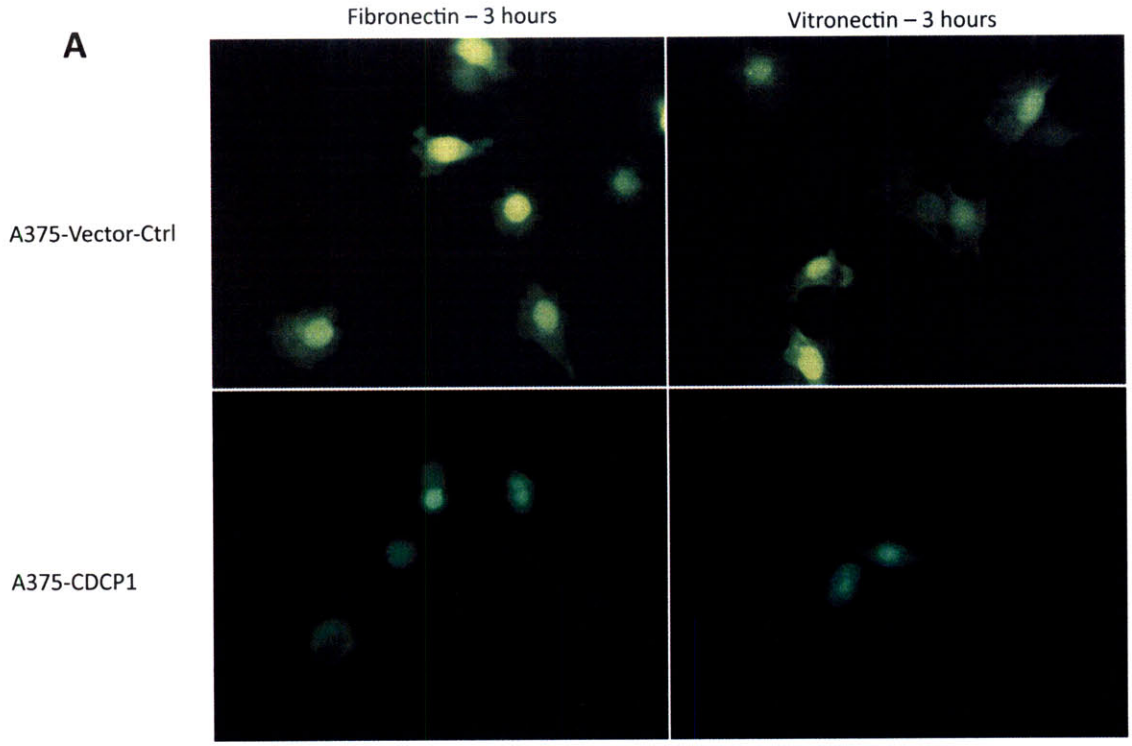

Figure 7. A375-CDCP1 cells fail to spread on fibronectin or vitronectin coated surfaces. Glass coverslides were coated with 5μg/ml fibronectin or vitronectin at 4^0C overnight, and A375-Vector-Ctrl cells or A375-CDCP1 cells were seeded on the slides and allowed to adhere for 3 hours before the cells were washed 3 times with PBS containing Ca^{++}/Mg^{++}. The cells were then fixed with 4% Paraformaldehyde for 15mins and imaged.

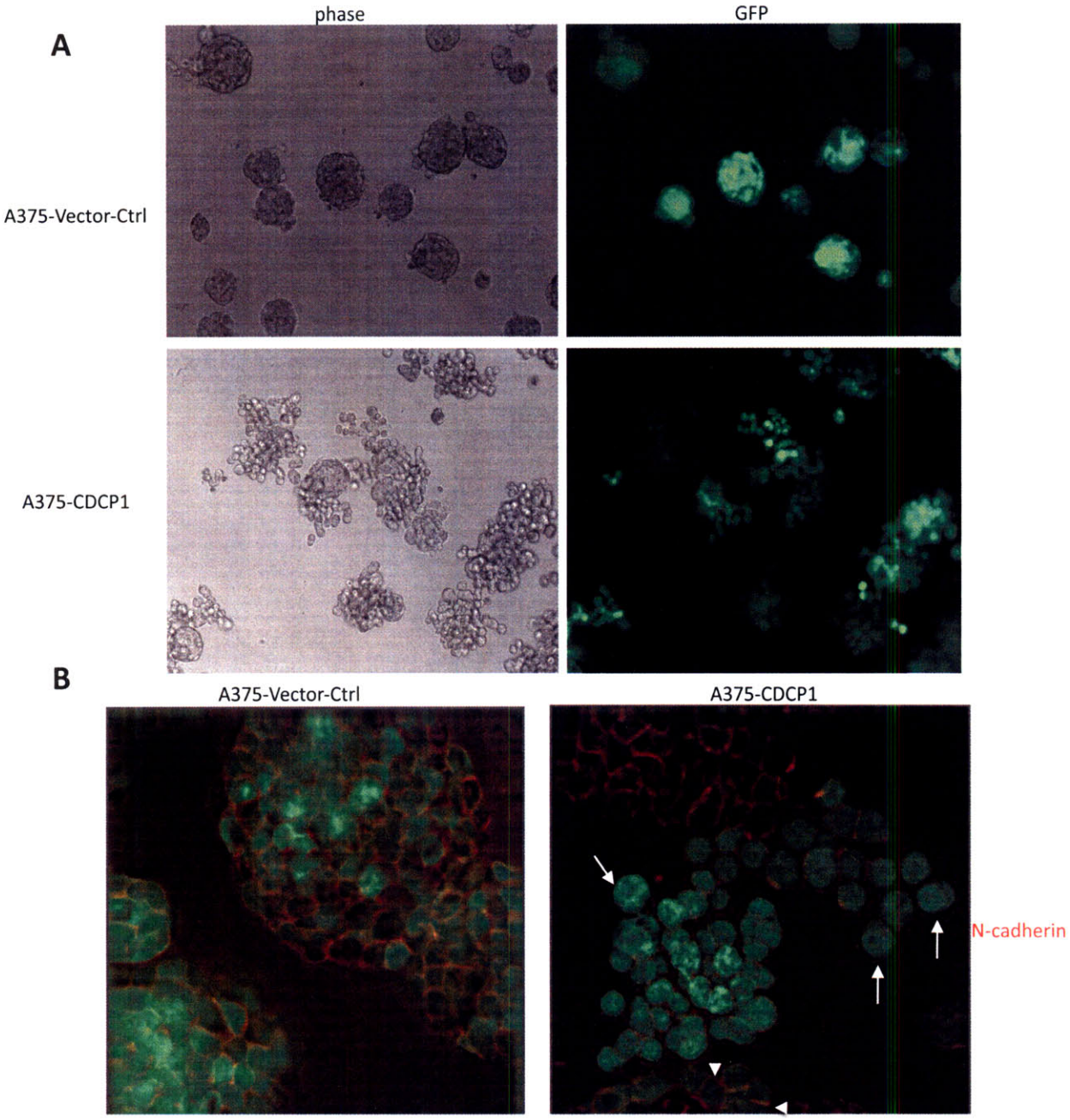

Figure 8. A375-Vector-Ctrl cells and A375-CDCP1 cells grow in distinctively different pattern when cultured in 3D Matrigel, and A375-CDCP1 cells show reduced N-cadherin staining at the "invasion front" and mislocalized β-catenin. In Matrigel assay, 8-well glass chamber slides were coated with 45µl of Matrigel at 4^0C, and were incubated at 37^0C for at least 30min to allow the gel to solidify. 3000 cells were then plated on top of the solidified Matrigel in the presence of 2% Matrigel in E4Hg-10 medium. The cells were cultured for 6-10 days. **(A)** A375-Vector-Ctrl cells grow as tight balls, while A375-CDCP1 cells showed scattered growth pattern. **(B)** Cell were fixed and stained with anti N-cadherin antibody (red). While A375-Vector-Ctrl cells show strong N-cadherin at cell-cell junctions, A375-CDCP1 cells show reduced N-cadherin at the "invasion front" (arrows), but retain N-cadherin if cells are attached (arrowheads).

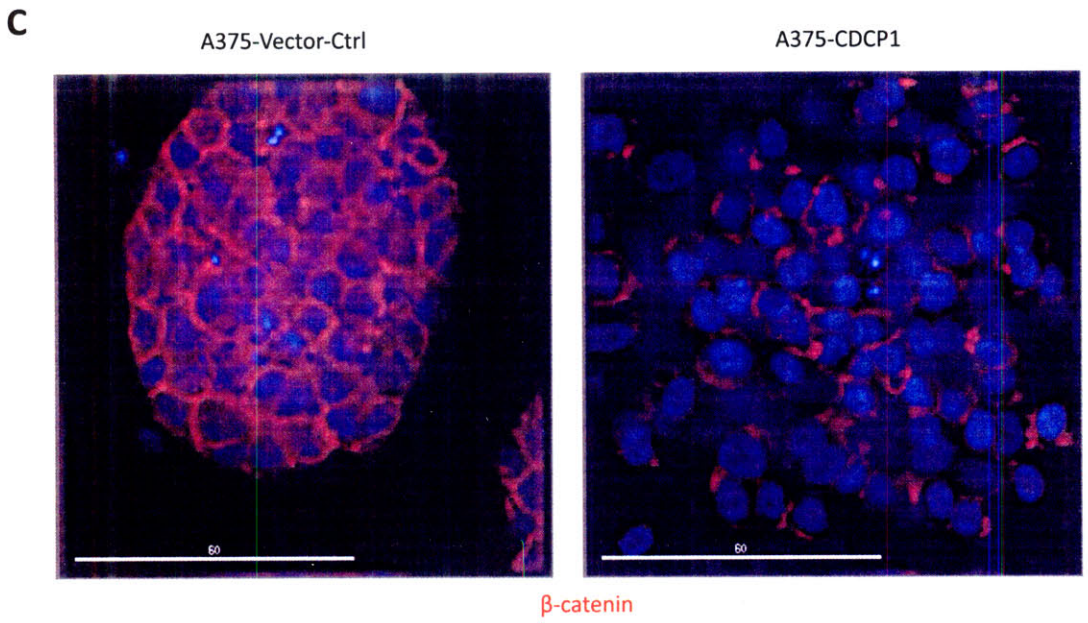

Figure 8. A375-Vector-Ctrl cells and A375-CDCP1 cells grow in distinctively different pattern when cultured in 3D Matrigel, and A375-CDCP1 cells show reduced N-cadherin staining at the "invasion front" and mislocalized β-catenin. (C) Cells were fixed and stained with anti β-catenin antibody (red). While β-catenin was localized at cell-cell junctions in A375-Vector-Ctrl cells, A375-CDCP1 cells showed mislocalization of β-catenin.

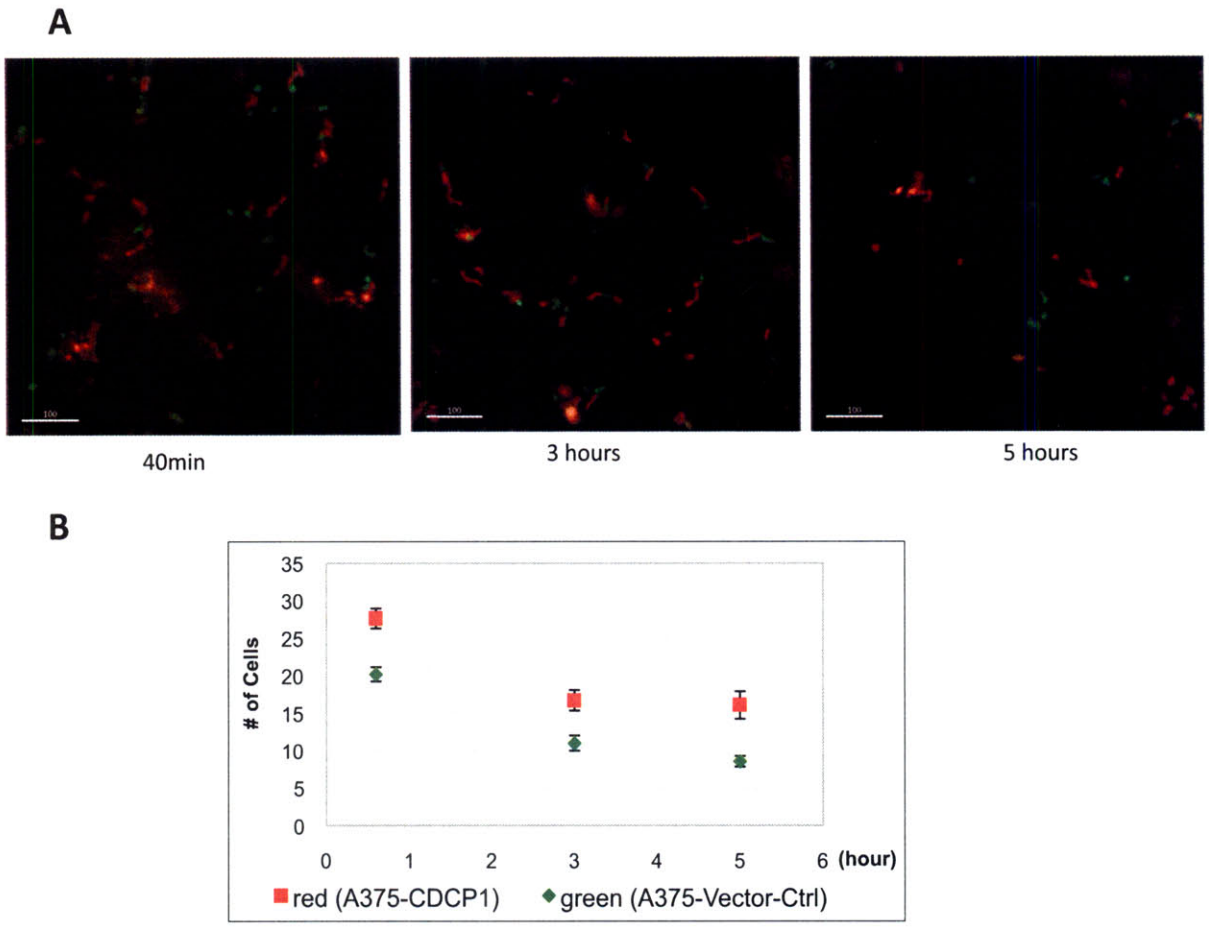

Figure 9. CDCP1 has a small effect on early "seeding" of cells in the lung. When investigating early events post intravenous injection, cells were labeled with CellTracker™ fluorescence dyes (red or green), mixed at equal ratio and injected into NOD/SCID mice via tail vein. At indicated time points, the mice were sacrificed and left lobes were imaged using DeltaVision microscope. 10-15 random fields were imaged, covering different areas of the lung. (A) More A375-CDCP1 cells (red) than A375-Vector-Ctrl cells (green) were retained in the lungs at 40min, 3 hours and 5 hours post tail vein injection. (B) Quantification of number of red (A375-CDCP1) and green (A375-Vector-Ctrl) cells in the lungs at different time points.

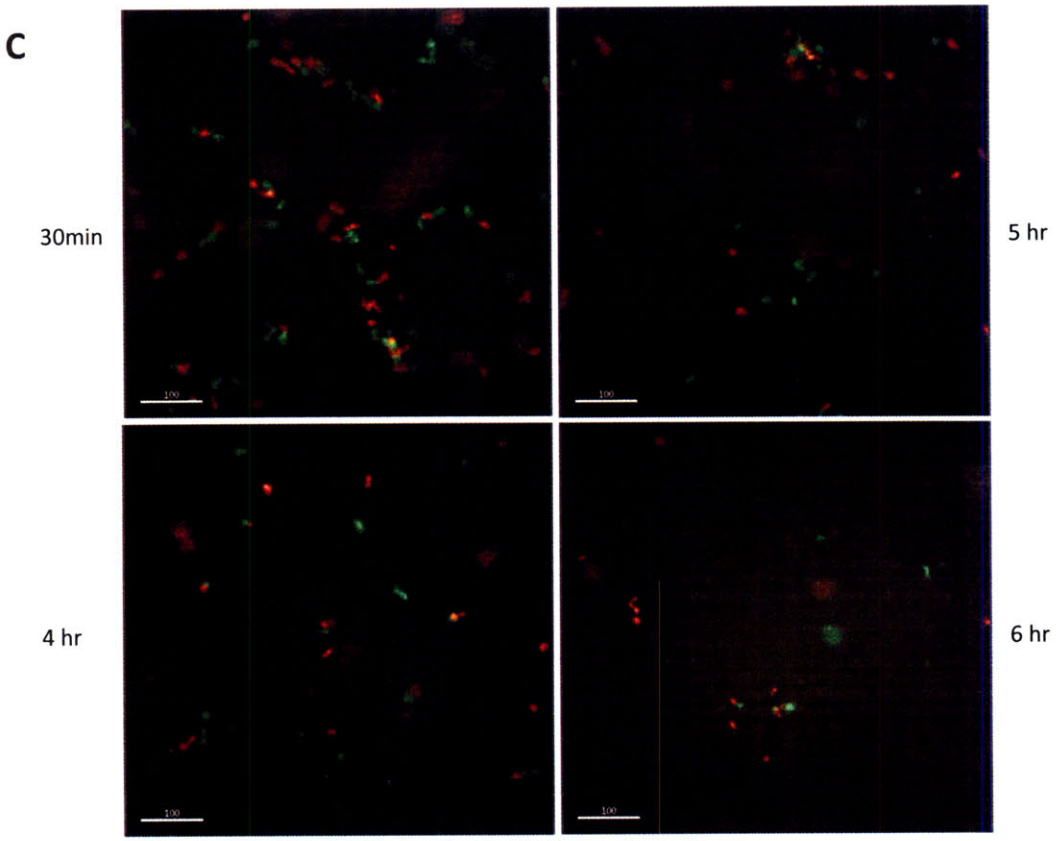

Figure 9. CDCP1 has a small effect on early "seeding" of cells in the lung. When investigating early events post intravenous injection, cells were labeled with CellTracker™ fluorescence dyes (red or green), mixed at equal ratio and injected into NOD/SCID mice via tail vein. At indicated time points, the mice were sacrificed and left lobes were imaged using DeltaVision microscope. 10-15 random fields were imaged, covering different areas of the lung. **(C)** However, a five fold reduction of surface CDCP1 in MA2 cells did not affect early retention of cells in the lungs. **(D)** Quantification of number of red (MA2-KD10) and green(MA2-Ctrl-KD) cells in the lungs at different time points.

CHAPTER 5

MOLECULAR MECHANISMS BY WHICH CDCP1 MAY FUNCTION TO ENHANCE METASTASIS

The work in this chapter was conceived by Hui Liu and Richard Hynes. Overexpression constructs for activated Src and activated Ras were generated by and/or obtained from Patrick Stern. The contents of this chapter were written by Hui Liu, with editing by Richard Hynes.

INTRODUCTION

In the previous chapters, I have described the identification of CDCP1 as a metastasis enhancer in vivo and we have found over-expression of CDCP1 causes cells to detach in 2D culture and grow in dispersive manner in 3D Matrigel culture. I am interested in further understanding how CDCP1 exerts such functions *in vitro* and *in vivo*, through elucidating the signaling pathway(s) that is (are) activated by CDCP1 overexpression.

Early work by Bhatt et al has shown that tyrosine phosphorylation of CDCP1 can be blocked using inhibitors to Src family kninases (SFKs), and that CDCP1 can be phosphorylated in vitro by Src, suggesting the potential involvement of SFKs (Bhatt et al., 2005). Work accomplished by others since I initially focused on CDCP1 has also provided useful information for our studies. When working on protein kinase Cδ (PKCδ), the Soltoff group found that Src, CDCP1 and PKCδ form stable signaling complexes when all are overexpressed. Interactions of PKCδ with CDCP1 are dependant on the C2 domain of PKCδ and the phosphorylation of CDCP1 by Src (Benes et al., 2005). Several tyrosine residues on CDCP1 were identified and some were shown to be important for complex formation: Y734→F mutation sharply reduced binding of CDCP1 to Src, and Y762→F mutation mildly decreased CDCP1 association with PKCδ. This paper built a framework on which models can be proposed to understand the cellular functions of CDCP1 as described in chapter 4.

Recently, Sakai's group showed that CDCP1 plays a functional role during lung adenocarcinoma (A549 cells) and gastric Scirrhous carcinoma (44As3 cells) metastasis (Uekita et al., 2007; Uekita et al., 2008). In agreement with Bhatt's work, they found that CDCP1 is tyrosine phosphorylated and can be immunoprecipitated from suspension A549 cells with antibody against Fyn (another member of the SFK family). Furthermore, wild-type, but not Y734F mutant form of CDCP1 is important for anoikis-resistance in lung carcinoma cells. Together, these data suggested that SFKs might be involved in CDCP1 functions (Figure 1A Summarizes all known molecules interacting with CDCP1 and their potential cellular functions). Therefore, I will introduce SFKs and PKCδ here, and describe their known activation mechanisms and their roles in tumor initiation and progression.

The Src family of protein tyrosine kinases

Src family kinases (SFKs) are non-receptor protein tyrosine kinases, playing pivotal roles in various aspects of cellular processes, such as cell adhesion, proliferation, angiogenesis, apoptosis-resistance, differentiation, migration and invasion (Martin, 2001; Parsons and Parsons, 2004; Thomas and Brugge, 1997). In this chapter, I will introduce the discovery of Src and the domain architectures of Src family kinase members, and I will focus on the activation mechanisms of SFKs and the involvement of SFKs in tumor progression and metastasis.

Intensive investigations using Rous Sarcoma virus identified *v-src* as the gene that is required for cell transformation (Lai et al., 1973; Martin et al., 1971; Wang et al., 1975) and the gene product is a phospho-protein $pp60^{v\text{-}src}$, which is a protein tyrosine kinase (Brugge and Erikson, 1977; Collett et al., 1978; Collett et al., 1980; Hunter and Sefton, 1980; Levinson et al., 1978; Purchio et al., 1978). A cellular homologue *c-src* in normal untransfomed cells was also identified (Oppermann et al., 1979; Stehelin et al., 1976a; Stehelin et al., 1976b). Sequence analysis comparing v-Src and c-Src revealed substantial differences at their C-termini, where a stretch of 12 different amino acids in v-Src replaced those of c-Src(Takeya and Hanafusa, 1983). This structural difference correlates with functional differences: while v-Src is constitutively active and expresses transforming ability, c-Src is less active and does not transform chicken fibroblast cells (Iba et al., 1984; Tanaka and Fujita, 1986).

These early studies led to the identification of the Src family of kinases, which include Src, Fyn and Yes, expressed in most tissues; and Blk, Gfr, Hck, Lck, and Lyn, predominantly in hematopoietic cells (Bolen and Brugge, 1997). They share the same domain structures (Figure1B), with an N-terminal unique region, an SH3 domain, an SH2 domain and the kinase domain (SH1 domain). The kinase is kept inactive by multiple intramolecular interactions and the activation of SFKs is achieved by disrupting those interactions, through phosphorylation/de-phosphorylation events and/or intermolecular associations.

Three major interactions keep Src in inactive conformation (Figure 1C, center): 1) Tyrosine530 at the C-terminus, when phosphorylated by Csk (c-Src Kinase) (Sicheri et al., 1997; Xu et al., 1997; Yamaguchi and Hendrickson, 1996) or by CHK (CSK homologous kinase)(Davidson et al., 1997), folds back and binds to the SH2 domain of Src (Sicheri et al.,

1997; Xu et al., 1997; Yamaguchi and Hendrickson, 1996). Phasphatases that remove the phosphate from Y530 can activate Src; and in fact, this is the tyrosine that is lost in v-Src, rendering it constitutively active; 2) A loop region (with sequence: $PX_4PX_{12}P$) from the kinase domain interacts with the SH3 domain, thus preventing the closing of N- and C-lobes of the kinase domain (Xu et al., 1999). Proteins competing with such interactions can potentially activate Src; and 3) Activation-loop with un-phosphorylated Tyr 419 forms a short α-helix that occludes the substrate-binding site (Bjorge et al., 2000; Ingley, 2008; Xu et al., 1999). Auto-phosphorylation of Y419 in trans will change the conformation of the α-helix and remove it from the binding site, thus achieving full activation of Src. Therefore, activation of SFK can be achieved by 1) disrupting intra-molecular interactions; 2) autophosphorylation of Y419 at the activation loop; and /or 3) de-phosphorylation of pY530 at the C-terminus (Chong et al., 2005).

Numerous proteins have been identified regulating the activities of Src, which can be divided into two sub-groups, one modulates Src activity through phosphorylation and de-phosphorylation events (Figure 1C, right), and the other functions as binding partners and competes with intra-molecular interactions described above (Figure 1C, left).

Kinases/phosphatases

As mentioned earlier, Csk and CHK are the major negative regulators of Src by phosphorylating the C-terminal tyrosine (pY530). On the other hand, activation-loop Y419 is auto-phosphorylated in trans by an identical or related SFK, and only when Y419 is phosphorylated can kinase achieve maximal activity (Chong et al., 2005).

Several phosphatases have been identified, among them, PTPalpha (protein tyrosine phosphatase alpha)(Ponniah et al., 1999; Su et al., 1999; Zheng et al., 1992) and SHP1 (tandem SH2 domain-containing protein tyrosine phosphatase) (Somani et al., 1997) have been shown to be rather specific for the C-terminal pY530, thus activating SFKs. Other phosphatases have also been identified, such as PEP (proline-enriched tyrosine phosphatase), TCPTP (T-cell protein tyrosine phosphatase), and CD45. They have been shown to remove phosphate from both the C-terminal site (equivalent to Y530), and the activation loop tyrosine, thus they can both activate and inhibit SFK activity depending on the cell types (Alexander, 2000; Bjorge et al., 2000; Ingley, 2008).

Src binding partners and adaptor proteins

Interactions of SFK with various proteins play important roles in regulating SFK activities and in bringing SFK to the proper subcellular locations (Bjorge et al., 2000; Thomas and Brugge, 1997). Proteins with specific PxxP motifs and phosphorylated-YEEI and related sequences can compete for binding to SH3 and SH2 domains, respectively, disturbing the intra-molecular interactions and allowing for SFK activation. For example, PDGFR can bind to the SH2 domain of Src and induce activation of Src (Alonso et al., 1995; Kypta et al., 1990), and Sin activates Src through interaction with the SH3 domain (Alexandropoulos and Baltimore, 1996). Recently, a class of transmembrane adaptor proteins, including Cbp and its related molecules such as LIME and LAT, has been identified to modulate SFK activities by complexing with other signaling molecules. In the case of Cbp, it was identified to recruit Csk to the membrane (Kawabuchi et al., 2000), and when tyrosine-phosphorylated, Cbp binds to both Csk and SFK (Lyn and Src), thus mediating the inactivation of SFKs. And interestingly, Cbp has been shown to reside in the lipid raft fraction of the plasma membranes (Ingley, 2008; Ingley et al., 2006; Oneyama et al., 2008). Recently, reversion induced LIM (RIL) has been shown to serve as an adaptor protein and interact with both Src and PTPL1, thus facilitating the de-phosphorylation of tyrosine at the activation loop, and reducing Src activities (Zhang et al., 2009). It is possible that more adaptor proteins are involved in modulating SFK activities, and identification and analysis of these adaptor proteins will further our understanding of the regulation of SFKs.

Roles of Src in tumor progression and metastasis

Numerous studies in colorectal carcinomas have shown the important contributions of SFKs to tumor formation and progression, and the function of SFKs have been described in many other types of malignancies, such as lung, skin, breast, ovarian, hepatocellular, pancreatic and gastric cancers (Biscardi et al., 1999; Frame, 2002; Ishizawar and Parsons, 2004; Parsons and Parsons, 2004; Summy and Gallick, 2003; Yeatman, 2004).

Early data have reported increased Src activities comparing colon carcinoma cells to normal colon (Bolen et al., 1987), adenomatous polyps to normal mucosa (Cartwright et al., 1990), and comparing liver metastasis to primary tumors and to normal tissues (Talamonti et al., 1993). Furthermore, it was shown that enhanced c-Src activity served as an independent

prognosis marker at all stages of colon carcinomas (Aligayer et al., 2002). These data suggest strong correlation between tumor formation/progression and Src activities (Russello and Shore, 2003).

Functional studies showed that Src is involved in various processes of tumor formation and progression. Irby et al showed that over-expression of c-Src enhanced subcutaneous tumor growth (Irby et al., 1997), while down-regulation of c-Src using antisense oligonucleotides slowed the tumor growth of HT29 cells (Staley et al., 1997), supporting a role of c-Src in cell proliferation.

SFKs also contribute to tumor metastasis. For example, colon carcinoma cells overexpressing SFK negative regulator Csk (described above) are defective in metastatic spread, although primary tumor formation was not affected (Nakagawa et al., 2000). Many different pathways can be activated to promote metastases. 1) SFKs have been shown to localize to integrin-mediated focal adhesions, and play pivotal roles in cell-ECM adhesion, spreading and cell migration (Abram and Courtneidge, 2000; Hynes, 1992; Thomas and Brugge, 1997); 2) SFKs can also contribute to the invasiveness of colon carcinoma cells through enhanced metalloprotease productions. Csk over-expressing cells mentioned above migrate to the same extent relative to control cells, but are defective in invasion through Matrigel, possibly due to diminished production of matrix metalloprotease 2 (MMP2) (Nakagawa et al., 2000). SW480 cells with constitutively active Src showed increased degradation of laminin1 due to transcriptional induction of urokinase receptor (Allgayer et al., 1999; Leupold et al., 2007); 3) Active Src can diminish cell-cell junctions, which could also be partly responsible for enhanced metastatic potential. For example, in colon tumor cells expressing constitutively active Src, there is a reduced surface N-cad expression and disrupted N-cadherin /β-catenin association, resulting in reduced cell-cell adhesion (Irby and Yeatman, 2002; Nam et al., 2002; Owens et al., 2000); 4) In addition, Src can also activate anoikis-resistance pathways. (Windham et al., 2002); 5) Src may also contribute to tumor formation and progression through elevated angiogenesis. v-Src has been shown to induce the production of vascular endothelial growth factor (VEGF) through the activation of STAT3 (Yu et al., 1995), Src kinase inhibitor treatment in pancreatic cancer reduced tumor burden and decreased metastasis, and inhibited endothelial cell migration and sprouting *in vitro* (Ischenko et al., 2007). It is clear that SFKs elicit a variety of activities, that individually or collectively, could contribute to tumor progression and metastasis.

Protein kinase Cδ (PKCδ)

Protein kinase C is a family of nine serine/threonine kinases that regulate cell proliferation, apoptosis, differentiation and cell motility. It can be classified into three groups, classical PKC or cPKC (include PKCα, βI, βII and γ), novel PKC (nPKC: PKCδ, ε, η, and θ) and atypical PKC (aPKC: PKCζ and PKCι), each with different requirement for activation. Members of the cPKC group need Ca^{++} and DAG (or phorbol esters); nPKC members are dependent on DAG but not on Ca^{++}, while neither Ca^{++} nor DAG activates aPKCs. Most cells express more than one family of PKCs – PKC isoforms α, δ and ε are most widely expressed, while the expression of the other PKCs are largely cell-type specific.

The mechanisms involved in the activation of PKCs have been extensively studied (Griner and Kazanietz, 2007; Jackson and Foster, 2004; Kikkawa et al., 2002; Newton, 2003; Steinberg, 2004), and a simplified view is presented here – phospholipase Cs (γ or β) coupled to receptor tyrosine kinases (RTKs) or G-protein-coupled receptors (GPCRs) are activated when cells are stimulated through RTKs or GPCRs, resulting in generation of diacylglycerol (DAG) at the membrane. The increased DAG production triggers the recruitment of cPKCs and nPKCs through the C1-domains at the regulatory region, and conformational changes upon localizing to the membrane induce the kinase activation (Griner and Kazanietz, 2007).

In addition to membrane-translocation, tyrosine phosphorylations have also been shown to modulate PKC activities, in particular, PKCδ activities (Kikkawa et al., 2002; Steinberg, 2004). However, the effect of tyrosine phosphorylation on the enzymatic activity of PKCδ is still controversial. On the one hand, activation of SFK and epidermal growth factor receptor signaling have been shown to result in tyrosine-phosphorylation of PKCδ, and a reduction in PKCδ activities (Denning et al., 1993; Denning et al., 1996; Joseloff et al., 2002). On the other hand, PKCδ can be phosphorylated on tyrosines *in vitro* or *in vivo* by Src, insulin receptor or platelet derived growth factor receptor b, resulting in enhanced PKCδ activities (Benes and Soltoff, 2001; Li et al., 1994a; Li et al., 1994b; Uekita et al., 2007). Many factors contribute to these apparently opposite results. Different cell types were used in these studies, and it is conceivable that the state of the cells – such as the presence and activation status of other signaling molecules – can well vary among different cells. In

addition, various upstream stimuli were applied to the cells, which, together, may result in different configurations of tyrosine residues that are phosphorylated on PKCδ. The precise configuration may dictate the properties of the enzyme (Steinberg, 2004).

The cellular functions of PKCδ have been controversial as well. However, compelling evidence from PKCδ knockout mice supports roles of PKCδ in suppressing cell proliferation and enhancing apoptosis. Two groups generated PKCδ knockout mice, which are viable and fertile, suggesting PKCδ is not required for normal development (Leitges et al., 2001; Mecklenbrauker et al., 2002; Miyamoto et al., 2002). Smooth muscle cells derived from the mice are resistant to cell death in response to various stimuli *in vitro*, suggesting a normal function of PKCδ in promoting apoptosis (Leitges et al., 2001). Also shown is loss of B-cell tolerance in PKCδ knockout mice, with enhanced B cell proliferation, and presence of auto-reactive antibodies (Mecklenbrauker et al., 2002; Miyamoto et al., 2002). In agreement with these studies, PKCδ has been shown to suppress cell proliferation, mediate apoptosis (Griner and Kazanietz, 2007; Hung et al., 2008; Mhaidat et al., 2007; Perletti et al., 1999; Sitailo et al., 2006), and function as a tumor suppressor (Aziz et al., 2006; Lu et al., 1997; Reddig et al., 1999). However, in other cases, PKCδ was shown to suppress apoptosis and enhance cell proliferation (Kiley et al., 1999a; Kiley et al., 1999b; Xia et al., 2009; Xia et al., 2007). And currently the reasons for these conflicting results are still not clear, although one can speculate that differences in cell types and the pre-existing signaling status of the cells may contribute to these contradictions.

EXPERIMENTAL GOALS AND APPROACHES

In the previous chapter, we found that CDCP1 alters the balance between cell proliferation and apoptosis, and allows the cells to grow in a dispersive manner; both properties potentially contribute to the enhanced metastatic abilities of melanoma cells. In this chapter, we will investigate the signaling pathway(s) activated by CDCP1 that contribute to such cellular effects. We will first focus on the possible involvement of SFKs in CDCP1-mediated metastasis and we will also try to investigate the potential function of PKCδ.

RESULTS

Extracellular and transmembrane domains are necessary for CDCP1 functions

We would like to dissect CDCP1 further to understand the structural features that are responsible for its functions. For this purpose, we constructed chimeric CDCP1 where the extracellular domain (including all three CUB domains) and transmembrane domain were replaced with those of IL2-receptor α (IL2Rα), generating Tac-CDCP1 (Berrier et al., 2002; LaFlamme et al., 1992). When A375 cells express the chimeric proteins, cells failed to detach in 2-D culture (Figure 2A). In 3D Matrigel, cells over-expressing Tac-CDCP1 remained as ball-like structures and failed to form "cluster-of-grapes" morphology (Figure 2B), although the proteins are expressed detected by anti-CDCP1 antibody in western blot (Figure 2C), and on the surface of the cells assayed by flow cytometry analysis using anti-IL2Rα antibody (Figure 2D). These data suggest that removing the extracellular domain and transmembrane domain abolished the functions associated with CDCP1, at least *in vitro*. It is possible that ligand(s) interactions and/or clustering of CDCP1s are necessary for the functions of CDCP1, and further experiments are needed to distinguish among these possibilities.

Mutation in tyrosine at position 743, 762 and 806 did not affect CDCP1 functions *in vitro*

Inspection of the cytoplasmic domain of CDCP1 reveals the presence of five tyrosines and two poly-proline motifs with typical PXXP sequences that are presumptive binding sites for SH3 domains. Several of the tyrosines have been reported to be phosphorylated by SFKs and serve as docking sites for SFKs and PKCδ, suggesting they may be important sites mediating CDCP1 functions.

To test the possible involvement of tyrosines (and phosphorylation of these tyrosines), we performed site-directed mutagenesis to obtain tyrosine-to-phenylalanine mutant forms of CDCP1 (Y734F, Y743F, Y762F and Y806F), and generated stable A375 cell lines expressing each of these mutants – A375-Y734F, A375-Y743F, A375-Y762F and A375-Y806F. Surface expression levels of these mutants are similar, comparing to wild type CDCP1 (A375-CDCP1)(Figure 3A).

In 2D culture, A375-Y743F, A375-Y762F and A375-Y806F, just like A375-CDCP1 cells, de-adhere from tissue culture plates and proliferate in suspension (Figure 3B). When subjected to 3D Matrigel assay, these cell lines also behave the same as A375-CDCP1 cells, forming

"cluster-of-grapes" morphology with scattered growth pattern (Figure 3C). These mutants also showed mislocalization of β-catenin in Matrigel (Figure 3D) and reduced N-cadherin staining at cell-cell junction (data not shown), although total expression levels of N-cadherin and beta-catenin are similar judging by western blotting (Figure 3E). These data indicated that these four tyrosine-to-phenylalanine mutations did not alter the activities of CDCP1 in our *in vitro* analysis.

Tyrosine 734 of CDCP1 is critical for the cell de-adhesion activities of CDCP1 *in vitro*, and scattered growth in Matrigel

In contrast to the aforementioned mutants, A375 cells overexpressing the Y734F mutant version of CDCP1 cells remain as adherent cells in tissue culture (Figure 4A). A375-Y734F cells fail to grow in dispersive manner in Matrigel. Instead, they grow as tight balls in 3D Matrigel just like A375-Vector-Ctrl cells (Figure 4B). Immuno-fluorescence staining revealed that the majority of N-cadherin and β-catenin are localized at the cell-cell junctions (Figure 4C). Our data showed that *in vitro*, the function of CDCP1 is dependent on the presence of tyrosine at amino acid position 734. When mutated, it completely abolished the functions of CDCP1 observed *in vitro*.

Mutation of tyrosine 734 to phenylalanine in CDCP1 abolished the metastasis-enhancing activity of CDCP1 *in vivo*.

With these *in vitro* results, we performed *In vivo* metastasis assays by injecting A375-Y734F, A375-CDCP1 cells or A375-Vector-Ctrl cells into NOD/SCID mice via the tail vein. In agreement with our *in vitro* work, A375-Y734F cells produced significantly reduced number of lung metastasis as compared with WT-CDCP1 (Figure 4D). In fact, there is no difference in number of lung metastasis formed by A375-Y734F cells or control cells, suggesting that mutation in Tyrosine-734 completely abolished the metastasis-enhancing activity of CDCP1 *in vivo* (Figure 4E).

Our work dissecting the functional motifs in CDCP1 showed that the extracellular and transmembrane domains are required for CDCP1 activities, indicating the potential involvement of CDCP1 ligand(s). We also identified a critical amino acid Y734 in the cytoplasmic tail of CDCP1 that mediates various functions of CDCP1, namely cell de-

adhesion in 2D culture, scattered growth in 3D matrigel, and enhanced metastasis *in vivo*. This is very interesting, especially in light of the work by Benes et al, where the same amino acid Y734, but not other tyrosines, was identified as the docking site for Src in the triple over-expression system (overexpress CDCP1, Src and PKCδ) (Benes et al., 2005), suggesting the potential involvement of Src family kinases in the functions of CDCP1.

Overexpression of CDCP1 enhances activation of Src family kinases (SFKs) and AKT

We next tested which Src family kinases are present in A375 melanoma cells using antibodies specific to Src, Fyn and Yes. Although A375 cells express all three members, Src is the most abundant (data not shown), and we decided to focus on Src.

To investigate the possible involvement of Src in the functions of CDCP1, we performed immuno-blotting using antibody recognizing the active form of SFKs (pY416) or total Src. We found that, in A375 cells over-expressing CDCP1, the abundance of pY416 increased while total Src remained the same, indicating enhanced SFK activity by overexpression of CDCP1. We also found that the serine 473-phosphorylated form of AKT (i.e. activated AKT) is increased in these cells comparing to A375-Vector-Ctrl cells, with the same total AKT expression (Figure 5).

Y734F mutation abolished enhanced SFK activation by CDCP

We next analyzed the activation status of SFKs and AKT in the mutant cell lines. We found that although over-expression of WT-CDCP1, A375-Y743F and A375-Y806F caused stronger activation of SFKs than A375-Vector-Ctrl cells (Figure 6, lower panel), even though total expression levels remained the same (Figure 6, upper panel). Importantly, cells over-expressing the Y734F mutant form of CDCP1 no longer showed increased SFK activation (Figure 6). In fact, the activation levels of SFKs in A375-Y734F cells were similar to those of A375-Vector-Ctrl cells, suggesting that higher SFK activation caused by CDCP1 is dependent on the presence of tyrosine 734.

The coincidence between loss of function (both *in vitro* and *in vivo*) and loss of SFK activation suggested that CDCP1 might exert its functions through hyper-activation of Src. We further tested the involvement of Src family kinases using pharmacological treatment.

PP_2 and Dasatinib treatment partly reverted "cluster-of-grape" growth of A375-CDCP1 cells into ball-like structures in 3D Matrigel culture

PP_2 and Dasatinib are Src family kinase inhibitors, which have been widely used. The IC_{50} of PP_2 for Lck and Fyn has been reported as 5nM in *in vitro* kinases assays, and as 0.55um in T cells (Hanke et al., 1996). However, in HT29 colon carcinoma cells, it was reported that 10um of PP_2 was used to reduce Src kinase activity to 75% of that in untreated cells (Nam et al., 2002). The IC_{50} of dasatinib for Src in a kinase assay is 0.6nM, and in cells is at 0.1-0.3μM range (Lombardo et al., 2004). We treated the cells with increasing concentrations of PP_2 (with non-functional analogue PP_3 as negative controls) and Dasatinib in 3D Matrigel culture, and colony morphologies were analyzed after 6 days. We found that when A375-CDCP1 cells were treated with 15um of PP2, the majority of the colonies lost the scattered pattern and reverted to ball-like structures, while treatment with 15um PP3 had no effect on the dispersive growth (Figure 7A). When using Dasatinib, we found that only at concentrations higher than reported (2um) did we observe such a reversion of morphology (Figure 7B). At this concentration, the average colony size for A375-Vector-Ctrl cells (mean diameter = 86.2±3.29) is smaller than that of control DMSO treated cells (mean diameter = 102.3±3.98, Figure 7C), indicating some reduction in cell proliferation.

Using pharmacological treatment, we have found that at concentrations similar to reported IC_{50} or higher than reported, Src family kinase inhibitors effectively inhibited the ability of A375-CDCP1 cells to grow in a scattered manner in 3D Matrigel. These data agreed with our previous finding that enhanced SFK activation correlates with 3D growth pattern and *in vivo* metastsis, further supporting our hypothesis that CDCP1 exerts its function through the activation of Src family kinases.

Over-expression of activated Src in A375 cells partly mimics the morphologies of A375-CDCP1 cells

To test this idea further, we expressed activated Src in A375 cells and subjected them to 3D Matrigel assay (Figure 8), and we found the cells partially mimic the morphology of A375-CDCP1 cells (but not cells expressing other oncogenes such as activated Ras or YAP). The

colonies became scattered in Src over-expressing cells, although not to the same degree as A375-CDCP1 cells, suggesting that activated Src can induce a similar change.

We also attempted to down-regulate Src expression levels using lentivirus-mediated knock-down. For this purpose, we obtained constructs from the Schlaepfer group (Wu et al., 2008) and subcloned them into pLentilox3.7-p. A375-CDCP1 cells were infected and selected with puromycin. We found that the puromycin-resistant cells initially proliferated extremely slowly, but started to proliferate after approximately 2 weeks in the presence of puromycin. When these cells were analyzed, we did not observe reduced Src expression. Based on our observation, we speculate that A375-CDCP1 cells may not tolerate reduced Src expression well. Therefore, cells which escaped shRNA knock-down were eventually selected, while cells with reduced Src were depleted in culture. At this point, we are not able to test if down-regulation of Src in A375-CDCP1 cells will effectively suppress the scattered growth of these cells and eventually suppress the metastases.

To summarize, we have shown 1) a CDCP1 point mutation that diminished hyper-activation of SFK also abolished the functions of CDCP1 *in vitro* and *in vivo*; 2) SFK inhibitors partly reverted scattered growth morphology of A375-CDCP1 cells and 3) A375 cells expressing activated Src partially mimic the growth pattern of those over-expressing CDCP1. All these data indicate that CDCP1 may exert its function through hyper-activation of Src family kinases.

Y734F mutation in CDCP1 does not significantly alter interactions between CDCP1 and Src using Triton-soluble cell lysate

We are interested in understanding the mechanism(s) by which CDCP1 activates SFKs. Tyrosine 734 of CDCP1 has been reported as a key docking site for Src, mutation of Y734 to phenylalanine severely diminished interaction between Src and CDCP1 when both were over-expressed (Benes et al., 2005). Upon binding, Src phosphorylated Y734 and other tyrosines of CDCP1, and phospho-Y762 was reported to be important for PKCδ recruitment. These data suggested a model that CDCP1 functions as a membrane adaptor protein, directly recruiting SFKs through Y734 and activating SFKs. We decided to test this model by comparing Src-CDCP1 interaction levels between A375 cells overexpressing WT-CDCP1 versus Y734F mutants using co-immunoprecipitation assays.

We first lysed the cells in 1% triton lysis buffer and used the triton-soluble fraction to perform immunoprecipitation. In two out of four experiments, we found a small reduction in interaction between CDCP1 and Src when anti-Src antibody was used (Figure 9A, upper panel). But in the other two experiments, similar levels of interaction were observed. However, we observed two interesting phenomena. First, the fraction of CDCP1 complexed with Src is very small comparing to the total amount of CDCP1 expressed by the cells (Figure 9A, lower panel), which makes the quantification unreliable. This is probably the major reason that we did not observe consistent reduction in CDCP1-Src interaction.

Intriguingly, we also found that, although the cells express similar levels of total Src (Figure 9B, lower panel), the amount of Src that is immunoprecipitated by anti-Src antibody is smaller in A375-CDCP1 cells relative to A375-Vector-Ctrl or A375-Y734F cells Figure 9B, top panel). When blotted with antibody specific to phosphorylated tyrosine 416, this fraction of Src is positive, suggesting that it is the active form of Src (Data not shown). It has long been observed that v-Src, which is constitutively active, is resistant to non-ionic detergent (such as Triton X-100 and NP-40) extraction in a kinase activity-dependent manner. However Triton X-100 can easily extract c-Src, which is normally kept inactive due to multiple intramolecular interactions (Burr et al., 1980; Fukui et al., 1991; Loeb et al., 1987). Because of the strong activation of Src shown in A375-CDCP1 cells, we wonder if our data reflect the activity-dependent Src solubility-change in non-ionic detergents. Further studies will be required to answer this question.

Our data supported the hypothesis that highly activated Src is important for the function of CDCP1. However, the exact mechanism by which CDCP1 activates Src awaits further investigation.

Potential Involvement of PKCδ

As shown by Benes et al, the C2 domain of PKCδ interacts with tyrosine-phosphorylated CDCP1, forming stable signal complexes when all three components (Src, PKCδ and CDCP1) are overexpressed. Such interactions are partly dependent on the presence of tyrosine 762 in CDCP1, since Y762F mutation in CDCP1 reduced interactions with PKCδ.

We are wondering if PKCδ is in the same pathway, therefore relaying signals initiated by CDCP1.

To test this hypothesis, we first treated A375-CDCP1 cells and vector control cells with rottlerin at concentration approximately its IC_{50} (3-6um), and allowed the cells to grow in Matrigel in the continuous presence of rottlerin for 6 days. We found that at 1um rottlerin, neither A375-CDCP1 nor A375-Vector-Ctrl cells were affected; however, both cell types treated with 2um rottlerin stopped proliferation, suggesting either a strong dependence on PKCδ for cell proliferation or inhibitory side-effects of rottlerin. Because of this, we are not able to conclude whether or not PKC δ is responsible for the scattered growth of A375-CDCP1 cells (Data not shown). We then made Y762F point mutation of CDCP1 and generated stable cell lines (A375-Y762F), and these cells behaved just like WT-CDCP1 – cells detached from plates and grew in suspension in 2D and formed "cluster-of-grapes" morphology in 3D Matrigel (Figure 3B, 3C).

Next, we generated stable PKCδ knock-down cell lines for both A375-CDCP1 cells and A375-Vector-Ctrl cells (A375-CDCP1-PKCδ KD7, KD8; and A375-Vector-Ctrl-PKCδ KD7, KD8 and KD10) (Figure 10A). When we grew the cells in 3D Matrigel, we did not observe major differences in the pattern of cell growth comparing A375-CDCP1-PKCδ KD7, KD8 to A375-CDCP1 cells expressing control knockdown construct (Figure 10B). However, A375-Vector-Ctrl cells with reduced PKCδ expression displayed "stellate" morphology with many "connector" cells between the balls. These "connector cells" showed mesenchymal cell morphology, rather than the typically observed amoeboid morphology (Figure 10C).

Potential Involvement of Akt

We also observed that the activation of Akt followed the same trend as that of SFK (Figure 11A), namely cells over-expressing the Y734F mutant showed reduced Akt activation comparing to wild-type CDCP1 and other mutants (Y743F, Y806F). In addition, A375 cells expressing constitutively active Akt also mimic the scattered growth pattern seen by expressing CDCP1 (Figure 11B). However, the significance of Akt activation has not been fully exploited, and is certainly of great interest to us.

DISSCUSSION

In this study, several lines of evidence suggest that CDCP1 functions through the activation of Src family kinases to exert metastasis-enhancing activities. 1) Overexpression of wild-type CDCP1 in A375 cells hyper-activates SFKs and allow the cells to grow in dispersive manner in 3D Matrigel culture; 2) PP2 and dasatinib, which are inhibitors of SFKs, can revert the scattered growth pattern of A375-CDCP1 cells into ball-like structures in Matrigel; 3) A375 cells expressing activated Src mimic the growth of A375-CDCP1 cells in Matrigel; and 4) A point mutation in CDCP1 (Y734F) abolished hyper-activation of SFKs elicited by WT-CDCP1, which coincides with loss of cell-detachment, loss of scattered growth and loss of metastasis-enhancing abilities of WT-CDCP1. Together, our data suggest activation of SFKs by CDCP1 is responsible for the cellular effects of CDCP1 and for the metastasis-enhancing activity of CDCP1.

Perhaps the above results are not surprising since Src is an important player during tumor progression (Ishizawar and Parsons, 2004; Summy and Gallick, 2003; Yeatman, 2004). One need only look at v-Src transformed fibroblasts to draw the similarity to the phenotypes we found with CDCP1. v-Src transformed fibroblasts round up and float in the culture medium, just as we saw with A375-CDCP1 cells. The mechanisms by which Src affects cell-ECM adhesion are through disassembly and turnover of focal adhesions (Chang et al., 1995; Fincham and Frame, 1998; Yeatman, 2004). In addition, in epithelial cells, Src disrupts adherens junctions mediated by E-cadherin by phosphorylation of E-cadherin followed by ubiquitin-mediated proteolysis, and by disrupting E-cadherin/β-catenin interactions (Avizienyte et al., 2002; Yeatman, 2004). A375 cells express N-cadherin as cell-cell adhesion molecules (rather than E-cadherins), and similar phosphorylation events have been shown for N-cadherin as well (Qi et al., 2006), in agreement with the observation of reduced cell-cell adhesion in 3D Matrigel in A375-CDCP1 cells. Our finding further supports the notion that Src plays pivotal roles during cancer metastasis.

In addition, our results suggest that CDCP1 is a new regulator of Src activities. We are very interested in the mechanisms by which CDCP1 activates Src. It was shown that when CDCP1, Src and PKCδ are overexpressed in U2-OS cells, they form stable complexes, which are dependent on the activity of Src. The Y734F mutation in CDCP1 reduced interactions between CDCP1 and Src (Benes et al., 2005). This paper suggested a simple

model; that CDCP1 activates Src by directly recruiting Src through tyrosine734. Based on this model, the Y734F mutation should decrease/diminish interactions between CDCP1 and Src in co-immunoprecipitation experiments. However, we did not find consistent reduction in Src-CDCP1 association comparing Y734F mutants to wild-type CDCP1. There are several possible explanations. First, inspection of the cytoplasmic tail of CDCP1 found two PxxP motifs, which are the consensus binding sequences for SH3 domains. It is possible that the Y734F mutation is not sufficient to abolish the protein-protein interactions between CDCP1 and Src, and the presence of multiple PxxP-SH3 domain interactions could compensate for loss of Y734 binding. In addition, we found that the amount of CDCP1 that interact with Src is very small, perhaps less than 1% of total CDCP1 levels, which conceivably contributed to the inconsistency in our co-IP quantifications.

Furthermore, we observed a CDCP1-dependent solubility change in Src – although A375-CDCP1 cells express similar levels of total Src relative to the A375-Y734F mutants, there was less Src present in the 1% Triton-soluble fraction, which complicated our data analysis. However, the last point is quite interesting – together with the result that CDCP1 overexpression causes stronger activation of SFKs, our data suggest an activity-dependent solubility change in Src. This observation is in agreement with early results, where constitutively active v-Src was found prominently associated with the Triton-insoluble fraction, while less active c-Src could be solublized easily in triton X-100. The triton X-100 insoluble fraction – which includes the cytoskeleton as well as membrane subfractions such as lipid rafts or detergent-resistant microdomains (DRMs) – is likely to play important roles in activating and coordinating signaling events. Many signaling molecules have been found associated with cytoskeleton or localized in detergent-insoluble membrane microdomains, including G protein- coupled receptors, integrins, T cell receptor complexes, Cbp, and SFKs themselves(Echarri et al., 2007; Resh, 2006; Simons and Toomre, 2000). Therefore, maybe CDCP1-dependent solubility change in Src reflects a significant change in localization and activation of Src.

Based on this information, we propose a model that CDCP1 functions as an adaptor protein, interacting with SFKs directly or indirectly, recruiting SFKs to the cytoskeleton and/or to lipid rafts/DRM fractions. Perhaps, it is in these locations that Src is activated.

Other circumstantial evidence may provide further support for this hypothesis. 1) CUB domains have previously been shown to be important for directing metalloprotease ADAMTS13 (a disintegrin and mellalloprotease with thrombospondin type I repeats 13) to lipid rafts (Shang et al., 2006); 2) CDCP1 can potentially be palmitoylated on the cysteines immediately C-terminal of the transmembrane domain, and many palmitoylated proteins are enriched in lipid rafts (Resh, 2006); 3) CDCP1 has been suggested to localize to the lipid rafts/DRM fraction (Alvares et al., 2008); and 4) Another adaptor protein, Cbp, which is localized in the lipid rafts and interacting with Src and Csk, bears similarities in its cytoplasmic domains to those of CDCP1. Both proteins have multiple tyrosines that are phosphorylated by Src, which can mediate phosphotyrosine-SH2 interactions (in the case of Cbp, it has been shown to interact with SH2 domains from both Src and Csk). Both proteins contain PxxP motifs that can mediate SH3 domain interactions (Ingley, 2008). Further experiments inspecting localization of CDCP1 and Src in the lipid rafts/DRM fractions or the cytoskeleton in A375 cells expressing wild-type CDCP1 or the Y734F mutant will be needed to test this hypothesis. In addition, identification of CDCP1-interacting proteins using an unbiased approach such as immunoprecipitation-mass spectrometry will be greatly useful. This experiment will identify proteins differentially interacting with wild-type CDCP1 or Y734F mutant, which will certainly shed light on the potential mechanisms CDCP1 employs to activate Src.

When delineating the potential signaling pathways activated by CDCP1, we also attempted to investigate the roles of PKCδ in our system. Our initial treatment with rottlerin was not informative because proliferation in these cells was highly sensitive to rottlerin treatment. At a concentration that is lower than reported IC_{50}, both A375-CDCP1 cells and A375-Vector-Ctrl cells failed completely to proliferate. However, down-regulation of PKCδ revealed some interesting phenomena. While reduction in PKCδ expression in A375-CDCP1 cells did not have visible effects in these cells, we found in A375 control cells (without over-expression of CDCP1), a subset of cells harboring PKCδ knock-down constructs change cell morphology in Matrigel, making "networks" of cells with mesenchymal-like morphology. This is interesting since PKCδ has been shown to inhibit cell migration – mouse fibroblasts derived from PKCδ knockout mice show enhanced motility and dominant-negative PKCδ mutants enhanced MCF-7 cell migration(Jackson et al., 2005). In addition,mammary carcinoma cells presenting this "stellate" morphology in Matrigel have been shown to be more aggressive cells compared to cells with other mophologies (Kenny et al., 2007). Our observation

suggests a potential effect of PKCδ in cell invasion and further experiments will be needed to address this possibility.

We also observed enhanced activation of Akt when A375 cells over-express WT-CDCP1, which was abolished by the point mutation Y734F - the same mutation that abolishes SFK activation. Given the essential roles of the PI3K/Akt pathway in cell survival (Duronio, 2008; Qiao et al., 2008), we are certainly interested in understanding its functions in CDCP1-mediated activities. Preliminary data showed that when A375 cells express constitutively active Akt, these cells also grow in scattered manner in Matrigel. We have obtained dominant-negative Akt (DN-Akt) and it will be interesting to see whether there is any effect on the cell morphology and growth pattern when A375-CDCP1 cells are infected to express DN-Akt, and if so, whether such an effect translates into *in vivo* metastases differences. We will also treat the A375-CDCP1 cells with PI3K pathway inhibitors such as Wortmannin and LY294002 in the 3D assays to investigate their effects on the growth patterns. This set of experiments will be useful to understand if Akt activation is downstream of CDCP1, and contributes to the functions of CDCP1.

Abram, C. L., and Courtneidge, S. A. (2000). Src family tyrosine kinases and growth factor signaling. Exp Cell Res *254*, 1-13.
Alexander, D. R. (2000). The CD45 tyrosine phosphatase: a positive and negative regulator of immune cell function. Semin Immunol *12*, 349-359.
Alexandropoulos, K., and Baltimore, D. (1996). Coordinate activation of c-Src by SH3- and SH2-binding sites on a novel p130Cas-related protein, Sin. Genes Dev *10*, 1341-1355.
Aligayer, H., Boyd, D. D., Heiss, M. M., Abdalla, E. K., Curley, S. A., and Gallick, G. E. (2002). Activation of Src kinase in primary colorectal carcinoma: an indicator of poor clinical prognosis. Cancer *94*, 344-351.
Allgayer, H., Wang, H., Gallick, G. E., Crabtree, A., Mazar, A., Jones, T., Kraker, A. J., and Boyd, D. D. (1999). Transcriptional induction of the urokinase receptor gene by a constitutively active Src. Requirement of an upstream motif (-152/-135) bound with Sp1. J Biol Chem *274*, 18428-18437.
Alonso, G., Koegl, M., Mazurenko, N., and Courtneidge, S. A. (1995). Sequence requirements for binding of Src family tyrosine kinases to activated growth factor receptors. J Biol Chem *270*, 9840-9848.
Alvares, S. M., Dunn, C. A., Brown, T. A., Wayner, E. E., and Carter, W. G. (2008). The role of membrane microdomains in transmembrane signaling through the epithelial glycoprotein Gp140/CDCP1. Biochim Biophys Acta *1780*, 486-496.
Avizienyte, E., Wyke, A. W., Jones, R. J., McLean, G. W., Westhoff, M. A., Brunton, V. G., and Frame, M. C. (2002). Src-induced de-regulation of E-cadherin in colon cancer cells requires integrin signalling. Nat Cell Biol *4*, 632-638.
Aziz, M. H., Wheeler, D. L., Bhamb, B., and Verma, A. K. (2006). Protein kinase C delta overexpressing transgenic mice are resistant to chemically but not to UV radiation-induced development of squamous cell carcinomas: a possible link to specific cytokines and cyclooxygenase-2. Cancer Res *66*, 713-722.
Benes, C., and Soltoff, S. P. (2001). Modulation of PKCdelta tyrosine phosphorylation and activity in salivary and PC-12 cells by Src kinases. Am J Physiol Cell Physiol *280*, C1498-1510.
Benes, C. H., Wu, N., Elia, A. E., Dharia, T., Cantley, L. C., and Soltoff, S. P. (2005). The C2 domain of PKCdelta is a phosphotyrosine binding domain. Cell *121*, 271-280.
Berrier, A. L., Martinez, R., Bokoch, G. M., and LaFlamme, S. E. (2002). The integrin beta tail is required and sufficient to regulate adhesion signaling to Rac1. J Cell Sci *115*, 4285-4291.
Bhatt, A. S., Erdjument-Bromage, H., Tempst, P., Craik, C. S., and Moasser, M. M. (2005). Adhesion signaling by a novel mitotic substrate of src kinases. Oncogene *24*, 5333-5343.
Biscardi, J. S., Tice, D. A., and Parsons, S. J. (1999). c-Src, receptor tyrosine kinases, and human cancer. Adv Cancer Res *76*, 61-119.
Bjorge, J. D., Jakymiw, A., and Fujita, D. J. (2000). Selected glimpses into the activation and function of Src kinase. Oncogene *19*, 5620-5635.
Bolen, J. B., and Brugge, J. S. (1997). Leukocyte protein tyrosine kinases: potential targets for drug discovery. Annu Rev Immunol *15*, 371-404.
Bolen, J. B., Veillette, A., Schwartz, A. M., Deseau, V., and Rosen, N. (1987). Analysis of pp60c-src in human colon carcinoma and normal human colon mucosal cells. Oncogene Res *1*, 149-168.
Brugge, J. S., and Erikson, R. L. (1977). Identification of a transformation-specific antigen induced by an avian sarcoma virus. Nature *269*, 346-348.

Burr, J. G., Dreyfuss, G., Penman, S., and Buchanan, J. M. (1980). Association of the src gene product of Rous sarcoma virus with cytoskeletal structures of chicken embryo fibroblasts. Proc Natl Acad Sci U S A *77*, 3484-3488.
Cartwright, C. A., Meisler, A. I., and Eckhart, W. (1990). Activation of the pp60c-src protein kinase is an early event in colonic carcinogenesis. Proc Natl Acad Sci U S A *87*, 558-562.
Chang, J. H., Gill, S., Settleman, J., and Parsons, S. J. (1995). c-Src regulates the simultaneous rearrangement of actin cytoskeleton, p190RhoGAP, and p120RasGAP following epidermal growth factor stimulation. J Cell Biol *130*, 355-368.
Chong, Y. P., Ia, K. K., Mulhern, T. D., and Cheng, H. C. (2005). Endogenous and synthetic inhibitors of the Src-family protein tyrosine kinases. Biochim Biophys Acta *1754*, 210-220.
Collett, M. S., Brugge, J. S., and Erikson, R. L. (1978). Characterization of a normal avian cell protein related to the avian sarcoma virus transforming gene product. Cell *15*, 1363-1369.
Collett, M. S., Purchio, A. F., and Erikson, R. L. (1980). Avian sarcoma virus-transforming protein, pp60src shows protein kinase activity specific for tyrosine. Nature *285*, 167-169.
Davidson, D., Chow, L. M., and Veillette, A. (1997). Chk, a Csk family tyrosine protein kinase, exhibits Csk-like activity in fibroblasts, but not in an antigen-specific T-cell line. J Biol Chem *272*, 1355-1362.
Denning, M. F., Dlugosz, A. A., Howett, M. K., and Yuspa, S. H. (1993). Expression of an oncogenic rasHa gene in murine keratinocytes induces tyrosine phosphorylation and reduced activity of protein kinase C delta. J Biol Chem *268*, 26079-26081.
Denning, M. F., Dlugosz, A. A., Threadgill, D. W., Magnuson, T., and Yuspa, S. H. (1996). Activation of the epidermal growth factor receptor signal transduction pathway stimulates tyrosine phosphorylation of protein kinase C delta. J Biol Chem *271*, 5325-5331.
Duronio, V. (2008). The life of a cell: apoptosis regulation by the PI3K/PKB pathway. Biochem J *415*, 333-344.
Echarri, A., Muriel, O., and Del Pozo, M. A. (2007). Intracellular trafficking of raft/caveolae domains: insights from integrin signaling. Semin Cell Dev Biol *18*, 627-637.
Fincham, V. J., and Frame, M. C. (1998). The catalytic activity of Src is dispensable for translocation to focal adhesions but controls the turnover of these structures during cell motility. EMBO J *17*, 81-92.
Frame, M. C. (2002). Src in cancer: deregulation and consequences for cell behaviour. Biochim Biophys Acta *1602*, 114-130.
Fukui, Y., O'Brien, M. C., and Hanafusa, H. (1991). Deletions in the SH2 domain of p60v-src prevent association with the detergent-insoluble cellular matrix. Mol Cell Biol *11*, 1207-1213.
Griner, E. M., and Kazanietz, M. G. (2007). Protein kinase C and other diacylglycerol effectors in cancer. Nat Rev Cancer *7*, 281-294.
Hanke, J. H., Gardner, J. P., Dow, R. L., Changelian, P. S., Brissette, W. H., Weringer, E. J., Pollok, B. A., and Connelly, P. A. (1996). Discovery of a novel, potent, and Src family-selective tyrosine kinase inhibitor. Study of Lck- and FynT-dependent T cell activation. J Biol Chem *271*, 695-701.
Hung, J. H., Lu, Y. S., Wang, Y. C., Ma, Y. H., Wang, D. S., Kulp, S. K., Muthusamy, N., Byrd, J. C., Cheng, A. L., and Chen, C. S. (2008). FTY720 induces apoptosis in hepatocellular carcinoma cells through activation of protein kinase C delta signaling. Cancer Res *68*, 1204-1212.
Hunter, T., and Sefton, B. M. (1980). Transforming gene product of Rous sarcoma virus phosphorylates tyrosine. Proc Natl Acad Sci U S A *77*, 1311-1315.
Hynes, R. O. (1992). Integrins: versatility, modulation, and signaling in cell adhesion. Cell *69*, 11-25.

Iba, H., Takeya, T., Cross, F. R., Hanafusa, T., and Hanafusa, H. (1984). Rous sarcoma virus variants that carry the cellular src gene instead of the viral src gene cannot transform chicken embryo fibroblasts. Proc Natl Acad Sci U S A *81*, 4424-4428.
Ingley, E. (2008). Src family kinases: regulation of their activities, levels and identification of new pathways. Biochim Biophys Acta *1784*, 56-65.
Ingley, E., Schneider, J. R., Payne, C. J., McCarthy, D. J., Harder, K. W., Hibbs, M. L., and Klinken, S. P. (2006). Csk-binding protein mediates sequential enzymatic down-regulation and degradation of Lyn in erythropoietin-stimulated cells. J Biol Chem *281*, 31920-31929.
Irby, R., Mao, W., Coppola, D., Jove, R., Gamero, A., Cuthbertson, D., Fujita, D. J., and Yeatman, T. J. (1997). Overexpression of normal c-Src in poorly metastatic human colon cancer cells enhances primary tumor growth but not metastatic potential. Cell Growth Differ *8*, 1287-1295.
Irby, R. B., and Yeatman, T. J. (2002). Increased Src activity disrupts cadherin/catenin-mediated homotypic adhesion in human colon cancer and transformed rodent cells. Cancer Res *62*, 2669-2674.
Ischenko, I., Guba, M., Yezhelyev, M., Papyan, A., Schmid, G., Green, T., Fennell, M., Jauch, K. W., and Bruns, C. J. (2007). Effect of Src kinase inhibition on metastasis and tumor angiogenesis in human pancreatic cancer. Angiogenesis *10*, 167-182.
Ishizawar, R., and Parsons, S. J. (2004). c-Src and cooperating partners in human cancer. Cancer Cell *6*, 209-214.
Jackson, D., Zheng, Y., Lyo, D., Shen, Y., Nakayama, K., Nakayama, K. I., Humphries, M. J., Reyland, M. E., and Foster, D. A. (2005). Suppression of cell migration by protein kinase Cdelta. Oncogene *24*, 3067-3072.
Jackson, D. N., and Foster, D. A. (2004). The enigmatic protein kinase Cdelta: complex roles in cell proliferation and survival. FASEB J *18*, 627-636.
Joseloff, E., Cataisson, C., Aamodt, H., Ocheni, H., Blumberg, P., Kraker, A. J., and Yuspa, S. H. (2002). Src family kinases phosphorylate protein kinase C delta on tyrosine residues and modify the neoplastic phenotype of skin keratinocytes. J Biol Chem *277*, 12318-12323.
Kawabuchi, M., Satomi, Y., Takao, T., Shimonishi, Y., Nada, S., Nagai, K., Tarakhovsky, A., and Okada, M. (2000). Transmembrane phosphoprotein Cbp regulates the activities of Src-family tyrosine kinases. Nature *404*, 999-1003.
Kenny, P. A., Lee, G. Y., Myers, C. A., Neve, R. M., Semeiks, J. R., Spellman, P. T., Lorenz, K., Lee, E. H., Barcellos-Hoff, M. H., Petersen, O. W., *et al.* (2007). The morphologies of breast cancer cell lines in three-dimensional assays correlate with their profiles of gene expression. Mol Oncol *1*, 84-96.
Kikkawa, U., Matsuzaki, H., and Yamamoto, T. (2002). Protein kinase C delta (PKC delta): activation mechanisms and functions. J Biochem *132*, 831-839.
Kiley, S. C., Clark, K. J., Duddy, S. K., Welch, D. R., and Jaken, S. (1999a). Increased protein kinase C delta in mammary tumor cells: relationship to transformtion and metastatic progression. Oncogene *18*, 6748-6757.
Kiley, S. C., Clark, K. J., Goodnough, M., Welch, D. R., and Jaken, S. (1999b). Protein kinase C delta involvement in mammary tumor cell metastasis. Cancer Res *59*, 3230-3238.
Kypta, R. M., Goldberg, Y., Ulug, E. T., and Courtneidge, S. A. (1990). Association between the PDGF receptor and members of the src family of tyrosine kinases. Cell *62*, 481-492.
LaFlamme, S. E., Akiyama, S. K., and Yamada, K. M. (1992). Regulation of fibronectin receptor distribution. J Cell Biol *117*, 437-447.
Lai, M. M., Duesberg, P. H., Horst, J., and Vogt, P. K. (1973). Avian tumor virus RNA: a comparison of three sarcoma viruses and their transformation-defective derivatives by oligonucleotide fingerprinting and DNA-RNA hybridization. Proc Natl Acad Sci U S A *70*, 2266-2270.

Leitges, M., Mayr, M., Braun, U., Mayr, U., Li, C., Pfister, G., Ghaffari-Tabrizi, N., Baier, G., Hu, Y., and Xu, Q. (2001). Exacerbated vein graft arteriosclerosis in protein kinase Cdelta-null mice. J Clin Invest *108*, 1505-1512.
Leupold, J. H., Asangani, I., Maurer, G. D., Lengyel, E., Post, S., and Allgayer, H. (2007). Src induces urokinase receptor gene expression and invasion/intravasation via activator protein-1/p-c-Jun in colorectal cancer. Mol Cancer Res *5*, 485-496.
Levinson, A. D., Oppermann, H., Levintow, L., Varmus, H. E., and Bishop, J. M. (1978). Evidence that the transforming gene of avian sarcoma virus encodes a protein kinase associated with a phosphoprotein. Cell *15*, 561-572.
Li, W., Mischak, H., Yu, J. C., Wang, L. M., Mushinski, J. F., Heidaran, M. A., and Pierce, J. H. (1994a). Tyrosine phosphorylation of protein kinase C-delta in response to its activation. J Biol Chem *269*, 2349-2352.
Li, W., Yu, J. C., Michieli, P., Beeler, J. F., Ellmore, N., Heidaran, M. A., and Pierce, J. H. (1994b). Stimulation of the platelet-derived growth factor beta receptor signaling pathway activates protein kinase C-delta. Mol Cell Biol *14*, 6727-6735.
Loeb, D. M., Woolford, J., and Beemon, K. (1987). pp60c-src has less affinity for the detergent-insoluble cellular matrix than do pp60v-src and other viral protein-tyrosine kinases. J Virol *61*, 2420-2427.
Lombardo, L. J., Lee, F. Y., Chen, P., Norris, D., Barrish, J. C., Behnia, K., Castaneda, S., Cornelius, L. A., Das, J., Doweyko, A. M., *et al.* (2004). Discovery of N-(2-chloro-6-methyl-phenyl)-2-(6-(4-(2-hydroxyethyl)- piperazin-1-yl)-2-methylpyrimidin-4- ylamino)thiazole-5-carboxamide (BMS-354825), a dual Src/Abl kinase inhibitor with potent antitumor activity in preclinical assays. J Med Chem *47*, 6658-6661.
Lu, Z., Hornia, A., Jiang, Y. W., Zang, Q., Ohno, S., and Foster, D. A. (1997). Tumor promotion by depleting cells of protein kinase C delta. Mol Cell Biol *17*, 3418-3428.
Martin, G. S. (2001). The hunting of the Src. Nat Rev Mol Cell Biol *2*, 467-475.
Martin, G. S., Venuta, S., Weber, M., and Rubin, H. (1971). Temperature-dependent alterations in sugar transport in cells infected by a temperature-sensitive mutant of Rous sarcoma virus. Proc Natl Acad Sci U S A *68*, 2739-2741.
Mecklenbrauker, I., Saijo, K., Zheng, N. Y., Leitges, M., and Tarakhovsky, A. (2002). Protein kinase Cdelta controls self-antigen-induced B-cell tolerance. Nature *416*, 860-865.
Mhaidat, N. M., Thorne, R. F., Zhang, X. D., and Hersey, P. (2007). Regulation of docetaxel-induced apoptosis of human melanoma cells by different isoforms of protein kinase C. Mol Cancer Res *5*, 1073-1081.
Miyamoto, A., Nakayama, K., Imaki, H., Hirose, S., Jiang, Y., Abe, M., Tsukiyama, T., Nagahama, H., Ohno, S., Hatakeyama, S., and Nakayama, K. I. (2002). Increased proliferation of B cells and auto-immunity in mice lacking protein kinase Cdelta. Nature *416*, 865-869.
Nakagawa, T., Tanaka, S., Suzuki, H., Takayanagi, H., Miyazaki, T., Nakamura, K., and Tsuruo, T. (2000). Overexpression of the csk gene suppresses tumor metastasis in vivo. Int J Cancer *88*, 384-391.
Nam, J. S., Ino, Y., Sakamoto, M., and Hirohashi, S. (2002). Src family kinase inhibitor PP2 restores the E-cadherin/catenin cell adhesion system in human cancer cells and reduces cancer metastasis. Clin Cancer Res *8*, 2430-2436.
Newton, A. C. (2003). Regulation of the ABC kinases by phosphorylation: protein kinase C as a paradigm. Biochem J *370*, 361-371.
Oneyama, C., Hikita, T., Enya, K., Dobenecker, M. W., Saito, K., Nada, S., Tarakhovsky, A., and Okada, M. (2008). The lipid raft-anchored adaptor protein Cbp controls the oncogenic potential of c-Src. Mol Cell *30*, 426-436.

Oppermann, H., Levinson, A. D., Varmus, H. E., Levintow, L., and Bishop, J. M. (1979). Uninfected vertebrate cells contain a protein that is closely related to the product of the avian sarcoma virus transforming gene (src). Proc Natl Acad Sci U S A *76*, 1804-1808.
Owens, D. W., McLean, G. W., Wyke, A. W., Paraskeva, C., Parkinson, E. K., Frame, M. C., and Brunton, V. G. (2000). The catalytic activity of the Src family kinases is required to disrupt cadherin-dependent cell-cell contacts. Mol Biol Cell *11*, 51-64.
Parsons, S. J., and Parsons, J. T. (2004). Src family kinases, key regulators of signal transduction. Oncogene *23*, 7906-7909.
Perletti, G. P., Marras, E., Concari, P., Piccinini, F., and Tashjian, A. H., Jr. (1999). PKCdelta acts as a growth and tumor suppressor in rat colonic epithelial cells. Oncogene *18*, 1251-1256.
Ponniah, S., Wang, D. Z., Lim, K. L., and Pallen, C. J. (1999). Targeted disruption of the tyrosine phosphatase PTPalpha leads to constitutive downregulation of the kinases Src and Fyn. Curr Biol *9*, 535-538.
Purchio, A. F., Erikson, E., Brugge, J. S., and Erikson, R. L. (1978). Identification of a polypeptide encoded by the avian sarcoma virus src gene. Proc Natl Acad Sci U S A *75*, 1567-1571.
Qi, J., Wang, J., Romanyuk, O., and Siu, C. H. (2006). Involvement of Src family kinases in N-cadherin phosphorylation and beta-catenin dissociation during transendothelial migration of melanoma cells. Mol Biol Cell *17*, 1261-1272.
Qiao, M., Sheng, S., and Pardee, A. B. (2008). Metastasis and AKT activation. Cell Cycle *7*, 2991-2996.
Reddig, P. J., Dreckschmidt, N. E., Ahrens, H., Simsiman, R., Tseng, C. P., Zou, J., Oberley, T. D., and Verma, A. K. (1999). Transgenic mice overexpressing protein kinase Cdelta in the epidermis are resistant to skin tumor promotion by 12-O-tetradecanoylphorbol-13-acetate. Cancer Res *59*, 5710-5718.
Resh, M. D. (2006). Palmitoylation of ligands, receptors, and intracellular signaling molecules. Sci STKE *2006*, re14.
Russello, S. V., and Shore, S. K. (2003). Src in human carcinogenesis. Front Biosci *8*, s1068-1073.
Shang, D., Zheng, X. W., Niiya, M., and Zheng, X. L. (2006). Apical sorting of ADAMTS13 in vascular endothelial cells and Madin-Darby canine kidney cells depends on the CUB domains and their association with lipid rafts. Blood *108*, 2207-2215.
Sicheri, F., Moarefi, I., and Kuriyan, J. (1997). Crystal structure of the Src family tyrosine kinase Hck. Nature *385*, 602-609.
Simons, K., and Toomre, D. (2000). Lipid rafts and signal transduction. Nat Rev Mol Cell Biol *1*, 31-39.
Sitailo, L. A., Tibudan, S. S., and Denning, M. F. (2006). The protein kinase C delta catalytic fragment targets Mcl-1 for degradation to trigger apoptosis. J Biol Chem *281*, 29703-29710.
Somani, A. K., Bignon, J. S., Mills, G. B., Siminovitch, K. A., and Branch, D. R. (1997). Src kinase activity is regulated by the SHP-1 protein-tyrosine phosphatase. J Biol Chem *272*, 21113-21119.
Staley, C. A., Parikh, N. U., and Gallick, G. E. (1997). Decreased tumorigenicity of a human colon adenocarcinoma cell line by an antisense expression vector specific for c-Src. Cell Growth Differ *8*, 269-274.
Stehelin, D., Guntaka, R. V., Varmus, H. E., and Bishop, J. M. (1976a). Purification of DNA complementary to nucleotide sequences required for neoplastic transformation of fibroblasts by avian sarcoma viruses. J Mol Biol *101*, 349-365.
Stehelin, D., Varmus, H. E., Bishop, J. M., and Vogt, P. K. (1976b). DNA related to the transforming gene(s) of avian sarcoma viruses is present in normal avian DNA. Nature *260*, 170-173.

Steinberg, S. F. (2004). Distinctive activation mechanisms and functions for protein kinase Cdelta. Biochem J *384*, 449-459.
Su, J., Muranjan, M., and Sap, J. (1999). Receptor protein tyrosine phosphatase alpha activates Src-family kinases and controls integrin-mediated responses in fibroblasts. Curr Biol *9*, 505-511.
Summy, J. M., and Gallick, G. E. (2003). Src family kinases in tumor progression and metastasis. Cancer Metastasis Rev *22*, 337-358.
Takeya, T., and Hanafusa, H. (1983). Structure and sequence of the cellular gene homologous to the RSV src gene and the mechanism for generating the transforming virus. Cell *32*, 881-890.
Talamonti, M. S., Roh, M. S., Curley, S. A., and Gallick, G. E. (1993). Increase in activity and level of pp60c-src in progressive stages of human colorectal cancer. J Clin Invest *91*, 53-60.
Tanaka, A., and Fujita, D. J. (1986). Expression of a molecularly cloned human c-src oncogene by using a replication-competent retroviral vector. Mol Cell Biol *6*, 3900-3909.
Thomas, S. M., and Brugge, J. S. (1997). Cellular functions regulated by Src family kinases. Annu Rev Cell Dev Biol *13*, 513-609.
Uekita, T., Jia, L., Narisawa-Saito, M., Yokota, J., Kiyono, T., and Sakai, R. (2007). CUB domain-containing protein 1 is a novel regulator of anoikis resistance in lung adenocarcinoma. Mol Cell Biol *27*, 7649-7660.
Uekita, T., Tanaka, M., Takigahira, M., Miyazawa, Y., Nakanishi, Y., Kanai, Y., Yanagihara, K., and Sakai, R. (2008). CUB-domain-containing protein 1 regulates peritoneal dissemination of gastric scirrhous carcinoma. Am J Pathol *172*, 1729-1739.
Wang, L. H., Duesberg, P., Beemon, K., and Vogt, P. K. (1975). Mapping RNase T1-resistant oligonucleotides of avian tumor virus RNAs: sarcoma-specific oligonucleotides are near the poly(A) end and oligonucleotides common to sarcoma and transformation-defective viruses are at the poly(A) end. J Virol *16*, 1051-1070.
Windham, T. C., Parikh, N. U., Siwak, D. R., Summy, J. M., McConkey, D. J., Kraker, A. J., and Gallick, G. E. (2002). Src activation regulates anoikis in human colon tumor cell lines. Oncogene *21*, 7797-7807.
Wu, L., Bernard-Trifilo, J. A., Lim, Y., Lim, S. T., Mitra, S. K., Uryu, S., Chen, M., Pallen, C. J., Cheung, N. K., Mikolon, D., *et al.* (2008). Distinct FAK-Src activation events promote alpha5beta1 and alpha4beta1 integrin-stimulated neuroblastoma cell motility. Oncogene *27*, 1439-1448.
Xia, S., Chen, Z., Forman, L. W., and Faller, D. V. (2009). PKCdelta survival signaling in cells containing an activated p21Ras protein requires PDK1. Cell Signal *21*, 502-508.
Xia, S., Forman, L. W., and Faller, D. V. (2007). Protein kinase C delta is required for survival of cells expressing activated p21RAS. J Biol Chem *282*, 13199-13210.
Xu, W., Doshi, A., Lei, M., Eck, M. J., and Harrison, S. C. (1999). Crystal structures of c-Src reveal features of its autoinhibitory mechanism. Mol Cell *3*, 629-638.
Xu, W., Harrison, S. C., and Eck, M. J. (1997). Three-dimensional structure of the tyrosine kinase c-Src. Nature *385*, 595-602.
Yamaguchi, H., and Hendrickson, W. A. (1996). Structural basis for activation of human lymphocyte kinase Lck upon tyrosine phosphorylation. Nature *384*, 484-489.
Yeatman, T. J. (2004). A renaissance for SRC. Nat Rev Cancer *4*, 470-480.
Yu, C. L., Meyer, D. J., Campbell, G. S., Larner, A. C., Carter-Su, C., Schwartz, J., and Jove, R. (1995). Enhanced DNA-binding activity of a Stat3-related protein in cells transformed by the Src oncoprotein. Science *269*, 81-83.
Zhang, Y., Tu, Y., Zhao, J., Chen, K., and Wu, C. (2009). Reversion-induced LIM interaction with Src reveals a novel Src inactivation cycle. J Cell Biol *184*, 785-792.

Zheng, X. M., Wang, Y., and Pallen, C. J. (1992). Cell transformation and activation of pp60c-src by overexpression of a protein tyrosine phosphatase. Nature *359*, 336-339.

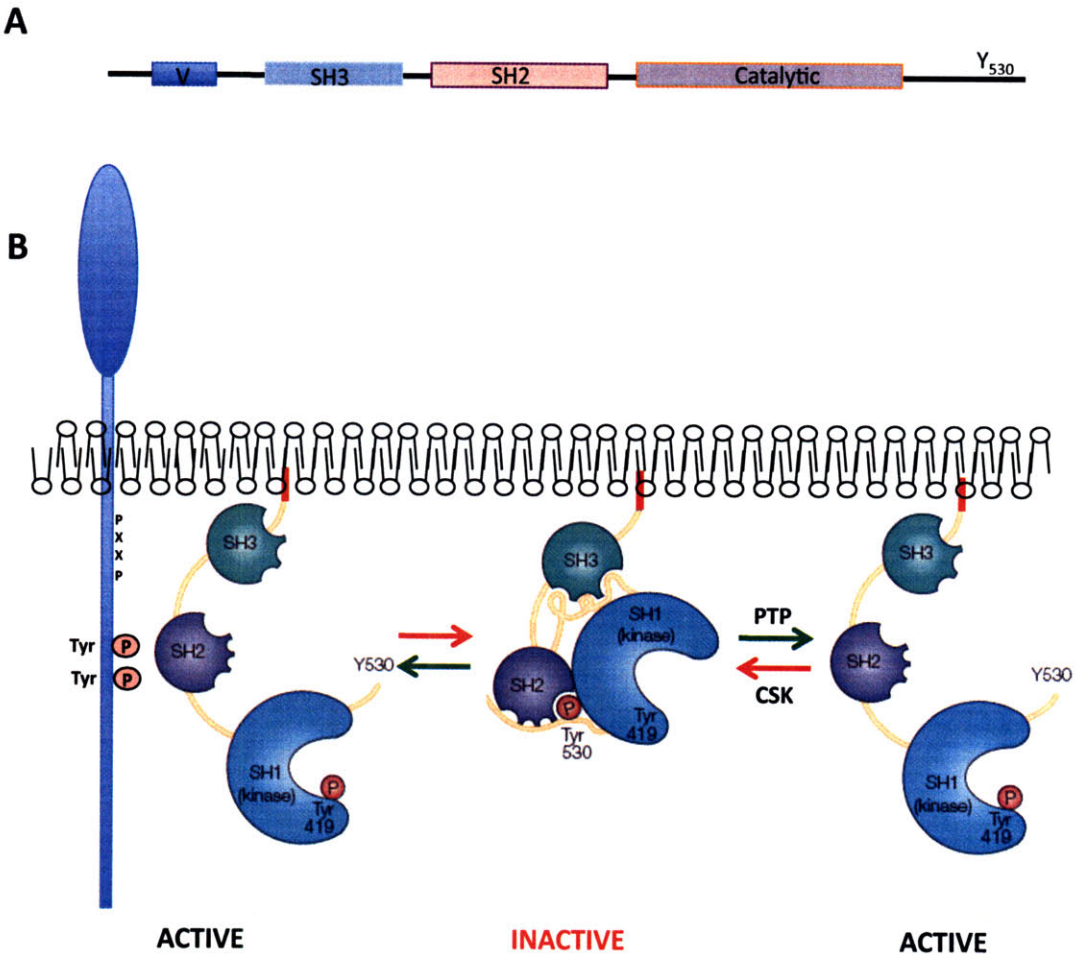

Figure 1. Schematic of the domain structures of Src family kinases (SFKs) and the potential activation mechanism (adapted from Yeatman T.J., 2004 and Bjorge J.D. et al, 2000). (A) All SFKs have the same domain architecture. From N-terminus to C-terminus: variable domain -SH3 domain -SH2 domain -SH1(catalytic) domain. **(B)** Activation mechanisms of SFKs (see text for details). Briefly, SFKs can be activated through phosphorylation-de phosphorylation events (right part) and/or binding to growth factors (depicted here, on the left) and/or other adaptor proteins.

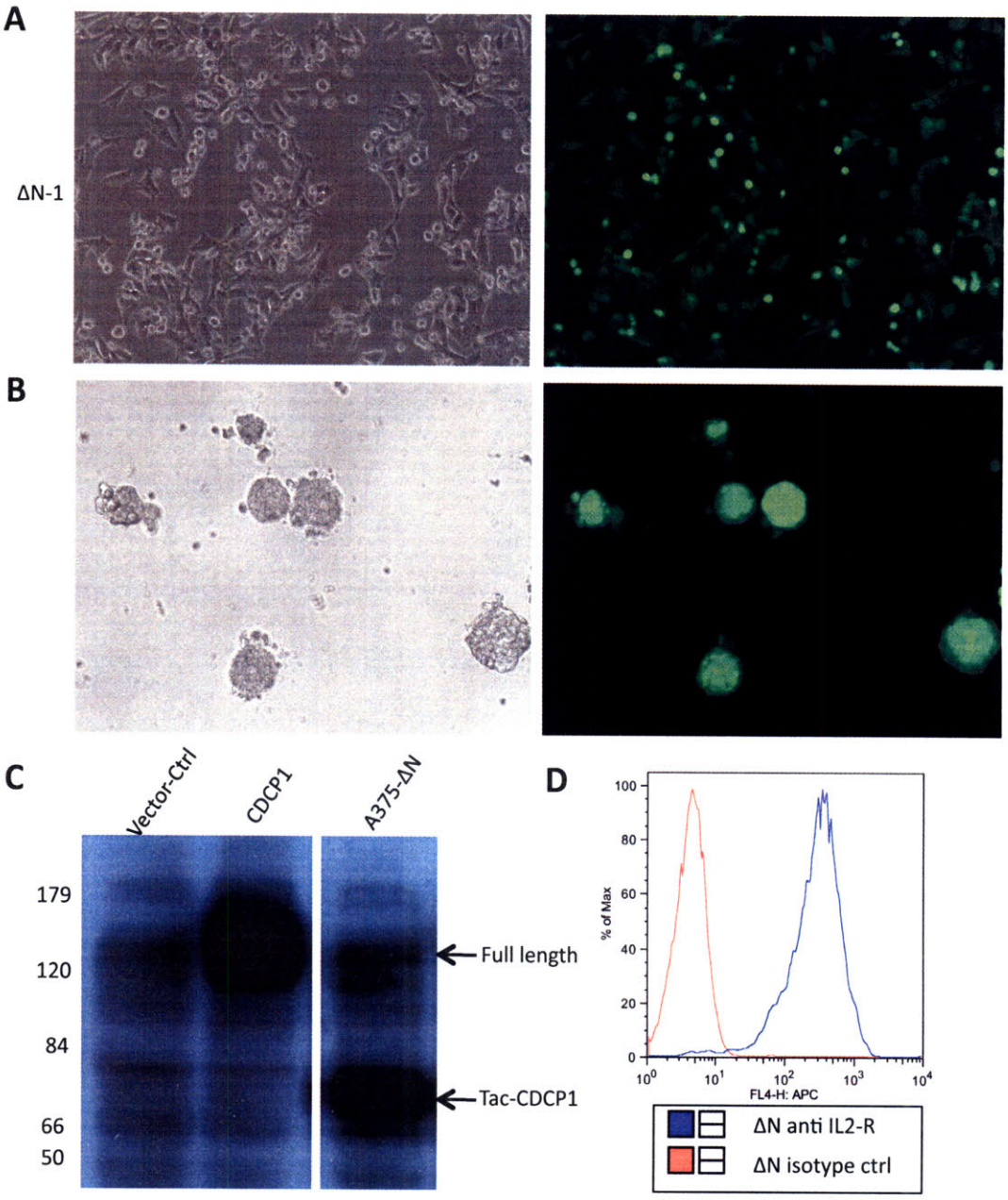

Figure 2. Extracellular and transmembrane domains are required for CDCP1 functions. (A) A375 cells over-expressing Tac-CDCP1 where extracellular and transmembrane domains were replaced with those from IL2 receptor-α no longer de-adhere from culture plates . **(B)** A375 cells over-expressing Tac-CDCP1 grow as tight balls in Matrigel culture. **(C)** Tac-CDCP1 expression was confirmed by western using polyclonal antibody against C-terminal of CDCP1. **(D)** Surface Tac-CDCP1 expression was detected using anti-IL2Rα antibody.

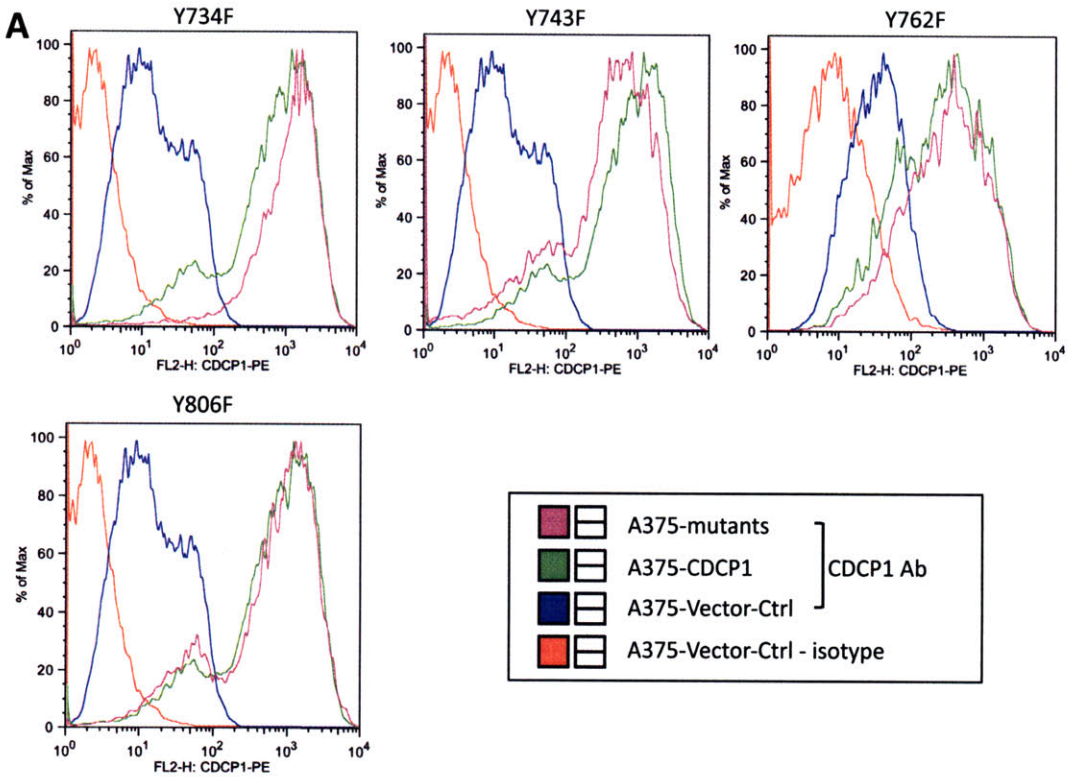

Figure 3. Tyrosine-to-phenylalanine mutations in Y743, Y762 and Y806 of CDCP1 have no effect on the functions of CDCP1 *in vitro*. (A) Surface expression of various mutants were confirmed using flow cytometry and compared to the expression levels of wild-type CDCP1. **(B)** Similar to cells over-expressing wild-type CDCP1, A375 cells over-expressing Y743F, Y762F or Y806F mutants de-adhere in 2D culture. **(C)** A375 cells over-expressing Y743F, Y762F and Y806F mutants grow in scattered manner in 3D Matrigel, just like cells expressing wild-type CDCP1. (See next two pages for figures B and C)

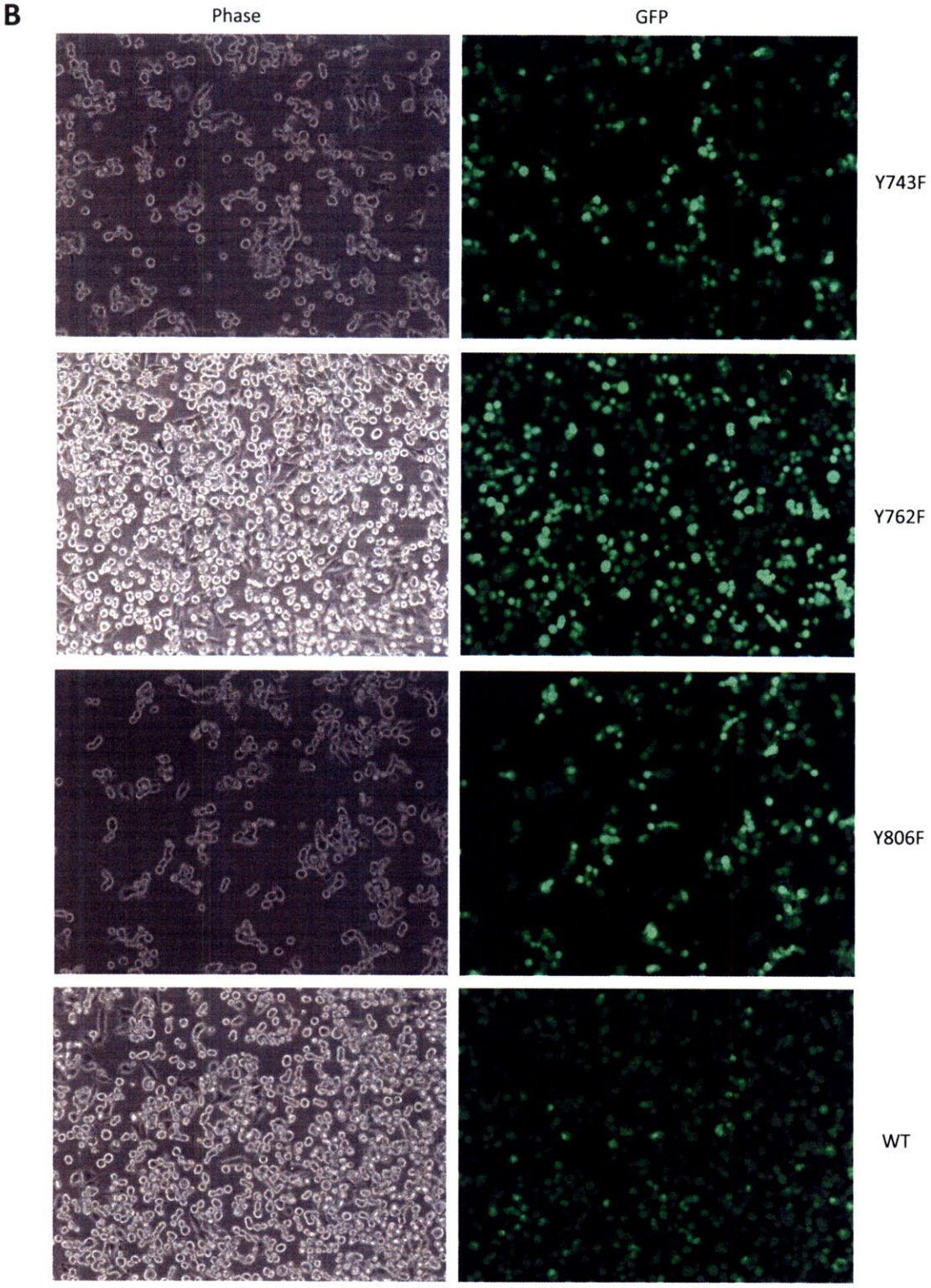
B
Phase
GFP
Y743F
Y762F
Y806F
WT

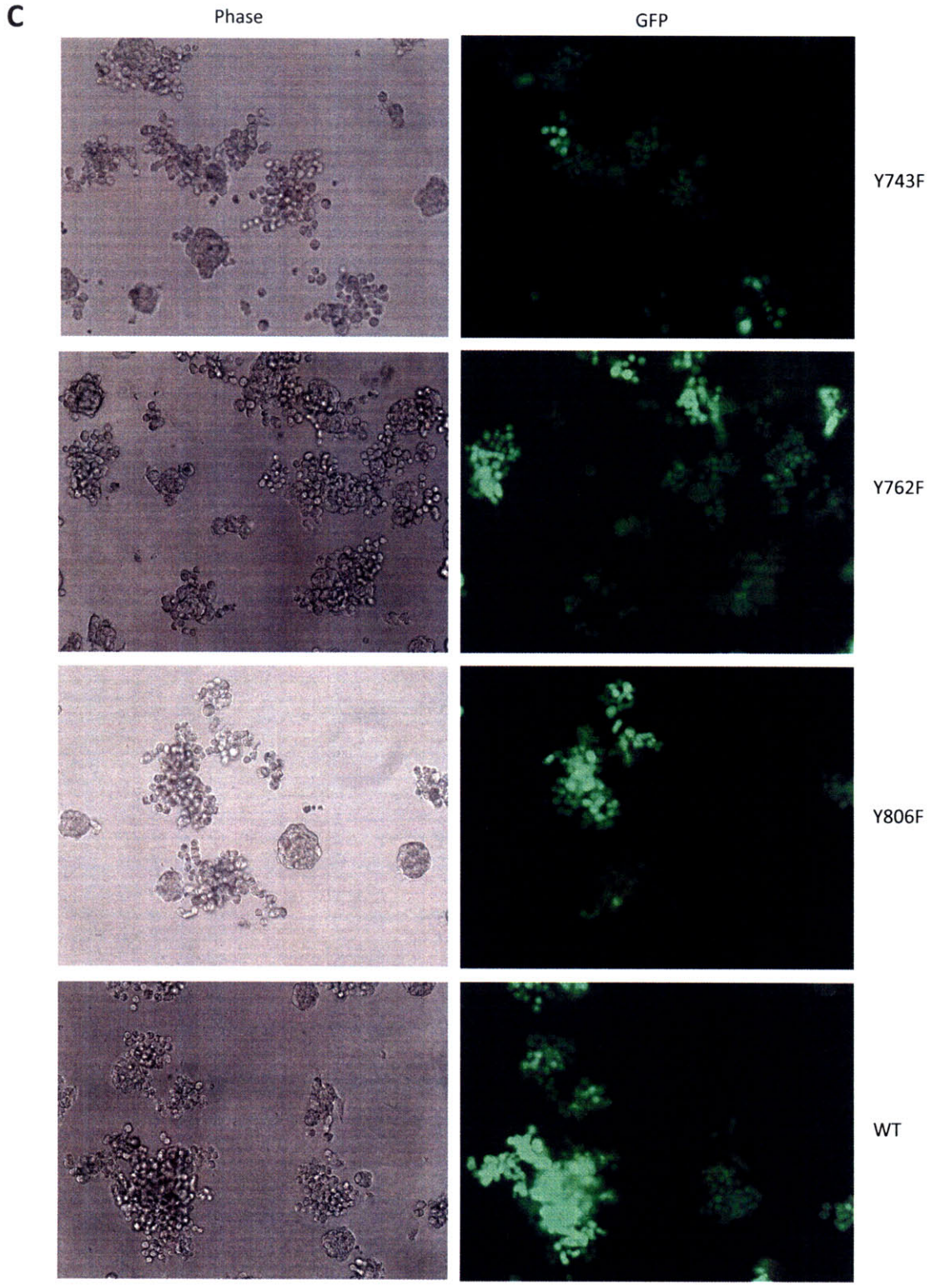
C
Phase
GFP
Y743F
Y762F
Y806F
WT

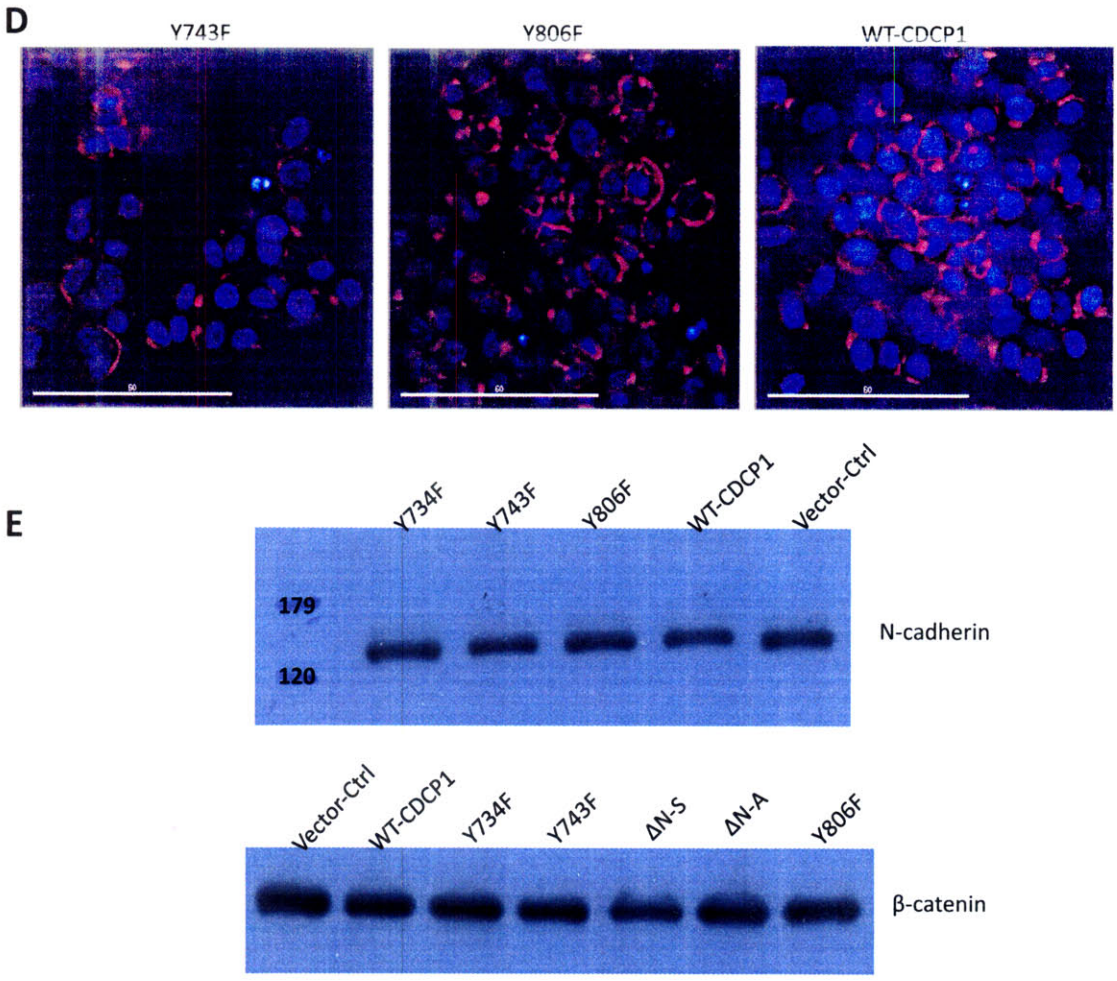

Figure 3. Tyrosine-to-phenylalanine mutations in Y743, Y762 and Y806 of CDCP1 have no effect on the functions of CDCP1 *in vitro*. **(D)** Immunofluorescence staining in Matrigel culture revealed mislocalization of β-catenin. **(E)** Western blotting shows that total expression levels of N-cadherin and β-catenin are similar comparing A375 cells expressing vector control, or wild-type CDCP1 or various mutants of CDCP1.

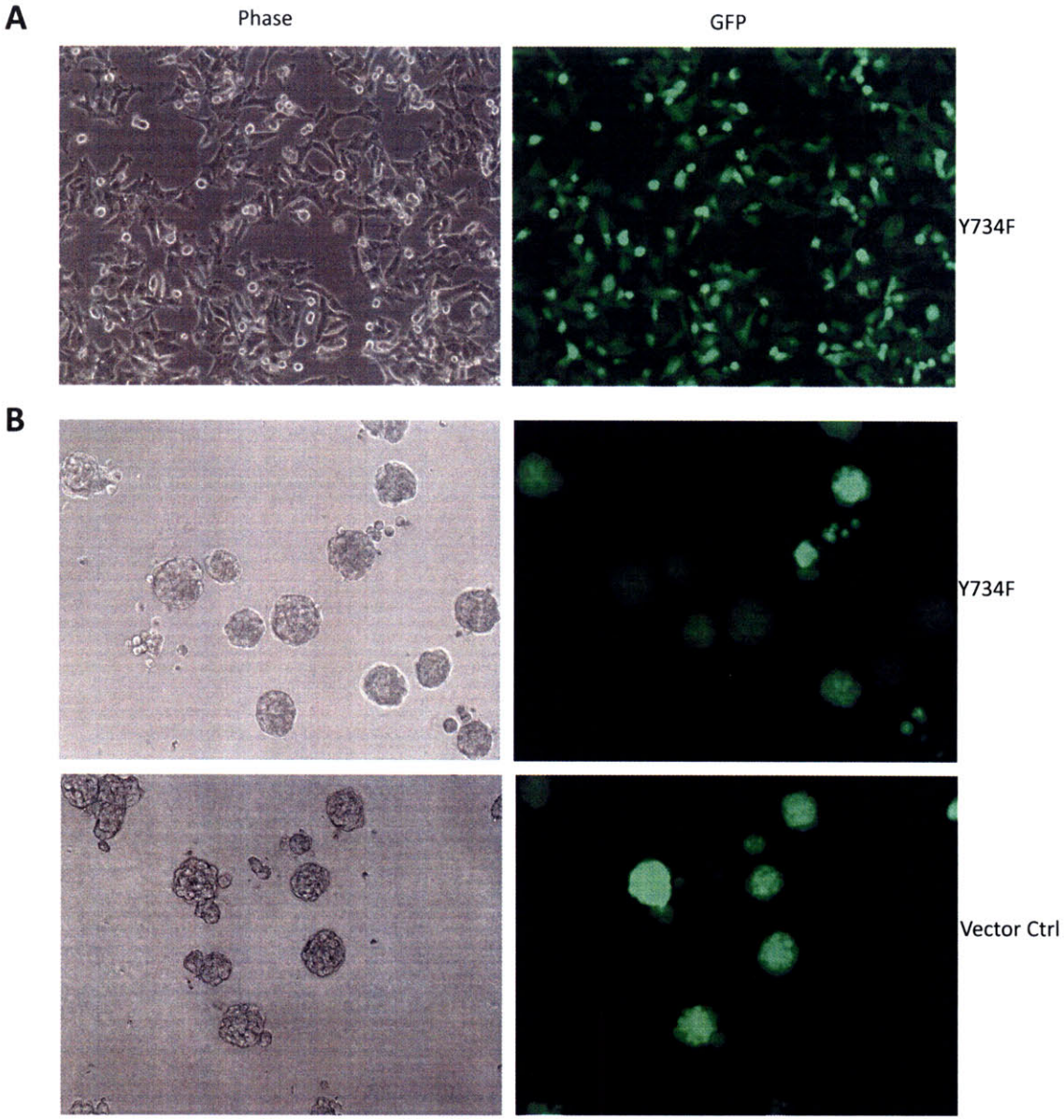

Figure 4. Tyrosine Y734 is necessary for all functions of CDCP1 *in vitro* and *in vivo*. (A) A375 cells over-expressing Y734F mutant form of CDCP1 no longer de-adhere from culture plates in 2D culture. **(B)** A375-Y734F cells completely lose "cluster-of-grape" pattern of growth in 3D, instead, they grow as a ball of cells in Matrigel, similar A375 cells expressing vector control.

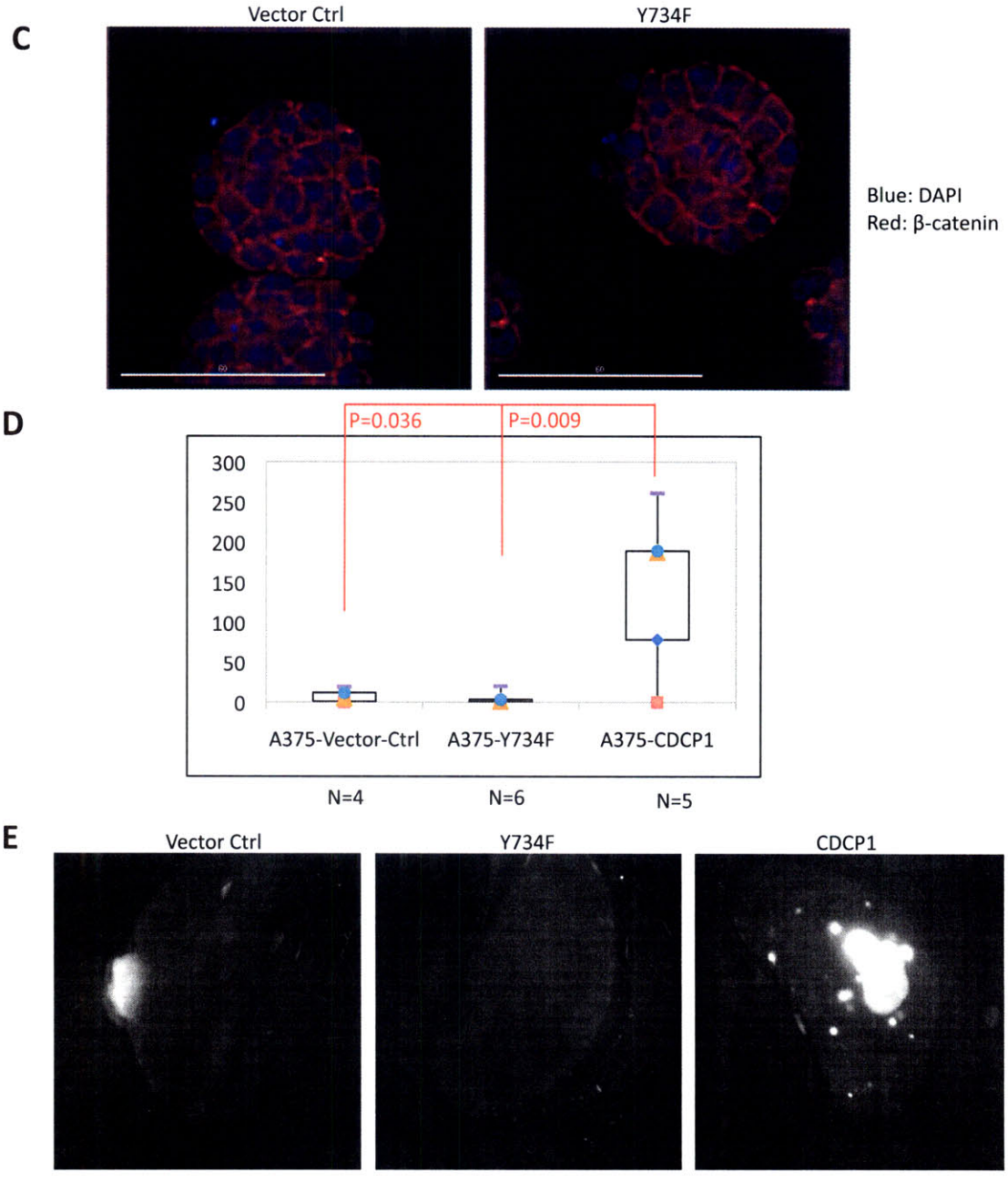

Figure 4. Tyrosine Y734 is necessary for all functions of CDCP1 *in vitro* and *in vivo*. (C) Immunofluorescence staining shows localization of β-catenin at cell-cell junctions in A375-Y734F cells. These data suggested that Y734 is necessary for *in vitro* functions of CDCP1 **(D)** Y734F point mutation completely abolished metastasis-enhancing activity of CDCP1 *in vivo*. A375-Vector-Ctrl, A375-CDCP1 or A375-Y734F cells were injected into NOD/SCID mice via tai vein and numbers of lung metastasis were recorded at the end of 10 weeks. Mice injected with A375-Y734F cells harbor significantly fewer lung tumors comparing to those injected with A375-CDCP1. There is no difference between the number of lung tumors in mice receiving A375-Vector-Ctrl or A375-Y734F cells. **(E)** Representative images of the left lobes from mice injected with A375-Vector-Ctrl cells (left), A375-Y734F cells (middle) or A375-CDCP1 cells (right).

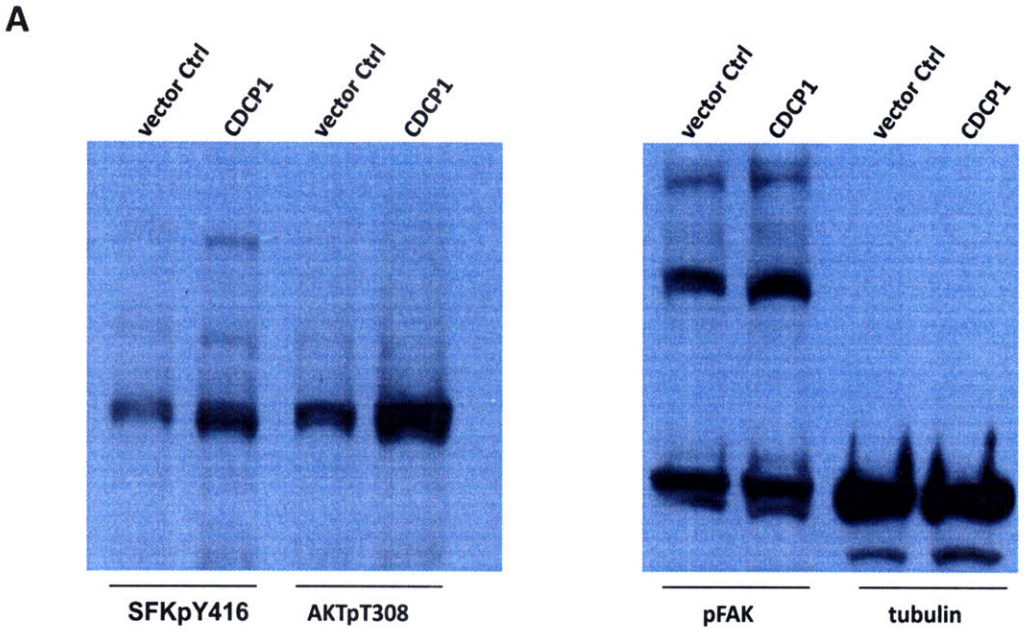

Figure 5. A375 cells over-expressing CDCP1 showed strong activation of SFKs and AKT, but comparable FAK activation relative to control cells.

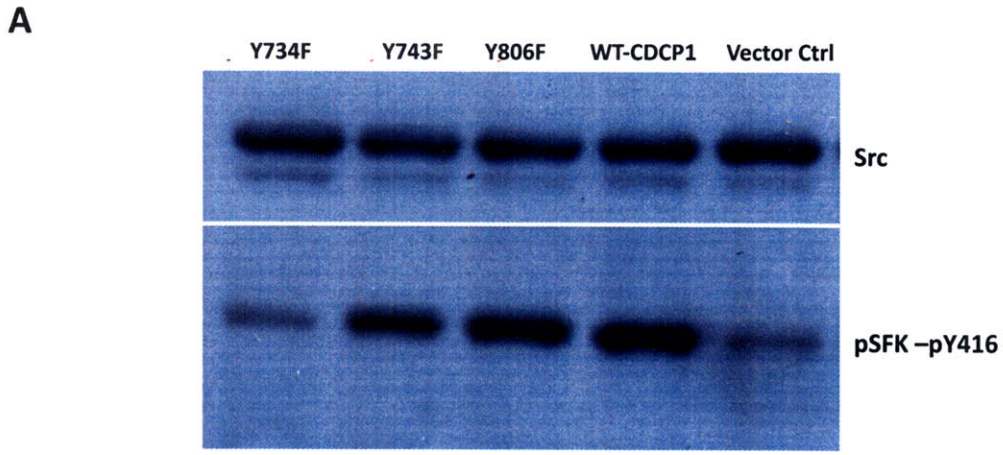

Figure 6. Y734F mutation that abolishes all functions of CDCP1 also abolished over activation of SFKs. Other point mutations (Y743F and Y806F) that have no effect on CDCP1 functions also showed no influence on the activation status of SFKs.

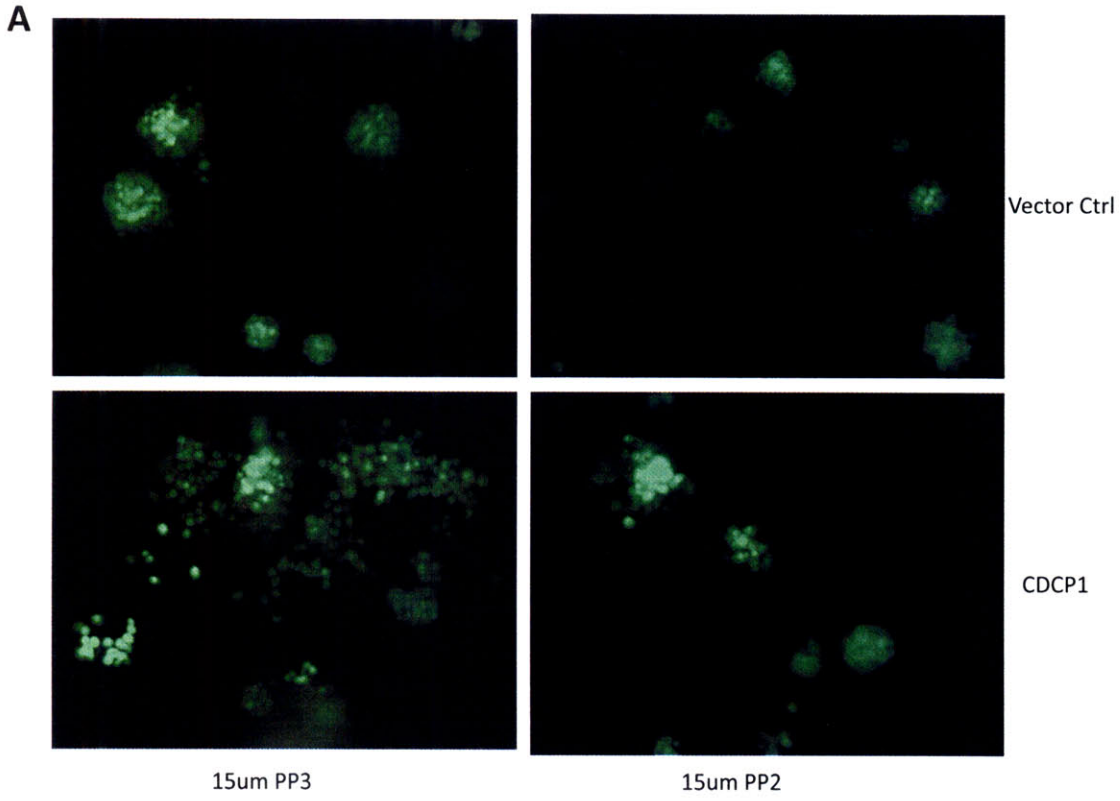

Figure 7. Inhibitors of SFKs blocked scattered growth of A375-CDCP1 cells in 3D Matrigel cultures. (A) PP2 treatment, but not PP3 treatment, reverted dispersive growth of CDCP1 over-expressing A375 cells to control "ball-like" structures.

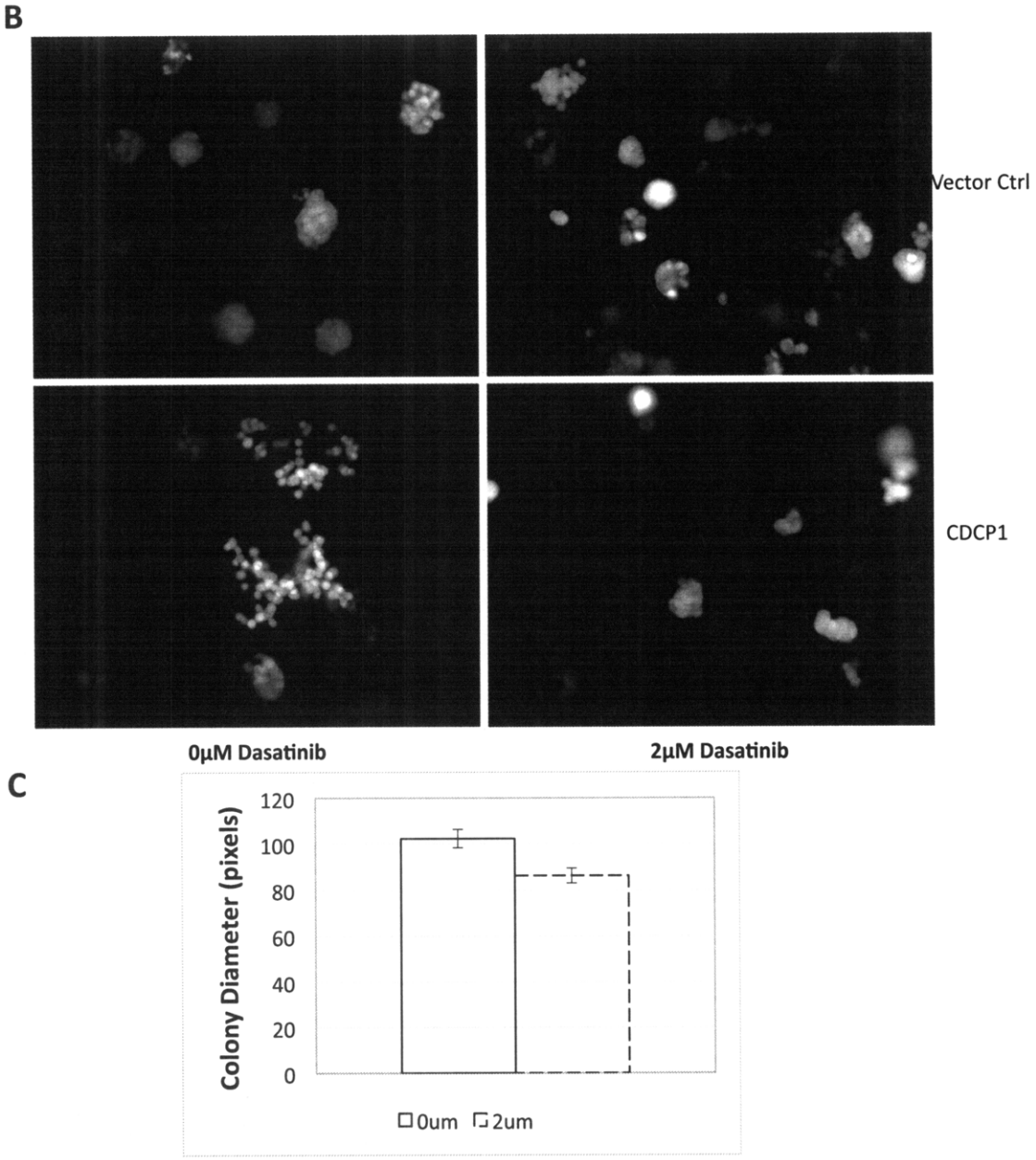

Figure 7. Inhibitors of SFKs blocked scattered growth of A375-CDCP1 cells in 3D Matrigel cultures. (B) Another SFK inhibitor – Dasatinib – also blocked the dispersive growth of CDCP1-overexpressing cells in 3D Matrigle. (C) Dasatinib has a small effect on colony size. The colony diameters of A375-Vector-Ctrl cells treated with Dasatinib are slightly smaller than control DMSO treated cells.

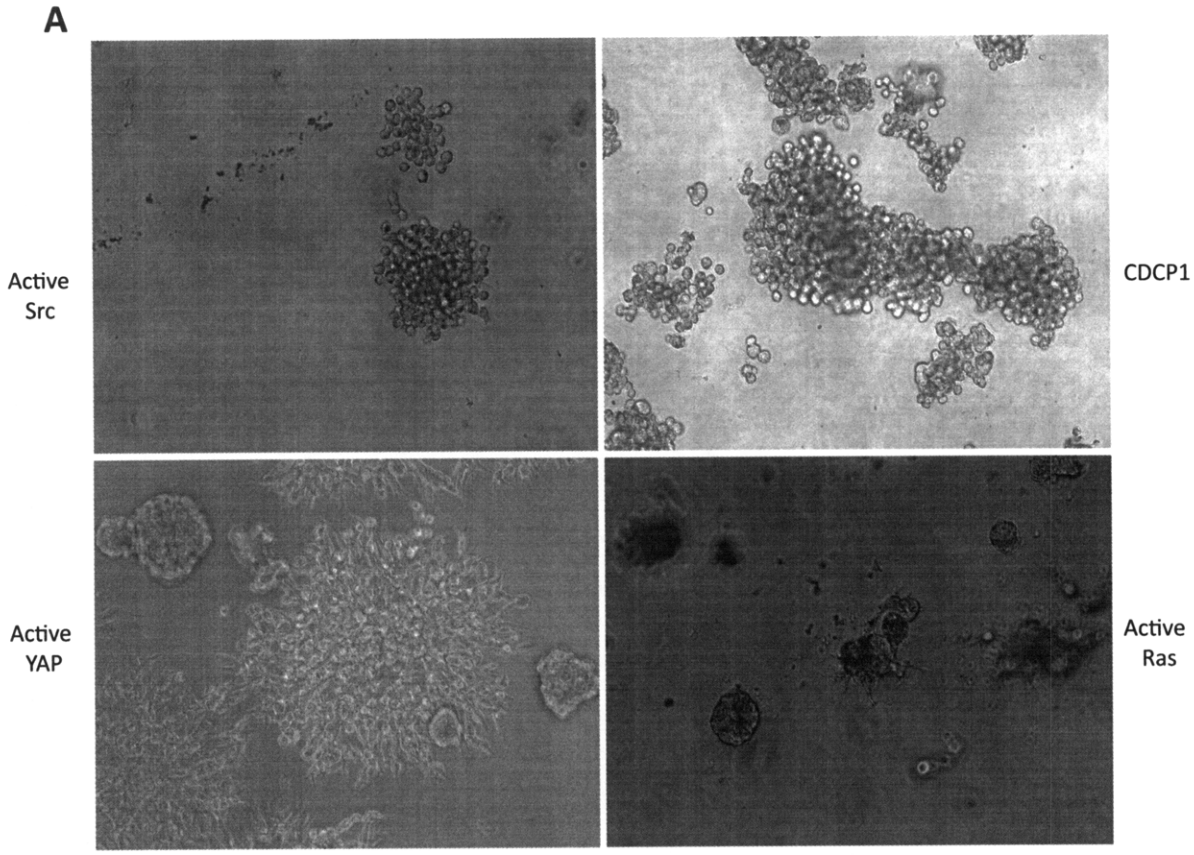

Figure 8. A375 cells expressing constitutively active Src partially mimics the growth pattern of A375-CDCP1 cells. A375 cells expressing constitutively active Ras or YAP display different phenotype in Matrigel, suggesting scattered growth is not a universal effect by oncogenes.

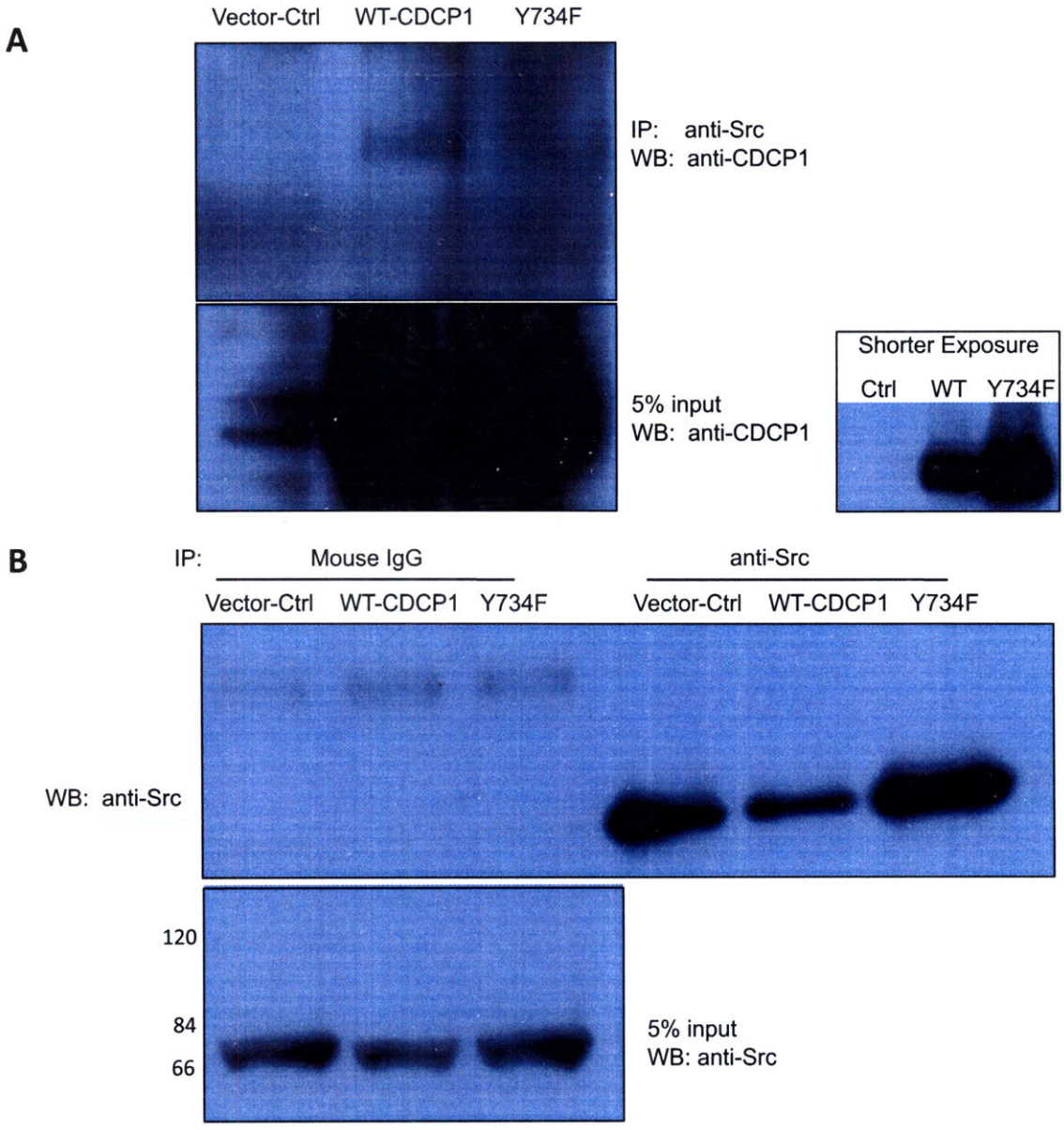

Figure 9. Y734F mutation in CDCP1 has little effect on binding to Src. In these co-immunoprecipitation (co-IP) experiments, equal number of cells were lysed in 1% Triton X-100 lysis buffer on ice for 30min, followed with centrifugation at 13000rpm at 4^{0}C using table-top centrifuge. Triton- soluble fractions were collected from each cell lysate and incubated with anti-Src antibody (or mouse IgG control (data not shown) for co-IP. **(A)** Association between CDCP1 (WT and Y734F) and Src was shown by co-immunoprecipitation with anti-Src antibody, followed by Western blot using anti-CDCP1 antibody in upper panel. Lower panel: 5% input for Co-IP, blotted with anti-CDCP1 antibody. (B) Western blotting using anti-Src antibody revealed that there is less soluble Src present in 1% Triton that can be immuno-precipitated using anti-Src antibody.
(IP: immunoprecipitation; WB: Western blot)

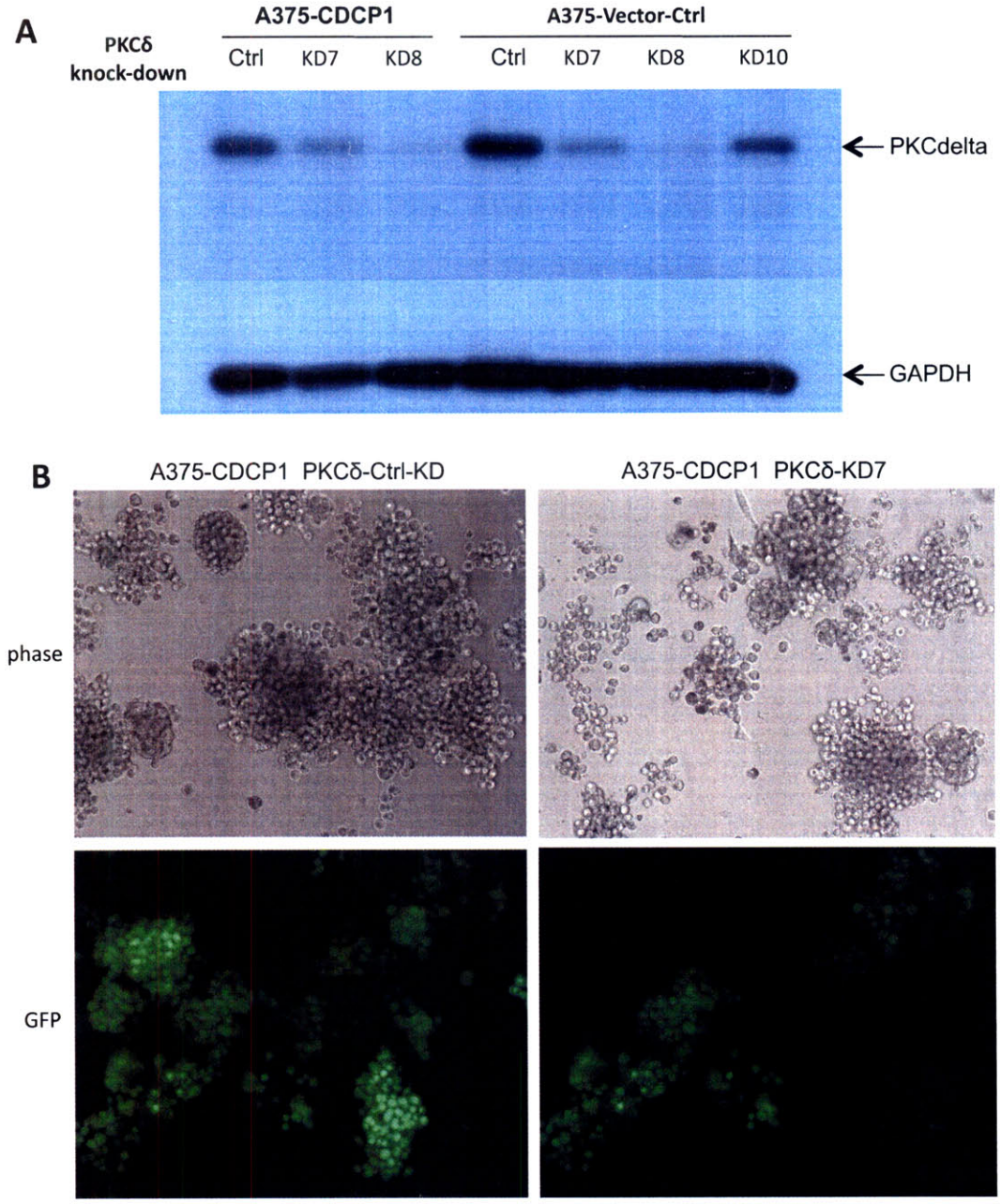

Figure 10. In 3D Matrigel, downregulation of PKCδ did not change growth pattern of A375-CDCP1 cells, but affected cell behavior in A375-Vector-Ctrl cells. (A) Western blot using anti-PKCδ antibody showed that reduced PKCδ expression using KD7, KD8 and KD10 siRNA constructs in A375-CDCP1 and A375-Vector-Ctrl cells. **(B)** In A375-CDCP1 over-expressing cells, reduction of PKCδ expression (KD7) did not affect scattered growth in Matrigel (Right panels) compared to A375-CDCP1-PKCδ-Ctrl-KD cells (Left panels).

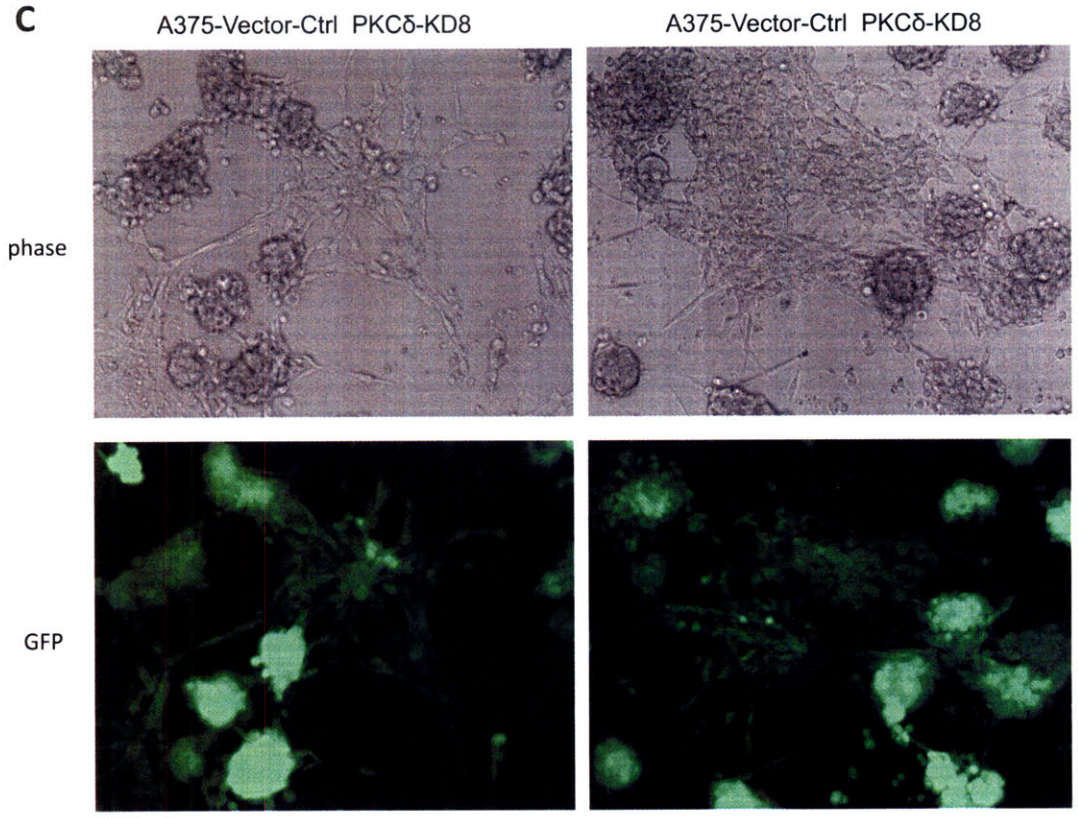

Figure 10. In 3D Matrigel, downregulation of PKCδ did not change growth pattern of A375-CDCP1 cells, but affected cell behavior in A375-Vector-Ctrl cells. (C) A375-Vector-Ctrl cells with reduced PKCδ expression form "Stellate" pattern with connector cells showing mesenchymal morphology in between balls of cells.

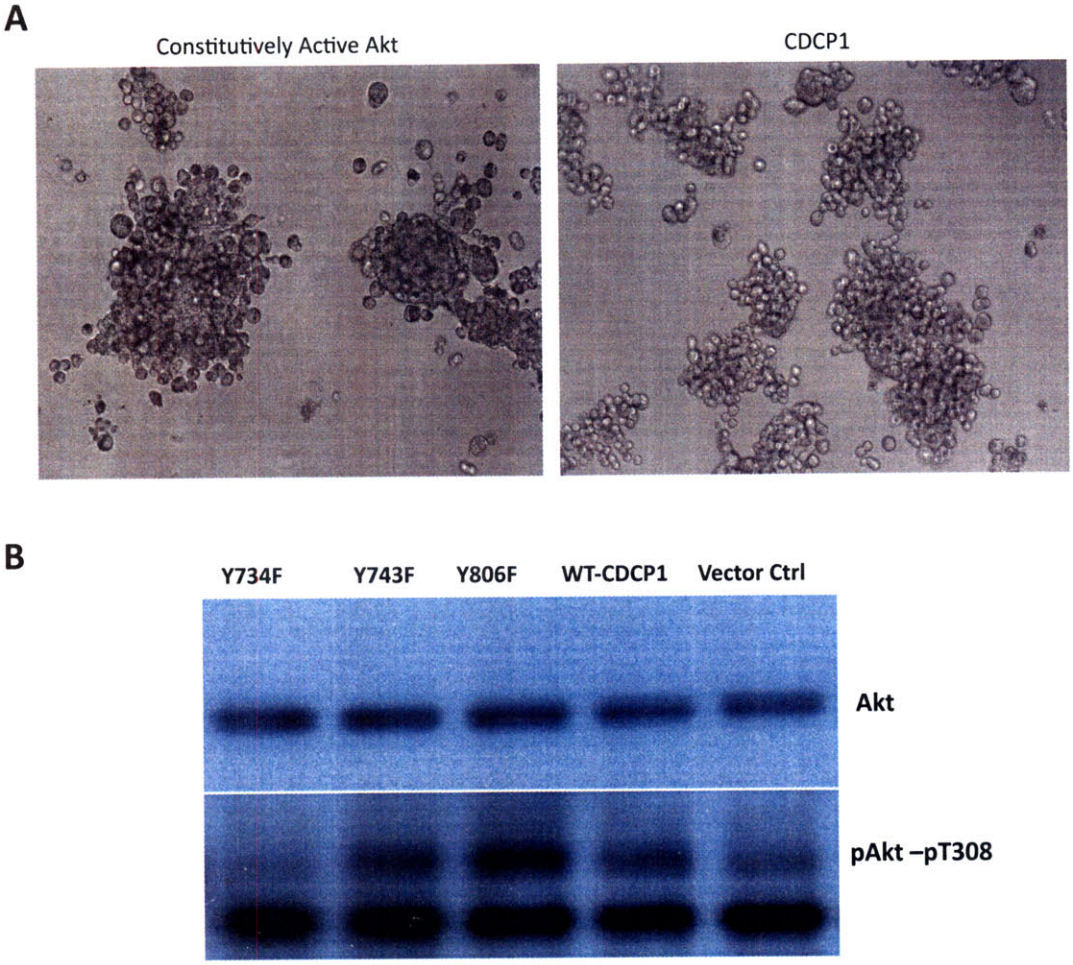

Figure 11. A375 cells expressing constitutively active Akt behave similarly to A375-CDCP1 cells in Matrigel and follow the same activation pattern seen with SFKs. (A) A375 cells expressing constitutively active Akt grow in scattered pattern in Matrigel (Left), similar to A375-CDCP1 cells (Right). (B) Western blot using antibody against activated Akt showed that A375 cells over-expressing wild-type CDCP1, Y743F or Y806F mutants have stronger activation of Akt compared to A375-Vector-Ctrl cells or cells over-expressing Y734F mutant.

CHAPTER 6.

DISCUSSION AND FUTURE DIRECTIONS

The contents of this chapter were written by Hui Liu, with editing by Richard Hynes.

Summary of Results

Nearly 90% of cancer mortality from solid tumors is due to metastasis of malignant cells to the distant vital organs. Currently our understanding of cancer metastasis has gone beyond observations and researchers have started to gain mechanistic insights into this devastating disease. Now we understand that not only the intrinsic propensities of tumor cells can partly determine their metastatic potentials, their abilities to adapt and to change their microenvironment also contribute greatly to the formation of metastases. Plasma membranes are situated in between tumor cells and their microenvironments, mediating the communications between them.

We decided to focus on plasma membranes and ask:

1) What are the intrinsic differences between tumor cells that form primary tumors equally well but have different metastatic potentials?
2) Are any of these differences functionally contributing to metastasis?
3) If so, what are the underlying mechanisms?

We began to address the first question by enriching for plasma membrane followed by quantitative mass spectrometry. We applied an interesting technique, colloidal silica coating of cells, to isolate plasma membrane while removing other internal organelle membranes (Chaney and Jacobson, 1983; Stolz and Jacobson, 1992), and we routinely achieve a 10-15 fold enrichment for plasma membrane proteins using integrin α2 as a marker. We also observe significant removal of major contaminant membranes, particularly ER membranes based on markers for these organelles. With this result, we began to analyze the identity of the proteins present in the plasma-membrane-enriched complex protein mixtures by performing mass spectrometry experiments. To reduce the complexity, we first separated the membrane-enriched protein mixture using 1D electrophoresis, followed by excision of 30 gel slices, thus reducing the complexity by 30-fold. Upon tryptic digestion, peptides from each gel band were further separated by reverse-phase HPLC, thus achieving 2-dimensional separation of initial membrane protein complex. As peptides were eluted from the column, they were introduced into the mass spectrometer by ion spray ionization, and data-dependent acquisition was performed to collect the information of the top 10 most abundant ions during each MS-MS/MS cycle. These data were searched against a human

database using Sequest software to elucidate the identity of these peptides and eventually match them to their parent proteins.

This approach yielded a list of proteins that are present in the plasma-membrane-enriched mixture. We categorized them in two ways. First, we grouped by number of peptides matching the identified proteins – either by single peptide, or two peptides, or more than two peptides. Although we applied stringent search criteria followed by visual inspection of the MS/MS spectrum, this method of categorization nevertheless provides a further measure of confidence. For proteins that were identified by more than 2 peptides (940 proteins in total), we are confident about their presence in the initial plasma membrane-enriched sample, while for proteins identified by a single peptide, we are not so sure. We also group these proteins based on their subcellular localization, which effectively is a measure of the plasma membrane isolation technique, and we found that approximately 30% of all detected proteins are membrane proteins.

To add quantitative power to mass spectrometry analysis, the initial protein identification was combined with differential metabolic labeling of proteins from poorly metastatic A375 cells and highly metastatic MA2 cells. We chose metabolic labeling since it is a convenient method with minimal human-introduced errors. However, we had to adjust our data collection method to obtain high-resolution information with our instrument, which is needed for quantitative analysis. We inserted a slower zoom scan step in between the conventional MS (survey) scan and MS/MS scan. This did not come without sacrifice – indeed, we reduced the number of peptides collected and analyzed by MS/MS from 10 to 5. Therefore, the amount of identity information we were able to extract is less than aforementioned, but we were able to obtain quantitative information instead. We found a total of approximately 530 proteins, 60% of which provided quantitative information.

Among the proteins that changed expression levels, we were pleased to find that some of these proteins have been shown previously to be involved in metastasis. Ultimately, we decided to pursue further a relatively novel protein, CDCP1, on the hypothesis that it is a potential metastasis enhancer. CDCP1 has previously been found to be unregulated in lung and colorectal cancer (Scherl-Mostageer et al., 2001), and in highly metastatic human epidermoid carcinoma cells relative to their poorly metastatic counterparts (Hooper et al., 2003). The phosphorylation status of CDCP1 seems to correlate with cell de-adhesion from

ECM substrates (Brown et al., 2004). It was also shown that CDCP1 could be tyrosine-phosphorylated by Src family kinases (Bhatt et al., 2005). However, at the time when we started to focus on CDCP1, it had not been shown that CDCP1 actually played any functional role in tumors or in metastasis formation.

When investigating surface expression levels of CDCP1 in poorly metastatic A375 cells, we noticed that two subpopulations – CDCP1^{low} and CDCP1^{high} – co-existed in culture, but only CDCP1^{high} cells were recovered from lung metastases. This prompted us to test whether CDCP1 can serve as a surface marker for cells with higher metastatic potential within a pool of A375 cells. We FACS-sorted A375-CDCP1^{high} and A375-CDCP1^{low}, and tested their metastatic abilities using tail-vein injection assays. We found that mice receiving A375-CDCP1^{high} cells harbored significantly more lung tumor nodules relative to mice receiving A375-CDCP1^{low} cells, suggesting that CDCP1 can indeed mark cells with higher metastatic potential.

We then began to examine the role of this protein in melanoma metastasis by downregulating CDCP1 expression in highly metastatic MA2 cells. When injected intravenously into NOD/SCID mice, MA2 cells expressing siRNA against CDCP1 exhibited significantly less metastasis in the lungs relative to the controls, whereas the size of subcutaneous tumors did not differ. We also overexpressed this protein in poorly metastatic A375 cells, and these cells formed significantly more tumor nodules in the lungs compared to control cells when introduced directly into the circulation. Subcutaneous tumor growth comparing cells overexpressing CDCP1 with control cells did not yield statistically significant change. These data showed for the first time, that CDCP1 plays a causal role in metastasis of melanoma cells.

We were curious about the cellular pathways in which CDCP1 might be involved to promote melanoma metastasis. Using two series of stable cell lines - MA2 cells with or without CDCP1 knockdown constructs, and A375 cells with or without overexpressing CDCP1 - we tested whether CDCP1 is involved in cell adhesion, migration/invasion, proliferation or soft agar formation. We observed that down-regulation of CDCP1 somewhat reduced the number of soft agar colony formed by MA2 cells; while overexpression of CDCP1 increased the number of colonies formed by A375 cells. These data suggested that CDCP1 might be involved in regulating the balance between cell proliferation and apoptosis. This finding was

further supported by immuno-histochemical staining of lung metastases for proliferation and apoptosis markers. Comparing lung metastases from MA2 cells harboring CDCP1 knockdown constructs to control MA2 cells, there was a small, yet statistically significant, reduction in proliferation index and increase in apoptosis, respectively. We speculate that altered balance by CDCP1 toward proliferation might contribute to its ability to enhance metastasis in the long run.

The other marked effect of CDCP1 is that CDCP1 overexpression caused the cells to detach from culture plates, and to proliferate as suspension cells – some cells are completely in suspension, and some cells tether loosely to the culture plate. A closer examination found that A375 cells overexpressing CDCP1 failed to spread on ECM proteins.

We then decided to adopt a 3-D Matrigel culture system that has been widely used for analyzing mammary carcinoma cells to study cellular alterations caused by CDCP1 overexpression. We found that, while A375 cells grow in 3D matrigel as balls with strong N-cadherin and β-catenin staining at cell-cell junctions, overexpression of CDCP1 caused the cells to scatter, and grow in a dispersive manner, with decreased N-cadherin and mislocalized β-catenin. Given that mammary gland cells behave similarly *in vivo* and in 3D Matrigel (Debnath and Brugge, 2005; Schmeichel and Bissell, 2003), we speculate that this scattered growth pattern may also occur in the lungs, and contribute to the large increase in numbers of lung metastases caused by overexpressing CDCP1.

We would like to dissect CDCP1 further to understand the structural features that are responsible for its functions. For this purpose, we constructed chimeric CDCP1 where the extracellular domain and transmembrane domain were replaced by those of IL2-receptor α (IL2Rα), generating Tac-CDCP1, along with four intracellular Y→F mutations: Y734F, Y743F, Y762F and Y806F. We found that Tac-CDCP1 and Y734F expressing cells no longer caused de-adhesion in 2D culture or dispersive growth in 3D Matrigel, suggesting that the extracellular and/or transmembrane domains, and tyrosine Y734 are necessary for CDCP1 functions. Remarkably, the Y734F mutation completely abolished the metastasis-enhancing activity of CDCP1, indicating that all functions of CDCP1 – in vitro de-adhesion and scattered growth, and in vivo metastasis-enhancing activity - are mediated through tyrosine 734.

We noticed that whenever we observed cell de-adhesion in culture, we also found scattered growth and loss of cell-cell adhesion in 3D; and that mutations that abolish one concomitantly remove the other; suggesting that CDCP1 may affect pathway(s) that regulate both cell-cell and cell-substrate adhesions. What could the pathway(s) be? Several results have provided clues to this question. Src family kinases have been reported to phosphorylate CDCP1 on tyrosine (Bhatt et al., 2005), and Y734F has been implicated in interacting with SFKs. Following recruitment of SFK, CDCP1 has been shown to be tyrosine-phosphorylated and mediate recruitment of PKCδ (Benes et al., 2005). These data point to the potential involvement of SFKs downstream of CDCP1, mediating CDCP1 functions.

We tested this hypothesis using several methods. First, we investigated signaling pathways activated by CDCP1, and found that CDCP1 overexpression hyper-activates Src. This enhanced activation is lost when cells express the Y734F mutant or Tac-CDCP1 mutant, but not other mutants, indicating a strong correlation between the activity of CDCP1 and activity of Src. Next, we grew A375 cells overexpressing CDCP1 in 3D Matrigel in the presence of SFK inhibitors (PP_2 or Dasatinib), and the morphology was observed. In this case, blocking SFKs inhibited scattered growth of these cells. We then expressed activated Src and found these cells mimic behaviors of cells overexpressing CDCP1. These data together suggested that the metastasis-enhancing function of CDCP1 is mediated by activation of Src family kinases.

Thus this thesis has answered, in part, the three questions we asked at the beginning of this research. We identified a list of proteins that are differentially expressed between tumor cells with high versus low metastatic abilities; we determined the functional involvement of CDCP1, and found it to be a novel metastasis-enhancer for melanoma cells; we investigated the cellular pathways that CDCP1 engages to promote metastasis and found that perhaps the changed balance between cell proliferation and cell death, and maybe scattered cell growth, contribute to enhanced metastases. We also found that CDCP1 exerts its functions, in part, by activation of Src family kinases.

Future Work

In many ways, the work described in this thesis remains ongoing. Mass spectrometry technology has advanced since the start of this project, and currently we are better equipped with high-resolution, high-accuracy instruments on-campus and around, and re-analysis of some of the samples will undoubtedly yield higher-confidence data with additional quantitative information. I described here a successful application of quantitative mass spectrometry to the plasma membrane proteome, and this technology has much broader use to study organelle proteomes – to first catalogue proteins present in each organelle and studying their dynamic changes upon stimulations. In fact, we have initiated investigation in secreted proteins, in particular, extracellular matrix proteins, using quantitative mass spectrometry.

As mentioned in chapter 1, we are interested in secreted and membrane proteins in the context of metastasis because these proteins represent interfaces between tumor-intrinsic abilities and their engagement with their microenvironment. In our system, we found that poorly metastatic human melanoma A375 cells proliferate at similar rate relative to highly metastatic MA2 cells in vitro, and subcutaneous tumors grow at similar rate in vivo; yet when introduced in the lungs via tail vein, there exist dramatic differences in their abilities to form tumors in the lungs. Tumor cells probably encounter very different situations in these two sites. At the subcutaneous site of the skin, a large number of tumor cells are embedded in the adipose tissue with ample tumor cell-cell interactions; and in the lungs, solitary cells are in contact with lung endothelium (experimental observations and personal communications with Dr. Sobolev). Conceptually, the fact that poorly metastatic tumor cells fail to manifest into tumors in the lung reflects lack of proliferation, and/or cell death of these cells in isolation and in a foreign environment. In other words, they are sensitive to their microenvironment. And conversely, highly metastatic cells are "indifferent" to their microenvironment due to intrinsic factors that compensate for lack of proper cell-cell and/or cell-matrix contacts (for example, increased activation of MAPK pathway for proliferation or Pi3K pathway for apoptosis-resistance), or due to their ability to make their own "home" or niche by secreting growth factors and extracellular matrix (ECM) proteins (by themselves or by inducing the stromal cells), or a combination of both.

We began to address these possibilities by first investigating membrane proteins and we found that upregulation of CDCP1 in highly metastatic cells enhances the activation of Src family kinase and activation of AKT, supporting our aforementioned hypothesis. And work

has been initiated to test whether highly metastatic cells are better at making their own "home" by investigating secreted proteins, in particular, ECM proteins. Similar to what we have accomplished in this thesis, we are interested in first cataloguing the ECM proteins that are present in the normal lungs, then quantitatively compare lung ECM proteins generated by highly metastatic cells to those from poorly metastatic cells. For quantification, instead of using metabolic labeling, which suits in vitro samples the best, we will apply chemical labeling using iTRAQ. This method is currently widely used. Another interesting question concerning secreted proteins in tumors is, where are these secreted proteins coming from? Are they secreted by tumor cells, or by the stromal cells? Our biological system of introducing human cells in immunocompromised mice, and mass spectrometry technology are particularly fit for answering these questions. Currently, microarray technology uses short probes that typically fail to discriminate between species. However, since mass spectrometry can tell precisely the amino acid sequence and assign the source of the protein to human-derived (tumor-derived) or mouse-(stroma-) derived, one single amino acid change can be detected by mass spectrometry. So even for ECM proteins that are highly conserved (for example 90% identical) between human and mouse sequences, one amino acid change for a 10-amino acid peptide will be easily discriminated.

Although sometimes suggested as "rivals", microarray analysis and quantitative mass spectrometry are nevertheless complementing each other. Combination of these two with intensive data mining should yield information not only concerning relative quantitative differences, but may also provide information on translational and post-translational modifications. We have recently generated microarray data using passage-matched A375 cells and MA2 cells grown in culture, and we will perform detailed comparisons between array and proteomics data in collaboration with the bioinformatics center.

Although we have shown that one of the proteins identified through the quantitative mass spectrometry screen is functionally involved in metastasis, many more proteins await discovery and/or confirmation. In fact, this presents the bottleneck between high-throughput analysis by proteomics works and (extremely) low-throughput biology confirmation for their roles in metastasis. Although currently there is no easy solution for this problem, application of 3D Matrigel culture might be a good middle ground. Kenny et al have used a large panel of breast cancer cell lines in 3D Matrigel culture and found that they generally fall into one of four categories – round, mass, grape and stellate morphologies. Interestingly, eight out of

nine cell lines that form "grape" structures with loose cell-cell adhesions are cells isolated from metastases; and six out of eight of the cell lines that form "Stellate" morphologies have previously been shown highly invasive in Boyden-Chamber invasion assays (Kenny et al., 2007). Therefore, there seems to be a correlation between the cell morphology in 3D cultures and their invasiveness. In addition, with currently available genome-wide cDNA libraries and siRNA libraries, this method can be easily coupled with high-throughput imaging analysis to test proteins that were identified through our work and genes identified from microarray studies for their involvement in metastasis. This method could effectively function as pre-*in vivo,* second-round functional screen and we shall expect more studies along this line in the next several years.

We found that CDCP1 is a surface marker for melanoma cells with high metastatic potential, and we would like to extend this work to clinical samples to determine if CDCP1 expression correlates with disease progression or patient survival. Currently we have obtained tissue arrays containing tumor samples and their normal counterparts; as well as tumor samples of different stages. Recent work by Ikeda et al has shown that in lung adenocarcinoma patients, significant positive correlation was observed between CDCP1 expression and poor prognosis, and there is also significant difference in disease-free survival between patients with high CDCP1 expression and those with low CDCP1 expression, strengthening our argument (Ikeda et al., 2009). So far, CDCP1 upregulation has been shown to be associated with enhanced tumor metastasis in lung and stomach cancers (Uekita et al., 2007; Uekita et al., 2008) and in melanoma (this work). These results certainly hint that CDCP1 may regulate tumor metastasis in a broader spectrum of cancers, and work along this line will be necessary to generalize its roles.

Using experimental metastasis assay, we found CDCP1 as a positive regulator of cancer metastasis. How do we explain such remarkable effects on metastasis by CDCP1? Our results from *in vitro* and *in vivo* characterization of cells with reduced or enhanced CDCP1 expression do not seem to offer a simple answer to this question; however, they provide several possibilities.

Experiments comparing cells overexpressing CDCP1 to control cells in early tail vein injection assays found a small yet consistent increase (less than 2 fold) in number of cells in the lungs 40min, 3 hours and 5 hours after tumor cell injections. This could be due to better

trapping in the lung microvescular bed, and/or due to better survival in the circulation and upon lodging in the lungs. Both ideas are supported by our data. Given that A375 cells overexpressing CDCP1 are bigger than control cells, it is conceivable that more CDCP1-overexpressing cells can be trapped in the lung microvasculature. Although I have not demonstrated a direct anoikis-resistance effect of CDCP1 in our cell system, such effects have been reported for both lung adenocarcinoma cells and gastric cancer cells (Uekita et al., 2007; Uekita et al., 2008). Together with our result that downregulation of CDCP1 somewhat reduces soft agar colony formation, these data support the possibility that CDCP1-overexpressing cells survive better in the circulation and upon lodging in the lung. This idea can be directly tested by staining cells for apoptosis shortly after tail-vein injection.

Obviously this initial less-than-2-fold difference cannot explain more than 5-fold difference in number of lung metastases that we observed after 5 weeks. It is possible that a function of CDCP1 in apoptosis-resistance continues to play a role between 5 hours and 5 weeks, which offers one explanation. This idea can be tested by investigating the number of cells undergoing apoptosis during the intermediate time points - such as after 2 days, one week, two weeks. Alternatively, CDCP1 could have a function in metastasis initiation to provide cells with proliferative power, which can also be tested by staining for proliferation marker Ki67 at intermediate time points.

It is also possible that additional functions of CDCP1 may participate. We observed de-adhesion from substrate and cell-cell dissociation in Matrigel when cells overexpress CDCP1, and we speculate that perhaps these properties allow the tumor cells to dissociate from the primary metastases and seed additional metastases in the lung, resulting in a significant increase in the number of lung tumors. Direct *in vivo* observation of such a process may not be feasible without long-term live imaging, but we can take advantage of "marking" tumor cells with a pool of ~100 barcodes, and assay for the presence of particular barcodes in a particular metastasis and in its surrounding metastases. In an example illustrated in Figure 1, the predominant tumors A and B could be dissected to test the presence of barcodes (for simplicity, tumor A or B harbor barcode A or B, respectively). Tumors surrounding A and B (indicated with red or blue arrows) could also be dissected and tested for the presence of these and other barcodes. If all these surrounding tumors are derived from individual cells initially seeded in the lung (and not by disseminating from tumor A or B), then there should be equal probability for the presence of these 100 barcodes.

However, if these metastases are indeed derived from A or B, barcode A or B should be enriched relative to other 98 barcodes, suggesting the role of CDCP1 in metastasis-to-metastasis dissemination.

In our assay, cells were artificially introduced into the circulation; therefore we test the functions of CDCP1 in later steps of cancer metastssis. Perhaps the next logical step is to use orthotopic models to confirm the function of CDCP1 in full metastasis. Currently a CDCP1 knockout mouse is not available yet, although target vector construction has begun by the NIH Knock Out Mouse Project (KOMP).

When analyzing molecular pathways that may mediate the activities of CDCP1, we found that activation of SFKs strongly correlates with CDCP1 functions, and CDCP1 overexpression in turn activates SFKs. We are interested in knowing the underlying mechanisms for CDCP1-mediated SFK activation. Work by Benes et al has suggested a loss of recruitment of Src by mutant Y734F form of CDCP1, suggesting that CDCP1 functions as an adaptor protein through Y734 to directly recruit SFKs. However, we were unable to confirm loss of interaction between Y734F mutant CDCP1 and Src, therefore we cannot confirm this simple activation model. The question is then, how does CDCP1 activate Src?

Although the previous model suggests that CDCP1 interacts with Src directly to compete for intramolecular SH2-phosphoTyrosine interactions that keep Src in inactive state, it is entirely possible that CDCP1 activates Src through indirect interactions to recruit Src activators. CDCP1 may interact with protein phosphatases such as SHP1 and PTPα through Y734. These protein phosphatases have been shown to remove the phospho-group from tyrosine 530 at the C-terminus of Src, releasing intramolecular interactions between SH2-phosphoTyrosine interactions, thus activating Src. To test this hypothesis, co-immunoprecipitation experiments using cells overexpressing either wild-type or Y734F mutant CDCP1 can be carried out. In such experiments, anti-CDCP1 antibody will be used for IP, and the resultant immunocomplexes can be blotted using anti-SHP1 or anti-PTPα antibodies. If indeed Y734 is involved in recruiting these Src activators, we expect to see reduced interaction between SHP1 or PTPα and Y734F mutant CDCP1, relative to wild-type CDCP1. Alternatively, an unbiased method is to apply SILAC-quantitative mass spectrometry to investigate proteins that immunoprecipitate with wild-type or Y734F mutant

CDCP1. Proteins that fail to interact with CDCP1 due to Y734F mutation will be under-represented in mass spectrometry analysis, while proteins that are not affected or non-specific proteins will be presented at 1:1 ratio.

As detailed in chapter 5, we found a CDCP1-dependent solubility change of Src in 1% Triton X-100, which correlates with the activity change of Src. It was also reported that CDCP1 is localized in lipid rafts of the plasma membrane (Alvares et al., 2008), and Src family kinases have also been shown to reside in lipid rafts (Simons and Toomre, 2000; Stefanova et al., 1991). These data suggest one possibility - that Src needs to localize to these triton-insoluble fractions to be activated. Based on this hypothesis, wild-type CDCP1 may interact with Src via direct interactions through both SH2 domain- and SH3 domain-mediated interactions, but only activate Src when both are localized to the detergent-resistant fraction. CDCP1 with Y734F mutation could therefore fail to activate Src because it itself fails to localize to the detergent-insoluble fraction, rather than failing to interact with Src. This hypothesis can be tested by 1) immunofluorescence staining of CDCP1 with Src and with activated SFKs to investigate co-localization eg with the cytoskeleton; and 2) biochemical fractionation of Triton X-100 lysate on sucrose gradient to test colocalization of CDCP1 with Src in the lipid raft fraction.

One question that we have not started to address is whether activation of Src by CDCP1 is dependent on the phosphorylation of CDCP1? This can be answered by investigating the phosphorylation status of wild-type CDCP1 (that activates Src) and Y734F mutant form of CDCP1 (that does not activate Src) by immunoprecipitating CDCP1 and blotting for tyrosine phosphorylation using 4G10 antibody. If Src activation is dependent on the phosphorylation of CDCP1, then we shall expect that tyrosine-phosphorylation in Y734F is reduced or diminished. If this is true, then there may exist a feed-forward loop between CDCP1 and Src – Src may mediate the initial phosphorylation of CDCP1, and upon phosphorylation, CDCP1 may further activate Src. This idea is supported by the following observations 1) Src has been shown to phosphorylate CDCP1 *in vitro* in kinase assays, and blocking SFKs using inhibitors reduced CDCP1 tyrosine-phosphorylation *in vivo*, suggesting that Src could be the initiating kinase, although that does not exclude the involvement of other kinases; 2) We found that not all cells that overexpress CDCP1 detach in 2D culture, an observation supported by the Bhatt's work. It was suggested by Bhatt et al that only in the tumor cells that have intrinsically high SFK activities did they find CDCP1 able to cause cell detachment

(Bhatt et al., 2005). Comparing the basal SFK activities in cells that detach or remain adherent when overexpressing CDCP1 might provide some insight in this manner.

In summary, we propose a model that CDCP1 functions as an adaptor protein, interacting with SFKs directly or indirectly in a phosphorylation-dependent manner, recruiting SFKs to the lipid raft/DRM fraction or to the cytoskeleton. Perhaps, it is in these locations that Src is activated. We are very interested in testing our hypothesis in the near future.

In addition to activation of SFKs, overexpressing CDCP1 in A375 cells also enhanced the activation of Akt. This is a very interesting phenomenon since the PI3K/Akt pathway has been shown to be involved in apoptosis resistance (Duronio, 2008), and work by the Sakai group has shown that down-regulation of CDCP1 in lung adenocarcinoma cells reduced their anoikis resistance (Uekita et al., 2007). We are interested to pursue this topic further to see if, indeed, the Akt pathway is downstream of CDCP1, mediating some of the effects we observed. We will combine pharmacological treatments with specific inactivation (by expressing dominant negative Akt, or siRNA-mediated knockdown) to address this question. So far, we have investigated roles of CDCP1 as a cell-intrinsic factor. However, several lines of evidence suggest that CDCP1 may be involved in communicating with the microenvironment in which the cells reside. First, we found that A375 overexpressing CDCP1 proliferate more slowly in tissue culture, and the sizes of subcutaneous tumors generated from these cells are slightly (but not significantly) smaller relative to those from control cells. However, when intravenously introduced into the lungs of the mice, these cells form significantly more metastases in the lungs, suggesting a tissue-specific effect of CDCP1 in balancing between proliferation and apoptosis. Secondly, we found that cells overexpressing Tac-CDCP1, where extracellular and transmembrane regions of CDCP1 were replaced with those from IL-2 α, no longer detach from tissue-culture plates and no longer grow in scattered manner in 3D Matrigel. In addition, CDCP1 contains extracellular CUB domains, which have been shown to be involved in protein-protein, or protein-carbohydrate interactions (Sieron et al., 2000; Tao et al., 2005; Tu et al., 2008). Together, these results indicate the potential existence of factors in the microenvironment that interact with CDCP1, dictating the functions of CDCP1. Identification of such factors (or CDCP1 ligands) and elucidating their localization in tumors (both the subcutaneous tumors and in the lungs where the metastases eventually arise) will be very interesting to further our understanding of tumor-microenvironment communications.

Concluding Remarks

The results from this thesis have contributed small pieces of knowledge to our current understanding of the problem of cancer metastasis. We have applied a new technology to answer an "old" question, which has yielded novel information; we have focused on one membrane protein CDCP1 and have shown its functions as a metastasis enhancer. We have uncovered some of the potential cellular and molecular pathways by which CDCP1 increases metastatic potential. We hope this type of research may open avenues to design specific blocking reagents in the effort to combat cancer metastasis.

REFERENCE

Alvares, S. M., Dunn, C. A., Brown, T. A., Wayner, E. E., and Carter, W. G. (2008). The role of membrane microdomains in transmembrane signaling through the epithelial glycoprotein Gp140/CDCP1. Biochim Biophys Acta *1780*, 486-496.

Benes, C. H., Wu, N., Elia, A. E., Dharia, T., Cantley, L. C., and Soltoff, S. P. (2005). The C2 domain of PKCdelta is a phosphotyrosine binding domain. Cell *121*, 271-280.

Bhatt, A. S., Erdjument-Bromage, H., Tempst, P., Craik, C. S., and Moasser, M. M. (2005). Adhesion signaling by a novel mitotic substrate of src kinases. Oncogene *24*, 5333-5343.

Brown, T. A., Yang, T. M., Zaitsevskaia, T., Xia, Y., Dunn, C. A., Sigle, R. O., Knudsen, B., and Carter, W. G. (2004). Adhesion or plasmin regulates tyrosine phosphorylation of a novel membrane glycoprotein p80/gp140/CUB domain-containing protein 1 in epithelia. J Biol Chem *279*, 14772-14783.

Chaney, L. K., and Jacobson, B. S. (1983). Coating cells with colloidal silica for high yield isolation of plasma membrane sheets and identification of transmembrane proteins. J Biol Chem *258*, 10062-10072.

Debnath, J., and Brugge, J. S. (2005). Modelling glandular epithelial cancers in three-dimensional cultures. Nat Rev Cancer *5*, 675-688.

Duronio, V. (2008). The life of a cell: apoptosis regulation by the PI3K/PKB pathway. Biochem J *415*, 333-344.

Hooper, J. D., Zijlstra, A., Aimes, R. T., Liang, H., Claassen, G. F., Tarin, D., Testa, J. E., and Quigley, J. P. (2003). Subtractive immunization using highly metastatic human tumor cells identifies SIMA135/CDCP1, a 135 kDa cell surface phosphorylated glycoprotein antigen. Oncogene *22*, 1783-1794.

Ikeda, J., Oda, T., Inoue, M., Uekita, T., Sakai, R., Okumura, M., Aozasa, K., and Morii, E. (2009). Expression of CUB domain containing protein (CDCP1) is correlated with prognosis and survival of patients with adenocarcinoma of lung. Cancer Sci *100*, 429-433.

Kenny, P. A., Lee, G. Y., Myers, C. A., Neve, R. M., Semeiks, J. R., Spellman, P. T., Lorenz, K., Lee, E. H., Barcellos-Hoff, M. H., Petersen, O. W., *et al.* (2007). The morphologies of breast cancer cell lines in three-dimensional assays correlate with their profiles of gene expression. Mol Oncol *1*, 84-96.

Scherl-Mostageer, M., Sommergruber, W., Abseher, R., Hauptmann, R., Ambros, P., and Schweifer, N. (2001). Identification of a novel gene, CDCP1, overexpressed in human colorectal cancer. Oncogene *20*, 4402-4408.

Schmeichel, K. L., and Bissell, M. J. (2003). Modeling tissue-specific signaling and organ function in three dimensions. J Cell Sci *116*, 2377-2388.

Sieron, A. L., Tretiakova, A., Jameson, B. A., Segall, M. L., Lund-Katz, S., Khan, M. T., Li, S., and Stocker, W. (2000). Structure and function of procollagen C-proteinase (mTolloid) domains determined by protease digestion, circular dichroism, binding to procollagen type I, and computer modeling. Biochemistry *39*, 3231-3239.

Simons, K., and Toomre, D. (2000). Lipid rafts and signal transduction. Nat Rev Mol Cell Biol *1*, 31-39.

Stefanova, I., Horejsi, V., Ansotegui, I. J., Knapp, W., and Stockinger, H. (1991). GPI-anchored cell-surface molecules complexed to protein tyrosine kinases. Science *254*, 1016-1019.

Stolz, D. B., and Jacobson, B. S. (1992). Examination of transcellular membrane protein polarity of bovine aortic endothelial cells in vitro using the cationic colloidal silica microbead membrane-isolation procedure. J Cell Sci *103 (Pt 1)*, 39-51.

Tao, Z., Peng, Y., Nolasco, L., Cal, S., Lopez-Otin, C., Li, R., Moake, J. L., Lopez, J. A., and Dong, J. F. (2005). Recombinant CUB-1 domain polypeptide inhibits the cleavage of ULVWF strings by ADAMTS13 under flow conditions. Blood *106*, 4139-4145.

Tu, C. F., Yan, Y. T., Wu, S. Y., Djoko, B., Tsai, M. T., Cheng, C. J., and Yang, R. B. (2008). Domain and functional analysis of a novel platelet-endothelial cell surface protein, SCUBE1. J Biol Chem *283*, 12478-12488.
Uekita, T., Jia, L., Narisawa-Saito, M., Yokota, J., Kiyono, T., and Sakai, R. (2007). CUB domain-containing protein 1 is a novel regulator of anoikis resistance in lung adenocarcinoma. Mol Cell Biol *27*, 7649-7660.
Uekita, T., Tanaka, M., Takigahira, M., Miyazawa, Y., Nakanishi, Y., Kanai, Y., Yanagihara, K., and Sakai, R. (2008). CUB-domain-containing protein 1 regulates peritoneal dissemination of gastric scirrhous carcinoma. Am J Pathol *172*, 1729-1739.

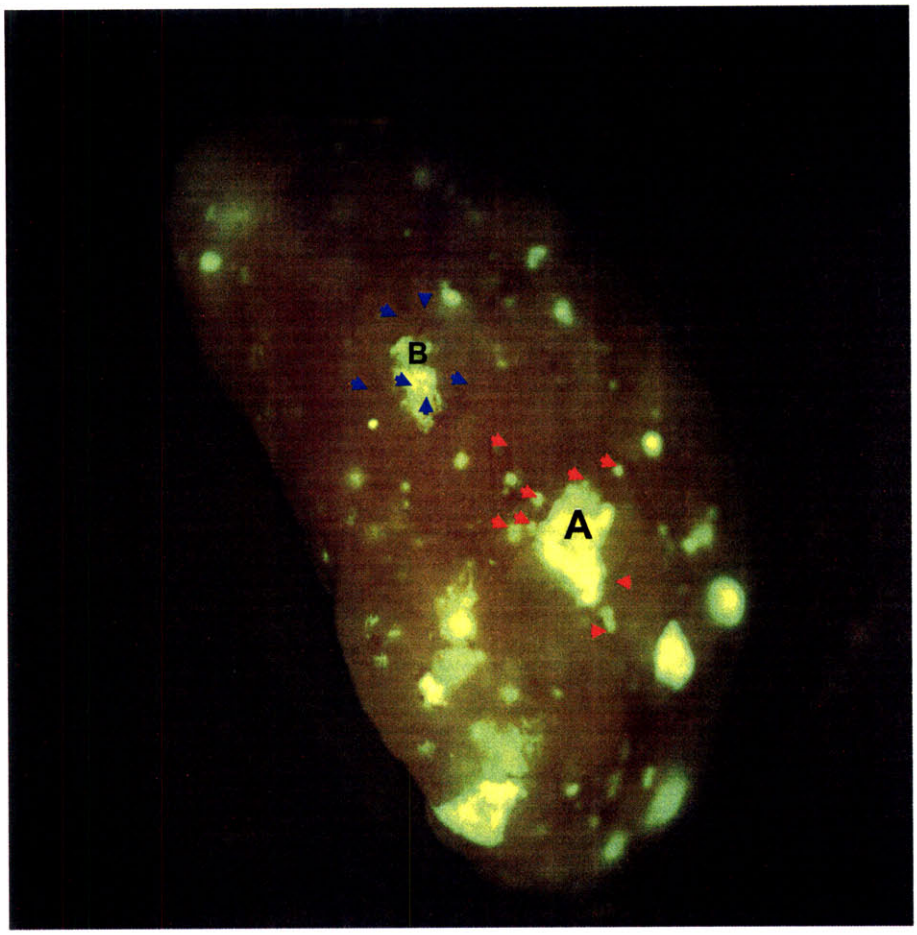

Figure 1. Proposed experiment to test the involvement of CDCP1 in seeding metastases from metastases. Briefly, A375-CDCP1 cells will be infected with a pool of barcodes before intravenous injection, and metastases A and B (in this example) will be dissected to test the presence of particular barcodes (A or B, respectively), and their surrounding tumor nodules (red and blue arrows) will also be assayed for the presence of barcodes. Significant enrichment for barcode A or B in these tumors suggest a role of CDCP1 in possible metastases-seeding-metastases dissemination.

APPENDIX A.

ROLE OF YES-ASSOCIATED PROTEIN (YAP) IN MELANOMA METASTASIS

The work in this chapter was conceived by Hui Liu and Richard Hynes. Overexpression construct for YAP was generated by Dr. Patrick Stern. The content of this chapter were written by Hui Liu, with editing by Richard Hynes.

When trying to understand the cellular mechanisms of CDCP1, it was overexpressed in mouse embryonic fibroblasts to generate stable cell line (MEF-CDCP1). We found that although control mouse embryonic fibroblasts (MEFs) formed one layer of cells and failed to proliferate when reaching confluence (contacted-inhibited cell proliferation), MEF-CDCP1 continued to proliferate, suggesting maybe CDCP1 is involved in contact-mediated inhibition of cell proliferation (Data not shown). I was intrigued by this observation, and I obtained construct encoding a transcription factor – Yes Associated Protein, or YAP from Dr. Stern, and generated retroviruses. YAP (Yorkie in Drosophila) is part of the newly discovered Hippo pathway that mediates contact-inhibited cell proliferation (Edgar, 2006; Zhao et al., 2008; Zhao et al., 2009). Therefore, it provided a positive control to test whether CDCP1 is involved in contact inhibition of MEFs.

Both MEFs and A375 cells were infected with YAP or control retroviruses to generate MEF-YAP and A375-YAP cells, as well as control cells (A375-MIGw and MEF-MIGw). When A375-YAP cells were grown in 3D Matrigel, they look dramatically different from the control cells. A375-YAP cells showed mesenchymal morphology and by day 8, clusters of spindly-shaped cells spreading out from the center were observed (Figure 1), indicating that A375-YAP cells have enhanced invasive activity. Transwell migration and invasion assays showed drastic enhancement in the cells' ability to migrate, and in their ability to invade through Matrigel-coated wells. While very few A375- control cells migrate or invaded through the transwell (Figure 2A, left), the whole bottom membranes were covered with migrated/invaded A375-YAP cells (Figure 2A, right). In addition, these migrated/invaded cells look different from the control – while control cells present amoeboid morphology, A375-YAP cells are mesenchymal. We also tested migration using scratch-wound assays, and we found markedly enhanced migration with A375-YAP cells relative to control cells, in agreement with transwell results (Figure 2B). These data showed that expression of YAP significantly enhanced the ability of cells to migrate and invade.

Next, we investigated cell proliferation *in vitro*. Equal numbers of cells were seeded on day 0 and harvested on day 3, and we found approximately 40% more A375-YAP cells compared to control cells, suggesting that YAP enhanced cell proliferation (Figure 3A).

To assess tumor cell growth at a subcutaneous site, we injected 0.5*10e6 A375-YAP cells or A375-MIGw control cells into the mice and dissected at different time points to measure

tumor growth rate. Initially (approximately 3 weeks and 5.5 weeks), tumors generated by A375-YAP cells are much bigger than those from control cells; however, by eight weeks, tumors from both cell types reached the same size (Figure 3B). These data suggesting that YAP provides a growth advantage at early time, are in agreement with in vitro proliferation data. However, such advantage is lost at later time points, and the reasons remain obscure at this moment.

In light of our *in vitro* migration/invasion and 3D culture results, we performed experimental metastasis assays to measure the abilities of A375-YAP cells to form lung tumors comparing to the control cells. Perhaps as expected (given the dramatic effects we observed *in vitro*), YAP expression significantly enhanced cell metastatic potential. While mice injected with 1*10e6 A375-MIGw cells on average harbored 4.3 ±1.67 lung metastasis, mice receiving the same number of A375-YAP cells contain 62.4±14.4 lung tumors, a more than 10-fold increase ($p= 0.0004$, Figure 4). In addition, we observed formation of tumors in the diaphragm underlying the lung, suggesting that tumor cells may have disseminated from the lung and lodged into the diaphragm.

Impressively, we also observed numerous green tumor cells disseminated from subcutaneous tumors generated by A375-YAP cells. We have found tumor cells in the lungs that were disseminated from the subcutaneous tumors as early as 3 weeks. Visual inspection using UV-dissecting microscope at the time of mouse dissection found that the number of tumor cells in the lungs seem to increase over time. At an early time point (3 weeks), we only see solitary cells in the lungs, and later (5 weeks), small clusters of green tumor cells could be found, indicating that these cells are proliferating. A thorough evaluation of the number of disseminated cells in the lungs remains to be carried out.

In summary, we have identified a gene that seems to posses "super metastatic" power. YAP has been mapped to 9qA1 region in mouse chromosome, which is frequently amplified in liver cancer, and has been shown to be a novel oncogene contributing to rapid tumor growth (Zender et al., 2006). Furthermore, work by Overholtzer et al showed that YAP functions as a potential oncogene in mammary epithelial cells, enhances colony formation in soft agar and induces epithelial-to-mesenchymal transition (Overholtzer et al., 2006). These studies have shown that YAP is a new oncogene. Our results suggest that YAP also contributes to tumor metastasis. In fact, we have never seen any single gene so "virulent" in

promoting melanoma migration/invasion *in vitro* and promoting metastasis from subcutaneous tumors *in vivo*. We are very interested in the mechanisms by which YAP functions to augment metastatic ability, and have started to gain insight by investigating the potential pathways that are important for YAP functions.

REFERENCES

Edgar, B. A. (2006). From cell structure to transcription: Hippo forges a new path. Cell *124*, 267-273.

Overholtzer, M., Zhang, J., Smolen, G. A., Muir, B., Li, W., Sgroi, D. C., Deng, C. X., Brugge, J. S., and Haber, D. A. (2006). Transforming properties of YAP, a candidate oncogene on the chromosome 11q22 amplicon. Proc Natl Acad Sci U S A *103*, 12405-12410.

Zender, L., Spector, M. S., Xue, W., Flemming, P., Cordon-Cardo, C., Silke, J., Fan, S. T., Luk, J. M., Wigler, M., Hannon, G. J., *et al.* (2006). Identification and validation of oncogenes in liver cancer using an integrative oncogenomic approach. Cell *125*, 1253-1267.

Zhao, B., Lei, Q. Y., and Guan, K. L. (2008). The Hippo-YAP pathway: new connections between regulation of organ size and cancer. Curr Opin Cell Biol *20*, 638-646.

Zhao, B., Lei, Q. Y., and Guan, K. L. (2009). Harness the power: new insights into the inhibition of YAP/Yorkie. Dev Cell *16*, 321-322.

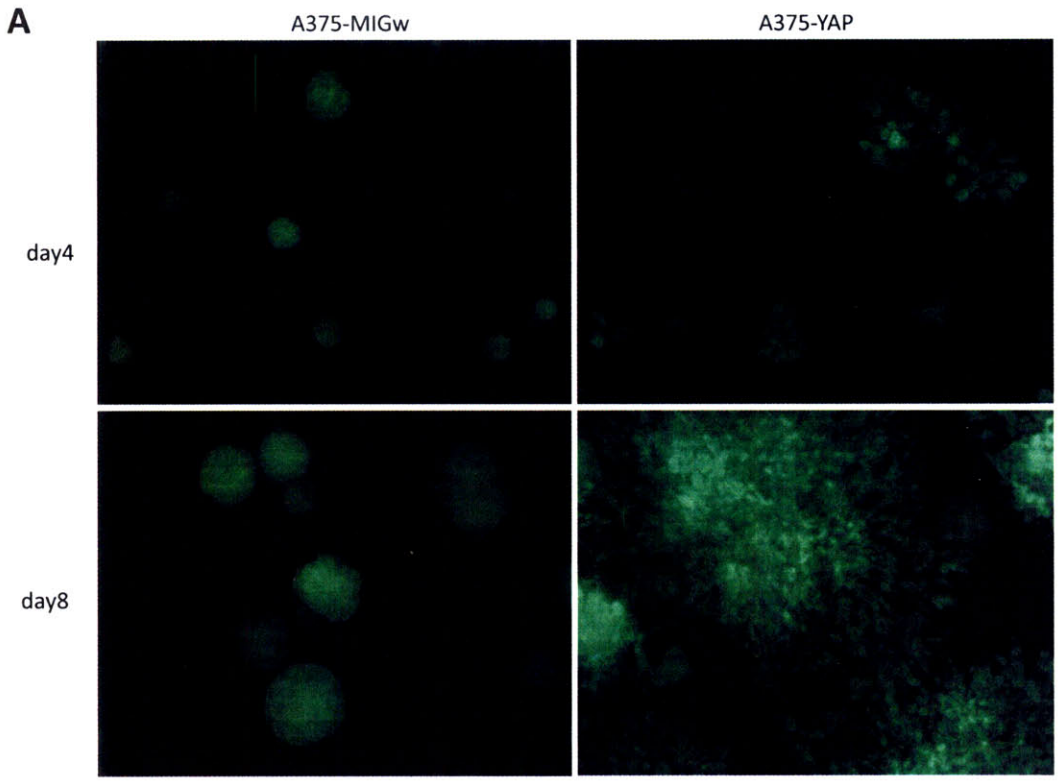

Figure 1. YAP-expressing A375 cells grow in markedly different pattern compared with A375 control cells in 3D Matrigel. While control cells grow as tight balls in Matrigel, A375-YAP cells showed stellate morphology.

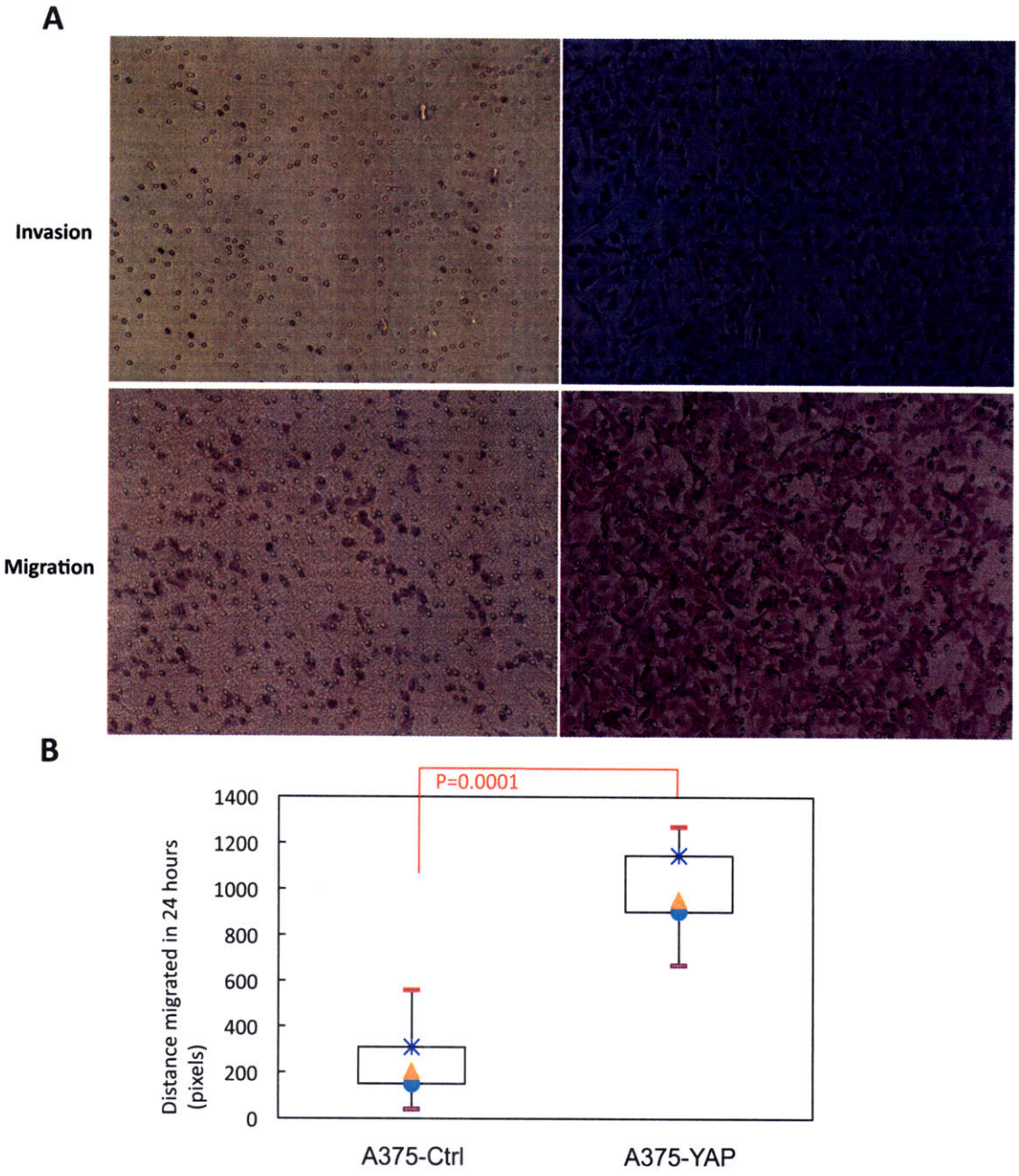

Figure 2. YAP significantly enhanced A375 cell migration and invasion. (A) Representative picture of the invasion assay (top) and migration assay (bottom) showed dramatically increased number of cells that invaded or migrated in transwell assays. **(B)** Scratch wound migration assay showed that A375-YAP cells migrate faster than A375-MIGw cells.

A

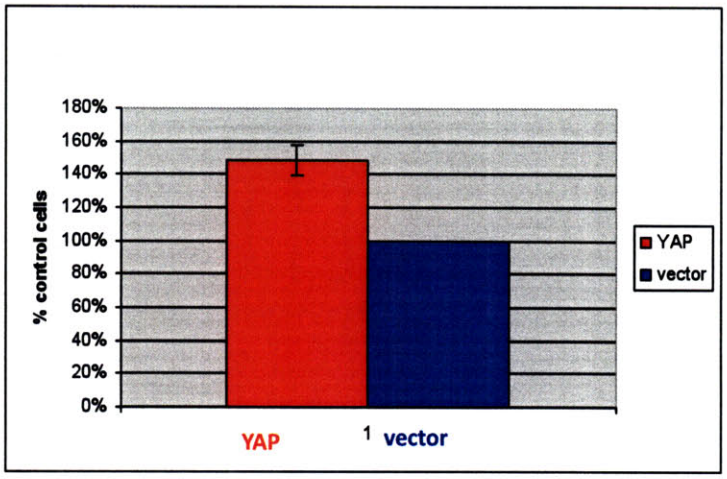

B

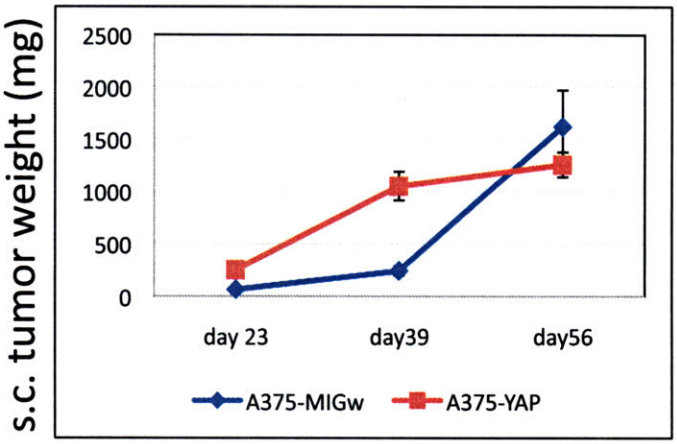

Figure 3. YAP significantly increases A375 cell proliferation and provides early advantage for tumor growth at the subcutaneous site. (A) Equal numbers of cells were seeded on day 0 and numbers of cells were counted on day3, and plotted as percent control cells. **(B)** 0.5*10e6 cells were injected at the subcutaneous site, and mice were dissected at indicated time points, and tumors were weighed. At 23 days and 39 days, tumors from A375-YAP cells are significantly bigger than those from control cells. However, by 8 weeks, tumor sizes are no longer different.

A

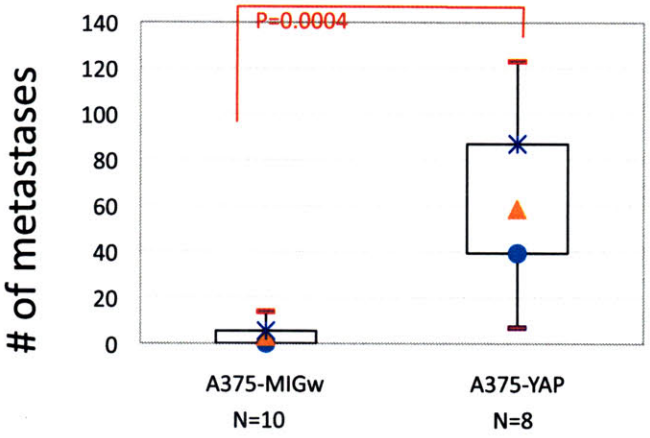

Figure 4. YAP significantly enhances lung metastasis and. NOD/SCID mice were injected with 1*10e6 cells via tail-vein and numbers of lung tumors were counted under UV dissecting microscope. YAP-expression significantly increased numbers of tumor nodules in the lung compared to control cells.

APPENDIX B.

METHODS USED FOR MASS SPECTROMETRY SAMPLE PREPARATION AND SAMPLE ANALYSIS

The content of this chapter were written by Hui Liu, with editing by Richard Hynes.

APPENDIX B. SILAC AND MASS SPECTROMETRY PROTOCOLS

SILAC medium was custom-made using the following formula:

	10L (mg)
L-Cystine	478.4
Glycine	300.0
L-histidine. HCl	382.0
L-phenylalanine	660.0
L-Serine	420.0
L-threonine	950.0
L-Tryptophan	160.0
L-Tyrosine	720.0
L-Valine	940.0
Isoleucine	1050.0
	10 L (g)
D-glucose	45
CaCl2	2
Fe(NO3)3. 9H2O	0.001
KCl	4
MgSO4. 7H2O	2
NaCl	64
NaH2PO4.H2O	1.24
Na Bicarbonate	22
Phenol Red	0.15
MEM vitamin stock	400ml
Adjust pH with concentrated HCl to 7.15	
Filter to sterilize and store in dark at 4^0C.	
Add the following before using	
Glutamine (100x)	
Leucine (60x: 6.3mg/ml)	Final
Methionine (100x: 3mg/ml)	
Arginine (100x: 8.4mg/ml)	
Lysine (14.6mg/ml)	Final 3.6mg/100ml
Dialyzed serum to 10%	
Sodium Pyrovate (100x)	
Pen/Strep (100x)	

Membrane Enrichment using Colloidal Silica beads

Reagents:
HBSS/5mMEDTA: 50ml HBSS + 0.5ml 0.5M stock. (warm up to 37^0C before use)
PMCB: 20mM MES/280mM Sorbitol/ 150mM NaCl, pH to 5.0-5.5
1% colloidal silica in PMCB: dilute from 30% provided by Dr. Donna Storz.
1mg/ml of polyacrytic acid (Sigma) in PMCB
Lysis buffer: 2.5mM imidazole (add protease inhibitor cocktail (Roche) before use)
100% Nycodenz (Sigma) : 10g in 5.5ml of lysis buffer containing protease inhibitors.
70% Nycodenz; dilute from 100%: 7ml 100% in 3ml lysis buffer, mix well.

Protocol:

1) Harvest cells
    a. Wash with 5ml of 37^0c HBSS/5mM EDTA. Rinse for the first two washes, and for the last wash, leave in 37^0C incubator for 7 min.
    b. Harvest A375 cells first by banning the plate with 5ml of HBSS/5mM EDTA, the cells should dislodge easily. Rinse with 5ml of HBSS/5mM EDTA and pool. MA2 cells do not dislodge as easily as A375, use 5ml glass pipette and pipette up and down gently to remove the cells. Again, rinse and pool.
    c. Before spinning down, take 10ul and count live and dead cells. Then spin 1100rpm for 3 min in the tissue culture room centrifuge.
    d. Place cells on ice for several minutes.

2) Coat cells with colloidal silica and polyacrytic acid (Do everything ON ICE).
    a. Resuspend cells in PMCB buffer to $1x10^7$/ml, keep on ice.
    b. In 50ml Falcon tube, add 5ml cold 1% colloidal silica. Use P1000, add cell suspension drop wise to the colloidal silica solution, swirl gently after each drop. Rock at 4C for 10-15 min. Then add 14ml of PMCB, mix gently once or twice. Repeat for the other cell line.
    c. Spin 1100rpm for 3min using the centrifuge in the chemical room at 4^0C. Aspirate the supernatant (Supt.)– milky white at this time. Shake the tube to dislodge the pellet before adding 35ml of PMCB, spin again and the supt. should be clear.
    d. Resuspend the cells in 1ml of PMCB, and keep on ice.
    e. In 50ml Falcon tube, add 5ml of 1mg/ml polyacy. Again, use P1000 to add cell suspension drop wise to the PAA solution, swirl gently after each drop. Then add 14ml of PMCB, mix gently.
    f. Spin 2000rpm for 3min using the centrifuge in the chemical room at 4^0C. Wash the pellet two more times with 20ml of PMCB at 2000rpm for 3min at 4^0C, aspirate the supernatant.

NOTE: Use 5ml 1% colloidal silica solution for every 10x10e6 cells.

3) Lyse cells (on ice).
    a. To each 10ml of lysis buffer (2.5mM Imidazole), add 1 tabelet of protease inhibitor cocktail (Roche), let dissolve and leave on ice.
    b. Add 0.5ml of lysis buffer to 0.5 $x10^6$ cells, leave on ice for 10-30min to swell.
    c. Transfer cells to pre-chilled parr bomb and increase pressure to 1500psi. Let the parr bomb sit on ice for 15min before releasing pressure to lyse the cells. Check cell lysis using trypan blue staining.

4) Fractionate cell lysate (all solutions 4^0C)
    a. Spin in the chemical room centrifuge at 2000rpm for 10mn at 4^0C. Take Supt,
    b. Resuspend pellet in same volume of lysis buffer as previous, save 50ul as Pellet I, pass through 26G needle to break up the clumps.
    c. To each 15ml Cortex glass centrifuge tube, add 2ml of 70% Nycodenz. Lay pellet from previous spin on top of Nycodenz, and centrifuge the solution at 28000rcf for 30min at 4^0C.
    d. After spinning, carefully take the top layer, middle layer (white), and bottom layer. Remove bottom layer as much as possible.
    e. Add 1ml of lysis buffer (containing protease inhibitors)t o collect the pellet and transfer into 1.5ml Eppendorf tube.
    f. Wash 4x with 2.5mM imidazole, pH7.0 (with protease inhibitors) in eppendorf tubess;
    g. Wash 3x with 100mM Na_2CO3, pH11.4 (with protease inhibitor); Centrifuge at 13000rpm in the tabletop centrifuge in the cold room for 5min to pellet. Freeze the final pellet with liquid nitrogen and store at -80^0C till use.

Sample Preparation and In-Gel Digestion

Thaw pellets collected from membrane preparation described above, and add 30µl of 2x SDS sample buffer (with β-mercaptoethanol). After heating at 95^{0}C for 5min with vortexing, the samples were loaded onto 4-20% gradient gel (Invitrogen) and electrophoresed at 150V till the front dye runs off. The gels were transferred to clean container, rinsed with autoclaved water and stained with SafeStain (Invitrogen), and 20-30 slices were cut from the gel. Following these steps, in-gel digestion was performed as described below.

1. Excision of protein bands from polyacrylamide gels
    a. Wash gel 2 with ddH20 ten minutes each
    b. Excise the band of interest. Cut as close to the protein band as possible to reduce the amount of "background" gel. Cut into 1mm x 1mm cubes and place in 0.65 ml tube (do not crush or clog pipet tips)

2. Washing gel pieces
    a. Wash the gel pieces with ~400µl of water,15 min.
    b. Wash with water/Acetonitrile 1:1, 15 min (vortex) (200µl+ 200 µl)
    c. Remove liquid, add acetonitrile to cover gel pieces (vortex)
    d. After pieces shrink and turn sticky white, remove acetonitrile
    e. Rehydrate in 100 mM NH_4HCO_3, vortex
    f. After 5 min, add equal volume of acetonitrile (to get 1:1 ratio) (vortex)
    g. Incubate 15 minutes then remove solvent
    h. Dry down in speed-vac
    i. Reduction and alkylation
    j. Rehydrate in 20mM DTT in 100 mM NH_4HCO_3
    k. Incubate at 65^{0}C for 30 min (vortex)
    l. Remove solvent, replace with same volume of 55 mM (10 mg/ml) iodoacetamide in 100 mM NH_4HCO_3
    m. Incubate 20 minutes at 37^{0}C in the dark
    n. Remove solvent
    o. Wash with $NH_4HCO_3$and Acetonitrile as in step 2e.
    p. All the Coomassie blue stain should be removed at this time. If residual Coomassie still remains, repeat wash with NH_4HCO_3/Acetonitrile (1:1) until no longer see blue color
    q. Gel pieces should be dried completely in speed-vac

3. In-gel Digestion
    a. Dilute 20 ug of Promega sequencing grade modified trypsin in 200 ul of 50 mM A NH_4HCO_3 (0.1 ug/ul) (trypsin solution)
    b. Dilute trypsin solution 1:10 in 50 mM AMBIC (10 ng/ul trypsin solution)
    c. Add 60 ul of 10 ng/ul trypsin solution to gel pieces and leave on ice for 1 hour. Check every 15min to make sure the solution is enough to cover the gel pieces.
    d. Incubate at 37°C overnight

4. Extraction of Peptides (never let the supernatant go dry, just concentrate (~10µl)
    a. Transfer the supt. Into a clean (low-binding) 0.6ml tube, dry in the speed-vec;
    b. Rinse with 50mM NH_4HCO_3, pool into the speed-vacing tube
    c. Add 100µl 50% acetonitrile /5% formic acid, vortex at R.T. for 30min, collect and pool into the tube in speed-vec;
    d. Rehydrate with 50µl 50mM NH_4HCO_3, vortex 10min, then add 100µl 50% MeCN/5%Formic acid, vortex at RT for 30min, collect supt and pool
    e. Rehydrate in minimum volume of 50mM AMBIC, vortex 10min, then add excess 100% acetonitrile, vortex for 20min, collect supt and pool;
    f. Dry down to ~5-10µl, and reconstitute with 0.1% formic acid in ddH_2O.

Mass spectrometry analysis of digested peptides

One-third peptides from each gel slice were analyzed using liquid chromatography tandem mass spectrometry (LC-MS/MS) with the LTQ ion-trap mass spectrometer from Thermo Finnigan. Each sample was loaded onto a 50 um (i.d.) by10 cm (length) fused silica C18 microcapillary column (New Objective, MA) using an Agilent 1100 (Agilent Corporation, CA) series binary HPLC pump with auto-sampler and nanoflow cell with an in-line flow splitter to achieve approximately 100nl/min flow at the tip of the column. Peptides were eluted with a 120min linear gradient as the following: 2% to 37.5% buffer B from 0 to 75 min, 37.5% to 75% buffer B from 75min to 105min, and 75% to 98% B from 105 min to 120 min (buffer B: 0.1% formic acid, 80% acetonitrile). Eluted peptides were introduced to LTQ mass spectrometer via electrospray ionization and data-dependent acquisition was performed, with exclusion list activated and top 10 ions are selected for fragmentation to obtain peptide sequence information.

Data collected by mass spectrometer were analyzed using Sequest software, searched against human database, which is maintained by the biopolymer lab at Koch Institute. When search peptides, we used filter of $\Delta Cn > 0.1$, and Xcorr value of 2, 2.5, 3.5 for peptides with +1, +2, or +3 charges, respectively and $p<0.0001$. We also visually inspected the spectrum when there were less than 3 peptides matched to the proteins.

SILAC and Identification of Proteins that are differentially expressed

Passage-matched A375 (low metastatic cells) and MA2 (high metastatic cells) were grown in "light" (Arg0, Lys 0) and "heavy" (Arg10, Lys 8) respectively, equal amount of total cell lysate from these two cell lines were mixed and plasma membrane preparations were made (Figure 3). A total of 80μg of membrane proteins were separated on 4-20% gel and 20 gel slices were cut and in-gel digested. Samples were analyzed with LC-MS/MS as mentioned above; with slight modification of sample-acquire method. Briefly, during gradient elution, following a MS scan, zoom scan spectrum and MS/MS spectrum were obtained for each of the top 5 abundant ions per data-dependent cycle. The zoom scan spectrum was included to get a high-resolution spectrum, which can be used by quantification software (PepQuan) to quantify peptides/proteins. Data were analyzed with Sequest for protein identification, and with PepQuan for protein quantification.

APPENDIX C.

PROTEINS IDENTIFIED THROUGH MASS SPECTROMETRY ANALYSIS

The work in The content of this chapter were written by Hui Liu.

Accession	Reference	MW	Peptide (Hits)	P (pro)
A0AVT1	UBA6_HUMAN (A0AVT1) Ubiquitin-like modifier-activating enzyme 6 OS=Homo sapiens GN=UBA6 PE=1 SV=	117895.2	2 (2 0 0 0 0)	1.65E-07
A0FGR8	ESYT2_HUMAN (A0FGR8) Extended synaptotagmin-2 OS=Homo sapiens GN=FAM62B PE=1 SV=1	102294.1	1 (1 0 0 0 0)	2.95E-07
A1L3U3	A1L3U3_HUMAN (A1L3U3) ABCA8 protein OS=Homo sapiens GN=ABCA8 PE=2 SV=1	183585.3	2 (2 0 0 0 0)	6.57E-09
A2A2L6	SERA_HUMAN (O43175) D-3-phosphoglycerate dehydrogenase OS=Homo sapiens GN=PHGDH PE=1 SV=4	26057.7	1 (1 0 0 0 0)	2.12E-05
A2BF29	A2BF29_HUMAN (A2BF29) Major histocompatibility complex class I B (Fragment) OS=Homo sapiens GN=HL	27751.5	2 (1 1 0 0 0)	1.47E-07
A4D0W6	A4D0W6_HUMAN (A4D0W6) Similar to ribosomal protein L18; 60S ribosomal protein L18 OS=Homo sapiens (	24907.0	1 (0 1 0 0 0)	1.88E-06
A4D0W6	A4D0W6_HUMAN (A4D0W6) Similar to ribosomal protein L18; 60S ribosomal protein L18 OS=Homo sapiens (	24907.0	1 (0 1 0 0 0)	2.22E-06
A4D0Y7	A4D0Y7_HUMAN (A4D0Y7) Similar to 40S ribosomal protein S2 OS=Homo sapiens GN=LOC392781 PE=3 SV	21055.3	5 (5 0 0 0 0)	3.78E-09
A4D1G5	A4D1G5_HUMAN (A4D1G5) Ribosomal protein S27 OS=Homo sapiens GN=LOC392748 PE=3 SV=1	16866.6	4 (4 0 0 0 0)	9.18E-08
A4D1Q5	A4D1Q5_HUMAN (A4D1Q5) Ribosomal protein L15 OS=Homo sapiens GN=LOC136321 PE=3 SV=1	23754.9	4 (4 0 0 0 0)	6.61E-11
A4D2P0	A4D2P0_HUMAN (A4D2P0) cDNA FLJ77333, highly similar to Homo sapiens ras-related C3 botulinum toxin s	23452.3	7 (7 0 0 0 0)	9.30E-09
A4URH5	A4URH5_HUMAN (A4URH5) MHC class I antigen (Fragment) OS=Homo sapiens GN=HLA-A PE=3 SV=1	31240.9	1 (1 0 0 0 0)	1.09E-09
A5D8X1	A5D8X1_HUMAN (A5D8X1) FLJ45422 protein OS=Homo sapiens GN=FLJ45422 PE=2 SV=1	18590.3	1 (0 1 0 0 0)	7.11E-06
A5JGZ4	A5JGZ4_HUMAN (A5JGZ4) Non-functional aryl hydrocarbon receptor interacting protein (Fragment) OS=Hom	40737.8	9 (9 0 0 0 0)	2.61E-08
A5JGZ4	A5JGZ4_HUMAN (A5JGZ4) Non-functional aryl hydrocarbon receptor interacting protein (Fragment) OS=Hom	40737.8	2 (2 0 0 0 0)	5.32E-08
A5YKK6	CNOT1_HUMAN (A5YKK6) CCR4-NOT transcription complex subunit 1 OS=Homo sapiens GN=CNOT1 PE=1	266765.7	2 (2 0 0 0 0)	1.97E-06
A6NBZ8	A6NBZ8_HUMAN (A6NBZ8) Putative uncharacterized protein ALB OS=Homo sapiens GN=ALB PE=4 SV=2	71657.7	3 (3 0 0 0 0)	7.58E-12
A6NDU1	A6NDU1_HUMAN (A6NDU1) Putative uncharacterized protein ENSP00000364356 (Fragment) OS=Homo sap	32767.3	1 (1 0 0 0 0)	1.82E-08
A6NDZ9	A6NDZ9_HUMAN (A6NDZ9) Putative uncharacterized protein PELP1 OS=Homo sapiens GN=PELP1 PE=4 S	110017.4	1 (1 0 0 0 0)	4.17E-09
A6NE05	A6NE05_HUMAN (A6NE05) Putative uncharacterized protein RPL26P6 OS=Homo sapiens GN=RPL26P6 PE	18243.2	4 (4 0 0 0 0)	4.50E-05
A6NEC0	A6NEC0_HUMAN (A6NEC0) Putative uncharacterized protein MAGOHB OS=Homo sapiens GN=MAGOHB P	12947.7	2 (2 0 0 0 0)	1.92E-05
A6NG51	A6NG51_HUMAN (A6NG51) Putative uncharacterized protein SPTAN1 OS=Homo sapiens GN=SPTAN1 PE=4	284770.7	4 (23 1 0 0 0)	5.45E-13
A6NGR5	A6NGR5_HUMAN (A6NGR5) Putative uncharacterized protein ENSP00000353405 OS=Homo sapiens PE=3 S	31277.3	2 (2 0 0 0 0)	2.73E-08
A6NGR5	A6NGR5_HUMAN (A6NGR5) Putative uncharacterized protein ENSP00000353405 OS=Homo sapiens PE=3 S	31277.3	4 (4 0 0 0 0)	2.15E-07
A6NHL2	TBAL3_HUMAN (A6NHL2) Tubulin alpha chain-like 3 OS=Homo sapiens GN=TUBAL3 PE=1 SV=2	49876.8	2 (2 0 0 0 0)	2.52E-10
A6NHQ2	FBRLL_HUMAN (A6NHQ2) rRNA/tRNA 2'-O-methyltransferase fibrillarin-like OS=Homo sapiens PE=3 SV=1	34654.0	1 (1 0 0 0 0)	9.59E-07
A6NK82	A6NK82_HUMAN (A6NK82) Putative uncharacterized protein COL4A1 OS=Homo sapiens GN=COL4A1 PE=4	160642.1	4 (4 0 0 0 0)	2.46E-11
A6NN38	A6NN38_HUMAN (A6NN38) Coactivator-associated arginine methyltransferase 1, isoform CRA_b OS=Homo s	65811.5	3 (3 0 0 0 0)	1.76E-08
A6NNZ2	TBB8B_HUMAN (A6NNZ2) Tubulin beta-8 chain B OS=Homo sapiens PE=3 SV=1	49540.7	4 (4 0 0 0 0)	1.85E-09
A6XMH5	A6XMH5_HUMAN (A6XMH5) Beta-2-microglobulin OS=Homo sapiens PE=4 SV=1	10392.4	2 (2 0 0 0 0)	1.14E-07
A7YDY3	A7YDY3_HUMAN (A7YDY3) BolA homolog 2 (E. coli) OS=Homo sapiens GN=BOLA2 PE=2 SV=1	16921.8	1 (1 0 0 0 0)	2.59E-07
A8K8Z5	A8K8Z5_HUMAN (A8K8Z5) cDNA FLJ76682, highly similar to Homo sapiens v-Ki-ras2 Kirsten rat sarcoma vira	21410.9	1 (1 0 0 0 0)	1.32E-05
A8MQ38	A8MQ38_HUMAN (A8MQ38) Putative uncharacterized protein NOL1 OS=Homo sapiens GN=NOL1 PE=4 SV=	93925.4	5 (5 0 0 0 0)	2.39E-08
A8MSK1	A8MSK1_HUMAN (A8MSK1) Lysyl-tRNA synthetase OS=Homo sapiens GN=KARS PE=3 SV=1	71451.6	1 (1 0 0 0 0)	5.87E-07
A8MT02	A8MT02_HUMAN (A8MT02) Putative uncharacterized protein SNRPB OS=Homo sapiens GN=SNRPB PE=4 S	29851.2	2 (2 0 0 0 0)	2.35E-08
A8MT80	A8MT80_HUMAN (A8MT80) Ribosomal protein L15 OS=Homo sapiens PE=3 SV=1	21971.5	2 (2 0 0 0 0)	1.20E-07
A8MTF2	A8MTF2_HUMAN (A8MTF2) Putative uncharacterized protein ENSP00000382149 (Fragment) OS=Homo sapi	32818.3	1 (1 0 0 0 0)	3.04E-05
A8MTH6	A8MTH6_HUMAN (A8MTH6) Putative uncharacterized protein SRI (Fragment) OS=Homo sapiens GN=SRI PE	23627.7	2 (2 0 0 0 0)	2.81E-06
A8MTN7	A8MTN7_HUMAN (A8MTN7) Putative uncharacterized protein NACA OS=Homo sapiens GN=NACA PE=4 SV	23367.7	2 (1 0 1 0 0)	4.91E-08
A8MUM5	A8MUM5_HUMAN (A8MUM5) Putative uncharacterized protein TOR1AIP1 OS=Homo sapiens GN=TOR1AIP1	66279.4	3 (3 0 0 0 0)	6.89E-10
A8MUS3	A8MUS3_HUMAN (A8MUS3) Putative uncharacterized protein RPL23A OS=Homo sapiens GN=RPL23A PE=	21902.5	2 (12 0 0 0 0)	1.67E-08
A8MUS3	A8MUS3_HUMAN (A8MUS3) Putative uncharacterized protein RPL23A OS=Homo sapiens GN=RPL23A PE=	21902.5	2 (2 0 0 0 0)	6.61E-08
A8MUT7	A8MUT7_HUMAN (A8MUT7) Putative uncharacterized protein ENSP00000380341 OS=Homo sapiens PE=3 S	44789.3	3 (2 1 0 0 0)	3.40E-07
A8MUW5	A8MUW5_HUMAN (A8MUW5) Putative uncharacterized protein FAM98B OS=Homo sapiens GN=FAM98B PE	45518.6	2 (2 0 0 0 0)	4.43E-07
A8MVJ4	A8MVJ4_HUMAN (A8MVJ4) Proteasome subunit alpha type (Fragment) OS=Homo sapiens GN=PSMA1 PE=	30147.3	2 (2 0 0 0 0)	2.07E-07
A8MWM6	A8MWM6_HUMAN (A8MWM6) Putative uncharacterized protein ENSP00000383763 (Fragment) OS=Homo sa	44849.5	1 (1 0 0 0 0)	1.09E-06
A8MWY5	A8MWY5_HUMAN (A8MWY5) Putative uncharacterized protein ENSP00000382197 OS=Homo sapiens PE=3	12651.0	3 (3 0 0 0 0)	5.21E-05
A8MXB0	MGN3_HUMAN (A8MXB0) Putative protein mago nashi homolog 3 OS=Homo sapiens GN=MAGOHP PE=5 S	17333.8	2 (2 0 0 0 0)	2.48E-07
A8MY04	A8MY04_HUMAN (A8MY04) Putative uncharacterized protein ENSP00000381447 (Fragment) OS=Homo sapi	32398.2	2 (2 0 0 0 0)	5.14E-07
A8MYK1	A8MYK1_HUMAN (A8MYK1) Putative uncharacterized protein MRPL23 OS=Homo sapiens GN=MRPL23 PE=	21828.7	1 (1 0 0 0 0)	3.81E-04
A9R9N7	A9R9N7_HUMAN (A9R9N7) Major histocompatibility complex, class I, A OS=Homo sapiens GN=HLA-A PE=3	41423.5	4 (4 0 0 0 0)	2.72E-07
B0QYK0	B0QYK0_HUMAN (B0QYK0) Ewing sarcoma breakpoint region 1 OS=Homo sapiens GN=EWSR1 PE=4 SV=1	64889.0	2 (2 0 0 0 0)	2.46E-08
B0YIW6	B0YIW6_HUMAN (B0YIW6) Coatomer subunit delta variant 2 (Archain 1, isoform CRA_a) OS=Homo sapiens (	61587.4	4 (4 0 0 0 0)	5.13E-08
B1AHD1	B1AHD1_HUMAN (B1AHD1) NHP2 non-histone chromosome protein 2-like 1 (S. cerevisiae) OS=Homo sapien	14617.9	2 (2 0 0 0 0)	4.69E-07
B1AK40	B1AK40_HUMAN (B1AK40) Fumarylacetoacetate hydrolase domain containing 1 OS=Homo sapiens GN=FAH	27110.9	5 (5 0 0 0 0)	1.26E-07
B1AM21	B1AM21_HUMAN (B1AM21) Guanine nucleotide binding protein (G protein), q polypeptide (Fragment) OS=Ho	19668.8	2 (2 0 0 0 0)	3.32E-10
B1AP13	B1AP13_HUMAN (B1AP13) CD55 molecule, decay accelerating factor for complement (Cromer blood group) (	49306.7	1 (1 0 0 0 0)	1.12E-06
B1B5Y2	B1B5Y2_HUMAN (B1B5Y2) Tyrosine-protein kinase receptor (Fragment) OS=Homo sapiens GN=IGF1R PE=2	155746.4	1 (1 0 0 0 0)	6.70E-08
B1PS43	B1PS43_HUMAN (B1PS43) Myosin heavy chain 11 smooth muscle isoform OS=Homo sapiens GN=MYH11 P	234090.7	2 (2 0 0 0 0)	2.45E-05
B2CI53	B2CI53_HUMAN (B2CI53) Solute carrier family 4 sodium bicarbonate cotransporter member 7 OS=Homo sapi	127278.0	7 (7 0 0 0 0)	1.07E-11
B2RAR6	B2RAR6_HUMAN (B2RAR6) cDNA, FLJ95068, highly similar to Homo sapiens eukaryotic translation elongatic	71406.3	2 (2 0 0 0 0)	6.37E-08
B2RBK5	B2RBK5_HUMAN (B2RBK5) cDNA, FLJ95559, Homo sapiens dynactin 2 (p50) (DCTN2), mRNA OS=Homo sa	44792.2	2 (2 0 0 0 0)	1.67E-11
B2RDW1	B2RDW1_HUMAN (B2RDW1) cDNA, FLJ96793, Homo sapiens ribosomal protein S27a (RPS27A), mRNA (Ri	17953.5	3 (3 0 0 0 0)	6.64E-08
B2REA7	B2REA7_HUMAN (B2REA7) Ribosomal protein L36a OS=Homo sapiens GN=RPL36A PE=4 SV=1	13219.1	2 (2 0 0 0 0)	1.46E-05
B2RWP9	B2RWP9_HUMAN (B2RWP9) MYH10 protein OS=Homo sapiens GN=MYH10 PE=2 SV=1	229887.5	6 (26 0 0 0 0)	7.08E-13
B2ZZ91	B2ZZ91_HUMAN (B2ZZ91) Golgin B1 OS=Homo sapiens GN=GOLGB1 PE=2 SV=1	376889.9	1 (1 0 0 0 0)	2.77E-05
B3KML9	B3KML9_HUMAN (B3KML9) cDNA FLJ11352 fis, clone HEMBA1000020, highly similar to Tubulin beta-2C cha	44573.6	8 (17 0 1 0 0)	1.58E-12
B3KNY2	B3KNY2_HUMAN (B3KNY2) cDNA FLJ30723 fis, clone FCBBF4000282, highly similar to Homo sapiens electr	37411.0	5 (5 0 0 0 0)	2.97E-10
B3KPJ9	B3KPJ9_HUMAN (B3KPJ9) cDNA FLJ31884 fis, clone NT2RP7002906, highly similar to Homo sapiens heat s	98051.4	4 (3 0 0 0 1)	6.94E-10
B3KPU1	B3KPU1_HUMAN (B3KPU1) cDNA FLJ32188 fis, clone PLACE6002056, highly similar to Guanine nucleotide-	25914.1	2 (2 0 0 0 0)	1.45E-05
B3KQ79	B3KQ79_HUMAN (B3KQ79) cDNA FLJ33051 fis, clone TRACH1000063, highly similar to B-cell receptor-asso	34730.3	7 (7 0 0 0 0)	1.13E-05
B3KRQ1	SSRA_HUMAN (P43307) Translocon-associated protein subunit alpha OS=Homo sapiens GN=SSR1 PE=1 SV	20919.5	2 (12 0 0 0 0)	4.65E-08
B3KSQ1	B3KSQ1_HUMAN (B3KSQ1) cDNA FLJ36768 fis, clone ADIPS1000064, highly similar to Synaptic glycoprotein	37442.6	2 (2 0 0 0 0)	2.82E-05
B3KSQ6	B3KSQ6_HUMAN (B3KSQ6) cDNA FLJ36801 fis, clone ADRGL2007810, highly similar to NADPH:adrenodoxi	41483.7	2 (2 0 0 0 0)	4.68E-11
B3KSR7	B3KSR7_HUMAN (B3KSR7) cDNA FLJ36831 fis, clone ASTRO2010615, highly similar to Calpain-5 (EC 3.4.22	64005.6	4 (4 0 0 0 0)	6.87E-10

B3KT15	B3KT15_HUMAN (B3KT15) cDNA FLJ37456 fis, clone BRAWH2011096, highly similar to 26S proteasome non	42915.1	2 (10 2 0 0 0)	1.77E-12
B3KTZ0	B3KTZ0_HUMAN (B3KTZ0) cDNA FLJ38980 fis, clone NT2RI2004884, highly similar to Guanine nucleotide-bi	38712.1	6 (6 0 0 0 0)	1.77E-09
B3KUY2	B3KUY2_HUMAN (B3KUY2) cDNA FLJ40895 fis, clone UTERU2002294, highly similar to Prostaglandin E syn	19436.2	2 (2 0 0 0 0)	1.21E-07
B3KX11	B3KX11_HUMAN (B3KX11) cDNA FLJ44436 fis, clone UTERU2019706, highly similar to T-complex protein 1 s	57909.1	6 (6 0 0 0 0)	6.33E-06
B3KXN4	B3KXN4_HUMAN (B3KXN4) cDNA FLJ45763 fis, clone N1ESE2000698, highly similar to WD repeat protein 1	62077.8	1 (1 0 0 0 0)	3.13E-06
B3KXY9	B3KXY9_HUMAN (B3KXY9) cDNA FLJ46359 fis, clone TESTI4049786, highly similar to Hexokinase-1 (EC 2.7	106183.4	2 (2 0 0 0 0)	1.36E-05
B3KY95	B3KY95_HUMAN (B3KY95) cDNA FLJ16143 fis, clone BRAMY2038516, highly similar to Protein disulfide-isor	53255.9	6 (6 0 0 0 0)	2.28E-10
B4DDR3	B4DDR3_HUMAN (B4DDR3) cDNA FLJ52148, highly similar to Apoptosis inhibitor 5 OS=Homo sapiens PE=2	37484.7	1 (1 0 0 0 0)	9.58E-06
B4DE31	B4DE31_HUMAN (B4DE31) cDNA FLJ54957, highly similar to Transketolase (EC 2.2.1.1) OS=Homo sapiens	68698.3	2 (12 0 0 0 0)	1.41E-09
B4DEA8	B4DEA8_HUMAN (B4DEA8) cDNA FLJ56425, highly similar to Very-long-chain specific acyl-CoAdehydrogena	75162.9	5 (5 0 0 0 0)	2.11E-10
B4DEH1	B4DEH1_HUMAN (B4DEH1) cDNA FLJ60436, highly similar to Homo sapiens dolichyl-phosphate mannosyltra	18346.9	4 (4 0 0 0 0)	2.37E-08
B4DEZ3	B4DEZ3_HUMAN (B4DEZ3) cDNA FLJ57958, highly similar to NADH dehydrogenase (ubiquinone) 1 alpha sul	14076.3	3 (3 0 0 0 0)	1.59E-09
B4DF76	B4DF76_HUMAN (B4DF76) cDNA FLJ59191, highly similar to NADH dehydrogenase (ubiquinone) 1 alpha sub	24865.8	2 (2 0 0 0 0)	4.80E-06
B4DFX8	B4DFX8_HUMAN (B4DFX8) cDNA FLJ56065, highly similar to Pyruvate kinase isozyme M1 (EC 2.7.1.40) OS=	65888.9	7 (17 0 0 0 0)	4.65E-12
B4DGE8	B4DGE8_HUMAN (B4DGE8) cDNA FLJ55467, highly similar to Septin-2 OS=Homo sapiens PE=2 SV=1	45432.3	6 (6 0 0 0 0)	1.36E-09
B4DGP8	B4DGP8_HUMAN (B4DGP8) cDNA FLJ55574, highly similar to Calnexin OS=Homo sapiens PE=2 SV=1	71458.0	8 (8 0 0 0 0)	2.06E-12
B4DGY2	B4DGY2_HUMAN (B4DGY2) cDNA FLJ59683, highly similar to Homo sapiens malignant T cell amplified sequ	20536.8	4 (4 0 0 0 0)	1.91E-06
B4DHQ3	B4DHQ3_HUMAN (B4DHQ3) cDNA FLJ56437, highly similar to Phosphoserine aminotransferase (EC 2.6.1.52	45326.5	3 (3 0 0 0 0)	8.06E-07
B4DI54	B4DI54_HUMAN (B4DI54) cDNA FLJ56386, highly similar to Heat shock 70 kDa protein 1L OS=Homo sapiens	77513.3	6 (6 0 0 0 0)	2.10E-09
B4DIM0	B4DIM0_HUMAN (B4DIM0) cDNA FLJ56442, highly similar to ATP-citrate synthase (EC 2.3.3.8) OS=Homo sa	125057.5	4 (14 0 0 0 0)	5.76E-10
B4DJ30	B4DJ30_HUMAN (B4DJ30) cDNA FLJ61290, highly similar to Neutral alpha-glucosidase AB OS=Homo sapien	112854.8	0 (10 0 0 0 0)	1.49E-09
B4DJ60	B4DJ60_HUMAN (B4DJ60) cDNA FLJ55072, highly similar to Succinate dehydrogenase (ubiquinone) flavopro	67207.0	2 (2 0 0 0 0)	1.24E-07
B4DJQ5	B4DJQ5_HUMAN (B4DJQ5) cDNA FLJ59211, highly similar to Glucosidase 2 subunit beta OS=Homo sapiens	60096.3	2 (2 0 0 0 0)	3.27E-08
B4DJV9	B4DJV9_HUMAN (B4DJV9) cDNA FLJ60607, highly similar to Acyl-protein thioesterase 1 (EC 3.1.2.-) OS=Hor	28260.3	2 (2 0 0 0 0)	1.78E-07
B4DKS0	B4DKS0_HUMAN (B4DKS0) cDNA FLJ53381, highly similar to Monocarboxylate transporter 1 OS=Homo sapi	51802.8	2 (2 0 0 0 0)	5.70E-08
B4DKW1	B4DKW1_HUMAN (B4DKW1) cDNA FLJ55703, highly similar to Solute carrier family 2, facilitated glucose tran	47789.2	4 (4 0 0 0 0)	5.34E-09
B4DL07	B4DL07_HUMAN (B4DL07) cDNA FLJ53353, highly similar to ATP-binding cassette sub-family D member 3 O	78410.0	1 (1 0 0 0 0)	3.94E-07
B4DL12	B4DL12_HUMAN (B4DL12) cDNA FLJ53754, highly similar to Transmembrane emp24 domain-containing prot	20046.5	5 (5 0 0 0 0)	3.49E-09
B4DLC0	B4DLC0_HUMAN (B4DLC0) cDNA FLJ58476, highly similar to Poly(rC)-binding protein 2 OS=Homo sapiens P	32144.4	4 (4 0 0 0 0)	8.10E-11
B4DLU5	B4DLU5_HUMAN (B4DLU5) cDNA FLJ60675, highly similar to ATP-dependent RNA helicase DDX3X (EC 3.6.	58737.6	1 (1 0 0 0 0)	2.83E-05
B4DLV7	B4DLV7_HUMAN (B4DLV7) cDNA FLJ60299, highly similar to Rab GDP dissociation inhibitor beta OS=Homo	51121.3	1 (1 0 0 0 0)	2.74E-07
B4DM70	B4DM70_HUMAN (B4DM70) cDNA FLJ54451, highly similar to Stress-induced-phosphoprotein 1 OS=Homo sa	59769.0	4 (4 0 0 0 0)	1.04E-06
B4DM97	B4DM97_HUMAN (B4DM97) cDNA FLJ55002, highly similar to Alpha-centractin OS=Homo sapiens PE=2 SV=	38250.7	2 (2 0 0 0 0)	2.04E-11
B4DMB1	B4DMB1_HUMAN (B4DMB1) cDNA FLJ53358, highly similar to Heterogeneous nuclear ribonucleoprotein R O	66966.3	5 (5 0 0 0 0)	2.22E-08
B4DMH5	B4DMH5_HUMAN (B4DMH5) cDNA FLJ55107, highly similar to Cell division control protein 42 homolog OS=H	26562.4	4 (4 0 0 0 0)	1.14E-05
B4DMJ2	B4DMJ2_HUMAN (B4DMJ2) cDNA FLJ50994, moderately similar to 60S ribosomal protein L4 OS=Homo sapie	27046.2	5 (5 0 0 0 0)	1.21E-08
B4DMJ5	B4DMJ5_HUMAN (B4DMJ5) cDNA FLJ53012, highly similar to Tubulin beta-7 chain OS=Homo sapiens PE=2	27289.9	9 (8 1 0 0 0)	1.35E-11
B4DMU8	B4DMU8_HUMAN (B4DMU8) cDNA FLJ53063, highly similar to Tubulin beta-7 chain OS=Homo sapiens PE=2	35897.4	2 (2 0 0 0 0)	3.00E-08
B4DNA3	B4DNA3_HUMAN (B4DNA3) cDNA FLJ53068, highly similar to Adenylyl cyclase-associated protein 1 OS=Hon	47091.3	1 (1 0 0 0 0)	1.27E-07
B4DNC0	B4DNC0_HUMAN (B4DNC0) cDNA FLJ61141, highly similar to Ras-related protein Rab-34 OS=Homo sapiens	30596.7	3 (3 0 0 0 0)	1.19E-09
B4DNH8	B4DNH8_HUMAN (B4DNH8) cDNA FLJ59138, highly similar to Annexin A2 OS=Homo sapiens PE=2 SV=1	21656.1	0 (10 0 0 0 0)	9.82E-11
B4DNK3	B4DNK3_HUMAN (B4DNK3) cDNA FLJ52127, highly similar to Multisynthetase complex auxiliary component p	29726.8	4 (4 0 0 0 0)	4.20E-08
B4DNK4	B4DNK4_HUMAN (B4DNK4) cDNA FLJ53368, highly similar to Pyruvate kinase isozymes M1/M2 (EC 2.7.1.40	49866.0	1 (1 0 0 0 0)	5.68E-05
B4DNL8	B4DNL8_HUMAN (B4DNL8) cDNA FLJ58851, highly similar to Galactosylgalactosylxylosyl protein 3-beta-gluc	34633.3	1 (1 0 0 0 0)	2.15E-09
B4DNV4	B4DNV4_HUMAN (B4DNV4) cDNA FLJ53071, highly similar to Heat shock 70 kDa protein 1 OS=Homo sapien	25262.9	1 (1 0 0 0 0)	7.69E-07
B4DNX1	B4DNX1_HUMAN (B4DNX1) cDNA FLJ53752, highly similar to Heat shock 70 kDa protein 1 OS=Homo sapien	45099.1	2 (2 0 0 0 0)	2.39E-09
B4DP54	B4DP54_HUMAN (B4DP54) cDNA FLJ52712, highly similar to Tubulin beta-6 chain OS=Homo sapiens PE=2 S	46671.6	2 (1 0 0 1 0)	6.67E-06
B4DP82	B4DP82_HUMAN (B4DP82) cDNA FLJ51018, highly similar to 60S ribosomal protein L4 OS=Homo sapiens PE	16561.4	2 (2 0 0 0 0)	1.39E-07
B4DPJ2	B4DPJ2_HUMAN (B4DPJ2) cDNA FLJ51518, highly similar to Annexin A11 OS=Homo sapiens PE=2 SV=1	45569.3	1 (1 0 0 0 0)	3.19E-06
B4DPZ4	B4DPZ4_HUMAN (B4DPZ4) cDNA FLJ60782, highly similar to Rho-GTPase-activating protein 1 OS=Homo sa	52722.6	1 (1 0 0 0 0)	1.41E-06
B4DQU4	B4DQU4_HUMAN (B4DQU4) cDNA FLJ60809, highly similar to Homo sapiens cytokeratin type II (K6HF), mRN	65321.0	2 (0 2 0 0 0)	1.47E-06
B4DR52	B4DR52_HUMAN (B4DR52) cDNA FLJ56787, highly similar to Histone H2B type 2-F OS=Homo sapiens PE=2	18029.7	2 (2 0 0 0 0)	1.01E-06
B4DR52	B4DR52_HUMAN (B4DR52) cDNA FLJ56787, highly similar to Histone H2B type 2-F OS=Homo sapiens PE=2	18029.7	3 (3 0 0 0 0)	1.05E-05
B4DR61	B4DR61_HUMAN (B4DR61) cDNA FLJ59739, highly similar to Protein transport protein Sec61 subunit alpha is	52915.0	1 (1 0 0 0 0)	2.85E-05
B4DRJ2	B4DRJ2_HUMAN (B4DRJ2) cDNA FLJ61353, highly similar to Apoptosis inhibitor 5 OS=Homo sapiens PE=2 S	58968.0	1 (1 0 0 0 0)	2.14E-05
B4DRS6	B4DRS6_HUMAN (B4DRS6) cDNA FLJ58980, highly similar to Sideroflexin-3 OS=Homo sapiens PE=2 SV=1,	36326.9	3 (3 0 0 0 0)	1.05E-10
B4DRT2	B4DRT2_HUMAN (B4DRT2) cDNA FLJ54536, highly similar to Mitochondrial 28S ribosomal protein S27 OS=H	49119.1	1 (1 0 0 0 0)	4.47E-09
B4DRY3	B4DRY3_HUMAN (B4DRY3) cDNA FLJ52228, highly similar to Mps one binder kinase activator-like 1A OS=Ho	25482.8	1 (1 0 0 0 0)	1.29E-04
B4DS71	B4DS71_HUMAN (B4DS71) cDNA FLJ57081, moderately similar to WD repeat protein 1 OS=Homo sapiens P	22409.6	2 (2 0 0 0 0)	2.68E-09
B4DS84	B4DS84_HUMAN (B4DS84) cDNA FLJ59747, highly similar to Ubiquitin carboxyl-terminal hydrolase 10 (EC 3.	87477.1	2 (2 0 0 0 0)	3.04E-05
B4DSR4	B4DSR4_HUMAN (B4DSR4) cDNA FLJ59973, highly similar to Elongation factor 1-gamma OS=Homo sapiens	18479.3	1 (1 0 0 0 0)	3.39E-07
B4DT29	B4DT29_HUMAN (B4DT29) cDNA FLJ51082, highly similar to Actin-like protein 3 OS=Homo sapiens PE=2 SV	40673.7	1 (1 0 0 0 0)	6.31E-07
B4DTE6	B4DTE6_HUMAN (B4DTE6) cDNA FLJ56243, highly similar to Melanoma-associated antigen 4 OS=Homo sap	37810.3	2 (2 0 0 0 0)	1.91E-06
B4DTG2	B4DTG2_HUMAN (B4DTG2) cDNA FLJ56389, highly similar to Elongation factor 1-gamma OS=Homo sapiens	56114.4	2 (2 0 0 0 0)	1.60E-09
B4DUJ2	B4DUJ2_HUMAN (B4DUJ2) cDNA FLJ54063, highly similar to Homo sapiens CD74 antigen, transcript variant	16659.2	1 (1 0 0 0 0)	1.17E-10
B4DUQ1	B4DUQ1_HUMAN (B4DUQ1) cDNA FLJ54552, highly similar to Heterogeneous nuclear ribonucleoprotein K O	48480.2	5 (5 0 0 0 0)	4.58E-10
B4DUT2	B4DUT2_HUMAN (B4DUT2) cDNA FLJ53206 OS=Homo sapiens PE=2 SV=1	88141.6	1 (1 0 0 0 0)	6.53E-06
B4DVX2	B4DVX2_HUMAN (B4DVX2) cDNA FLJ55373, highly similar to Isoleucyl-tRNA synthetase, cytoplasmic (EC 6.	87692.8	3 (3 0 0 0 0)	4.76E-09
B4DW28	B4DW28_HUMAN (B4DW28) cDNA FLJ58953, highly similar to 40S ribosomal protein S20 OS=Homo sapiens	15995.4	6 (6 0 0 0 0)	5.19E-08
B4DW52	B4DW52_HUMAN (B4DW52) cDNA FLJ55253, highly similar to Actin, cytoplasmic 1 OS=Homo sapiens PE=2	38608.2	2 (2 0 0 0 0)	3.58E-09
B4DW52	AT1B3_HUMAN (P54709) Sodium/potassium-transporting ATPase subunit beta-3 OS=Homo sapiens GN=ATP	38608.2	2 (1 1 0 0 0)	5.08E-09
B4DW52	B4DW52_HUMAN (B4DW52) cDNA FLJ55253, highly similar to Actin, cytoplasmic 1 OS=Homo sapiens PE=2	38608.2	1 (0 1 0 0 0)	2.49E-05
B4DW74	B4DW74_HUMAN (B4DW74) cDNA FLJ50711, moderately similar to Ras-related protein Rap-1b OS=Homo sa	16023.3	6 (6 0 0 0 0)	2.01E-07
B4DWB5	B4DWB5_HUMAN (B4DWB5) cDNA FLJ53931, highly similar to Bifunctional 3'-phosphoadenosine5'-phospho	69987.9	5 (5 0 0 0 0)	9.97E-08
B4DWQ5	B4DWQ5_HUMAN (B4DWQ5) cDNA FLJ51655, highly similar to Actin-like protein 2 OS=Homo sapiens PE=2	34485.9	1 (1 0 0 0 0)	2.08E-07
B4DWW4	B4DWW4_HUMAN (B4DWW4) cDNA FLJ55599, highly similar to DNA replication licensing factor MCM3 (MCN	95848.4	3 (3 0 0 0 0)	6.68E-09

B4DX78	B4DX78_HUMAN (B4DX78) cDNA FLJ55484, highly similar to ATP-dependent RNA helicase DDX39 (EC 3.6.1	53662.4	5 (5 0 0 0 0)	1.33E-06
B4DXJ1	B4DXJ1_HUMAN (B4DXJ1) cDNA FLJ56334, highly similar to SEC13-related protein OS=Homo sapiens PE=2	40720.8	2 (2 0 0 0 0)	3.11E-06
B4DXL5	K2C1_HUMAN (P04264) Keratin, type II cytoskeletal 1 OS=Homo sapiens GN=KRT1 PE=1 SV=5	37475.9	1 (1 0 0 0 0)	9.75E-06
B4DZ53	B4DZ53_HUMAN (B4DZ53) cDNA FLJ59643, highly similar to Neutral alpha-glucosidase AB OS=Homo sapien	96467.2	2 (2 0 0 0 0)	1.85E-07
B4DZA5	B4DZA5_HUMAN (B4DZA5) cDNA FLJ57678, highly similar to Transmembrane protein 16F OS=Homo sapien	107961.2	1 (1 0 0 0 0)	1.46E-07
B4E040	B4E040_HUMAN (B4E040) cDNA FLJ55177, highly similar to Ras-related protein Ral-B OS=Homo sapiens PE	25950.3	2 (2 0 0 0 0)	4.26E-05
B4E132	B4E132_HUMAN (B4E132) cDNA FLJ53122, highly similar to ATP-dependent RNA helicase DDX3Y (EC 3.6.1	44813.9	3 (3 0 0 0 0)	4.66E-06
B4E1T7	B4E1T7_HUMAN (B4E1T7) cDNA FLJ58665, highly similar to Serine/threonine-protein phosphatase 2A 55 kD	52966.2	2 (2 0 0 0 0)	3.22E-05
B4E299	B4E299_HUMAN (B4E299) cDNA FLJ54574, highly similar to Staphylococcal nuclease domain-containing pro	99616.5	4 (4 0 0 0 0)	6.56E-08
B4E2P2	B4E2P2_HUMAN (B4E2P2) cDNA FLJ52061, highly similar to Translocon-associated protein subunit gamma (	22595.9	1 (1 0 0 0 0)	1.48E-05
B4E3A0	B4E3A0_HUMAN (B4E3A0) cDNA FLJ54253, highly similar to Ras-related protein Rab-34 OS=Homo sapiens	26703.6	2 (2 0 0 0 0)	4.56E-08
B4E3A0	B4E3A0_HUMAN (B4E3A0) cDNA FLJ54253, highly similar to Ras-related protein Rab-34 OS=Homo sapiens	26703.6	2 (2 0 0 0 0)	1.13E-07
B5BU72	B5BU72_HUMAN (B5BU72) Phosphatidylinositol-binding clathrin assembly protein isoform 2 OS=Homo sapien	66351.9	1 (1 0 0 0 0)	7.79E-08
B5MDF5	B5MDF5_HUMAN (B5MDF5) Putative uncharacterized protein RANP1 OS=Homo sapiens GN=RANP1 PE=4	26207.5	1 (11 0 0 0 0)	2.76E-08
B5ME97	B5ME97_HUMAN (B5ME97) Putative uncharacterized protein SEPT10 (Fragment) OS=Homo sapiens GN=SE	59750.3	2 (0 2 0 0 0)	4.11E-06
B5MEC5	B5MEC5_HUMAN (B5MEC5) Putative uncharacterized protein SLC38A1 OS=Homo sapiens GN=SLC38A1 PE	58729.6	1 (1 0 0 0 0)	5.31E-06
O00116	ADAS_HUMAN (O00116) Alkyldihydroxyacetonephosphate synthase, peroxisomal OS=Homo sapiens GN=AG	72865.9	5 (5 0 0 0 0)	1.27E-08
O00154	BACH_HUMAN (O00154) Cytosolic acyl coenzyme A thioester hydrolase OS=Homo sapiens GN=ACOT7 PE=	41769.4	5 (15 0 0 0 0)	1.34E-10
O00161	SNP23_HUMAN (O00161) Synaptosomal-associated protein 23 OS=Homo sapiens GN=SNAP23 PE=1 SV=1	23339.5	0 (10 0 0 0 0)	7.63E-10
O00186	STXB3_HUMAN (O00186) Syntaxin-binding protein 3 OS=Homo sapiens GN=STXBP3 PE=2 SV=2	67720.9	3 (3 0 0 0 0)	1.83E-11
O00232	PSD12_HUMAN (O00232) 26S proteasome non-ATPase regulatory subunit 12 OS=Homo sapiens GN=PSMD	52870.6	0 (10 0 0 0 0)	2.94E-08
O00425	IF2B3_HUMAN (O00425) Insulin-like growth factor 2 mRNA-binding protein 3 OS=Homo sapiens GN=IGF2BP	63680.7	1 (1 0 0 0 0)	4.63E-05
O00461	GOLI4_HUMAN (O00461) Golgi integral membrane protein 4 OS=Homo sapiens GN=GOLIM4 PE=1 SV=1	81831.2	1 (1 0 0 0 0)	1.73E-05
O00483	NDUA4_HUMAN (O00483) NADH dehydrogenase [ubiquinone] 1 alpha subcomplex subunit 4 OS=Homo sapi	9363.9	5 (5 0 0 0 0)	1.36E-07
O00487	PSDE_HUMAN (O00487) 26S proteasome non-ATPase regulatory subunit 14 OS=Homo sapiens GN=PSMD1	34554.6	2 (2 0 0 0 0)	1.65E-08
O00487	TBA1A_HUMAN (Q71U36) Tubulin alpha-1A chain OS=Homo sapiens GN=TUBA1A PE=1 SV=1	34554.6	2 (2 0 0 0 0)	1.93E-08
O00541	PESC_HUMAN (O00541) Pescadillo homolog 1 OS=Homo sapiens GN=PES1 PE=1 SV=1	67960.1	2 (2 0 0 0 0)	2.64E-05
O00567	NOL5A_HUMAN (O00567) Nucleolar protein 5A OS=Homo sapiens GN=NOL5A PE=1 SV=4	66008.8	3 (3 0 0 0 0)	2.66E-07
O00592	PODXL_HUMAN (O00592) Podocalyxin-like protein 1 OS=Homo sapiens GN=PODXL PE=2 SV=1	55561.6	1 (1 0 0 0 0)	2.53E-05
O00625	PIR_HUMAN (O00625) Pirin OS=Homo sapiens GN=PIR PE=1 SV=1; GDPD1_HUMAN (Q8N9F7) Glycerophe	32093.3	2 (2 0 0 0 0)	1.03E-06
O14521	DHSD_HUMAN (O14521) Succinate dehydrogenase [ubiquinone] cytochrome b small subunit, mitochondrial C	17031.9	1 (1 0 0 0 0)	7.56E-06
O14657	PSDE_HUMAN (O00487) 26S proteasome non-ATPase regulatory subunit 14 OS=Homo sapiens GN=PSMD1	37954.8	1 (1 0 0 0 0)	1.65E-08
O14660	O14660_HUMAN (O14660) GARS-AIRS-GART (Fragment) OS=Homo sapiens PE=2 SV=1	10725.8	2 (2 0 0 0 0)	6.16E-10
O14662	STX16_HUMAN (O14662) Syntaxin-16 OS=Homo sapiens GN=STX16 PE=2 SV=3; FBRLL_HUMAN (A6NHQ	37008.3	2 (1 1 0 0 0)	8.89E-07
O14672	ADA10_HUMAN (O14672) ADAM 10 OS=Homo sapiens GN=ADAM10 PE=1 SV=1	84087.7	5 (5 0 0 0 0)	1.43E-08
O14735	CDIPT_HUMAN (O14735) CDP-diacylglycerol--inositol 3-phosphatidyltransferase OS=Homo sapiens GN=CDI	23523.1	1 (1 0 0 0 0)	3.66E-07
O14744	ANM5_HUMAN (O14744) Protein arginine N-methyltransferase 5 OS=Homo sapiens GN=PRMT5 PE=1 SV=4	72637.7	4 (4 0 0 0 0)	6.51E-10
O14763	TR10B_HUMAN (O14763) Tumor necrosis factor receptor superfamily member 10B OS=Homo sapiens GN=T	47819.7	3 (3 0 0 0 0)	8.18E-10
O14818	PSA7_HUMAN (O14818) Proteasome subunit alpha type-7 OS=Homo sapiens GN=PSMA7 PE=1 SV=1	27869.6	1 (1 0 0 0 0)	2.50E-06
O14828	SCAM3_HUMAN (O14828) Secretory carrier-associated membrane protein 3 OS=Homo sapiens GN=SCAMP	38262.4	3 (3 0 0 0 0)	2.22E-08
O14908	GIPC1_HUMAN (O14908) PDZ domain-containing protein GIPC1 OS=Homo sapiens GN=GIPC1 PE=1 SV=2	36026.7	2 (2 0 0 0 0)	4.83E-11
O14949	QCR8_HUMAN (O14949) Cytochrome b-c1 complex subunit 8 OS=Homo sapiens GN=UQCRQ PE=1 SV=4	9900.1	2 (2 0 0 0 0)	5.21E-06
O14979	HNRDL_HUMAN (O14979) Heterogeneous nuclear ribonucleoprotein D-like OS=Homo sapiens GN=HNRPDL	46409.0	1 (0 1 0 0 0)	6.49E-05
O14980	XPO1_HUMAN (O14980) Exportin-1 OS=Homo sapiens GN=XPO1 PE=1 SV=1	123306.1	2 (2 0 0 0 0)	3.71E-07
O15031	PLXB2_HUMAN (O15031) Plexin-B2 OS=Homo sapiens GN=PLXNB2 PE=1 SV=3	204996.1	8 (8 0 0 0 0)	1.09E-10
O15143	ARC1B_HUMAN (O15143) Actin-related protein 2/3 complex subunit 1B OS=Homo sapiens GN=ARPC1B PE=	40923.4	1 (1 0 0 0 0)	7.32E-06
O15145	ARPC3_HUMAN (O15145) Actin-related protein 2/3 complex subunit 3 OS=Homo sapiens GN=ARPC3 PE=1	20533.4	4 (4 0 0 0 0)	3.00E-08
O15160	RPAC1_HUMAN (O15160) DNA-directed RNA polymerases I and III subunit RPAC1 OS=Homo sapiens GN=P	39225.1	3 (3 0 0 0 0)	1.91E-09
O15260	SURF4_HUMAN (O15260) Surfeit locus protein 4 OS=Homo sapiens GN=SURF4 PE=1 SV=3	30373.8	2 (2 0 0 0 0)	3.77E-08
O15305	PMM2_HUMAN (O15305) Phosphomannomutase 2 OS=Homo sapiens GN=PMM2 PE=1 SV=1	28064.2	4 (4 0 0 0 0)	1.50E-07
O15327	INP4B_HUMAN (O15327) Type II inositol-3,4-bisphosphate 4-phosphatase OS=Homo sapiens GN=INPP4B PI	104671.5	1 (1 0 0 0 0)	3.03E-06
O15400	STX7_HUMAN (O15400) Syntaxin-7 OS=Homo sapiens GN=STX7 PE=1 SV=4	29797.3	1 (1 0 0 0 0)	1.15E-06
O15439	MRP4_HUMAN (O15439) Multidrug resistance-associated protein 4 OS=Homo sapiens GN=ABCC4 PE=1 SV	149431.6	2 (2 0 0 0 0)	1.22E-06
O15498	YKT6_HUMAN (O15498) Synaptobrevin homolog YKT6 OS=Homo sapiens GN=YKT6 PE=1 SV=1	22403.4	1 (1 0 0 0 0)	8.30E-06
O43143	DHX15_HUMAN (O43143) Putative pre-mRNA-splicing factor ATP-dependent RNA helicase DHX15 OS=Hom	90875.3	9 (9 0 0 0 0)	1.56E-08
O43157	PLXB1_HUMAN (O43157) Plexin-B1 OS=Homo sapiens GN=PLXNB1 PE=1 SV=3	232148.9	2 (2 0 0 0 0)	3.63E-09
O43169	CYB5B_HUMAN (O43169) Cytochrome b5 type B OS=Homo sapiens GN=CYB5B PE=1 SV=2	16322.0	1 (1 0 0 0 0)	5.49E-07
O43175	SERA_HUMAN (O43175) D-3-phosphoglycerate dehydrogenase OS=Homo sapiens GN=PHGDH PE=1 SV=4	56614.5	8 (8 0 0 0 0)	2.56E-08
O43175	SERA_HUMAN (O43175) D-3-phosphoglycerate dehydrogenase OS=Homo sapiens GN=PHGDH PE=1 SV=4	56614.5	1 (1 0 0 0 0)	3.53E-08
O43242	PSMD3_HUMAN (O43242) 26S proteasome non-ATPase regulatory subunit 3 OS=Homo sapiens GN=PSMD3	60939.6	4 (4 0 0 0 0)	2.23E-08
O43252	PAPS1_HUMAN (O43252) Bifunctional 3'-phosphoadenosine 5'-phosphosulfate synthetase 1 OS=Homo sapie	70787.8	2 (2 0 0 0 0)	3.79E-06
O43399	TPD54_HUMAN (O43399) Tumor protein D54 OS=Homo sapiens GN=TPD52L2 PE=1 SV=2	22224.3	4 (4 0 0 0 0)	5.14E-06
O43633	CHM2A_HUMAN (O43633) Charged multivesicular body protein 2a OS=Homo sapiens GN=CHMP2A PE=1 S	25087.9	1 (1 0 0 0 0)	3.10E-07
O43676	NDUB3_HUMAN (O43676) NADH dehydrogenase [ubiquinone] 1 beta subcomplex subunit 3 OS=Homo sapie	11394.7	1 (1 0 0 0 0)	3.60E-06
O43684	BUB3_HUMAN (O43684) Mitotic checkpoint protein BUB3 OS=Homo sapiens GN=BUB3 PE=1 SV=1	37131.2	5 (5 0 0 0 0)	5.08E-08
O43752	STX6_HUMAN (O43752) Syntaxin-6 OS=Homo sapiens GN=STX6 PE=1 SV=1	29157.8	1 (1 0 0 0 0)	5.77E-08
O43776	SYNC_HUMAN (O43776) Asparaginyl-tRNA synthetase, cytoplasmic OS=Homo sapiens GN=NARS PE=1 SV	62902.6	2 (2 0 0 0 0)	9.36E-08
O43809	CPSF5_HUMAN (O43809) Cleavage and polyadenylation specificity factor subunit 5 OS=Homo sapiens GN=N	26210.7	6 (6 0 0 0 0)	2.53E-08
O43837	IDH3B_HUMAN (O43837) Isocitrate dehydrogenase [NAD] subunit beta, mitochondrial OS=Homo sapiens GN	42156.6	1 (1 0 0 0 0)	2.98E-09
O60262	GBG7_HUMAN (O60262) Guanine nucleotide-binding protein G(I)/G(S)/G(O) subunit gamma-7 OS=Homo sap	7517.0	2 (2 0 0 0 0)	1.01E-11
O60462	NRP2_HUMAN (O60462) Neuropilin-2 OS=Homo sapiens GN=NRP2 PE=1 SV=2	104792.0	3 (3 0 0 0 0)	6.99E-08
O60506	HNRPQ_HUMAN (O60506) Heterogeneous nuclear ribonucleoprotein Q OS=Homo sapiens GN=SYNCRIP PE	69559.6	8 (8 0 0 0 0)	7.21E-10
O60645	EXOC3_HUMAN (O60645) Exocyst complex component 3 OS=Homo sapiens GN=EXOC3 PE=1 SV=2	86789.9	1 (1 0 0 0 0)	4.00E-05
O60669	MOT2_HUMAN (O60669) Monocarboxylate transporter 2 OS=Homo sapiens GN=SLC16A7 PE=2 SV=1	52152.2	1 (1 0 0 0 0)	9.48E-07
O60701	UGDH_HUMAN (O60701) UDP-glucose 6-dehydrogenase OS=Homo sapiens GN=UGDH PE=1 SV=1	54989.3	3 (3 0 0 0 0)	1.20E-06
O60739	EIF1B_HUMAN (O60739) Eukaryotic translation initiation factor 1b OS=Homo sapiens GN=EIF1B PE=1 SV=2	12815.7	2 (2 0 0 0 0)	2.95E-09

O60749	SNX2_HUMAN (O60749) Sorting nexin-2 OS=Homo sapiens GN=SNX2 PE=1 SV=2	58434.8	2 (2 0 0 0 0)	7.32E-08
O60941	DTNB_HUMAN (O60941) Dystrobrevin beta OS=Homo sapiens GN=DTNB PE=1 SV=1	71309.7	1 (1 0 0 0 0)	6.86E-07
O75044	FNBP2_HUMAN (O75044) SLIT-ROBO Rho GTPase-activating protein 2 OS=Homo sapiens GN=SRGAP2 PE	120804.7	2 (2 0 0 0 0)	2.94E-08
O75056	SDC3_HUMAN (O75056) Syndecan-3 OS=Homo sapiens GN=SDC3 PE=2 SV=2	45469.4	1 (1 0 0 0 0)	1.45E-05
O75116	ROCK2_HUMAN (O75116) Rho-associated protein kinase 2 OS=Homo sapiens GN=ROCK2 PE=1 SV=3	160810.9	2 (2 0 0 0 0)	5.93E-08
O75165	DJC13_HUMAN (O75165) DnaJ homolog subfamily C member 13 OS=Homo sapiens GN=DNAJC13 PE=1 SV	254266.4	1 (1 0 0 0 0)	5.28E-06
O75352	MPU1_HUMAN (O75352) Mannose-P-dolichol utilization defect 1 protein OS=Homo sapiens GN=MPDU1 PE=	26620.5	3 (3 0 0 0 0)	4.34E-06
O75367	H2AY_HUMAN (O75367) Core histone macro-H2A.1 OS=Homo sapiens GN=H2AFY PE=1 SV=4	39592.5	2 (2 0 0 0 0)	1.01E-08
O75369	FLNB_HUMAN (O75369) Filamin-B OS=Homo sapiens GN=FLNB PE=1 SV=1	278018.3	3 (3 0 0 0 0)	1.02E-08
O75396	SC22B_HUMAN (O75396) Vesicle-trafficking protein SEC22b OS=Homo sapiens GN=SEC22B PE=1 SV=3	24724.8	8 (8 0 0 0 0)	3.16E-10
O75431	MTX2_HUMAN (O75431) Metaxin-2 OS=Homo sapiens GN=MTX2 PE=1 SV=1	29744.1	2 (2 0 0 0 0)	1.28E-06
O75436	VP26A_HUMAN (O75436) Vacuolar protein sorting-associated protein 26A OS=Homo sapiens GN=VPS26A P	38145.8	1 (1 0 0 0 0)	3.30E-06
O75475	PSIP1_HUMAN (O75475) PC4 and SFRS1-interacting protein OS=Homo sapiens GN=PSIP1 PE=1 SV=1	60066.7	1 (1 0 0 0 0)	2.42E-05
O75477	ERLN1_HUMAN (O75477) Erlin-1 OS=Homo sapiens GN=ERLIN1 PE=2 SV=1	38901.4	6 (6 0 0 0 0)	9.71E-08
O75487	GPC4_HUMAN (O75487) Glypican-4 OS=Homo sapiens GN=GPC4 PE=1 SV=4	62371.8	2 (2 0 0 0 0)	1.60E-06
O75489	NDUS3_HUMAN (O75489) NADH dehydrogenase [ubiquinone] iron-sulfur protein 3, mitochondrial OS=Homo	30222.7	8 (8 0 0 0 0)	9.05E-10
O75506	HSBP1_HUMAN (O75506) Heat shock factor-binding protein 1 OS=Homo sapiens GN=HSBP1 PE=1 SV=1	8538.2	1 (1 0 0 0 0)	1.93E-04
O75683	SURF6_HUMAN (O75683) Surfeit locus protein 6 OS=Homo sapiens GN=SURF6 PE=1 SV=3	41425.7	1 (1 0 0 0 0)	2.74E-07
O75694	NU155_HUMAN (O75694) Nuclear pore complex protein Nup155 OS=Homo sapiens GN=NUP155 PE=1 SV=	155099.8	2 (2 0 0 0 0)	1.10E-07
O75695	XRP2_HUMAN (O75695) Protein XRP2 OS=Homo sapiens GN=RP2 PE=1 SV=4	39615.5	2 (2 0 0 0 0)	6.72E-07
O75746	CMC1_HUMAN (O75746) Calcium-binding mitochondrial carrier protein Aralar1 OS=Homo sapiens GN=SLC2	74715.0	7 (6 0 1 0 0)	4.49E-07
O75821	EIF3G_HUMAN (O75821) Eukaryotic translation initiation factor 3 subunit G OS=Homo sapiens GN=EIF3G PE	35588.9	3 (3 0 0 0 0)	4.19E-09
O75923	DYSF_HUMAN (O75923) Dysferlin OS=Homo sapiens GN=DYSF PE=1 SV=1	237142.3	1 (1 0 0 0 0)	1.21E-08
O75934	SPF27_HUMAN (O75934) Pre-mRNA-splicing factor SPF27 OS=Homo sapiens GN=BCAS2 PE=1 SV=1	26115.0	3 (3 0 0 0 0)	3.14E-07
O75947	ATP5H_HUMAN (O75947) ATP synthase subunit d, mitochondrial OS=Homo sapiens GN=ATP5H PE=1 SV=3	18479.5	9 (9 0 0 0 0)	6.93E-07
O75955	FLOT1_HUMAN (O75955) Flotillin-1 OS=Homo sapiens GN=FLOT1 PE=1 SV=3	47325.7	3 (3 0 0 0 0)	4.16E-07
O75964	ATP5L_HUMAN (O75964) ATP synthase subunit g, mitochondrial OS=Homo sapiens GN=ATP5L PE=1 SV=3	11421.2	2 (12 0 0 0 0)	3.78E-10
O76021	RL1D1_HUMAN (O76021) Ribosomal L1 domain-containing protein 1 OS=Homo sapiens GN=RSL1D1 PE=1	54939.0	9 (9 0 0 0 0)	9.04E-09
O76021	RL1D1_HUMAN (O76021) Ribosomal L1 domain-containing protein 1 OS=Homo sapiens GN=RSL1D1 PE=1	54939.0	1 (1 0 0 0 0)	1.37E-05
O76094	SRP72_HUMAN (O76094) Signal recognition particle 72 kDa protein OS=Homo sapiens GN=SRP72 PE=1 SV	74560.1	1 (1 0 0 0 0)	1.65E-13
O94788	AL1A2_HUMAN (O94788) Retinal dehydrogenase 2 OS=Homo sapiens GN=ALDH1A2 PE=2 SV=3	56688.0	2 (2 0 0 0 0)	2.12E-08
O94832	MYO1D_HUMAN (O94832) Myosin-Id OS=Homo sapiens GN=MYO1D PE=1 SV=2	116128.6	1 (1 0 0 0 0)	1.97E-05
O94905	ERLN2_HUMAN (O94905) Erlin-2 OS=Homo sapiens GN=ERLIN2 PE=1 SV=1	37815.5	4 (4 0 0 0 0)	9.74E-09
O94910	LPHN1_HUMAN (O94910) Latrophilin-1 OS=Homo sapiens GN=LPHN1 PE=1 SV=1	162612.9	2 (2 0 0 0 0)	2.72E-07
O94911	ABCA8_HUMAN (O94911) ATP-binding cassette sub-family A member 8 OS=Homo sapiens GN=ABCA8 PE=	179128.9	4 (4 0 0 0 0)	5.14E-09
O95183	VAMP5_HUMAN (O95183) Vesicle-associated membrane protein 5 OS=Homo sapiens GN=VAMP5 PE=1 SV=	12796.7	2 (2 0 0 0 0)	6.10E-08
O95202	LETM1_HUMAN (O95202) LETM1 and EF-hand domain-containing protein 1, mitochondrial OS=Homo sapien	83302.0	1 (1 0 0 0 0)	9.64E-08
O95232	CROP_HUMAN (O95232) Cisplatin resistance-associated overexpressed protein OS=Homo sapiens GN=CRC	51435.1	1 (1 0 0 0 0)	1.58E-08
O95292	VAPB_HUMAN (O95292) Vesicle-associated membrane protein-associated protein B/C OS=Homo sapiens GN	27211.1	2 (2 0 0 0 0)	5.87E-07
O95295	SNAPN_HUMAN (O95295) SNARE-associated protein Snapin OS=Homo sapiens GN=SNAPIN PE=1 SV=1	14864.9	2 (2 0 0 0 0)	1.40E-08
O95297	MPZL1_HUMAN (O95297) Myelin protein zero-like protein 1 OS=Homo sapiens GN=MPZL1 PE=1 SV=1	29064.0	1 (1 0 0 0 0)	2.29E-05
O95298	NDUC2_HUMAN (O95298) NADH dehydrogenase [ubiquinone] 1 subunit C2 OS=Homo sapiens GN=NDUFC2	14178.4	2 (2 0 0 0 0)	6.00E-07
O95486	SC24A_HUMAN (O95486) Protein transport protein Sec24A OS=Homo sapiens GN=SEC24A PE=1 SV=2	119673.9	2 (2 0 0 0 0)	4.37E-09
O95571	ETHE1_HUMAN (O95571) Protein ETHE1, mitochondrial OS=Homo sapiens GN=ETHE1 PE=1 SV=2	27855.1	5 (5 0 0 0 0)	1.93E-09
O95573	ACSL3_HUMAN (O95573) Long-chain-fatty-acid--CoA ligase 3 OS=Homo sapiens GN=ACSL3 PE=1 SV=3	80368.3	2 (2 0 0 0 0)	1.41E-12
O95747	OXSR1_HUMAN (O95747) Serine/threonine-protein kinase OSR1 OS=Homo sapiens GN=OXSR1 PE=1 SV=	57986.2	2 (2 0 0 0 0)	9.42E-10
O95747	OXSR1_HUMAN (O95747) Serine/threonine-protein kinase OSR1 OS=Homo sapiens GN=OXSR1 PE=1 SV=	57986.2	1 (1 0 0 0 0)	3.53E-06
O95831	AIFM1_HUMAN (O95831) Apoptosis-inducing factor 1, mitochondrial OS=Homo sapiens GN=AIFM1 PE=1 SV	66859.0	2 (2 0 0 0 0)	5.16E-07
O95837	GNA14_HUMAN (O95837) Guanine nucleotide-binding protein subunit alpha-14 OS=Homo sapiens GN=GNA	41544.2	1 (0 1 0 0 0)	1.25E-07
O96000	NDUBA_HUMAN (O96000) NADH dehydrogenase [ubiquinone] 1 beta subcomplex subunit 10 OS=Homo sapi	20763.2	4 (4 0 0 0 0)	6.48E-07
O96008	TOM40_HUMAN (O96008) Mitochondrial import receptor subunit TOM40 homolog OS=Homo sapiens GN=TO	37869.2	4 (4 0 0 0 0)	1.88E-07
O96011	PX11B_HUMAN (O96011) Peroxisomal membrane protein 11B OS=Homo sapiens GN=PEX11B PE=1 SV=1	28413.2	7 (7 0 0 0 0)	9.01E-09
P00338	LDHA_HUMAN (P00338) L-lactate dehydrogenase A chain OS=Homo sapiens GN=LDHA PE=1 SV=2	36665.4	5 (5 0 0 0 0)	3.60E-10
P00387	NB5R3_HUMAN (P00387) NADH-cytochrome b5 reductase 3 OS=Homo sapiens GN=CYB5R3 PE=1 SV=3	34212.7	2 (2 0 0 0 0)	3.20E-07
P00403	COX2_HUMAN (P00403) Cytochrome c oxidase subunit 2 OS=Homo sapiens GN=MT-CO2 PE=1 SV=1	25548.2	5 (5 0 0 0 0)	4.36E-07
P00492	HPRT_HUMAN (P00492) Hypoxanthine-guanine phosphoribosyltransferase OS=Homo sapiens GN=HPRT1 P	24563.6	1 (1 0 0 0 0)	6.71E-10
P00505	AATM_HUMAN (P00505) Aspartate aminotransferase, mitochondrial OS=Homo sapiens GN=GOT2 PE=1 SV=	47445.3	11 (11 0 0 0 0)	7.97E-09
P00533	EGFR_HUMAN (P00533) Epidermal growth factor receptor OS=Homo sapiens GN=EGFR PE=1 SV=2	134190.2	1 (1 0 0 0 0)	1.33E-08
P00558	PGK1_HUMAN (P00558) Phosphoglycerate kinase 1 OS=Homo sapiens GN=PGK1 PE=1 SV=3	44586.2	10 (10 0 0 0 0)	2.79E-09
P01111	RASN_HUMAN (P01111) GTPase NRas OS=Homo sapiens GN=NRAS PE=1 SV=1	21215.5	1 (1 0 0 0 0)	3.65E-05
P01112	RASH_HUMAN (P01112) GTPase HRas OS=Homo sapiens GN=HRAS PE=1 SV=1	21284.6	8 (8 0 0 0 0)	1.41E-08
P01116	RASK_HUMAN (P01116) GTPase KRas OS=Homo sapiens GN=KRAS PE=1 SV=1	21642.0	3 (3 0 0 0 0)	2.09E-06
P01903	2DRA_HUMAN (P01903) HLA class II histocompatibility antigen, DR alpha chain OS=Homo sapiens GN=HLA	28588.7	8 (8 0 0 0 0)	2.58E-11
P01908	HA21_HUMAN (P01908) HLA class II histocompatibility antigen, DQ(1) alpha chain OS=Homo sapiens PE=2 S	28087.4	2 (2 0 0 0 0)	9.88E-10
P02533	K1C14_HUMAN (P02533) Keratin, type I cytoskeletal 14 OS=Homo sapiens GN=KRT14 PE=1 SV=3	51589.5	5 (5 0 0 0 0)	3.52E-08
P02538	K2C6A_HUMAN (P02538) Keratin, type II cytoskeletal 6A OS=Homo sapiens GN=KRT6A PE=1 SV=3	60008.3	2 (2 0 0 0 0)	1.85E-05
P02545	LMNA_HUMAN (P02545) Lamin-A/C OS=Homo sapiens GN=LMNA PE=1 SV=1	74094.8	3 (23 0 0 0 0)	2.51E-09
P02647	APOA1_HUMAN (P02647) Apolipoprotein A-I OS=Homo sapiens GN=APOA1 PE=1 SV=1	30758.9	2 (2 0 0 0 0)	5.22E-08
P02786	TFR1_HUMAN (P02786) Transferrin receptor protein 1 OS=Homo sapiens GN=TFRC PE=1 SV=2	84818.0	1 (1 0 0 0 0)	9.55E-09
P03928	ATP8_HUMAN (P03928) ATP synthase protein 8 OS=Homo sapiens GN=MT-ATP8 PE=1 SV=1	7986.2	3 (3 0 0 0 0)	1.31E-05
P04004	VTNC_HUMAN (P04004) Vitronectin OS=Homo sapiens GN=VTN PE=1 SV=1	54271.2	1 (1 0 0 0 0)	2.32E-08
P04075	ALDOA_HUMAN (P04075) Fructose-bisphosphate aldolase A OS=Homo sapiens GN=ALDOA PE=1 SV=2	39395.3	4 (4 0 0 0 0)	1.74E-08
P04083	ANXA1_HUMAN (P04083) Annexin A1 OS=Homo sapiens GN=ANXA1 PE=1 SV=2;	38690.0	6 (16 0 0 0 0)	7.09E-12
P04156	PRIO_HUMAN (P04156) Major prion protein OS=Homo sapiens GN=PRNP PE=1 SV=1	27643.2	3 (3 0 0 0 0)	1.02E-07
P04179	SODM_HUMAN (P04179) Superoxide dismutase [Mn], mitochondrial OS=Homo sapiens GN=SOD2 PE=1 SV=	24706.6	2 (2 0 0 0 0)	1.31E-06
P04183	KITH_HUMAN (P04183) Thymidine kinase, cytosolic OS=Homo sapiens GN=TK1 PE=1 SV=2	25452.0	1 (1 0 0 0 0)	7.38E-05

P04233	HG2A_HUMAN (P04233) HLA class II histocompatibility antigen gamma chain OS=Homo sapiens GN=CD74 F	33493.7	1 (1 0 0 0 0)	1.15E-07
P04264	K2C1_HUMAN (P04264) Keratin, type II cytoskeletal 1 OS=Homo sapiens GN=KRT1 PE=1 SV=5	65977.9	6 (36 0 0 0 0)	1.18E-11
P04406	G3P_HUMAN (P04406) Glyceraldehyde-3-phosphate dehydrogenase OS=Homo sapiens GN=GAPDH PE=1 S	36030.4	9 (9 0 0 0 0)	6.00E-09
P04792	HSPB1_HUMAN (P04792) Heat shock protein beta-1 OS=Homo sapiens GN=HSPB1 PE=1 SV=2	22768.5	8 (8 0 0 0 0)	2.38E-08
P04843	RPN1_HUMAN (P04843) Dolichyl-diphosphooligosaccharide--protein glycosyltransferase subunit 1 OS=Homo	68526.9	2 (22 0 0 0 0)	5.86E-13
P04844	RPN2_HUMAN (P04844) Dolichyl-diphosphooligosaccharide--protein glycosyltransferase subunit 2 OS=Homo	69241.1	4 (4 0 0 0 0)	1.31E-06
P05023	AT1A1_HUMAN (P05023) Sodium/potassium-transporting ATPase subunit alpha-1 OS=Homo sapiens GN=AT	112824.1	7 (27 0 0 0 0)	4.09E-13
P05026	AT1B1_HUMAN (P05026) Sodium/potassium-transporting ATPase subunit beta-1 OS=Homo sapiens GN=ATP	35038.9	5 (5 0 0 0 0)	1.43E-09
P05106	ITB3_HUMAN (P05106) Integrin beta-3 OS=Homo sapiens GN=ITGB3 PE=1 SV=2	87000.4	1 (11 0 0 0 0)	5.45E-07
P05109	S10A8_HUMAN (P05109) Protein S100-A8 OS=Homo sapiens GN=S100A8 PE=1 SV=1	10827.7	2 (2 0 0 0 0)	1.31E-05
P05198	IF2A_HUMAN (P05198) Eukaryotic translation initiation factor 2 subunit 1 OS=Homo sapiens GN=EIF2S1 PE=	36089.4	4 (4 0 0 0 0)	1.36E-08
P05362	ICAM1_HUMAN (P05362) Intercellular adhesion molecule 1 OS=Homo sapiens GN=ICAM1 PE=1 SV=2	57789.0	1 (1 0 0 0 0)	1.04E-08
P05386	RLA1_HUMAN (P05386) 60S acidic ribosomal protein P1 OS=Homo sapiens GN=RPLP1 PE=1 SV=1	11506.7	2 (2 0 0 0 0)	2.10E-07
P05387	RLA2_HUMAN (P05387) 60S acidic ribosomal protein P2 OS=Homo sapiens GN=RPLP2 PE=1 SV=1	11657.9	2 (2 0 0 0 0)	9.01E-08
P05556	ITB1_HUMAN (P05556) Integrin beta-1 OS=Homo sapiens GN=ITGB1 PE=1 SV=2	88357.0	4 (4 0 0 0 0)	8.27E-08
P05787	K2C8_HUMAN (P05787) Keratin, type II cytoskeletal 8 OS=Homo sapiens GN=KRT8 PE=1 SV=7	53671.2	2 (0 2 0 0 0)	1.90E-05
P06213	INSR_HUMAN (P06213) Insulin receptor OS=Homo sapiens GN=INSR PE=1 SV=2	156206.1	2 (2 0 0 0 0)	6.14E-07
P06396	GELS_HUMAN (P06396) Gelsolin OS=Homo sapiens GN=GSN PE=1 SV=1	85644.3	0 (10 0 0 0 0)	7.00E-11
P06576	ATPB_HUMAN (P06576) ATP synthase subunit beta, mitochondrial OS=Homo sapiens GN=ATP5B PE=1 SV=	56524.7	1 (11 0 0 0 0)	2.85E-13
P06733	ENOA_HUMAN (P06733) Alpha-enolase OS=Homo sapiens GN=ENO1 PE=1 SV=2	47139.4	2 (21 11 0 0 0)	5.88E-14
P06737	PYGL_HUMAN (P06737) Glycogen phosphorylase, liver form OS=Homo sapiens GN=PYGL PE=1 SV=4	97087.1	2 (2 0 0 0 0)	2.41E-07
P06744	G6PI_HUMAN (P06744) Glucose-6-phosphate isomerase OS=Homo sapiens GN=GPI PE=1 SV=4	63107.3	3 (3 0 0 0 0)	2.17E-09
P06748	NPM_HUMAN (P06748) Nucleophosmin OS=Homo sapiens GN=NPM1 PE=1 SV=2	32554.9	2 (2 0 0 0 0)	4.72E-08
P06756	ITAV_HUMAN (P06756) Integrin alpha-V OS=Homo sapiens GN=ITGAV PE=1 SV=2	115964.5	7 (17 0 0 0 0)	7.43E-09
P07195	LDHB_HUMAN (P07195) L-lactate dehydrogenase B chain OS=Homo sapiens GN=LDHB PE=1 SV=2	36615.2	0 (10 0 0 0 0)	1.49E-09
P07203	GPX1_HUMAN (P07203) Glutathione peroxidase 1 OS=Homo sapiens GN=GPX1 PE=1 SV=3	31782.1	2 (2 0 0 0 0)	1.65E-08
P07305	H10_HUMAN (P07305) Histone H1.0 OS=Homo sapiens GN=H1F0 PE=1 SV=3	20850.2	4 (4 0 0 0 0)	1.73E-07
P07477	TRY1_HUMAN (P07477) Trypsin-1 OS=Homo sapiens GN=PRSS1 PE=1 SV=1	26541.1	1 (1 0 0 0 0)	7.37E-04
P07686	HEXB_HUMAN (P07686) Beta-hexosaminidase subunit beta OS=Homo sapiens GN=HEXB PE=1 SV=3	63071.3	1 (1 0 0 0 0)	1.07E-04
P07737	PROF1_HUMAN (P07737) Profilin-1 OS=Homo sapiens GN=PFN1 PE=1 SV=2	15044.6	1 (1 0 0 0 0)	1.03E-07
P07741	APT_HUMAN (P07741) Adenine phosphoribosyltransferase OS=Homo sapiens GN=APRT PE=1 SV=2	19595.4	2 (2 0 0 0 0)	1.71E-07
P07814	SYEP_HUMAN (P07814) Bifunctional aminoacyl-tRNA synthetase OS=Homo sapiens GN=EPRS PE=1 SV=3	170539.3	2 (12 0 0 0 0)	4.90E-10
P07910	HNRPC_HUMAN (P07910) Heterogeneous nuclear ribonucleoproteins C1/C2 OS=Homo sapiens GN=HNRNP	33649.6	6 (6 0 0 0 0)	1.41E-07
P07942	LAMB1_HUMAN (P07942) Laminin subunit beta-1 OS=Homo sapiens GN=LAMB1 PE=1 SV=1	197935.7	5 (5 0 0 0 0)	1.74E-10
P07954	FUMH_HUMAN (P07954) Fumarate hydratase, mitochondrial OS=Homo sapiens GN=FH PE=1 SV=3	54602.2	1 (1 0 0 0 0)	1.73E-05
P08183	MDR1_HUMAN (P08183) Multidrug resistance protein 1 OS=Homo sapiens GN=ABCB1 PE=1 SV=2	141373.3	1 (1 0 0 0 0)	2.24E-06
P08195	4F2_HUMAN (P08195) 4F2 cell-surface antigen heavy chain OS=Homo sapiens GN=SLC3A2 PE=1 SV=2	57909.0	7 (17 0 0 0 0)	9.50E-13
P08238	HS90B_HUMAN (P08238) Heat shock protein HSP 90-beta OS=Homo sapiens GN=HSP90AB1 PE=1 SV=4	83212.2	5 (5 0 0 0 0)	1.25E-08
P08240	SRPR_HUMAN (P08240) Signal recognition particle receptor subunit alpha OS=Homo sapiens GN=SRPR PE	69767.4	1 (1 0 0 0 0)	4.49E-05
P08572	CO4A2_HUMAN (P08572) Collagen alpha-2(IV) chain OS=Homo sapiens GN=COL4A2 PE=1 SV=4	167448.4	2 (2 0 0 0 0)	2.29E-05
P08582	TRFM_HUMAN (P08582) Melanotransferrin OS=Homo sapiens GN=MFI2 PE=1 SV=1	80190.5	9 (19 0 0 0 0)	6.78E-11
P08670	VIME_HUMAN (P08670) Vimentin OS=Homo sapiens GN=VIM PE=1 SV=4	53619.2	6 (15 0 0 0 1)	3.08E-08
P08708	RS17_HUMAN (P08708) 40S ribosomal protein S17 OS=Homo sapiens GN=RPS17 PE=1 SV=2	15540.4	5 (5 0 0 0 0)	4.76E-06
P09211	GSTP1_HUMAN (P09211) Glutathione S-transferase P OS=Homo sapiens GN=GSTP1 PE=1 SV=2	23341.0	1 (1 0 0 0 0)	4.94E-05
P09382	LEG1_HUMAN (P09382) Galectin-1 OS=Homo sapiens GN=LGALS1 PE=1 SV=2	14706.2	2 (2 0 0 0 0)	9.09E-08
P09417	DHPR_HUMAN (P09417) Dihydropteridine reductase OS=Homo sapiens GN=QDPR PE=1 SV=2	25773.0	1 (1 0 0 0 0)	1.08E-05
P09429	HMGB1_HUMAN (P09429) High mobility group protein B1 OS=Homo sapiens GN=HMGB1 PE=1 SV=3	24878.2	3 (3 0 0 0 0)	6.16E-10
P09471	GNAO_HUMAN (P09471) Guanine nucleotide-binding protein G(o) subunit alpha OS=Homo sapiens GN=GNA	40024.9	6 (6 0 0 0 0)	2.55E-10
P09543	CN37_HUMAN (P09543) 2',3'-cyclic-nucleotide 3'-phosphodiesterase OS=Homo sapiens GN=CNP PE=1 SV=	47548.7	7 (7 0 0 0 0)	1.83E-07
P09651	ROA1_HUMAN (P09651) Heterogeneous nuclear ribonucleoprotein A1 OS=Homo sapiens GN=HNRNPA1 PE	38822.1	4 (4 0 0 0 0)	5.01E-10
P09661	RU2A_HUMAN (P09661) U2 small nuclear ribonucleoprotein A' OS=Homo sapiens GN=SNRPA1 PE=1 SV=2	28398.1	1 (1 0 0 0 0)	3.43E-05
P09874	PARP1_HUMAN (P09874) Poly [ADP-ribose] polymerase 1 OS=Homo sapiens GN=PARP1 PE=1 SV=4	113012.4	3 (13 0 0 0 0)	9.70E-11
P0C7M2	RA1L3_HUMAN (P0C7M2) Putative heterogeneous nuclear ribonucleoprotein A1-like protein 3 OS=Homo sap	34202.3	5 (5 0 0 0 0)	2.05E-09
P0C7M2	RA1L3_HUMAN (P0C7M2) Putative heterogeneous nuclear ribonucleoprotein A1-like protein 3 OS=Homo sap	34202.3	1 (1 0 0 0 0)	9.56E-06
P0C7P4	UCRIL_HUMAN (P0C7P4) Cytochrome b-c1 complex subunit Rieske-like protein 1 OS=Homo sapiens GN=UC	30796.1	2 (2 0 0 0 0)	9.15E-06
P10114	RAP2A_HUMAN (P10114) Ras-related protein Rap-2a OS=Homo sapiens GN=RAP2A PE=1 SV=1	20602.3	3 (2 1 0 0 0)	1.10E-07
P10301	RRAS_HUMAN (P10301) Ras-related protein R-Ras OS=Homo sapiens GN=RRAS PE=1 SV=1	23465.9	2 (2 0 0 0 0)	7.20E-07
P10515	ODP2_HUMAN (P10515) Dihydrolipoyllysine-residue acetyltransferase component of pyruvate dehydrogenase	68953.3	4 (4 0 0 0 0)	1.79E-10
P10599	THIO_HUMAN (P10599) Thioredoxin OS=Homo sapiens GN=TXN PE=1 SV=3	11729.7	5 (5 0 0 0 0)	3.63E-09
P10606	COX5B_HUMAN (P10606) Cytochrome c oxidase subunit 5B, mitochondrial OS=Homo sapiens GN=COX5B F	13686.9	2 (2 0 0 0 0)	7.90E-07
P10809	CH60_HUMAN (P10809) 60 kDa heat shock protein, mitochondrial OS=Homo sapiens GN=HSPD1 PE=1 SV=	61016.5	5 (5 0 0 0 0)	1.17E-09
P11047	LAMC1_HUMAN (P11047) Laminin subunit gamma-1 OS=Homo sapiens GN=LAMC1 PE=1 SV=2	177491.8	6 (6 0 0 0 0)	3.13E-11
P11142	HSP7C_HUMAN (P11142) Heat shock cognate 71 kDa protein OS=Homo sapiens GN=HSPA8 PE=1 SV=1	70854.4	4 (14 0 0 0 0)	1.14E-10
P11172	PYR5_HUMAN (P11172) Uridine 5'-monophosphate synthase OS=Homo sapiens GN=UMPS PE=1 SV=1	52188.7	5 (5 0 0 0 0)	1.83E-11
P11177	ODPB_HUMAN (P11177) Pyruvate dehydrogenase E1 component subunit beta, mitochondrial OS=Homo sapi	39208.1	2 (2 0 0 0 0)	1.01E-06
P11217	PYGM_HUMAN (P11217) Glycogen phosphorylase, muscle form OS=Homo sapiens GN=PYGM PE=1 SV=6	97030.8	2 (2 0 0 0 0)	8.25E-08
P11233	RALA_HUMAN (P11233) Ras-related protein Ral-A OS=Homo sapiens GN=RALA PE=1 SV=1	23552.0	6 (6 0 0 0 0)	1.60E-10
P11233	RALA_HUMAN (P11233) Ras-related protein Ral-A OS=Homo sapiens GN=RALA PE=1 SV=1	23552.0	2 (2 0 0 0 0)	3.24E-09
P11498	PYC_HUMAN (P11498) Pyruvate carboxylase, mitochondrial OS=Homo sapiens GN=PC PE=1 SV=2	129551.6	1 (1 0 0 0 0)	7.91E-07
P11586	C1TC_HUMAN (P11586) C-1-tetrahydrofolate synthase, cytoplasmic OS=Homo sapiens GN=MTHFD1 PE=1 S	101495.6	2 (2 0 0 0 0)	1.30E-10
P11766	ADHX_HUMAN (P11766) Alcohol dehydrogenase class-3 OS=Homo sapiens GN=ADH5 PE=1 SV=4	39698.4	2 (2 0 0 0 0)	1.25E-09
P12235	ADT1_HUMAN (P12235) ADP/ATP translocase 1 OS=Homo sapiens GN=SLC25A4 PE=1 SV=4	33043.2	6 (5 1 0 0 0)	2.50E-09
P12270	TPR_HUMAN (P12270) Nucleoprotein TPR OS=Homo sapiens GN=TPR PE=1 SV=3	267129.4	5 (5 0 0 0 0)	1.83E-07
P12814	ACTN1_HUMAN (P12814) Alpha-actinin-1 OS=Homo sapiens GN=ACTN1 PE=1 SV=2	102992.7	4 (4 0 0 0 0)	3.78E-10
P12956	KU70_HUMAN (P12956) ATP-dependent DNA helicase 2 subunit 1 OS=Homo sapiens GN=XRCC6 PE=1 SV=	69799.2	4 (14 0 0 0 0)	1.00E-08
P13010	KU86_HUMAN (P13010) ATP-dependent DNA helicase 2 subunit 2 OS=Homo sapiens GN=XRCC5 PE=1 SV=	82652.4	8 (8 0 0 0 0)	6.85E-12

P13073	COX41_HUMAN (P13073) Cytochrome c oxidase subunit 4 isoform 1, mitochondrial OS=Homo sapiens GN=C	19564.1	6 (6 0 0 0 0)	6.78E-09
P13164	IFM1_HUMAN (P13164) Interferon-induced transmembrane protein 1 OS=Homo sapiens GN=IFITM1 PE=1 S	13955.3	3 (3 0 0 0 0)	4.36E-10
P13591	NCAM1_HUMAN (P13591) Neural cell adhesion molecule 1 OS=Homo sapiens GN=NCAM1 PE=1 SV=3	94515.2	3 (3 0 0 0 0)	2.21E-06
P13639	EF2_HUMAN (P13639) Elongation factor 2 OS=Homo sapiens GN=EEF2 PE=1 SV=4	95277.1	6 (16 0 0 0 0)	2.12E-08
P13645	K1C10_HUMAN (P13645) Keratin, type I cytoskeletal 10 OS=Homo sapiens GN=KRT10 PE=1 SV=4	59474.8	0 (20 0 0 0 0)	6.58E-12
P13646	K1C13_HUMAN (P13646) Keratin, type I cytoskeletal 13 OS=Homo sapiens GN=KRT13 PE=1 SV=3	49555.5	8 (8 0 0 0 0)	6.72E-08
P13647	K2C5_HUMAN (P13647) Keratin, type II cytoskeletal 5 OS=Homo sapiens GN=KRT5 PE=1 SV=3	62340.0	1 (1 0 0 0 0)	5.92E-07
P13647	K2C5_HUMAN (P13647) Keratin, type II cytoskeletal 5 OS=Homo sapiens GN=KRT5 PE=1 SV=3	62340.0	2 (2 0 0 0 0)	2.93E-06
P13761	2B17_HUMAN (P13761) HLA class II histocompatibility antigen, DRB1-7 beta chain OS=Homo sapiens GN=H	29803.0	5 (5 0 0 0 0)	7.73E-07
P13807	GYS1_HUMAN (P13807) Glycogen [starch] synthase, muscle OS=Homo sapiens GN=GYS1 PE=1 SV=2	83732.5	1 (1 0 0 0 0)	7.57E-07
P13984	T2FB_HUMAN (P13984) General transcription factor IIF subunit 2 OS=Homo sapiens GN=GTF2F2 PE=1 SV=	28362.9	1 (1 0 0 0 0)	6.01E-06
P13987	CD59_HUMAN (P13987) CD59 glycoprotein OS=Homo sapiens GN=CD59 PE=1 SV=1	14167.8	4 (4 0 0 0 0)	4.83E-07
P14136	GFAP_HUMAN (P14136) Glial fibrillary acidic protein OS=Homo sapiens GN=GFAP PE=1 SV=1	49849.7	2 (0 2 0 0 0)	1.40E-07
P14174	MIF_HUMAN (P14174) Macrophage migration inhibitory factor OS=Homo sapiens GN=MIF PE=1 SV=4	12468.2	1 (1 0 0 0 0)	5.25E-04
P14406	CX7A2_HUMAN (P14406) Cytochrome c oxidase polypeptide 7A2, mitochondrial OS=Homo sapiens GN=COX	9390.1	3 (3 0 0 0 0)	7.67E-08
P14625	ENPL_HUMAN (P14625) Endoplasmin OS=Homo sapiens GN=HSP90B1 PE=1 SV=1	92411.2	9 (9 0 0 0 0)	8.11E-07
P14649	MYL6B_HUMAN (P14649) Myosin light chain 6B OS=Homo sapiens GN=MYL6B PE=1 SV=1	22749.7	3 (3 0 0 0 0)	3.30E-07
P14866	HNRPL_HUMAN (P14866) Heterogeneous nuclear ribonucleoprotein L OS=Homo sapiens GN=HNRNPL PE=	64092.4	3 (3 0 0 0 0)	3.34E-06
P14868	SYDC_HUMAN (P14868) Aspartyl-tRNA synthetase, cytoplasmic OS=Homo sapiens GN=DARS PE=1 SV=2	57100.1	2 (2 0 0 0 0)	4.71E-06
P15151	PVR_HUMAN (P15151) Poliovirus receptor OS=Homo sapiens GN=PVR PE=1 SV=2	45273.9	2 (2 0 0 0 0)	2.59E-08
P15559	NQO1_HUMAN (P15559) NAD(P)H dehydrogenase [quinone] 1 OS=Homo sapiens GN=NQO1 PE=1 SV=1	30848.0	2 (2 0 0 0 0)	2.28E-08
P16070	CD44_HUMAN (P16070) CD44 antigen OS=Homo sapiens GN=CD44 PE=1 SV=2	81503.4	5 (5 0 0 0 0)	1.32E-08
P16152	CBR1_HUMAN (P16152) Carbonyl reductase [NADPH] 1 OS=Homo sapiens GN=CBR1 PE=1 SV=3	30355.9	1 (1 0 0 0 0)	2.44E-08
P16401	H15_HUMAN (P16401) Histone H1.5 OS=Homo sapiens GN=HIST1H1B PE=1 SV=3	22566.5	7 (7 0 0 0 0)	1.89E-07
P16403	H12_HUMAN (P16403) Histone H1.2 OS=Homo sapiens GN=HIST1H1C PE=1 SV=2	21351.8	7 (7 0 0 0 0)	8.36E-08
P16615	AT2A2_HUMAN (P16615) Sarcoplasmic/endoplasmic reticulum calcium ATPase 2 OS=Homo sapiens GN=ATI	114682.7	9 (9 0 0 0 0)	2.31E-10
P17066	HSP76_HUMAN (P17066) Heat shock 70 kDa protein 6 OS=Homo sapiens GN=HSPA6 PE=1 SV=2	70984.4	4 (4 0 0 0 0)	1.29E-08
P17096	HMGA1_HUMAN (P17096) High mobility group protein HMG-I/HMG-Y OS=Homo sapiens GN=HMGA1 PE=1	11669.2	2 (2 0 0 0 0)	2.86E-10
P17301	ITA2_HUMAN (P17301) Integrin alpha-2 OS=Homo sapiens GN=ITGA2 PE=1 SV=1	129213.8	5 (5 0 0 0 0)	1.78E-07
P17612	KAPCA_HUMAN (P17612) cAMP-dependent protein kinase catalytic subunit alpha OS=Homo sapiens GN=PR	40564.0	2 (2 0 0 0 0)	2.63E-08
P17661	DESM_HUMAN (P17661) Desmin OS=Homo sapiens GN=DES PE=1 SV=3	53503.2	3 (3 0 0 0 0)	6.44E-05
P17813	EGLN_HUMAN (P17813) Endoglin OS=Homo sapiens GN=ENG PE=1 SV=2	70533.2	3 (3 0 0 0 0)	4.73E-09
P17844	DDX5_HUMAN (P17844) Probable ATP-dependent RNA helicase DDX5 OS=Homo sapiens GN=DDX5 PE=1	69104.8	9 (9 0 0 0 0)	7.09E-08
P17980	PRS6A_HUMAN (P17980) 26S protease regulatory subunit 6A OS=Homo sapiens GN=PSMC3 PE=1 SV=3	49172.5	4 (4 0 0 0 0)	7.02E-11
P17987	TCPA_HUMAN (P17987) T-complex protein 1 subunit alpha OS=Homo sapiens GN=CCT1 PE=1 SV=1	60305.7	1 (1 0 0 0 0)	6.19E-05
P18077	RL35A_HUMAN (P18077) 60S ribosomal protein L35a OS=Homo sapiens GN=RPL35A PE=1 SV=2	12529.8	2 (2 0 0 0 0)	3.11E-05
P18084	ITB5_HUMAN (P18084) Integrin beta-5 OS=Homo sapiens GN=ITGB5 PE=2 SV=1	87996.2	1 (1 0 0 0 0)	7.80E-05
P18085	ARF4_HUMAN (P18085) ADP-ribosylation factor 4 OS=Homo sapiens GN=ARF4 PE=1 SV=3	20497.7	7 (7 0 0 0 0)	2.82E-07
P18206	VINC_HUMAN (P18206) Vinculin OS=Homo sapiens GN=VCL PE=1 SV=4	123721.9	5 (5 0 0 0 0)	9.61E-09
P18621	RL17_HUMAN (P18621) 60S ribosomal protein L17 OS=Homo sapiens GN=RPL17 PE=1 SV=3	21383.3	8 (8 0 0 0 0)	1.53E-10
P18669	PGAM1_HUMAN (P18669) Phosphoglycerate mutase 1 OS=Homo sapiens GN=PGAM1 PE=1 SV=2	28785.9	7 (7 0 0 0 0)	3.64E-10
P19013	K2C4_HUMAN (P19013) Keratin, type II cytoskeletal 4 OS=Homo sapiens GN=KRT4 PE=1 SV=4	57249.9	5 (5 0 0 0 0)	3.07E-09
P19022	CADH2_HUMAN (P19022) Cadherin-2 OS=Homo sapiens GN=CDH2 PE=1 SV=4	99747.4	1 (1 0 0 0 0)	3.54E-08
P19256	LFA3_HUMAN (P19256) Lymphocyte function-associated antigen 3 OS=Homo sapiens GN=CD58 PE=1 SV=1	28128.9	1 (1 0 0 0 0)	2.44E-07
P19338	NUCL_HUMAN (P19338) Nucleolin OS=Homo sapiens GN=NCL PE=1 SV=3	76568.5	11 (11 0 0 0 0)	1.82E-11
P19525	E2AK2_HUMAN (P19525) Interferon-induced, double-stranded RNA-activated protein kinase OS=Homo sapie	62055.7	1 (1 0 0 0 0)	1.20E-06
P20020	AT2B1_HUMAN (P20020) Plasma membrane calcium-transporting ATPase 1 OS=Homo sapiens GN=ATP2B1	138667.9	5 (15 0 0 0 0)	4.23E-10
P20042	IF2B_HUMAN (P20042) Eukaryotic translation initiation factor 2 subunit 2 OS=Homo sapiens GN=EIF2S2 PE=	38364.4	1 (1 0 0 0 0)	3.21E-06
P20309	ACM3_HUMAN (P20309) Muscarinic acetylcholine receptor M3 OS=Homo sapiens GN=CHRM3 PE=1 SV=1	66085.9	2 (2 0 0 0 0)	5.57E-07
P20339	RAB5A_HUMAN (P20339) Ras-related protein Rab-5A OS=Homo sapiens GN=RAB5A PE=1 SV=2	23643.8	8 (8 0 0 0 0)	1.91E-07
P20340	RAB6A_HUMAN (P20340) Ras-related protein Rab-6A OS=Homo sapiens GN=RAB6A PE=1 SV=3	23577.9	5 (5 0 0 0 0)	1.65E-07
P20618	PSB1_HUMAN (P20618) Proteasome subunit beta type-1 OS=Homo sapiens GN=PSMB1 PE=1 SV=2	26472.4	4 (4 0 0 0 0)	1.02E-08
P20645	MPRD_HUMAN (P20645) Cation-dependent mannose-6-phosphate receptor OS=Homo sapiens GN=M6PR P	30973.4	2 (2 0 0 0 0)	1.11E-11
P20648	ATP4A_HUMAN (P20648) Potassium-transporting ATPase alpha chain 1 OS=Homo sapiens GN=ATP4A PE=2	114045.4	1 (1 0 0 0 0)	4.35E-06
P20674	COX5A_HUMAN (P20674) Cytochrome c oxidase subunit 5A, mitochondrial OS=Homo sapiens GN=COX5A P	16751.7	4 (4 0 0 0 0)	1.57E-08
P20700	LMNB1_HUMAN (P20700) Lamin-B1 OS=Homo sapiens GN=LMNB1 PE=1 SV=2	66367.7	3 (23 0 0 0 0)	1.18E-09
P21283	VATC1_HUMAN (P21283) V-type proton ATPase subunit C 1 OS=Homo sapiens GN=ATP6V1C1 PE=1 SV=4	43914.0	1 (1 0 0 0 0)	4.34E-05
P21291	CSRP1_HUMAN (P21291) Cysteine and glycine-rich protein 1 OS=Homo sapiens GN=CSRP1 PE=1 SV=3	20553.8	7 (7 0 0 0 0)	1.27E-09
P21333	FLNA_HUMAN (P21333) Filamin-A OS=Homo sapiens GN=FLNA PE=1 SV=4	280561.4	1 (71 0 0 0 0)	1.14E-10
P21589	5NTD_HUMAN (P21589) 5'-nucleotidase OS=Homo sapiens GN=NT5E PE=1 SV=1	63327.6	3 (23 0 0 0 0)	2.97E-12
P21796	VDAC1_HUMAN (P21796) Voltage-dependent anion-selective channel protein 1 OS=Homo sapiens GN=VDA	30753.6	9 (5 4 0 0 0)	6.18E-10
P21860	ERBB3_HUMAN (P21860) Receptor tyrosine-protein kinase erbB-3 OS=Homo sapiens GN=ERBB3 PE=1 SV=	148002.2	1 (1 0 0 0 0)	2.61E-08
P21926	CD9_HUMAN (P21926) CD9 antigen OS=Homo sapiens GN=CD9 PE=1 SV=4	25399.0	2 (2 0 0 0 0)	1.17E-05
P21964	COMT_HUMAN (P21964) Catechol O-methyltransferase OS=Homo sapiens GN=COMT PE=1 SV=2	30017.6	2 (2 0 0 0 0)	8.51E-06
P22061	PIMT_HUMAN (P22061) Protein-L-isoaspartate(D-aspartate) O-methyltransferase OS=Homo sapiens GN=PC	24634.6	1 (1 0 0 0 0)	3.57E-09
P22087	FBRL_HUMAN (P22087) rRNA 2'-O-methyltransferase fibrillarin OS=Homo sapiens GN=FBL PE=1 SV=2	33763.4	2 (12 0 0 0 0)	2.02E-11
P22307	NLTP_HUMAN (P22307) Non-specific lipid-transfer protein OS=Homo sapiens GN=SCP2 PE=1 SV=2	58955.7	5 (5 0 0 0 0)	1.07E-06
P22314	UBA1_HUMAN (P22314) Ubiquitin-like modifier-activating enzyme 1 OS=Homo sapiens GN=UBA1 PE=1 SV=	117774.5	3 (3 0 0 0 0)	5.64E-08
P22626	ROA2_HUMAN (P22626) Heterogeneous nuclear ribonucleoproteins A2/B1 OS=Homo sapiens GN=HNRNPA2	37406.7	7 (7 0 0 0 0)	2.72E-10
P22695	QCR2_HUMAN (P22695) Cytochrome b-c1 complex subunit 2, mitochondrial OS=Homo sapiens GN=UQCRC	48412.9	2 (2 0 0 0 0)	3.58E-08
P23193	TCEA1_HUMAN (P23193) Transcription elongation factor A protein 1 OS=Homo sapiens GN=TCEA1 PE=1 SV	33948.0	2 (2 0 0 0 0)	2.58E-08
P23246	SFPQ_HUMAN (P23246) Splicing factor, proline- and glutamine-rich OS=Homo sapiens GN=SFPQ PE=1 SV=	76101.8	1 (1 0 0 0 0)	6.40E-06
P23284	PPIB_HUMAN (P23284) Peptidyl-prolyl cis-trans isomerase B OS=Homo sapiens GN=PPIB PE=1 SV=2	23727.5	0 (10 0 0 0 0)	1.98E-05
P23396	RS3_HUMAN (P23396) 40S ribosomal protein S3 OS=Homo sapiens GN=RPS3 PE=1 SV=2	26671.4	4 (14 0 0 0 0)	3.26E-11
P23470	PTPRG_HUMAN (P23470) Receptor-type tyrosine-protein phosphatase gamma OS=Homo sapiens GN=PTPR	161926.0	1 (1 0 0 0 0)	1.79E-06
P23528	COF1_HUMAN (P23528) Cofilin-1 OS=Homo sapiens GN=CFL1 PE=1 SV=3	18490.7	8 (8 0 0 0 0)	4.24E-08

P23634	AT2B4_HUMAN (P23634) Plasma membrane calcium-transporting ATPase 4 OS=Homo sapiens GN=ATP2B4	137832.9	6 (6 0 0 0 0)	2.41E-10
P23919	KTHY_HUMAN (P23919) Thymidylate kinase OS=Homo sapiens GN=DTYMK PE=1 SV=4	23804.5	1 (1 0 0 0 0)	4.79E-05
P24539	AT5F1_HUMAN (P24539) ATP synthase subunit b, mitochondrial OS=Homo sapiens GN=ATP5F1 PE=1 SV=2	28890.3	8 (8 0 0 0 0)	4.85E-09
P24752	THIL_HUMAN (P24752) Acetyl-CoA acetyltransferase, mitochondrial OS=Homo sapiens GN=ACAT1 PE=1 SV	45170.7	7 (7 0 0 0 0)	3.71E-09
P24941	CDK2_HUMAN (P24941) Cell division protein kinase 2 OS=Homo sapiens GN=CDK2 PE=1 SV=2	33908.0	1 (1 0 0 0 0)	5.96E-06
P25398	RS12_HUMAN (P25398) 40S ribosomal protein S12 OS=Homo sapiens GN=RPS12 PE=1 SV=2	14516.5	5 (5 0 0 0 0)	3.56E-06
P25685	DNJB1_HUMAN (P25685) DnaJ homolog subfamily B member 1 OS=Homo sapiens GN=DNAJB1 PE=1 SV=4	38020.4	2 (2 0 0 0 0)	1.45E-06
P25705	ATPA_HUMAN (P25705) ATP synthase subunit alpha, mitochondrial OS=Homo sapiens GN=ATP5A1 PE=1 SV	59713.7	2 (12 0 0 0 0)	1.47E-10
P25787	PSA2_HUMAN (P25787) Proteasome subunit alpha type-2 OS=Homo sapiens GN=PSMA2 PE=1 SV=2	25882.3	3 (3 0 0 0 0)	4.04E-10
P25789	PSA4_HUMAN (P25789) Proteasome subunit alpha type-4 OS=Homo sapiens GN=PSMA4 PE=1 SV=1	29465.2	2 (2 0 0 0 0)	3.79E-06
P26006	ITA3_HUMAN (P26006) Integrin alpha-3 OS=Homo sapiens GN=ITGA3 PE=1 SV=3	118622.2	9 (9 0 0 0 0)	5.31E-12
P26368	U2AF2_HUMAN (P26368) Splicing factor U2AF 65 kDa subunit OS=Homo sapiens GN=U2AF2 PE=1 SV=4	53467.3	1 (1 0 0 0 0)	8.48E-06
P26373	RL13_HUMAN (P26373) 60S ribosomal protein L13 OS=Homo sapiens GN=RPL13 PE=1 SV=4	24246.5	4 (4 0 0 0 0)	3.09E-06
P26447	S10A4_HUMAN (P26447) Protein S100-A4 OS=Homo sapiens GN=S100A4 PE=1 SV=1	11720.7	4 (4 0 0 0 0)	7.73E-06
P26639	SYTC_HUMAN (P26639) Threonyl-tRNA synthetase, cytoplasmic OS=Homo sapiens GN=TARS PE=1 SV=3	83382.0	1 (1 0 0 0 0)	5.05E-08
P27105	STOM_HUMAN (P27105) Erythrocyte band 7 integral membrane protein OS=Homo sapiens GN=STOM PE=1	31710.7	6 (6 0 0 0 0)	1.81E-07
P27144	KAD4_HUMAN (P27144) Adenylate kinase isoenzyme 4, mitochondrial OS=Homo sapiens GN=AK3L1 PE=1 S	25252.2	2 (2 0 0 0 0)	2.25E-07
P27348	1433T_HUMAN (P27348) 14-3-3 protein theta OS=Homo sapiens GN=YWHAQ PE=1 SV=1	27746.8	2 (2 0 0 0 0)	8.54E-08
P27348	1433T_HUMAN (P27348) 14-3-3 protein theta OS=Homo sapiens GN=YWHAQ PE=1 SV=1	27746.8	1 (1 0 0 0 0)	4.72E-06
P27695	APEX1_HUMAN (P27695) DNA-(apurinic or apyrimidinic site) lyase OS=Homo sapiens GN=APEX1 PE=1 SV=	35532.2	7 (7 0 0 0 0)	1.10E-07
P27708	PYR1_HUMAN (P27708) CAD protein OS=Homo sapiens GN=CAD PE=1 SV=3	242827.1	6 (6 0 0 0 0)	5.48E-10
P27816	MAP4_HUMAN (P27816) Microtubule-associated protein 4 OS=Homo sapiens GN=MAP4 PE=1 SV=2	120944.1	3 (3 0 0 0 0)	2.18E-09
P28066	PSA5_HUMAN (P28066) Proteasome subunit alpha type-5 OS=Homo sapiens GN=PSMA5 PE=1 SV=3	26394.2	5 (5 0 0 0 0)	1.79E-09
P28072	PSB6_HUMAN (P28072) Proteasome subunit beta type-6 OS=Homo sapiens GN=PSMB6 PE=1 SV=4	25341.5	2 (2 0 0 0 0)	3.76E-07
P28074	PSB5_HUMAN (P28074) Proteasome subunit beta type-5 OS=Homo sapiens GN=PSMB5 PE=1 SV=3	28462.2	4 (4 0 0 0 0)	2.83E-07
P28482	MK01_HUMAN (P28482) Mitogen-activated protein kinase 1 OS=Homo sapiens GN=MAPK1 PE=1 SV=3	41363.3	6 (4 2 0 0 0)	4.98E-10
P28838	AMPL_HUMAN (P28838) Cytosol aminopeptidase OS=Homo sapiens GN=LAP3 PE=1 SV=3	56130.9	1 (1 0 0 0 0)	3.93E-08
P29317	EPHA2_HUMAN (P29317) Ephrin type-A receptor 2 OS=Homo sapiens GN=EPHA2 PE=1 SV=1	108184.8	7 (17 0 0 0 0)	2.61E-13
P29320	EPHA3_HUMAN (P29320) Ephrin type-A receptor 3 OS=Homo sapiens GN=EPHA3 PE=1 SV=2	110060.2	7 (7 0 0 0 0)	2.77E-10
P29323	EPHB2_HUMAN (P29323) Ephrin type-B receptor 2 OS=Homo sapiens GN=EPHB2 PE=1 SV=5	117416.9	4 (4 0 0 0 0)	3.52E-07
P29992	GNA11_HUMAN (P29992) Guanine nucleotide-binding protein subunit alpha-11 OS=Homo sapiens GN=GNA1	42096.6	6 (6 0 0 0 0)	7.97E-10
P30041	PRDX6_HUMAN (P30041) Peroxiredoxin-6 OS=Homo sapiens GN=PRDX6 PE=1 SV=3	25019.2	2 (2 0 0 0 0)	7.66E-05
P30042	ES1_HUMAN (P30042) ES1 protein homolog, mitochondrial OS=Homo sapiens GN=C21orf33 PE=1 SV=3	28152.7	4 (4 0 0 0 0)	4.88E-09
P30044	PRDX5_HUMAN (P30044) Peroxiredoxin-5, mitochondrial OS=Homo sapiens GN=PRDX5 PE=1 SV=3	22012.5	4 (4 0 0 0 0)	1.41E-08
P30048	PRDX3_HUMAN (P30048) Thioredoxin-dependent peroxide reductase, mitochondrial OS=Homo sapiens GN=	27675.2	2 (2 0 0 0 0)	6.31E-06
P30084	ECHM_HUMAN (P30084) Enoyl-CoA hydratase, mitochondrial OS=Homo sapiens GN=ECHS1 PE=1 SV=4	31367.1	9 (9 0 0 0 0)	5.11E-09
P30101	PDIA3_HUMAN (P30101) Protein disulfide-isomerase A3 OS=Homo sapiens GN=PDIA3 PE=1 SV=4	56746.8	2 (2 0 0 0 0)	9.22E-07
P30461	1B13_HUMAN (P30461) HLA class I histocompatibility antigen, B-13 alpha chain OS=Homo sapiens GN=HLA	40449.1	8 (8 0 0 0 0)	3.98E-08
P30519	HMOX2_HUMAN (P30519) Heme oxygenase 2 OS=Homo sapiens GN=HMOX2 PE=1 SV=2	36009.9	2 (2 0 0 0 0)	3.14E-08
P30711	GSTT1_HUMAN (P30711) Glutathione S-transferase theta-1 OS=Homo sapiens GN=GSTT1 PE=1 SV=4	27317.6	1 (1 0 0 0 0)	1.04E-09
P30825	CTR1_HUMAN (P30825) High affinity cationic amino acid transporter 1 OS=Homo sapiens GN=SLC7A1 PE=1	67594.3	4 (4 0 0 0 0)	1.00E-07
P31689	DNJA1_HUMAN (P31689) DnaJ homolog subfamily A member 1 OS=Homo sapiens GN=DNAJA1 PE=1 SV=2	44839.5	2 (2 0 0 0 0)	5.52E-07
P31930	QCR1_HUMAN (P31930) Cytochrome b-c1 complex subunit 1, mitochondrial OS=Homo sapiens GN=UQCRC	52612.5	2 (2 0 0 0 0)	7.22E-06
P31939	PUR9_HUMAN (P31939) Bifunctional purine biosynthesis protein PURH OS=Homo sapiens GN=ATIC PE=1 S	64575.5	3 (3 0 0 0 0)	1.10E-08
P31942	HNRH3_HUMAN (P31942) Heterogeneous nuclear ribonucleoprotein H3 OS=Homo sapiens GN=HNRNPH3 P	36903.0	2 (2 0 0 0 0)	3.78E-06
P31943	HNRH1_HUMAN (P31943) Heterogeneous nuclear ribonucleoprotein H OS=Homo sapiens GN=HNRNPH1 PE	49198.4	4 (4 0 0 0 0)	4.02E-09
P31946	1433B_HUMAN (P31946) 14-3-3 protein beta/alpha OS=Homo sapiens GN=YWHAB PE=1 SV=3	28064.8	6 (6 0 0 0 0)	1.58E-08
P31949	S10AB_HUMAN (P31949) Protein S100-A11 OS=Homo sapiens GN=S100A11 PE=1 SV=2	11732.8	3 (3 0 0 0 0)	4.05E-07
P32119	PRDX2_HUMAN (P32119) Peroxiredoxin-2 OS=Homo sapiens GN=PRDX2 PE=1 SV=5	21878.2	0 (10 0 0 0 0)	2.32E-10
P32969	RL9_HUMAN (P32969) 60S ribosomal protein L9 OS=Homo sapiens GN=RPL9 PE=1 SV=1	21849.8	7 (7 0 0 0 0)	1.64E-11
P32970	CD70_HUMAN (P32970) CD70 antigen OS=Homo sapiens GN=CD70 PE=1 SV=2	21104.9	1 (1 0 0 0 0)	1.21E-07
P33176	KINH_HUMAN (P33176) Kinesin-1 heavy chain OS=Homo sapiens GN=KIF5B PE=1 SV=1	109616.9	7 (17 0 0 0 0)	4.54E-11
P33527	MRP1_HUMAN (P33527) Multidrug resistance-associated protein 1 OS=Homo sapiens GN=ABCC1 PE=1 SV=	171450.5	3 (3 0 0 0 0)	2.90E-09
P33992	MCM5_HUMAN (P33992) DNA replication licensing factor MCM5 OS=Homo sapiens GN=MCM5 PE=1 SV=5	82233.3	2 (2 0 0 0 0)	2.89E-07
P34741	SDC2_HUMAN (P34741) Syndecan-2 OS=Homo sapiens GN=SDC2 PE=1 SV=2	22146.2	2 (2 0 0 0 0)	6.93E-07
P34897	GLYM_HUMAN (P34897) Serine hydroxymethyltransferase, mitochondrial OS=Homo sapiens GN=SHMT2 PE	55957.8	5 (5 0 0 0 0)	1.65E-08
P34932	HSP74_HUMAN (P34932) Heat shock 70 kDa protein 4 OS=Homo sapiens GN=HSPA4 PE=1 SV=4	94271.1	1 (1 0 0 0 0)	1.26E-06
P35030	TRY3_HUMAN (P35030) Trypsin-3 OS=Homo sapiens GN=PRSS3 PE=1 SV=2	32508.0	1 (1 0 0 0 0)	7.29E-06
P35052	GPC1_HUMAN (P35052) Glypican-1 OS=Homo sapiens GN=GPC1 PE=1 SV=1	61611.1	1 (1 0 0 0 0)	2.43E-09
P35221	CTNA1_HUMAN (P35221) Catenin alpha-1 OS=Homo sapiens GN=CTNNA1 PE=1 SV=1	100008.6	0 (10 0 0 0 0)	2.82E-09
P35222	CTNB1_HUMAN (P35222) Catenin beta-1 OS=Homo sapiens GN=CTNNB1 PE=1 SV=1	85442.3	7 (7 0 0 0 0)	1.29E-08
P35232	PHB_HUMAN (P35232) Prohibitin OS=Homo sapiens GN=PHB PE=1 SV=1	29785.9	7 (7 0 0 0 0)	9.28E-08
P35249	RFC4_HUMAN (P35249) Replication factor C subunit 4 OS=Homo sapiens GN=RFC4 PE=1 SV=2	39656.9	1 (1 0 0 0 0)	3.22E-08
P35250	RFC2_HUMAN (P35250) Replication factor C subunit 2 OS=Homo sapiens GN=RFC2 PE=1 SV=3	39132.1	4 (4 0 0 0 0)	4.16E-07
P35268	RL22_HUMAN (P35268) 60S ribosomal protein L22 OS=Homo sapiens GN=RPL22 PE=1 SV=2	14777.8	2 (2 0 0 0 0)	1.64E-07
P35268	RL22_HUMAN (P35268) 60S ribosomal protein L22 OS=Homo sapiens GN=RPL22 PE=1 SV=2	14777.8	1 (1 0 0 0 0)	2.70E-05
P35270	SPRE_HUMAN (P35270) Sepiapterin reductase OS=Homo sapiens GN=SPR PE=1 SV=1	28030.8	4 (4 0 0 0 0)	4.44E-11
P35527	K1C9_HUMAN (P35527) Keratin, type I cytoskeletal 9 OS=Homo sapiens GN=KRT9 PE=1 SV=2	62091.8	5 (14 1 0 0 0)	1.44E-10
P35579	MYH9_HUMAN (P35579) Myosin-9 OS=Homo sapiens GN=MYH9 PE=1 SV=4	226390.6	4 (43 0 0 0 1)	4.33E-14
P35613	BASI_HUMAN (P35613) Basigin OS=Homo sapiens GN=BSG PE=1 SV=2	42174.1	0 (10 0 0 0 0)	2.80E-12
P35659	DEK_HUMAN (P35659) Protein DEK OS=Homo sapiens GN=DEK PE=1 SV=1	42648.0	2 (2 0 0 0 0)	3.86E-07
P35908	K22E_HUMAN (P35908) Keratin, type II cytoskeletal 2 epidermal OS=Homo sapiens GN=KRT2 PE=1 SV=1	65825.4	0 (19 1 0 0 0)	2.60E-13
P36404	ARL2_HUMAN (P36404) ADP-ribosylation factor-like protein 2 OS=Homo sapiens GN=ARL2 PE=1 SV=4	20864.9	1 (1 0 0 0 0)	7.66E-05
P36405	ARL3_HUMAN (P36405) ADP-ribosylation factor-like protein 3 OS=Homo sapiens GN=ARL3 PE=1 SV=2	20442.8	1 (1 0 0 0 0)	2.15E-06
P36551	HEM6_HUMAN (P36551) Coproporphyrinogen III oxidase, mitochondrial OS=Homo sapiens GN=CPOX PE=1	50120.1	4 (4 0 0 0 0)	7.81E-08
P36957	ODO2_HUMAN (P36957) Dihydrolipoyllysine-residue succinyltransferase component of 2-oxoglutarate dehydr	48698.6	2 (2 0 0 0 0)	1.18E-08

P37108	SRP14_HUMAN (P37108) Signal recognition particle 14 kDa protein OS=Homo sapiens GN=SRP14 PE=1 SV	14560.8	1 (1 0 0 0 0)	1.33E-08
P37198	NUP62_HUMAN (P37198) Nuclear pore glycoprotein p62 OS=Homo sapiens GN=NUP62 PE=1 SV=3	53222.5	2 (2 0 0 0 0)	1.28E-06
P37802	TAGL2_HUMAN (P37802) Transgelin-2 OS=Homo sapiens GN=TAGLN2 PE=1 SV=3	22377.2	7 (7 0 0 0 0)	5.03E-08
P38159	HNRPG_HUMAN (P38159) Heterogeneous nuclear ribonucleoprotein G OS=Homo sapiens GN=RBMX PE=1	42306.3	1 (1 0 0 0 0)	1.79E-05
P39023	RL3_HUMAN (P39023) 60S ribosomal protein L3 OS=Homo sapiens GN=RPL3 PE=1 SV=2	46079.8	8 (8 0 0 0 0)	2.24E-08
P39060	COIA1_HUMAN (P39060) Collagen alpha-1(XVIII) chain OS=Homo sapiens GN=COL18A1 PE=1 SV=5	178076.4	1 (1 0 0 0 0)	4.08E-07
P40121	CAPG_HUMAN (P40121) Macrophage-capping protein OS=Homo sapiens GN=CAPG PE=1 SV=1	38493.6	2 (2 0 0 0 0)	1.39E-07
P40227	TCPZ_HUMAN (P40227) T-complex protein 1 subunit zeta OS=Homo sapiens GN=CCT6A PE=1 SV=3	57987.7	4 (4 0 0 0 0)	9.94E-07
P40616	ARL1_HUMAN (P40616) ADP-ribosylation factor-like protein 1 OS=Homo sapiens GN=ARL1 PE=1 SV=1	20404.5	3 (3 0 0 0 0)	1.78E-05
P40763	STAT3_HUMAN (P40763) Signal transducer and activator of transcription 3 OS=Homo sapiens GN=STAT3 PE	88011.4	2 (2 0 0 0 0)	2.44E-07
P40926	MDHM_HUMAN (P40926) Malate dehydrogenase, mitochondrial OS=Homo sapiens GN=MDH2 PE=1 SV=3	35480.7	3 (3 0 0 0 0)	1.09E-05
P41219	PERI_HUMAN (P41219) Peripherin OS=Homo sapiens GN=PRPH PE=1 SV=2	53618.5	3 (2 0 1 0 0)	3.18E-07
P41240	CSK_HUMAN (P41240) Tyrosine-protein kinase CSK OS=Homo sapiens GN=CSK PE=1 SV=1	50671.8	2 (2 0 0 0 0)	5.81E-07
P42126	D3D2_HUMAN (P42126) 3,2-trans-enoyl-CoA isomerase, mitochondrial OS=Homo sapiens GN=DCI PE=1 SV	32795.2	2 (2 0 0 0 0)	5.46E-08
P42765	THIM_HUMAN (P42765) 3-ketoacyl-CoA thiolase, mitochondrial OS=Homo sapiens GN=ACAA2 PE=1 SV=2	41897.7	1 (1 0 0 0 0)	1.40E-08
P42766	RL35_HUMAN (P42766) 60S ribosomal protein L35 OS=Homo sapiens GN=RPL35 PE=1 SV=2	14542.6	2 (2 0 0 0 0)	3.92E-06
P43007	SATT_HUMAN (P43007) Neutral amino acid transporter A OS=Homo sapiens GN=SLC1A4 PE=1 SV=1	55687.8	4 (4 0 0 0 0)	3.35E-08
P43034	LIS1_HUMAN (P43034) Platelet-activating factor acetylhydrolase IB subunit alpha OS=Homo sapiens GN=PAF	46608.2	5 (5 0 0 0 0)	9.47E-10
P43121	MUC18_HUMAN (P43121) Cell surface glycoprotein MUC18 OS=Homo sapiens GN=MCAM PE=1 SV=2	71562.7	2 (12 0 0 0 0)	7.97E-09
P43243	MATR3_HUMAN (P43243) Matrin-3 OS=Homo sapiens GN=MATR3 PE=1 SV=2	94564.7	2 (2 0 0 0 0)	4.46E-09
P43304	GPDM_HUMAN (P43304) Glycerol-3-phosphate dehydrogenase, mitochondrial OS=Homo sapiens GN=GPD2	80782.6	8 (8 0 0 0 0)	1.26E-09
P43307	SSRA_HUMAN (P43307) Translocon-associated protein subunit alpha OS=Homo sapiens GN=SSR1 PE=1 SV	32215.4	4 (4 0 0 0 0)	4.65E-08
P43362	MAGA9_HUMAN (P43362) Melanoma-associated antigen 9 OS=Homo sapiens GN=MAGEA9 PE=2 SV=1	35066.0	1 (1 0 0 0 0)	1.61E-06
P43487	RANG_HUMAN (P43487) Ran-specific GTPase-activating protein OS=Homo sapiens GN=RANBP1 PE=1 SV=	23295.6	3 (3 0 0 0 0)	4.36E-07
P43490	NAMPT_HUMAN (P43490) Nicotinamide phosphoribosyltransferase OS=Homo sapiens GN=NAMPT PE=1 SV	55486.6	1 (1 0 0 0 0)	5.76E-04
P43686	PRS6B_HUMAN (P43686) 26S protease regulatory subunit 6B OS=Homo sapiens GN=PSMC4 PE=1 SV=2	47336.6	3 (3 0 0 0 0)	6.18E-11
P45880	VDAC2_HUMAN (P45880) Voltage-dependent anion-selective channel protein 2 OS=Homo sapiens GN=VDAC	31546.5	6 (6 0 0 0 0)	4.15E-08
P46063	RECQ1_HUMAN (P46063) ATP-dependent DNA helicase Q1 OS=Homo sapiens GN=RECQL PE=1 SV=3	73410.0	1 (1 0 0 0 0)	3.33E-05
P46776	RL27A_HUMAN (P46776) 60S ribosomal protein L27a OS=Homo sapiens GN=RPL27A PE=1 SV=2	16551.0	2 (2 0 0 0 0)	9.28E-06
P46781	RS9_HUMAN (P46781) 40S ribosomal protein S9 OS=Homo sapiens GN=RPS9 PE=1 SV=3	22577.6	3 (3 0 0 0 0)	2.48E-05
P46782	RS5_HUMAN (P46782) 40S ribosomal protein S5 OS=Homo sapiens GN=RPS5 PE=1 SV=4	22862.1	7 (7 0 0 0 0)	5.60E-08
P46934	NEDD4_HUMAN (P46934) E3 ubiquitin-protein ligase NEDD4 OS=Homo sapiens GN=NEDD4 PE=1 SV=2	114864.9	1 (1 0 0 0 0)	2.43E-05
P46939	UTRO_HUMAN (P46939) Utrophin OS=Homo sapiens GN=UTRN PE=1 SV=2	394219.4	7 (7 0 0 0 0)	6.01E-08
P46940	IQGA1_HUMAN (P46940) Ras GTPase-activating-like protein IQGAP1 OS=Homo sapiens GN=IQGAP1 PE=1	189132.9	11 (11 0 0 0 0)	4.41E-11
P47755	CAZA2_HUMAN (P47755) F-actin-capping protein subunit alpha-2 OS=Homo sapiens GN=CAPZA2 PE=1 SV	32928.6	2 (2 0 0 0 0)	2.82E-11
P47756	CAPZB_HUMAN (P47756) F-actin-capping protein subunit beta OS=Homo sapiens GN=CAPZB PE=1 SV=4	31330.8	2 (2 0 0 0 0)	1.32E-05
P47895	AL1A3_HUMAN (P47895) Aldehyde dehydrogenase family 1 member A3 OS=Homo sapiens GN=ALDH1A3 P	56072.9	0 (10 0 0 0 0)	8.64E-11
P47897	SYQ_HUMAN (P47897) Glutaminyl-tRNA synthetase OS=Homo sapiens GN=QARS PE=1 SV=1	87743.0	3 (13 0 0 0 0)	8.59E-10
P48047	ATPO_HUMAN (P48047) ATP synthase subunit O, mitochondrial OS=Homo sapiens GN=ATP5O PE=1 SV=1	23262.7	3 (3 0 0 0 0)	1.44E-07
P48059	LIMS1_HUMAN (P48059) LIM and senescent cell antigen-like-containing domain protein 1 OS=Homo sapiens	37225.9	2 (2 0 0 0 0)	3.32E-08
P48643	TCPE_HUMAN (P48643) T-complex protein 1 subunit epsilon OS=Homo sapiens GN=CCT5 PE=1 SV=1	59632.9	3 (3 0 0 0 0)	8.21E-09
P48735	IDHP_HUMAN (P48735) Isocitrate dehydrogenase [NADP], mitochondrial OS=Homo sapiens GN=IDH2 PE=1	50876.9	1 (0 1 0 0 0)	1.11E-04
P49023	PAXI_HUMAN (P49023) Paxillin OS=Homo sapiens GN=PXN PE=1 SV=2	64491.9	1 (1 0 0 0 0)	4.77E-07
P49207	RL34_HUMAN (P49207) 60S ribosomal protein L34 OS=Homo sapiens GN=RPL34 PE=1 SV=3	13284.5	2 (2 0 0 0 0)	6.67E-06
P49257	LMAN1_HUMAN (P49257) Protein ERGIC-53 OS=Homo sapiens GN=LMAN1 PE=1 SV=2	57513.1	1 (1 0 0 0 0)	5.91E-06
P49411	EFTU_HUMAN (P49411) Elongation factor Tu, mitochondrial OS=Homo sapiens GN=TUFM PE=1 SV=2	49510.2	6 (6 0 0 0 0)	1.24E-08
P49419	AL7A1_HUMAN (P49419) Alpha-aminoadipic semialdehyde dehydrogenase OS=Homo sapiens GN=ALDH7A1	55331.5	3 (3 0 0 0 0)	1.02E-06
P49588	SYAC_HUMAN (P49588) Alanyl-tRNA synthetase, cytoplasmic OS=Homo sapiens GN=AARS PE=1 SV=2	106743.3	2 (2 0 0 0 0)	2.57E-06
P49720	PSB3_HUMAN (P49720) Proteasome subunit beta type-3 OS=Homo sapiens GN=PSMB3 PE=1 SV=2	22933.5	3 (2 1 0 0 0)	2.14E-09
P49721	PSB2_HUMAN (P49721) Proteasome subunit beta type-2 OS=Homo sapiens GN=PSMB2 PE=1 SV=1	22821.7	10 (9 0 0 1 0)	4.73E-09
P49770	EI2BB_HUMAN (P49770) Translation initiation factor eIF-2B subunit beta OS=Homo sapiens GN=EIF2B2 PE=	38964.9	2 (2 0 0 0 0)	9.43E-06
P49773	HINT1_HUMAN (P49773) Histidine triad nucleotide-binding protein 1 OS=Homo sapiens GN=HINT1 PE=1 SV	13793.1	5 (5 0 0 0 0)	6.82E-06
P49790	NU153_HUMAN (P49790) Nuclear pore complex protein Nup153 OS=Homo sapiens GN=NUP153 PE=1 SV=2	153842.5	1 (1 0 0 0 0)	4.11E-06
P49792	RBP2_HUMAN (P49792) E3 SUMO-protein ligase RanBP2 OS=Homo sapiens GN=RANBP2 PE=1 SV=2	357972.3	2 (2 0 0 0 0)	2.55E-08
P49795	RGS19_HUMAN (P49795) Regulator of G-protein signaling 19 OS=Homo sapiens GN=RGS19 PE=1 SV=1	24619.6	4 (4 0 0 0 0)	2.56E-07
P49902	5NTC_HUMAN (P49902) Cytosolic purine 5'-nucleotidase OS=Homo sapiens GN=NT5C2 PE=1 SV=1	64928.4	1 (1 0 0 0 0)	5.28E-08
P49915	GUAA_HUMAN (P49915) GMP synthase [glutamine-hydrolyzing] OS=Homo sapiens GN=GMPS PE=1 SV=1	76667.1	7 (7 0 0 0 0)	6.25E-11
P50213	IDH3A_HUMAN (P50213) Isocitrate dehydrogenase [NAD] subunit alpha, mitochondrial OS=Homo sapiens GN	39566.1	1 (1 0 0 0 0)	5.36E-07
P50402	EMD_HUMAN (P50402) Emerin OS=Homo sapiens GN=EMD PE=1 SV=1	28975.9	1 (1 0 0 0 0)	1.79E-05
P50443	S26A2_HUMAN (P50443) Sulfate transporter OS=Homo sapiens GN=SLC26A2 PE=1 SV=1	81597.0	9 (9 0 0 0 0)	3.55E-07
P50454	SERPH_HUMAN (P50454) Serpin H1 OS=Homo sapiens GN=SERPINH1 PE=1 SV=2	46411.3	1 (1 0 0 0 0)	6.09E-06
P50479	PDLI4_HUMAN (P50479) PDZ and LIM domain protein 4 OS=Homo sapiens GN=PDLIM4 PE=1 SV=2	35375.7	4 (4 0 0 0 0)	5.59E-09
P50502	F10A1_HUMAN (P50502) Hsc70-interacting protein OS=Homo sapiens GN=ST13 PE=1 SV=2	41305.5	1 (1 0 0 0 0)	3.86E-10
P50570	DYN2_HUMAN (P50570) Dynamin-2 OS=Homo sapiens GN=DNM2 PE=1 SV=2	98003.3	2 (2 0 0 0 0)	8.46E-10
P50750	CDK9_HUMAN (P50750) Cell division protein kinase 9 OS=Homo sapiens GN=CDK9 PE=1 SV=3	42750.2	1 (1 0 0 0 0)	1.65E-06
P50895	LU_HUMAN (P50895) Lutheran blood group glycoprotein OS=Homo sapiens GN=BCAM PE=1 SV=2	67362.7	7 (7 0 0 0 0)	2.55E-10
P50991	TCPD_HUMAN (P50991) T-complex protein 1 subunit delta OS=Homo sapiens GN=CCT4 PE=1 SV=4	57887.9	4 (4 0 0 0 0)	9.25E-11
P50991	TCPD_HUMAN (P50991) T-complex protein 1 subunit delta OS=Homo sapiens GN=CCT4 PE=1 SV=4	57887.9	2 (2 0 0 0 0)	7.53E-10
P51148	RAB5C_HUMAN (P51148) Ras-related protein Rab-5C OS=Homo sapiens GN=RAB5C PE=1 SV=2	23467.8	7 (7 0 0 0 0)	6.67E-09
P51149	RAB7A_HUMAN (P51149) Ras-related protein Rab-7a OS=Homo sapiens GN=RAB7A PE=1 SV=1	23474.9	2 (12 0 0 0 0)	5.47E-11
P51159	RB27A_HUMAN (P51159) Ras-related protein Rab-27A OS=Homo sapiens GN=RAB27A PE=1 SV=3	24852.3	1 (1 0 0 0 0)	3.91E-08
P51648	AL3A2_HUMAN (P51648) Fatty aldehyde dehydrogenase OS=Homo sapiens GN=ALDH3A2 PE=1 SV=1	54813.0	4 (4 0 0 0 0)	2.88E-09
P51665	PSD7_HUMAN (P51665) 26S proteasome non-ATPase regulatory subunit 7 OS=Homo sapiens GN=PSMD7 P	37002.5	1 (1 0 0 0 0)	2.41E-06
P51668	UB2D1_HUMAN (P51668) Ubiquitin-conjugating enzyme E2 D1 OS=Homo sapiens GN=UBE2D1 PE=1 SV=1	16591.4	1 (1 0 0 0 0)	1.42E-05
P51690	ARSE_HUMAN (P51690) Arylsulfatase E OS=Homo sapiens GN=ARSE PE=1 SV=2	65626.2	1 (1 0 0 0 0)	8.08E-07
P51812	KS6A3_HUMAN (P51812) Ribosomal protein S6 kinase alpha-3 OS=Homo sapiens GN=RPS6KA3 PE=1 SV=	83683.1	4 (4 0 0 0 0)	3.34E-11

P51970	NDUA8_HUMAN (P51970) NADH dehydrogenase [ubiquinone] 1 alpha subcomplex subunit 8 OS=Homo sapie	20092.1	1 (1 0 0 0 0)	5.01E-05
P52209	6PGD_HUMAN (P52209) 6-phosphogluconate dehydrogenase, decarboxylating OS=Homo sapiens GN=PGD	53106.0	1 (1 0 0 0 0)	2.72E-05
P52272	HNRPM_HUMAN (P52272) Heterogeneous nuclear ribonucleoprotein M OS=Homo sapiens GN=HNRNPM PE	77464.3	8 (8 0 0 0 0)	1.02E-07
P52564	MP2K6_HUMAN (P52564) Dual specificity mitogen-activated protein kinase kinase 6 OS=Homo sapiens GN=M	37468.2	1 (1 0 0 0 0)	1.98E-10
P52907	CAZA1_HUMAN (P52907) F-actin-capping protein subunit alpha-1 OS=Homo sapiens GN=CAPZA1 PE=1 SV	32902.3	3 (3 0 0 0 0)	2.03E-08
P52943	CRIP2_HUMAN (P52943) Cysteine-rich protein 2 OS=Homo sapiens GN=CRIP2 PE=1 SV=1	22478.0	2 (2 0 0 0 0)	1.14E-11
P53582	AMPM1_HUMAN (P53582) Methionine aminopeptidase 1 OS=Homo sapiens GN=METAP1 PE=1 SV=2	43187.3	1 (1 0 0 0 0)	3.81E-06
P53597	SUCA_HUMAN (P53597) Succinyl-CoA ligase [GDP-forming] subunit alpha, mitochondrial OS=Homo sapiens	35025.3	2 (2 0 0 0 0)	1.04E-06
P53621	COPA_HUMAN (P53621) Coatomer subunit alpha OS=Homo sapiens GN=COPA PE=1 SV=2	138257.8	4 (4 0 0 0 0)	8.49E-07
P53794	SC5A3_HUMAN (P53794) Sodium/myo-inositol cotransporter OS=Homo sapiens GN=SLC5A3 PE=2 SV=2	79641.4	3 (3 0 0 0 0)	2.28E-10
P53985	MOT1_HUMAN (P53985) Monocarboxylate transporter 1 OS=Homo sapiens GN=SLC16A1 PE=1 SV=2	53922.9	2 (2 0 0 0 0)	1.39E-07
P53992	SC24C_HUMAN (P53992) Protein transport protein Sec24C OS=Homo sapiens GN=SEC24C PE=1 SV=2	118239.2	1 (1 0 0 0 0)	2.36E-06
P54136	SYRC_HUMAN (P54136) Arginyl-tRNA synthetase, cytoplasmic OS=Homo sapiens GN=RARS PE=1 SV=2	75331.0	7 (16 0 1 0 0)	3.10E-09
P54577	SYYC_HUMAN (P54577) Tyrosyl-tRNA synthetase, cytoplasmic OS=Homo sapiens GN=YARS PE=1 SV=4	59106.2	1 (1 0 0 0 0)	7.04E-07
P54652	HSP72_HUMAN (P54652) Heat shock-related 70 kDa protein 2 OS=Homo sapiens GN=HSPA2 PE=1 SV=1	69978.0	5 (13 2 0 0 0)	4.63E-13
P54707	AT12A_HUMAN (P54707) Potassium-transporting ATPase alpha chain 2 OS=Homo sapiens GN=ATP12A PE=	115437.2	3 (3 0 0 0 0)	1.73E-09
P54709	AT1B3_HUMAN (P54709) Sodium/potassium-transporting ATPase subunit beta-3 OS=Homo sapiens GN=ATP	31492.1	0 (10 0 0 0 0)	3.67E-09
P54753	EPHB3_HUMAN (P54753) Ephrin type-B receptor 3 OS=Homo sapiens GN=EPHB3 PE=1 SV=2	110259.3	4 (4 0 0 0 0)	8.58E-13
P54760	EPHB4_HUMAN (P54760) Ephrin type-B receptor 4 OS=Homo sapiens GN=EPHB4 PE=1 SV=2	108201.5	1 (1 0 0 0 0)	1.08E-07
P54762	EPHB1_HUMAN (P54762) Ephrin type-B receptor 1 OS=Homo sapiens GN=EPHB1 PE=1 SV=1	109814.6	1 (1 0 0 0 0)	9.71E-06
P54819	KAD2_HUMAN (P54819) Adenylate kinase isoenzyme 2, mitochondrial OS=Homo sapiens GN=AK2 PE=1 SV	26460.8	4 (4 0 0 0 0)	5.75E-08
P54886	P5CS_HUMAN (P54886) Delta-1-pyrroline-5-carboxylate synthetase OS=Homo sapiens GN=ALDH18A1 PE=	87247.7	3 (3 0 0 0 0)	4.91E-08
P55011	S12A2_HUMAN (P55011) Solute carrier family 12 member 2 OS=Homo sapiens GN=SLC12A2 PE=1 SV=1	131363.9	2 (12 0 0 0 0)	6.11E-14
P55039	DRG2_HUMAN (P55039) Developmentally-regulated GTP-binding protein 2 OS=Homo sapiens GN=DRG2 PE	40720.4	4 (4 0 0 0 0)	2.58E-07
P55060	XPO2_HUMAN (P55060) Exportin-2 OS=Homo sapiens GN=CSE1L PE=1 SV=3	110346.5	2 (2 0 0 0 0)	1.11E-12
P55072	TERA_HUMAN (P55072) Transitional endoplasmic reticulum ATPase OS=Homo sapiens GN=VCP PE=1 SV=	89265.9	2 (2 0 0 0 0)	5.67E-09
P55290	CAD13_HUMAN (P55290) Cadherin-13 OS=Homo sapiens GN=CDH13 PE=1 SV=1	78238.1	1 (1 0 0 0 0)	6.55E-06
P55789	ALR_HUMAN (P55789) FAD-linked sulfhydryl oxidase ALR OS=Homo sapiens GN=GFER PE=1 SV=2	23434.1	1 (1 0 0 0 0)	5.12E-05
P55884	EIF3B_HUMAN (P55884) Eukaryotic translation initiation factor 3 subunit B OS=Homo sapiens GN=EIF3B PE	92423.8	0 (10 0 0 0 0)	3.33E-14
P56134	ATPK_HUMAN (P56134) ATP synthase subunit f, mitochondrial OS=Homo sapiens GN=ATP5J2 PE=2 SV=3	10910.7	2 (2 0 0 0 0)	7.93E-08
P56192	SYMC_HUMAN (P56192) Methionyl-tRNA synthetase, cytoplasmic OS=Homo sapiens GN=MARS PE=1 SV=	101052.0	9 (9 0 0 0 0)	5.13E-09
P56537	IF6_HUMAN (P56537) Eukaryotic translation initiation factor 6 OS=Homo sapiens GN=EIF6 PE=1 SV=1	26582.2	1 (1 0 0 0 0)	6.88E-05
P57088	TMM33_HUMAN (P57088) Transmembrane protein 33 OS=Homo sapiens GN=TMEM33 PE=1 SV=2	27959.8	3 (3 0 0 0 0)	5.10E-06
P57105	SYJ2B_HUMAN (P57105) Synaptojanin-2-binding protein OS=Homo sapiens GN=SYNJ2BP PE=1 SV=2	15918.2	1 (1 0 0 0 0)	6.02E-07
P57721	PCBP3_HUMAN (P57721) Poly(rC)-binding protein 3 OS=Homo sapiens GN=PCBP3 PE=2 SV=1	35915.6	1 (1 0 0 0 0)	8.35E-09
P59665	DEF1_HUMAN (P59665) Neutrophil defensin 1 OS=Homo sapiens GN=DEFA1 PE=1 SV=1	10194.2	4 (4 0 0 0 0)	1.44E-05
P59768	GBG2_HUMAN (P59768) Guanine nucleotide-binding protein G(I)/G(S)/G(O) subunit gamma-2 OS=Homo sap	7845.0	3 (3 0 0 0 0)	7.89E-09
P59998	ARPC4_HUMAN (P59998) Actin-related protein 2/3 complex subunit 4 OS=Homo sapiens GN=ARPC4 PE=1 S	19654.3	3 (3 0 0 0 0)	1.75E-06
P60174	TPIS_HUMAN (P60174) Triosephosphate isomerase OS=Homo sapiens GN=TPI1 PE=1 SV=2	26652.7	2 (2 0 0 0 0)	3.35E-05
P60468	SC61B_HUMAN (P60468) Protein transport protein Sec61 subunit beta OS=Homo sapiens GN=SEC61B PE=	9968.1	1 (1 0 0 0 0)	4.19E-06
P60660	MYL6_HUMAN (P60660) Myosin light polypeptide 6 OS=Homo sapiens GN=MYL6 PE=1 SV=2	16919.1	2 (2 0 0 0 0)	2.73E-06
P60842	IF4A1_HUMAN (P60842) Eukaryotic initiation factor 4A-I OS=Homo sapiens GN=EIF4A1 PE=1 SV=1	46124.6	0 (10 0 0 0 0)	3.50E-10
P60900	PSA6_HUMAN (P60900) Proteasome subunit alpha type-6 OS=Homo sapiens GN=PSMA6 PE=1 SV=1	27381.8	4 (4 0 0 0 0)	4.05E-10
P60903	S10AA_HUMAN (P60903) Protein S100-A10 OS=Homo sapiens GN=S100A10 PE=1 SV=2	11195.5	2 (2 0 0 0 0)	6.72E-06
P60953	CDC42_HUMAN (P60953) Cell division control protein 42 homolog OS=Homo sapiens GN=CDC42 PE=1 SV=	21296.9	1 (1 0 0 0 0)	9.15E-05
P60981	DEST_HUMAN (P60981) Destrin OS=Homo sapiens GN=DSTN PE=1 SV=3	18493.5	2 (2 0 0 0 0)	3.11E-08
P61006	RAB8A_HUMAN (P61006) Ras-related protein Rab-8A OS=Homo sapiens GN=RAB8A PE=1 SV=1	23653.2	5 (5 0 0 0 0)	1.05E-09
P61009	SPCS3_HUMAN (P61009) Signal peptidase complex subunit 3 OS=Homo sapiens GN=SPCS3 PE=2 SV=1	20300.5	4 (4 0 0 0 0)	2.81E-07
P61019	RAB2A_HUMAN (P61019) Ras-related protein Rab-2A OS=Homo sapiens GN=RAB2A PE=1 SV=1	23530.8	9 (9 0 0 0 0)	2.19E-09
P61020	RAB5B_HUMAN (P61020) Ras-related protein Rab-5B OS=Homo sapiens GN=RAB5B PE=1 SV=1	23691.9	6 (6 0 0 0 0)	8.54E-08
P61026	RAB10_HUMAN (P61026) Ras-related protein Rab-10 OS=Homo sapiens GN=RAB10 PE=1 SV=1	22526.6	6 (5 0 0 1 0)	1.83E-07
P61081	UBC12_HUMAN (P61081) NEDD8-conjugating enzyme Ubc12 OS=Homo sapiens GN=UBE2M PE=1 SV=1	20886.7	7 (7 0 0 0 0)	3.54E-07
P61106	RAB14_HUMAN (P61106) Ras-related protein Rab-14 OS=Homo sapiens GN=RAB14 PE=1 SV=4	23881.9	0 (10 0 0 0 0)	1.06E-09
P61221	ABCE1_HUMAN (P61221) ATP-binding cassette sub-family E member 1 OS=Homo sapiens GN=ABCE1 PE=	67271.1	4 (4 0 0 0 0)	8.34E-10
P61247	RS3A_HUMAN (P61247) 40S ribosomal protein S3a OS=Homo sapiens GN=RPS3A PE=1 SV=2	29925.8	2 (2 0 0 0 0)	8.21E-05
P61513	RL37A_HUMAN (P61513) 60S ribosomal protein L37a OS=Homo sapiens GN=RPL37A PE=1 SV=2	10268.5	2 (2 0 0 0 0)	3.27E-06
P61586	RHOA_HUMAN (P61586) Transforming protein RhoA OS=Homo sapiens GN=RHOA PE=1 SV=1	21754.1	8 (8 0 0 0 0)	6.95E-10
P61604	CH10_HUMAN (P61604) 10 kDa heat shock protein, mitochondrial OS=Homo sapiens GN=HSPE1 PE=1 SV=	10924.9	1 (1 0 0 0 0)	8.53E-08
P61758	PFD3_HUMAN (P61758) Prefoldin subunit 3 OS=Homo sapiens GN=VBP1 PE=1 SV=3	22643.5	1 (1 0 0 0 0)	2.40E-09
P61803	DAD1_HUMAN (P61803) Dolichyl-diphosphooligosaccharide--protein glycosyltransferase subunit DAD1 OS=H	12488.6	2 (2 0 0 0 0)	2.31E-06
P61964	WDR5_HUMAN (P61964) WD repeat-containing protein 5 OS=Homo sapiens GN=WDR5 PE=1 SV=1	36565.5	2 (2 0 0 0 0)	5.71E-08
P61981	1433G_HUMAN (P61981) 14-3-3 protein gamma OS=Homo sapiens GN=YWHAG PE=1 SV=2	28284.9	4 (4 0 0 0 0)	1.45E-09
P62070	RRAS2_HUMAN (P62070) Ras-related protein R-Ras2 OS=Homo sapiens GN=RRAS2 PE=1 SV=1	23384.7	4 (4 0 0 0 0)	1.11E-06
P62081	RS7_HUMAN (P62081) 40S ribosomal protein S7 OS=Homo sapiens GN=RPS7 PE=1 SV=1	22113.3	4 (4 0 0 0 0)	2.48E-09
P62140	PP1B_HUMAN (P62140) Serine/threonine-protein phosphatase PP1-beta catalytic subunit OS=Homo sapiens	37162.6	6 (6 0 0 0 0)	3.18E-07
P62191	PRS4_HUMAN (P62191) 26S protease regulatory subunit 4 OS=Homo sapiens GN=PSMC1 PE=1 SV=1	49153.8	1 (1 0 0 0 0)	1.09E-06
P62241	RS8_HUMAN (P62241) 40S ribosomal protein S8 OS=Homo sapiens GN=RPS8 PE=1 SV=2	24190.2	2 (12 0 0 0 0)	2.91E-09
P62244	RS15A_HUMAN (P62244) 40S ribosomal protein S15a OS=Homo sapiens GN=RPS15A PE=1 SV=2	14830.0	5 (5 0 0 0 0)	3.37E-11
P62249	RS16_HUMAN (P62249) 40S ribosomal protein S16 OS=Homo sapiens GN=RPS16 PE=1 SV=2	16435.0	3 (3 0 0 0 0)	4.23E-07
P62258	1433E_HUMAN (P62258) 14-3-3 protein epsilon OS=Homo sapiens GN=YWHAE PE=1 SV=1	29155.4	2 (2 0 0 0 0)	1.13E-08
P62263	RS14_HUMAN (P62263) 40S ribosomal protein S14 OS=Homo sapiens GN=RPS14 PE=1 SV=3	16262.5	4 (4 0 0 0 0)	9.24E-08
P62266	RS23_HUMAN (P62266) 40S ribosomal protein S23 OS=Homo sapiens GN=RPS23 PE=1 SV=3	15797.7	4 (4 0 0 0 0)	1.75E-07
P62269	RS18_HUMAN (P62269) 40S ribosomal protein S18 OS=Homo sapiens GN=RPS18 PE=1 SV=3	17707.9	3 (3 0 0 0 0)	1.19E-05
P62277	RS13_HUMAN (P62277) 40S ribosomal protein S13 OS=Homo sapiens GN=RPS13 PE=1 SV=2	17211.7	1 (1 0 0 0 0)	5.45E-06
P62280	RS11_HUMAN (P62280) 40S ribosomal protein S11 OS=Homo sapiens GN=RPS11 PE=1 SV=3	18419.0	2 (2 0 0 0 0)	1.26E-07
P62314	SMD1_HUMAN (P62314) Small nuclear ribonucleoprotein Sm D1 OS=Homo sapiens GN=SNRPD1 PE=1 SV=	13273.4	5 (5 0 0 0 0)	2.87E-07

P62316	SMD2_HUMAN (P62316) Small nuclear ribonucleoprotein Sm D2 OS=Homo sapiens GN=SNRPD2 PE=1 SV=	13518.2	3 (3 0 0 0 0)	5.80E-05
P62318	SMD3_HUMAN (P62318) Small nuclear ribonucleoprotein Sm D3 OS=Homo sapiens GN=SNRPD3 PE=1 SV=	13907.3	2 (2 0 0 0 0)	4.49E-07
P62333	PRS10_HUMAN (P62333) 26S protease regulatory subunit S10B OS=Homo sapiens GN=PSMC6 PE=1 SV=1	44145.2	7 (7 0 0 0 0)	2.64E-09
P62424	RL7A_HUMAN (P62424) 60S ribosomal protein L7a OS=Homo sapiens GN=RPL7A PE=1 SV=2	29977.0	5 (5 0 0 0 0)	5.55E-12
P62495	ERF1_HUMAN (P62495) Eukaryotic peptide chain release factor subunit 1 OS=Homo sapiens GN=ETF1 PE=	49000.2	9 (9 0 0 0 0)	2.61E-12
P62701	RS4X_HUMAN (P62701) 40S ribosomal protein S4, X isoform OS=Homo sapiens GN=RPS4X PE=1 SV=2	29579.1	6 (6 0 0 0 0)	2.54E-07
P62736	ACTA_HUMAN (P62736) Actin, aortic smooth muscle OS=Homo sapiens GN=ACTA2 PE=1 SV=1	41981.8	4 (4 0 0 0 0)	2.28E-07
P62753	RS6_HUMAN (P62753) 40S ribosomal protein S6 OS=Homo sapiens GN=RPS6 PE=1 SV=1	28663.0	10 (9 0 1 0 0)	1.00E-10
P62805	H4_HUMAN (P62805) Histone H4 OS=Homo sapiens GN=HIST1H4A PE=1 SV=2	11360.4	5 (25 0 0 0 0)	4.88E-09
P62820	RAB1A_HUMAN (P62820) Ras-related protein Rab-1A OS=Homo sapiens GN=RAB1A PE=1 SV=3	22663.4	2 (2 0 0 0 0)	7.20E-07
P62829	RL23_HUMAN (P62829) 60S ribosomal protein L23 OS=Homo sapiens GN=RPL23 PE=1 SV=1	14856.1	7 (5 2 0 0 0)	2.77E-07
P62834	RAP1A_HUMAN (P62834) Ras-related protein Rap-1A OS=Homo sapiens GN=RAP1A PE=1 SV=1	20973.7	7 (7 0 0 0 0)	1.32E-08
P62847	RS24_HUMAN (P62847) 40S ribosomal protein S24 OS=Homo sapiens GN=RPS24 PE=1 SV=1	15413.4	3 (3 0 0 0 0)	2.10E-07
P62851	RS25_HUMAN (P62851) 40S ribosomal protein S25 OS=Homo sapiens GN=RPS25 PE=1 SV=1	13733.7	4 (4 0 0 0 0)	5.18E-06
P62857	RS28_HUMAN (P62857) 40S ribosomal protein S28 OS=Homo sapiens GN=RPS28 PE=1 SV=1	7836.2	3 (3 0 0 0 0)	2.34E-06
P62861	RS30_HUMAN (P62861) 40S ribosomal protein S30 OS=Homo sapiens GN=FAU PE=1 SV=1	6643.8	3 (3 0 0 0 0)	4.77E-07
P62873	GBB1_HUMAN (P62873) Guanine nucleotide-binding protein G(I)/G(S)/G(T) subunit beta-1 OS=Homo sapiens	37353.0	2 (2 0 0 0 0)	2.97E-08
P62873	GBB1_HUMAN (P62873) Guanine nucleotide-binding protein G(I)/G(S)/G(T) subunit beta-1 OS=Homo sapiens	37353.0	1 (1 0 0 0 0)	1.29E-05
P62888	RL30_HUMAN (P62888) 60S ribosomal protein L30 OS=Homo sapiens GN=RPL30 PE=1 SV=2	12775.7	1 (1 0 0 0 0)	1.19E-06
P62899	RL31_HUMAN (P62899) 60S ribosomal protein L31 OS=Homo sapiens GN=RPL31 PE=1 SV=1	14453.9	1 (1 0 0 0 0)	7.61E-09
P62906	RL10A_HUMAN (P62906) 60S ribosomal protein L10a OS=Homo sapiens GN=RPL10A PE=1 SV=2	24815.5	9 (8 1 0 0 0)	7.21E-07
P62913	RL11_HUMAN (P62913) 60S ribosomal protein L11 OS=Homo sapiens GN=RPL11 PE=1 SV=2	20239.7	6 (6 0 0 0 0)	6.42E-09
P62917	RL8_HUMAN (P62917) 60S ribosomal protein L8 OS=Homo sapiens GN=RPL8 PE=1 SV=2	28007.3	2 (2 0 0 0 0)	2.47E-06
P63096	GNAI1_HUMAN (P63096) Guanine nucleotide-binding protein G(i), alpha-1 subunit OS=Homo sapiens GN=GN	40335.3	7 (7 0 0 0 0)	2.29E-07
P63096	BXDC1_HUMAN (Q9H7B2) Brix domain-containing protein 1 OS=Homo sapiens GN=BXDC1 PE=1 SV=2	40335.3	4 (4 0 0 0 0)	9.07E-07
P63104	1433Z_HUMAN (P63104) 14-3-3 protein zeta/delta OS=Homo sapiens GN=YWHAZ PE=1 SV=1	27727.7	3 (3 0 0 0 0)	3.25E-08
P63167	DYL1_HUMAN (P63167) Dynein light chain 1, cytoplasmic OS=Homo sapiens GN=DYNLL1 PE=1 SV=1	10359.1	2 (2 0 0 0 0)	2.04E-07
P63173	RL38_HUMAN (P63173) 60S ribosomal protein L38 OS=Homo sapiens GN=RPL38 PE=1 SV=2	8212.7	8 (8 0 0 0 0)	2.62E-08
P63208	SKP1_HUMAN (P63208) S-phase kinase-associated protein 1 OS=Homo sapiens GN=SKP1 PE=1 SV=2	18646.3	4 (4 0 0 0 0)	2.09E-08
P63218	GBG5_HUMAN (P63218) Guanine nucleotide-binding protein G(I)/G(S)/G(O) subunit gamma-5 OS=Homo sap	7313.8	1 (0 1 0 0 0)	2.64E-06
P63220	RS21_HUMAN (P63220) 40S ribosomal protein S21 OS=Homo sapiens GN=RPS21 PE=1 SV=1	9105.6	1 (1 0 0 0 0)	4.74E-07
P63241	IF5A1_HUMAN (P63241) Eukaryotic translation initiation factor 5A-1 OS=Homo sapiens GN=EIF5A PE=1 SV=	16821.4	1 (1 0 0 0 0)	1.53E-07
P63244	GBLP_HUMAN (P63244) Guanine nucleotide-binding protein subunit beta-2-like 1 OS=Homo sapiens GN=GN	35054.6	7 (7 0 0 0 0)	2.15E-08
P68871	HBB_HUMAN (P68871) Hemoglobin subunit beta OS=Homo sapiens GN=HBB PE=1 SV=2	15988.3	1 (1 0 0 0 0)	1.06E-04
P69905	HBA_HUMAN (P69905) Hemoglobin subunit alpha OS=Homo sapiens GN=HBA1 PE=1 SV=2	15247.9	2 (2 0 0 0 0)	2.12E-08
P78347	GTF2I_HUMAN (P78347) General transcription factor II-I OS=Homo sapiens GN=GTF2I PE=1 SV=2	112346.2	1 (1 0 0 0 0)	1.53E-07
P78358	CTG1B_HUMAN (P78358) Cancer/testis antigen 1 OS=Homo sapiens GN=CTAG1A PE=1 SV=1	17981.0	2 (2 0 0 0 0)	1.00E-08
P78371	TCPB_HUMAN (P78371) T-complex protein 1 subunit beta OS=Homo sapiens GN=CCT2 PE=1 SV=4	57452.3	5 (5 0 0 0 0)	1.69E-11
P78386	KRT85_HUMAN (P78386) Keratin, type II cuticular Hb5 OS=Homo sapiens GN=KRT85 PE=1 SV=1	55766.5	2 (2 0 0 0 0)	3.30E-05
P78527	PRKDC_HUMAN (P78527) DNA-dependent protein kinase catalytic subunit OS=Homo sapiens GN=PRKDC P	468786.9	0 (20 0 0 0 0)	3.72E-11
P82650	RT22_HUMAN (P82650) 28S ribosomal protein S22, mitochondrial OS=Homo sapiens GN=MRPS22 PE=1 SV	41254.4	2 (2 0 0 0 0)	8.69E-09
P82650	IF2A_HUMAN (P05198) Eukaryotic translation initiation factor 2 subunit 1 OS=Homo sapiens GN=EIF2S1 PE=	41254.4	2 (2 0 0 0 0)	1.36E-08
P83731	RL24_HUMAN (P83731) 60S ribosomal protein L24 OS=Homo sapiens GN=RPL24 PE=1 SV=1	17767.9	11 (11 0 0 0 0)	3.46E-09
P83916	CBX1_HUMAN (P83916) Chromobox protein homolog 1 OS=Homo sapiens GN=CBX1 PE=1 SV=1	21404.6	1 (1 0 0 0 0)	1.16E-07
P84077	ARF1_HUMAN (P84077) ADP-ribosylation factor 1 OS=Homo sapiens GN=ARF1 PE=1 SV=2	20683.7	6 (6 0 0 0 0)	8.55E-09
P84098	RL19_HUMAN (P84098) 60S ribosomal protein L19 OS=Homo sapiens GN=RPL19 PE=1 SV=1	23451.3	11 (11 0 0 0 0)	8.99E-14
P84103	SFRS3_HUMAN (P84103) Splicing factor, arginine/serine-rich 3 OS=Homo sapiens GN=SFRS3 PE=1 SV=1	19317.9	1 (1 0 0 0 0)	3.65E-07
P98160	PGBM_HUMAN (P98160) Basement membrane-specific heparan sulfate proteoglycan core protein OS=Homo	468501.1	8 (8 0 0 0 0)	1.60E-10
Q00325	MPCP_HUMAN (Q00325) Phosphate carrier protein, mitochondrial OS=Homo sapiens GN=SLC25A3 PE=1 SV	40068.8	2 (2 0 0 0 0)	1.03E-07
Q00610	CLH1_HUMAN (Q00610) Clathrin heavy chain 1 OS=Homo sapiens GN=CLTC PE=1 SV=5	191491.7	8 (8 0 0 0 0)	1.91E-08
Q00839	HNRPU_HUMAN (Q00839) Heterogeneous nuclear ribonucleoprotein U OS=Homo sapiens GN=HNRNPU PE	90457.0	4 (4 0 0 0 0)	1.23E-10
Q01082	SPTB2_HUMAN (Q01082) Spectrin beta chain, brain 1 OS=Homo sapiens GN=SPTBN1 PE=1 SV=2	274437.2	2 (12 0 0 0 0)	5.32E-11
Q01518	CAP1_HUMAN (Q01518) Adenylyl cyclase-associated protein 1 OS=Homo sapiens GN=CAP1 PE=1 SV=4	51822.8	4 (4 0 0 0 0)	5.04E-07
Q01546	K22O_HUMAN (Q01546) Keratin, type II cytoskeletal 2 oral OS=Homo sapiens GN=KRT76 PE=2 SV=1	65830.1	1 (0 0 0 0 1)	1.75E-04
Q01650	LAT1_HUMAN (Q01650) Large neutral amino acids transporter small subunit 1 OS=Homo sapiens GN=SLC7A	54974.4	4 (4 0 0 0 0)	6.14E-13
Q01813	K6PP_HUMAN (Q01813) 6-phosphofructokinase type C OS=Homo sapiens GN=PFKP PE=1 SV=2	85541.6	3 (3 0 0 0 0)	7.66E-08
Q02127	PYRD_HUMAN (Q02127) Dihydroorotate dehydrogenase, mitochondrial OS=Homo sapiens GN=DHODH PE=	42841.0	5 (5 0 0 0 0)	1.22E-13
Q02539	H11_HUMAN (Q02539) Histone H1.1 OS=Homo sapiens GN=HIST1H1A PE=1 SV=3	21828.9	2 (2 0 0 0 0)	1.13E-07
Q02543	RL18A_HUMAN (Q02543) 60S ribosomal protein L18a OS=Homo sapiens GN=RPL18A PE=1 SV=2	20748.9	6 (6 0 0 0 0)	5.43E-07
Q02978	M2OM_HUMAN (Q02978) Mitochondrial 2-oxoglutarate/malate carrier protein OS=Homo sapiens GN=SLC25A	34039.9	3 (3 0 0 0 0)	4.92E-11
Q03113	GNA12_HUMAN (Q03113) Guanine nucleotide-binding protein subunit alpha-12 OS=Homo sapiens GN=GNA1	44251.5	2 (0 2 0 0 0)	2.26E-06
Q03252	LMNB2_HUMAN (Q03252) Lamin-B2 OS=Homo sapiens GN=LMNB2 PE=1 SV=3	67647.6	3 (3 0 0 0 0)	8.98E-07
Q04837	SSB_HUMAN (Q04837) Single-stranded DNA-binding protein, mitochondrial OS=Homo sapiens GN=SSBP1 P	17249.0	2 (2 0 0 0 0)	1.34E-07
Q04941	PLP2_HUMAN (Q04941) Proteolipid protein 2 OS=Homo sapiens GN=PLP2 PE=1 SV=1	16679.7	2 (2 0 0 0 0)	5.14E-08
Q05193	DYN1_HUMAN (Q05193) Dynamin-1 OS=Homo sapiens GN=DNM1 PE=1 SV=2	97347.1	1 (1 0 0 0 0)	9.41E-05
Q05519	SFR11_HUMAN (Q05519) Splicing factor, arginine/serine-rich 11 OS=Homo sapiens GN=SFRS11 PE=1 SV=1	53510.2	2 (2 0 0 0 0)	9.90E-07
Q05639	EF1A2_HUMAN (Q05639) Elongation factor 1-alpha 2 OS=Homo sapiens GN=EEF1A2 PE=1 SV=1	50438.4	6 (16 0 0 0 0)	5.97E-09
Q06210	GFPT1_HUMAN (Q06210) Glucosamine--fructose-6-phosphate aminotransferase [isomerizing] 1 OS=Homo sa	78756.4	1 (1 0 0 0 0)	1.13E-06
Q06830	PRDX1_HUMAN (Q06830) Peroxiredoxin-1 OS=Homo sapiens GN=PRDX1 PE=1 SV=1	22096.3	11 (11 0 0 0 0)	2.46E-07
Q07020	RL18_HUMAN (Q07020) 60S ribosomal protein L18 OS=Homo sapiens GN=RPL18 PE=1 SV=2	21621.1	7 (7 0 0 0 0)	3.70E-09
Q07065	CKAP4_HUMAN (Q07065) Cytoskeleton-associated protein 4 OS=Homo sapiens GN=CKAP4 PE=1 SV=2	65982.9	0 (20 0 0 0 0)	1.10E-11
Q07666	KHDR1_HUMAN (Q07666) KH domain-containing, RNA-binding, signal transduction-associated protein 1 OS=	48197.2	1 (1 0 0 0 0)	5.86E-08
Q07954	LRP1_HUMAN (Q07954) Prolow-density lipoprotein receptor-related protein 1 OS=Homo sapiens GN=LRP1 P	504243.2	1 (1 0 0 0 0)	2.85E-05
Q07955	SFRS1_HUMAN (Q07955) Splicing factor, arginine/serine-rich 1 OS=Homo sapiens GN=SFRS1 PE=1 SV=2	27727.8	2 (2 0 0 0 0)	6.35E-06
Q08170	SFRS4_HUMAN (Q08170) Splicing factor, arginine/serine-rich 4 OS=Homo sapiens GN=SFRS4 PE=1 SV=2	56645.3	1 (1 0 0 0 0)	5.79E-07
Q08211	DHX9_HUMAN (Q08211) ATP-dependent RNA helicase A OS=Homo sapiens GN=DHX9 PE=1 SV=4	140868.9	4 (4 0 0 0 0)	2.40E-07

Q08945	SSRP1_HUMAN (Q08945) FACT complex subunit SSRP1 OS=Homo sapiens GN=SSRP1 PE=1 SV=1	81024.3	1 (1 0 0 0 0)	1.80E-06
Q08AM6	VAC14_HUMAN (Q08AM6) Protein VAC14 homolog OS=Homo sapiens GN=VAC14 PE=1 SV=1	87916.8	1 (1 0 0 0 0)	6.00E-06
Q08J23	NSUN2_HUMAN (Q08J23) tRNA (cytosine-5-)-methyltransferase NSUN2 OS=Homo sapiens GN=NSUN2 PE=	86415.9	1 (1 0 0 0 0)	1.26E-05
Q09028	RBBP4_HUMAN (Q09028) Histone-binding protein RBBP4 OS=Homo sapiens GN=RBBP4 PE=1 SV=3	47626.1	3 (3 0 0 0 0)	2.59E-10
Q09666	AHNK_HUMAN (Q09666) Neuroblast differentiation-associated protein AHNAK OS=Homo sapiens GN=AHNA	628705.2	6 (15 0 1 0 0)	7.63E-10
Q0IIN1	Q0IIN1_HUMAN (Q0IIN1) Keratin 77 OS=Homo sapiens GN=KRT77 PE=2 SV=1	61764.4	1 (0 1 0 0 0)	1.26E-04
Q0VAB1	Q0VAB1_HUMAN (Q0VAB1) Translocase of inner mitochondrial membrane 50 homolog (S. cerevisiae) OS=Ho	50447.2	5 (5 0 0 0 0)	3.43E-11
Q10567	AP1B1_HUMAN (Q10567) AP-1 complex subunit beta-1 OS=Homo sapiens GN=AP1B1 PE=1 SV=1	104540.3	2 (2 0 0 0 0)	1.17E-04
Q12788	TBL3_HUMAN (Q12788) WD repeat-containing protein SAZD OS=Homo sapiens GN=TBL3 PE=1 SV=1	56011.4	2 (2 0 0 0 0)	2.53E-07
Q12792	TWF1_HUMAN (Q12792) Twinfilin-1 OS=Homo sapiens GN=TWF1 PE=1 SV=2	42182.6	6 (6 0 0 0 0)	1.74E-09
Q12800	TFCP2_HUMAN (Q12800) Alpha-globin transcription factor CP2 OS=Homo sapiens GN=TFCP2 PE=1 SV=2	57219.8	1 (1 0 0 0 0)	1.25E-07
Q12840	KIF5A_HUMAN (Q12840) Kinesin heavy chain isoform 5A OS=Homo sapiens GN=KIF5A PE=1 SV=2	117305.4	5 (5 0 0 0 0)	2.59E-08
Q12846	STX4_HUMAN (Q12846) Syntaxin-4 OS=Homo sapiens GN=STX4 PE=1 SV=2	34158.9	2 (2 0 0 0 0)	6.27E-06
Q12905	ILF2_HUMAN (Q12905) Interleukin enhancer-binding factor 2 OS=Homo sapiens GN=ILF2 PE=1 SV=2	43035.2	4 (4 0 0 0 0)	3.03E-11
Q12906	ILF3_HUMAN (Q12906) Interleukin enhancer-binding factor 3 OS=Homo sapiens GN=ILF3 PE=1 SV=3	95279.2	2 (12 0 0 0 0)	1.99E-10
Q12907	LMAN2_HUMAN (Q12907) Vesicular integral-membrane protein VIP36 OS=Homo sapiens GN=LMAN2 PE=1	40203.1	2 (2 0 0 0 0)	6.14E-06
Q12929	EPS8_HUMAN (Q12929) Epidermal growth factor receptor kinase substrate 8 OS=Homo sapiens GN=EPS8 P	91824.5	2 (2 0 0 0 0)	6.34E-11
Q12931	TRAP1_HUMAN (Q12931) Heat shock protein 75 kDa, mitochondrial OS=Homo sapiens GN=TRAP1 PE=1 SV	80059.8	2 (12 0 0 0 0)	4.40E-10
Q12955	ANK3_HUMAN (Q12955) Ankyrin-3 OS=Homo sapiens GN=ANK3 PE=1 SV=1	480106.0	3 (3 0 0 0 0)	2.69E-07
Q12965	MYO1E_HUMAN (Q12965) Myosin-Ie OS=Homo sapiens GN=MYO1E PE=1 SV=2	126982.0	2 (2 0 0 0 0)	2.42E-06
Q12979	ABR_HUMAN (Q12979) Active breakpoint cluster region-related protein OS=Homo sapiens GN=ABR PE=1 SV	97635.3	1 (1 0 0 0 0)	4.31E-07
Q12981	SEC20_HUMAN (Q12981) Vesicle transport protein SEC20 OS=Homo sapiens GN=BNIP1 PE=1 SV=3	26115.9	1 (1 0 0 0 0)	4.40E-05
Q13011	ECH1_HUMAN (Q13011) Delta(3,5)-Delta(2,4)-dienoyl-CoA isomerase, mitochondrial OS=Homo sapiens GN=	35793.4	1 (1 0 0 0 0)	1.00E-07
Q13077	TRAF1_HUMAN (Q13077) TNF receptor-associated factor 1 OS=Homo sapiens GN=TRAF1 PE=1 SV=1	46134.0	4 (4 0 0 0 0)	9.03E-07
Q13151	ROA0_HUMAN (Q13151) Heterogeneous nuclear ribonucleoprotein A0 OS=Homo sapiens GN=HNRNPA0 PE	30821.8	4 (4 0 0 0 0)	3.27E-10
Q13155	MCA2_HUMAN (Q13155) Multisynthetase complex auxiliary component p38 OS=Homo sapiens GN=JTV1 PE	35326.3	5 (5 0 0 0 0)	4.15E-08
Q13185	CBX3_HUMAN (Q13185) Chromobox protein homolog 3 OS=Homo sapiens GN=CBX3 PE=1 SV=4	20798.4	3 (3 0 0 0 0)	2.48E-09
Q13263	TIF1B_HUMAN (Q13263) Transcription intermediary factor 1-beta OS=Homo sapiens GN=TRIM28 PE=1 SV=	88493.5	2 (2 0 0 0 0)	4.22E-05
Q13283	G3BP1_HUMAN (Q13283) Ras GTPase-activating protein-binding protein 1 OS=Homo sapiens GN=G3BP1 P	52132.1	4 (2 0 2 0 0)	1.34E-12
Q13308	PTK7_HUMAN (Q13308) Tyrosine-protein kinase-like 7 OS=Homo sapiens GN=PTK7 PE=1 SV=2	118316.9	1 (1 0 0 0 0)	1.06E-08
Q13347	EIF3I_HUMAN (Q13347) Eukaryotic translation initiation factor 3 subunit I OS=Homo sapiens GN=EIF3I PE=1	36478.6	6 (6 0 0 0 0)	7.52E-06
Q13363	CTBP1_HUMAN (Q13363) C-terminal-binding protein 1 OS=Homo sapiens GN=CTBP1 PE=1 SV=2	47505.6	2 (2 0 0 0 0)	5.52E-06
Q13418	ILK_HUMAN (Q13418) Integrin-linked protein kinase OS=Homo sapiens GN=ILK PE=1 SV=2	51386.0	4 (4 0 0 0 0)	3.93E-06
Q13425	SNTB2_HUMAN (Q13425) Beta-2-syntrophin OS=Homo sapiens GN=SNTB2 PE=1 SV=1	57913.1	2 (2 0 0 0 0)	1.09E-06
Q13428	TCOF_HUMAN (Q13428) Treacle protein OS=Homo sapiens GN=TCOF1 PE=1 SV=2	152013.1	4 (4 0 0 0 0)	1.05E-05
Q13449	LSAMP_HUMAN (Q13449) Limbic system-associated membrane protein OS=Homo sapiens GN=LSAMP PE=	37370.2	2 (2 0 0 0 0)	5.83E-07
Q13557	KCC2D_HUMAN (Q13557) Calcium/calmodulin-dependent protein kinase type II delta chain OS=Homo sapien	56333.6	2 (2 0 0 0 0)	1.66E-08
Q13601	KRR1_HUMAN (Q13601) KRR1 small subunit processome component homolog OS=Homo sapiens GN=KRR	43637.7	1 (1 0 0 0 0)	1.04E-06
Q13618	CUL3_HUMAN (Q13618) Cullin-3 OS=Homo sapiens GN=CUL3 PE=1 SV=2	88873.5	2 (2 0 0 0 0)	7.68E-08
Q13637	RAB32_HUMAN (Q13637) Ras-related protein Rab-32 OS=Homo sapiens GN=RAB32 PE=1 SV=3	24981.7	1 (1 0 0 0 0)	4.08E-06
Q13724	GCS1_HUMAN (Q13724) Mannosyl-oligosaccharide glucosidase OS=Homo sapiens GN=GCS1 PE=1 SV=5	91860.9	4 (4 0 0 0 0)	4.87E-09
Q13740	CD166_HUMAN (Q13740) CD166 antigen OS=Homo sapiens GN=ALCAM PE=1 SV=2	65061.2	1 (1 0 0 0 0)	2.25E-04
Q13838	UAP56_HUMAN (Q13838) Spliceosome RNA helicase BAT1 OS=Homo sapiens GN=BAT1 PE=1 SV=1	48960.0	1 (11 0 0 0 0)	6.07E-08
Q13868	EXOS2_HUMAN (Q13868) Exosome complex exonuclease RRP4 OS=Homo sapiens GN=EXOSC2 PE=1 SV	32768.1	1 (1 0 0 0 0)	6.14E-05
Q14008	CKAP5_HUMAN (Q14008) Cytoskeleton-associated protein 5 OS=Homo sapiens GN=CKAP5 PE=1 SV=3	225350.5	9 (9 0 0 0 0)	4.86E-08
Q14019	COTL1_HUMAN (Q14019) Coactosin-like protein OS=Homo sapiens GN=COTL1 PE=1 SV=3	15935.0	1 (1 0 0 0 0)	1.35E-04
Q14103	HNRPD_HUMAN (Q14103) Heterogeneous nuclear ribonucleoprotein D0 OS=Homo sapiens GN=HNRNPD P	38410.3	2 (2 0 0 0 0)	1.89E-07
Q14118	DAG1_HUMAN (Q14118) Dystroglycan OS=Homo sapiens GN=DAG1 PE=1 SV=1	97519.9	6 (6 0 0 0 0)	3.16E-08
Q14152	EIF3A_HUMAN (Q14152) Eukaryotic translation initiation factor 3 subunit A OS=Homo sapiens GN=EIF3A PE=	166467.5	1 (1 0 0 0 0)	7.85E-08
Q14156	EFR3A_HUMAN (Q14156) Protein EFR3 homolog A OS=Homo sapiens GN=EFR3A PE=1 SV=2	92865.0	2 (2 0 0 0 0)	2.64E-07
Q14160	LAP4_HUMAN (Q14160) Protein LAP4 OS=Homo sapiens GN=SCRIB PE=1 SV=3	174823.4	1 (1 0 0 0 0)	1.90E-06
Q14165	MLEC_HUMAN (Q14165) Malectin OS=Homo sapiens GN=MLEC PE=1 SV=1	32213.6	1 (1 0 0 0 0)	2.20E-05
Q14204	DYHC1_HUMAN (Q14204) Cytoplasmic dynein 1 heavy chain 1 OS=Homo sapiens GN=DYNC1H1 PE=1 SV=	532071.8	4 (4 0 0 0 0)	2.21E-09
Q14232	EI2BA_HUMAN (Q14232) Translation initiation factor eIF-2B subunit alpha OS=Homo sapiens GN=EIF2B1 PE	33690.8	5 (5 0 0 0 0)	9.21E-07
Q14247	SRC8_HUMAN (Q14247) Src substrate cortactin OS=Homo sapiens GN=CTTN PE=1 SV=2	61548.6	6 (3 3 0 0 0)	1.44E-09
Q14254	FLOT2_HUMAN (Q14254) Flotillin-2 OS=Homo sapiens GN=FLOT2 PE=1 SV=1	41659.3	5 (5 0 0 0 0)	1.08E-10
Q14254	FLOT2_HUMAN (Q14254) Flotillin-2 OS=Homo sapiens GN=FLOT2 PE=1 SV=1	41659.3	1 (1 0 0 0 0)	4.24E-06
Q14331	FRG1_HUMAN (Q14331) Protein FRG1 OS=Homo sapiens GN=FRG1 PE=1 SV=1	29154.1	1 (1 0 0 0 0)	3.21E-06
Q14344	GNA13_HUMAN (Q14344) Guanine nucleotide-binding protein subunit alpha-13 OS=Homo sapiens GN=GNA	44021.7	2 (12 0 0 0 0)	1.59E-09
Q14376	GALE_HUMAN (Q14376) UDP-glucose 4-epimerase OS=Homo sapiens GN=GALE PE=1 SV=2	38257.3	1 (1 0 0 0 0)	4.24E-07
Q14376	ARMC1_HUMAN (Q9NVT9) Armadillo repeat-containing protein 1 OS=Homo sapiens GN=ARMC1 PE=1 SV=	38257.3	1 (1 0 0 0 0)	4.59E-07
Q14444	CAPR1_HUMAN (Q14444) Caprin-1 OS=Homo sapiens GN=CAPRIN1 PE=1 SV=2	78318.2	1 (1 0 0 0 0)	5.92E-07
Q14498	RBM39_HUMAN (Q14498) RNA-binding protein 39 OS=Homo sapiens GN=RBM39 PE=1 SV=2	59342.8	1 (0 1 0 0 0)	1.22E-08
Q14532	K1H2_HUMAN (Q14532) Keratin, type I cuticular Ha2 OS=Homo sapiens GN=KRT32 PE=1 SV=2	50286.2	1 (1 0 0 0 0)	2.73E-06
Q14533	KRT81_HUMAN (Q14533) Keratin, type II cuticular Hb1 OS=Homo sapiens GN=KRT81 PE=1 SV=2	54935.8	5 (5 0 0 0 0)	1.31E-05
Q14627	I13R2_HUMAN (Q14627) Interleukin-13 receptor alpha-2 chain OS=Homo sapiens GN=IL13RA2 PE=2 SV=1	44147.8	3 (3 0 0 0 0)	2.82E-07
Q14690	RRP5_HUMAN (Q14690) Protein RRP5 homolog OS=Homo sapiens GN=PDCD11 PE=1 SV=3	208569.2	1 (1 0 0 0 0)	2.85E-05
Q14692	BMS1_HUMAN (Q14692) Ribosome biogenesis protein BMS1 homolog OS=Homo sapiens GN=BMS1 PE=1 S	145715.5	1 (1 0 0 0 0)	1.56E-09
Q14847	LASP1_HUMAN (Q14847) LIM and SH3 domain protein 1 OS=Homo sapiens GN=LASP1 PE=1 SV=2	29698.2	3 (3 0 0 0 0)	6.02E-08
Q14964	RB39A_HUMAN (Q14964) Ras-related protein Rab-39A OS=Homo sapiens GN=RAB39 PE=2 SV=2	24990.7	1 (0 0 1 0 0)	4.27E-06
Q14974	IMB1_HUMAN (Q14974) Importin subunit beta-1 OS=Homo sapiens GN=KPNB1 PE=1 SV=2	97108.2	7 (7 0 0 0 0)	1.77E-09
Q14CN4	K2C72_HUMAN (Q14CN4) Keratin, type II cytoskeletal 72 OS=Homo sapiens GN=KRT72 PE=1 SV=2	55842.5	1 (0 1 0 0 0)	2.63E-06
Q15005	SPCS2_HUMAN (Q15005) Signal peptidase complex subunit 2 OS=Homo sapiens GN=SPCS2 PE=2 SV=3	24986.7	5 (5 0 0 0 0)	8.15E-06
Q15020	SART3_HUMAN (Q15020) Squamous cell carcinoma antigen recognized by T-cells 3 OS=Homo sapiens GN=	109865.3	1 (1 0 0 0 0)	4.19E-07
Q15029	U5S1_HUMAN (Q15029) 116 kDa U5 small nuclear ribonucleoprotein component OS=Homo sapiens GN=EFT	109366.4	6 (6 0 0 0 0)	1.17E-08
Q15041	AR6P1_HUMAN (Q15041) ADP-ribosylation factor-like protein 6-interacting protein 1 OS=Homo sapiens GN=A	23347.4	1 (1 0 0 0 0)	4.26E-05

Q15056	IF4H_HUMAN (Q15056) Eukaryotic translation initiation factor 4H OS=Homo sapiens GN=EIF4H PE=1 SV=5	27368.4	1 (1 0 0 0 0)	1.68E-06
Q15057	ACAP2_HUMAN (Q15057) ARFGAP with coiled-coil, ANK repeat and PH domain-containing protein 2 OS=Hor	87973.2	1 (1 0 0 0 0)	7.63E-10
Q15075	EEA1_HUMAN (Q15075) Early endosome antigen 1 OS=Homo sapiens GN=EEA1 PE=1 SV=1	162366.4	2 (2 0 0 0 0)	2.11E-06
Q15149	PLEC1_HUMAN (Q15149) Plectin-1 OS=Homo sapiens GN=PLEC1 PE=1 SV=3	531465.9	8 (18 0 0 0 0)	1.28E-10
Q15233	NONO_HUMAN (Q15233) Non-POU domain-containing octamer-binding protein OS=Homo sapiens GN=NON	54197.4	2 (2 0 0 0 0)	3.90E-06
Q15286	RAB35_HUMAN (Q15286) Ras-related protein Rab-35 OS=Homo sapiens GN=RAB35 PE=1 SV=1	23010.8	8 (7 1 0 0 0)	2.36E-10
Q15323	K1H1_HUMAN (Q15323) Keratin, type I cuticular Ha1 OS=Homo sapiens GN=KRT31 PE=1 SV=3	47207.1	7 (7 0 0 0 0)	1.09E-06
Q15363	TMED2_HUMAN (Q15363) Transmembrane emp24 domain-containing protein 2 OS=Homo sapiens GN=TME	22746.4	3 (3 0 0 0 0)	1.03E-06
Q15365	PCBP1_HUMAN (Q15365) Poly(rC)-binding protein 1 OS=Homo sapiens GN=PCBP1 PE=1 SV=2	37474.0	8 (8 0 0 0 0)	2.96E-13
Q15369	ELOC_HUMAN (Q15369) Transcription elongation factor B polypeptide 1 OS=Homo sapiens GN=TCEB1 PE=	12465.0	2 (2 0 0 0 0)	8.54E-09
Q15370	ELOB_HUMAN (Q15370) Transcription elongation factor B polypeptide 2 OS=Homo sapiens GN=TCEB2 PE=	13124.6	2 (2 0 0 0 0)	4.12E-08
Q15459	SF3A1_HUMAN (Q15459) Splicing factor 3 subunit 1 OS=Homo sapiens GN=SF3A1 PE=1 SV=1	88830.8	1 (1 0 0 0 0)	4.68E-06
Q15738	NSDHL_HUMAN (Q15738) Sterol-4-alpha-carboxylate 3-dehydrogenase, decarboxylating OS=Homo sapiens (	41873.6	3 (3 0 0 0 0)	6.69E-10
Q15813	TBCE_HUMAN (Q15813) Tubulin-specific chaperone E OS=Homo sapiens GN=TBCE PE=1 SV=1	59309.1	3 (3 0 0 0 0)	1.56E-06
Q15836	VAMP3_HUMAN (Q15836) Vesicle-associated membrane protein 3 OS=Homo sapiens GN=VAMP3 PE=1 SV=	11302.0	3 (3 0 0 0 0)	1.52E-10
Q15907	RB11B_HUMAN (Q15907) Ras-related protein Rab-11B OS=Homo sapiens GN=RAB11B PE=1 SV=4	24473.5	11 (11 0 0 0 0)	1.83E-10
Q15907	RB11B_HUMAN (Q15907) Ras-related protein Rab-11B OS=Homo sapiens GN=RAB11B PE=1 SV=4	24473.5	4 (4 0 0 0 0)	2.85E-07
Q16181	SEPT7_HUMAN (Q16181) Septin-7 OS=Homo sapiens GN=SEPT7 PE=1 SV=2	50648.0	6 (6 0 0 0 0)	1.42E-09
Q16401	PSMD5_HUMAN (Q16401) 26S proteasome non-ATPase regulatory subunit 5 OS=Homo sapiens GN=PSMD5	56160.5	1 (1 0 0 0 0)	2.13E-06
Q16527	CSRP2_HUMAN (Q16527) Cysteine and glycine-rich protein 2 OS=Homo sapiens GN=CSRP2 PE=1 SV=3	20939.9	3 (3 0 0 0 0)	3.11E-09
Q16543	CDC37_HUMAN (Q16543) Hsp90 co-chaperone Cdc37 OS=Homo sapiens GN=CDC37 PE=1 SV=1	44440.1	2 (2 0 0 0 0)	5.62E-05
Q16630	CPSF6_HUMAN (Q16630) Cleavage and polyadenylation specificity factor subunit 6 OS=Homo sapiens GN=C	59173.5	1 (1 0 0 0 0)	3.18E-07
Q16666	IF16_HUMAN (Q16666) Gamma-interferon-inducible protein Ifi-16 OS=Homo sapiens GN=IFI16 PE=1 SV=3	88199.5	3 (3 0 0 0 0)	1.46E-04
Q16718	NDUA5_HUMAN (Q16718) NADH dehydrogenase [ubiquinone] 1 alpha subcomplex subunit 5 OS=Homo sapi	13450.2	2 (2 0 0 0 0)	1.04E-05
Q16719	KYNU_HUMAN (Q16719) Kynureninase OS=Homo sapiens GN=KYNU PE=1 SV=1	52318.3	2 (2 0 0 0 0)	2.50E-12
Q16795	NDUA9_HUMAN (Q16795) NADH dehydrogenase [ubiquinone] 1 alpha subcomplex subunit 9, mitochondrial (	42482.6	3 (3 0 0 0 0)	1.32E-06
Q16822	PPCKM_HUMAN (Q16822) Phosphoenolpyruvate carboxykinase [GTP], mitochondrial OS=Homo sapiens GN	70591.7	1 (1 0 0 0 0)	1.51E-08
Q16890	TPD53_HUMAN (Q16890) Tumor protein D53 OS=Homo sapiens GN=TPD52L1 PE=1 SV=1	22435.1	2 (2 0 0 0 0)	1.46E-06
Q16891	IMMT_HUMAN (Q16891) Mitochondrial inner membrane protein OS=Homo sapiens GN=IMMT PE=1 SV=1	83626.5	9 (9 0 0 0 0)	2.13E-13
Q1KMD3	HNRL2_HUMAN (Q1KMD3) Heterogeneous nuclear ribonucleoprotein U-like protein 2 OS=Homo sapiens GN=	85052.2	3 (3 0 0 0 0)	3.13E-07
Q2KHP4	Q2KHP4_HUMAN (Q2KHP4) HSPA5 protein OS=Homo sapiens GN=HSPA5 PE=2 SV=1	72377.6	2 (2 0 0 0 0)	1.89E-07
Q2M389	K1033_HUMAN (Q2M389) UPF0681 protein KIAA1033 OS=Homo sapiens GN=KIAA1033 PE=1 SV=1	136330.2	1 (1 0 0 0 0)	1.26E-07
Q2VIR3	IF2GL_HUMAN (Q2VIR3) Eukaryotic translation initiation factor 2 subunit 3-like protein OS=Homo sapiens PE=	51196.3	4 (4 0 0 0 0)	1.86E-08
Q2Y0W8	S4A8_HUMAN (Q2Y0W8) Electroneutral sodium bicarbonate exchanger 1 OS=Homo sapiens GN=SLC4A8 PE	122858.3	1 (0 0 1 0 0)	2.84E-06
Q30154	2B51_HUMAN (Q30154) HLA class II histocompatibility antigen, DRB5 beta chain OS=Homo sapiens GN=HLA	30037.0	1 (1 0 0 0 0)	4.82E-04
Q31612	1B73_HUMAN (Q31612) HLA class I histocompatibility antigen, B-73 alpha chain OS=Homo sapiens GN=HLA	40410.0	2 (2 0 0 0 0)	1.66E-05
Q32P44	EML3_HUMAN (Q32P44) Echinoderm microtubule-associated protein-like 3 OS=Homo sapiens GN=EML3 P	95137.6	2 (2 0 0 0 0)	7.56E-05
Q32Q14	Q32Q14_HUMAN (Q32Q14) NDUFA7 protein (Fragment) OS=Homo sapiens GN=NDUFA7 PE=2 SV=1	13502.2	1 (1 0 0 0 0)	4.51E-08
Q32Q82	Q32Q82_HUMAN (Q32Q82) PCBP2 protein OS=Homo sapiens GN=PCBP2 PE=2 SV=1	35324.2	1 (1 0 0 0 0)	1.66E-07
Q3LXA3	DHAK_HUMAN (Q3LXA3) Dihydroxyacetone kinase OS=Homo sapiens GN=DAK PE=2 SV=1	58940.2	3 (3 0 0 0 0)	4.15E-09
Q3MHD2	LSM12_HUMAN (Q3MHD2) Protein LSM12 homolog OS=Homo sapiens GN=LSM12 PE=1 SV=2	21687.1	3 (3 0 0 0 0)	9.97E-09
Q3SY84	K2C71_HUMAN (Q3SY84) Keratin, type II cytoskeletal 71 OS=Homo sapiens GN=KRT71 PE=1 SV=2	57214.0	2 (0 2 0 0 0)	1.12E-06
Q3SY84	K2C71_HUMAN (Q3SY84) Keratin, type II cytoskeletal 71 OS=Homo sapiens GN=KRT71 PE=1 SV=2	57214.0	1 (0 1 0 0 0)	1.77E-06
Q3ZCU9	Q3ZCU9_HUMAN (Q3ZCU9) STIP1 protein OS=Homo sapiens GN=STIP1 PE=2 SV=1	68003.3	2 (2 0 0 0 0)	2.28E-08
Q49A26	NP60_HUMAN (Q49A26) Nuclear protein NP60 OS=Homo sapiens GN=NP60 PE=1 SV=2	60509.1	1 (0 1 0 0 0)	4.40E-05
Q49AP7	Q49AP7_HUMAN (Q49AP7) C1orf212 protein OS=Homo sapiens GN=C1orf212 PE=4 SV=1	10732.6	3 (3 0 0 0 0)	6.65E-05
Q4LE56	Q4LE56_HUMAN (Q4LE56) MYO1C variant protein (Fragment) OS=Homo sapiens GN=MYO1C variant protei	124977.9	7 (16 1 0 0 0)	9.10E-09
Q4LE64	Q4LE64_HUMAN (Q4LE64) NUMA1 variant protein (Fragment) OS=Homo sapiens GN=NUMA1 variant protei	238712.5	4 (14 0 0 0 0)	1.34E-11
Q4LE83	Q4LE83_HUMAN (Q4LE83) FASN variant protein (Fragment) OS=Homo sapiens GN=FASN variant protein PE	277192.9	7 (17 0 0 0 0)	4.39E-11
Q504R6	Q504R6_HUMAN (Q504R6) RAB13 protein (Fragment) OS=Homo sapiens GN=RAB13 PE=2 SV=1	27181.9	4 (4 0 0 0 0)	7.90E-09
Q53GF9	Q53GF9_HUMAN (Q53GF9) Full-length cDNA 5-PRIME end of clone CS0DF013YM24 of Fetal brain of Homo	25620.3	2 (2 0 0 0 0)	1.54E-08
Q53GL6	Q53GL6_HUMAN (Q53GL6) RNA binding protein (Autoantigenic, hnRNP-associated with lethal yellow) long is	32530.7	2 (2 0 0 0 0)	3.46E-06
Q53GQ0	DHB12_HUMAN (Q53GQ0) Estradiol 17-beta-dehydrogenase 12 OS=Homo sapiens GN=HSD17B12 PE=1 SV	34302.2	2 (2 0 0 0 0)	4.88E-08
Q53GS9	SNUT2_HUMAN (Q53GS9) U4/U6.U5 tri-snRNP-associated protein 2 OS=Homo sapiens GN=USP39 PE=1 SV	65339.8	1 (1 0 0 0 0)	9.50E-06
Q53H29	Q53H29_HUMAN (Q53H29) Nucleoporin 54kDa variant (Fragment) OS=Homo sapiens PE=2 SV=1	55529.5	2 (2 0 0 0 0)	4.76E-08
Q546F9	Q546F9_HUMAN (Q546F9) Mitochondrial aspartate-glutamate carrier protein OS=Homo sapiens GN=SLC25A	74256.9	6 (6 0 0 0 0)	3.46E-08
Q562R1	ACTBL_HUMAN (Q562R1) Beta-actin-like protein 2 OS=Homo sapiens GN=ACTBL2 PE=1 SV=2	41976.0	1 (1 0 0 0 0)	1.87E-05
Q58FF7	H90B3_HUMAN (Q58FF7) Putative heat shock protein HSP 90-beta-3 OS=Homo sapiens GN=HSP90AB3P P	68282.0	1 (1 0 0 0 0)	6.26E-06
Q58FF8	H90B2_HUMAN (Q58FF8) Putative heat shock protein HSP 90-beta 2 OS=Homo sapiens GN=HSP90AB2P P	44321.1	6 (0 6 0 0 0)	1.20E-08
Q58FF8	H90B2_HUMAN (Q58FF8) Putative heat shock protein HSP 90-beta 2 OS=Homo sapiens GN=HSP90AB2P P	44321.1	2 (2 0 0 0 0)	4.83E-07
Q58FG0	HS905_HUMAN (Q58FG0) Putative heat shock protein HSP 90-alpha A5 OS=Homo sapiens GN=HSP90AA5P	38713.8	4 (4 0 0 0 0)	1.14E-06
Q58FG1	HS904_HUMAN (Q58FG1) Putative heat shock protein HSP 90-alpha A4 OS=Homo sapiens GN=HSP90AA4P	47682.2	2 (0 2 0 0 0)	2.44E-08
Q58FG1	HS904_HUMAN (Q58FG1) Putative heat shock protein HSP 90-alpha A4 OS=Homo sapiens GN=HSP90AA4P	47682.2	3 (0 3 0 0 0)	2.80E-07
Q59E85	Q59E85_HUMAN (Q59E85) Caveolin (Fragment) OS=Homo sapiens PE=2 SV=1	25053.1	2 (2 0 0 0 0)	8.34E-06
Q59E93	Q59E93_HUMAN (Q59E93) Membrane alanine aminopeptidase variant (Fragment) OS=Homo sapiens PE=2 S	110523.4	2 (12 0 0 0 0)	5.09E-08
Q59EI9	Q59EI9_HUMAN (Q59EI9) ADP,ATP carrier protein, liver isoform T2 variant (Fragment) OS=Homo sapiens PE	35360.6	2 (2 0 0 0 0)	4.17E-08
Q59EL4	Q59EL4_HUMAN (Q59EL4) PRPF4 protein variant (Fragment) OS=Homo sapiens PE=2 SV=1	59984.3	3 (3 0 0 0 0)	3.61E-07
Q59EP1	Q59EP1_HUMAN (Q59EP1) Annexin A11 variant (Fragment) OS=Homo sapiens PE=2 SV=1	54858.4	1 (1 0 0 0 0)	5.14E-04
Q59ES3	Q59ES3_HUMAN (Q59ES3) Solute carrier family 1 (Neutral amino acid transporter), member 5 variant (Fragm	57353.9	7 (7 0 0 0 0)	4.62E-09
Q59EV6	Q59EV6_HUMAN (Q59EV6) Carrier family 6 , member 8 variant (Fragment) OS=Homo sapiens GN=PPGB PE	56083.9	1 (1 0 0 0 0)	9.80E-06
Q59F66	Q59F66_HUMAN (Q59F66) DEAD box polypeptide 17 isoform p82 variant (Fragment) OS=Homo sapiens PE=	81016.9	1 (1 0 0 0 0)	8.71E-09
Q59F99	Q59F99_HUMAN (Q59F99) Staufen isoform b variant (Fragment) OS=Homo sapiens PE=2 SV=1	64705.8	2 (2 0 0 0 0)	1.77E-07
Q59FF0	Q59FF0_HUMAN (Q59FF0) EBNA-2 co-activator variant (Fragment) OS=Homo sapiens PE=2 SV=1	107366.4	1 (1 0 0 0 0)	5.69E-04
Q59G24	Q59G24_HUMAN (Q59G24) Activated RNA polymerase II transcription cofactor 4 variant (Fragment) OS=Hom	15125.8	1 (1 0 0 0 0)	2.83E-05
Q59GB4	Q59GB4_HUMAN (Q59GB4) Dihydropyrimidinase-like 2 variant (Fragment) OS=Homo sapiens PE=2 SV=1	68141.6	1 (1 0 0 0 0)	1.40E-05
Q59GD6	Q59GD6_HUMAN (Q59GD6) Transducin beta-like 3 variant (Fragment) OS=Homo sapiens PE=2 SV=1	91180.7	2 (2 0 0 0 0)	2.32E-06

Q59GK9	Q59GK9_HUMAN (Q59GK9) Ribosomal protein L21 variant (Fragment) OS=Homo sapiens PE=2 SV=1	18879.3	3 (3 0 0 0 0)	1.12E-11
Q59GM9	Q59GM9_HUMAN (Q59GM9) Phosphorylase (Fragment) OS=Homo sapiens PE=2 SV=1	98766.8	9 (19 0 0 0 0)	1.00E-11
Q59GW5	Q59GW5_HUMAN (Q59GW5) Tripartite motif-containing 25 variant (Fragment) OS=Homo sapiens PE=2 SV=	72203.4	2 (2 0 0 0 0)	6.44E-07
Q59GX6	Q59GX6_HUMAN (Q59GX6) DEAD/H (Asp-Glu-Ala-Asp/His) box polypeptide 3 variant (Fragment) OS=Homo	74532.8	2 (2 0 0 0 0)	4.47E-09
Q59GX9	Q59GX9_HUMAN (Q59GX9) Ribosomal protein L5 variant (Fragment) OS=Homo sapiens PE=2 SV=1	35181.3	1 (1 0 0 0 0)	3.81E-08
Q59GY2	Q59GY2_HUMAN (Q59GY2) Ribosomal protein L4 variant (Fragment) OS=Homo sapiens PE=2 SV=1	48965.2	2 (2 0 0 0 0)	4.22E-08
Q59HH3	Q59HH3_HUMAN (Q59HH3) Phosphoribosylglycinamide formyltransferase, phosphoribosylglycinamide synthe	112067.5	4 (4 0 0 0 0)	4.61E-09
Q5HY50	Q5HY50_HUMAN (Q5HY50) Ribosomal protein L10 (Fragment) OS=Homo sapiens GN=RPL10 PE=2 SV=1	26575.9	5 (5 0 0 0 0)	1.69E-07
Q5HYE4	Q5HYE4_HUMAN (Q5HYE4) Putative uncharacterized protein DKFZp686F1612 OS=Homo sapiens GN=DKFZ	94577.8	2 (2 0 0 0 0)	1.37E-06
Q5HYI7	MTX3_HUMAN (Q5HYI7) Metaxin-3 OS=Homo sapiens GN=MTX3 PE=2 SV=2	35071.3	2 (2 0 0 0 0)	1.75E-11
Q5HYN5	CT451_HUMAN (Q5HYN5) Cancer/testis antigen 45-1 OS=Homo sapiens GN=CT45-1 PE=2 SV=1	21259.0	6 (6 0 0 0 0)	1.01E-07
Q5JNZ5	RS26L_HUMAN (Q5JNZ5) Putative 40S ribosomal protein S26-like 1 OS=Homo sapiens GN=RPS26L1 PE=5	12994.0	5 (5 0 0 0 0)	6.13E-08
Q5JPE7	NOMO2_HUMAN (Q5JPE7) Nodal modulator 2 OS=Homo sapiens GN=NOMO2 PE=1 SV=1	139351.0	1 (1 0 0 0 0)	4.81E-05
Q5JVF3	PCID2_HUMAN (Q5JVF3) PCI domain-containing protein 2 OS=Homo sapiens GN=PCID2 PE=1 SV=2	45999.9	1 (1 0 0 0 0)	4.69E-10
Q5JWF2	GNAS1_HUMAN (Q5JWF2) Guanine nucleotide-binding protein G(s) subunit alpha isoforms XLas OS=Homo s	110955.6	6 (6 0 0 0 0)	1.13E-08
Q5M7Z5	Q5M7Z5_HUMAN (Q5M7Z5) GRHPR protein (Fragment) OS=Homo sapiens GN=GRHPR PE=2 SV=1	36801.0	5 (5 0 0 0 0)	1.92E-08
Q5RI15	FA36A_HUMAN (Q5RI15) Protein FAM36A OS=Homo sapiens GN=FAM36A PE=2 SV=2	13282.8	2 (2 0 0 0 0)	8.35E-09
Q5RKV6	EXOS6_HUMAN (Q5RKV6) Exosome complex exonuclease MTR3 OS=Homo sapiens GN=EXOSC6 PE=1 SV	28217.7	1 (1 0 0 0 0)	2.78E-05
Q5SQP8	Q5SQP8_HUMAN (Q5SQP8) C-terminal binding protein 2 OS=Homo sapiens GN=CTBP2 PE=3 SV=1	56066.6	1 (1 0 0 0 0)	4.89E-06
Q5T1C6	THEM4_HUMAN (Q5T1C6) Thioesterase superfamily member 4 OS=Homo sapiens GN=THEM4 PE=1 SV=1	27111.6	1 (1 0 0 0 0)	3.34E-06
Q5T1D1	Q5T1D1_HUMAN (Q5T1D1) Novel protein similar to ribosomal protein L29 RPL29 (Fragment) OS=Homo sapi	18700.4	2 (2 0 0 0 0)	2.25E-08
Q5T4L4	Q5T4L4_HUMAN (Q5T4L4) Ribosomal protein S27 (Metallopanstimulin 1) OS=Homo sapiens GN=RPS27 PE=	7351.7	2 (2 0 0 0 0)	4.62E-07
Q5T7Y6	Q5T7Y6_HUMAN (Q5T7Y6) S100 calcium binding protein A1 (S100 calcium binding protein A1, isoform CRA	15884.7	2 (2 0 0 0 0)	2.59E-08
Q5T9B7	Q5T9B7_HUMAN (Q5T9B7) Adenylate kinase 1 OS=Homo sapiens GN=AK1 PE=2 SV=1	23396.1	2 (2 0 0 0 0)	9.94E-07
Q5VTR2	BRE1A_HUMAN (Q5VTR2) E3 ubiquitin-protein ligase BRE1A OS=Homo sapiens GN=RNF20 PE=1 SV=2	113592.1	1 (1 0 0 0 0)	1.72E-09
Q5VVL5	Q5VVL5_HUMAN (Q5VVL5) RNA terminal phosphate cyclase domain 1 (RNA terminal phosphate cyclase dom	40683.2	2 (2 0 0 0 0)	8.95E-07
Q5VW36	K1797_HUMAN (Q5VW36) Uncharacterized protein KIAA1797 OS=Homo sapiens GN=KIAA1797 PE=2 SV=1	199942.4	1 (1 0 0 0 0)	2.69E-09
Q5VWZ2	LYPL1_HUMAN (Q5VWZ2) Lysophospholipase-like protein 1 OS=Homo sapiens GN=LYPLAL1 PE=1 SV=3	26299.4	4 (4 0 0 0 0)	1.49E-05
Q5VYJ4	RUEL1_HUMAN (Q5VYJ4) Putative small nuclear ribonucleoprotein polypeptide E-like protein 1 OS=Homo sa	10671.5	3 (3 0 0 0 0)	1.23E-06
Q5W9G2	Q5W9G2_HUMAN (Q5W9G2) LAR (Fragment) OS=Homo sapiens GN=LAR PE=2 SV=1	213832.9	1 (1 0 0 0 0)	7.59E-05
Q66LE6	2ABD_HUMAN (Q66LE6) Serine/threonine-protein phosphatase 2A 55 kDa regulatory subunit B delta isoform	52009.6	2 (2 0 0 0 0)	5.16E-09
Q68CP5	Q68CP5_HUMAN (Q68CP5) Putative uncharacterized protein DKFZp781K1922 OS=Homo sapiens GN=DKFZ	20230.8	7 (7 0 0 0 0)	1.17E-08
Q6DN03	H2B2C_HUMAN (Q6DN03) Putative histone H2B type 2-C OS=Homo sapiens GN=HIST2H2BC PE=5 SV=3	21458.2	2 (2 0 0 0 0)	3.10E-06
Q6GMV3	CB079_HUMAN (Q6GMV3) Uncharacterized protein C2orf79 OS=Homo sapiens GN=C2orf79 PE=1 SV=1	15795.3	1 (1 0 0 0 0)	1.02E-06
Q6IBS0	TWF2_HUMAN (Q6IBS0) Twinfilin-2 OS=Homo sapiens GN=TWF2 PE=1 SV=2	39523.3	5 (5 0 0 0 0)	3.12E-09
Q6IPH7	Q6IPH7_HUMAN (Q6IPH7) RPL14 protein OS=Homo sapiens GN=RPL14 PE=2 SV=1	23772.2	8 (8 0 0 0 0)	2.67E-09
Q6IQ22	RAB12_HUMAN (Q6IQ22) Putative Ras-related protein Rab-12 OS=Homo sapiens GN=RAB12 PE=5 SV=3	27231.1	2 (2 0 0 0 0)	3.03E-04
Q6LAP8	Q6LAP8_HUMAN (Q6LAP8) Mitochondrial citrate transport protein (Fragment) OS=Homo sapiens PE=2 SV=1	34765.5	3 (3 0 0 0 0)	7.03E-06
Q6NT97	Q6NT97_HUMAN (Q6NT97) Regulator of chromosome condensation 1 OS=Homo sapiens GN=RCC1 PE=2 S	48115.1	6 (6 0 0 0 0)	2.67E-09
Q6NUS1	Q6NUS1_HUMAN (Q6NUS1) PDCD6IP protein OS=Homo sapiens GN=PDCD6IP PE=1 SV=1	96757.6	1 (1 0 0 0 0)	2.81E-08
Q6NVC0	Q6NVC0_HUMAN (Q6NVC0) SLC25A5 protein (Fragment) OS=Homo sapiens GN=SLC25A5 PE=2 SV=1	35271.4	3 (3 0 0 0 0)	1.33E-08
Q6NVV1	R13AX_HUMAN (Q6NVV1) Putative 60S ribosomal protein L13a-like MGC87657 OS=Homo sapiens PE=5 SV	12126.9	2 (2 0 0 0 0)	5.37E-09
Q6NXE6	ARMC6_HUMAN (Q6NXE6) Armadillo repeat-containing protein 6 OS=Homo sapiens GN=ARMC6 PE=1 SV=	54107.5	1 (1 0 0 0 0)	4.69E-09
Q6NZI2	PTRF_HUMAN (Q6NZI2) Polymerase I and transcript release factor OS=Homo sapiens GN=PTRF PE=1 SV=	43449.9	1 (1 0 0 0 0)	3.01E-08
Q6P1X6	CH082_HUMAN (Q6P1X6) UPF0598 protein C8orf82 OS=Homo sapiens GN=C8orf82 PE=2 SV=2	23874.1	2 (2 0 0 0 0)	1.53E-07
Q6P2Q9	PRP8_HUMAN (Q6P2Q9) Pre-mRNA-processing-splicing factor 8 OS=Homo sapiens GN=PRPF8 PE=1 SV=2	273424.6	2 (2 0 0 0 0)	2.32E-09
Q6P4Q7	CNNM4_HUMAN (Q6P4Q7) Metal transporter CNNM4 OS=Homo sapiens GN=CNNM4 PE=1 SV=2	86651.1	1 (1 0 0 0 0)	1.75E-07
Q6PI48	SYDM_HUMAN (Q6PI48) Aspartyl-tRNA synthetase, mitochondrial OS=Homo sapiens GN=DARS2 PE=1 SV=	73516.3	1 (1 0 0 0 0)	1.34E-05
Q6S8J3	A26CA_HUMAN (Q6S8J3) ANKRD26-like family C member 1A OS=Homo sapiens GN=A26C1A PE=1 SV=3	121285.6	5 (5 0 0 0 0)	1.41E-10
Q6U841	S4A10_HUMAN (Q6U841) Sodium-driven chloride bicarbonate exchanger OS=Homo sapiens GN=SLC4A10 P	125865.8	2 (2 0 0 0 0)	9.80E-07
Q6U8A4	Q6U8A4_HUMAN (Q6U8A4) Ubiquitin carboxyl-terminal hydrolase (Fragment) OS=Homo sapiens PE=2 SV=1	128921.8	2 (2 0 0 0 0)	8.21E-08
Q6UVK1	CSPG4_HUMAN (Q6UVK1) Chondroitin sulfate proteoglycan 4 OS=Homo sapiens GN=CSPG4 PE=1 SV=1	250339.4	9 (19 0 0 0 0)	2.03E-11
Q6UWE0	LRSM1_HUMAN (Q6UWE0) E3 ubiquitin-protein ligase LRSAM1 OS=Homo sapiens GN=LRSAM1 PE=1 SV=	83541.1	2 (2 0 0 0 0)	8.58E-07
Q6YHK3	CD109_HUMAN (Q6YHK3) CD109 antigen OS=Homo sapiens GN=CD109 PE=1 SV=2	161586.8	5 (5 0 0 0 0)	1.39E-12
Q6ZMR3	LDH6A_HUMAN (Q6ZMR3) L-lactate dehydrogenase A-like 6A OS=Homo sapiens GN=LDHAL6A PE=2 SV=1	36484.2	2 (2 0 0 0 0)	9.12E-09
Q6ZRM8	Q6ZRM8_HUMAN (Q6ZRM8) cDNA FLJ46245 fis, clone TESTI4020596, highly similar to Homo sapiens calpa	77259.8	6 (6 0 0 0 0)	3.47E-10
Q6ZTT1	Q6ZTT1_HUMAN (Q6ZTT1) cDNA FLJ44241 fis, clone THYMU3008436, highly similar to 6-phosphofructokina	93160.6	1 (1 0 0 0 0)	5.28E-06
Q6ZUX7	LHPL2_HUMAN (Q6ZUX7) Lipoma HMGIC fusion partner-like 2 protein OS=Homo sapiens GN=LHFPL2 PE=2	24469.3	2 (2 0 0 0 0)	1.70E-05
Q71U36	TBA1A_HUMAN (Q71U36) Tubulin alpha-1A chain OS=Homo sapiens GN=TUBA1A PE=1 SV=1	50103.7	7 (7 0 0 0 0)	1.54E-11
Q71U36	TBA1A_HUMAN (Q71U36) Tubulin alpha-1A chain OS=Homo sapiens GN=TUBA1A PE=1 SV=1	50103.7	1 (11 0 0 0 0)	5.12E-11
Q71UI9	H2AV_HUMAN (Q71UI9) Histone H2A.V OS=Homo sapiens GN=H2AFV PE=1 SV=3	13500.5	4 (4 0 0 0 0)	2.86E-09
Q7KZS6	Q7KZS6_HUMAN (Q7KZS6) Tubulin, beta, 4 OS=Homo sapiens GN=hCG_2042771 PE=2 SV=1	88324.5	4 (2 0 2 0 0)	1.05E-09
Q7L0Y3	MRRP1_HUMAN (Q7L0Y3) Mitochondrial ribonuclease P protein 1 OS=Homo sapiens GN=RG9MTD1 PE=1 S	47316.7	2 (2 0 0 0 0)	1.38E-05
Q7L2E3	DHX30_HUMAN (Q7L2E3) Putative ATP-dependent RNA helicase DHX30 OS=Homo sapiens GN=DHX30 PE	133854.7	1 (1 0 0 0 0)	3.40E-05
Q7L2H7	EIF3M_HUMAN (Q7L2H7) Eukaryotic translation initiation factor 3 subunit M OS=Homo sapiens GN=EIF3M P	42475.8	0 (10 0 0 0 0)	1.48E-08
Q7L576	CYFP1_HUMAN (Q7L576) Cytoplasmic FMR1-interacting protein 1 OS=Homo sapiens GN=CYFIP1 PE=1 SV=	145088.6	7 (6 1 0 0 0)	9.06E-09
Q7Z406	MYH14_HUMAN (Q7Z406) Myosin-14 OS=Homo sapiens GN=MYH14 PE=1 SV=1	227861.2	7 (5 2 0 0 0)	4.74E-07
Q7Z434	MAVS_HUMAN (Q7Z434) Mitochondrial antiviral-signaling protein OS=Homo sapiens GN=MAVS PE=1 SV=2	56493.2	1 (1 0 0 0 0)	5.27E-08
Q7Z460	CLAP1_HUMAN (Q7Z460) CLIP-associating protein 1 OS=Homo sapiens GN=CLASP1 PE=1 SV=1	169345.6	2 (2 0 0 0 0)	1.48E-12
Q7Z4V5	HDGR2_HUMAN (Q7Z4V5) Hepatoma-derived growth factor-related protein 2 OS=Homo sapiens GN=HDGFR	74272.3	2 (2 0 0 0 0)	1.39E-08
Q7Z5G4	GOGA7_HUMAN (Q7Z5G4) Golgin subfamily A member 7 OS=Homo sapiens GN=GOLGA7 PE=1 SV=2	15814.0	4 (4 0 0 0 0)	1.09E-09
Q7Z6Z7	HUWE1_HUMAN (Q7Z6Z7) E3 ubiquitin-protein ligase HUWE1 OS=Homo sapiens GN=HUWE1 PE=1 SV=3	481588.9	1 (1 0 0 0 0)	1.20E-05
Q7Z7H5	TMED4_HUMAN (Q7Z7H5) Transmembrane emp24 domain-containing protein 4 OS=Homo sapiens GN=TME	25926.4	3 (2 1 0 0 0)	1.69E-05
Q86SE5	RALYL_HUMAN (Q86SE5) RNA-binding Raly-like protein OS=Homo sapiens GN=RALYL PE=2 SV=2	32310.6	2 (0 2 0 0 0)	7.84E-07
Q86SE5	RALYL_HUMAN (Q86SE5) RNA-binding Raly-like protein OS=Homo sapiens GN=RALYL PE=2 SV=2	32310.6	1 (0 1 0 0 0)	1.18E-06
Q86UK7	ZN598_HUMAN (Q86UK7) Zinc finger protein 598 OS=Homo sapiens GN=ZNF598 PE=1 SV=1	98575.4	1 (1 0 0 0 0)	4.73E-07

Q86UP2	KTN1_HUMAN (Q86UP2) Kinectin OS=Homo sapiens GN=KTN1 PE=1 SV=1	156178.8	2 (2 0 0 0 0)	4.17E-09
Q86UU1	PHLB1_HUMAN (Q86UU1) Pleckstrin homology-like domain family B member 1 OS=Homo sapiens GN=PHLD	151067.9	1 (1 0 0 0 0)	3.76E-06
Q86V81	THOC4_HUMAN (Q86V81) THO complex subunit 4 OS=Homo sapiens GN=THOC4 PE=1 SV=3	26871.6	1 (1 0 0 0 0)	6.24E-04
Q86VP6	CAND1_HUMAN (Q86VP6) Cullin-associated NEDD8-dissociated protein 1 OS=Homo sapiens GN=CAND1 P	136288.8	4 (14 0 0 0 0)	4.48E-10
Q86VX2	COMD7_HUMAN (Q86VX2) COMM domain-containing protein 7 OS=Homo sapiens GN=COMMD7 PE=1 SV=	22525.6	1 (1 0 0 0 0)	5.95E-05
Q86W42	THOC6_HUMAN (Q86W42) THO complex subunit 6 homolog OS=Homo sapiens GN=THOC6 PE=2 SV=1	37511.1	2 (2 0 0 0 0)	6.56E-06
Q86XC7	Q86XC7_HUMAN (Q86XC7) Importin 5 OS=Homo sapiens GN=IPO5 PE=2 SV=1	125506.8	1 (1 0 0 0 0)	7.74E-06
Q86Y38	XYLT1_HUMAN (Q86Y38) Xylosyltransferase 1 OS=Homo sapiens GN=XYLT1 PE=1 SV=1	107501.6	1 (1 0 0 0 0)	1.40E-04
Q86Y39	NDUAB_HUMAN (Q86Y39) NADH dehydrogenase [ubiquinone] 1 alpha subcomplex subunit 11 OS=Homo sa	14842.5	3 (3 0 0 0 0)	9.37E-07
Q86Y46	K2C73_HUMAN (Q86Y46) Keratin, type II cytoskeletal 73 OS=Homo sapiens GN=KRT73 PE=1 SV=1	58886.8	2 (2 0 0 0 0)	4.88E-07
Q86Y56	HEAT2_HUMAN (Q86Y56) HEAT repeat-containing protein 2 OS=Homo sapiens GN=HEATR2 PE=1 SV=2	93474.2	1 (1 0 0 0 0)	1.54E-05
Q86Y82	STX12_HUMAN (Q86Y82) Syntaxin-12 OS=Homo sapiens GN=STX12 PE=1 SV=1	31622.3	2 (2 0 0 0 0)	3.52E-08
Q86YB8	ERO1B_HUMAN (Q86YB8) ERO1-like protein beta OS=Homo sapiens GN=ERO1LB PE=1 SV=2	53509.2	1 (1 0 0 0 0)	7.65E-05
Q8IU81	I2BP1_HUMAN (Q8IU81) Interferon regulatory factor 2-binding protein 1 OS=Homo sapiens GN=IRF2BP1 PE	61649.1	5 (5 0 0 0 0)	4.10E-11
Q8IVF7	FMNL3_HUMAN (Q8IVF7) Formin-like protein 3 OS=Homo sapiens GN=FMNL3 PE=1 SV=3	117138.9	2 (2 0 0 0 0)	6.07E-11
Q8IWE2	NXP20_HUMAN (Q8IWE2) Protein NOXP20 OS=Homo sapiens GN=FAM114A1 PE=1 SV=1	60787.3	2 (2 0 0 0 0)	3.11E-10
Q8IWX8	CHERP_HUMAN (Q8IWX8) Calcium homeostasis endoplasmic reticulum protein OS=Homo sapiens GN=CHE	103508.2	1 (1 0 0 0 0)	1.30E-05
Q8IXI1	MIRO2_HUMAN (Q8IXI1) Mitochondrial Rho GTPase 2 OS=Homo sapiens GN=RHOT2 PE=1 SV=2	68074.8	2 (2 0 0 0 0)	1.81E-05
Q8IY81	RRMJ3_HUMAN (Q8IY81) Putative rRNA methyltransferase 3 OS=Homo sapiens GN=FTSJ3 PE=1 SV=1	96516.2	3 (3 0 0 0 0)	2.22E-12
Q8IZL9	CCRK_HUMAN (Q8IZL9) Cell cycle-related kinase OS=Homo sapiens GN=CCRK PE=1 SV=1	38670.3	1 (0 1 0 0 0)	1.87E-04
Q8IZQ5	SELH_HUMAN (Q8IZQ5) Selenoprotein H OS=Homo sapiens GN=SELH PE=2 SV=2	23295.2	2 (2 0 0 0 0)	1.32E-07
Q8N0W4	NLGNX_HUMAN (Q8N0W4) Neuroligin-4, X-linked OS=Homo sapiens GN=NLGN4X PE=1 SV=1	91857.0	1 (1 0 0 0 0)	2.07E-06
Q8N0X7	SPG20_HUMAN (Q8N0X7) Spartin OS=Homo sapiens GN=SPG20 PE=1 SV=1	72787.8	1 (1 0 0 0 0)	1.57E-06
Q8N1C8	Q8N1C8_HUMAN (Q8N1C8) HSPA9 protein (Fragment) OS=Homo sapiens GN=HSPA9 PE=2 SV=1	73808.0	1 (1 0 0 0 0)	3.53E-11
Q8N1F7	NUP93_HUMAN (Q8N1F7) Nuclear pore complex protein Nup93 OS=Homo sapiens GN=NUP93 PE=1 SV=2	93429.7	2 (2 0 0 0 0)	1.75E-07
Q8N1G4	LRC47_HUMAN (Q8N1G4) Leucine-rich repeat-containing protein 47 OS=Homo sapiens GN=LRRC47 PE=1 S	63433.9	9 (9 0 0 0 0)	7.77E-15
Q8N2Q7	NLGN1_HUMAN (Q8N2Q7) Neuroligin-1 OS=Homo sapiens GN=NLGN1 PE=1 SV=2	93775.9	1 (0 1 0 0 0)	7.36E-07
Q8N3R9	MPP5_HUMAN (Q8N3R9) MAGUK p55 subfamily member 5 OS=Homo sapiens GN=MPP5 PE=1 SV=3	77245.6	1 (1 0 0 0 0)	3.44E-07
Q8N442	GUF1_HUMAN (Q8N442) GTP-binding protein GUF1 homolog OS=Homo sapiens GN=GUF1 PE=1 SV=1	74281.3	1 (1 0 0 0 0)	1.76E-07
Q8N5K1	CISD2_HUMAN (Q8N5K1) CDGSH iron sulfur domain-containing protein 2 OS=Homo sapiens GN=CISD2 PE	15268.5	2 (2 0 0 0 0)	1.21E-08
Q8N5L2	Q8N5L2_HUMAN (Q8N5L2) AXL receptor tyrosine kinase OS=Homo sapiens GN=AXL PE=2 SV=1	98302.2	1 (1 0 0 0 0)	2.48E-05
Q8N6E1	Q8N6E1_HUMAN (Q8N6E1) Ribosomal protein L15 (Fragment) OS=Homo sapiens PE=2 SV=1	25646.0	2 (2 0 0 0 0)	1.08E-10
Q8N7V9	Q8N7V9_HUMAN (Q8N7V9) cDNA FLJ40287 fis, clone TESTI2027909, highly similar to 5'-AMP-ACTIVATED	38508.4	1 (1 0 0 0 0)	4.09E-06
Q8N999	CL029_HUMAN (Q8N999) Uncharacterized protein C12orf29 OS=Homo sapiens GN=C12orf29 PE=2 SV=2	37466.0	1 (1 0 0 0 0)	2.42E-06
Q8N9N7	LRC57_HUMAN (Q8N9N7) Leucine-rich repeat-containing protein 57 OS=Homo sapiens GN=LRRC57 PE=2 S	26737.3	5 (5 0 0 0 0)	9.79E-07
Q8NB49	AT11C_HUMAN (Q8NB49) Probable phospholipid-transporting ATPase IG OS=Homo sapiens GN=ATP11C PE	129394.2	1 (1 0 0 0 0)	4.76E-07
Q8NBU5	ATAD1_HUMAN (Q8NBU5) ATPase family AAA domain-containing protein 1 OS=Homo sapiens GN=ATAD1 P	40718.0	1 (1 0 0 0 0)	5.05E-07
Q8NC51	PAIRB_HUMAN (Q8NC51) Plasminogen activator inhibitor 1 RNA-binding protein OS=Homo sapiens GN=SEF	44938.5	9 (19 0 0 0 0)	1.30E-09
Q8NCN5	PDPR_HUMAN (Q8NCN5) Pyruvate dehydrogenase phosphatase regulatory subunit, mitochondrial OS=Homo	99300.7	1 (1 0 0 0 0)	7.92E-06
Q8NFJ5	RAI3_HUMAN (Q8NFJ5) Retinoic acid-induced protein 3 OS=Homo sapiens GN=GPRC5A PE=1 SV=2	40225.0	1 (1 0 0 0 0)	6.36E-07
Q8NFQ8	TOIP2_HUMAN (Q8NFQ8) Torsin-1A-interacting protein 2 OS=Homo sapiens GN=TOR1AIP2 PE=1 SV=1	51232.2	3 (3 0 0 0 0)	1.93E-10
Q8NFW8	NEUA_HUMAN (Q8NFW8) N-acylneuraminate cytidylyltransferase OS=Homo sapiens GN=CMAS PE=1 SV=2	48348.7	3 (3 0 0 0 0)	1.69E-08
Q8NG11	TSN14_HUMAN (Q8NG11) Tetraspanin-14 OS=Homo sapiens GN=TSPAN14 PE=2 SV=1	30670.6	3 (3 0 0 0 0)	2.97E-06
Q8NHW5	RLA0L_HUMAN (Q8NHW5) 60S acidic ribosomal protein P0-like OS=Homo sapiens PE=2 SV=1	34342.7	5 (5 0 0 0 0)	6.05E-08
Q8NHW5	RLA0L_HUMAN (Q8NHW5) 60S acidic ribosomal protein P0-like OS=Homo sapiens PE=2 SV=1	34342.7	1 (1 0 0 0 0)	1.59E-05
Q8NI61	Q8NI61_HUMAN (Q8NI61) Ribosomal protein S2 OS=Homo sapiens GN=OK/KNS-cl.7 PE=2 SV=1	21707.7	1 (1 0 0 0 0)	9.27E-08
Q8TAA3	PSA7L_HUMAN (Q8TAA3) Proteasome subunit alpha type-7-like OS=Homo sapiens GN=PSMA8 PE=1 SV=3	28512.1	2 (2 0 0 0 0)	1.57E-05
Q8TAT6	NPL4_HUMAN (Q8TAT6) Nuclear protein localization protein 4 homolog OS=Homo sapiens GN=NPLOC4 PE	68077.0	3 (3 0 0 0 0)	5.81E-08
Q8TD43	TRPM4_HUMAN (Q8TD43) Transient receptor potential cation channel subfamily M member 4 OS=Homo sapi	134215.5	1 (0 1 0 0 0)	1.16E-05
Q8TDB8	GTR14_HUMAN (Q8TDB8) Solute carrier family 2, facilitated glucose transporter member 14 OS=Homo sapie	56283.6	2 (2 0 0 0 0)	1.78E-06
Q8TDN6	BXDC2_HUMAN (Q8TDN6) Brix domain-containing protein 2 OS=Homo sapiens GN=BXDC2 PE=1 SV=2	41375.0	3 (3 0 0 0 0)	3.07E-06
Q8WTT2	NOC3L_HUMAN (Q8WTT2) Nucleolar complex protein 3 homolog OS=Homo sapiens GN=NOC3L PE=1 SV=	92489.7	2 (2 0 0 0 0)	1.00E-08
Q8WU19	Q8WU19_HUMAN (Q8WU19) TUBA1B protein OS=Homo sapiens GN=TUBA1B PE=2 SV=1	37194.1	2 (2 0 0 0 0)	5.50E-09
Q8WU19	Q8WU19_HUMAN (Q8WU19) TUBA1B protein OS=Homo sapiens GN=TUBA1B PE=2 SV=1	37194.1	2 (2 0 0 0 0)	5.83E-07
Q8WUD1	RAB2B_HUMAN (Q8WUD1) Ras-related protein Rab-2B OS=Homo sapiens GN=RAB2B PE=1 SV=1	24199.2	1 (1 0 0 0 0)	6.96E-07
Q8WUK0	PTPM1_HUMAN (Q8WUK0) Protein-tyrosine phosphatase mitochondrial 1 OS=Homo sapiens GN=PTPMT1 P	22829.2	1 (1 0 0 0 0)	1.01E-04
Q8WVC6	DCAKD_HUMAN (Q8WVC6) Dephospho-CoA kinase domain-containing protein OS=Homo sapiens GN=DCAI	26533.3	1 (1 0 0 0 0)	1.23E-05
Q8WVM8	SCFD1_HUMAN (Q8WVM8) Sec1 family domain-containing protein 1 OS=Homo sapiens GN=SCFD1 PE=1 S	72334.1	1 (1 0 0 0 0)	4.79E-08
Q8WVX7	Q8WVX7_HUMAN (Q8WVX7) Ribosomal protein S19 (Fragment) OS=Homo sapiens PE=2 SV=1	17271.2	7 (7 0 0 0 0)	2.09E-09
Q8WVY7	UBCP1_HUMAN (Q8WVY7) Ubiquitin-like domain-containing CTD phosphatase 1 OS=Homo sapiens GN=UB	36781.2	1 (1 0 0 0 0)	2.15E-05
Q8WW12	PCNP_HUMAN (Q8WW12) PEST proteolytic signal-containing nuclear protein OS=Homo sapiens GN=PCNP	18913.4	1 (1 0 0 0 0)	6.58E-07
Q8WWC4	CB047_HUMAN (Q8WWC4) Uncharacterized protein C2orf47, mitochondrial OS=Homo sapiens GN=C2orf47	32524.0	4 (4 0 0 0 0)	2.50E-06
Q8WWI5	CTL1_HUMAN (Q8WWI5) Choline transporter-like protein 1 OS=Homo sapiens GN=SLC44A1 PE=1 SV=1	73253.4	2 (2 0 0 0 0)	3.91E-09
Q8WWM7	ATX2L_HUMAN (Q8WWM7) Ataxin-2-like protein OS=Homo sapiens GN=ATXN2L PE=1 SV=2	113303.8	2 (2 0 0 0 0)	1.62E-08
Q8WY22	BRI3B_HUMAN (Q8WY22) BRI3-binding protein OS=Homo sapiens GN=BRI3BP PE=1 SV=1	27817.8	2 (2 0 0 0 0)	1.07E-12
Q92499	DDX1_HUMAN (Q92499) ATP-dependent RNA helicase DDX1 OS=Homo sapiens GN=DDX1 PE=1 SV=2	82379.9	3 (3 0 0 0 0)	1.43E-07
Q92520	FAM3C_HUMAN (Q92520) Protein FAM3C OS=Homo sapiens GN=FAM3C PE=1 SV=1	24664.6	8 (7 1 0 0 0)	1.02E-10
Q92522	H1X_HUMAN (Q92522) Histone H1x OS=Homo sapiens GN=H1FX PE=1 SV=1	22473.6	2 (2 0 0 0 0)	3.97E-09
Q92542	NICA_HUMAN (Q92542) Nicastrin OS=Homo sapiens GN=NCSTN PE=1 SV=2	78361.7	3 (3 0 0 0 0)	1.07E-06
Q92616	GCN1L_HUMAN (Q92616) Translational activator GCN1 OS=Homo sapiens GN=GCN1L1 PE=1 SV=5	292555.8	2 (2 0 0 0 0)	1.72E-09
Q92804	RBP56_HUMAN (Q92804) TATA-binding protein-associated factor 2N OS=Homo sapiens GN=TAF15 PE=1 SV	61792.9	2 (2 0 0 0 0)	2.41E-08
Q92888	ARHG1_HUMAN (Q92888) Rho guanine nucleotide exchange factor 1 OS=Homo sapiens GN=ARHGEF1 PE	102371.5	5 (5 0 0 0 0)	1.96E-07
Q92979	NEP1_HUMAN (Q92979) Probable ribosome biogenesis protein NEP1 OS=Homo sapiens GN=EMG1 PE=1 S	26703.2	1 (1 0 0 0 0)	1.38E-05
Q93034	CUL5_HUMAN (Q93034) Cullin-5 OS=Homo sapiens GN=CUL5 PE=1 SV=4	90897.5	3 (3 0 0 0 0)	1.96E-08
Q93096	TP4A1_HUMAN (Q93096) Protein tyrosine phosphatase type IVA 1 OS=Homo sapiens GN=PTP4A1 PE=1 SV	19802.2	2 (2 0 0 0 0)	2.79E-10
Q969G5	PRDBP_HUMAN (Q969G5) Protein kinase C delta-binding protein OS=Homo sapiens GN=PRKCDBP PE=1 S	27609.5	3 (3 0 0 0 0)	1.02E-07

Q969Q5	RAB24_HUMAN (Q969Q5) Ras-related protein Rab-24 OS=Homo sapiens GN=RAB24 PE=2 SV=1	23109.4	1 (1 0 0 0 0)	4.00E-05
Q969S9	EFG2_HUMAN (Q969S9) Elongation factor G 2, mitochondrial OS=Homo sapiens GN=GFM2 PE=2 SV=1	86546.3	1 (1 0 0 0 0)	7.63E-06
Q96A08	H2B1A_HUMAN (Q96A08) Histone H2B type 1-A OS=Homo sapiens GN=HIST1H2BA PE=1 SV=3	14158.8	3 (3 0 0 0 0)	1.02E-08
Q96A26	F162A_HUMAN (Q96A26) UPF0389 protein FAM162A OS=Homo sapiens GN=FAM162A PE=1 SV=2	17331.2	2 (2 0 0 0 0)	7.31E-07
Q96AG4	LRC59_HUMAN (Q96AG4) Leucine-rich repeat-containing protein 59 OS=Homo sapiens GN=LRRC59 PE=1 S	34908.9	2 (2 0 0 0 0)	1.32E-07
Q96AH8	RAB7B_HUMAN (Q96AH8) Ras-related protein Rab-7b OS=Homo sapiens GN=RAB7B PE=2 SV=1	22496.6	1 (1 0 0 0 0)	2.05E-05
Q96B97	SH3K1_HUMAN (Q96B97) SH3 domain-containing kinase-binding protein 1 OS=Homo sapiens GN=SH3KBP1	73081.8	3 (3 0 0 0 0)	7.20E-11
Q96C36	P5CR2_HUMAN (Q96C36) Pyrroline-5-carboxylate reductase 2 OS=Homo sapiens GN=PYCR2 PE=1 SV=1	33615.7	1 (1 0 0 0 0)	1.31E-07
Q96D71	REPS1_HUMAN (Q96D71) RalBP1-associated Eps domain-containing protein 1 OS=Homo sapiens GN=REPS	80720.4	2 (2 0 0 0 0)	4.07E-05
Q96DA0	YP003_HUMAN (Q96DA0) Uncharacterized protein UNQ773/PRO1567 OS=Homo sapiens GN=UNQ773/PRO	22724.6	1 (1 0 0 0 0)	1.95E-05
Q96DA6	TIM14_HUMAN (Q96DA6) Mitochondrial import inner membrane translocase subunit TIM14 OS=Homo sapien	12490.7	1 (1 0 0 0 0)	1.01E-04
Q96DB5	RMD1_HUMAN (Q96DB5) Regulator of microtubule dynamics protein 1 OS=Homo sapiens GN=FAM82B PE=	35785.4	1 (1 0 0 0 0)	2.74E-07
Q96EK6	GNA1_HUMAN (Q96EK6) Glucosamine 6-phosphate N-acetyltransferase OS=Homo sapiens GN=GNPNAT1 P	20735.6	2 (2 0 0 0 0)	5.15E-06
Q96ER9	CCD51_HUMAN (Q96ER9) Coiled-coil domain-containing protein 51 OS=Homo sapiens GN=CCDC51 PE=2 S	45782.8	2 (2 0 0 0 0)	1.36E-07
Q96EY8	MMAB_HUMAN (Q96EY8) Cob(I)yrinic acid a,c-diamide adenosyltransferase, mitochondrial OS=Homo sapien	27371.0	3 (3 0 0 0 0)	4.07E-08
Q96GQ7	DDX27_HUMAN (Q96GQ7) Probable ATP-dependent RNA helicase DDX27 OS=Homo sapiens GN=DDX27 P	89779.2	1 (1 0 0 0 0)	6.32E-06
Q96I99	SUCB2_HUMAN (Q96I99) Succinyl-CoA ligase [GDP-forming] subunit beta, mitochondrial OS=Homo sapiens	46481.5	3 (3 0 0 0 0)	1.14E-12
Q96IH1	Q96IH1_HUMAN (Q96IH1) FSCN1 protein (Fragment) OS=Homo sapiens GN=FSCN1 PE=2 SV=1	55101.4	6 (6 0 0 0 0)	2.32E-07
Q96J84	KIRR1_HUMAN (Q96J84) Kin of IRRE-like protein 1 OS=Homo sapiens GN=KIRREL PE=1 SV=2	83484.0	5 (5 0 0 0 0)	9.69E-07
Q96JB6	LOXL4_HUMAN (Q96JB6) Lysyl oxidase homolog 4 OS=Homo sapiens GN=LOXL4 PE=1 SV=1	84429.1	6 (6 0 0 0 0)	4.06E-08
Q96JJ7	TXD10_HUMAN (Q96JJ7) Protein disulfide-isomerase TXNDC10 OS=Homo sapiens GN=TXNDC10 PE=1 SV	51839.0	2 (2 0 0 0 0)	8.47E-07
Q96L92	SNX27_HUMAN (Q96L92) Sorting nexin-27 OS=Homo sapiens GN=SNX27 PE=1 SV=2	61226.6	1 (1 0 0 0 0)	2.47E-07
Q96P70	IPO9_HUMAN (Q96P70) Importin-9 OS=Homo sapiens GN=IPO9 PE=1 SV=3	115888.8	2 (2 0 0 0 0)	2.74E-08
Q96PK6	RBM14_HUMAN (Q96PK6) RNA-binding protein 14 OS=Homo sapiens GN=RBM14 PE=1 SV=2	69449.0	1 (1 0 0 0 0)	4.03E-07
Q96PY5	FMNL2_HUMAN (Q96PY5) Formin-like protein 2 OS=Homo sapiens GN=FMNL2 PE=1 SV=2	123322.2	1 (1 0 0 0 0)	3.40E-09
Q96QK1	VPS35_HUMAN (Q96QK1) Vacuolar protein sorting-associated protein 35 OS=Homo sapiens GN=VPS35 PE=	91649.1	2 (2 0 0 0 0)	2.99E-07
Q96QV6	H2A1A_HUMAN (Q96QV6) Histone H2A type 1-A OS=Homo sapiens GN=HIST1H2AA PE=1 SV=3	14224.9	2 (2 0 0 0 0)	3.60E-05
Q96RP9	EFG1_HUMAN (Q96RP9) Elongation factor G 1, mitochondrial OS=Homo sapiens GN=GFM1 PE=1 SV=2	83418.5	1 (1 0 0 0 0)	6.70E-08
Q96RS2	Q96RS2_HUMAN (Q96RS2) Laminin receptor-like protein LAMRL5 OS=Homo sapiens GN=LAMR1P15 PE=2	32975.5	3 (3 0 0 0 0)	4.62E-10
Q96S19	CP013_HUMAN (Q96S19) UPF0585 protein C16orf13 OS=Homo sapiens GN=C16orf13 PE=2 SV=2	22563.7	2 (2 0 0 0 0)	2.15E-04
Q96S52	PIGS_HUMAN (Q96S52) GPI transamidase component PIG-S OS=Homo sapiens GN=PIGS PE=1 SV=3	61617.3	2 (2 0 0 0 0)	6.36E-08
Q96S59	RANB9_HUMAN (Q96S59) Ran-binding protein 9 OS=Homo sapiens GN=RANBP9 PE=1 SV=1	77798.1	1 (1 0 0 0 0)	1.11E-07
Q96S97	MYADM_HUMAN (Q96S97) Myeloid-associated differentiation marker OS=Homo sapiens GN=MYADM PE=1	35250.3	1 (1 0 0 0 0)	9.03E-06
Q99456	K1C12_HUMAN (Q99456) Keratin, type I cytoskeletal 12 OS=Homo sapiens GN=KRT12 PE=1 SV=1	53478.5	1 (0 1 0 0 0)	3.85E-05
Q99536	VAT1_HUMAN (Q99536) Synaptic vesicle membrane protein VAT-1 homolog OS=Homo sapiens GN=VAT1 PE	41893.5	2 (2 0 0 0 0)	6.87E-11
Q99569	PKP4_HUMAN (Q99569) Plakophilin-4 OS=Homo sapiens GN=PKP4 PE=1 SV=1	134186.1	1 (1 0 0 0 0)	1.79E-06
Q99575	POP1_HUMAN (Q99575) Ribonucleases P/MRP protein subunit POP1 OS=Homo sapiens GN=POP1 PE=1 S	114636.0	6 (6 0 0 0 0)	2.15E-08
Q99584	S10AD_HUMAN (Q99584) Protein S100-A13 OS=Homo sapiens GN=S100A13 PE=1 SV=1	11464.1	4 (4 0 0 0 0)	3.02E-06
Q99623	PHB2_HUMAN (Q99623) Prohibitin-2 OS=Homo sapiens GN=PHB2 PE=1 SV=2	33275.9	11 (11 0 0 0 0)	1.22E-09
Q99643	C560_HUMAN (Q99643) Succinate dehydrogenase cytochrome b560 subunit, mitochondrial OS=Homo sapien	18597.8	2 (2 0 0 0 0)	2.31E-05
Q99653	CHP1_HUMAN (Q99653) Calcium-binding protein p22 OS=Homo sapiens GN=CHP PE=1 SV=3	22442.4	3 (3 0 0 0 0)	6.27E-08
Q99700	ATX2_HUMAN (Q99700) Ataxin-2 OS=Homo sapiens GN=ATXN2 PE=1 SV=2	140195.9	1 (1 0 0 0 0)	1.14E-05
Q99714	HCD2_HUMAN (Q99714) 3-hydroxyacyl-CoA dehydrogenase type-2 OS=Homo sapiens GN=HSD17B10 PE=	26906.1	3 (13 0 0 0 0)	2.92E-09
Q99798	ACON_HUMAN (Q99798) Aconitate hydratase, mitochondrial OS=Homo sapiens GN=ACO2 PE=1 SV=2	85372.0	2 (2 0 0 0 0)	2.78E-07
Q99816	TS101_HUMAN (Q99816) Tumor susceptibility gene 101 protein OS=Homo sapiens GN=TSG101 PE=1 SV=2	43916.5	8 (8 0 0 0 0)	9.07E-09
Q99828	CIB1_HUMAN (Q99828) Calcium and integrin-binding protein 1 OS=Homo sapiens GN=CIB1 PE=1 SV=4	21689.9	2 (2 0 0 0 0)	5.16E-06
Q99832	TCPH_HUMAN (Q99832) T-complex protein 1 subunit eta OS=Homo sapiens GN=CCT7 PE=1 SV=2	59329.0	2 (2 0 0 0 0)	1.18E-05
Q99848	EBP2_HUMAN (Q99848) Probable rRNA-processing protein EBP2 OS=Homo sapiens GN=EBNA1BP2 PE=1	34830.4	1 (1 0 0 0 0)	4.26E-05
Q99873	ANM1_HUMAN (Q99873) Protein arginine N-methyltransferase 1 OS=Homo sapiens GN=PRMT1 PE=1 SV=2	41488.5	3 (3 0 0 0 0)	3.99E-07
Q99986	VRK1_HUMAN (Q99986) Serine/threonine-protein kinase VRK1 OS=Homo sapiens GN=VRK1 PE=1 SV=1	45447.5	1 (1 0 0 0 0)	3.63E-05
Q9BPW8	NIPS1_HUMAN (Q9BPW8) Protein NipSnap homolog 1 OS=Homo sapiens GN=NIPSNAP1 PE=1 SV=1	33288.9	2 (2 0 0 0 0)	8.58E-06
Q9BQ61	CS043_HUMAN (Q9BQ61) Uncharacterized protein C19orf43 OS=Homo sapiens GN=C19orf43 PE=1 SV=1	18408.2	2 (2 0 0 0 0)	1.54E-04
Q9BQC6	RT63_HUMAN (Q9BQC6) Ribosomal protein 63, mitochondrial OS=Homo sapiens GN=MRP63 PE=2 SV=1	12258.5	1 (1 0 0 0 0)	4.66E-08
Q9BQG0	MBB1A_HUMAN (Q9BQG0) Myb-binding protein 1A OS=Homo sapiens GN=MYBBP1A PE=1 SV=2	148761.2	7 (7 0 0 0 0)	3.78E-07
Q9BRG1	VPS25_HUMAN (Q9BRG1) Vacuolar protein-sorting-associated protein 25 OS=Homo sapiens GN=VPS25 PE	20734.5	3 (3 0 0 0 0)	1.66E-05
Q9BRX8	CJ058_HUMAN (Q9BRX8) Uncharacterized protein C10orf58 OS=Homo sapiens GN=C10orf58 PE=1 SV=3	25747.4	6 (6 0 0 0 0)	2.09E-07
Q9BSD7	CA057_HUMAN (Q9BSD7) Nucleoside-triphosphatase C1orf57 OS=Homo sapiens GN=C1orf57 PE=1 SV=1	20700.1	4 (4 0 0 0 0)	6.83E-11
Q9BSJ8	ESYT1_HUMAN (Q9BSJ8) Extended synaptotagmin-1 OS=Homo sapiens GN=FAM62A PE=1 SV=1	122780.1	7 (17 0 0 0 0)	4.09E-11
Q9BTE7	DCNL5_HUMAN (Q9BTE7) DCN1-like protein 5 OS=Homo sapiens GN=DCUN1D5 PE=1 SV=1	27490.6	6 (6 0 0 0 0)	4.66E-11
Q9BTV4	TMM43_HUMAN (Q9BTV4) Transmembrane protein 43 OS=Homo sapiens GN=TMEM43 PE=1 SV=1	44847.3	4 (4 0 0 0 0)	5.10E-06
Q9BUL8	PDC10_HUMAN (Q9BUL8) Programmed cell death protein 10 OS=Homo sapiens GN=PDCD10 PE=1 SV=1	24685.8	3 (3 0 0 0 0)	3.36E-06
Q9BUQ8	DDX23_HUMAN (Q9BUQ8) Probable ATP-dependent RNA helicase DDX23 OS=Homo sapiens GN=DDX23 P	95524.0	1 (1 0 0 0 0)	7.41E-08
Q9BV20	EI2BL_HUMAN (Q9BV20) Translation initiation factor eIF-2B subunit alpha/beta/delta-like protein OS=Homo sa	39125.4	1 (1 0 0 0 0)	3.68E-07
Q9BVC6	TM109_HUMAN (Q9BVC6) Transmembrane protein 109 OS=Homo sapiens GN=TMEM109 PE=1 SV=1	26193.6	6 (6 0 0 0 0)	1.74E-05
Q9BVK6	TMED9_HUMAN (Q9BVK6) Transmembrane emp24 domain-containing protein 9 OS=Homo sapiens GN=TME	25088.9	3 (2 1 0 0 0)	2.56E-05
Q9BVP2	GNL3_HUMAN (Q9BVP2) Guanine nucleotide-binding protein-like 3 OS=Homo sapiens GN=GNL3 PE=1 SV=	61958.5	3 (3 0 0 0 0)	3.45E-09
Q9BW27	NUP85_HUMAN (Q9BW27) Nucleoporin NUP85 OS=Homo sapiens GN=NUP85 PE=1 SV=1	74971.2	1 (1 0 0 0 0)	6.55E-06
Q9BWH2	FUND2_HUMAN (Q9BWH2) FUN14 domain-containing protein 2 OS=Homo sapiens GN=FUNDC2 PE=1 SV=	20662.7	2 (2 0 0 0 0)	2.10E-07
Q9BX79	STRA6_HUMAN (Q9BX79) Stimulated by retinoic acid gene 6 protein homolog OS=Homo sapiens GN=STRA6	73455.9	3 (3 0 0 0 0)	1.51E-07
Q9BY32	ITPA_HUMAN (Q9BY32) Inosine triphosphate pyrophosphatase OS=Homo sapiens GN=ITPA PE=1 SV=2	21431.9	3 (3 0 0 0 0)	3.99E-11
Q9BZE4	NOG1_HUMAN (Q9BZE4) Nucleolar GTP-binding protein 1 OS=Homo sapiens GN=GTPBP4 PE=1 SV=3	73917.9	2 (2 0 0 0 0)	1.19E-06
Q9BZF9	UACA_HUMAN (Q9BZF9) Uveal autoantigen with coiled-coil domains and ankyrin repeats OS=Homo sapiens	162403.8	1 (1 0 0 0 0)	3.95E-07
Q9BZK3	NACP1_HUMAN (Q9BZK3) Putative nascent polypeptide-associated complex subunit alpha-like protein OS=H	23291.9	1 (0 1 0 0 0)	5.16E-07
Q9BZL1	UBL5_HUMAN (Q9BZL1) Ubiquitin-like protein 5 OS=Homo sapiens GN=UBL5 PE=1 SV=1	8541.4	2 (2 0 0 0 0)	4.49E-05
Q9C004	SPY4_HUMAN (Q9C004) Protein sprouty homolog 4 OS=Homo sapiens GN=SPRY4 PE=1 SV=2	32519.7	4 (4 0 0 0 0)	4.56E-07
Q9GZL7	WDR12_HUMAN (Q9GZL7) WD repeat-containing protein 12 OS=Homo sapiens GN=WDR12 PE=1 SV=2	47677.7	1 (1 0 0 0 0)	1.96E-06

Q9GZM7	TINAL_HUMAN (Q9GZM7) Tubulointerstitial nephritis antigen-like OS=Homo sapiens GN=TINAGL1 PE=1 SV=	52353.0	1 (1 0 0 0 0)	1.48E-09
Q9GZT3	SLIRP_HUMAN (Q9GZT3) SRA stem-loop-interacting RNA-binding protein, mitochondrial OS=Homo sapiens (	12341.4	5 (5 0 0 0 0)	1.48E-10
Q9GZT9	EGLN1_HUMAN (Q9GZT9) Egl nine homolog 1 OS=Homo sapiens GN=EGLN1 PE=1 SV=1	45991.9	2 (2 0 0 0 0)	1.26E-07
Q9GZZ1	NAT13_HUMAN (Q9GZZ1) N-acetyltransferase 13 OS=Homo sapiens GN=NAT13 PE=1 SV=1	19386.0	5 (5 0 0 0 0)	8.40E-08
Q9H009	NACA2_HUMAN (Q9H009) Nascent polypeptide-associated complex subunit alpha-2 OS=Homo sapiens GN=	23208.8	1 (0 1 0 0 0)	1.62E-05
Q9H081	MIS12_HUMAN (Q9H081) Protein MIS12 homolog OS=Homo sapiens GN=MIS12 PE=1 SV=1	24124.3	4 (4 0 0 0 0)	1.88E-07
Q9H0A0	NAT10_HUMAN (Q9H0A0) N-acetyltransferase 10 OS=Homo sapiens GN=NAT10 PE=1 SV=1	115630.7	2 (2 0 0 0 0)	3.08E-08
Q9H0F7	ARL6_HUMAN (Q9H0F7) ADP-ribosylation factor-like protein 6 OS=Homo sapiens GN=ARL6 PE=1 SV=1	21084.2	1 (1 0 0 0 0)	6.23E-07
Q9H0S4	DDX47_HUMAN (Q9H0S4) Probable ATP-dependent RNA helicase DDX47 OS=Homo sapiens GN=DDX47 PI	50614.8	2 (0 2 0 0 0)	2.12E-07
Q9H1C7	CE032_HUMAN (Q9H1C7) UPF0467 protein C5orf32 OS=Homo sapiens GN=C5orf32 PE=2 SV=1	10623.8	1 (1 0 0 0 0)	3.02E-05
Q9H246	CA021_HUMAN (Q9H246) Uncharacterized protein C1orf21 OS=Homo sapiens GN=C1orf21 PE=1 SV=1	13856.7	1 (1 0 0 0 0)	4.13E-10
Q9H3Z4	DNJC5_HUMAN (Q9H3Z4) DnaJ homolog subfamily C member 5 OS=Homo sapiens GN=DNAJC5 PE=1 SV=	22134.3	2 (2 0 0 0 0)	2.02E-08
Q9H488	OFUT1_HUMAN (Q9H488) GDP-fucose protein O-fucosyltransferase 1 OS=Homo sapiens GN=POFUT1 PE=	43927.2	5 (5 0 0 0 0)	2.35E-09
Q9H4B7	TBB1_HUMAN (Q9H4B7) Tubulin beta-1 chain OS=Homo sapiens GN=TUBB1 PE=1 SV=1	50294.6	4 (4 0 0 0 0)	1.65E-07
Q9H4M9	EHD1_HUMAN (Q9H4M9) EH domain-containing protein 1 OS=Homo sapiens GN=EHD1 PE=1 SV=2	60588.8	3 (3 0 0 0 0)	8.21E-08
Q9H5V8	CDCP1_HUMAN (Q9H5V8) CUB domain-containing protein 1 OS=Homo sapiens GN=CDCP1 PE=1 SV=1	92815.5	2 (2 0 0 0 0)	2.51E-10
Q9H5Y7	SLIK6_HUMAN (Q9H5Y7) SLIT and NTRK-like protein 6 OS=Homo sapiens GN=SLITRK6 PE=2 SV=3	95048.9	3 (3 0 0 0 0)	1.97E-06
Q9H7B2	BXDC1_HUMAN (Q9H7B2) Brix domain-containing protein 1 OS=Homo sapiens GN=BXDC1 PE=1 SV=2	35560.2	2 (2 0 0 0 0)	9.07E-07
Q9H845	ACAD9_HUMAN (Q9H845) Acyl-CoA dehydrogenase family member 9, mitochondrial OS=Homo sapiens GN=	68716.8	3 (3 0 0 0 0)	6.17E-10
Q9H853	TBA4B_HUMAN (Q9H853) Putative tubulin-like protein alpha-4B OS=Homo sapiens GN=TUBA4B PE=5 SV=2	27533.7	3 (3 0 0 0 0)	1.27E-07
Q9H8M5	CNNM2_HUMAN (Q9H8M5) Metal transporter CNNM2 OS=Homo sapiens GN=CNNM2 PE=2 SV=2	96561.8	1 (1 0 0 0 0)	9.75E-06
Q9H9B4	SFXN1_HUMAN (Q9H9B4) Sideroflexin-1 OS=Homo sapiens GN=SFXN1 PE=1 SV=4	35596.4	4 (4 0 0 0 0)	6.82E-09
Q9H9L3	I20L2_HUMAN (Q9H9L3) Interferon-stimulated 20 kDa exonuclease-like 2 OS=Homo sapiens GN=ISG20L2 P	39129.6	2 (2 0 0 0 0)	3.41E-10
Q9HAV7	GRPE1_HUMAN (Q9HAV7) GrpE protein homolog 1, mitochondrial OS=Homo sapiens GN=GRPEL1 PE=1 SV	24263.9	2 (2 0 0 0 0)	4.82E-06
Q9HB66	Q9HB66_HUMAN (Q9HB66) McKusick-Kaufman syndrome, isoform CRA_a OS=Homo sapiens GN=MKKS PE	7258.9	1 (1 0 0 0 0)	4.23E-05
Q9HB71	CYBP_HUMAN (Q9HB71) Calcyclin-binding protein OS=Homo sapiens GN=CACYBP PE=1 SV=2	26193.7	2 (2 0 0 0 0)	2.35E-04
Q9HBA0	TRPV4_HUMAN (Q9HBA0) Transient receptor potential cation channel subfamily V member 4 OS=Homo sapi	98218.6	2 (2 0 0 0 0)	1.10E-06
Q9HBB3	Q9HBB3_HUMAN (Q9HBB3) 60S ribosomal protein L6 OS=Homo sapiens PE=2 SV=1	32870.7	5 (5 0 0 0 0)	1.50E-09
Q9HCJ1	ANKH_HUMAN (Q9HCJ1) Progressive ankylosis protein homolog OS=Homo sapiens GN=ANKH PE=1 SV=2	54205.5	2 (2 0 0 0 0)	4.35E-06
Q9HD33	RM47_HUMAN (Q9HD33) 39S ribosomal protein L47, mitochondrial OS=Homo sapiens GN=MRPL47 PE=2 S	29432.0	1 (1 0 0 0 0)	6.51E-05
Q9HDC9	APMAP_HUMAN (Q9HDC9) Adipocyte plasma membrane-associated protein OS=Homo sapiens GN=APMAP	46450.9	2 (2 0 0 0 0)	1.06E-05
Q9NP72	RAB18_HUMAN (Q9NP72) Ras-related protein Rab-18 OS=Homo sapiens GN=RAB18 PE=1 SV=1	22962.6	2 (2 0 0 0 0)	1.01E-06
Q9NP90	RAB9B_HUMAN (Q9NP90) Ras-related protein Rab-9B OS=Homo sapiens GN=RAB9B PE=1 SV=1	22705.0	2 (0 2 0 0 0)	1.09E-06
Q9NPA0	CO024_HUMAN (Q9NPA0) UPF0480 protein C15orf24 OS=Homo sapiens GN=C15orf24 PE=1 SV=1	26453.5	1 (1 0 0 0 0)	4.63E-05
Q9NPD3	EXOS4_HUMAN (Q9NPD3) Exosome complex exonuclease RRP41 OS=Homo sapiens GN=EXOSC4 PE=1 S	26366.5	3 (3 0 0 0 0)	7.06E-06
Q9NPE3	NOP10_HUMAN (Q9NPE3) H/ACA ribonucleoprotein complex subunit 3 OS=Homo sapiens GN=NOP10 PE=1	7701.0	4 (4 0 0 0 0)	2.08E-07
Q9NPH3	IL1AP_HUMAN (Q9NPH3) Interleukin-1 receptor accessory protein OS=Homo sapiens GN=IL1RAP PE=1 SV=	65376.8	1 (1 0 0 0 0)	4.73E-06
Q9NQ48	LZTL1_HUMAN (Q9NQ48) Leucine zipper transcription factor-like protein 1 OS=Homo sapiens GN=LZTFL1 P	34571.1	1 (1 0 0 0 0)	6.69E-09
Q9NQ88	CL005_HUMAN (Q9NQ88) Uncharacterized protein C12orf5 OS=Homo sapiens GN=C12orf5 PE=1 SV=1	30043.1	1 (1 0 0 0 0)	5.60E-06
Q9NQC3	RTN4_HUMAN (Q9NQC3) Reticulon-4 OS=Homo sapiens GN=RTN4 PE=1 SV=2	129851.2	2 (2 0 0 0 0)	3.20E-07
Q9NQG5	RPR1B_HUMAN (Q9NQG5) Regulation of nuclear pre-mRNA domain-containing protein 1B OS=Homo sapien	36877.2	7 (7 0 0 0 0)	7.34E-12
Q9NR30	DDX21_HUMAN (Q9NR30) Nucleolar RNA helicase 2 OS=Homo sapiens GN=DDX21 PE=1 SV=5	87290.5	7 (7 0 0 0 0)	1.26E-06
Q9NR31	SAR1A_HUMAN (Q9NR31) GTP-binding protein SAR1a OS=Homo sapiens GN=SAR1A PE=1 SV=1	22352.5	1 (1 0 0 0 0)	2.36E-07
Q9NR45	SIAS_HUMAN (Q9NR45) Sialic acid synthase OS=Homo sapiens GN=NANS PE=1 SV=2	40281.5	1 (1 0 0 0 0)	8.48E-05
Q9NSD9	SYFB_HUMAN (Q9NSD9) Phenylalanyl-tRNA synthetase beta chain OS=Homo sapiens GN=FARSB PE=1 SV	66087.7	1 (1 0 0 0 0)	7.60E-07
Q9NT62	ATG3_HUMAN (Q9NT62) Autophagy-related protein 3 OS=Homo sapiens GN=ATG3 PE=1 SV=1	35841.5	1 (1 0 0 0 0)	1.87E-07
Q9NT99	LRC4B_HUMAN (Q9NT99) Leucine-rich repeat-containing protein 4B OS=Homo sapiens GN=LRRC4B PE=2	76385.8	2 (2 0 0 0 0)	2.78E-05
Q9NTJ4	MA2C1_HUMAN REVERSED - (Q9NTJ4) Alpha-mannosidase 2C1 OS=Homo sapiens GN=MAN2C1 PE=1 SV	115761.7	1 (0 1 0 0 0)	5.41E-07
Q9NTK5	OLA1_HUMAN (Q9NTK5) Obg-like ATPase 1 OS=Homo sapiens GN=OLA1 PE=1 SV=2	44715.4	1 (1 0 0 0 0)	4.62E-11
Q9NUJ3	T11L1_HUMAN (Q9NUJ3) T-complex protein 11-like protein 1 OS=Homo sapiens GN=TCP11L1 PE=2 SV=1	56998.8	1 (1 0 0 0 0)	1.69E-05
Q9NUP9	LIN7C_HUMAN (Q9NUP9) Lin-7 homolog C OS=Homo sapiens GN=LIN7C PE=1 SV=1	21820.5	1 (1 0 0 0 0)	7.23E-07
Q9NV31	IMP3_HUMAN (Q9NV31) U3 small nucleolar ribonucleoprotein protein IMP3 OS=Homo sapiens GN=IMP3 PE	21836.6	2 (2 0 0 0 0)	3.83E-11
Q9NV96	CC50A_HUMAN (Q9NV96) Cell cycle control protein 50A OS=Homo sapiens GN=TMEM30A PE=1 SV=1	40657.7	1 (1 0 0 0 0)	4.23E-05
Q9NVA1	UQCC_HUMAN (Q9NVA1) Ubiquinol-cytochrome c reductase complex chaperone CBP3 homolog OS=Homo s	34549.6	1 (1 0 0 0 0)	6.18E-05
Q9NVA2	SEP11_HUMAN (Q9NVA2) Septin-11 OS=Homo sapiens GN=SEPT11 PE=1 SV=3	49367.2	4 (4 0 0 0 0)	2.20E-10
Q9NVH1	DJC11_HUMAN (Q9NVH1) DnaJ homolog subfamily C member 11 OS=Homo sapiens GN=DNAJC11 PE=2 S	63238.9	1 (1 0 0 0 0)	2.03E-05
Q9NVI7	ATD3A_HUMAN (Q9NVI7) ATPase family AAA domain-containing protein 3A OS=Homo sapiens GN=ATAD3A	71324.8	3 (3 0 0 0 0)	8.86E-09
Q9NVT9	ARMC1_HUMAN (Q9NVT9) Armadillo repeat-containing protein 1 OS=Homo sapiens GN=ARMC1 PE=1 SV=	31260.8	2 (2 0 0 0 0)	4.59E-07
Q9NW08	RPC2_HUMAN (Q9NW08) DNA-directed RNA polymerase III subunit RPC2 OS=Homo sapiens GN=POLR3B	127702.4	2 (2 0 0 0 0)	8.59E-09
Q9NW13	RBM28_HUMAN (Q9NW13) RNA-binding protein 28 OS=Homo sapiens GN=RBM28 PE=1 SV=3	85684.8	1 (1 0 0 0 0)	2.13E-08
Q9NX08	COMD8_HUMAN (Q9NX08) COMM domain-containing protein 8 OS=Homo sapiens GN=COMMD8 PE=1 SV=	21077.0	2 (2 0 0 0 0)	2.55E-07
Q9NX24	NHP2_HUMAN (Q9NX24) H/ACA ribonucleoprotein complex subunit 2 OS=Homo sapiens GN=NHP2 PE=1 SV	17189.9	3 (3 0 0 0 0)	5.06E-06
Q9NX58	LYAR_HUMAN (Q9NX58) Cell growth-regulating nucleolar protein OS=Homo sapiens GN=LYAR PE=1 SV=2	43587.9	2 (2 0 0 0 0)	3.08E-06
Q9NX63	CHCH3_HUMAN (Q9NX63) Coiled-coil-helix-coiled-coil-helix domain-containing protein 3, mitochondrial OS=H	26136.2	7 (7 0 0 0 0)	1.09E-12
Q9NXF1	TEX10_HUMAN (Q9NXF1) Testis-expressed sequence 10 protein OS=Homo sapiens GN=TEX10 PE=1 SV=2	105607.8	2 (2 0 0 0 0)	4.41E-08
Q9NXR1	NDE1_HUMAN (Q9NXR1) Nuclear distribution protein nudE homolog 1 OS=Homo sapiens GN=NDE1 PE=1 S	38784.6	2 (2 0 0 0 0)	2.75E-07
Q9NXS2	QPCTL_HUMAN (Q9NXS2) Glutaminyl-peptide cyclotransferase-like protein OS=Homo sapiens GN=QPCTL P	42837.2	1 (1 0 0 0 0)	1.07E-05
Q9NXU5	ARL15_HUMAN (Q9NXU5) ADP-ribosylation factor-like protein 15 OS=Homo sapiens GN=ARL15 PE=2 SV=1	22861.5	4 (4 0 0 0 0)	1.17E-08
Q9NXV6	CARF_HUMAN (Q9NXV6) CDKN2A-interacting protein OS=Homo sapiens GN=CDKN2AIP PE=1 SV=2	61016.9	2 (2 0 0 0 0)	1.92E-06
Q9NY12	GAR1_HUMAN (Q9NY12) H/ACA ribonucleoprotein complex subunit 1 OS=Homo sapiens GN=GAR1 PE=1 S	22334.2	4 (4 0 0 0 0)	4.40E-09
Q9NY35	CLDN1_HUMAN (Q9NY35) Claudin domain-containing protein 1 OS=Homo sapiens GN=CLDND1 PE=2 SV=1	28584.1	2 (2 0 0 0 0)	5.05E-09
Q9NYL4	FKB11_HUMAN (Q9NYL4) FK506-binding protein 11 OS=Homo sapiens GN=FKBP11 PE=2 SV=1	22166.3	2 (2 0 0 0 0)	1.07E-06
Q9NZ45	CISD1_HUMAN (Q9NZ45) CDGSH iron sulfur domain-containing protein 1 OS=Homo sapiens GN=CISD1 PE=	12191.2	3 (3 0 0 0 0)	1.83E-10
Q9NZI8	IF2B1_HUMAN (Q9NZI8) Insulin-like growth factor 2 mRNA-binding protein 1 OS=Homo sapiens GN=IGF2BP	63417.2	2 (2 0 0 0 0)	1.94E-08
Q9NZM1	MYOF_HUMAN (Q9NZM1) Myoferlin OS=Homo sapiens GN=FER1L3 PE=1 SV=1	234558.8	7 (27 0 0 0 0)	2.99E-11
Q9NZU0	FLRT3_HUMAN (Q9NZU0) Leucine-rich repeat transmembrane protein FLRT3 OS=Homo sapiens GN=FLRT3	72957.6	2 (2 0 0 0 0)	1.07E-05

Q9NZW5	MPP6_HUMAN (Q9NZW5) MAGUK p55 subfamily member 6 OS=Homo sapiens GN=MPP6 PE=1 SV=2	61078.9	1 (1 0 0 0 0)	2.41E-05
Q9P035	PTAD1_HUMAN (Q9P035) Protein tyrosine phosphatase-like protein PTPLAD1 OS=Homo sapiens GN=PTPL	43131.6	2 (2 0 0 0 0)	2.94E-10
Q9P0L0	VAPA_HUMAN (Q9P0L0) Vesicle-associated membrane protein-associated protein A OS=Homo sapiens GN=	27875.2	2 (2 0 0 0 0)	9.81E-08
Q9P0M6	H2AW_HUMAN (Q9P0M6) Core histone macro-H2A.2 OS=Homo sapiens GN=H2AFY2 PE=2 SV=3	40033.4	2 (2 0 0 0 0)	1.38E-10
Q9P258	RCC2_HUMAN (Q9P258) Protein RCC2 OS=Homo sapiens GN=RCC2 PE=1 SV=2	56049.3	2 (2 0 0 0 0)	5.36E-07
Q9P273	TEN3_HUMAN (Q9P273) Teneurin-3 OS=Homo sapiens GN=ODZ3 PE=2 SV=3	300757.7	3 (3 0 0 0 0)	2.62E-08
Q9P2B2	FPRP_HUMAN (Q9P2B2) Prostaglandin F2 receptor negative regulator OS=Homo sapiens GN=PTGFRN PE=	98494.7	6 (6 0 0 0 0)	1.98E-08
Q9P2J5	SYLC_HUMAN (Q9P2J5) Leucyl-tRNA synthetase, cytoplasmic OS=Homo sapiens GN=LARS PE=1 SV=2	134379.5	8 (8 0 0 0 0)	1.24E-09
Q9P2J5	SYLC_HUMAN (Q9P2J5) Leucyl-tRNA synthetase, cytoplasmic OS=Homo sapiens GN=LARS PE=1 SV=2	134379.5	1 (1 0 0 0 0)	1.56E-07
Q9UBF2	COPG2_HUMAN (Q9UBF2) Coatomer subunit gamma-2 OS=Homo sapiens GN=COPG2 PE=1 SV=1	97559.7	2 (2 0 0 0 0)	8.24E-07
Q9UBG0	MRC2_HUMAN (Q9UBG0) C-type mannose receptor 2 OS=Homo sapiens GN=MRC2 PE=1 SV=1	166548.2	1 (1 0 0 0 0)	6.87E-08
Q9UBI6	GBG12_HUMAN (Q9UBI6) Guanine nucleotide-binding protein G(I)/G(S)/G(O) subunit gamma-12 OS=Homo s	8001.2	3 (3 0 0 0 0)	7.14E-07
Q9UBP9	GULP1_HUMAN (Q9UBP9) PTB domain-containing engulfment adapter protein 1 OS=Homo sapiens GN=GU	34468.5	2 (2 0 0 0 0)	1.33E-05
Q9UBQ0	VPS29_HUMAN (Q9UBQ0) Vacuolar protein sorting-associated protein 29 OS=Homo sapiens GN=VPS29 PE	20492.7	2 (2 0 0 0 0)	8.74E-05
Q9UBT2	SAE2_HUMAN (Q9UBT2) SUMO-activating enzyme subunit 2 OS=Homo sapiens GN=UBA2 PE=1 SV=2	71179.3	2 (2 0 0 0 0)	8.66E-09
Q9UBU9	NXF1_HUMAN (Q9UBU9) Nuclear RNA export factor 1 OS=Homo sapiens GN=NXF1 PE=1 SV=1	70138.8	3 (3 0 0 0 0)	1.96E-07
Q9UBX3	DIC_HUMAN (Q9UBX3) Mitochondrial dicarboxylate carrier OS=Homo sapiens GN=SLC25A10 PE=2 SV=2	31262.3	2 (2 0 0 0 0)	8.15E-07
Q9UDW1	QCR9_HUMAN (Q9UDW1) Cytochrome b-c1 complex subunit 9 OS=Homo sapiens GN=UQCR10 PE=1 SV=3	7303.8	2 (2 0 0 0 0)	3.63E-08
Q9UFW8	CGBP1_HUMAN (Q9UFW8) CGG triplet repeat-binding protein 1 OS=Homo sapiens GN=CGGBP1 PE=1 SV=	18808.6	2 (2 0 0 0 0)	2.89E-05
Q9UGJ0	AAKG2_HUMAN (Q9UGJ0) 5'-AMP-activated protein kinase subunit gamma-2 OS=Homo sapiens GN=PRKAG	63026.8	2 (2 0 0 0 0)	7.04E-07
Q9UHB9	SRP68_HUMAN (Q9UHB9) Signal recognition particle 68 kDa protein OS=Homo sapiens GN=SRP68 PE=1 S	70685.7	2 (2 0 0 0 0)	4.18E-07
Q9UHD1	CHRD1_HUMAN (Q9UHD1) Cysteine and histidine-rich domain-containing protein 1 OS=Homo sapiens GN=C	37465.7	4 (4 0 0 0 0)	1.51E-08
Q9UHD8	SEPT9_HUMAN (Q9UHD8) Septin-9 OS=Homo sapiens GN=SEPT9 PE=1 SV=2	65360.9	2 (2 0 0 0 0)	8.12E-08
Q9UHN6	TMEM2_HUMAN (Q9UHN6) Transmembrane protein 2 OS=Homo sapiens GN=TMEM2 PE=1 SV=1	154275.9	4 (24 0 0 0 0)	2.21E-09
Q9UI12	VATH_HUMAN (Q9UI12) V-type proton ATPase subunit H OS=Homo sapiens GN=ATP6V1H PE=1 SV=1	55847.1	1 (1 0 0 0 0)	8.80E-06
Q9UI14	PRAF1_HUMAN (Q9UI14) Prenylated Rab acceptor protein 1 OS=Homo sapiens GN=RABAC1 PE=1 SV=1	20634.8	2 (2 0 0 0 0)	2.83E-07
Q9UI30	TR112_HUMAN (Q9UI30) TRM112-like protein OS=Homo sapiens GN=AD-001 PE=1 SV=1	14190.3	4 (4 0 0 0 0)	5.86E-10
Q9UIQ6	LCAP_HUMAN (Q9UIQ6) Leucyl-cystinyl aminopeptidase OS=Homo sapiens GN=LNPEP PE=1 SV=3	117274.2	2 (2 0 0 0 0)	3.56E-07
Q9UIU0	Q9UIU0_HUMAN (Q9UIU0) Dihydropyridine receptor alpha 2 subunit OS=Homo sapiens GN=CACNA2D1 PE=	125228.9	3 (3 0 0 0 0)	5.97E-07
Q9UJZ1	STML2_HUMAN (Q9UJZ1) Stomatin-like protein 2 OS=Homo sapiens GN=STOML2 PE=1 SV=1	38510.2	6 (6 0 0 0 0)	2.15E-12
Q9UK41	VPS28_HUMAN (Q9UK41) Vacuolar protein sorting-associated protein 28 homolog OS=Homo sapiens GN=VP	25408.7	2 (2 0 0 0 0)	5.61E-07
Q9UL25	RAB21_HUMAN (Q9UL25) Ras-related protein Rab-21 OS=Homo sapiens GN=RAB21 PE=1 SV=3	24332.3	9 (7 2 0 0 0)	3.74E-08
Q9UL26	RB22A_HUMAN (Q9UL26) Ras-related protein Rab-22A OS=Homo sapiens GN=RAB22A PE=1 SV=2	21841.2	2 (2 0 0 0 0)	2.31E-06
Q9ULL4	PLXB3_HUMAN (Q9ULL4) Plexin-B3 OS=Homo sapiens GN=PLXNB3 PE=1 SV=2	206714.5	1 (1 0 0 0 0)	4.95E-07
Q9UMF0	ICAM5_HUMAN (Q9UMF0) Intercellular adhesion molecule 5 OS=Homo sapiens GN=ICAM5 PE=1 SV=2	97270.1	2 (2 0 0 0 0)	5.65E-08
Q9UMR2	DD19B_HUMAN (Q9UMR2) ATP-dependent RNA helicase DDX19B OS=Homo sapiens GN=DDX19B PE=1 S	53892.9	2 (2 0 0 0 0)	2.44E-07
Q9UNK0	STX8_HUMAN (Q9UNK0) Syntaxin-8 OS=Homo sapiens GN=STX8 PE=2 SV=2	26890.0	1 (1 0 0 0 0)	4.55E-07
Q9UNQ2	DIMT1_HUMAN (Q9UNQ2) Probable dimethyladenosine transferase OS=Homo sapiens GN=DIMT1L PE=1 S	35214.1	4 (4 0 0 0 0)	1.10E-07
Q9UPN3	MACF1_HUMAN (Q9UPN3) Microtubule-actin cross-linking factor 1, isoforms 1/2/3/5 OS=Homo sapiens GN=I	620038.5	5 (5 0 0 0 0)	1.32E-09
Q9UQQ2	SH2B3_HUMAN (Q9UQQ2) SH2B adapter protein 3 OS=Homo sapiens GN=SH2B3 PE=2 SV=2	63185.7	1 (1 0 0 0 0)	3.41E-08
Q9Y221	NIP7_HUMAN (Q9Y221) 60S ribosome subunit biogenesis protein NIP7 homolog OS=Homo sapiens GN=NIP	20449.5	1 (1 0 0 0 0)	1.70E-10
Q9Y224	CN166_HUMAN (Q9Y224) UPF0568 protein C14orf166 OS=Homo sapiens GN=C14orf166 PE=1 SV=1	28050.7	9 (9 0 0 0 0)	2.21E-09
Q9Y230	RUVB2_HUMAN (Q9Y230) RuvB-like 2 OS=Homo sapiens GN=RUVBL2 PE=1 SV=3	51124.6	5 (5 0 0 0 0)	2.64E-10
Q9Y265	RUVB1_HUMAN (Q9Y265) RuvB-like 1 OS=Homo sapiens GN=RUVBL1 PE=1 SV=1	50196.4	7 (7 0 0 0 0)	1.44E-08
Q9Y266	NUDC_HUMAN (Q9Y266) Nuclear migration protein nudC OS=Homo sapiens GN=NUDC PE=1 SV=1	38219.1	4 (4 0 0 0 0)	7.43E-09
Q9Y277	VDAC3_HUMAN (Q9Y277) Voltage-dependent anion-selective channel protein 3 OS=Homo sapiens GN=VDA	30639.3	1 (1 0 0 0 0)	7.91E-07
Q9Y295	DRG1_HUMAN (Q9Y295) Developmentally-regulated GTP-binding protein 1 OS=Homo sapiens GN=DRG1 PE	40516.9	7 (7 0 0 0 0)	9.91E-09
Q9Y2A7	NCKP1_HUMAN (Q9Y2A7) Nck-associated protein 1 OS=Homo sapiens GN=NCKAP1 PE=1 SV=1	128706.6	5 (5 0 0 0 0)	1.99E-07
Q9Y2L1	RRP44_HUMAN (Q9Y2L1) Exosome complex exonuclease RRP44 OS=Homo sapiens GN=DIS3 PE=1 SV=2	108934.0	1 (1 0 0 0 0)	5.03E-08
Q9Y2Q3	GSTK1_HUMAN (Q9Y2Q3) Glutathione S-transferase kappa 1 OS=Homo sapiens GN=GSTK1 PE=1 SV=3	25480.3	4 (4 0 0 0 0)	7.97E-09
Q9Y2R0	CCD56_HUMAN (Q9Y2R0) Coiled-coil domain-containing protein 56 OS=Homo sapiens GN=CCDC56 PE=1 S	11724.1	1 (1 0 0 0 0)	2.63E-05
Q9Y2V2	CHSP1_HUMAN (Q9Y2V2) Calcium-regulated heat stable protein 1 OS=Homo sapiens GN=CARHSP1 PE=1	15882.0	1 (1 0 0 0 0)	8.31E-11
Q9Y2W1	TR150_HUMAN (Q9Y2W1) Thyroid hormone receptor-associated protein 3 OS=Homo sapiens GN=THRAP3 P	108600.8	1 (1 0 0 0 0)	1.06E-07
Q9Y2X3	NOL5_HUMAN (Q9Y2X3) Nucleolar protein 5 OS=Homo sapiens GN=NOL5 PE=1 SV=1	59540.6	2 (2 0 0 0 0)	4.40E-07
Q9Y383	LC7L2_HUMAN (Q9Y383) Putative RNA-binding protein Luc7-like 2 OS=Homo sapiens GN=LUC7L2 PE=1 SV	46485.6	1 (1 0 0 0 0)	2.89E-06
Q9Y3A5	SBDS_HUMAN (Q9Y3A5) Ribosome maturation protein SBDS OS=Homo sapiens GN=SBDS PE=1 SV=4	28745.3	7 (7 0 0 0 0)	2.03E-12
Q9Y3A6	TMED5_HUMAN (Q9Y3A6) Transmembrane emp24 domain-containing protein 5 OS=Homo sapiens GN=TME	25988.2	4 (4 0 0 0 0)	1.29E-07
Q9Y3B4	PM14_HUMAN (Q9Y3B4) Pre-mRNA branch site protein p14 OS=Homo sapiens GN=SF3B14 PE=1 SV=1	14575.6	6 (6 0 0 0 0)	3.10E-08
Q9Y3B7	RM11_HUMAN (Q9Y3B7) 39S ribosomal protein L11, mitochondrial OS=Homo sapiens GN=MRPL11 PE=2 SV	20670.5	4 (4 0 0 0 0)	1.10E-06
Q9Y3C1	NOP16_HUMAN (Q9Y3C1) Nucleolar protein 16 OS=Homo sapiens GN=NOP16 PE=1 SV=2	21175.1	4 (4 0 0 0 0)	1.02E-06
Q9Y3I0	CV028_HUMAN (Q9Y3I0) UPF0027 protein C22orf28 OS=Homo sapiens GN=C22orf28 PE=1 SV=1	55175.0	6 (6 0 0 0 0)	1.62E-06
Q9Y3U8	RL36_HUMAN (Q9Y3U8) 60S ribosomal protein L36 OS=Homo sapiens GN=RPL36 PE=1 SV=3	12245.9	4 (4 0 0 0 0)	1.59E-06
Q9Y490	TLN1_HUMAN (Q9Y490) Talin-1 OS=Homo sapiens GN=TLN1 PE=1 SV=3	269596.3	0 (40 0 0 0 0)	1.13E-10
Q9Y4F1	FARP1_HUMAN (Q9Y4F1) FERM, RhoGEF and pleckstrin domain-containing protein 1 OS=Homo sapiens GN	118558.8	3 (3 0 0 0 0)	1.45E-08
Q9Y4L1	HYOU1_HUMAN (Q9Y4L1) Hypoxia up-regulated protein 1 OS=Homo sapiens GN=HYOU1 PE=1 SV=1	111266.2	3 (3 0 0 0 0)	4.37E-07
Q9Y512	SAM50_HUMAN (Q9Y512) Sorting and assembly machinery component 50 homolog OS=Homo sapiens GN=	51943.4	1 (1 0 0 0 0)	1.21E-07
Q9Y584	TIM22_HUMAN (Q9Y584) Mitochondrial import inner membrane translocase subunit Tim22 OS=Homo sapiens	20017.9	2 (2 0 0 0 0)	8.75E-08
Q9Y5B9	SP16H_HUMAN (Q9Y5B9) FACT complex subunit SPT16 OS=Homo sapiens GN=SUPT16H PE=1 SV=1	119838.3	4 (4 0 0 0 0)	4.73E-06
Q9Y5L4	TIM13_HUMAN (Q9Y5L4) Mitochondrial import inner membrane translocase subunit Tim13 OS=Homo sapiens	10493.0	2 (2 0 0 0 0)	2.72E-08
Q9Y5M8	SRPRB_HUMAN (Q9Y5M8) Signal recognition particle receptor subunit beta OS=Homo sapiens GN=SRPRB	29683.8	4 (4 0 0 0 0)	1.22E-07
Q9Y625	GPC6_HUMAN (Q9Y625) Glypican-6 OS=Homo sapiens GN=GPC6 PE=2 SV=1	62695.0	3 (3 0 0 0 0)	6.08E-09
Q9Y639	NPTN_HUMAN (Q9Y639) Neuroplastin OS=Homo sapiens GN=NPTN PE=1 SV=1	31271.9	3 (3 0 0 0 0)	4.99E-06
Q9Y696	CLIC4_HUMAN (Q9Y696) Chloride intracellular channel protein 4 OS=Homo sapiens GN=CLIC4 PE=1 SV=4	28753.8	1 (1 0 0 0 0)	1.98E-07
Q9Y6A4	CP080_HUMAN (Q9Y6A4) UPF0468 protein C16orf80 OS=Homo sapiens GN=C16orf80 PE=2 SV=1	22760.0	3 (3 0 0 0 0)	3.09E-08
Q9Y6E2	BZW2_HUMAN (Q9Y6E2) Basic leucine zipper and W2 domain-containing protein 2 OS=Homo sapiens GN=B	48132.0	2 (2 0 0 0 0)	2.02E-10
Q9Y6M1	IF2B2_HUMAN (Q9Y6M1) Insulin-like growth factor 2 mRNA-binding protein 2 OS=Homo sapiens GN=IGF2BP	61804.5	1 (0 1 0 0 0)	5.52E-07

Q9Y6M4	KC1G3_HUMAN (Q9Y6M4) Casein kinase I isoform gamma-3 OS=Homo sapiens GN=CSNK1G3 PE=1 SV=2	51356.0	1 (1 0 0 0 0)	6.79E-09
Q9Y6W3	CAN7_HUMAN (Q9Y6W3) Calpain-7 OS=Homo sapiens GN=CAPN7 PE=1 SV=1	92593.9	1 (1 0 0 0 0)	6.87E-06

APPENDIX D.

MATERIALS AND METHODS

The content of this chapter were written by Hui Liu.

MOLECULAR BIOLOGY PROTOCOLS

All molecular biology methods were performed according to standard molecular biology techniques. All restriction enzymes were obtained from New England Biolabs.

Cloning of wild type CDCP1 and point mutants into retrovirus vector

1) Cloning of CDCP1 from cDNA derived from MA2 cells using primers:

Forward: 5'-CACGAATTCGCCACCATGGCCGGCCTGAACTGC-3'
Reverse: 5'-CAGATGCGGCCGCTTATTCTGCTGGCTCCATGGG-3'

PCR reactions is performed as the following using Pfu polymerase (Stratgene):

Step1: 95^{0}C, 2min
Step2: 95^{0}C, 30 seconds
Step3: 59^{0}C, 30 seconds
Step4: 72^{0}C, 3min
Step5: Repeat step 2 to 4 for a total 30 cycles
Step6: 72^{0}C, 15min
Step7: 4^{0}C

PCR products were cloned into pcDNA3.1(+) vector via EcoRI and NotI and sequences were confirmed using a set of three primers:

T7 primer: 5'-TAATACGACTCACTATAGGG-3'
CDCP1 F2 primer: 5'-GAGGTGTTCAAGCTGGAGGAC-3'
CDCP1 F3 primer: 5'-CTCTATCAAGCAGATCCAGGTG-3'

2) To clone CDCP1 into retrovirus vector, CDCP1 inserts were excised via EcoRI-XhoI and cloned into pMIGw vector through EcoRI and XhoI sites. pMIGw vector was kindly provided by Dr. Patrick Stern. To minimize recombination of the retrovirus, Stbl3 bacteria (Invitrogen) were used for transformation and all bacteria were cultured at 30^{0}C.

3) Site-directed Mutagenesis using QuikChange XL kit (Stratagene)

Primers for Y734F point mutation:
Y734F- F: 5'- GAC TCC CAT GTG TTT GCA GTC ATG GAG GAC-3'
Y734F-R: 5'- GTC CTC CAT GAC TGC AAA CAC ATG GGA GTC-3'
Primers for Y743F point mutation:
Y743F-F: 5'- GAG GAC ACC ATG GTA TTT GGG CAT CTG CTA CAG-3'
Y743F-R: 5'- CTG TAG CAG ATG CCC AAA TAC CAT GGT GTC CTC -3'
Primers for Y762F point mutation:
Y762F-F: 5'- GAG GTG GAC ACC TTC CGG CCG TTC CAG -3'
Y762F-R: 5'- CTG GAA CGG CCG GAA GGT GTC CAC CTC -3
Primers for Y806F point mutation:
Y806F-F: 5'- CT GAG AGT GAA CCG TTC ACC TTC TCC CAT CCC-3'
Y806F-R: 5'- GGG ATG GGA GAA GGT GAA CGG TTC ACT CTC AG-3'

All mutagenses were performed in pcDNA3.1(+) vector, and sequences were confirmed before excision of the insert via EcoRI and XhoI sites. Inserts were cloned into pMIGw vector via EcoRI and XhoI sites.

Generation of CDCP1 knockdown constructs:

miR30-based RNAi constructs were developed for the Hannon-Elledge libraries (Stegmeier et al. PNAS 102(37), p. 13212) and were obtained from Dr. Patrick Stern. The following primers correspond to KD6 and KD10 described in the thesis.

KD6:
5'TGCTGTTGACAGTGAGCGACCTGTTACATCGTCATTTCTATAGTGAAGCCACAGATGTA
TAGAAATGACGATGTAACAGGGTGCCTACTGCCTCGGA-3'
KD10:
5'TGCTGTTGACAGTGAGCGCCCTGAGAATCACTTTGTCATATAGTGAAGCCACAGATGT
ATATGACAAAGTGATTCTCAGGATGCCTACTGCCTCGGA-3'

PKCδ knockdown lentiviral constructs were obtained from OpenBiosystem (catalog number: RHS4533).

Hairpin sequence for PKCδ KD7
CCGGGGCCGCTTTGAACTCTACCGTCTCGAGACGGTAGAGTTCAAAGCGGCCTTTTT
Hairpin sequence for PKCδ KD8
CCGGCAAGGCTACAAATGCAGGCAACTCGAGTTGCCTGCATTTGTAGCCTTGTTTTT
Hairpin sequence for PKCδ KD10
CCGGGCAGGGATTAAAGTGTGAAGACTCGAGTCTTCACACTTTAATCCCTGCTTTTT

CELL CULTURE

A375 cells and all derivatives were grown in E4Hg-10 medium, which contains basal E4Hg medium and Glutamine and 10% fetal bovine serum. Cells were harvested in the absence of trypsin using PBS/5mMEDTA.

Drug selections
MA2 cells infected with RNAi knockdown constructs were selected with 2.5μg/ml of puromycin two days after virus infection. A375-vector control and A375-CDCP1 cells that harbor siRNA constructs for PKCδ were selected with 5μg/ml of puromycin.

Retrovirus and Lentivirus Production
The day before transfection, 293 cells were plated into 6-well plate to approximately 25% confluence. On the day of transfection, a total of 4μg of plasmids were used for each well, with 2ug being the target vector, and 1.33μg of vector containing retrovirus or lentivirus Gag/Pol and 0.73μg of vector containing virus Envelope. Transfection was performed using Fugene 6 (Roche) at ratio of 4:1 between Fugene 6 and vector. One day after transfection, the medium was changed and fresh 2ml of E4Hg-10 were added. Two days and three days after transfection, virus particles in the supernatant were collected by filtering through 2μm filter, and were used directly, or were stored at -80^{0}C till use.

Cell Infection
The day before cell injected, cells were plated in 6-well culture plates at approximately 25% confluence. On the day of injection, 1ml of virus supernatant were add to the cell, with 1μl of 5mg/ml polyBrene, and covered with Saran wrap. The plates were centrifuged in the table-top centrifuge at 30^{0}C for 2 hours before returning to the incubator. The next day after infection, the supernatant containing virus were removed and fresh medium were applied.

3-D Matrigel Culture –"on-top" method
We closely follow the protocol published by Debnath J, et al, Methods 30 (2003) 256–268. Briefly, Matrigel (BD Biosciences) were thawed overnight on ice at 4^{0}C and mixed well using pre-chilled pipette tips before use. Place 8-well glass chamber slides (NUNK, catalog # 177402) on ice, and dispense 45μl of Matrigel in each well, spread with pipette tip till reaching all corners. Incubate the glass slides at 37^{0}C for at least 30min. In the meanwhile, harvest and count cells and make single-cell suspension of 25000cell/ml in E4Hg-10. Mix 200μl of this cell suspension with 200μl of E4Hg-10 containing 4% Matrigel and dispense the whole 400μl into each well in 8-well chamber slides. Place the chamber slides in 37^{0}C, 5% CO_2 incubator, change medium every 4 days and photograph on day 6 or day 10.

CELLULAR BIOLOGY PROTOCOLS

Adhesion Assay
96-well tissue culture plates were coated with 50μl of human plasma Fibronectin, vitronectin, or 20μg/ml poly-D-lysine diluted in PBS. The concentrations of each ECM proteins were indicated in the

experiments. After overnight coating at 4^0C, the plates were washed washed with PBS and blocked with 5% BSA, before 50,000 cells were added to each well and incubated at 37^0C for indicated time period. At the end of the adhesion assays, the plates were inverted on paper towel and allowed to drain, and plates were washed carefully for three times with serum-free medium. Cells remain adherent were fixed with formalin and stained with crystal violet before they were lysed in 0.1% Triton X-100. Absorbance was recorded at A490 as indicator of cell numbers. In all cases, number of cells remain adherent on poly-D-lysine (PLD)-coated wells were set as 100%.

Transwell Migration / Invasion Assay
Cells were serum-starved for 24 hours before harvesting using PBS/EDTA, and washed with serum-free E4Hg and diluted to 5*10e5/ml in serum-free medium. 500µl of E4Hg-10 (with 10% serum) were added to the bottom of the transwell (8µm pore, Costar, catalog # 3422 for migration assay, BD BioCoat Matrigel Invasion chamber, catalog #: 354480, 8um pore size for invasion assay) and 200µl of cell suspension were added to the top of filter. The plates were returned to 370C incubator and after 24 hours, cells on top of the filter were removed using cotton swap (QTip), and the cells were fixed in formalin for 10min before staining with 0.1% crystal violet for 30min. Numbers of cells that have migrated/invaded to the bottom of the filter were counted.

Scratch Migration Assay
Cells were grown to confluent in 6-well plate and a scratch wound was made by attaching P20 pipette tip to the vacuum line and aspirating cells, and the plates were washed three times with PBS and replaced with E4Hg containing 2% serum. Pictures were taken at the time of scratching (time 0) and after 24 hours (time24), distances of the open wounds were measured using OpenLab for time0 (D0) and time 24 (D24). Distances migrated by the cells were calculated as (D0-D24)/2.

Soft Agar Colony Assay
In 24-weel plate, add 0.5ml of 0.4% agar diluted in E4Hg-10, and let cool to solidify (base agar). Harvest cells and dilute to 1.2*10e4cells/ml in E4Hg-10, and mix at 1:1 with 0.4% agar, and add 0.5ml of the cell mixture to the top of base agar. After 7 days, number of colonies were counted under microscope.

Anoikis Assay
Coat tissue culture plates with 12mg/ml of polyHEMA (Sigma) – for 24-well plate, add 100µl/well, and for 6-well plate, add 500µl/well – and let evaporate in the hood till dry. The plates were washed with PBS before 1*10e5 cells in 3ml serum-free E4Hg medium were added. The cells were returned to 37^0C incubator and after 24, 48, 72 hours, cells were harvested and resuspended in 100µl of Annexin V binding buffer (BD Pharmingen™, Annexin V-PE Apoptosis Detection Kit I, Catalog # 559763), and 10µl of 7- AAD and 5µl of Annexin V were added to the cells and incubated at room temperature for 15 minutes in dark. After that, 400µl of 1X binding buffer were added to the cells and analyzed by flow cytometry within 30 minutes.

MOUSE INJECTION

Subcutaneous injection
8- to 10-week-old NOD/SCID mice were anesthetized with an intraperitoneal injection of Avertin/tribomethanol (Sigma). 200µl of cell suspension (2.5*10e6 cells/ml) was injected to the subcutaneous just above the pelvis of the mouse using 26G needle attached to 1ml syringe.

Tail-Vein injection
6- to 8-week-old NOD/SCID mice were kept in the mouse restraint, and 200µl of cell suspension (5*10e6 cells/ml) was injected to the vein of the tail using 30G needle attached to 1ml syringe.